Aziz M. Malek
Amr S. Azzouz
Mohsen M. Baligh
John T. Germaine

Undrained Cyclic Simple Shear Behavior of Clay with Application to Pile Foundations Supporting Tension Leg Platforms

MIT Sea Grant
College Program

Massachusetts
Institute of Technology
Cambridge, MA 02139

MITSG 87-20
August, 1987

UNDRAINED CYCLIC SIMPLE SHEAR BEHAVIOR OF CLAY WITH APPLICATION TO PILE FOUNDATIONS SUPPORTING TENSION LEG PLATFORMS

Aziz M. Malek

Amr S. Azzouz

Mohsen M. Baligh

John T. Germaine

$ 18.00

MIT Sea Grant
College Program

Massachusetts Institute
of Technology
77 Massachusetts Ave.
Cambridge, MA 02139

MITSG 87-20
August, 1987
NA84AA-D-00046
R/O 25

AUTHORS

Aziz M. Malek is a graduate Research Assistant in the MIT Department of Civil Engineering.

Amr S. Azzouz is the Vice Dean for Research and Academic Affairs at Kuwait University, Kuwait. He contributed to this project while an Associate Professor in the MIT Department of Civil Engineering.

Mohsen M. Baligh is Professor of Civil Engineering in the MIT Department of Civil Engineering.

John T. Germaine is Director of the Geotechnical Engineering Laboratory in the MIT Department of Civil Engineering.

ACKNOWLEDGEMENT

This research has been sponsored primarily by the National Oceanic and Atmospheric Administration through the MIT Sea Grant College Program, grant number NA84AA-D00046.

ABSTRACT

The objective of this study is to develop a basic understanding of the behavior of clays under combined static and cyclic loading conditions with particular application to deep water compliant offshore structures. The research attempts to identify and evaluate the effects of important factors on the behavior of clay elements subjected to the complex loading history typical of a Tension Leg Platform (TLP) foundation system in order to develop more rational and reliable methods for analyzing and predicting the behavior of pile shafts supporting such platforms.

A comprehensive laboratory testing program, consisting of the design and development of necessary testing equipment and the performance of an extensive number of cyclic direct simple shear (DSS) tests, was conducted on resedimented samples of Boston Blue Clay (BBC) with OCR values of 1, 1.4, 2 and 4. After consolidating the samples under K_0-conditions to the desired stress levels, they were subjected in a drained fashion to a horizontal average static (sustained) shear stress. The samples were then sheared in an undrained stress-controlled mode using sinusoidal waves with a constant period of 10 seconds.

Results, presented in a normalized format to allow generalizations and comparisons with other clays, show that there is a unified definition of failure in undrained cyclic DSS mode of shearing independent of the value of the average static shear stress acting on the soil during undrained cyclic shearing. Samples with different OCR values sheared under various shear stress combinations reach failure when the effective stress path approaches the maximum obliquity line from monotonic undrained DSS tests. Moreover, for normally consolidated BBC, there is a threshold shear stress level below which failure in stress-controlled undrained cyclic DSS shearing does not occur, even after subjecting the soil to a very large number of cycles.

A hypothesis of "Apparent Overconsolidation" (AOCR) due to undrained cyclic loading is presented, and implemented in a framework for predicting the undrained cyclic behavior of slightly overconsolidated clay samples from the basic results obtained on normally consolidated samples. The AOCR hypothesis is also incorporated in a superposition method for improving prediction of tests with variable cyclic shear stress levels. Comparisons with DSS test results indicate that the AOCR framework provides good predictions of the number of cycles at failure as well as evolution of shear strains during undrained cyclic DSS shearing.

RELATED REPORTS

This report is one of a series of MIT reports published as a result of Sea Grant sponsored research on offshore piles and marine soils. Other reports and unpublished theses related to this project are listed below. MITSG reports may be purchased from the MIT Sea Grant Program (617) 253-5944. For theses, microfiche only is available from Sea Grant. Paper copies of theses may be ordered from: MIT Libraries Microreproduction Lab (617) 253-5668.

Azzouz, A.S., M.M. Baligh, and C.C. Ladd. CONE PENETRATION AND ENGINEERING PROPERTIES OF THE SOFT ORINOCO CLAY. MITSG 82-11. 55 pp. $5.00.

Baligh, M.M, et al. PIEZOCONE PENETROMETER. MITSG 81-10. 21 pp. $3.50

Baligh, M.M., A.S. Azzouz, and R.T. Martin. CONE PENETRATION TESTS OFFSHORE THE VENEZUELAN COAST. MITSG 80-21. 164 pp. $8.00.

Baligh, M.M. and J.N. Levadoux. PORE PRESSURE DISSIPATION AFTER CONE PENETRATION. MITSG 80-13. 368 pp. $8.00.

Baligh, M.M., V. Vivatrat, and C.C. Ladd. EXPLORATION AND EVALUATION OF ENGINEERING PROPERTIES FOR FOUNDATION DESIGN OF OFFSHORE STRUCTURES. MITSG 79-8. 268 pp. $8.00.

Gadinsky, S.P. "Evaluation of the Engineering Properties of Clays with the Piezocone Penetrometer." Thesis, Department of Civil Engineering, MIT, 1983.

Germaine, J.T. "Development of the Directional Shear Cell for Measuring Cross Anisotropic Clay Properties." Thesis, Department of Civil Engineering, MIT, 1982.

Ghantous, I.B. "Prediction of In Situ Consolidation Parameters of Boston Blue Clay." Thesis, Department of Civil Engineering, MIT, 1982.

Kavvadas, M. "Non-Linear Consolidation Around Driven Piles in Clays." Thesis, Department of Civil Engineering, MIT, 1982.

Kavvadas, M. "Stress-Strain Models for Soils Based on Plasticity Theory." Thesis, Department of Civil Engineering, MIT, 1980.

Levadoux, J.N. "Pore Pressures in Clay Due to Cone Penetration." Thesis, Department of Civil Engineering, MIT, 1980.

Levadoux, J.N. and M.M. Baligh. PORE PRESSURES DURING CONE PENETRATION IN CLAYS. MITSG 80-12. 310 pp. $8.00.

Malek, A.M. "Compositional and Engineering Properties of Offshore Venezuelan Clay." Thesis, Department of Civil Engineering, MIT, 1983.

Mishu, R. "Evaulation of the Compositional and Engineering Properties of Offshore Venezuelan Soils: Tuy Cariaco Clays." Thesis, Department of Civil Engineering, MIT, 1982.

Morrison, M.J. "In Situ Measurements on a Model Pile in Clay." Thesis, Department of Civil Engineering, MIT 1984.

Stanichevsky, M.S. "A Study of End-Bearing Piles in the Boston Waterfront Area." Thesis, Department of Civil Engineering, MIT, 1982.

Urdaneta Lafee, E. "Evaluation of the Effects of Sample Disturbances on the Undrained Stress-Strain-Strength Properties of the Offshore Orinoco Clay." Thesis, Department of Civil Engineering, MIT, 1980.

TABLE OF CONTENTS

LIST OF SYMBOLS

Prefix Δ indicates a change

Suffix f indicates a final or failure condition

A bar over a stress indicates an effective stress.

GENERAL

BBC	Boston Blue Clay
z	Depth below mudline

INDEX AND CLASSIFICATION PROPERTIES

e	Void ratio
e_o	Initial void ratio
G_s	Specific gravity
LI	Liquidity Index
PI	Plasticity index
S	Degree of saturation
w	Water content
w_L	Liquid Limit
w_N	Natural water content
w_P	Plastic limit

STRESSES, STRAINS, MODULI, AND STRENGTH PARAMETERS

B	Skempton's pore pressure parameter $B = \Delta u/\Delta\sigma_c$
E_u	Undrained secant E
E_{50}	E half way to failure
G	Undrained shear modulus
K_c	$\bar{\sigma}_{hc}/\bar{\sigma}_{vc}$
K_o	Coefficient of earth pressure at rest (in situ)

LIST OF SYMBOLS

OCR	Overconsolidation ratio = $\bar{\sigma}_{vm}/\bar{\sigma}_{vo}$, $\bar{\sigma}_{vm}/\bar{\sigma}_{vc}$
p, $\bar{p}$	$1/2(\sigma_v + \sigma_h)$, $1/2(\bar{\sigma}_v + \bar{\sigma}_h)$
q	$1/2\ (\sigma_v - \sigma_h)$
q_f	$1/2\ (\sigma_1 - \sigma_3)_f$
S_t	Sensitivity = s_u(Undisturbed)/s_u(Remolded)
s_u	Undrained monotonic shear strength
s_u(NC)	Undrained monotonic normally consolidated shear strength
s_u(OC)	Undrained monotonic overconsolidated shear strength
s_u(DSS)	s_u from direct simple shear test
s_u(TC)	s_u from triaxial compression test
s_u(TE)	s_u from triaxial extension test
u	Pore water pressure
$\dot{\epsilon}$	Strain rate
ϵ_a	Axial strain
γ_{ave}	Average shear strain
γ_c	cyclic shear strain
γ, γ_f	Shear strain, shear strain at failure
σ, $\bar{\sigma}$	Normal total stress, normal effective stress
σ_c	Confining pressure
$\bar{\sigma}_c$	Consolidation pressure (isotropic)
σ_h	Horizontal normal stress
$\bar{\sigma}_{hc}$	Horizontal consolidation stress
σ_v	Vertical normal stress
τ	Shear stress
τ_{ave}	Average shear stress

LIST OF SYMBOLS

τ_c	Cyclic shear stress
τ_{ff}	τ on failure plane at failure
τ_h	τ on horizontal plane (direct simple shear test)
τ_m	Mooring shear stress
ϕ, $\overline{\phi}$	Slope of Mohr-Coulomb failure envelope
$\overline{\phi}_{MO}$	$\text{Tan}^{-1}(\tau/\overline{\sigma}_v)$ at maximum obliquity in monotonic DSS test
$\Delta u, \Delta u_f$	Excess pore pressure, excess pore pressure at failure

CONSOLIDATION PARAMETERS

ε_v	Vertical strain
$\overline{\sigma}_{vc}$	Vertical consolidation stress
$\overline{\sigma}_{vo}$	Initial vertical effective stress
$\overline{\sigma}_{vm}$	Maximum past pressure

CONSOLIDATION AND STRENGTH TESTS

CIUC	Isotropically consolidated undrained triaxial compression test
CK_oUC	K_o-consolidated undrained triaxial compression test
CK_oUE	K_o-consolidated undrained triaxial extension test
CK_oUDSS	K_o-consolidated undrained direct simple shear test
CK_oUCDSS	K_o-consolidated undrained cyclic direct simple shear test
DSS	Direct simple shear
TC	Triaxial compression
TE	Triaxial extension
UU	Unconsolidated-undrained shear test
UUC	UUC triaxial compression test

LIST OF SYMBOLS

CYCLIC TESTS

N	Number of cycles
N_f	Number of cycles at failure
$\overline{N}$	N/N_f
$\Delta\overline{u}$	$\Delta u/\Delta u_f$

LIST OF TABLES

LIST OF FIGURES

LIST OF FIGURES

LIST OF FIGURES

LIST OF FIGURES

LIST OF FIGURES

LIST OF FIGURES

LIST OF FIGURES

LIST OF FIGURES

LIST OF FIGURES

LIST OF FIGURES

LIST OF FIGURES

LIST OF FIGURES

LIST OF FIGURES

CHAPTER 1

INTRODUCTION

1.1 BACKGROUND

1.1.1 Introduction

Mankind has constantly explored the earth for various resources, including minerals and energy. Land was initially targeted for exploration and production before the oceans because of its easier accessibility and because of the limited available offshore technology. As the resources on land are dwindling or becoming more difficult to extract, mankind is turning to the oceans, which cover 70% of the surface of the earth.

The oceans include a vast amount of resources including food, minerals, and energy. Food is the oldest resource to be extracted from the oceans, although not to its full potential. Minerals cannot presently be extracted economically, but because of their abundance, technologies are being developed to enable future development of marine mining. Marine energy sources include hydrocarbon in the form of oil and gas, as well as thermal and kinetic energy in the ocean waters which have become the focus of recent research programs.[1]

Oil and gas represent the most developed ocean-based resource, about 90% of the value of all sub-sea mineral production.[2] The oil and gas resources of the offshore continental margins are quite significant, and the ocean frontiers are estimated to contain approximately 30% of the total

---

[1]Ronald L. Geer, "Engineering Challenges for Off-Shore Exploration and Production in the '80's," Proceedings of the Third International Conference on Behavior of Off-Shore Structures, M.I.T., Cambridge, MA, Vol. 2 Supplement, 1982, p. 1.

[2]Ibid, p.1.

hydrocarbon resource of the world.[3]

Because of the large offshore reserves of hydrocarbon, offshore oil and gas production will play an important role in the world energy supply. This, along with the future increase in production of food and minerals from the oceans, will require building an increasing number of offshore structures fulfilling numerous and diverse functions. Currently, the majority of offshore structures have been built for oil and gas exploration, drilling, production, temporary storage, and distribution, as well as living quarters.

Figures 1.1 and 1.2 show the evolution of platforms into deeper waters. Prior to 1947, wells were drilled from structures in inland lakes in the U.S.A. and in Lake Maracaibo in Venezuela. In 1947, the first platform was constructed in the open sea, out of sight of land, in 6 meters (20 feet) of water. Between 1947 and 1975, the height of offshore platforms increased steadily to 144 meters (474 feet), as the water depth overlying potentially rewarding offshore sites increased. Figure 1.2 shows a sudden increase in size of deep water platforms with the installation of the Hondo platform in 1976 off California in 260 meters (850 feet) of water, and the Cognac platform in 1978 in the Gulf of Mexico in 312 meters (1025 feet) of water. Both Hondo and Cognac are fixed steel jacket platforms, which are submerged trusses connected to the sea floor by driven piles, and supporting the drilling and operations platform. The Cognac platform remains the tallest steel jacket structure to date, and has held this record for nine years. Bullwinkle, a steel jacket type platform under

---

[3]Michel T. Halbouty, "Petroleum Still Leader in the Energy Race," Offshore, 20 June 1981, pp. 49-52.

construction, will be installed in 412 meters (1350 feet) of water in the Gulf of Mexico, in the fall of 1987, and will cause another sharp increase in platform water depth as shown in Figure 1.2.[4] There are over 2000 major offshore structures worldwide, most of which are steel jacket type platforms. About 17 concrete gravity structures have been built in the North Sea, and are among the largest and most complex structures.[5]

As the worldwide demand for energy increases, and as hydrocarbon reserves are discovered in deeper waters, more platforms will be built in deep water (greater than 1000 feet). Exploration wells have been drilled already in waters deeper than 2500 feet, and in the North Sea off Norway, significant discoveries were made in over 1100 feet of water.[6]

As the water depth increases, fixed platforms connected rigidly to the sea floor, including piled steel jacket platforms and gravity platforms, become more flexible. Such structures have their first natural frequency close to the dominant wave frequency, hence involve large dynamic amplifications. In order to avoid this, the rigidity of the structures should be increased. Stiffness and fatigue criteria, not strength, become dominant in the design process. Fixed steel jacket platforms have been proposed up to water depths of 1500 feet, assuming the bottom section is widened to increase the structural rigidity and therefore lower the first

---

[4]M. Lawson and J. Tuchman, "Gulf Platforms Head for Record Depths," Engineering News Records, Vol. 218, No. 11, 12 March 1987, p. 10.

[5]Griff C. Lee, "Design and Construction of Deep Water Jacket Platforms," Proceedings of the Third International Conference on Behavior of Off-Shore Structures, M.I.T., Cambridge, MA, Vol. 1, 1982, pp. 4-5.

[6]Geer, p. 3.

natural frequency.[7] However, the cost of increasing the rigidity of fixed offshore structures becomes prohibitive for large water depths and the development of new design concepts becomes necessary.

Compliant structures, which are not rigidly connected to the sea floor, have been proposed for deep waters. These structures involve flexible lateral connections, hence a first natural frequency much smaller than the characteristic wave frequency. The proposed designs include the following: Articulated or Buoyant Towers, Guyed Towers, Catenary Anchored Floaters, and Tension Leg Platforms (or TLP), and are shown in Figure 1.3. Huslid, Gudmestad, and Alm-Paulsen (1982), and Fay (1985) described the advantages and disadvantages of these alternate deep water structures for the North Sea. Articulated Towers are structures connected to the foundation template via an articulated joint, and are kept in a stable vertical position through a built-in buoyancy in the structure itself. Guyed Towers are flexible jacket type structures which rely on guylines for lateral stability. Catenary Anchored Floaters or Catenary Moored Platforms are floating platforms which are held to the bottom seafloor by catenary cables under tension, providing a stabilizing buoyancy. Tension Leg Platforms consist of a buoyant structure connected to the sea bottom by vertical tension legs, the latter being connected to piles driven into the soil. The legs consist of tethers which are tensioned to pull the hull down and provide vertical as well as lateral stability. The Guyed Tower and the Tension Leg Platform concepts are more promising than the other two designs, and both types have already been constructed.

---

[7]Lee, p. 10.

In 1983, the first Guyed Tower, the Lena Tower, was installed by Exxon in 1000 feet of water in the Gulf of Mexico.[8] The first Tension Leg Platform, shown in Figure 1.4, was installed in 1984 by Conoco in 485 feet of water in the Hutton field, the North Sea.[9] Conoco is currently working on the second tension leg platform to be installed in the Green Canyon field in the Gulf of Mexico, in 537 meters (1760 feet) of water, by 1989.[10]

Because of the large water depths and the peculiarities of the new concepts, compliant offshore structures offer new challenges in design and installation. Structural innovations and new materials are needed, as well as new and improved methods for geotechnical exploration, analysis, design, and installation of offshore foundations.

1.1.2 Foundation Design Considerations for Deep Water Compliant Structures

Buoyant Towers, Guyed Towers, and Tension Leg Platforms rely on piled foundations to resist the environmental forces (wind, waves, currents, earthquakes, ice). Bea, Dover, and Audibert (1982) reviewed existing pile design considerations for various deep water platforms, including jacket structures, and summarized special loading conditions for each type of structure:

Jacket platforms have piled foundations which are subjected to large axial compression loads and minor repeated load components. Load reversals

---

[8] M.S. Glasscock et al., "Design of the Lena Guyed Tower," Proceedings of the Sixteenth Annual Off-Shore Technology Conference, Houston, Texas, Vol. 1, Paper No. 4650, 1984, p. 19.

[9] H.Bradshaw, E.G. Stokes and M.J. Leece, "Hutton TLP Installation," Proceedings of the Seventeenth Annual Off-Shore Technology Conference, Houston, Texas, Vol. 2, Paper No. 4913, 1985, p. 159.

[10] Lawson and Tuchman, p. 10.

are limited to the top of the piles, and are not critical. Large lateral loads also act on the pile heads. Guyed Towers built on piles subject these piles to the same loading conditions as jacket platforms, namely large static axial compression loads with large repeated components, except that lateral loads on the piles are small since the structure relies on the guylines for lateral stability. Important axial load reversals occur. Bouyant Towers are supported by piles which are acted upon by small axial compression loading and large cyclic components, leading to important load reversals along a substantial portion of the pile length. Lateral loads can be important. Finally, Tension Leg Platforms are supported by several pile groups. These piles are acted upon by extremely large axial tension forces due to the pre-tensioning of the tethers creating the buoyancy forces acting on the platform. Large cyclic tensile loads are superimposed on the static tension bias. Minimal lateral loads act on the piles, which experience very little or no load reversal.[11]

Wave effects on the four platform types of compliant structures described above cause significant cyclic loading of their pile foundations and hence can represent an important consideration in pile design. In the case of the Tension Leg Platform, the combination of static and cyclic tensile loads, which tend to pull the piles out of the seafloor, is critical. The high construction cost of the foundations of platforms in deep waters prohibits the designer from being too conservative. This is why the soil properties must be understood with more certainty, which requires better estimates of the environmental loads, better site

---

[11]R.G. Bea, A.R. Dover and J.M.E. Audibert, "Pile Foundation Design Considerations for Deepwater Fixed Structures," Proceedings of the Third International Conference on Behavior of Off-Shore Structures, M.I.T., Cambridge, MA, Vol. 1, 1982, p. 134-135.

exploration, including geophysical surveys, in situ testing, and soil sampling, and better understanding of the behavior of soils under sustained and cyclic loads.[12]

This report is concerned with the cyclic properties of clayey deposits supporting Tension Leg Platform (TLP) piles. Fine grained deposits have been chosen because they often represent critical and common seafloor conditions. The TLP type of loading has been chosen because it is the most severe and the most unusual (tensile pile loads), and because TLP platforms are one of the most promising types of deep water structures. The following section describes in some detail the loading of a typical TLP pile.

1.1.3 Typical Loading of a TLP Pile

After installation of the piles in a TLP foundation, the TLP platform is connected to the foundation template with tethers under tension to counterbalance the buoyancy of the structure and hence provide its lateral stability. This imposes a large tensile load at the pile head, which in turn is resisted by means of shear stresses at the pile-soil interface. Figure 1.5(a) shows a typical TLP pile with the tensile mooring force F_m, and the corresponding mooring shear stresses τ_m, that generally decrease with depth z along the pile. Thereafter, a cyclic load F_c, caused principally by waves (but can also include wind and earthquake effects) is applied to the pile, leading to a cyclic variation in the stress distribution along the pile. Figure 1.5(b) illustrates the shear stress

---

[12] Ibid.

history for a soil element located at depth z, adjacent to the pile wall. During calm sea conditions, loading typically consists of an average shear stress equal to the mooring stress τ_m, over which are superimposed small variable cyclic shear stresses. During a storm, there is a surge in the mean sea level causing an increase in mean shear stress from τ_m to τ_{ave}. This increase in average shear stress is accompanied by large variable or cyclic shear stresses caused by wave loading. Storm loading represents a critical condition for pile design and storm-induced shear stresses are very complex involving wide bands of frequencies and amplitudes.

The prediction of the cyclic load capacity of TLP piles is very important in TLP design. This requires a thorough understanding of the cyclic behavior of soil elements surrounding the piles, when subjected to a variable time load history such as the one in Figure 1.5(b).

1.2 PURPOSE OF THE RESEARCH

The objective of the report is to investigate and determine the behavior of offshore sediments under the complex loading imposed by compliant offshore structures. The research attempts to achieve a better understanding of the important factors controlling the behavior of offshore piles subjected to a combined static and repeated loading typical of Tension Leg Platforms, in order to develop more rational and reliable methods for analysis and prediction.

Research consists of an extensive laboratory cyclic testing program on samples of Boston Blue Clay, using a Direct Simple Shear (DSS) apparatus modified for cyclic loading. The testing procedure and the type of loading are chosen to simulate the stresses imposed on soil elements at the

interface of TLP piles on the DSS samples.

Whereas the research program is aimed at Tension Leg Platforms, its results are applicable to all deep water offshore structures since all are connected to the seafloor by piled foundations which are acted upon by a combination of sustained and cyclic loads.

1.3 OUTLINE OF THE REPORT

Chapter 1 provides background information and defines the report objectives.

Chapter 2 presents a summary of previous studies conducted to investigate the behavior of clays subjected to cyclic loading.

Chapter 3 describes a framework for predicting the behavior of TLP piles under cyclic loading.

Chapter 4 describes the equipment used in the experimental program, outlines the testing procedure, and gives a summary of the performed tests.

Chapter 5 presents the results of undrained Direct Simple Shear (DSS) tests on normally consolidated samples of Boston Blue Clay (BBC). The following behavioral aspects are studied: the effects of τ_{ave} and τ_c, the failure conditions and modes, the existence of a threshold shear stress below which failure does not take place, and others.

Chapter 6 gives the results of undrained cyclic DSS tests on overconsolidated BBC.

Chapter 7 presents a hypothesis for apparent overconsolidation (AOCR) due to undrained cyclic loading. This hypothesis is used in predicting the cyclic behavior of slightly overconsolidated samples from test results on

normally consolidated clays. An improved method for predicting the results of cyclic tests with variable load levels is also presented.

Chapter 8 summarizes the important results of this study and presents its main conclusions.

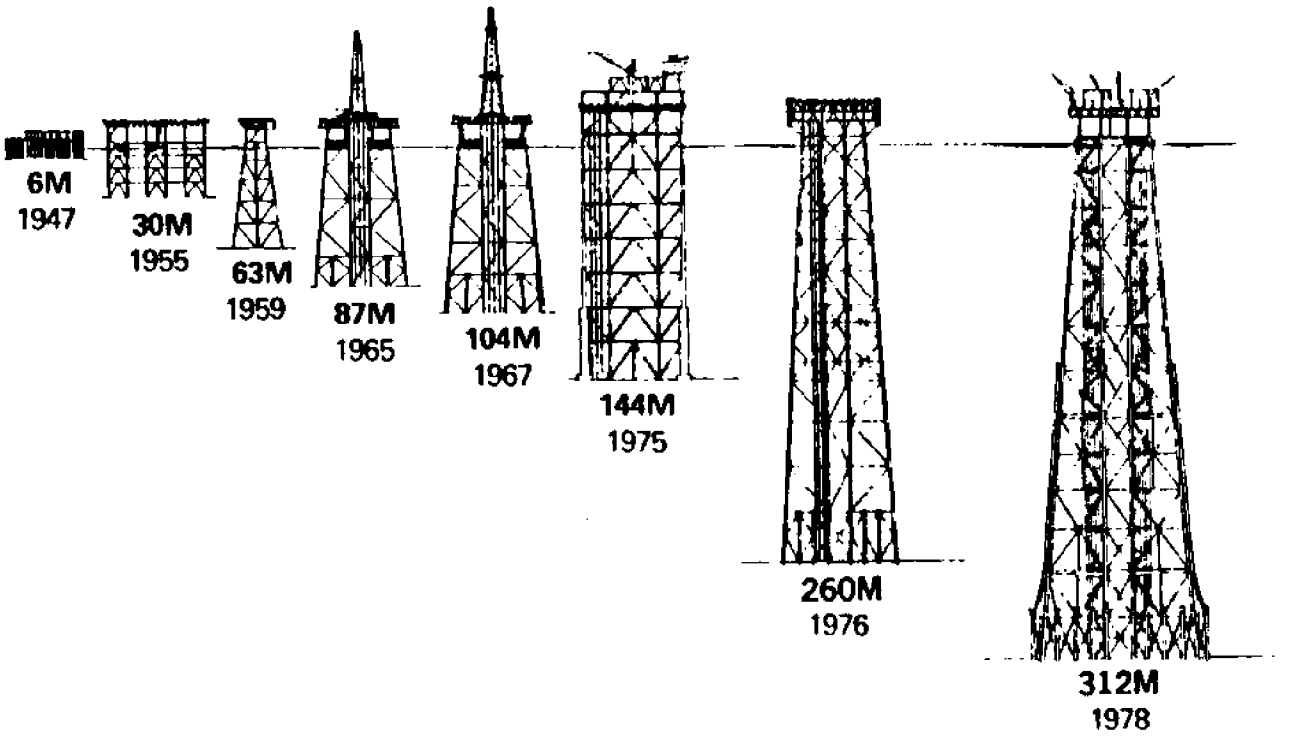

Figure 1.1 Offshore Jacket Platform Development (from G.C. Lee, 1982)

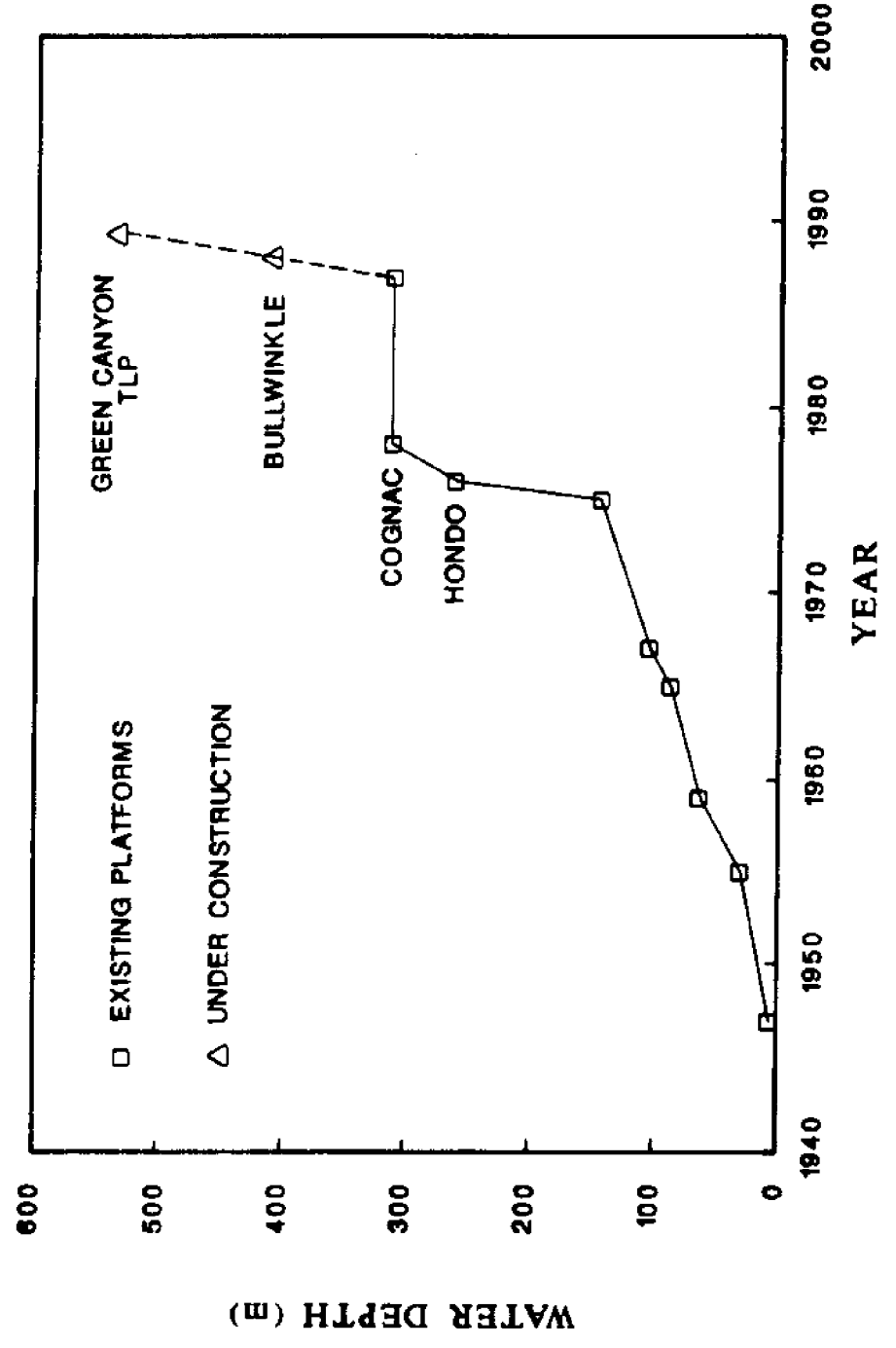

Figure 1.2 Offshore Platform Evolution

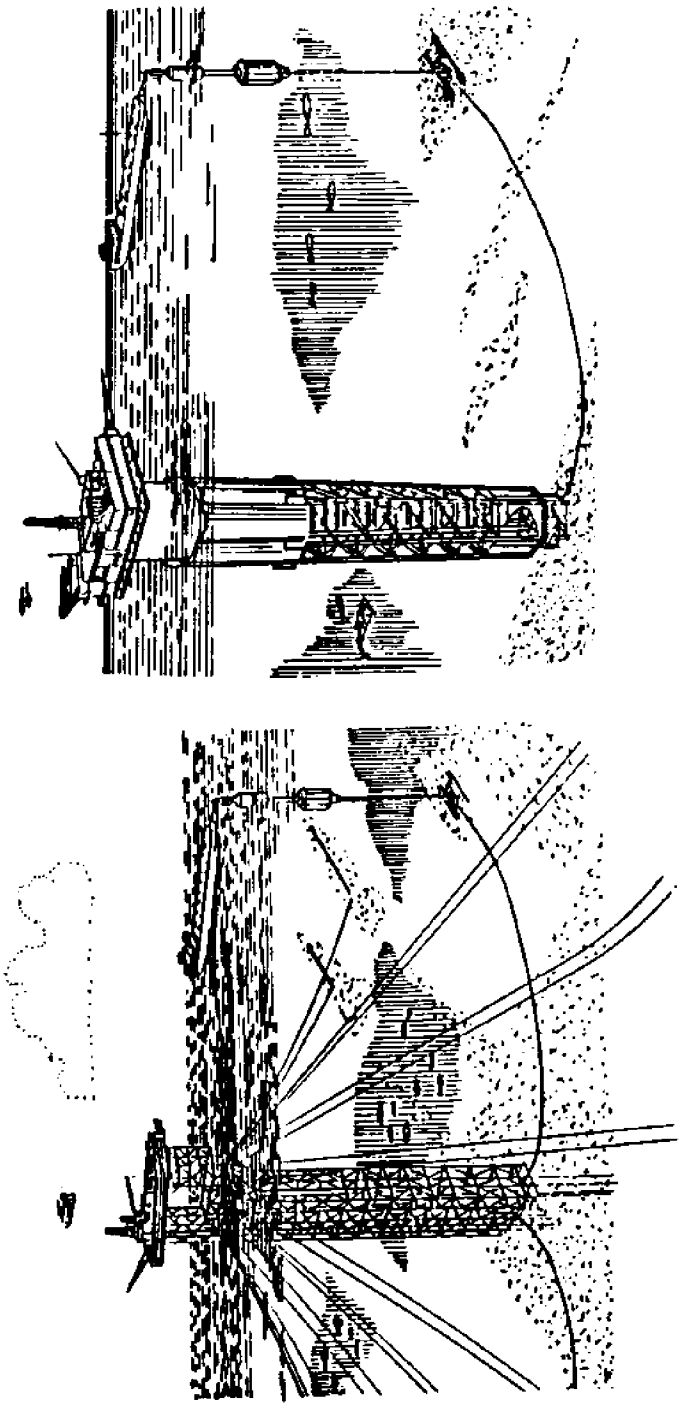

(a) The Guyed Tower Structure (b) The Buoyant Tower Structure

Figure 1.3 Compliant Offshore Structure Concepts (from C.E. Fay, 1985)

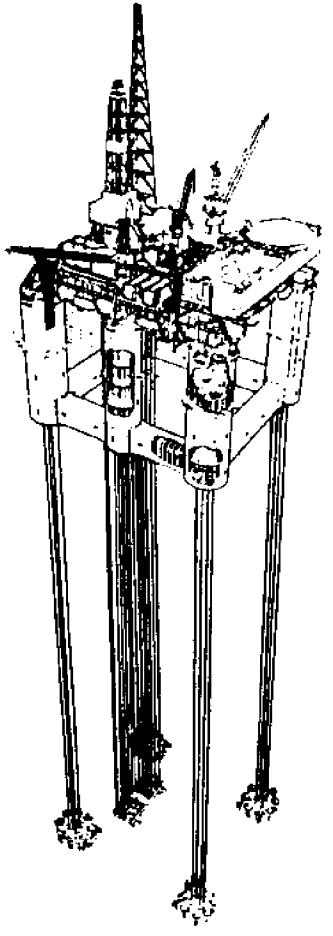

(c) The Tension Leg Platform (TLP)

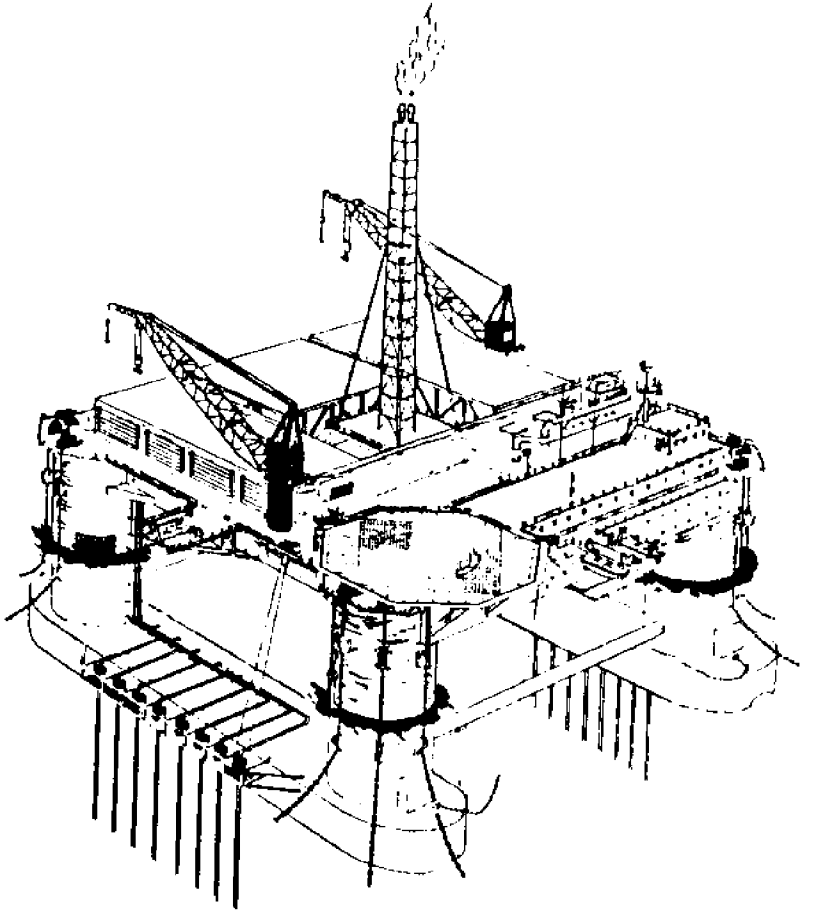

(d) The Catenary Anchored Floater (CAF)

Figure 1.3 (continued) Compliant Offshore Structure Concepts (from C.E. Fay, 1985)

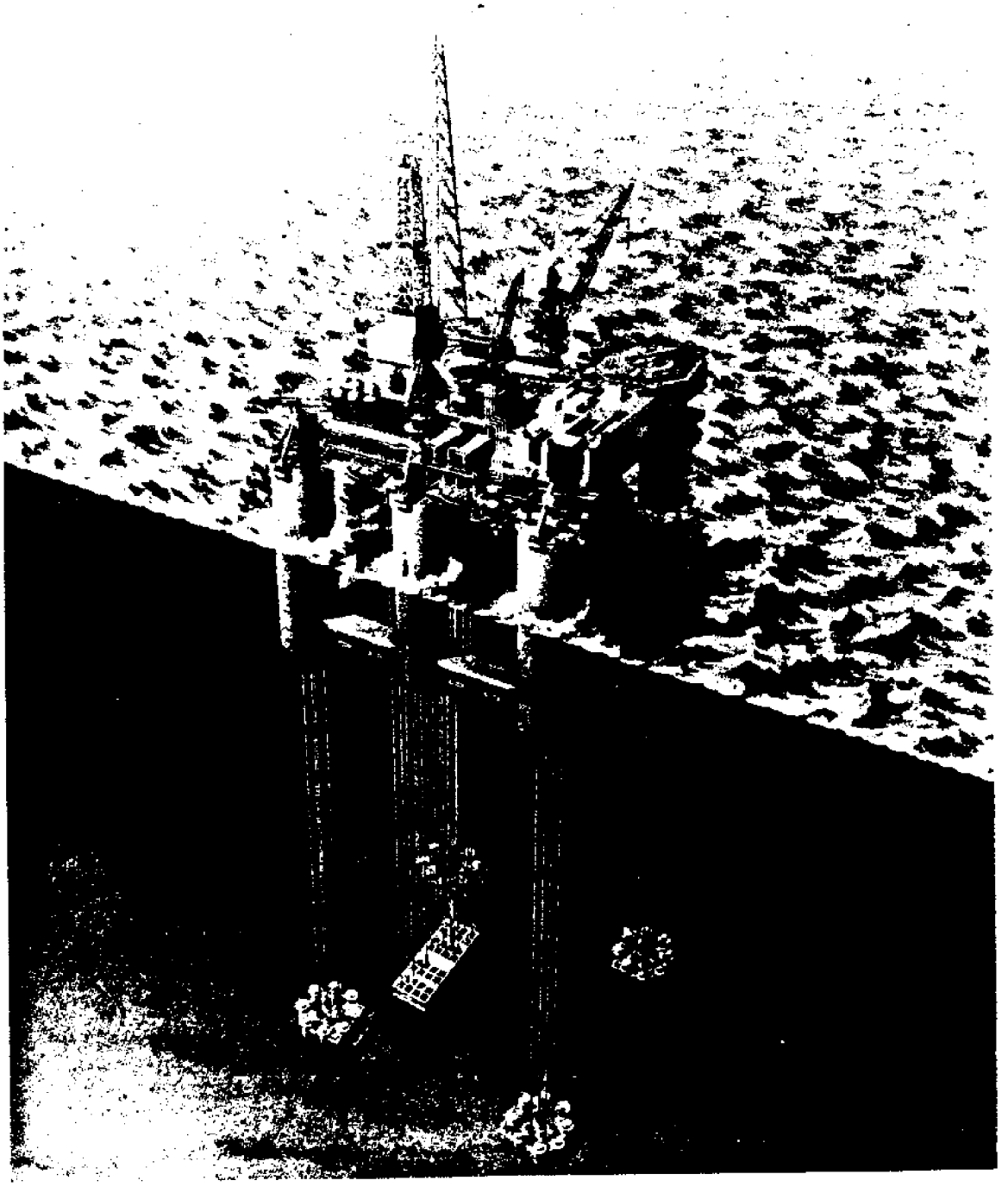

Figure 1.4 Hutton TLP Concept Showing Well Template, Foundation Templates, Floating Platform, and Marine Pipeline. (from Kelland et al., 1985)

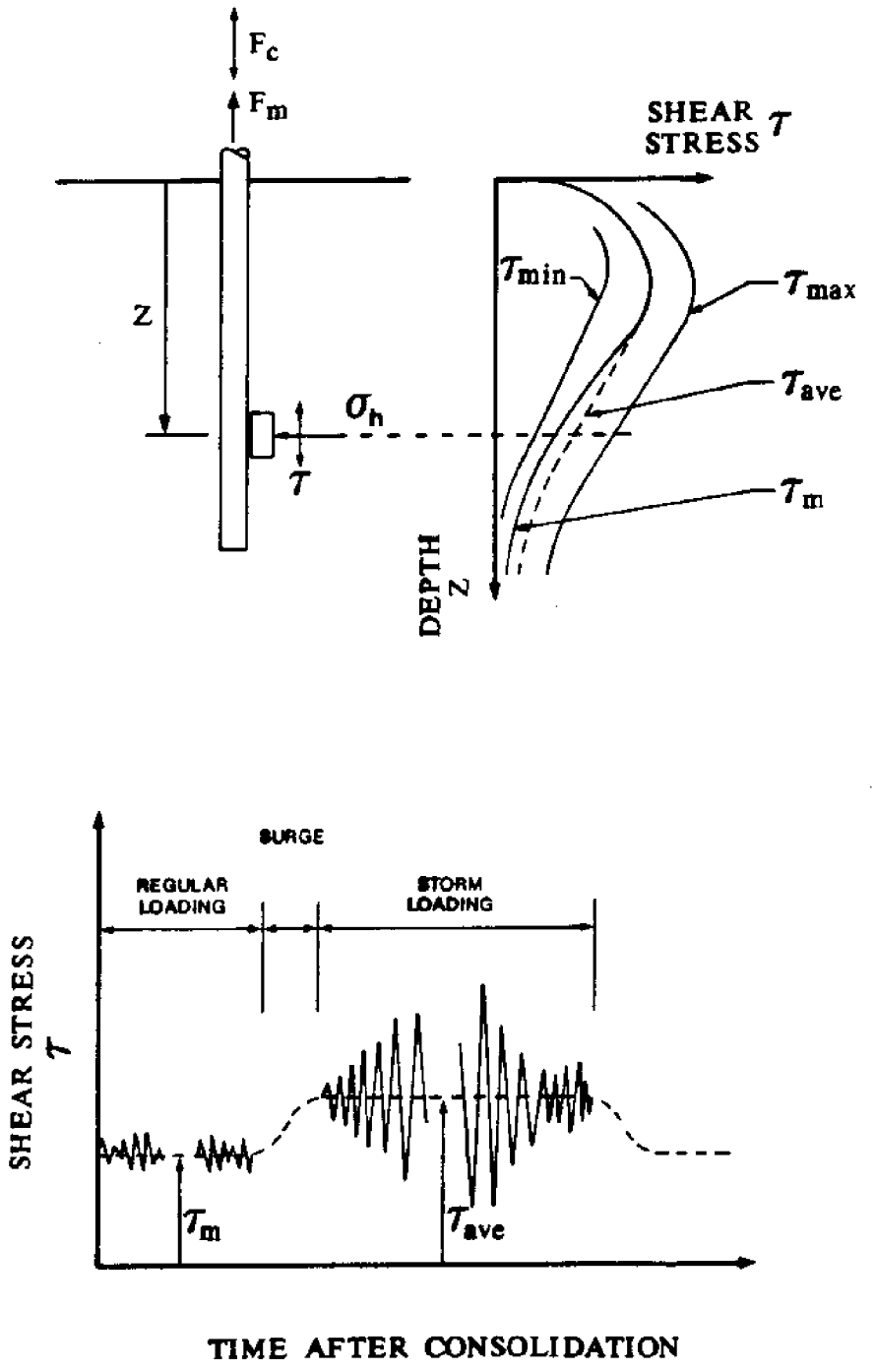

Figure 1.5 a) Typical Shear Stress Distribution Along TLP Pile
b) Typical Time History of Shear Stress at Depth z Along TLP Pile

CHAPTER 2

A LITERATURE REVIEW OF CYCLIC BEHAVIOR OF CLAYS UNDER TLP LOADING CONDITIONS

2.1 INTRODUCTION

The cyclic behavior of clays has previously been studied by numerous researchers. Most of the previous work has been related to clay behavior under dynamic loads (traffic loads on highways, earthquake resistant structures, etc.), and under cyclic loads due to waves and winds in offshore structures.

Appendix A presents a comprehensive summary of important publications dealing with the cyclic behavior of clays. The current research is concerned with the behavior of clays in undrained cyclic direct simple shearing (DSS), with cyclic loading typical of Tension Leg Platforms (TLP). Therefore, this chapter will only present a summary of previous laboratory testing programs dealing with stress-controlled cyclic DSS tests.

The following sections present a partial summary of the work of Andersen at the Norwegian Geotechnical Institute, Dyvik and Zimmie at the Rensselaer Polytechnic Institute, and Goulois at MIT. Only those topics which are directly related to the current research are included.

2.2 SUMMARY OF ANDERSEN'S WORK

The Norwegian Geotechnical Institute (NGI) has devoted a comprehensive effort over the last 10 to 15 years to the understanding of the important soil-structure interaction aspects affecting the foundation performance of

offshore structures. The work initially concentrated on gravity structures, but has recently focused on deep-water platforms. Of interest herein are the efforts carried out by Andersen and his co-workers related to the laboratory investigation of clay behavior under cyclic loading conditions (Andersen, 1975, 1976; Andersen et al., 1980), which included an extensive number of triaxial and direct simple shear tests mostly on Drammen clay. Drammen Clay is a plastic clay with an average natural water content, liquid limit and plasticity index of 52%, 55%, and 27%, respectively.

Samples tested in the Geonor direct simple shear device, of particular relevance to the current research, were initially K_o-consolidated to stress levels greater than the preconsolidation pressure and then unloaded to the desired overconsolidation ratio, OCR, with the majority of the tests run at OCR's equal to 1, 4, and 10. Static (i.e. monotonic) undrained tests were first performed to establish the stress-strain-strength characteristics of Drammen clay under monotonic loading conditions. The basic cyclic testing program consisted of constant volume (i.e. undrained), stress-controlled tests with horizontal cyclic shear stresses, τ_c (see Figure 1.5 for notations), alternating between equal positive and negative values (i.e., two-way loading), which were mostly kept constant throughout each test. A few two-way loading tests were, however, conducted where the samples were subjected to variable cyclic shear stress levels during shearing to simulate storm loading conditions. Sinusoidal as well as trapezoidal cyclic wave pulses with a period of 10 seconds were used. Upon completion of the cyclic tests, undrained monotonic tests were performed, without allowing the samples to drain, in order to investigate the effect of cyclic loading on subsequent undrained static strength.

The major findings of the NGI two-way loading DSS testing programs are presented in Figures 2.1 through 2.4 and are summarized below:

1. During cyclic shearing, samples experience two-way symmetrical cyclic shear strains, γ_c, with no permanent strains. Figure 2.1(a) shows that the magnitude of γ_c increases with increasing number of cycles, N. However, this rate of increase is a function of the cyclic shear stress level, τ_{hc}/τ_{hf} ($\tau_{hc}=\tau_c$=cyclic horizontal shear stress; $\tau_{hf}=s_u$=monotonic undrained shear strength). For a low cyclic shear stress level, γ_c becomes essentially constant with N, whereas for high stress levels, γ_c increases rapidly to failure (defined herein as $\gamma_c = \pm 3\%$).

2. Permanent excess pore pressures, u_p, develop in the samples as a result of undrained cyclic shearing. The magnitude of excess pore pressures increases with the cyclic shear stress level and with the number of cycles (Figure 2.1(b)).

3. The stress-strain response during cyclic shearing is hysteretic in nature (Figure 2.2), with the size of the hysteresis loops increasing with N. The secant modulus, defined as the slope of the line connecting the peaks of the hysteresis loop, decreases as the number of cycles increases.

4. The number of cycles to failure, N_f (corresponding to $\gamma_c = \pm 3\%$) decreases rapidly with increasing cyclic shear stress level. The relationship between N_f and τ_{hc}/τ_{hf} is shown in Figure 2.3, and is a function of the overconsolidation ratio of the clay. For example, at a value of τ_{hc}/τ_{hf} of $\pm$ 0.5, the number of cycles to failure for the normally consolidated Drammen clay (OCR=1) is about 50 times larger than that corresponding to OCR=10.

5. Utilizing the results of stress-controlled tests, it is possible to construct contour lines of equal cyclic shear strain, γ_c, as a function

of cyclic shear stress level and N. Such contours are referred to as the S-N diagrams, and a set corresponding to the normally consolidated Drammen clay is illustrated in Figure 2.4. Based on these S-N diagrams, Andersen developed a procedure for predicting the results of variable cyclic stress level tests from those performed with constant τ_c. The procedure, valid for two-way symmetrical loading, is based on the assumption that the previous history of cycling is contained in the knowledge of the cyclic shear strain at any cycle number less than that to failure. The details of the Andersen superposition technique, which gives good predictions of N_f and γ_c at intermediate cycles, are given in Chapter 3.

6. The effect of undrained cycling on subsequent monotonic behavior was also investigated by Andersen. The results indicate that for overconsolidated clays, the effective stress-strength parameters, $\bar{\phi}$ and $\bar{c}$ are not influenced by previous undrained cyclic loading. However, for normally consolidated clay, undrained cyclic loading causes the samples to behave as overconsolidated in subsequent monotonic shearing. A detailed summary of these results is given in Chapter 6.

2.3 SUMMARY OF THE WORK OF DYVIK AND ZIMMIE

Dyvik and Zimmie (1981) conducted constant volume (undrained) cyclic DSS tests on Gulf of Mexico Clay (PI=75%) and on reconstituted Pacific Illite (PI=56%). Symmetrical, two-way stress-controlled cyclic tests, with a period of 4 seconds, were performed using a Geonor DSS apparatus, modified for cyclic testing. All specimens were consolidated into the normally consolidated range, after which they were cycled undrained.

The range of cyclic shear stress level, τ_c, expressed as a percentage

of the undrained monotonic DSS strength varied between 0.42 and 0.65 for the Gulf of Mexico clay, and between 0.37 and 0.58 for the Pacific Illite.

Figures 2.5(a) and (b) show the relationship between the cyclic shear strain γ_c (one half the peak to peak strain) and the number of cycles, for both clays. The shear strain gradually increases, and reaches large values at failure (in excess of 10%), except for tests with low values of the cyclic shear stress ratio. Three tests with $\tau_c/s_u < 0.44$ do not fail, but reach stabilizing strain values.

Figure 2.6(a) and (b) show the excess pore pressure normalized by the vertical consolidation stress, versus the cycle number, for both clays. The excess pore pressure increases with number of cycles until failure or termination of the test.

Figure 2.7(a) and (b) show contours of equal cyclic shear strain in a cyclic shear stress ratio versus number of cycles space. The curves seem to converge to a threshold stress boundary below which no failure occurs. The value of the threshold is about 0.42 for Gulf of Mexico Clay, and 0.45 for the Pacific Illite.

Figure 2.8 plots contours of equal normalized excess pore pressure as a function of the cyclic shear stress level, τ_c/s_u, and cycle number, N, for reconstituted Pacific Illite. The excess pore pressure contours are similar to the curves of equal cyclic shear strain shown in the S-N curves in Figures 2.7(a) and (b). These excess pore pressure contours were used to predict the number of cycles to failure N_f for tests with variable τ_c, by ensuring continuity of excess pore pressure as τ_c is varied (as opposed to the Andersen superposition procedure which ensures continuity of cyclic shear strains). The N_f values obtained using the pore pressure method are slightly higher than those obtained using the Andersen method,

but are in good agreement with measured data.

2.4 SUMMARY OF THE WORK OF GOULOIS

At MIT, Goulois (1982) focused on the study of the behavior of a single tension pile in clay subjected to the storm loading conditions typical of a TLP foundation system (see Figure 1.5). His work included three main parts. The first was a theoretical study of the cyclic interaction between a TLP pile and the surrounding clay using elasto-plastic models. The second was an experimental investigation of the effect of average shear stresses on the cyclic behavior of normally consolidated plastic Drammen clay, and consisted of twelve constant volume stress-controlled direct simple shear tests subjected to both τ_{ave} and τ_c. Finally, the third part involved the development of a computer algorithm for predicting the cyclic behavior of tension piles by incorporating the soil degradation data obtained from the DSS tests into a pile model. Only the results of the experimental program, which are of direct importance to the present research, are summarized below.

Goulois' work extended NGI's previous results to the case of $\tau_{ave} \neq 0$, and hence represents the first attempt at investigating the behavior of a clay element adjacent to a TLP pile shaft using the Geonor DSS device. The testing procedure, illustrated in Figure 2.9, consisted of first consolidating the clay samples under K_o-normally consolidated conditions to a stress level of 392.4 kPa, which is well beyond the maximum past pressure of approximately 100 kPa. Shortly after the application of the last consolidation increment, the average shear stress, τ_{ave}, was applied in a drained fashion. The samples were left to creep under the application of

τ_{ave} for 19 hours, after which constant volume (or undrained) cyclic shearing was performed. Cycling was trapezoidal in shape, with a period of 10 seconds in all but two tests for which the period was 12 seconds. Cyclic loading was limited to 2000 cycles or to a failure condition defined either by γ_{ave} reaching 15% or γ_c reaching ± 3%. Ten tests were performed with constant τ_{ave} and τ_c, and two with constant τ_{ave} but variable τ_c. The range of different values of τ_{ave} and τ_c investigated by Goulois is presented in Figure 2.10, which shows that the values of the average shear stress ratio, τ_{ave}/s_u, where s_u is the undrained monotonic DSS strength, varied between 0.3 and 0.7. The values of the cyclic shear stress ratio, τ_c/s_u, varied between 0.3 and 0.6. Figure 2.9 shows the loading stages and notations.

An example of the results obtained by Goulois is presented in Figure 2.11, which shows the evolution of shear strain (solid lines) and excess pore pressures (dotted lines) with time (i.e., number of cycles) from four tests. The deformations plotted in this figure are the envelopes of γ_{max} and γ_{min} (expressed in percent with respect to the end of the K_o-consolidation sample height). Results in Figure 2.11 show the following:

1. The average, or permanent, component of strain, γ_{ave}, represented by the average of the deformation bands in Figure 2.11, is much larger than the cyclic strain, γ_c (given by half of the band's width). Moreover, the values of γ_c did not significantly change as samples approached failure (i.e., γ_{ave}=15%). In other words, the width of the deformation bands in Figure 2.11 is essentially constant. This is significantly different from the behavior of soil elements subjected to a symmetrical two-way loading (i.e., τ_{ave}=0) presented earlier in Figure 2.1 where no permanent shear

strain was accumulated.

2. As time increases, the deformation curves exhibit a very rapid increase. Samples 1 and 11 did not accumulate enough strains to reach failure, and tests were stopped after 1500 and 2000 cycles, respectively.

3. The excess pore pressure curves show a very rapid increase with number of cycles, followed by a slower, almost linear region to failure.

4. The influence of τ_c and τ_{ave} on the evolution of strains and pore pressures can be identified by comparing the results of the four tests in Figure 2.11 (i.e., Test 3 vs. 11, and 7 vs. 11).

In order to present the results in a coherent manner allowing extrapolations to new stress conditions, Goulois introduced the concept of 3-D strain contour, which is an extension of the work done by Andersen for τ_{ave}=0. The 3-D strain contour consists of the average strain, γ_{ave}, corresponding to given values of τ_c and τ_{ave} after N shear cycles, and is presented in normalized τ_c-normalized τ_{ave}-log N plot. Surfaces are then obtained by joining points of equal γ_{ave}, creating the iso-γ_{ave} network. Similar surfaces can also be obtained for constant γ_c, the iso-γ_c network.

Since 3-D surfaces are difficult to present graphically, cross-sections at specific values of N would yield curves of iso-γ_{ave} and iso-γ_c as a function of τ_{ave}/s_u and τ_c/s_u. Figure 2.12(a) and (b) show typical iso-γ_{ave} and iso-γ_c contours for the case of N=50 cycles. The degradation of a specific iso-γ contour with number of cycles may be presented by plotting the iso-γ curves at different cycle umbers in a τ_{ave}/s_u and τ_c/s_u space. Figure 2.13(a) and (b) show the degradation of the contours corresponding to γ_{ave}=4% and γ_c=0.5%, respectively.

Goulois also introduced a superposition method for estimating the

results of tests with variable τ_c for the case of $\tau_{ave} \neq 0$. Goulois' method is identical to Andersen's method, which applies only to the case of $\tau_{ave}=0$, except that the continuity of γ_{ave} is ensured rather than that of γ_c. Goulois evaluated his superposition procedure by comparing its predictions with the evolution of γ_{ave} versus N from two tests with constant τ_{ave} and variable τ_c with a fit on γ_{ave}. The maximum error was about 20%, and the number of cycles at failure was predicted with a 10% error on the conservative side.

In summary, Goulois' experimental contribution lies in the concept of 3-D strain contour diagrams which allow interpolation and extrapolation over a wide range of data, as well as visualization of the degradation which occurs during cycling. Also, the extension of Andersen's procedure with a fit on γ_{ave} to the case of $\tau_{ave} \neq 0$ allows satisfactory estimates of clay behavior under constant τ_{ave} and variable τ_c.

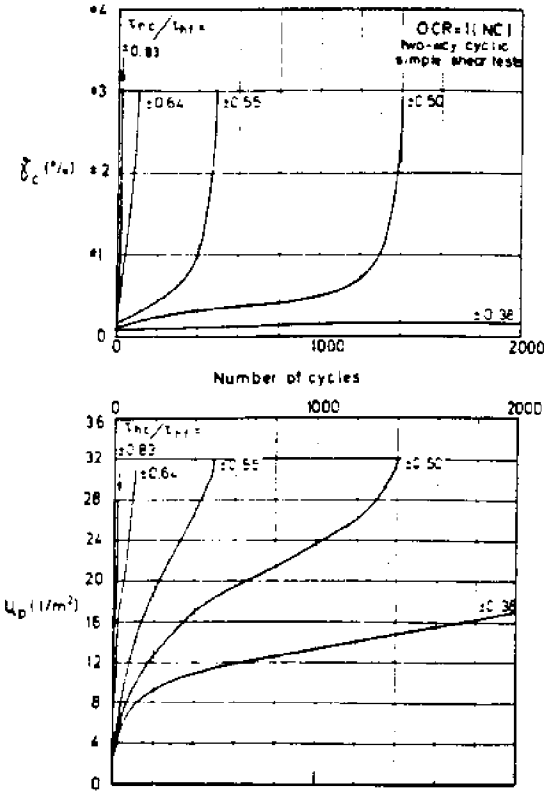

Figure 2.1 Results of Undrained Two-Way Cyclic DSS Tests on Normally Consolidated Drammen Clay:
a) Cyclic Shear Strain versus Number of Cycles
b) Excess Pore Pressure versus Number of Cycles
(from Andersen, 1975)

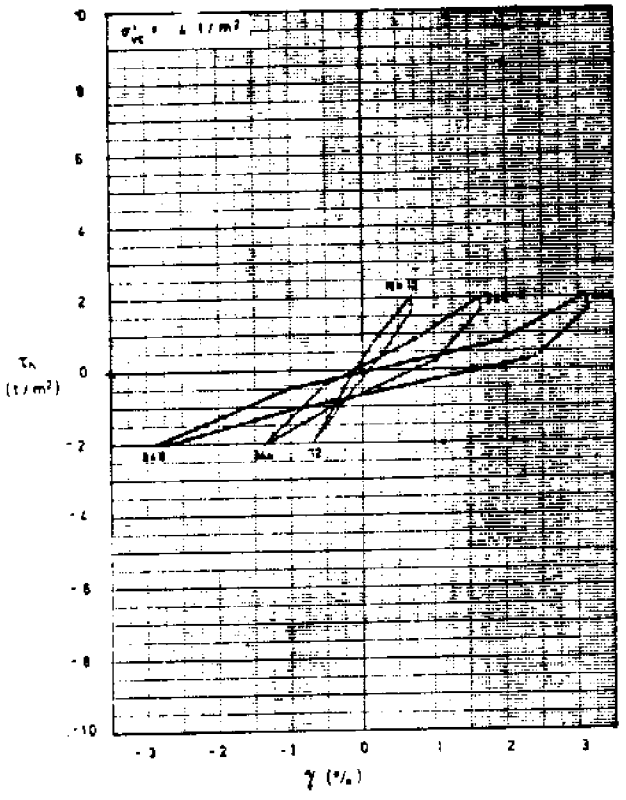

Figure 2.2 Typical Stress Strain Curve from Undrained Two-Way Cyclic DSS Tests on Normally Consolidated Drammen Clay (from Andersen, 1975)

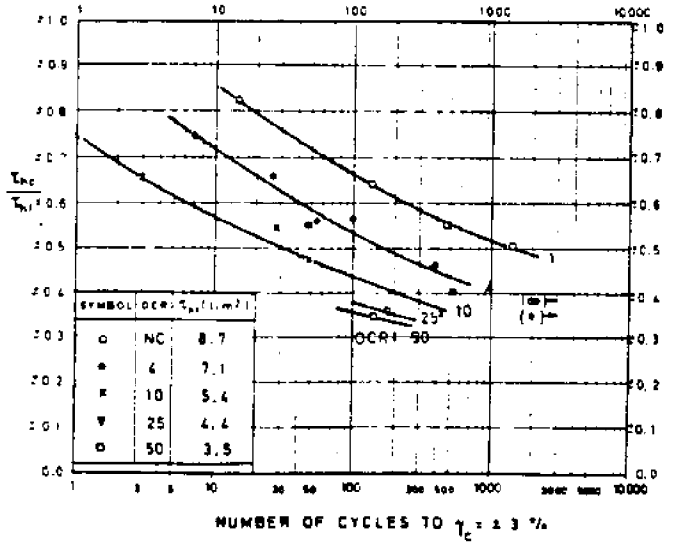

Figure 2.3 Number of Cycles at Failure (γ_c=±3%) as a Function of the Cyclic Shear Stress Level in Undrained Two-Way Cyclic DSS Tests on Drammen Clay with OCR=1, 4, 10, 25, and 50 (from Andersen, 1975)

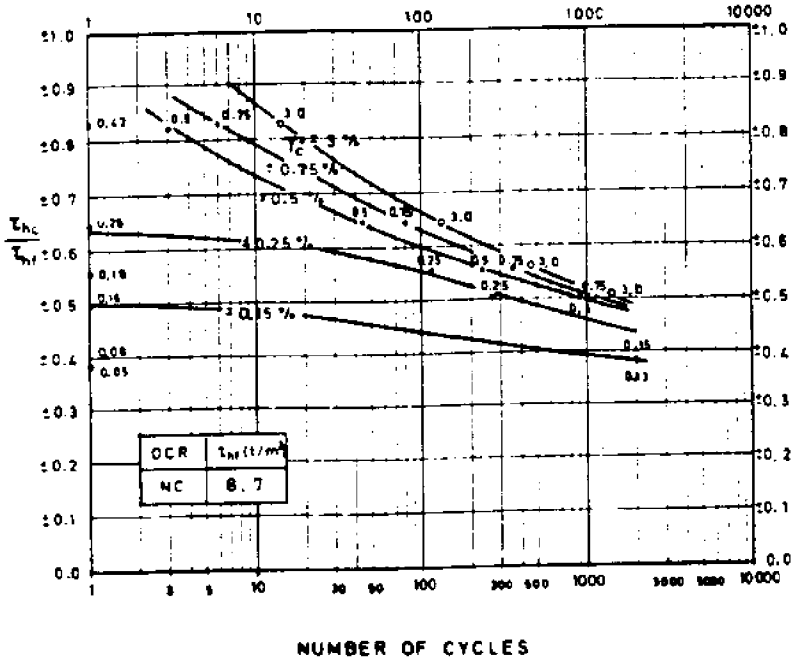

Figure 2.4 S-N Curves for Normally Consolidated Drammen Clay (from Andersen, 1975)

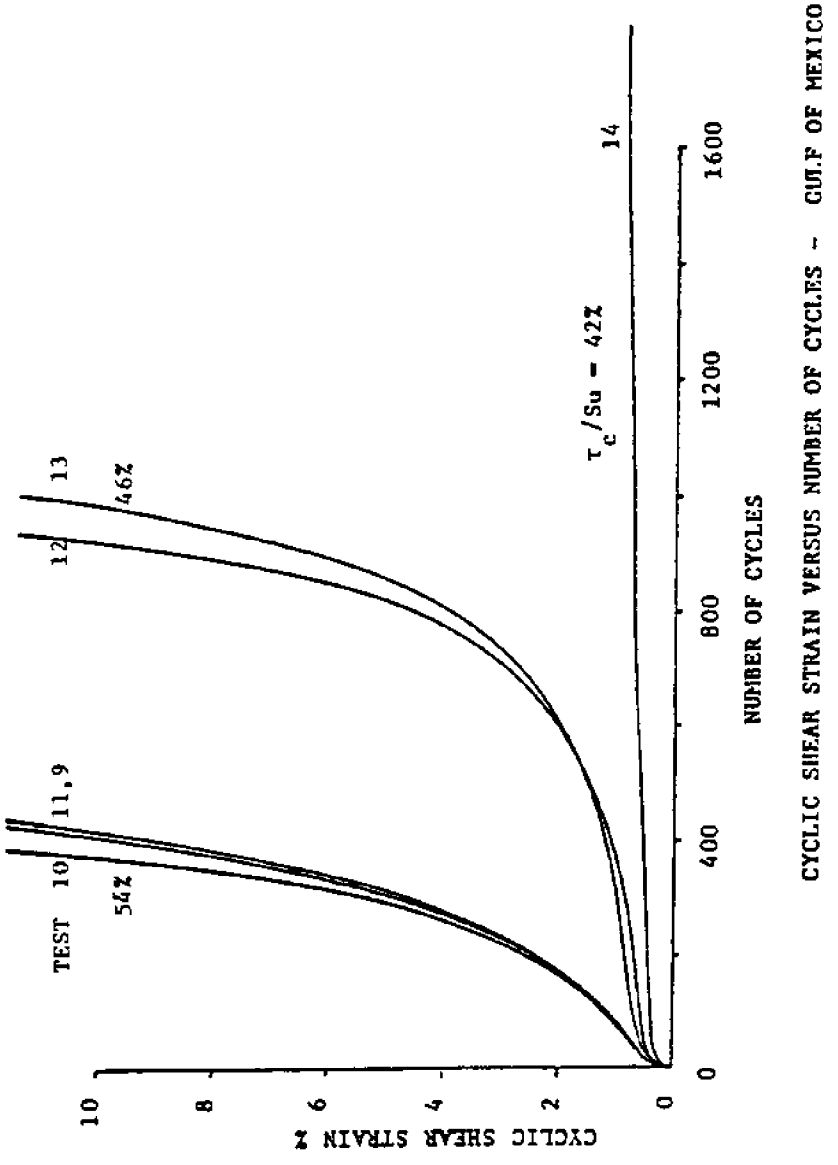

Figure 2.5 Cyclic Shear Strain versus Number of Cycles in Undrained Two-Way Cyclic DSS Tests on:
a) Normally Consolidated Gulf of Mexico Clay
(from Dyvic and Zimmie, 1981)

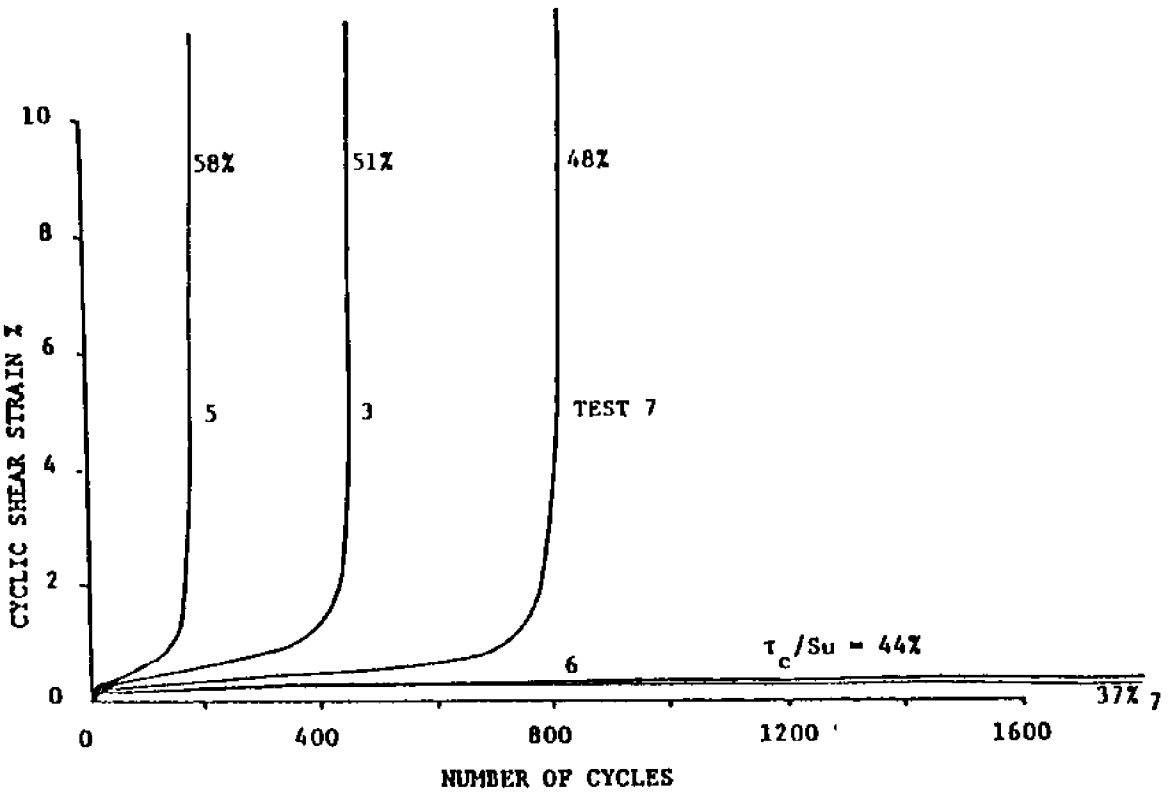

Figure 2.5 Cyclic Shear Strain versus Number of Cycles in Undrained Two-Way Cyclic DSS Tests on:
b) Normally Consolidated Pacific Illite
(from Dyvic and Zimmie, 1981)

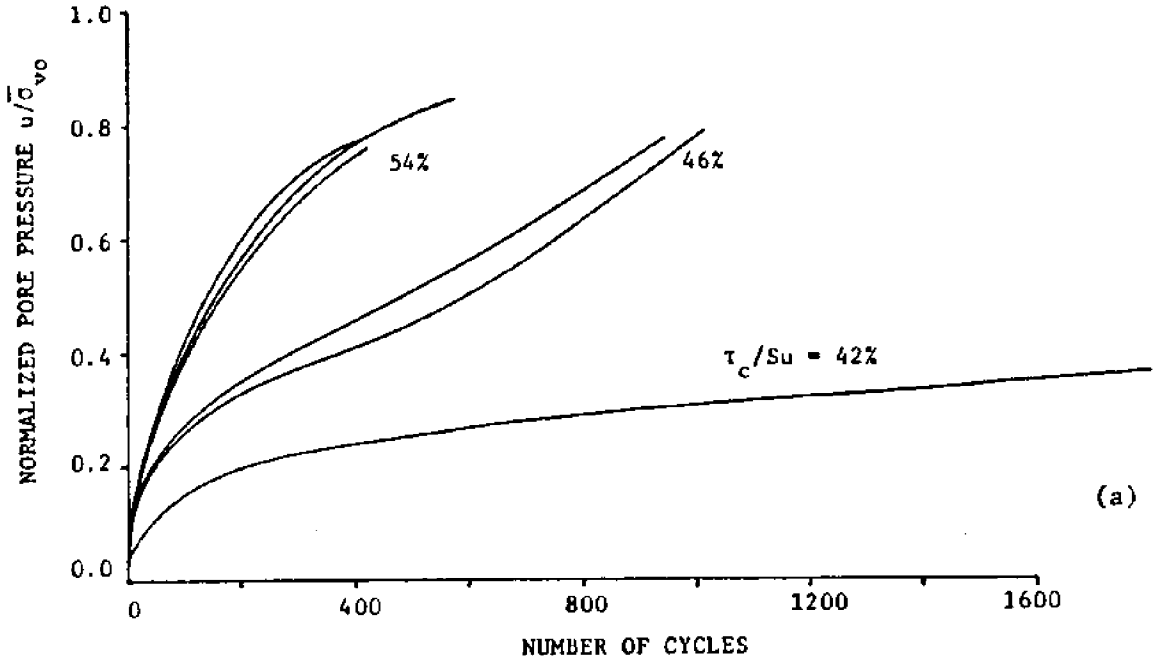

NORMALIZED PORE PRESSURE VERSUS NUMBER OF CYCLES - GULF OF MEXICO CLAY

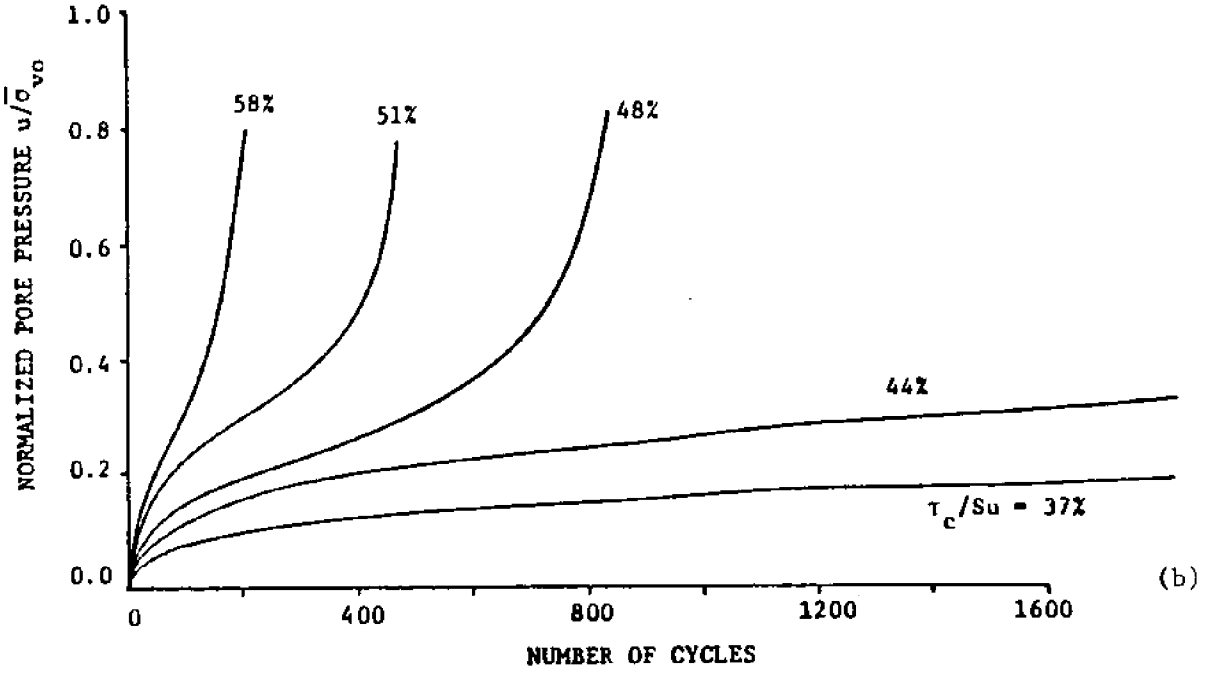

NORMALIZED PORE PRESSURE VERSUS NUMBER OF CYCLES - PACIFIC ILLITE

Figure 2.6 Normalized Excess Pore Pressure versus Number of Cycles in Undrained Two-Way Cyclic DSS Tests on:
a) Normally Consolidated Gulf of Mexico Clay
b) Normally Consolidated Pacific Illite
(from Dyvic and Zimmie, 1981)

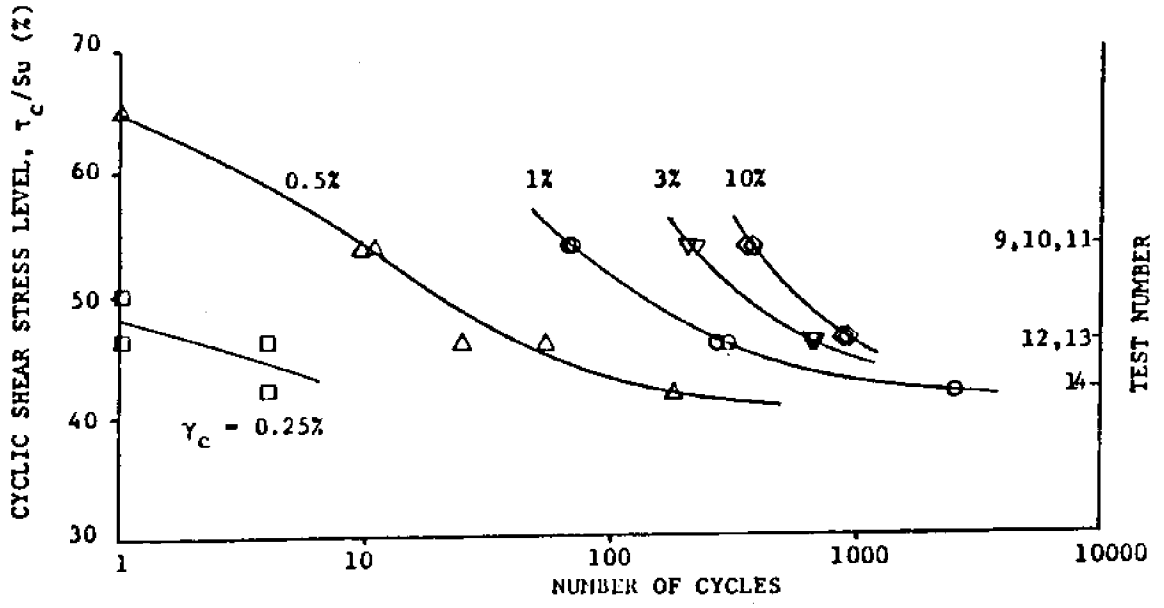

(a) CYCLIC SHEAR STRESS LEVEL VERSUS NUMBER OF CYCLES TO VARIOUS SHEAR STRAIN LEVELS - GULF OF MEXICO CLAY

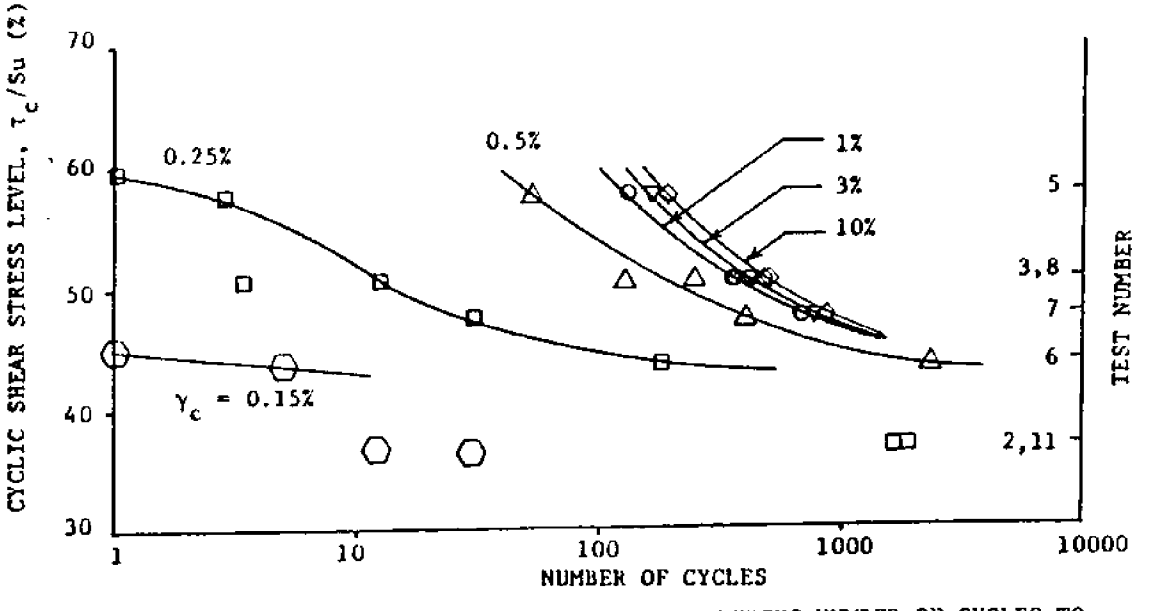

(b) CYCLIC SHEAR STRESS LEVEL VERSUS NUMBER OF CYCLES TO VARIOUS SHEAR STRAIN LEVELS - PACIFIC ILLITE

Figure 2.7 a) S-N Curves for Normally Consolidated Gulf of Mexico Clay
b) S-N Curves for Normally Consolidated Pacific Illite
(from Dyvic and Zimmie, 1981)

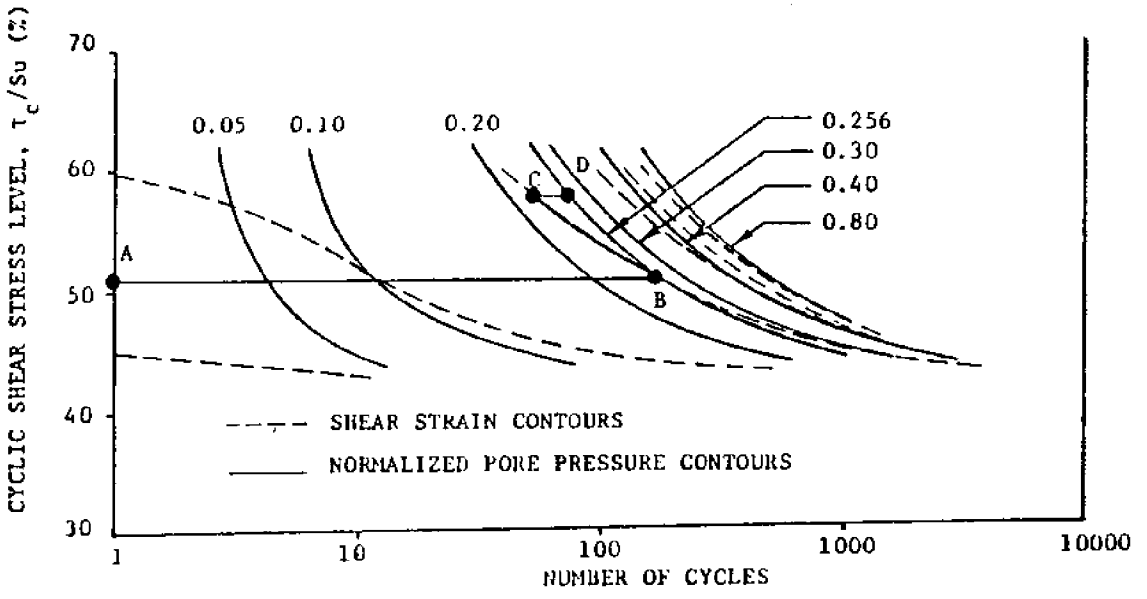

CYCLIC SHEAR STRESS LEVEL VERSUS NUMBER OF CYCLES TO VARIOUS SHEAR STRAIN LEVELS AND NORMALIZED PORE PRESSURES PACIFIC ILLITE

Figure 2.8 Contours of Equal Excess Pore Pressure in a Cyclic Shear Stress Ratio versus Number of Cycles Space for Normally Consolidated Pacific Illite
(from Dyvic and Zimmie, 1981)

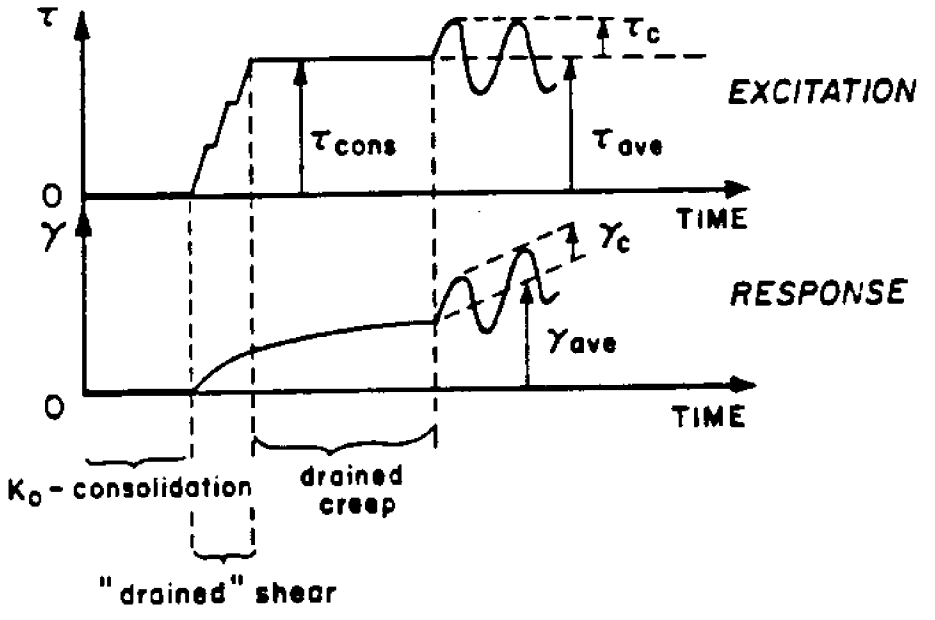

Figure 2.9 Test Procedure and Notations of Undrained Cyclic DSS Tests on Normally Consolidated Drammen Clay with $\tau_{ave} \neq 0$ (from Goulois, 1982)

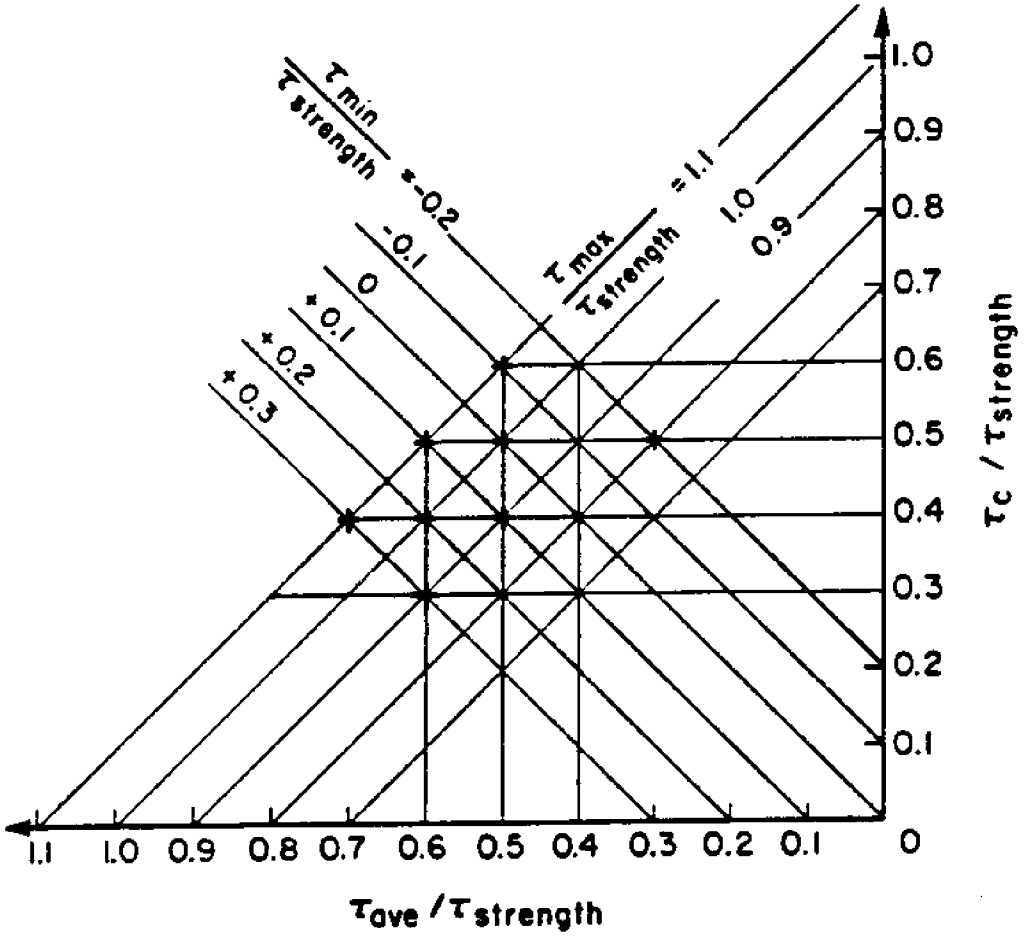

Figure 2.10 Summary of Undrained Cyclic DSS Tests on Normally Consolidated Drammen Clay with $\tau_{ave} \neq 0$ (from Goulois, 1982)

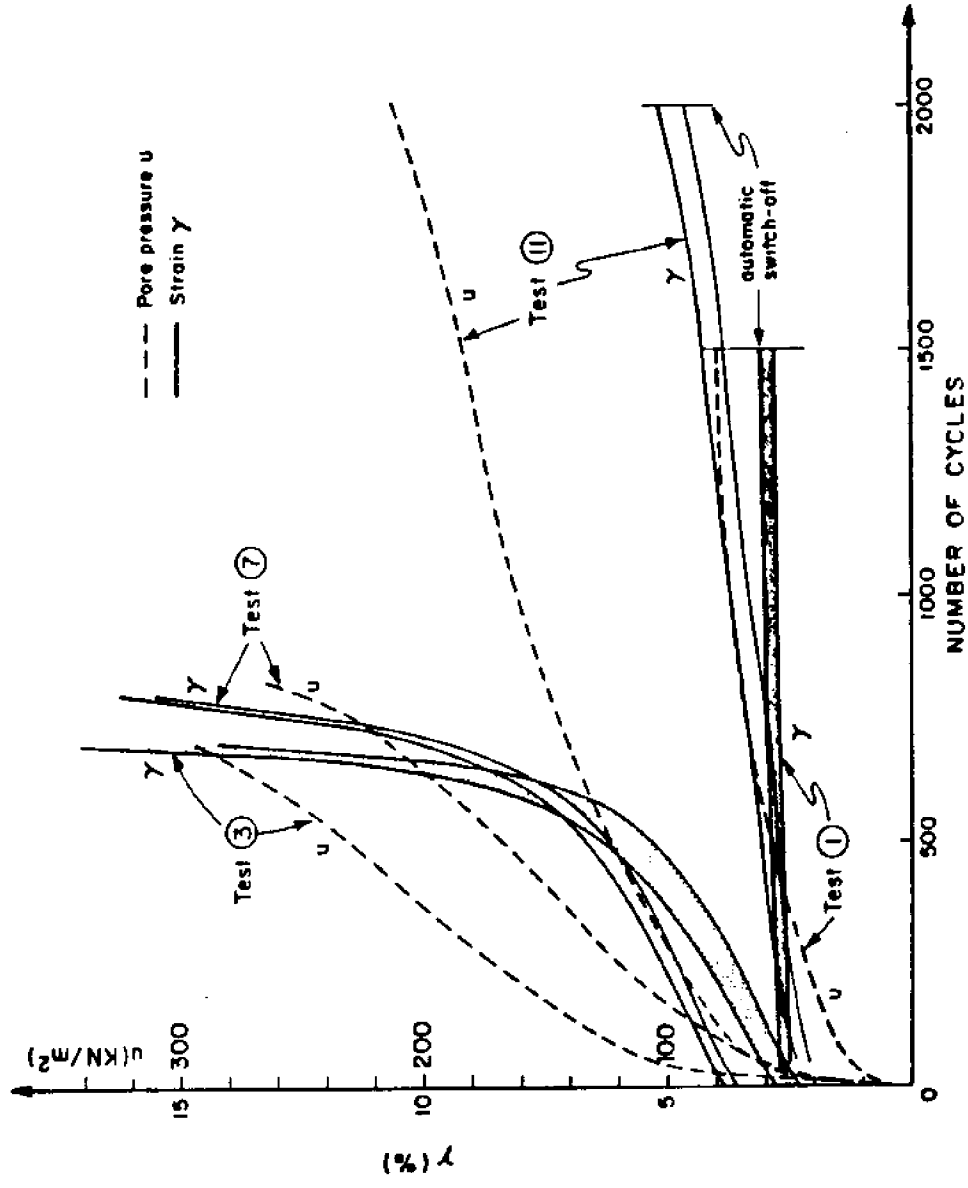

Figure 2.11 Shear Strain and Excess Pore Pressure versus Number of Cycles from Undrained Cyclic DSS Tests on Normally Consolidated Drammen Clay with $\tau_{ave} \neq 0$ (from Goulois, 1982)

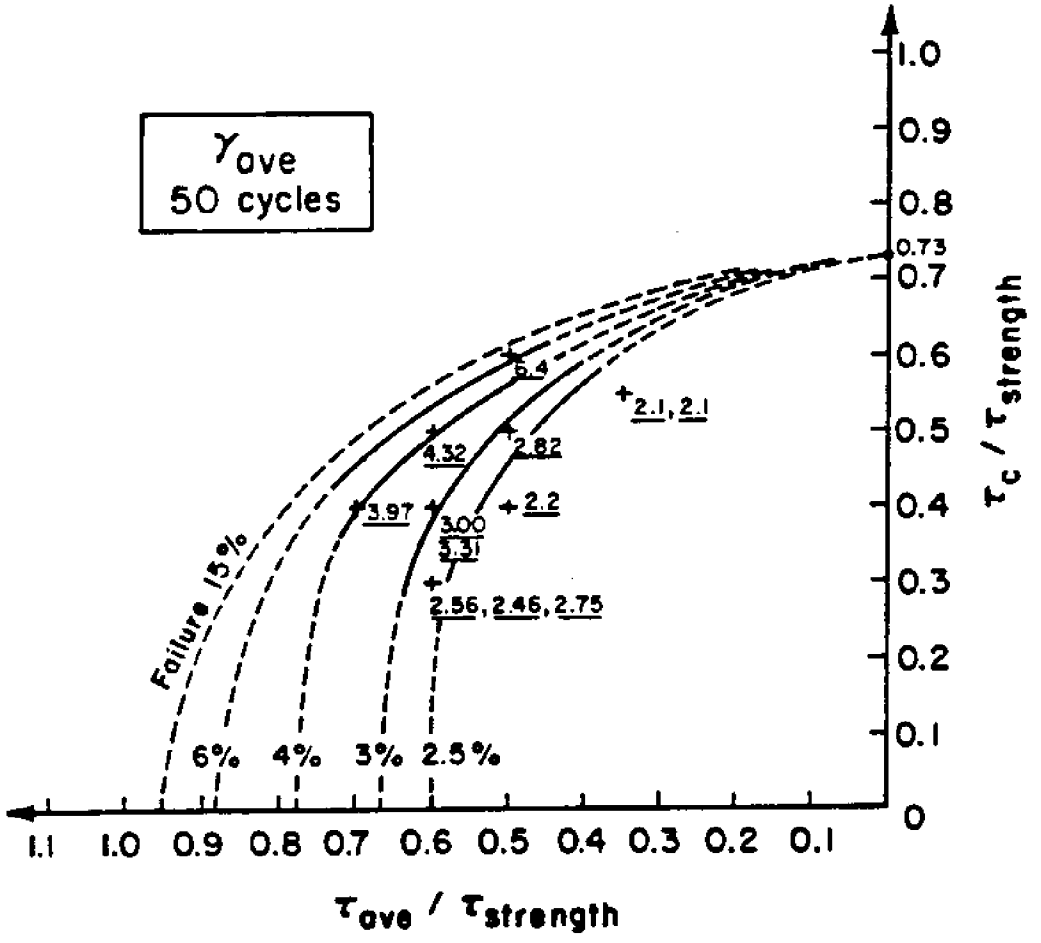

Figure 2.12 Sections of Iso-γ Network from Undrained Cyclic DSS Tests on Normally Consolidated Drammen Clay with $\tau_{ave} \neq 0$:
a) Iso-γ_{ave} Network at N=50
(from Goulois, 1982)

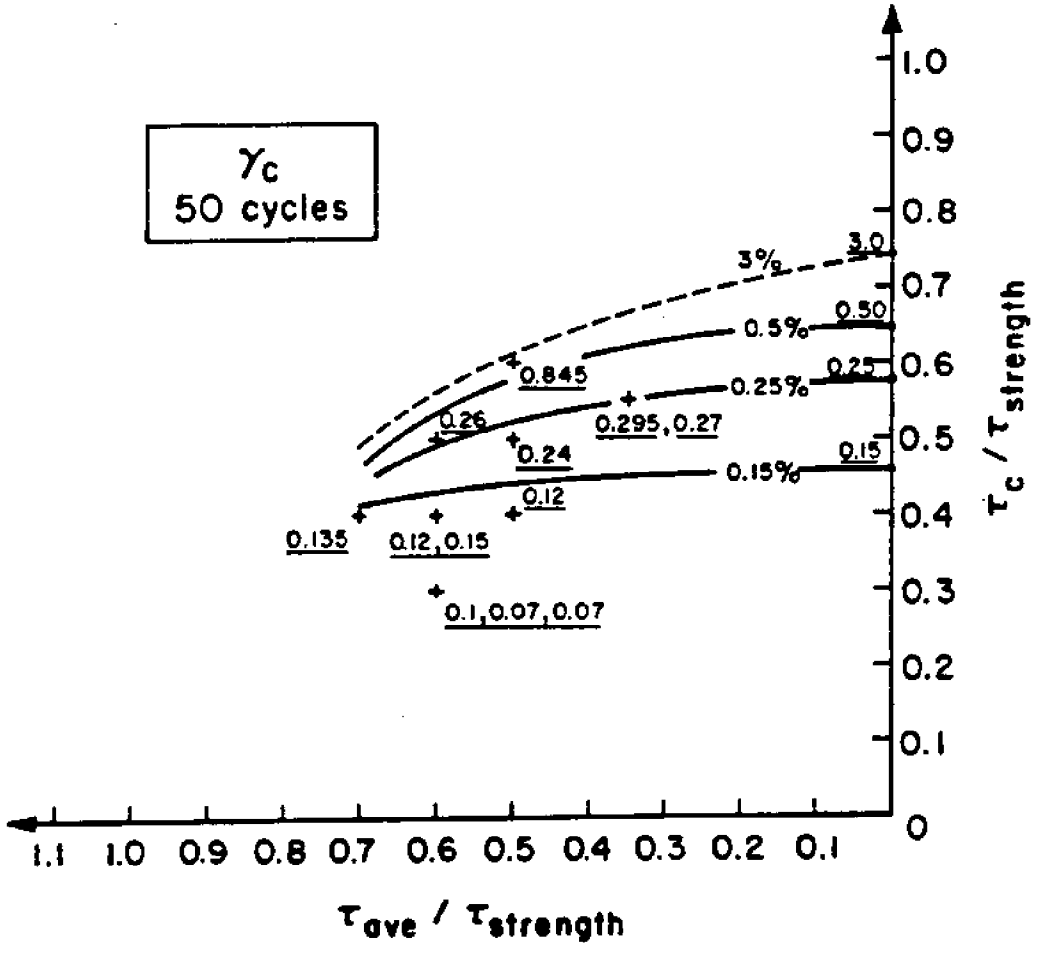

Figure 2.12 Sections of Iso-γ Network from Undrained Cyclic DSS Tests on Normally Consolidated Drammen Clay with $\tau_{ave} \neq 0$:
b) Iso-γ_c Network at N=50
(from Goulois, 1982)

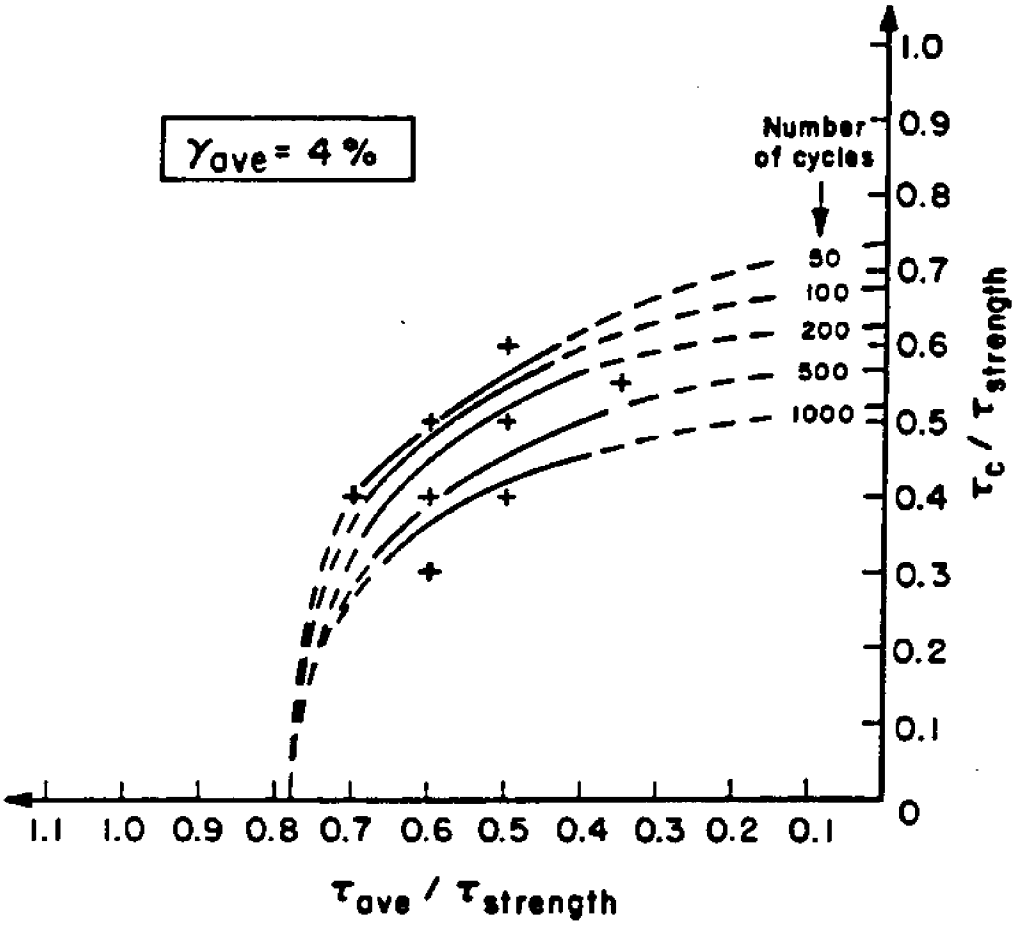

Figure 2.13 Iso-γ Network from Undrained Cyclic DSS Tests on Normally Consolidated Drammen Clay with $\tau_{ave} \neq 0$:
a) Sections of Iso-γ_{ave} Surface for γ_{ave}=4% at Various Number of Cycles
(from Goulois, 1982)

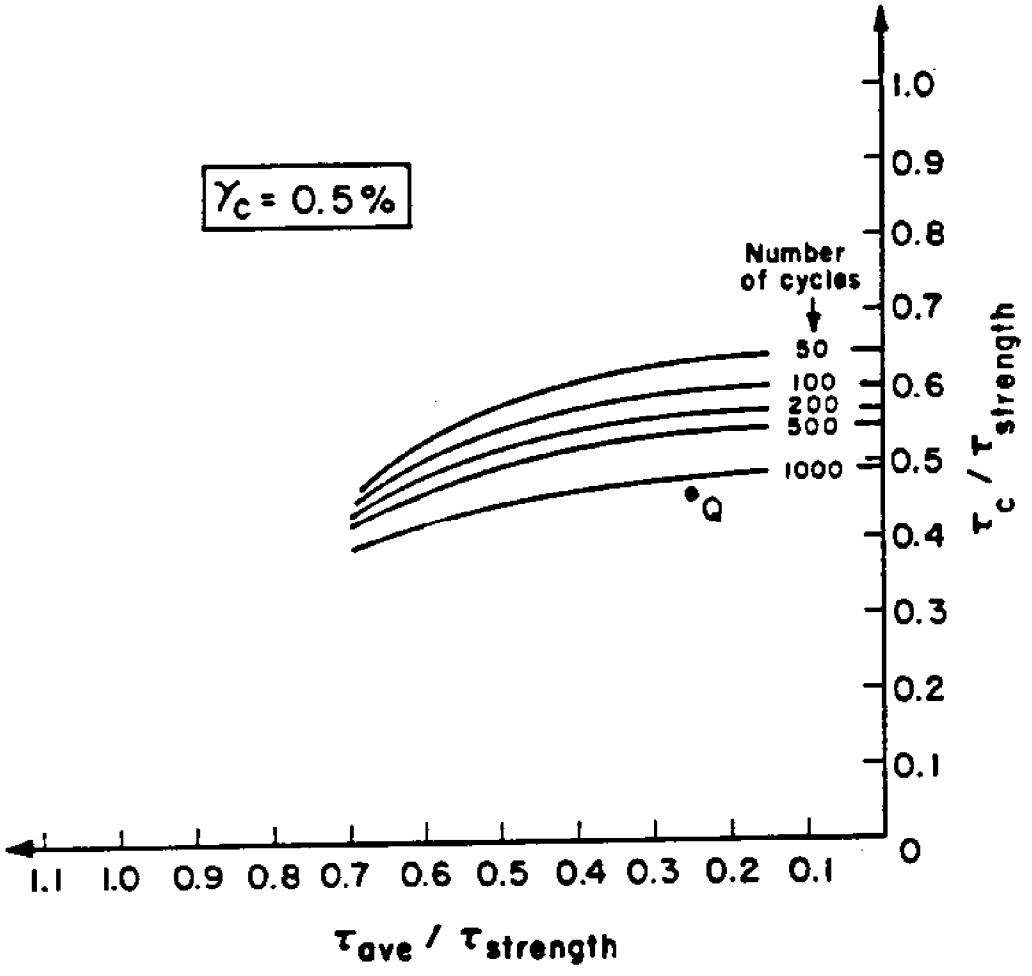

Figure 2.13 Iso-γ Network from Undrained Cyclic DSS Tests on Normally Consolidated Drammen Clay with $\tau_{ave} \neq 0$:
b) Sections of Iso-γ_c Surface for γ_c=0.5% at Various Number of Cycles
(from Goulois, 1982)

CHAPTER 3

RESEARCH FRAMEWORK FOR TLP PILES PERFORMANCE PREDICTIONS

3.1 PREDICTION OBJECTIVES

Prediction of the cyclic load capacity of TLP piles requires a thorough understanding of the cyclic behavior of soil elements surrounding the piles. This report presents the results of an experimental program aimed at developing a better understanding of clay behavior under cyclic loading and determining the important mechanisms and factors governing the cyclic resistance of TLP piles in clay.

3.1.1 Necessary Steps in the Prediction Process

Figure 3.1 shows the sequence of events that requires investigation in order to identify and quantify the important aspects affecting the static and cyclic axial response of a single pile in a TLP foundation system:

a) In situ conditions prior to pile driving, which depend primarily on the stress (or strain) history of the clay deposit, given by the overconsolidation ratio, OCR.

b) Changes in stresses and soil properties due to pile installation. Pile installation induces significant shearing (remolding) of the soil. In deposits having low to moderate degrees of overconsolidation ($OCR \leq 4$), pile installation causes high excess pore pressures and a significant reduction in effective stresses.

c) Changes in stresses and soil properties due to consolidation after pile driving and during the process of dissipation of

excess pore pressures. In deposits having low to moderate degrees of overconsolidation, the consolidation process increases the effective stresses in the vicinity of the pile-soil interface and hence increases the shaft resistance of the pile.

d) Changes in stresses and soil properties during loading of the pile with the static mooring tensile force.

e) Changes in stresses and soil properties due to the cyclic loading created by wave action.

Most studies ignore the effects of events (a) through (c) on the cyclic response of piles. In other words, these studies assume that the initial in situ conditions are not altered by pile driving and the subsequent dissipation of pore pressures and soil consolidation. However, research in the last ten years at the Massachusetts Institute of Technology (MIT) has concentrated on events (a) through (c) above. Contributions involved a theoretical study based on the Strain Path Method (Levadoux, 1980; Kavvadas, 1982) complemented by an in situ experimental investigation of pile shaft behavior based on a newly developed device, the Piezo-Lateral Stress cell (PLS cell; Morrison, 1984). The PLS cell measures the pore pressure and total radial stress simultaneously at the same location on the shaft of a long model pile (3.8 cm in diameter) which is pushed into the soil at a steady rate.[1] It provides continuous readings of the excess pore pressure Δu and the total radial stress σ_r during steady state penetration as well as during the consolidation phase when installation is halted. It can also be used to study the pile shaft response in subsequent shearing

---

[1] a velocity of 2 cm/sec was the standard rate used to ensure undrained penetration of the deposit.

following complete dissipation of the installation induced pore pressures. This work confirmed the importance of the radial effective stress $\bar{\sigma}_{rc}$, at the pile soil interface after installation and consolidation, with regards to the response of pile shafts in clays.

Whittle (1987), as part of a parallel MIT research program aimed at predicting the behavior of piles supporting tension leg platforms, has developed a generalized constitutive mode, the MIT-E3 model, for simulating the behavior of soils under monotonic and cyclic loading. This model was evaluated by comparisons with the results of monotonic triaxial and direct simple shear (DSS) tests of resedimented Boston Blue Clay, and was found to give good predictions. Also, comparisons with the results of undrained cyclic DSS tests conducted as part of this report indicated that the model is capable of predicting the essential features of soil behavior during cyclic loading. The model provides good qualitative predictions of cyclic degradation, pore pressure generation, and strain accumulation (in stress-controlled tests, or shear stress reduction in strain-controlled tests) with number of cycles.

In order to make predictions of actual or field performance of TLP piles, Whittle implemented the MIT-E3 model in the framework of the Strain Path Method and made predictions of effective stresses and pore pressures at the various stages of a driven pile. His results were evaluated using field data from the PLS cell in Boston Blue Clay at the MIT field testing site in Saugus, MA (Morrison, 1984), and compared favorably with the field data for penetration, consolidation, and monotonic shearing.

Of special interest to this report is Whittle's prediction of the pile shaft behavior for undrained axial loading using the MIT-E3 model in conjunction with the stress field predicted at the end of pile

consolidation. Figure 3.2 shows the variation of shear strength τ with radial distance r away from the pile with radius R, for initial undisturbed OCR values of 1.0, 1.5, 2.0 and 4.0, as predicted by MIT-E3 for DSS mode of shearing. The shear strength is normalized by the strength at the pile-soil interface, and increases monotonically with radial distance from the pile shaft. The figure also shows the shear stress variation with r, $\tau(r)$, required for equilibrium under an imposed shear stress τ_{shaft} at the pile-soil interface. This equilibrium line was constructed assuming vertical equilibrium which is given by:

$$\tau_{shaft} \cdot R = \tau(r) \cdot r \qquad (3.1)$$

It can be seen from the figure that a soil element at the pile-soil interface has the largest applied shear stress and the smallest shear strength, indicating that failure will occur in the soil element next to the pile shaft (assuming no slippage occurs at the interface). Figure 3.3 shows the effective stress paths and stress-strain curves for the soil element adjacent to the pile shaft, for initial undisturbed OCR values of 1.0, 1.5, 2.0 and 4.0. The results are normalized by $\bar{\sigma}_{vo}$ and the peak strength values $\tau/\bar{\sigma}_{vo}$ range from 0.11 at OCR=1.0 to 0.31 at OCR=4.0. Using the approach suggested by Azzouz and Baligh (1984), the same results are presented in Figure 3.4, normalized with respect to the effective radial stress at the end of consolidation $\bar{\sigma}_{rc}$. It can be seen that normalization by $\bar{\sigma}_{rc}$ leads to monotonic behavior that is independent of the initial OCR of the clay (same peak resistance equal to 0.26 for all OCR values). The figure also shows MIT-E3 predictions for K_o-consolidated undrained direct simple shear tests on Boston Blue Clay at OCR=1.0 and 1.2. Comparison of the solid curves (subsequent shear after pile installation and

consolidation) with the dashed curves (undisturbed shear) indicates that undrained monotonic shearing after pile installation and consolidation causes the soil to behave as if it were undisturbed at an equivalent OCR between 1.0 and 1.2, when normalized with respect to the radial stress at the end of consolidation. This important result has the following consequences:

1. The performance of pile shafts during rapid monotonic axial loading can be estimated on the basis of the undrained monotonic behavior of K_o-normally to very slightly overconsolidated clay (OCR$\leq$1.2). This result applies to deposits with in situ OCR values up to 4.0;

2. Assessment of pile capacity requires accurate and reliable determination of $\bar{\sigma}_{rc}$, the radial effective stress at the end of consolidation.

3.1.2 Focus of the Research

In the preceding section, it has been established that, after normalization by $\bar{\sigma}_{rc}$, the undrained monotonic response of the soil adjacent to cylindrical pile shafts (following driving and consolidation in deposits with in situ OCR$\leq$4) closely resembles the behavior of a K_o-normally to very slightly overconsolidated clay in a DSS mode of shearing. This suggests that, if the effective stresses at the end of consolidation can be reasonably well estimated, then the behavior of pile shafts during undrained cyclic loading can also be interpreted from the behavior of normally to very slightly overconsolidated clay subjected to undrained cyclic DSS shearing. This hypothesis provides the rationale for the main thrust of the experimental program conducted in this research involving measurements of the undrained cyclic behavior of K_o-normally consolidated

clays in laboratory DSS tests.

This report is only concerned with the behavior, under axial loading, of soil elements at the interface of the TLP pile. The axial load history (Figures 3.1(d) and 3.1(f)) following consolidation involves two phases: first, the tensile mooring force induces shear stresses along the shaft under mostly drained conditions; then, cyclic loading, due to storm waves, causes cyclic shear stresses, which may occur under undrained or partially drained conditions when subjected to the mooring and wave induced repeated loadings (steps d and e in Figure 3.1).

The TLP pile is subjected to variable and complicated wave loading throughout the design life of the structure. At each depth z below mudline, the soil is subjected to different time histories of shear stresses. Figure 3.5(a) shows the distribution of the mooring shear stresses τ_m, decreasing with depth z along the pile. Figure 3.5(b) illustrates the shear stress history of a soil element located at depth z adjacent to the pile wall. During calm sea conditions, loading typically consists of an average shear stress equal to τ_m, over which are superimposed small variable cyclic shear stresses due to wave loading. However, during storm loading, the shear stresses vary and increase drastically and hence lead to critical loading conditions of the pile. Therefore, the current research focuses on storm loading conditions.

During a storm, there is a surge in the mean sea level causing an increase in mean shear stress level, accompanied by large variable shear stresses caused by storm waves. The storm induced shear stresses are almost random and very complex in shape (frequencies as well as amplitudes). Attempts to faithfully duplicate a given storm loading condition in an experimental program are very difficult to achieve and

would serve little purpose at this stage when reliable rational design methods are needed. Instead, a more fundamental and systematic experimental study that incorporates important characteristics of this variable loading was conducted. Figure 3.5(b) shows various loading characteristics investigated herein:

- τ_{ave}, which is the average shear stress at any depth z, during the storm. The value of τ_{ave} is generally larger than τ_m because of the storm surge;

- τ_c, the variable component of shear stresses involving changing amplitudes, but with constant average value equal to τ_{ave}.

Therefore, this study specifically does not include changes in the frequency of the applied wave loading. This means that studies of rate effects during cyclic loading are beyond the scope of this investigation.

In order to study the effect of variable shear stresses due to storm wave loading on a given soil element, a systematic investigation can only consider the behavior of the soil under a uniform cyclic loading as shown in Figure 3.5(c). A superposition or integration scheme is then required to predict the combined effect of N_1 cycles at τ_{c1} followed by N_2 cycles at τ_{c2} +...+ N_i cycles at τ_{ci} representing the various components of the actual storm loading.

This scheme of superimposing the effects of wave packages of equal cyclic stresses is very important and must be carefully examined since it will determine whether the predicted behavior of the soil under variable storm loading is correct or not. This is especially complicated by the highly nonlinear nature of soils.

3.2 TYPES OF EXPERIMENTS

In order to study the effect of cyclic shearing on an element of clay, various tests can be used in the laboratory. The triaxial test has been used extensively in research related to earthquakes and liquefaction as well as offshore cyclic loading. However, the mode of shearing of the soil around a pile is very similar to that in the Direct Simple Shear (DSS) test.[2] It can be seen in Figure 3.6 that the DSS provides the best simulation of the shearing conditions around piles.

At any time during DSS testing, one can control:

- the stress history (vertical effective stress $\bar{\sigma}_v$ and shear stress τ),
- the strain history (vertical strain ε_v and shear strain γ),
- a combination of $\bar{\sigma}_v$ and γ, or ε_v and τ.

The focus of the present research is on the undrained cyclic behavior of clays since undrained storm loading is believed to be the most critical type of loading of moderately overconsolidated offshore clay deposits. Perfectly undrained storm loading seldom occurs because storms tend to last a period of several days over which some drainage can occur, especially if non-cohesive soil layers are present at the foundation site. However, partial drainage during shearing is very difficult to quantify and duplicate in the laboratory, and is replaced in this experimental study by the more severe case of no drainage. Therefore, a value of ε_v=0 (Figure 3.6) is imposed during shearing. This limits the remaining testing options to either stress-controlled DSS tests where the stress history of τ is

---

[2] M.F. Randolph, C.P. Wroth, "Application of the Failure State in Undrained Simple Shear to the Shaft Capacity of Driven Piles," Geotechnique, Vol. 31, No. 1, 1981, p. 144.

known and specified, or strain-controlled DSS tests where the history of γ is known and specified. The right choice is the one whose results can easily be incorporated in the integration process mentioned in section 3.1.2, in order to predict undrained behavior under general variable loading conditions.

3.2.1 Typical Cyclic DSS Behavior

3.2.1.1 Stress-controlled tests

Figure 3.7 shows the time history of shear stresses applied in a stress-controlled DSS test, as well as a schematic response of the sample. Also shown are the definitions of the various terms related to DSS testing.

Figure 3.8 shows typical results from an actual cyclic DSS test with nonzero average (i.e., $\tau_{ave} \neq 0$) as well as cyclic shear stress components. The major features indicated by Figure 3.8 are:

- a continuous buildup of pore pressure with the number of cycles, N,
- a significant increase in average shear strain, $\Delta\gamma_{ave}$, with N,
- a modest increase in cyclic shear strain, γ_c, with N, indicating a gradual degradation of stiffness.

3.2.1.2 Strain-controlled tests

Figure 3.9 gives the time history of shear strain applied in a strain-controlled DSS test, as well as a schematic response of the sample. Also shown are definitions and notations.

Figure 3.10 shows typical results from an actual strain-controlled DSS test, with zero average shear strain (i.e., $\Delta\gamma_{ave}=0$) and nonzero cyclic shear strain. The major features are:

- a very sharp increase followed by a continuous buildup of pore pressure with N,

- a decrease in cyclic shear stress as well as a decrease in stiffness with N.

3.2.2 Stress vs Strain-Controlled Tests

Results in Figures 3.8 and 3.10 indicate that clay behavior in stress-controlled tests is different from that in strain-controlled ones. In actual situations, the imposed loading conditions at a soil element at any depth z along the pile are not necessarily stress-controlled (constant τ_c) nor strain-controlled (constant γ_c). This is due to the fact that, at the top of the pile, the load is not cyclic with constant amplitude, but rather variable with changing amplitudes and frequencies. Also, the pile-soil interface provides an inelastic shaft resistance, leading to unsteady and non-uniform load transfer characteristics along the pile length.

3.3 SUPERPOSITION OF CYCLIC LOADING DATA

As mentioned earlier, laboratory testing programs conducted to investigate the behavior of soil under variable loading were actually performed for uniform cyclic loading rather than irregular (random) loading. Data from uniform cyclic loading tests have then been utilized to predict behavior under irregular loading conditions using certain integration schemes. This section reviews integration methods adopted in dynamic studies (earthquake and liquefaction analyses), as well as in cyclic studies for gravity offshore platforms subjected to cyclic wave

loading.

3.3.1 Fatigue of Materials

All materials subjected to repeated loads lose strength, or stiffness, or both with increasing number of cycles. This weakening is called fatigue, and is conveniently represented by S-N diagrams. Figure 3.11 shows S-N curves for various materials, which are plots of the cyclic stress ratio (uniform cyclic stress divided by the static strength) versus number of cycles to cause failure. The trend is the same for all material, ranging from steel to soils, namely that the number of cycles to cause failure increases with decreasing cyclic stress ratio. The large scatter in the data for soils is mainly due to material differences (sand versus clay), and also due to differences in the testing procedure. However, even the data from steel, which are obtained from identical laboratory specimens, shows a large error band in contrast to what one would expect from well machined identical steel specimens. The S-N curves for steel show that for a given cyclic stress ratio, there is a difference of a factor of ten in the number of cycles causing failure, and at any given cycle number, there is a range of 20% between the lowest and highest stress level. Figure 3.11 shows that there is almost as much scatter for metal specimens as for soils, which is a useful observation to remember when evaluating the results of cyclic tests on soils.

3.3.2 Dynamic Analyses

The most widely used superposition method in dynamic analyses is the equivalent uniform number of cycles method. The method has been described and used by various investigators in analyses of liquefaction potential and

seismic stability of soils (Seed and Idriss, 1967; Seed, Lee and Idriss, 1969; Seed and Idriss, 1971; Donovan, 1971; Lee and Chan, 1972; Faccioli 1973; Seed et al. 1975). Annaki and Lee (1977) have reviewed the method along with its basic assumptions, and have provided some experimental verification for its applicability.

The method is based on the approach of Palmgren (1924) and Miner (1945) methods of extrapolating the effects of repeated loading from regular to irregular cyclic stress levels, on the strength of materials. The method is logical, simple, and convenient, and has been found to be reasonably satisfactory for many conditions. "The basic premise of the Palmgren-Miner hypothesis is the assumption that the energy applied during any stress cycle has an accumulative damaging effect on the material. This damaging effect is assumed to be directly proportional to the energy level of the particular cycle and independent of where in the time history that particular stress pulse is applied."[4]

Figure 3.12 shows how the equivalent uniform cycle concept is used. The damage or strength deterioration behavior due to continued cyclic loading must be available. This information can be obtained from laboratory tests with constant cyclic stress levels and presented in the form of S-N curves shown in Figures 3.12(c) and 3.12(d). S is defined as the uniform cyclic stress intensity (usually as a percentage of strength), and N is the number of uniform cycles to cause a specified degree of damage, which is typically measured by the cyclic strain reached after N cycles. All points

---

[3]M. Annaki, K.L. Lee, "Equivalent Uniform Cycle Concept for Soil Dynamics," Journal of the Geotechnical Engineering Division, ASCE, Vol. 103, No. GT6, June 1977, pp. 549-551.

[4]Ibid, p. 551.

on the same S-N curve are equivalent to each other since they all correspond to the same fatigue damage or cyclic strength degradation. In the case of Figures 3.12(c) and (d), the S-N curve shown corresponds to failure, and N_{if} cycles are required to cause failure at stress level S_i.

Figure 3.12(a) shows the actual time history of dynamic loading expressed in terms of variable stress, S, versus time, t. This loading is divided into a number i of packages each involving N_i cycles of fixed intensity S_i. The relative amount of damage caused by the ith package is $D_i = N_i/N_{if}$. The method then assumes that the cumulative damage, D, due to i packages is the sum of D_i, that is $D = \sum_i N_i/N_{if}$.

As a corollary of this hypothesis and for purposes of implementation in laboratory testing, the actual loading history, shown in Figure 3.12(a), can be replaced by an equivalent cyclic loading described by a number of cycles N_{eq} of intensity S_e, which has the same damage potential. In order to estimate the equivalent loading, S_e is customarily chosen as a "reasonable" average cyclic stress, and is expressed as $S_e = RS_{max}$ where S_{max} is the maximum stress in the given irregular stress pattern, and R is a dimensionless factor (usually chosen between 0.65 and 0.85). Next, the S-N curve in Figure 3.12(d) is used to obtain N_e, the number of uniform cycles with intensity S_e leading to failure. Assuming linearity, the number of uniform cycles of level S_e which have a damaging effect equivalent to the entire irregular stress time history shown in Figure 3.12(a) is:

$$N_{eq} = N_e \sum_i \frac{N_i}{N_{if}} \tag{3.2}$$

In order to evaluate the equivalent uniform cycle method described above, Annaki and Lee performed laboratory tests with irregular cyclic stress levels and compared their results with method predictions. Tests

were run on three different soils (sand, clayey sand, clay) using the triaxial apparatus. Their results show that there is "good agreement" between the experimental results and those predicted by the N-equivalent method. The scatter in test results on sand was higher than clay and involved differences in the number of cycles to failure, N_f (at a given S) on the order of 10. They finally conclude that "while the damage potential or equivalent cyclic concept may not be exactly valid for all cases, its continued use in the field of seismic stability analyses of soils seems to be a valid pragmatic approach."[5]

3.3.3 Irregular Cyclic Wave Loading

The equivalent uniform number of cycles method was used in offshore soil engineering in a study by Lee and Focht (1975) of the liquefaction potential of the Ekofisk Tank in the North Sea.

Andersen (1975), as part of a research program aimed at investigating the effects of repeated loading on clay deposits supporting offshore gravity platforms, proposed a method for predicting the response of clays subjected to variable loading on the basis of laboratory tests performed with constant cyclic stress levels. His method was developed for the case where the average component of stress is zero ($\tau_{ave}=0$ as defined in Figure 3.5(b) and utilizes S-N curves obtained by running stress controlled cyclic DSS tests, Figure 3.13(b). There are four S-N curves (or strain contours) corresponding to four different damage values expressed by the cyclic shear strain, γ_c= 0.5%, 1%, 1.5% and 3%. In cyclic DSS tests with $\tau_{ave}=0$, it was found that $\gamma_c=3\%$ corresponds to failure (i.e., $\gamma_f=3\%$). Figure 3.13(a) shows the N=1 curve relating the cyclic stress ratio to the corresponding

---

[5]Ibid., p. 562.

cyclic strain γ_c after one cycle. According to Andersen (1975), the two diagrams in Figure 3.13 can be used to predict the effect of variable cyclic loading according to the following procedure:

For a sample subjected to N=100 cycles of shearing with τ_{hc}/τ_{hf}= ±0.45 and τ_{ave}=0, Figure 3.13(b) shows that the path moves from point A to point B, hence the sample reaches a cyclic shear strain, γ_c= ± 1%. If the cyclic stress level is then increased to ± 0.50, the path follows the strain contour γ_c= ± 1.0% up to the cyclic stress level of ± 0.50 (point C) and the clay experiences an immediate increase in shear strain, $\Delta\gamma_c$. The value of $\Delta\gamma_c$ is found from the curve for N=1, Figure 3.13(a), and the path moves from point C to point D, Figure 3.13(b). If the sample is then subjected to 100 cycles, the path moves horizontally from point D (N=70) to point E (N=170). From the strain contours it can be seen that the predicted cyclic shear strain, γ_c is about ± 1.6%."[6]

The main assumption in this hypothesis is that at any point in the history of cycling, knowledge of the current cyclic shear strain is enough to predict all aspects of subsequent behavior (or, that all effects of previous cyclic history are inherently incorporated in the current cyclic shear strain). Andersen used his procedure to predict the behavior of four DSS tests with variable cyclic loading. His predictions agreed favorably with the measured values.

For applications to TLP piles, Goulois (1982) extended Andersen's procedure to cyclic shearing with $\tau_{ave}\neq 0$. In order to ensure continuity of

---

[6]K.H. Andersen, Research Report, Repeated Loading on Clay: Summary and Interpretation of Test Results, NGI Report No. 74037-9, 15 October 1975, p. 923.

τ_{ave} as the cyclic stress ratio is increased, Goulois uses S-N curves with iso-γ_{ave} rather than iso-γ_c. Predictions of this method were compared to results of two cyclic DSS tests conducted with $\tau_{ave} \neq 0$ and variable levels of cyclic shearing and were found to be "very satisfactory" with an error in the number of cycles to failure within 10%.[7]

3.4 SUMMARY AND CHOICE OF EXPERIMENTAL PROGRAM

Most researchers have used results of stress-controlled laboratory tests with a constant cyclic stress level to predict the behavior of soils under variable (irregular) loading (Sections 3.3.2 and 3.3.3). Predictions of cyclic behavior under irregular seismic or wave loading are then obtained by various superposition methods based on S-N curves from stress-controlled tests. In view of the reasonable success achieved by this approach, the research program conducted herein consists mainly of stress-controlled undrained direct simple shear tests. The results of these tests can then form the basis for predicting the behavior under irregular undrained storm loading using an adequate superposition method. The tests are performed on resedimented Boston Blue Clay (BBC), and mainly consist of undrained cyclic DSS tests on normally consolidated samples. The study focuses on the effects of varying τ_{ave} and τ_c with τ_{ave} equal to the mooring shear stress τ_m. The applied frequency of cyclic testing is fixed at 0.1 Hz since it is typical of storm ocean waves. Additional tests are performed to study the effects of overconsolidation.

---

[7] A.M. Goulois, "Contribution to the Study of Tension Piles Under Cyclic Loading," Ph.D thesis, MIT, Cambridge, MA, 1982, p. 211.

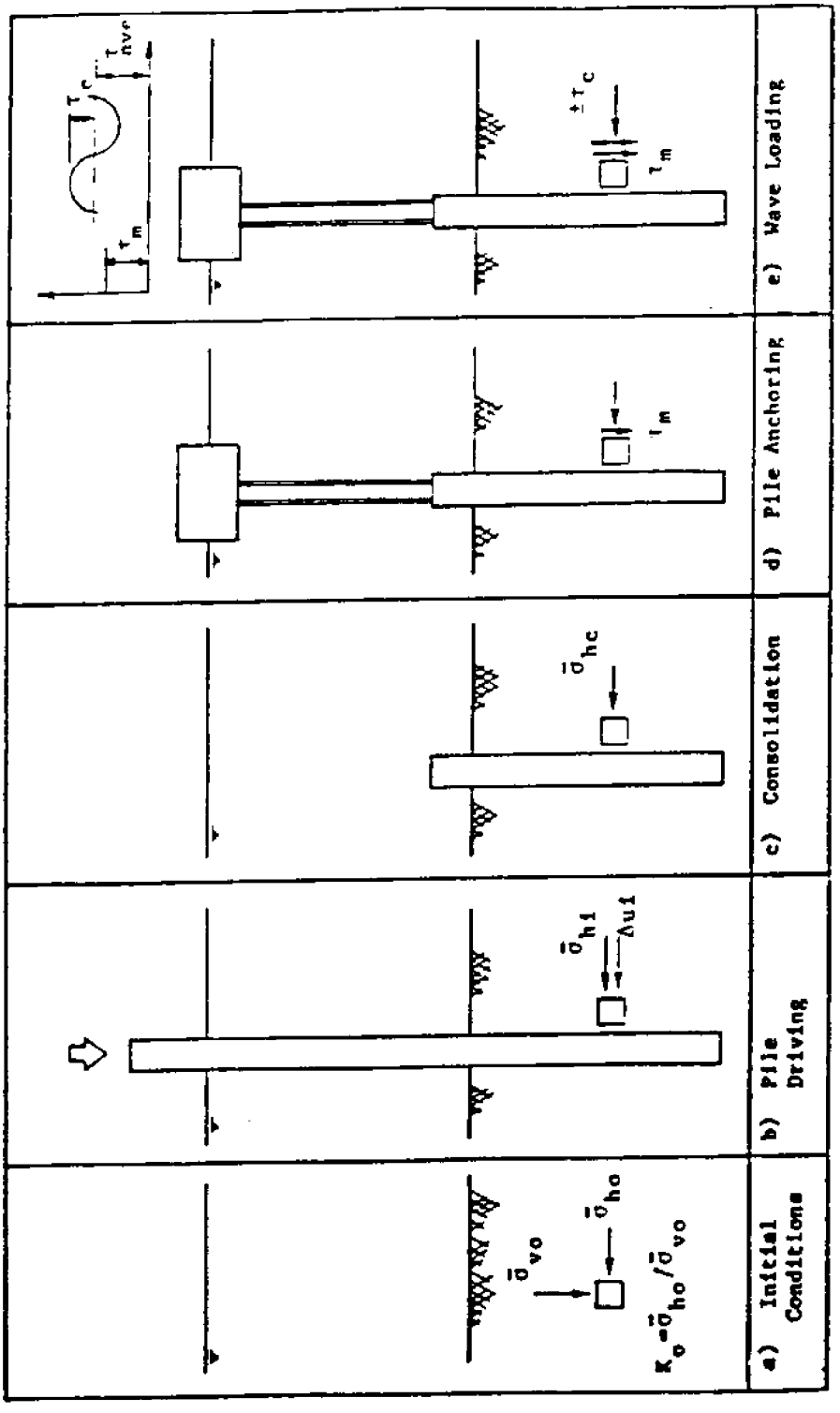

Figure 3.1 Different Phases in the Life of a TLP Pile

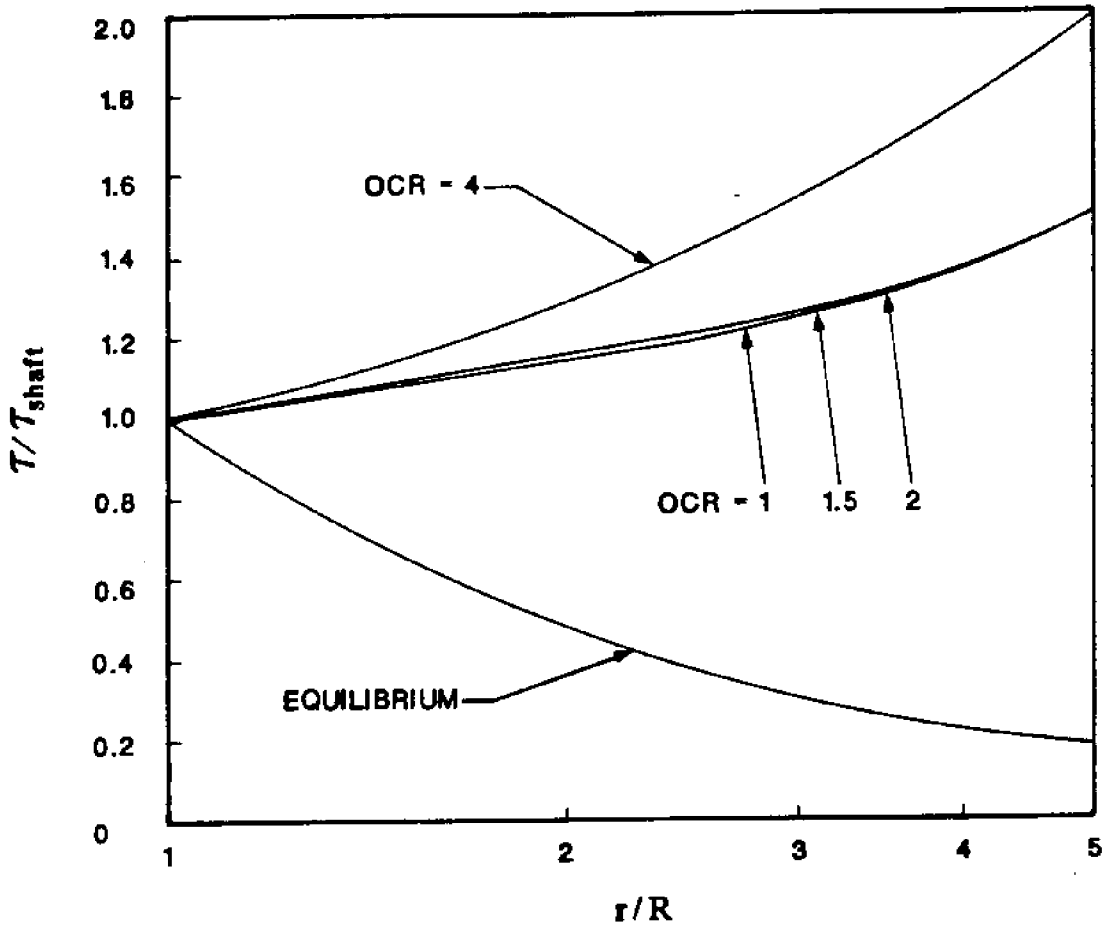

Figure 3.2 MIT-E3 Predictions of the Variation of Shear Strength of Soil Around the Pile Shaft at the End of Consolidation (from Whittle, 1987)

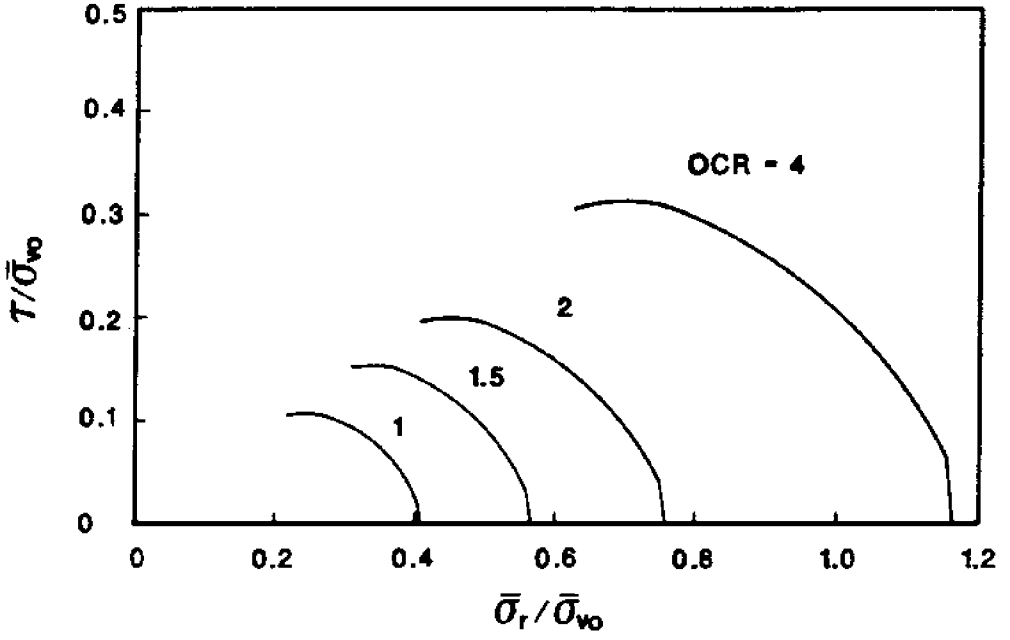

(A) EFFECTIVE STRESS PATHS

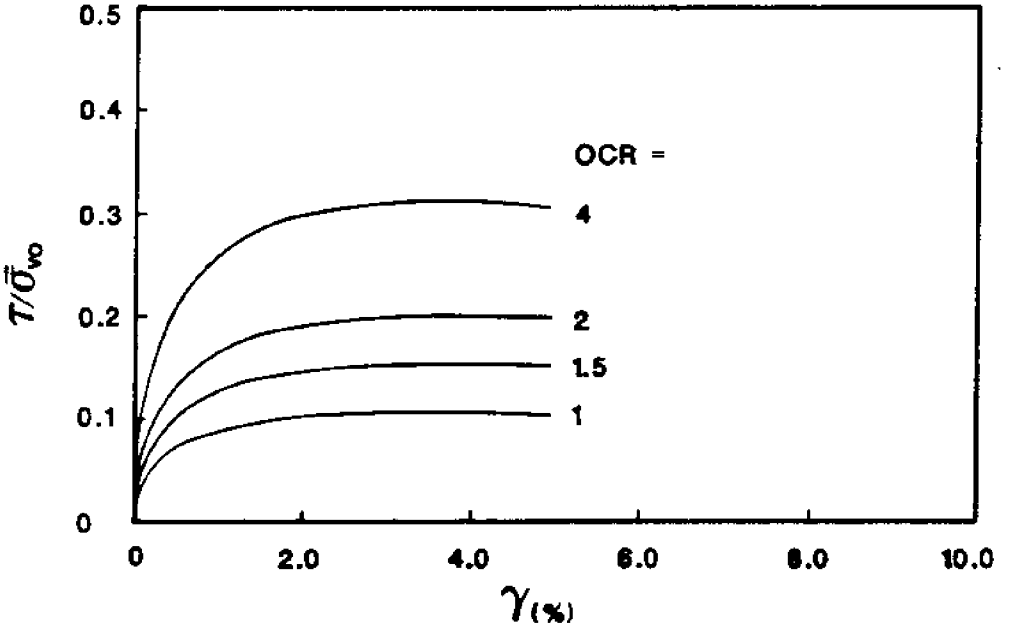

(B) STRESS-STRAIN CURVES

Figure 3.3 Undrained Shear Behavior of Soil Elements at the Pile Shaft (from Whittle, 1987)

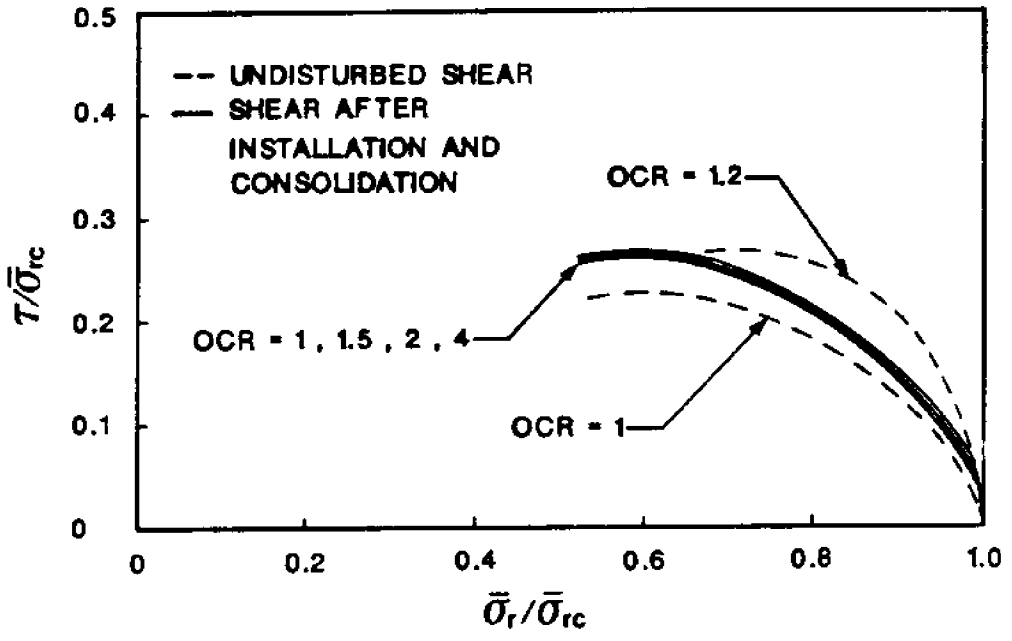

(A) EFFECTIVE STRESS PATH

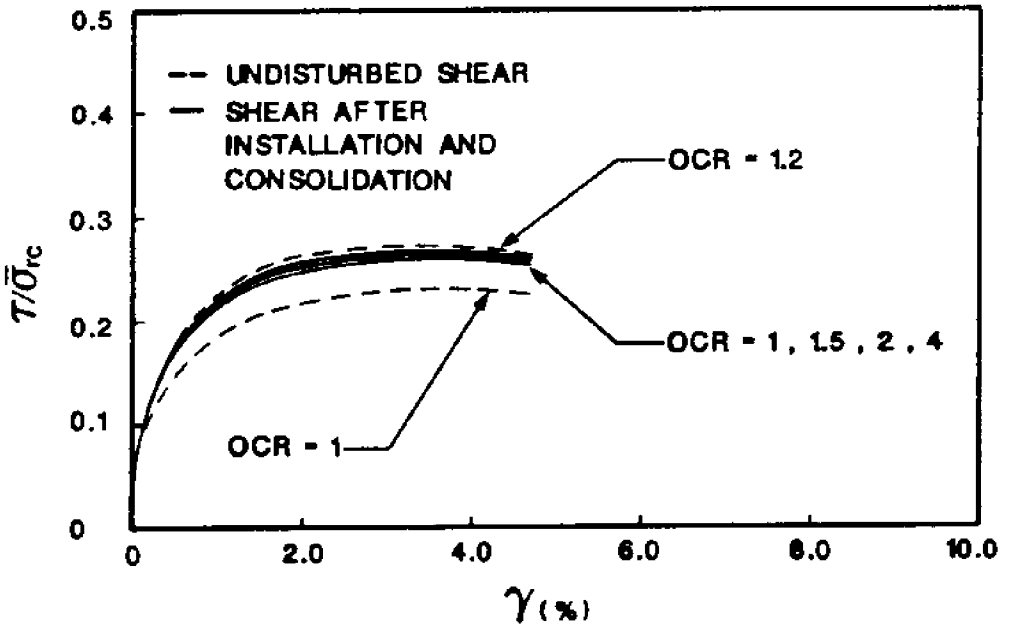

(B) STRESS-STRAIN CURVE

Figure 3.4 Undrained Shear of Soil Elements at the Pile Shaft (from Whittle, 1987)

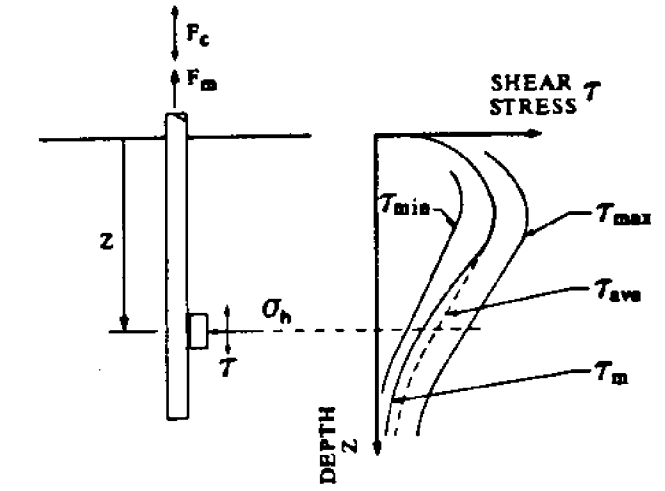

(a)

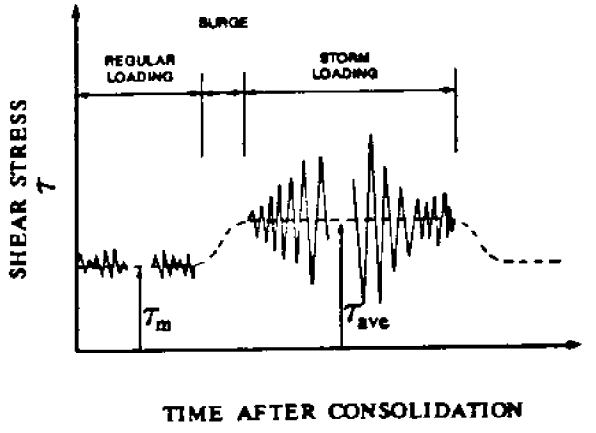

(b)

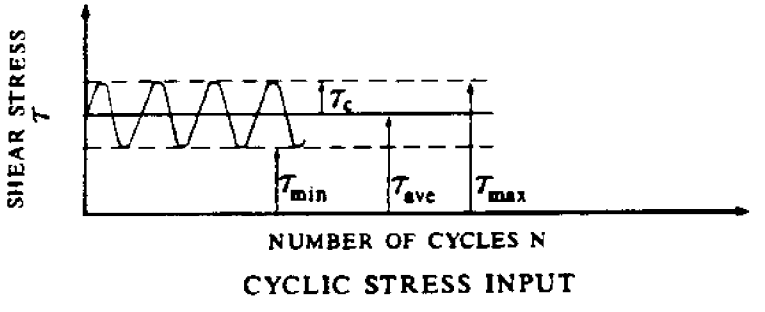

(c)

CYCLIC STRESS INPUT

Figure 3.5 a) Typical Shear Stress Distribution Along TLP Pile
b) Typical Time History of Shear Stress at Depth z Along TLP Pile
c) Uniform Cyclic Loading

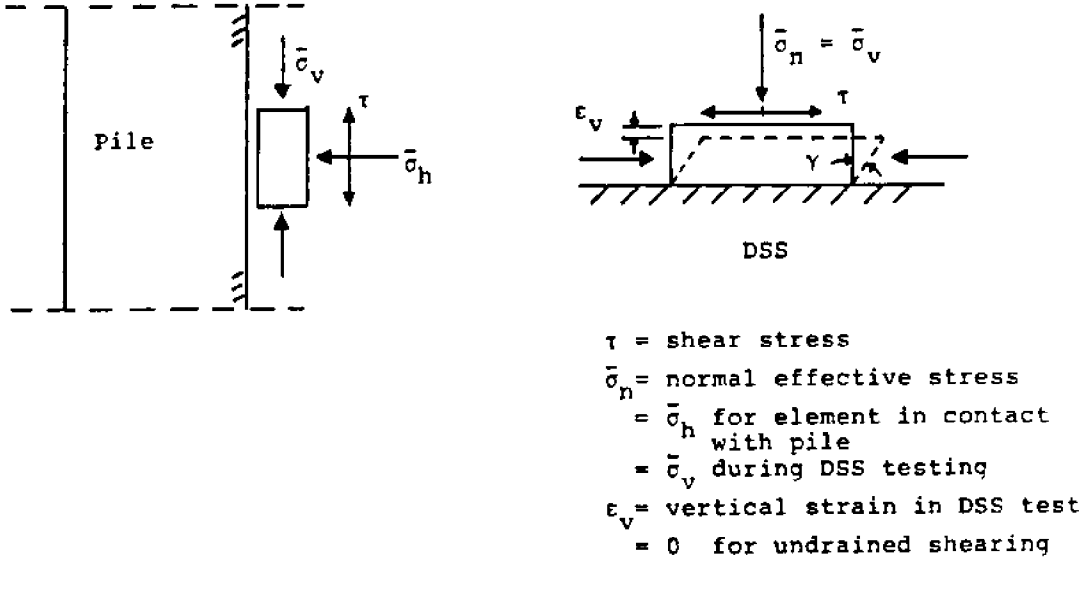

τ = shear stress

$\bar{\sigma}_n$ = normal effective stress
= $\bar{\sigma}_h$ for element in contact with pile
= $\bar{\sigma}_v$ during DSS testing

ε_v = vertical strain in DSS test
= 0 for undrained shearing

Figure 3.6 Simulation of Cyclic Shearing at the Pile Shaft by Means of DSS Cyclic Testing

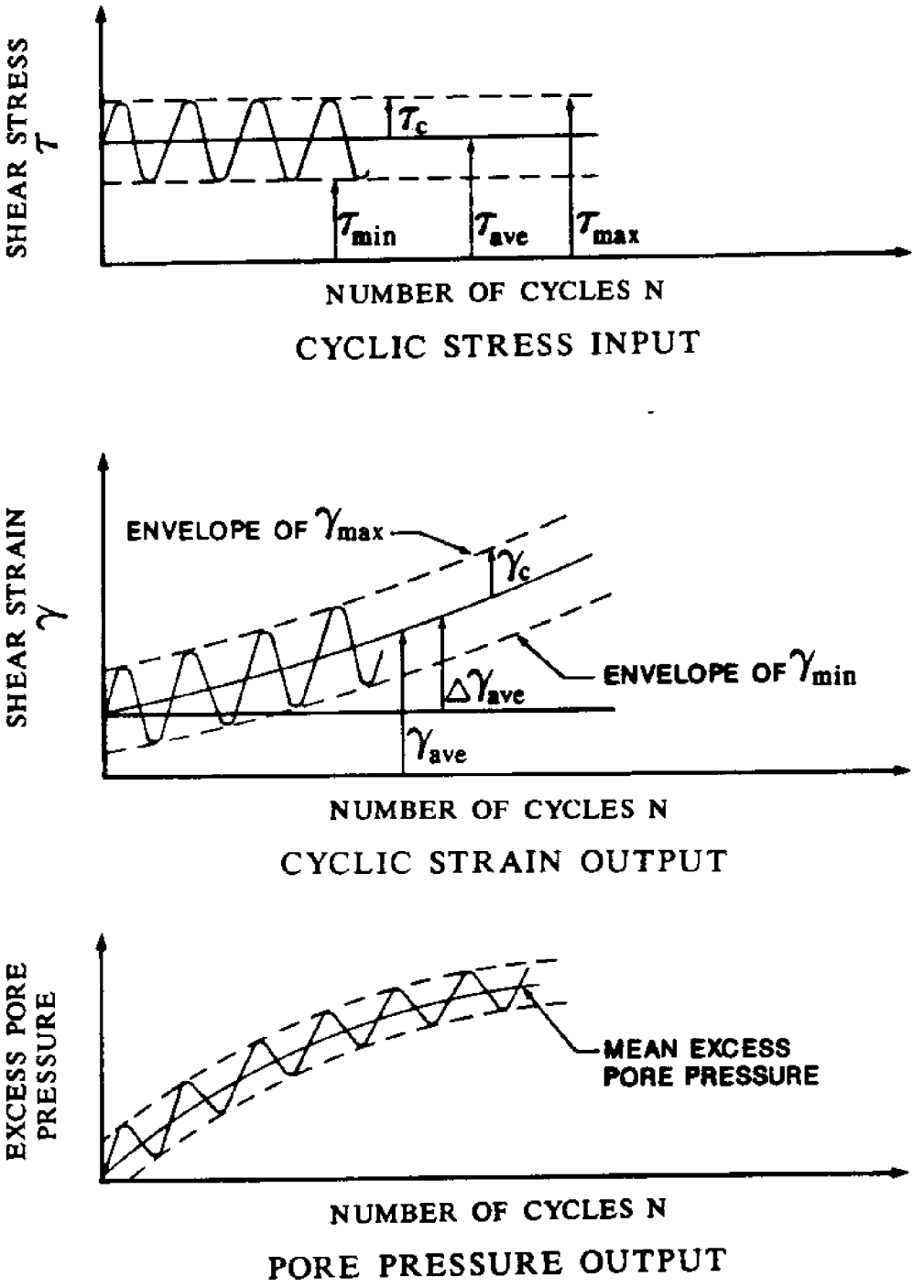

Figure 3.7 Stress-Controlled DSS Testing: Notations

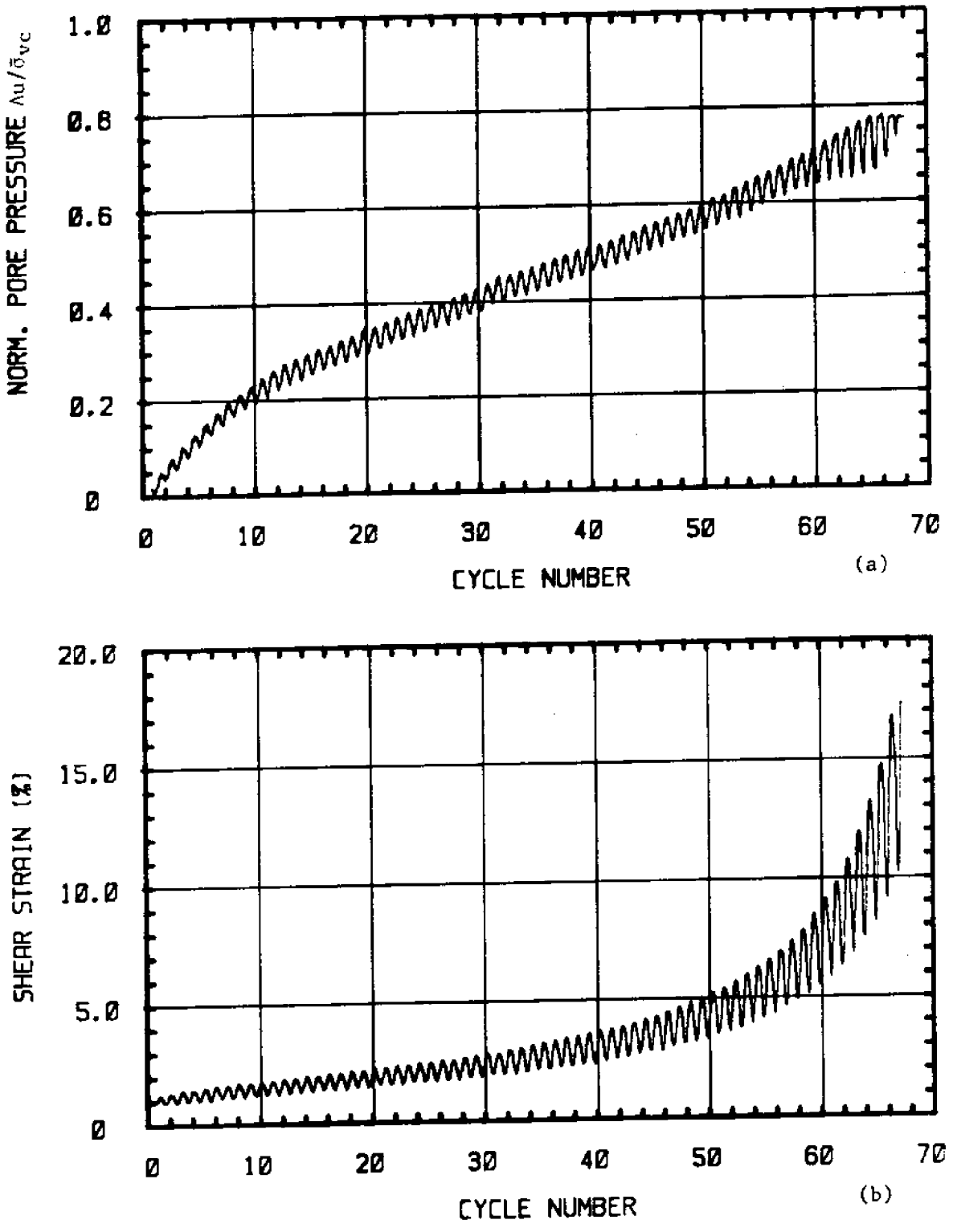

Figure 3.8 Typical Results of Stress-Controlled DSS Tests
a) Normalized Excess Pore Pressure versus Cycle Number
b) Shear Strain versus Cycle Number
Test C-18: N.C. BBC, $\tau_{ave}/s_u(NC)=0.39$, $\tau_c/s_u(NC)=0.60$

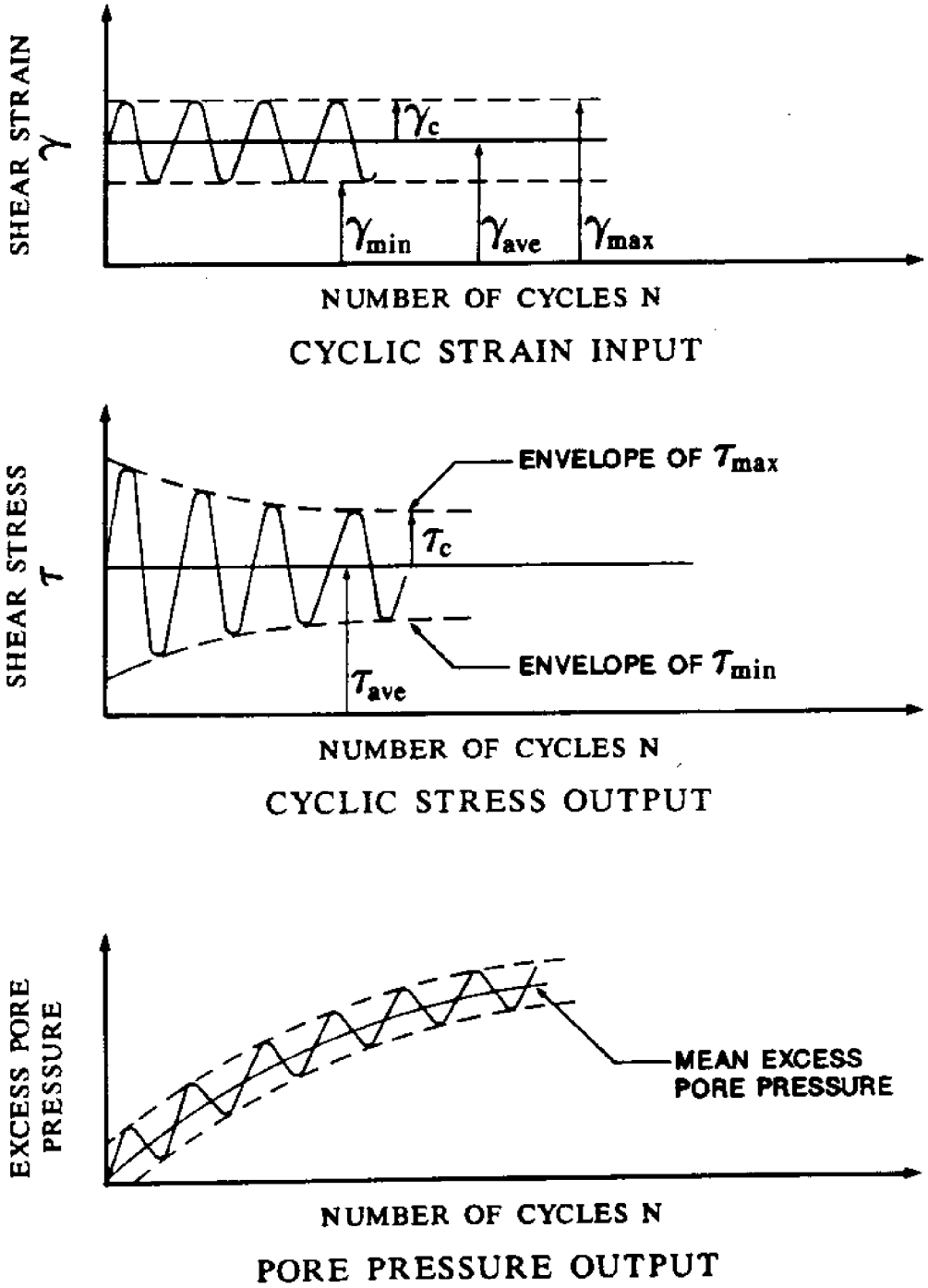

Figure 3.9 Strain-Controlled DSS Testing: Notations

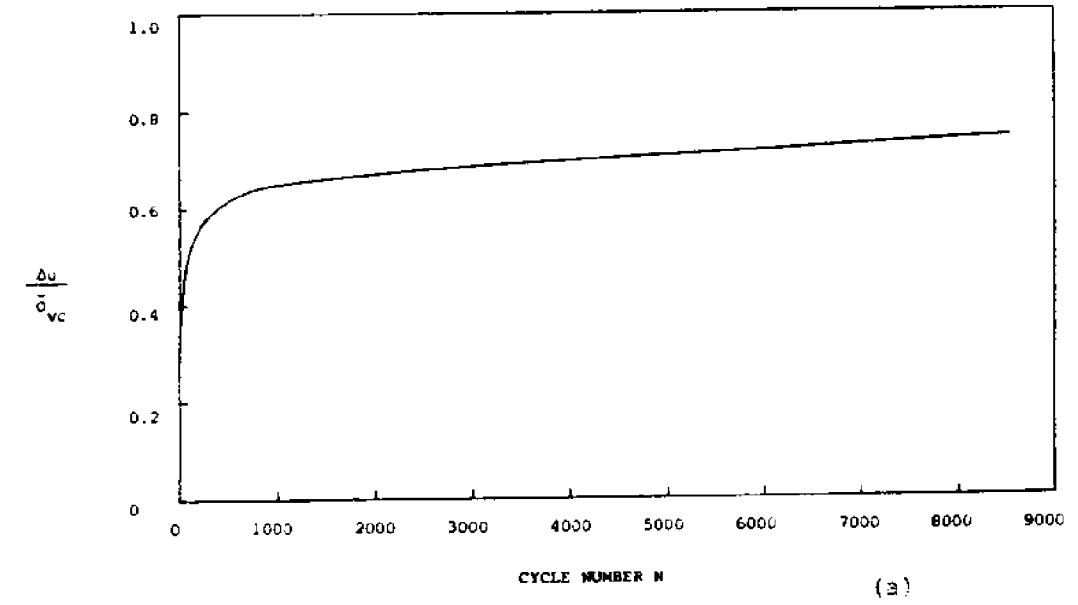

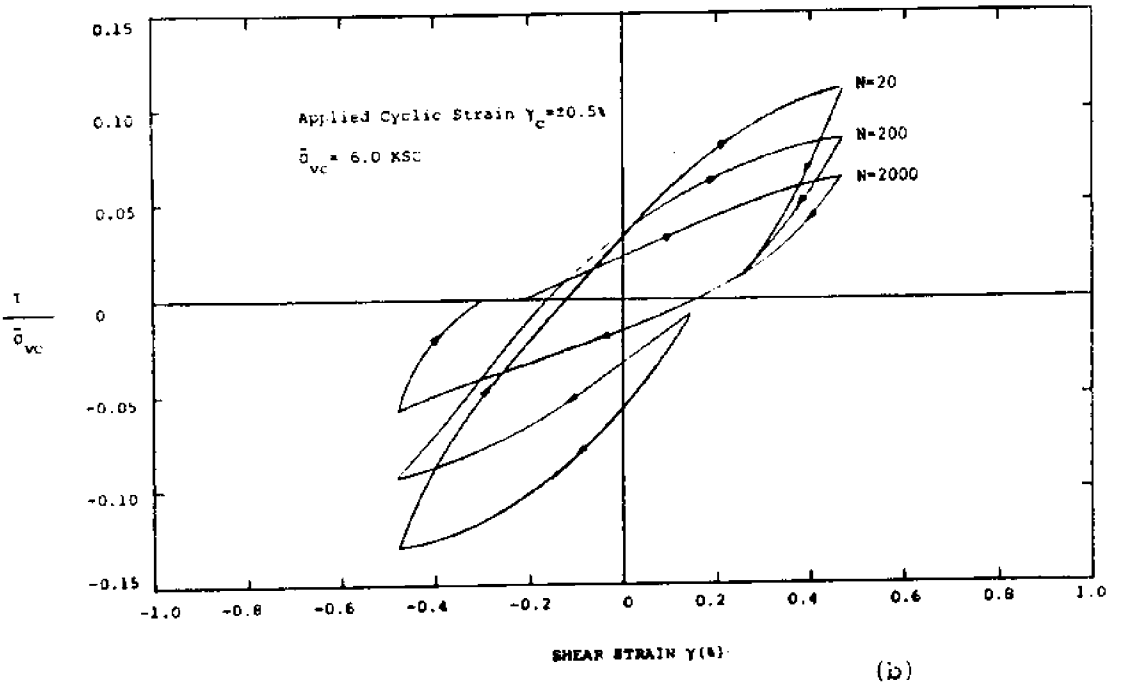

Figure 3.10 Typical Results of Strain-Controlled DSS Tests
a) Normalized Excess Pore Pressure versus Cycle Number
b) Normalized Shear Stress versus Shear Strain
Test C-21: N.C. BBC, $\bar{\sigma}_{vc}$=6.0 Kg/cm^2, γ_c=±0.5%

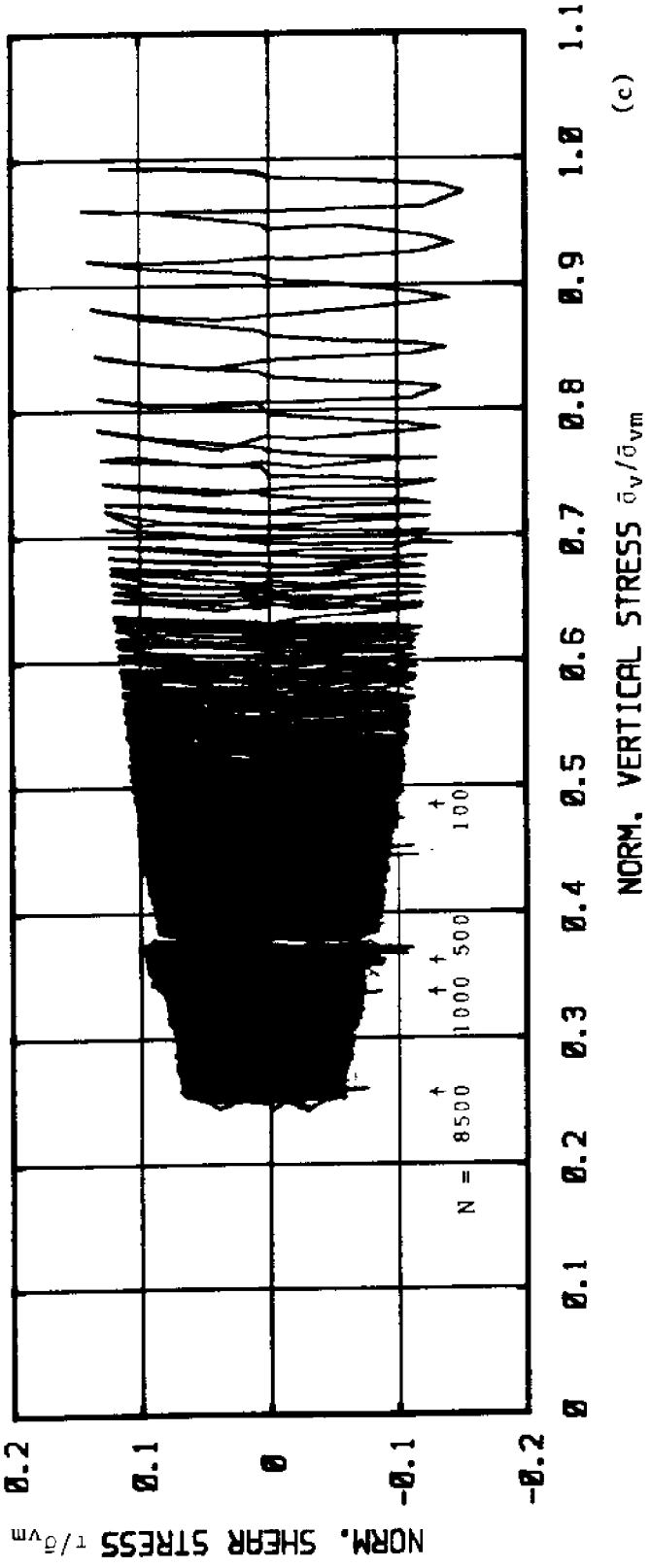

Figure 3.10 c) Normalized Stress Path, Strain-Controlled Test C-21

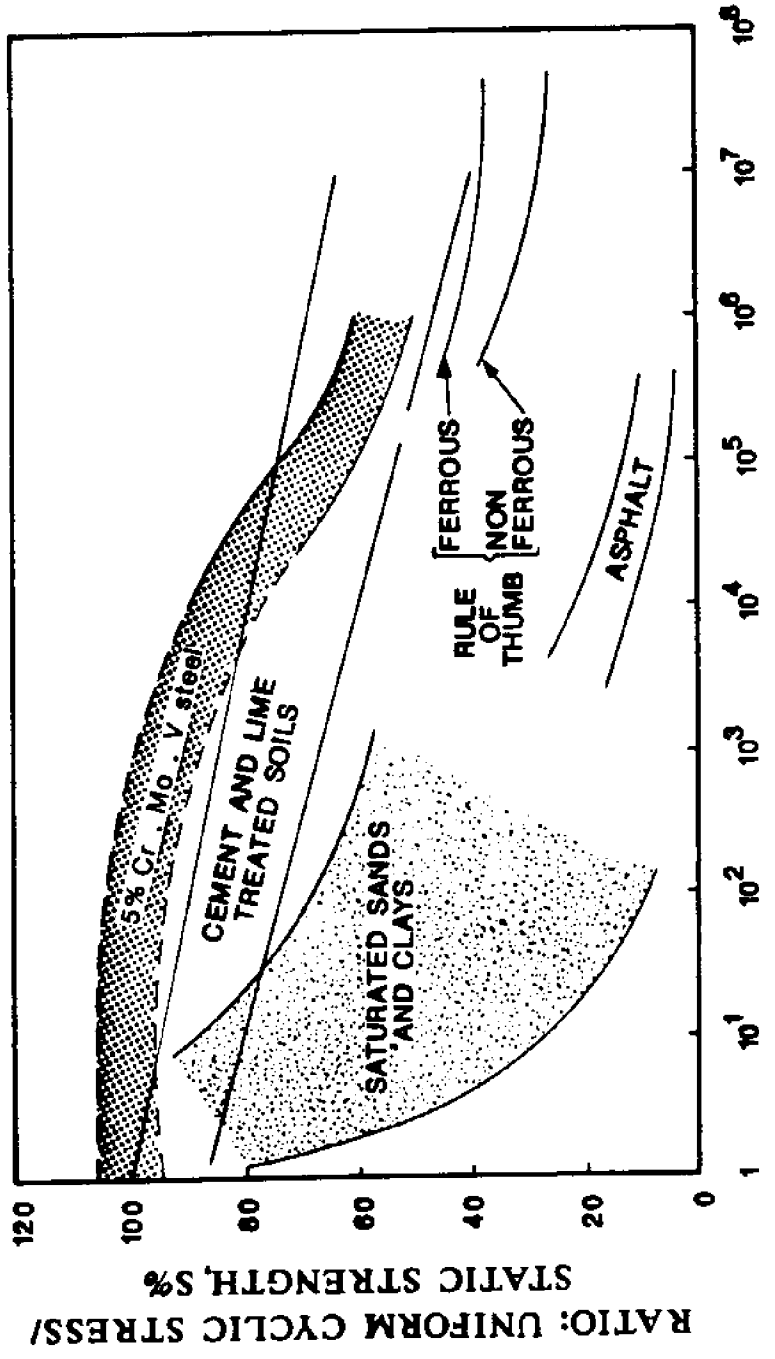

Figure 3.11 S-N Curves for Various Materials (redrawn from Annaki and Lee, 1977)

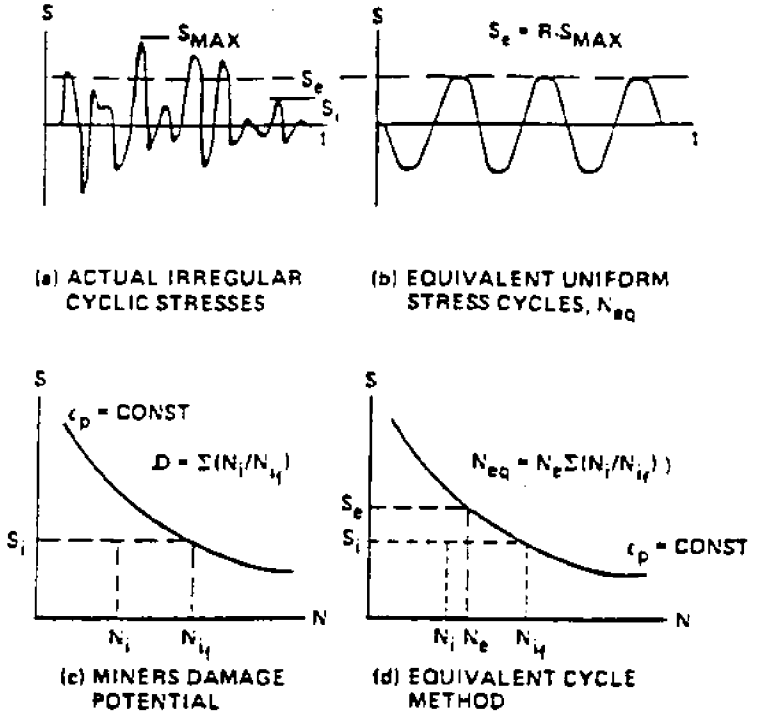

(from Annaki and Lee 1977)

Figure 3.12 Uniform Equivalent Number of Cycles Method of Superposition in Seismic Analyses

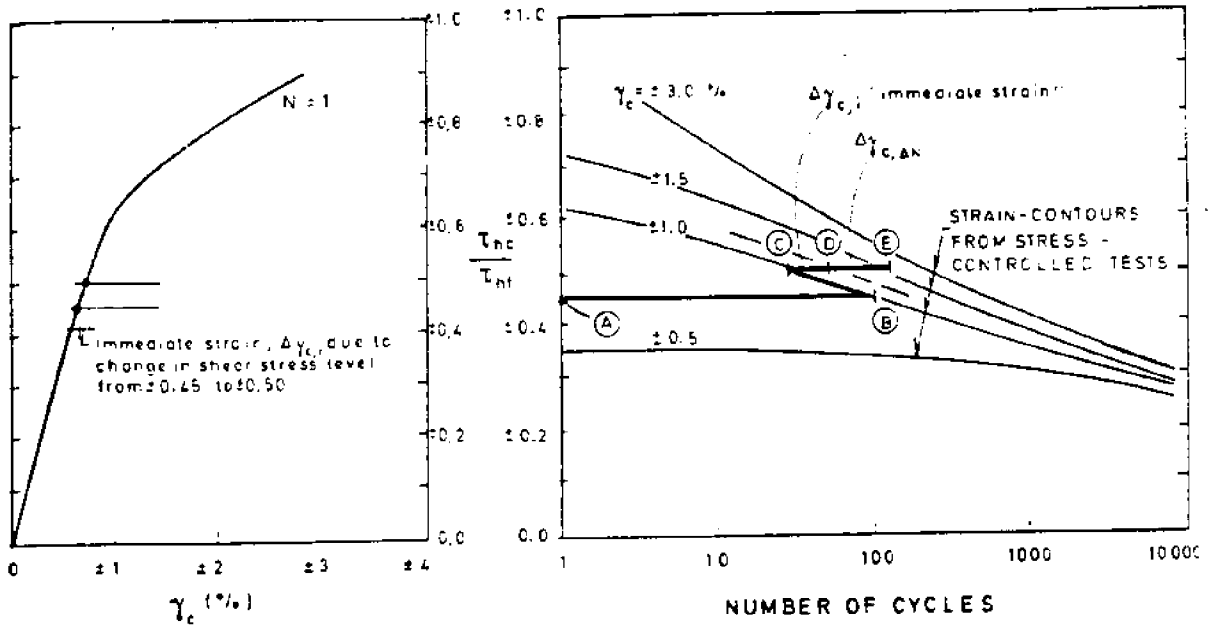

(a) (b)

(from Andersen 1975)

Figure 3.13 Andersen's Superposition Procedure for Gravity Platform Studies

CHAPTER 4

EQUIPMENT DESCRIPTION, EXPERIMENTAL PROCEDURE AND SUMMARY OF TESTING PROGRAM

4.1 THE GEONOR APPARATUS FOR MONOTONIC DIRECT SIMPLE SHEAR TESTING

Previous direct simple shear (DSS) research and testing at the Massachusetts Institute of Technology (MIT) was done using the Geonor Model 4 Direct Simple Shear Apparatus. This machine was developed at the Norwegian Geotechnical Institute, and is very similar to the one described by Bjerrum and Landva (1966). The DSS apparatus was built for testing undisturbed samples of soils under conditions of simple shear and plane strain (i.e., uniform strain throughout the soil sample and no change in the horizontal cross-sectional area). Plane strain conditions occur often in practical situations and cannot be simulated in the laboratory by means of conventional testing devices (e.g., triaxial test). The simple shearing mode imposed by the DSS test causes slippage on horizontal planes and hence simulates the shearing conditions along horizontal failure surfaces in slope stability analyses. Also, the DSS mode of shearing is the closest to the shearing mode of a soil element adjacent to a pile shaft (see Chapter 3). For a full description of this apparatus, the reader is referred to Ladd and Edgers (1972).

4.1.1 DSS Testing Description

Figures 4.1 and 4.2 schematically show the original Geonor Model 4 DSS device. After trimming, the soil sample is held by a wire-reinforced rubber membrane between top cap and pedestal, and is placed in a water bath in the DSS device (Figure 4.2). Drainage is provided at the top and bottom

of the sample, by means of porous stones communicating with the water bath. Two sample sizes can be tested, 35 cm^2 or 50 cm^2 in area with a height ranging from 1 to 2 cm. The first phase of the test is to consolidate the sample by load increments to the desired stress state. Throughout this process, the wire-reinforced membrane prevents lateral deformations, hence, the consolidation is performed under one dimensional loading conditions (K_o consolidation). The consolidation stress, recorded by means of a vertical proving ring, is applied by a dead weight lever arm system. Anisotropic, non K_o consolidation can be achieved by applying a horizontal shear stress during the consolidation phase, using the dead weight and pulley system. The second phase consists of shearing the sample by applying a horizontal load to the top cap. This can be done by either controlling the rate of displacement, using the gear box, or controlling the horizontal force on the top cap. The generated force is measured using a horizontal proving ring. Shearing can be performed under drained or undrained conditions. Because of the difficulties in sealing the sample, undrained shearing is carried out by imposing a condition of no volume change during shearing. Due to the high radial stiffness of the wire membrane, changes in the area of the specimen are very small and negligible compared to changes in height. Therefore, constant volume is achieved by keeping the sample height constant, which is done by adjusting the vertical stress. During this constant volume shearing, the measured pore pressures in the sample are zero. Vertical load adjustments were done manually in the original Geonor apparatus, and accounted for apparatus and porous stones compressibility during the correction phase. Later, the manual system was replaced by an automatic feedback system connected to a stepping motor which did not correct for apparatus compressibility. The constant volume

test is equivalent to an undrained test, and the change in applied vertical stress is equal to the change in pore pressure which would have occurred in the sample if it had been prevented from draining for a condition of constant applied vertical stress (see Section 4.2.3). A strain rate of 5% per hour is usually used in strain-controlled monotonic tests.

4.2 THE MIT APPARATUS FOR CYCLIC DIRECT SIMPLE SHEAR TESTING

Several modifications to the original MIT DSS device were necessary to allow cyclic DSS testing. These modifications fall in various categories and are described below.

4.2.1 Modification to the Geonor Model 4 Apparatus

The most significant change is the replacement of the shear gear box (0005, in Figure 4.1), responsible for application of the monotonic shear displacement, by an MTS hydraulic actuator connected to a closed-loop servo-hydraulic feedback system. Additional modifications were made to the DSS device and can be seen in Figure 4.3. The two proving rings were replaced by Data Instruments load cells. A 450 Kg capacity load cell for the vertical load was added to stiffen the measuring system, thus decreasing the response time of the height controller. The second load cell, 225 Kg in capacity, stiffens the horizontal loading system allowing displacement control by the MTS system without compliance corrections. Special mounts (C and D in Figure 4.3) were designed for these load cells to provide stiff, but moment free connections, both in tension and compression.

In addition to the load cell mounts, a structural bracket (A in Figure 4.3) was fabricated for the MTS actuator. This bracket is

compatible with the gear box mount needed for the static testing, thereby allowing quick exchange of the two systems. A new dead weight hanger (B in Figure 4.3), and connection to the height control mechanism were designed to be compatible with the geometric constraints imposed by the new actuator. Finally, a twin ball bearing assembly (E in Figure 4.3) was designed to apply positive and negative shear to the sample without backlash. This assembly is also designed to provide no resistance to the vertical motion of the upper cap, which takes place during sample consolidation prior to shear.

4.2.2 The MTS System

An MTS system was installed in order to allow cyclic DSS testing. The system consists of an actuator, controller, control unit, and hydraulic pump. The actuator has a 500 Kg capacity over a 10 cm stroke. It is regulated by a servovalve and powered by a 3/4 GPM (2.84 ℓ/min) pump at 3,000 psi (21,000 KPa) of pressure. The servovalve, controller and control unit constitute a closed loop system capable of performing displacement or load controlled testing. The control pulse is generated by a simple signal generator, but the controller can also be linked to an external signal source, such as a computer activated analog device.

After assembling all the MTS components, the system was calibrated and its performance was evaluated. The internal LVDT in the actuator as well as the horizontal load cell were calibrated, and all the adjustments in the electrical components (Controller and Control Unit) were done. As a result of these calibrations, the system is capable of running stress-controlled cyclic DSS tests to a maximum horizontal force of ± 175

Kg, corresponding to a maximum shear stress of ± 5 kg/cm^2, and strain-controlled cyclic DSS tests to a maximum displacement of ± 1.0 cm corresponding to approximately ± 50% shear strain (depending on the preshear sample height). An internal limit detector circuit and external limit switches ensure that the maximum load and maximum displacement respectively are never exceeded. The minimum horizontal force than can be applied to the sample is 0.175 Kg, corresponding to a horizontal shear stress of 0.005 Kg/cm^2, and the minimum horizontal displacement is 0.001 cm, corresponding to about 0.06% shear strain. The average as well as the cyclic stress (in stress-controlled tests), or strain (in strain-controlled tests) can be varied separately. The Control Unit has a built-in mini function generator, which is capable of producing sinusoidal, triangular, or square waveforms at frequencies varying between 0.01 and 1110 Hz. The testing frequency however cannot exceed 1 Hz. because of friction and inertia effects in the DSS device. A counter in the Control Unit keeps track of the cycles applied up to 100,000 cycles.

The performance of the DSS-MTS system was checked and evaluated. This was done by running a series of stress-controlled as well as strain-controlled tests, on a rubber sample placed in the device. The sample was subjected to known cyclic loading of various shapes, frequencies, mean values and cyclic values, and the response was monitored on an oscilloscope. After careful adjustment of the gain, rate and stability of the feedback control, it was found that the actual stresses (in stress-controlled tests) and the actual displacements (in strain-controlled tests) measured externally on the oscilloscope were identical to the specified input value applied by the MTS system.

4.2.3 Pedestal with Pore Pressure Measurements

As was mentioned in Section 4.1.1, undrained DSS shearing is achieved by shearing at constant volume while allowing drainage in the soil. The equivalence between undrained shearing and constant volume shearing, which is the same as constant height shearing in the DSS (since the sample area is unchanged), can be explained as follows.

At the end of consolidation, the pore pressure in the sample is zero since drainage is allowed. Immediately after shearing starts, shear induced pore pressures are generated in the sample, causing the sample height to change, if they are allowed to dissipate. However, the sample height is constantly monitored, and the onset of sample height change is detected and the vertical load is immediately varied until the tendency for height change stops. In order to keep the sample height constant, the change in vertical load must cancel the shear-induced pore pressures by generating equal but opposite volumetric pore pressures, leaving a net zero pore pressure in the sample. This condition of zero pore pressure ensures zero pressure gradient, resulting in the sample not compressing nor dilating, and hence constant volume. The vertical stress measured with the outside proving ring (or load cell) is therefore the vertical effective stress, and the difference between the vertical preshear consolidation stress and the measured effective vertical stress is equal to the shear-induced pore pressure in a truly undrained DSS test where drainage is prevented.

Monotonic undrained DSS tests are sheared at a strain rate not exceeding 5% per hour, which is slow enough to permit manual or automatic vertical stress adjustments with a slow response time. However, in a cyclic test with a period of 10 seconds and a cyclic strain value of ± 3%,

the strain rate can reach 4000% per hour which is 800 times faster than the monotonic strain rate. At this strain rate, it is necessary to use a height adjustment mechanism with a very small response time, and it becomes necessary to measure the pore pressure in the cyclic DSS sample in order to ensure zero pore pressures, and hence undrained conditions.

A special pedestal was designed and fabricated for this purpose, and is shown in Figure 4.4. The top surface of the pedestal is impervious and knurled to prevent slippage of the specimen. A flush mounted fine ceramic porous stone contacts the bottom of the sample, and is hydraulically connected to a miniature pressure transducer. Two O-rings are placed around the bottom of the wire-reinforced membrane in order to seal the bottom of the sample, and therefore obtain accurate pressure measurements. The sample is only drained at the top via a porous stone connected to a water bath.

The porous stone and transducer were deaired, and subsequently saturated with deaired water, in order to achieve a high degree of saturation leading to an instantaneous pore pressure response. The pore transducer is capable of accurately and instantaneously measuring changes in pore pressure in the sample.

4.2.4 Height Adjustment Mechanism

The height adjustment mechanism used in monotonic DSS tests previous to this research consisted of an automatic feedback system connected to a stepping motor. This old system had several problems, the major ones being a slow response time, and frequent shifts in the initial or zero value of

the sample height. These limitations could be circumvented while running slow monotonic tests, but caused major problems during fast cyclic DSS tests. A height adjustment mechanism capable of detecting very small changes, and capable of almost instantaneous vertical stress changes was required for cyclic testing. Therefore, a new digital control system, consisting of an Electrocraft motor and Controller connected to the data acquisition computer (described in the next section) has replaced the old one. The system reads the sample height and vertical stress, computes the apparatus compressibility correction, and sends the feedback voltage necessary to keep a constant height. The system has an instantaneous response, and its performance during cyclic tests was found to be perfect.

4.2.5 Development of the Data Acquisition and Reduction System

Cyclic testing generates a very large amount of data and therefore requires automated data acquisition and reduction systems. Data acquisition using strip chart recorders has the advantage of providing continuous data, but the disadvantage of creating an enormous amount of strip charts, especially for tests with large number of cycles. Also, reduction of such data requires manual reading of the strip chart record or digitizing of discrete points along the record for later reduction using a computer. This digitizing process not only defeats the purpose of taking continuous readings, but is very time consuming, especially for tests with hundreds or thousands of cycles. The most efficient method of data acquisition is to use a computer with an analog to digital converter, for reading the data and storing it on permanent media such as disk or tape. The time interval between successive readings can be varied, and depends on the speed of the

computer, the software package used, and the number of different devices to be read. The choice of hardware should be carefully studied, and should be tailored to the particular application.

An Analog Devices Macsym 150 computer, with multitasking capability, was chosen for reading, storing, and reducing the data from the various transducers in the cyclic DSS apparatus (vertical and horizontal load cells, vertical and horizontal displacement transducers, pore pressure transducer, and input voltage). Analog to digital cards are used for reading the data, and a digital to analog card is used for sending control voltages to the height adjustment mechanism. Three separate software codes were developed, the first for data acquisition, the second for data reduction, and the third for plotting the results.

The data acquisition code reads 12 sets of data in each 10-second cycle (i.e., one set every 0.83 seconds) and stores them in memory. Each set consists of the cycle number, the input voltage, the vertical load, the vertical displacement, the horizontal load, the horizontal displacement, and the measured pore pressure at the base of the sample. The raw data from every cycle is later stored on disk, while important test information necessary for control is displayed in real time. The sample height is simultaneously monitored in a continuous fashion, as part of a separate task, and the appropriate control voltage is sent to the Electrocraft controller to either increase or decrease the vertical stress, ensuring constant sample volume.

The data reduction code is a separate program that reads the raw data from disk, reduces it, and prints it in a tabulated format. For each cycle of interest, there are 12 values of horizontal stress and strain, vertical stress and strain, and measured pore pressure, corresponding to the 12 sets

of readings taken along each cycle by means of the data acquisition program. Because of the enormous amount of data generated during each test, the code allows reduction of only selected cycles, that is to reduce data every 1,2,..., 5,...,10, ..., x number of cycles if necessary. The printout also includes for each cycle the average shear stress and shear strain, the cyclic shear stress and shear strain, as well as the average computed (vertical stress difference) and measured pore pressures.

Plotting the results is done by first using a modified version of the data reduction program to print the reduced data to a disk file, and then using the disk file as input for a plotting program developed by Lutz (1985), for the Macsym 150 computer.

4.3 RESEDIMENTED BOSTON BLUE CLAY

The aim of this research is to develop a better understanding of clay behavior under cyclic loading rather than the determination of the cyclic strength of a particular clay for a specific design problem. Boston Blue Clay, which has been studied and tested extensively at MIT, provided a good reference clay for research purposes, hence, samples of resedimented Boston Blue Clay (RBBC) were used in this cyclic DSS testing program.

4.3.1 Resedimentation Procedure

Resedimented Boston Blue Clay has been used routinely at MIT (Ladd and Lambe, 1963; Ladd, 1964; Wissa and Heiberg, 1969; Ladd et al., 1971; Ladd and Edgers, 1972; Germaine, 1982; Bensari, 1984; O'Neill, 1985; Fayad, 1986). The resedimentation equipment and procedure have been constantly

upgraded, the latest improvements being attributed to Germaine (1982) to ensure production of saturated samples.

The resedimentation process consists of mixing dry deaired BBC clay powder with deaired water in an upper vacuum chamber. Sodium chloride (NaCl) is added to the mixture to produce a final slurry salt concentration of 16 g/l to control the segregation of the particles. After mixing, the slurry is rained into a lower vacuum chamber for consolidation. Dead weights are used up to a vertical stress of 0.063 kg/cm^2, and a rigid loading frame with an air activated piston is used for higher stresses. A load increment ratio of one is used, and each stress level is maintained until the end of primary consolidation. The sample is subjected to a maximum consolidation stress of 1 kg/cm^2, which is maintained for one cycle of secondary compression, after which the vertical stress is decreased to an overconsolidation ratio of 4. Water is removed from the chamber before the last load is removed, and the chamber is taken to the humid room for trimming immediately after load release. The cake of resedimented BBC is removed from the consolidation chamber by excavating a trench around the circumference of the sample and lifting the chamber without applying any shear stresses to the clay. The cake is then divided into individual DSS samples which are plastic wrapped and sealed with hot wax, and stored in the humid room for later testing.[1]

Germaine (1982) has evaluated the quality of resedimented samples

---

[1]J.T. Germaine, "Development of the Directional Shear Cell for Measuring Cross Anisotropic Clay Properties," Sc.D. Thesis, MIT, Department of Civil Engineering, Cambridge, MA, 1982, pp. 82-87.

obtained by using the above technique. Uniformity within each batch was confirmed by the absence of siltation, or the separation of silt and clay size particles. This was checked by measuring the water content variation with depth in each batch, (which was very small, on the order of 1%), by slow drying vertical slices of clay from each batch (which showed no difference in color due to stratification), and by performing x-ray diffraction tests on samples from different depths in each batch (which showed no change in either quartz or clay peaks). Batch to batch uniformity was confirmed by comparing the consolidation characteristics, compressibility and rate of consolidation, and the water content between batches, both of which showed very small changes. Full saturation of the batches was confirmed by Germaine from direct measurements of weight and volume, to compute the degree of saturation from the phase relation, and from measurements of Skempton's B parameter in triaxial tests. Finally, Germaine compared the properties of BBC samples obtained using the above procedure, with those of previous research programs, and found them to be similar.[2]

From the above quality evaluation of BBC, it follows that the latest technique for resedimenting Boston Blue Clay, which was described above, produces very uniform and repeatable batches of fully saturated clay, with properties very close to previous research BBC. Therefore, two batches of RBBC (Nos. 111 and 112) were completed for this research, and yielded 64 fully saturated DSS samples with very uniform properties and known stress history.

---

[2]Ibid, pp. 126-134.

4.3.2 Index Properties

Boston Blue Clay is a lean sensitive clay exhibiting normalized behavior. Table 4.1 summarizes the index properties for the two batches of RBBC.

The water content in each batch is very uniform, and the difference between the average value of each batch is also small (only 0.8%). The average water content for the two batches was 39.3% with a standard deviation of 0.7%, which compares very favorably with the values obtained by Germaine (1982) and Ladd and Edgers (1972).

Two Atterberg limits tests were performed on each batch. The samples used in each test included trimmings from three different DSS samples. The Atterberg limits values differ slightly between batches, with a maximum difference less than 1.5% in the plasticity index. The combined values for the two batches give a liquid limit of 44.1%, a plastic limit of 22.7%, and a plasticity index of 21.4%, which are close to the values of Germaine (1982) and Ladd and Edgers (1972).

4.3.3 Engineering Properties

Five monotonic K_o-consolidated undrained direct simple shear (CK_oUDSS) tests were performed, four on samples from batch No. 111, and one on a sample from batch No. 112. These tests were done in order to determine the undrained strength of the batches, and obtain a measure of strength uniformity. Table 4.2 gives important information about the tests, and summarizes their results. The five tests were performed on normally consolidated samples, at different vertical consolidation stresses (3, 4 and 6 Kg/cm^2), using the test procedure described in Section 4.1.1. Tests S-1 and S-2 were run using the old height adjustment mechanism,

whereas tests S-3, S-4, and S-5 were run using the computer controlled Electrocraft height adjustment mechanism with correction for apparatus and stone compressibility (see Section 4.2.4). The normalized undrained DSS shear strength, defined as the maximum horizontal shear stress divided by the preshear vertical consolidation stress, $\tau_{h(max)}/\overline{\sigma}_{vc}$, is given in the Table and ranges between 0.192 and 0.222.

Figure 4.5 plots shear stress versus shear strain, excess pore pressure versus shear strain, stress paths, and measured pore pressure versus shear strain. The stress strain curves in Figure 4.5(a) show similar trends, namely a stiff response at low strains, with a peak occuring between 5% and 10% shear strain, followed by strain softening for strain values above 15%. Tests S-1 and S-5 however peaked at a rather small strain value of 2.5% and 3.5%. The pore pressure curves in Figure 4.5(b) are very consistent, with the normalized excess pore pressure reaching large values ranging between 0.7 to 0.8 for strains greater than 20% to 25%. The stress paths in Figure 4.5(c) are very similar, showing a constant decrease in vertical effective stress with increasing strain. Test S-5 however shows an initial increase in vertical stress, leading to negative pore pressures, followed by a constant decrease in vertical stress. At large strains, all stress paths converge to the maximum obliquity line, which passes through the origin of the stress path space, and makes a 30° angle with the vertical effective stress axis. The measured pore pressure at the base of the sample is plotted in Figure 4.5(d). Except for test S-2, the values are very small and negligible compared to the vertical stress difference $\overline{\sigma}_{vc}-\overline{\sigma}_{v}$. This confirms the fact that constant volume tests are identical to undrained tests, and that the excess pore pressure in the undrained DSS test can be computed as the

difference in vertical effective stress during shearing (see Section 4.2.3). The measured pore pressure during tests S-1 and S-2, using the old constant height mechanism, show more scatter than the measured values in tests S-3, S-4, and S-5, which used the new Electrocraft system. This scatter is related to the slow response and the constant zero shift of the old system, which had to be changed for cyclic tests. The performance of the new constant height mechanism is very good, as demonstrated by tests S-3, S-4, and S-5. The data shows a trend of increasing measured pore pressure with increasing shear strain, which is mainly attributed to an increasing uncertainty in apparatus and stone compressibility with decreasing vertical stress. Because of this increasing uncertainty, the error in apparatus compressibility, used for maintaining a constant sample height, increases and results in a maximum measured pore pressure equal to 6% of the computed excess pore pressure, at a shear strain γ_c=30%.

The data from the five monotonic undrained DSS tests are consistent, and plot within a narrow band (Figure 4.5), indicating uniformity in the two RBBC batches. The normalized undrained monotonic DSS strength, $\tau_{h(max)}/\bar{\sigma}_{vc}$, equals 0.205 ± 0.013 SD, which compares very well with the value of 0.20 ± 0.01 SD reported by Ladd and Edgers (1972)[3]. This average value will be used as a reference strength in cyclic DSS tests.

4.4 CYCLIC DSS TESTING PROCEDURE AND NOTATIONS

This section describes the testing procedure during stress-controlled undrained cyclic direct simple shear testing. Sample trimming and

---

[3]C.C. Ladd, L. Edgers, "Consolidated Undrained Direct Simple Shear Tests on Saturated Clays," Research Report R72-82, Soils Publication No. 284, Department of Civil Engineering, MIT, Cambridge, MA, 1972, p. 61.

positioning in the testing apparatus is similar to that of monotonic DSS tests, except that the pedestal with built-in pore pressure transducer, described in Section 4.2.3, is used. The pore pressure is measured at the base of the sample, and drainage is allowed at the top only. Figure 4.6 shows the testing sequence and notations.

First, the sample is consolidated under K_o conditions to the desired consolidation stress, $\bar{\sigma}_{vc}$. In the case of a normally consolidated sample, the vertical consolidation stress is increased to at least 1.5 to 2 times the maximum past pressure, as recommended by the SHANSEP[4] approach (Ladd and Foott, 1974), in order to minimize the effects of sample disturbance. Overconsolidated samples are obtained by first consolidating the sample to a minimum of 1.5 to 2 times the maximum past pressure for a period of 24 hours, and then unloading to the desired overconsolidation ratio.

The second step, labeled drained shear in Figure 4.6, is the application of the average shear stress, τ_{ave}, on the sample. This is done in a drained fashion, using the horizontal force dead weight system shown in Figure 4.1. Three hours after applying the last consolidation increment, the horizontal stress is increased while the sample pore pressure is monitored and kept below 2% of the vertical consolidation stress, and thus ensuring mostly drained conditions. This is done by varying the magnitude of the applied horizontal stress increment and/or the time interval between increments (a maximum horizontal stress increment of 0.086 kg/cm^2, corresponding to a weight of 3 kg, applied at an interval of 6 minutes was found to be adequate for RBBC). The sample is allowed to

---

[4]SHANSEP is an acronym for Stress History and Normalized Soil Engineering Properties.

consolidate under the applied average shear stress for a period of 24 hours starting from the time the last consolidation load was applied. During this period, the vertical strain as well as the shear strain stabilize. At the end of the 24 hour period, the rate of strain development is small enough so that during undrained shearing, the tendency for deformation due to secondary compression and drained creep are small compared to the shear-induced deformations.

The third step, labeled undrained cyclic loading in Figure 4.6, is to subject the sample to the horizontal cyclic shear stress component, τ_c, under undrained conditions. A sinusoidal cyclic shear stress with a period of 10 seconds and an amplitude τ_c is applied using the MTS equipment. Cycling is continued until the sample fails or until a specified number of cycles is reached for non failing tests.

A typical sample response is shown in Figure 4.6. At the end of the drained creep period, the sample accumulates a shear strain γ_{dc} due to the application of the drained average shear stress. The response of the sample during the cyclic phase includes two components, the average shear strain γ_{ave} and the cyclic shear strain γ_c. The figure also defines $\Delta\gamma_{ave}=\gamma_{ave}-\gamma_{dc}$, which is the shear strain due to the application of τ_c alone, and which does not include the drained creep component of shear.

4.4.1 Limitations of the Testing Procedure

Figure 3.6 in Chapter 3 compared the stress system applied to the soil sample in the DSS apparatus to that of an element of soil next to the pile shaft, and section 3.2 indicated that the DSS test provides the best simulation of pile loading condition. However, there are two major differences between laboratory and field conditions which must be pointed

out:

1. After pile driving and consolidation, theoretical analyses (Whittle, 1987) indicate that soil elements adjacent to the pile shaft are under the following stress state: a major principal effective stress $\bar{\sigma}_{rc}$ acting radially, an intermediate effective principal stress $\bar{\sigma}_z$ acting vertically, and a minor effective principal stress $\bar{\sigma}_\theta$ acting tangentially. The DSS sample however is subjected to K_o condition with equal intermediate and minor principal stresses, and does not allow control over the intermediate effective stress.

2. In the laboratory, the DSS sample is trimmed and placed in the apparatus with planes of isotropy (i.e. the horizontal planes of deposition) perpendicular to the direction of the vertical consolidation stress $\bar{\sigma}_{vc}$. In case of normally consolidated clays, the latter direction (vertical) coincides with the orientation of the major principal stress. Hence, during subsequent DSS shearing, the horizontal shear stress is applied parallel to the planes of isotropy. In the field, after pile driving and consolidation, a soil element adjacent to the pile shaft has its major principal stress perpendicular to the pile shaft, and the shear stress (due to axial pile loading) acts parallel to the pile shaft (i.e. vertical). If the planes of isotropy in the field are parallel to the pile shaft, then the DSS test would be properly accounting for the effects of inherent soil anisotropy. However, the planes of isotropy in the field after pile installation and consolidation cannot be estimated with certainty because pile driving causes severe remolding of the soil, changing its fabric and the initial direction of inherent anisotropy. Existing data suggest that these planes of isotropy are close to being vertical, and hence almost parallel to the direction of shear (Strain Path

Method[5]). Also, as reported in Section 3.1.1, Whittle (1987) has shown that DSS shearing on normally to slightly overconsolidated (OCR<1.2) samples, sheared in a direction parallel to the planes of isotropy, produces stress-strain curves and stress paths (normalized by the vertical consolidation stress) which are similar to the stress-strain curves and stress paths (normalized by the horizontal stress after driving and consolidation) of soil elements adjacent to the pile shaft when sheared in a direction parallel to the pile (see Figure 3.4). The curves in the figure correspond to predictions for clays with different OCR values and indicate that, after installation disturbances, the soil behavior is very close to predictions for the undisturbed (regular) DSS test results. This indicates that the effects of inherent anisotropy on the disturbed soil behavior are not significant, and that DSS testing, with the planes of inherent isotropy parallel to the direction of shear, is appropriate for predicting pile behavior.

3. The Geonor DSS apparatus cannot impose uniform stresses on the sample. Theoretical analyses assuming linear elastic samples have shown that the stresses imposed on the DSS sample are not uniform (e.g. Lucks et al., 1972; Wright et al., 1978; and Shen et al., 1978). However, results of tests on real soil samples using different height to diameter ratios by Vucetic and Lacasse (1982) have shown that the non-uniformities do not affect the measured soil behavior.

Airey and Wood (1987) performed DSS tests on normally consolidated Kaolin using two different DSS devices: the regular Geonor apparatus and

---

[5]M.M. Baligh, "Strain Path Method," Journal of Geotechnical Engineering, ASCE, Vol. 111, No. 9, September 1985.

an instrumented circular simple shear apparatus with five load cells capable of measuring the stress distribution at the base of the sample. Their results indicate that for constant volume DSS tests, the shear strains were uniform and the volumetric strains were zero up to a shear strain of 11%. They conclude that, because of the non-uniformities in the standard DSS test sample, the shear strength determined from the average stresses which are measured at the boundaries of the sample, underpredicts the simple shear values by about 10%.

4.5 SUMMARY OF THE DSS TESTING PROGRAM

The cyclic experimental program conducted as part of this report consisted of K_o-consolidated undrained cyclic direct simple shear tests (CK_oUCDSS tests). Thirty-nine tests were performed in a stress-controlled mode of shearing and one test was strain-controlled. The majority of the tests were conducted on normally consolidated samples, with only eight tests performed on overconsolidated samples (up to OCR=4). In the stress-controlled tests, the average shear stress component τ_{ave} and the cyclic shear stress component τ_c were applied separately, with 23 tests performed with $\tau_{ave}=0$, and 16 tests with $\tau_{ave}\neq 0$. Three of the tests were conducted with variable τ_c values. Tables 4.3 and 4.4 list all the stress-controlled tests, along with the maximum consolidation stress $\bar{\sigma}_{vm}$, the overconsolidation ratio OCR, and the average and cyclic components of shear stress τ_{ave} and τ_c (expressed as a percentage of the monotonic undrained normally consolidated DSS strength, $s_u(NC)$). The results of these tests are presented in Chapters 5, 6, and 7.

TABLE 4.1

INDEX AND COMPOSITIONAL PROPERTIES OF
RESEDIMENTED BOSTON BLUE CLAY

RESEDIMENTED BOSTON BLUE CLAY WATER CONTENT

Batch Number	Number of Observations	Water Content (%) Average	Standard Deviation
111	19	39.46	0.48
112	17	39.16	0.79
Combining batches 111 & 112		39.32	0.65
Ladd and Edgers (1972)		37	2
Germaine (1982)		40.24	0.64

RESEDIMENTED BOSTON BLUE CLAY ATTERBERG LIMITS

Reference	Liquid Limit (%)	Plastic Limit (%)	Plasticity Index (%)
Batch 111	44.35	22.85	21.50
Batch 112	43.80	22.60	21.20
Combining batches 111 & 112	44.08	22.73	21.35
Ladd and Edgers (1972)	41	20	21
Germaine (1982)	41.8	21.6	20.20

BOSTON BLUE CLAY COMPOSITIONAL PROPERTIES
(from Ladd and Edgers, 1972)

Specific Gravity	2.78
Percent Clay Fraction	50%
Quartz	15-20%
Chlorite	5%
Illite	30-45%

TABLE 4.2

SUMMARY OF MONOTONIC UNDRAINED DSS TESTS
ON NORMALLY CONSOLIDATED BBC

						At Maximum τ_h					
TEST NO.	BATCH No.	$\bar{w}_N$ (%)	$\bar{\sigma}_{vc}$ Kg/cm^2	OCR	ε_v(%) at $\bar{\sigma}_{vc}$	γ (%)	$\frac{\tau_h}{\bar{\sigma}_{vc}}$	$\frac{\bar{\sigma}_v}{\bar{\sigma}_{vc}}$	$\bar{\phi}$	$\frac{E_{u50}}{s_u}$	COMMENTS
S-1	111	39.78	3.08	1.0	10.1	2.43	0.201	0.592	18.8°	243	Peak shear stress reached at low shear strain
S-2	111	39.71	3.09	1.0	8.1	10.7	0.192	0.447	23.2°	63	Good test
S-3	111	39.22	4.00	1.0	10.8	6.80	0.214	0.515	22.6°	80	Excellent test
S-4	111	39.52	4.00	1.0	10.0	6.85	0.195	0.505	21.1°	99	Excellent test
S-5	112	39.21	6.00	1.0	16.4	3.52	0.222	0.678	18.1°	159	Good test

$$s_u/\bar{\sigma}_{vc} = \tau_{hmax}/\bar{\sigma}_{vc} = 0.205 \pm 0.013 \text{ SD}$$

TABLE 4.3

SUMMARY OF UNDRAINED CYCLIC DSS TESTS
WITH $\tau_{ave}=0$

TEST NO.	$\bar{\sigma}_{vm}$ Kg/cm^2	OCR	$\frac{\tau_{ave}}{s_u}$*	$\frac{\tau_c}{s_u}$*	Failure	COMMENTS
C-1	4.00	1.0	0	0.25	YES	Average test, load cell zero shift
C-2	4.00	1.0	0	0.50	YES	Average test, load cell zero shift
C-3	4.00	1.0	0	0.62	--	No data, failure of data acquis. system
C-4	8.00	1.0	0	0.62	YES	Previous shear, same as sample C-3
C-5	6.13	1.0	0	0.56	YES	Good test
C-6	4.08	1.0	0	0.70	YES	Good test
C-7	4.08	1.0	0	0.85	YES	Good test
C-22	6.01	1.0	0	0.25	NO after 10,000 cycles	Excellent test
C-23	6.01	1.0	0	0.35	NO after 10,000 cycles	Excellent test, same sample as C-22
C-24	6.00	1.0	0	0.57	YES	Excellent test, same sample as C-23
C-26	6.00	1.38	0	0.60	YES	Excellent test
C-27	6.01	1.38	0	0.76	YES	Excellent test
C-28	6.01	1.0	0	0.56 0.71	YES	Excellent test, variable cyclic loading
C-29	4.00	1.0	0	0.56	NO after 29 cycles	Excellent test, test stopped after 29 cycles
C-30	8.01	1.0	0	0.56	YES	Experimental problems, same sample as C-29

* $s_u = s_u(NC) = 0.205\ \bar{\sigma}_{vc}$ for OCR = 1

$s_u = s_u(OC) = s_u(NC)\ (OCR)^{m-1}$ $m = 0.8$ for OCR > 1

(from Ladd and Edgers, 1972)

TABLE 4.3 (continued)

SUMMARY OF UNDRAINED CYCLIC DSS TESTS
WITH $\tau_{ave}=0$

TEST NO.	$\bar{\sigma}_{vm}$ Kg/cm^2	OCR	$\frac{\tau_{ave}}{s_u}$*	$\frac{\tau_c}{s_u}$*	Failure	COMMENTS
C-31	6.00	4	0	0.55	YES	Experimental problems with height adjustment mechanism
C-32	6.00	4	0	0.50	YES	Excellent test
C-33	6.01	2	0	0.56	YES	Excellent test
C-34	6.01	2	0	0.70	YES	Excellent test
C-35	6.01	2	0	0.56	YES	Excellent test
C-36	6.00	2	0	0.85	YES	Excellent test
C-37	6.00	1	0	0.50 0.64	YES	Excellent test, variable cyclic loading
C-38	6.00	1	0	0.50 0.70 0.56	YES	Excellent test, variable cyclic loading

* $s_u = s_u(NC) = 0.205\ \bar{\sigma}_{vc}$ for OCR = 1

$s_u = s_u(OC) = s_u(NC)\ (OCR)^{m-1}$ $m = 0.8$ for OCR > 1

(from Ladd and Edgers, 1972)

TABLE 4.4

SUMMARY OF UNDRAINED CYCLIC DSS TESTS
WITH $\tau_{ave} \neq 0$

TEST NO.	$\bar{\sigma}_{vm}$ Kg/cm2	OCR	$\frac{\tau_{ave}}{s_u}$*	$\frac{\tau_c}{s_u}$*	Failure	COMMENTS
C-8	4.09	1	0.45	0.46	YES	Good test
C-9	4.08	1	0.45	0.46	YES	Good test
C-10	4.08	1	0.69	0.40	YES	Excellent test
C-11	4.09	1	0.69	0.40	YES	Excellent test
C-12	6.13	1	0.49	0.40	YES	Excellent test
C-13	6.12	1	0.59	0.40	YES	Excellent test
C-14	6.13	1	0.59	0.41	YES	Excellent test
C-15	6.14	1	0.59	0.50	YES	Excellent test
C-16	6.13	1	0.49	0.60	YES	Excellent test
C-17	6.12	1	0.59	0.30	NO after 10,000 cycles	Excellent test
C-18	6.13	1	0.39	0.60	YES	Excellent test
C-19	6.00	1	0.50	0.51	YES	Excellent test
C-20	6.00	1	0.40	0.51	YES	Excellent test
C-25	6.01	1	0.35	0.35	NO after 15,000 cycles	Excellent test
C-39	6.02	1	0.15	0.38	NO after 100,000 cycles	Excellent test
C-40	6.01	1	0.80	0.20	NO after 30,000 cycles	Excellent test

* $s_u = s_u(NC) = 0.205\ \bar{\sigma}_{vc}$ for OCR = 1

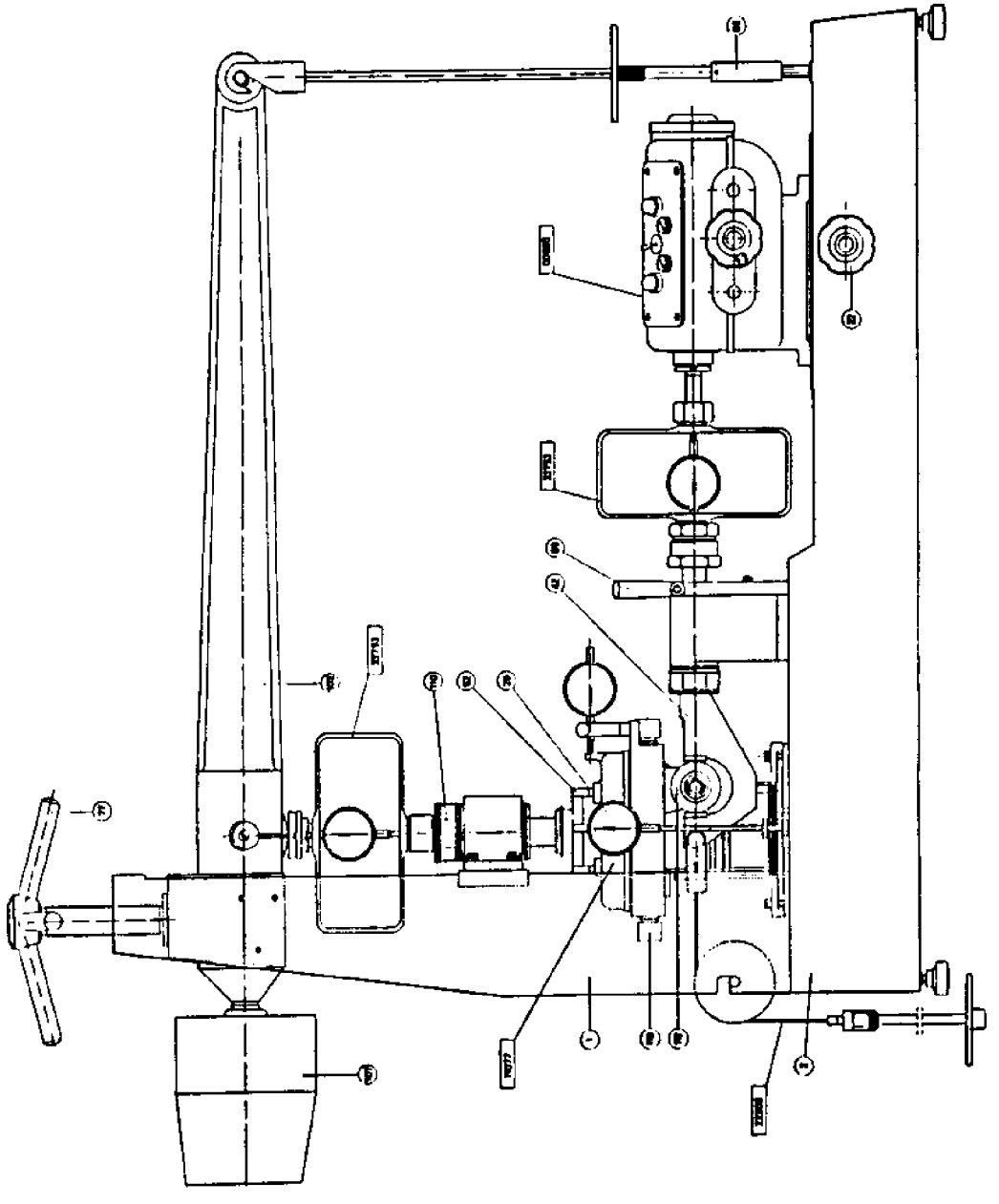

Figure 4.1 Diagram of the Geonor Model 4 Direct Simple Shear Apparatus

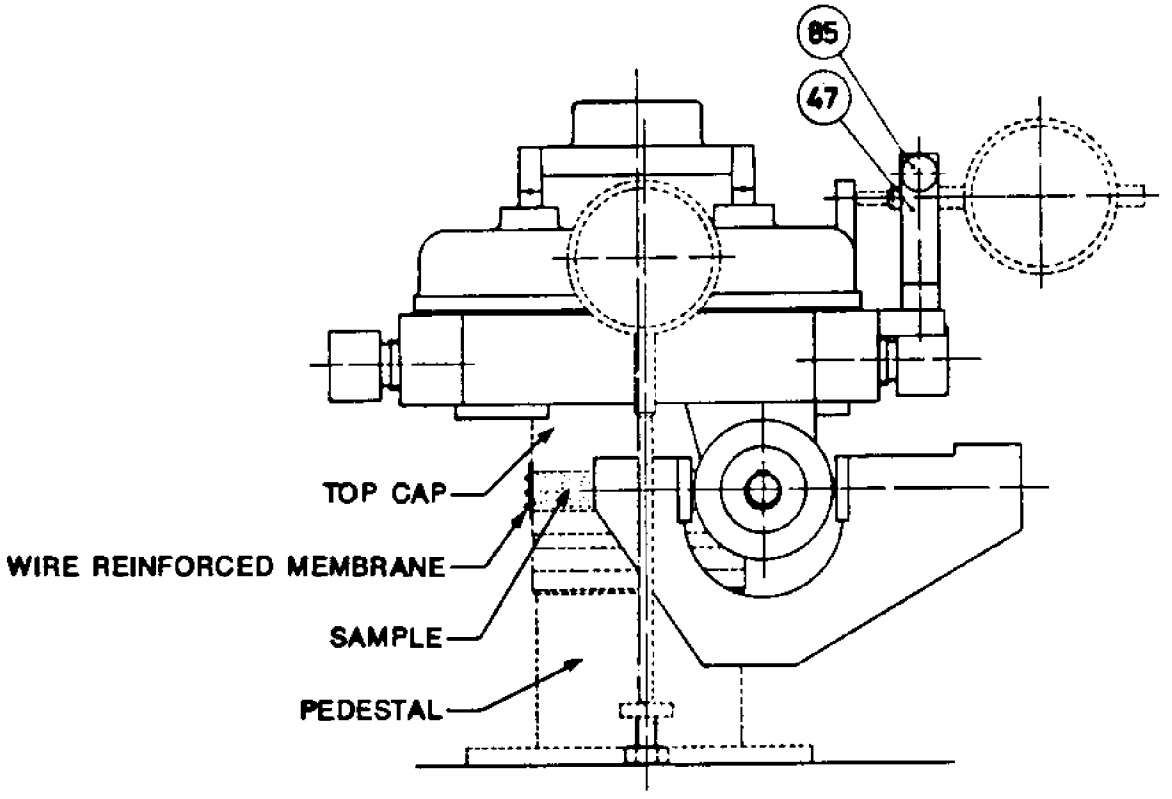

Figure 4.2 Geonor Model 4 Direct Simple Shear Sample Assembly

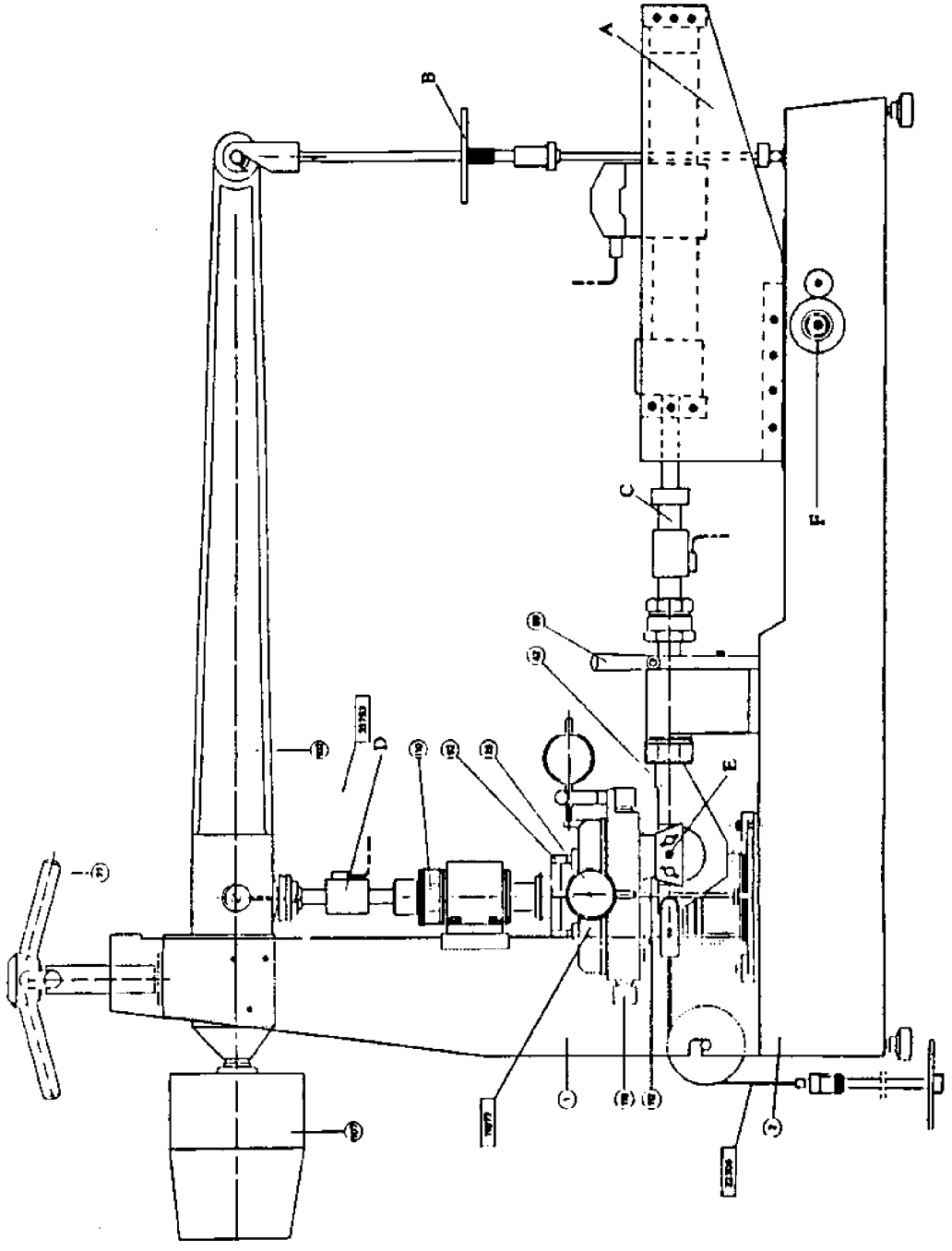

Figure 4.3 Geonor Direct Simple Shear Apparatus Modified for Cyclic Shear Loading

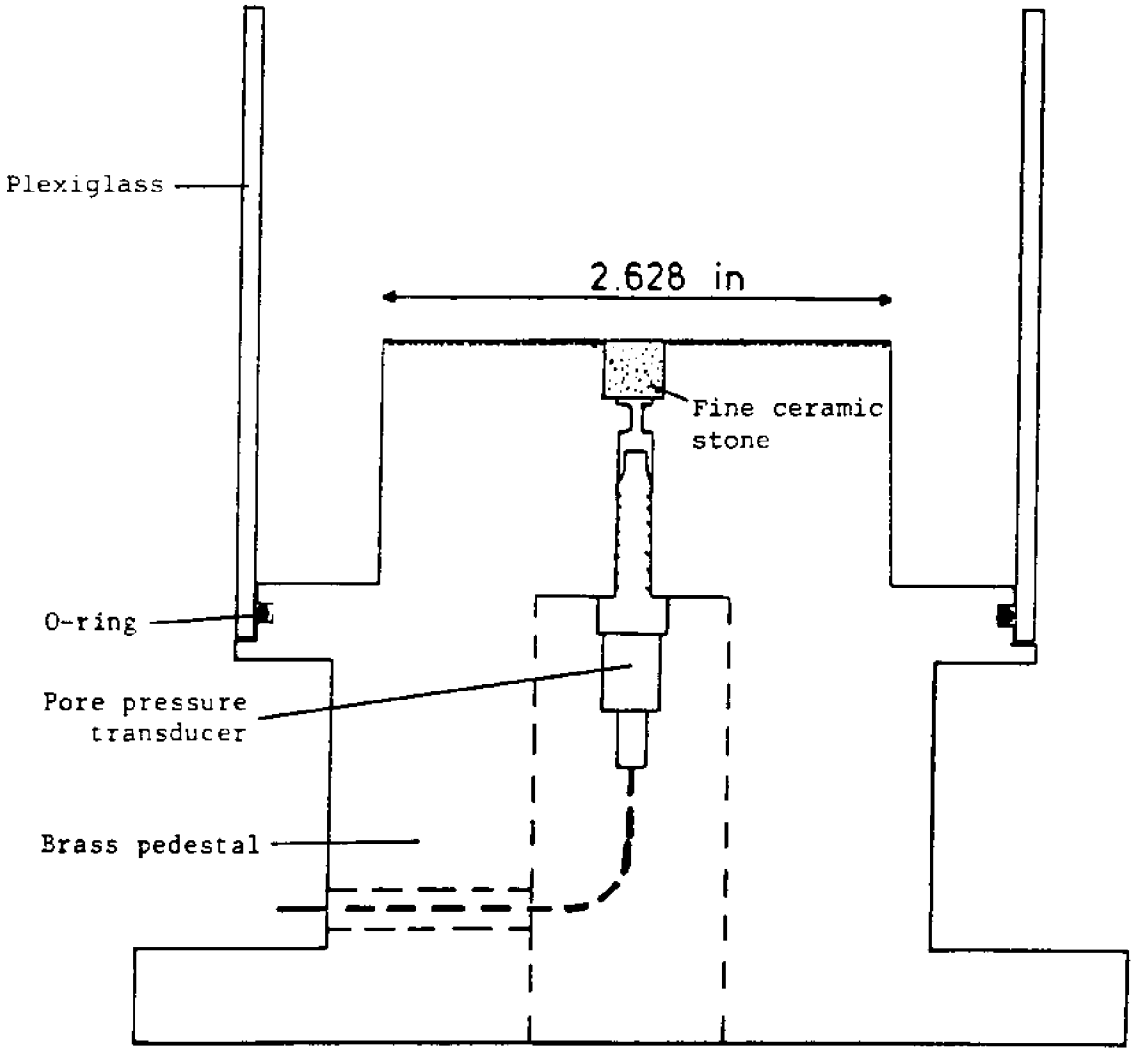

Figure 4.4 DSS Pedestal Showing Details of the Pressure Transducer and Fine Ceramic Stone System for Measuring the Pore Pressure at the Base of the Sample

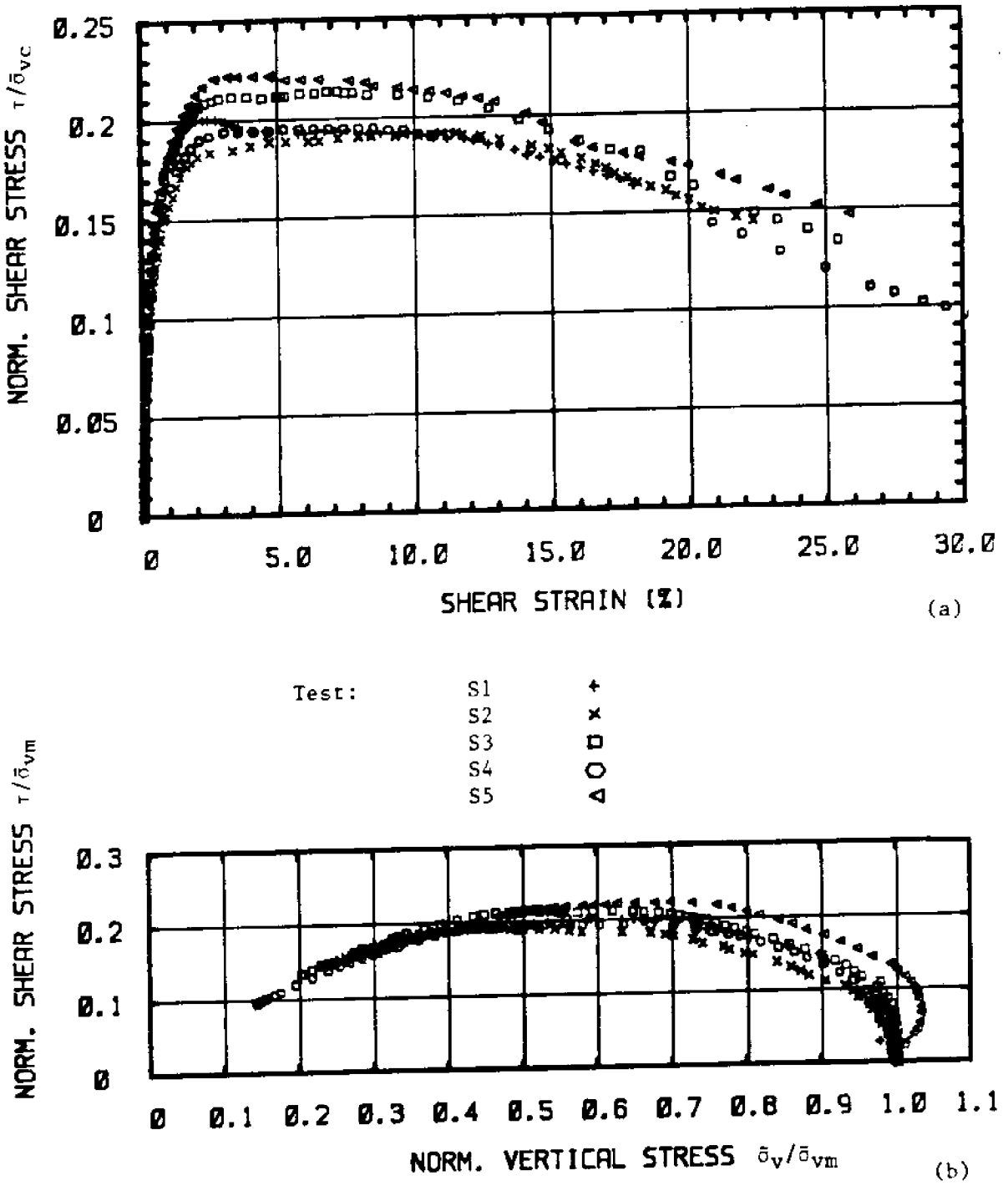

Figure 4.5 Results of Monotonic CK_oUDSS Tests on N.C. BBC
a) Normalized Shear Stress versus Shear Strain
b) Normalized Stress Paths

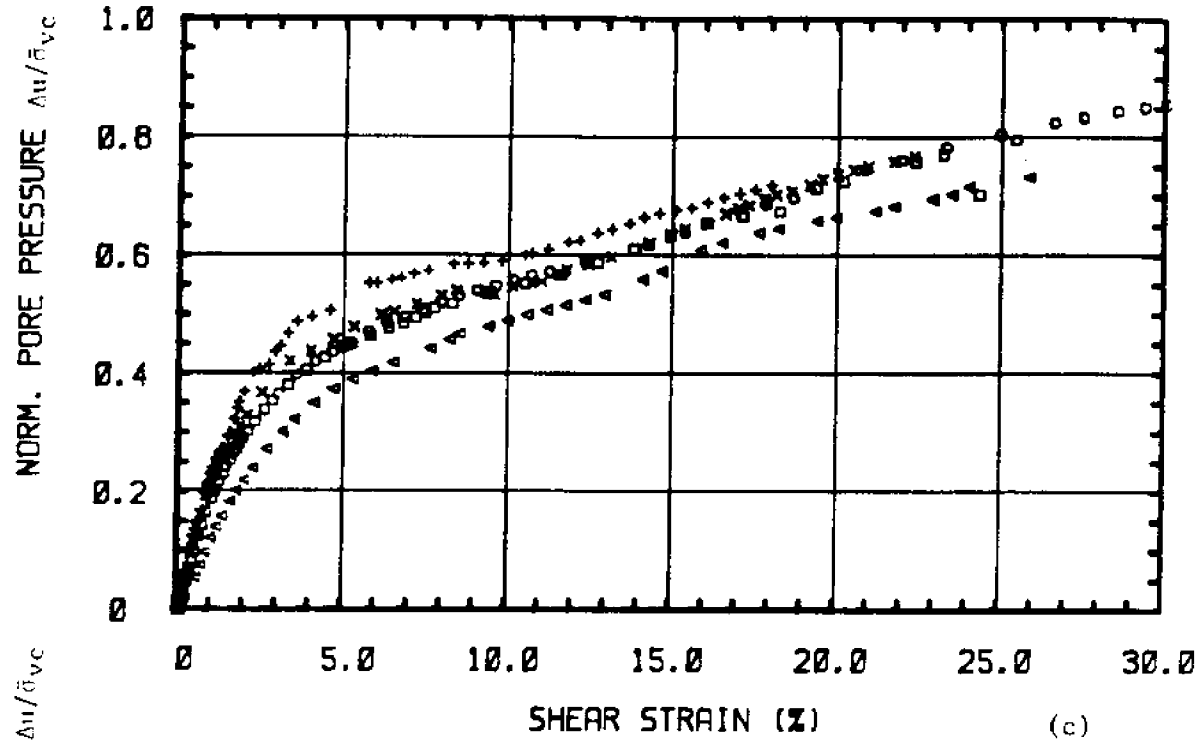

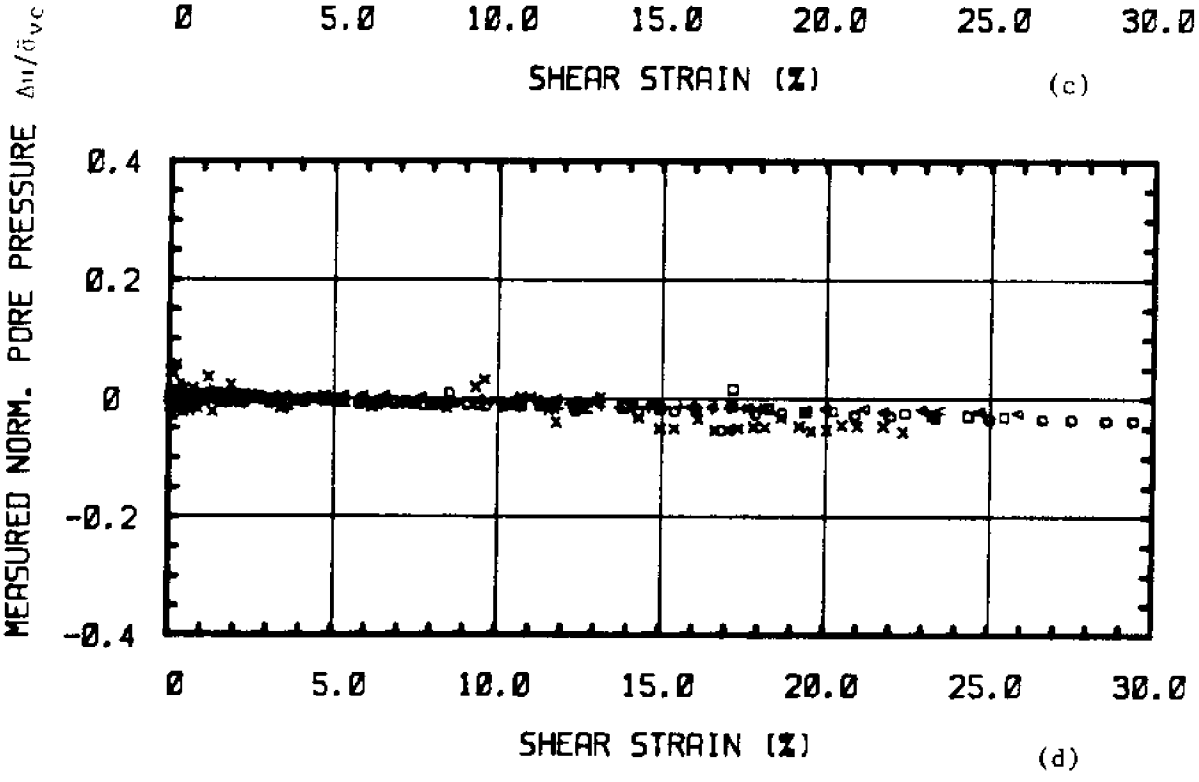

Test: S1 + S2 × S3 □ S4 ○ S5 ◁

Figure 4.5 c) Normalized Excess Pore Pressure (computed as the difference in vertical stress) versus Shear Strain
d) Normalized Pore Pressure Measured at the Base of the Sample versus Shear Strain

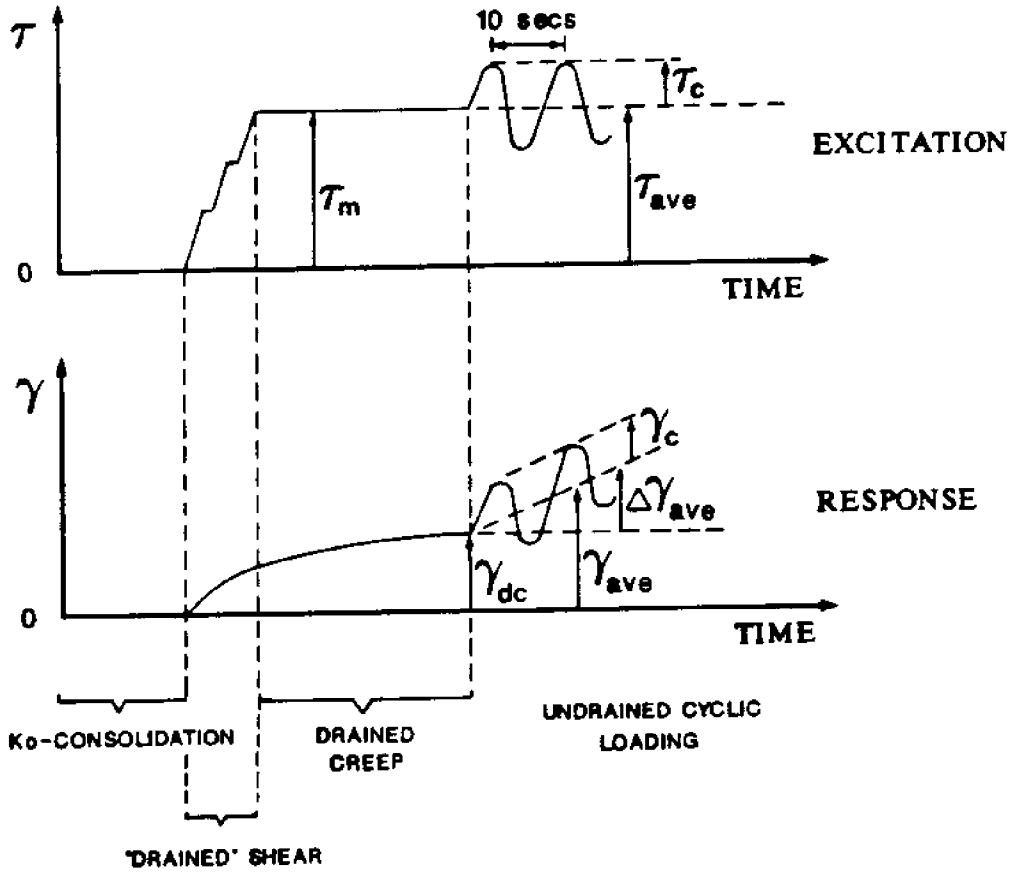

Figure 4.6 Stress-Controlled Undrained Cyclic DSS Test Loading and Notations

CHAPTER 5

UNDRAINED CYCLIC BEHAVIOR OF NORMALLY CONSOLIDATED RESEDIMENTED BOSTON BLUE CLAY

This chapter presents the results of undrained cyclic direct simple shear tests (CK_oUCDSS) on normally consolidated samples of resedimented Boston Blue Clay (RBBC). All the tests reported in this chapter were performed in a stress-controlled fashion, with varying values of average shear stress, τ_{ave}, and cyclic shear stress, τ_c. The value of τ_{ave} was applied after the last consolidation stress increment, and was kept constant throughout cycling, except in the case of three tests with variable τ_c. Thus, the results of the tests correspond to field conditions with the mooring stress τ_m equal to the average shear stress τ_{ave}. All specimens were cycled at a frequency of 0.1 Hz., or a period of 10 seconds, using a sinusoidal cyclic stress with cyclic amplitude τ_c. All samples were cycled until failure except for seven specimens, six of which did not fail after application of 10,000 to 100,000 cycles.

A convenient way of summarizing the tests is shown in Figure 5.1, which plots the cyclic stress ratio $\tau_c/s_u(NC)$ versus the average stress ratio $\tau_{ave}/s_u(NC)$ for each test. The undrained monotonic normally consolidated DSS strength, $s_u(NC)$, is used as a reference strength for normalization, and is given by the following expression:

$$s_u(NC) = 0.205 \cdot \bar{\sigma}_{vc} \qquad (5.1)$$

where $\bar{\sigma}_{vc}$ is the vertical effective consolidation stress. The figure shows lines of equal $\tau_{max}/s_u(NC)$, where $\tau_{max}=\tau_{ave} + \tau_c$, and indicates that tests were conducted with $\tau_{max}/s_u(NC)$ exceeding unity. This is possible because

of the high strain rate during cyclic DSS tests as compared to the rate of shearing in standard monotonic tests performed to obtain s_u(NC). The figure identifies two regions: a failure zone where specimens reach failure, and a non-failure zone where cycling can be performed in an undrained mode for very large number of cycles. The threshold stress boundary which separates these two zones is examined in detail in Section 5.3. It is drawn in the figure however, so that the closeness of each test relative to this threshold boundary can be assessed easily.

5.1 BASIC TEST RESULTS

This section presents the results of the tests which were cycled to failure. Results of tests with zero average stress will be presented first, followed by the results of tests with nonzero average stress.

The results will be presented in terms of:

1. The horizontal shear stress τ (Kg/cm^2), computed as the horizontal force divided by the area of the sample, with no membrane correction;

2. The shear strain γ (%), computed as the horizontal displacement divided by the sample height at the end of consolidation;

3. The excess pore pressure Δu (Kg/cm^2), computed as the change in vertical effective stress, starting from the end of consolidation. $\Delta u = \bar{\sigma}_{vc} - \bar{\sigma}_v$, where $\bar{\sigma}_{vc}$ is the vertical effective stress at the end of consolidation, and $\bar{\sigma}_v$ is the vertical effective stress.

In order to facilitate comparisons between results of various tests, all stresses and excess pore pressures are normalized by the vertical effective consolidation stress $\bar{\sigma}_{vc}$, except in the stress path plots where the shear stress and the vertical effective stress are normalized by the maximum consolidation stress $\bar{\sigma}_{vm}$ (which equals $\bar{\sigma}_{vc}$ for normally

consolidated tests).

5.1.1 Results of tests with $\tau_{ave}/s_u(NC)=0$

Table 4.3 in Chapter 4 summarized all tests with zero average stress. Some of the early tests had experimental problems, such as failure of the data acquisition system or fluctuation of the applied stresses due to poor testing procedure, and their results are not presented herein. Also, some of the tests in Table 4.3 were performed on presheared samples, and their results are not reported either.

Table 5.1 lists six good tests, C-2, C-5, C-6, C-7, C-29, and C-30, with zero average stress ratio, performed on normally consolidated samples until failure, and Figure 5.2 plots the position of the six tests in a cyclic stress ratio versus average stress ratio space. For each test, the table gives the following information: the test number, the vertical consolidation stress $\bar{\sigma}_{vc}$ which ranges between 4 and 8 Kg/cm^2 and equals the maximum past pressures $\bar{\sigma}_{vm}$ (because the samples are normally consolidated), the average stress ratio $\tau_{ave}/s_u(NC)$ which equals zero for all tests, the cyclic stress ratio $\tau_c/s_u(NC)$ which ranges between 0.5 and 0.85, and finally information at ± 3% cyclic shear strain (or 6% peak to peak strain) including the number of cycles required to reach this strain value, the normalized excess pore pressure $\Delta u/\bar{\sigma}_{vc}$, and the average shear strain γ_{ave} (%) at 6% peak to peak strain.

Figures 5.3, 5.4, 5.5, 5.6, 5.7, and 5.8 show results of tests C-2, C-5, C-6, C-7, C-29 and C-30 respectively. Each figure includes four plots: (a) normalized excess pore pressure $\Delta u/\bar{\sigma}_{vc}$ versus the number of cycles N;

(b) shear strain γ (%) versus the number of cycles N;

(c) normalized shear stress $\tau/\bar{\sigma}_{vc}$ versus shear strain γ (%) at selected cycles;

(d) effective stress path, which plots normalized shear stress $\tau/\bar{\sigma}_{vm}$ versus normalized vertical effective stress $\bar{\sigma}_v/\bar{\sigma}_{vm}$.

Results from all tests show the following general trends:

1. The average normalized excess pore pressure versus number of cycles increases rapidly in the first cycles, and then increases steadily to failure. There is a cyclic component of excess pore pressure, which is very small compared to the average excess pore pressure. At failure, the excess pore pressure stabilizes at its maximum value. The cyclic nature of excess pore pressure can be clearly seen in tests C-6 and C-7 because the physical scale of the plot is large enough compared to the total number of cycles, causing separation between cycles.

2. The shear strain versus number of cycles shows a maximum and minimum within each cycle, which are in phase with the applied shear stress. The shear strain plots are symmetrical, with the average strain very close to zero, due to the symmetrical two-way cyclic loading imposed on the samples. The shear strain increases steadily with number of cycles until it reaches a value of ± 3% cyclic shear strain (or 6% peak to peak shear strain), after which it increases very rapidly and reaches values in excess of ± 10%. The sample fails due to increasing cyclic shear strain component γ_c(%). Andersen (1975) and other investigators have defined failure in two way symmetrical cyclic DSS tests as the point at which the cyclic shear strain reaches a value of ± 3%, and Table 5.1 presents pertinent information at this traditional failure state. However, in this research, failure will be defined differently as discussed subsequently in Section 5.2.

3. The normalized shear stress versus shear strain plots, at selected number of cycles, show the same trend for all tests. The cyclic strain is small at low number of cycles, and increases with increasing number of cycles while the maximum cyclic stress remains constant. Hysteresis loops are formed, and increase in size as the cycle number increases. For a given cycle, the secant modulus is defined as the slope of the line connecting the peaks of the hysteresis loop. The secant modulus gradually decreases with number of cycles, and at ± 3% cyclic shear strain the secant modulus is 2.5% to 20% the secant modulus at cycle number one, and continues to decrease with increasing cyclic strain.

4. The effective stress paths consistently exhibit a decrease in the vertical effective stress with increasing number of cycles. This decrease occurs rapidly in early cycles, then becomes slower until the effective stress path reaches a final position at failure.

Tests C-2, C-5, C-6 and C-7 utilized the old height adjustment mechanism which had a slow response time and was not very accurate (see Section 4.2.4). This is why the curves of normalized excess pore pressure versus cycle number are not very smooth, especially for tests C-6 and C-7 which failed in small number of cycles (less than 50) and required very fast height adjustments. Tests C-29 and C-30 were performed using the new Electrocraft height adjustment mechanism which is very responsive and precise, yielding very smooth excess pore pressure curves. However, some experimental difficulties were encountered at the end of test C-30, which led to the failure of the height adjustment mechanism at cycle 128. This resulted in drainage being allowed after cycle 128, which explains the atypical behavior in the excess pore pressure versus number of cycles and in the stress path (see Figure 5.8(a) and (d)).

The horizontal displacement readings taken during tests C-2, C-5, C-6, and C-7, were very noisy due to ground loop problems in the data acquisition system. This resulted in scatter or fluctuations in the measured shear strain, especially in tests C-2 and C-5 (see Figures 5.3(b) and 5.4(b)). This problem was later corrected by using a specially designed filter to eliminate all electrical noise from the horizontal displacement readings.

Tests C-5, C-29, and C-30 are tests with identical values of cyclic stress ratio $\tau_c/s_u(NC)$ which equals 0.56. Tests C-5 was performed on a sample which was normally consolidated to $\overline{\sigma}_{vc}$=6.13 Kg/cm^2, and was cycled to failure in about 160 cycles. Test C-29 was performed on a sample which was normally consolidated to $\overline{\sigma}_{vc}$=4.00 Kg/cm^2, and was cycled for 29 cycles only, without reaching failure. Test C-30 was performed on the same sample as test C-29 after reconsolidating it into the virgin compression range at $\overline{\sigma}_{vc}$=8.01 Kg/cm^2, and the specimen was cycled until failure was reached in about 139 cycles. The results of the three tests are in excellent agreement up to cycle number 128 for test C-30 (because of the experimental problem described earlier). The normalized excess pore pressure versus cycle number curves are almost identical for all three tests, and the shear strain versus cycle number curves are identical for tests C-29 and C-30, and indicate slightly smaller cyclic strains than in test C-5 because of the data acquisition noise problem described earlier. The results of these three tests prove that the cyclic DSS apparatus, which was used in this research, can provide good repeatability of test results. Also, the fact that test C-30 was performed on a sample of RBBC which was previously sheared cyclically, and then reconsolidated into the virgin compression range, proves that the clay exhibits normalized behavior even under cyclic

loading, and reconfirms the applicability of the SHANSEP approach.

5.1.2 Results of Tests with $\tau_{ave}/s_u(NC) \neq 0$

Table 4.4 in Chapter 4 summarized all cyclic undrained DSS tests performed with non-zero average shear stress. Table 5.2 provides the details of twelve tests with OCR=1, listed in Table 4.4, and which have reached failure. These are tests C-8 through C-16 and C-18 through C-20, which were performed on normally consolidated samples of RBBC. For each test, Table 5.2 gives the following information: the test number, the vertical consolidation stress $\bar{\sigma}_{vc}$ which equals the maximum past pressure $\bar{\sigma}_{vm}$ and ranges between 4 and 6 Kg/cm^2, the average stress ratio $\tau_{ave}/s_u(NC)$ which ranges between 0.39 and 0.69, the cyclic stress ratio $\tau_c/s_u(NC)$ which ranges between 0.40 and 0.60, and finally information at 15% average shear strain including the number of cycles, the normalized excess pore pressure $\Delta u/\bar{\sigma}_{vc}$, and the cyclic shear strain $\gamma_c(\%)$. Figure 5.9 plots the position of the twelve tests in a cyclic stress ratio versus average stress ratio space. All the tests lie in the failure zone, and eight of them have maximum shear stress values equal to or exceeding the monotonic undrained DSS strength $s_u(NC)$.

Figures 5.10 through 5.21 present the results of tests C-8 through C-16 and C-18 through C-20 respectively. Each figure includes four plots:

(a) normalized excess pore pressure $\Delta u/\bar{\sigma}_{vc}$ versus the number of cycles N;

(b) shear strain $\gamma(\%)$ versus the number of cycles N;

(c) normalized shear stress $\tau/\bar{\sigma}_{vc}$ versus shear strain $\gamma(\%)$ at selected cycles;

(d) effective stress path, which plots normalized shear stress $\tau/\bar{\sigma}_{vm}$

versus normalized vertical effective stress $\bar{\sigma}_v/\bar{\sigma}_{vm}$.

Results of all the tests show the following general trends:

1. The average normalized excess pore pressure versus number of cycles increases rapidly in early cycles, and then more gradually until failure. The excess pore pressure is cyclic in nature, with a small cyclic component compared to the average one. At failure, the minimum excess pore pressure in each cycle seems to stabilize or increase slowly, while the maximum value continues to increase at a faster rate.

The excess pore pressure curves of tests C-8 and C-9 show a much larger cyclic component than other tests, and a zone where the excess pore pressure was constant with increasing number of cycles (see Figures 5.10(a) and 5.11(a)). This is not believed to represent true clay behavior, but results from testing imperfections. Vertical stresses were applied by a dead weight lever arm system which involved a dead zone during which the vertical stress remained constant despite the fact that the height adjustment mechanism was attempting to change it. Within this dead zone, the vertical stress could not be changed very quickly, resulting in a large cyclic component of excess pore pressure. This problem was corrected in later tests, resulting in smooth excess pore pressure curves with smaller cyclic components.

2. The shear strain versus number of cycles increases gradually with cycle number until failure. For all the tests, the shear strain at the beginning of cycle one is not zero, but is equal to the drained creep shear strain $\gamma_{dc}(\%)$ resulting from the drained application of the average shear stress τ_{ave}. The cyclic component of shear strain, $\gamma_c(\%)$, varies with the cyclic stress ratio, and increases slightly with cycle number. The average shear strain $\gamma_{ave}(\%)$ is much larger than the cyclic shear strain, and

increases gradually until failure occurs, and $\gamma_{ave}(\%)$ exceeds 15% shear strain. Previously, Goulois (1982) has defined failure, in cyclic undrained DSS tests with non-zero average shear stress, as the point at which the average shear strain $\gamma_{ave}(\%)$ reaches 15%, and Table 5.2 has presented pertinent information at this traditional failure point. However, as in the case of cyclic DSS tests with zero τ_{ave}, failure will be defined differently in Section 5.2.

3. The plots of normalized shear stress versus shear strain at selected cycle numbers show a large increase in average strain with a much smaller increase in cyclic strain as the cycle number increases. The secant modulus decreases with increasing cycle number, but less than in the case of tests with zero average stress. At 15% average shear strain, the secant modulus is 1.7% to 14% of the secant modulus at cycle one.

4. The effective stress paths are very consistent, showing similar trends to those of tests with zero average shear stress. There is a constant decrease in effective vertical stress with cyclic shearing. In early cycles, the rate of decrease is higher than in the middle of the test. Also, before failure, the rate of decrease in vertical effective stress increases again, and at failure, the effective stress path reaches a final position. The effective stress path of tests C-8 and C-9 show an unusual behavior near the end of the test due to the lever arm experimental problem which was described earlier.

5.1.3 Effect of $\tau_c/s_{u(NC)}$ and $\tau_{ave}/s_{u(NC)}$

This section compares the number of cycles at failure, N_f, of different tests with different values of the average and cyclic stress ratios. Sections 5.1.1 and 5.1.2 have given the previous definition of

failure which is ± 3% cyclic shear strain for tests with zero τ_{ave}, and 15% average shear strain for tests with non-zero τ_{ave}. However, in this research, the definition of failure is different, and is based on the concept of maximum obliquity, as will be explained in Section 5.2. Hence, all quoted values of N_f in this section as well as the rest of this report, are based on the maximum obliquity definition of failure, and not the traditional one. The advantage of this method is that it adopts the same failure criterion for tests with $\tau_{ave}=0$ as well as $\tau_{ave}\neq 0$.

Figure 5.22 summarizes results of tests C-2, C-5, C-6, and C-7 with $\tau_{ave}=0$ and $\tau_c/s_u(NC)$ varying between 0.5 and 0.85. Figure 5.22(a) plots the average normalized excess pore pressure versus the cycle number, and Figure 5.22(b) plots the envelope of maximum shear strain versus the number of cycles (the maximum strain envelope being a curve connecting the points of maximum shear strain). Clearly, by increasing the cyclic stress ratio $\tau_c/s_u(NC)$, both the excess pore pressures and the cyclic shear strains increase for any cycle number. Furthermore, the number of cycles required to reach failure increases as the cyclic shear stress ratio decreases.

Figure 5.23 plots results of tests C-10, C-11, C-12, C-13, and C-14 which have equal $\tau_c/s_u(NC)=0.4$, and different $\tau_{ave}/s_u(NC)$ values. Figure 5.23(a) shows the average normalized excess pore pressure, and Figure 5.23(b) shows envelopes of minimum and maximum shear strain. Tests C-10 and C-11 are identical tests and show excellent agreement in their results. Tests C-13 and C-14 also involved identical loading but show differences in response which can be attributed to the variability between samples. Despite the small discrepancy between tests C-13 and C-14, the figure shows a definite trend of decreasing number of cycles to failure with increasing $\tau_{ave}/s_u(NC)$ (C-12 fails after 1827 cycles, C-13 and C-14 after an average

value of 666 cycles, and C-10 and C-11 after an average value of 306 cycles). Also, increasing $\tau_{ave}/s_u(NC)$ causes a more rapid buildup of excess pore pressure.

Figure 5.24 shows the effects of increasing $\tau_c/s_u(NC)$ in the case of tests with non-zero average shear stress. The figure plots results of tests C-13, C-14, C-15, and C-17. Test C-17 does not fail after 10,000 cycles whereas tests C-13 and C-14 fail after 666 cycles, and test C-15 fails only after 80 cycles (complete results of test C-17 are presented in Section 5.3). It is also evident from this figure that increasing $\tau_c/s_u(NC)$ decreases the number of cycles to failure and causes a more rapid increase in excess pore pressure.

Finally, Figure 5.25 plots the position of tests C-10, C-11, C-12, and C-16 on a $\tau_c/s_u(NC)$ versus $\tau_{ave}/s_u(NC)$ space, and compares their number of cycles to failure, N_f. Tests C-10 and C-11 are identical, and comparison of their N_f with that of test C-12 indicates that a 20% increase in the average shear stress ratio leads to a one order of magnitude decrease in N_f. However, comparison of N_f in tests C-12 and C-16 indicates that a 20% increase in cyclic shear stress ratio leads to two orders of magnitude decrease in N_f. This means that the number of cycles to failure is more sensitive to changes in $\tau_c/s_u(NC)$ rather than changes in $\tau_{ave}/s_u(NC)$.

5.2 DEFINITION OF FAILURE

5.2.1 Effective Stress Paths to Failure

The effective stress paths from tests C-5, C-7, and C-30 with $\tau_{ave}=0$, and tests C-15, C-16, C-18, C-19, and C-20 with $\tau_{ave}\neq 0$ are shown in Figures 5.26 through 5.33 respectively. In all these tests, the effective

stress path moves towards the origin rather quickly in the first couple of cycles, corresponding to the rapid excess pore pressure increase at small number of cycles. Throughout the tests, the stress path is almost vertical with small increases in excess pore pressure with every cycle. In the case of tests with $\tau_{ave}=0$, when failure is reached, the effective stress path ceases its migration towards the origin as can be seen in Figures 5.26 and 5.27. In the case of tests with $\tau_{ave}\neq 0$, the maximum peak of the effective stress path seems to reach a stationary point at failure, while the minimum peak still moves towards the origin, as shown in Figures 5.29 through 5.33. For all the tests, a straight line connecting the stationary peak of the effective stress path at failure to the origin define a failure envelope. This envelope has been drawn in each of the figures, and its inclination varies between 28° and 34°. At failure, the effective stress path either touches the failure envelope, or moves along it, but never crosses it. Beyond the failure point, the effective stress path may cross over the failure line due to the very high strain rate of shearing (strain rates in excess of ± 3% in 5 seconds, or half the period of cycling), and due to nonuniformities and inaccuracies in the DSS sample at large shear strains (greater than 15%). This is not problematic since the post-failure behavior is not of interest.

Figure 5.34 plots the stationary location of the effective stress path when failure is reached for all the tests listed in Tables 5.1 and 5.2 except tests C-2, C-6, C-8, C-9, and C-30 which either used the old MIT height adjustment mechanism, or experienced experimental problems. There is some scatter, but an average failure envelope with a 30.0° ± 1.2° inclination can be drawn through all the points. This angle is also equal to the maximum obliquity measured in monotonic undrained DSS tests, shown

in Figure 5.35.

Therefore, it can be concluded that, for any value of $\tau_{ave}/s_u(NC)$, failure in stress-controlled undrained cyclic DSS tests occurs when effective stresses reach the Maximum Obliquity (MO) line. For resedimented Boston Blue Clay, this line has an inclination of $\bar{\phi}_{MO}=30.0°$ ± 1.2° on a $\tau/\bar{\sigma}_{vm}$ versus $\bar{\sigma}_v/\bar{\sigma}_{vm}$ plot. This result provides a consistent definition of failure, independently of the value of the average shear stress ratio, hence allowing direct comparison of results of tests conducted with or without $\tau_{ave}\neq 0$.

The definition of failure on the basis of maximum obliquity is different from the definition used by previous researchers. Andersen (1975) defined failure in the case of tests with $\tau_{ave}=0$ as occuring when γ_c reaches ± 3%, and Goulois (1982) defined failure in tests with $\tau_{ave}\neq 0$ as occuring when γ_{ave} reaches 15%. However, for RBBC, the difference between the number of cycles to failure, N_f, based on the maximum obliquity definition and that based on $\gamma_c=\pm$ 3% or $\gamma_{ave}=15\%$ is small:

Tests with $\tau_{ave}=0$: $N_f(MO) - N_f(\gamma_c=3\%) = 4$ cycles

Tests with $\tau_{ave}<0$: $N_f(\gamma_{ave}=15\%) - N_f(MO) = 2$ to 3 cycles

Therefore, the two definitions of failure yield values of N_f which are very close (within a couple of cycles).

5.2.2 Pore Pressure at Failure

Figure 5.36 shows the maximum obliquity (MO) line on a plot of $\tau/\bar{\sigma}_{vm}$ versus $\bar{\sigma}_v/\bar{\sigma}_{vm}$. All normally consolidated tests start at $\bar{\sigma}_v/\bar{\sigma}_{vm}=1$. After N cycles at given values of τ_{ave} and τ_c, the stress path migrates towards the origin by an amount $\Delta u/\bar{\sigma}_{vm}$ which is the average normalized pore pressure generated during cycle N. As cycling continues, and failure is

approached, the stress path reaches the maximum obliquity line, and the value of pore pressure at failure is Δu_f. From the geometry in Figure 5.36, it is possible to write the following expression for Δu_f:

$$\frac{\Delta u_f}{\bar{\sigma}_{vm}} = 1 - \frac{\tau_{ave} + \tau_c}{\bar{\sigma}_{vm} \tan\bar{\phi}_{MO}}$$

which is equivalent to:

$$\frac{\Delta u_f}{\bar{\sigma}_{vc}} = 1 - \frac{\tau_{ave} + \tau_c}{\bar{\sigma}_{vc} \tan\bar{\phi}_{MO}} \qquad (5.2)$$

for normally consolidated clays.

For RBBC with $s_u/\bar{\sigma}_{vm}(NC)=0.205$, and $\bar{\phi}_{MO} = 30°$, Equation 5.2 can be rewritten as:

$$\Delta u_f = \left[1 - \frac{0.205(\tau_{ave}/s_u(NC) + \tau_c/s_u(NC))}{\tan 30°} \right] \bar{\sigma}_{vc} \qquad (5.3)$$

Therefore, knowing the stress ratios $\tau_{ave}/s_u(NC)$ and $\tau_c/s_u(NC)$, as well as the vertical consolidation stress $\bar{\sigma}_{vc}$, Equation 5.3 enables estimates of the excess pore pressure at failure, Δu_f, to be obtained for normally-consolidated samples.

5.3 THRESHOLD SHEAR STRESS LEVEL

In the context of the present research program, the threshold shear stress level is defined as the combination of $\tau_{ave}/s_u(NC)$ and $\tau c/s_u(NC)$ below which failure does not occur in stress-controlled undrained direct simple shear loading. The existence of such a threshold level is crucial for tension leg platform stability since its absence means that with continued cyclic loading, failure progresses downwards along the pile, thus resulting in increased deformations and potential pullout of the pile.

In the course of investigating the effects of the average and cyclic

shear stress ratios on cyclic clay behavior, failure, as defined by reaching the maximum obliquity line in a stress path plot, did not occur for certain combinations of $\tau_{ave}/s_u(NC)$ and $\tau_c/s_u(NC)$ even after subjecting the soil to a very large number of undrained cycles. Test C-17, with $\tau_{ave}/s_u(NC) = 0.59$ and $\tau_c/s_u(NC) = 0.30$, was the first no-failure test, during which strains and pore pressures were stabilizing with increasing number of cycles, up to N=10,000 cycles.

A total of six stress-controlled cyclic DSS tests with small cyclic shear stresses were performed in order to better define the threshold region in the $\tau_{ave}/s_u(NC)$ versus $\tau_c/s_u(NC)$ space. Two of the tests were performed with $\tau_{ave}=0$, and the other four with $\tau_{ave}\neq 0$, and their details can be found in Table 5.3. For each test, the table lists the test number, the vertical consolidation stress $\bar{\sigma}_{vc}$ in Kg/cm^2, the average shear stress ratio $\tau_{ave}/s_u(NC)$, the cyclic shear stress ratio $\tau_c/s_u(NC)$, and finally information at the maximum cycle number reached, including the normalized excess pore pressure $\Delta u/\bar{\sigma}_{vc}$, and the cyclic shear stress $\gamma_c(\%)$ for tests with zero τ_{ave}, or the average shear strain $\gamma_{ave}(\%)$ for tests with non-zero τ_{ave}.

Figures 5.37 through 5.42 plot normalized excess pore pressure versus cycle number, shear strain versus cycle number, and stress path at selected number of cycles for tests C-22, C-23, C-17, C-39, and C-40 respectively. Because the tests involve a large number of cycles, the plots do not show every cycle, but every 100th cycle for tests C-22, C-23, C-17, C-25, and C-40, and every 1000th for test C-39. There are missing data in Figures 5.37, 5.39, 5.41, and 5.42 due to occasional failures of the data acquisition computer system during testing. Very little change occurred in these periods, hence the computer failures are not critical.

Tests C-22 and C-23 were performed on the same sample and in reality correspond to one test with zero average shear stress, and two different cyclic stress ratios. The sample was first subjected to 10,000 cycles at $\tau_c/s_u(NC)=0.25$ followed by 10,000 cycles at $\tau_c/s_u(NC)=0.35$, which explains why the values of excess pore pressure and shear strain, at cycle one in test C-23, are not equal to zero. The tests involved small cyclic shear strains, with values very close to the minimum measurable strain of the data acquisition system used (1 Least Significant Bit corresponds to 0.1% shear strain). This explains the measured scatter in the shear strain data, and the fact that no increase in shear strain with cycle number can be accurately detected in Figures 5.37(b) and 5.38(b) (a small real increase is masked by the scatter caused by measurement inaccuracies). All six tests did not fail after large numbers of cycles (10,000 cycles in the case of tests C-17, C-22, and C-23, 15,000 cycles in the case of test C-25, 100,000 cycles in the case of test C-39, and 32,000 cycles in the case of test C-40), but rather developed cyclic strains that stabilized. Throughout cycling, the excess pore pressure was increasing at a rather slow rate with increasing number of cycles. The stress path plots indicate that, when cycling was stopped, the effective stress path was far from reaching the maximum obliquity line, hence failure. Comparison of the excess pore pressure at a given cycle number, between test C-39 and tests C-22, C-23, C-17, C-25, and test C-40 shows a higher excess pore pressure level in test C-39. This indicates that the loading conditions in test C-39 are the most severe. Figure 5.43 plots the excess pore pressure versus the logarithm of cycle number for test C-39, and shows a linear increase in excess pore pressure with log N between cycle 1,000 and 100,000. The estimated value of the excess pore pressure at failure according to

Equation 5.3 (in Section 5.2.2) is also shown in Figure 5.43. Extrapolation of the straight line in Figure 5.43 beyond cycle number 100,000 indicates no failure in one million cycles, and potential failure in about 8 million cycles of undrained shearing. While the exact cycle number at failure is not known, extrapolation of the data for one logarithmic cycle of N can be done with confidence, leading to the conclusion that Test C-39 does not fail in one million cycles. This, coupled with the fact that test C-39 has the most severe loading conditions among the six non-failing tests, leads to the conclusion that all six tests listed in Table 5.3 do not fail in one million cycles.

Figure 5.44 shows the six tests along with a curve showing a proposed no-failure boundary. Combinations of $\tau_{ave}/s_u(NC)$ and $\tau_c/s_u(NC)$ below this boundary correspond to no failure conditions, while combinations above the threshold lead to failure.

5.4 EQUAL STRAIN AND FAILURE CONTOURS FOR TESTS WITH $\tau_{ave}=0$

Results from cyclic undrained stress-controlled DSS tests with $\tau_{ave}=0$ are summarized in Figure 5.45 which plots the cyclic stress ratio $\tau_c/s_u(NC)$ versus the logarithm of cycle number. The plot is traditionally referred to as an S-N diagram, and shows four iso-γ_c curves, or curves of equal cyclic shear strain, corresponding to progressively higher values of γ_c. A curve corresponding to failure, which is defined as the stress state corresponding to maximum obliquity is also shown. These curves were obtained by using the results of all the tests run on N.C. RBBC samples with $\tau_{ave}=0$, and by selecting from each test the appropriate number of cycles corresponding to the desired γ_c. For example, during test C-5 (with

τ_c=0.56 s_u(NC)), the sample reached a cyclic shear strain of 0.3% after 20 cycles, 0.5% after 70 cycles, 1% after 125 cycles, and finally a strain of 3% after 160 cycles. These data are plotted in the figure as four points at τ_c/s_u(NC)=0.56 and N=20, 70, 125, and 160 respectively. The iso-γ_c curves can be used to determine the cyclic shear strain resulting from the application of N cycles at a given constant cyclic shear stress level τ_c/s_u(NC). Also, the maximum obliquity (MO) curve can be used to obtain the number of cycles to failure, N_f, for any given cyclic stress ratio τ_c/s_u(NC).

5.5 EFFECT OF τ_{ave} ON CONTOURS OF NUMBER OF CYCLES AT FAILURE

Figure 5.46 plots contours of equal numbers of cycles to failure, or iso-N_f curves, for various combinations of average and cyclic shear stress ratios. These curves were obtained from the knowledge of N_f, the number of cycles required to reach maximum obliquity, as well as τ_{ave}/s_u(NC) and τ_c/s_u(NC) for all the undrained cyclic DSS tests performed with $\tau_{ave}\neq 0$. The curve of $N_f>10^6$ is the threshold shear stress boundary. All the other contours of various N_f values (N_f=10, 50, 100, 1000) are constructed by connecting points of equal N_f values in the τ_c/s_u(NC) versus τ_{ave}/s_u(NC) space.

It is important to observe that the iso-N_f contours are smooth and continuous in the region close to τ_{ave}=0. This indicates that the definition of failure, based on effective stresses reaching maximum obliquity leads to consistent results for tests performed with τ_{ave}=0 and those with $\tau_{ave}\neq 0$, despite the very different strains at failure in the two cases. In all tests conducted in this study, the effective stress paths

reached the maximum obliquity line of 30.0° ± 1.2° when γ_c=± 3% in the case of τ_{ave}=0, and γ_{ave}=12% in the case of $\tau_{ave}\neq 0$. The continuity and consistency of the iso-N_f curves in Figure 4.46 provide a check on the proposed unified definition of failure in terms of effective stresses.

Another important observation is the fact that all iso-N_f curves are parallel to each other and to the threshold shear stress boundary. This has a very important practical consequence, namely that knowledge of N_f from tests with τ_{ave}=0 as well as the threshold shear stress boundary, is sufficient to draw iso-N_f contours, and hence predict N_f, for cases of $\tau_{ave}\neq 0$. Any desired N_f contour can be obtained by locating the value of $\tau_c/s_u(NC)$ which would lead to failure in N_f cycles with zero average shear stress, and then drawing a curve parallel to the threshold boundary.

5.6 NORMALIZED RESULTS

5.6.1 Normalized Excess Pore Pressure Plots

Having a predictable and consistent definition of the pore pressure at failure, normalized excess pore pressure plots versus normalized number of cycles can be prepared and compared for various testing conditions. The test results were thus normalized as follows:

$$\overline{\Delta u} = \Delta u/\Delta u_f \qquad (5.4)$$

$$\overline{N} = N/N_f \qquad (5.5)$$

where Δu : excess pore pressure during undrained cyclic shearing

Δu_f: excess pore pressure at failure.

N : number of cycles

N_f: number of cycles at failure

Figure 5.47 presents plots of $\overline{\Delta u}$ vs. $\overline{N}$ from five tests with $\tau_{ave}=0$ (C-2, C-5, C-6, C-7, C-30), with $\tau_c/s_u(NC)$ values ranging from 0.5 to 0.85. Figure 5.48 shows plots of $\overline{\Delta u}$ vs. $\overline{N}$ from 12 tests with $\tau_{ave}\neq 0$ (C-8, C-9, C-10, C-11, C-12, C-13, C-14, C-15, C-16, C-18, C-19, C-20), with $\tau_{ave}/s_u(NC)$ ranging from 0.39 to 0.69, and $\tau_c/s_u(NC)$ ranging from 0.4 to 0.6. The number of cycles to failure in the seventeen tests ranges from 11 to 1827. In both figures, the normalized curves exhibit similar trends and fall within consistent bands.

Comparing the two figures, it appears that results of tests with $\tau_{ave}=0$ plot within the scatter of those with $\tau_{ave}\neq 0$, except for $\overline{N}>0.5$ where they are slightly higher. This discrepancy is believed to be due to experimental imperfections in the early tests with $\tau_{ave}=0$, performed using the old MIT height adjustment mechanism instead of the newer, more accurate Electrocraft system.

In summary, normalized plots of $\overline{\Delta u}$ vs. $\overline{N}$ from stress-controlled undrained cyclic DSS tests on resedimented Boston Blue Clay fall within a narrow band, with an average that can be fitted by the expression:

$$\overline{\Delta u} = 0.94\ \overline{N}^{(0.623)} \qquad (5.6)$$

5.6.2 Normalized Strain Plots

Figure 5.49 presents plots of $\gamma_c(\%)$ vs. $\overline{N}$ from the five tests with $\tau_{ave}=0$, and Figure 5.50 presents plots of $\Delta\gamma_{ave}(\%) = \gamma_{ave}(\%) - \gamma_{dc}(\%)$ vs. $\overline{N}$ from the twelve tests with $\tau_{ave}\neq 0$. In each figure, the normalized curves plot within a well defined band despite the large variation in τ_{ave}, τ_c, and N_f for each test. The mean curve in each band can be fitted by the equations:

$$\tau_{ave}=0: \quad \gamma_c(\%) = 0.127\, e^{3.751\,\bar{N}} \tag{5.7}$$

$$\tau_{ave}\neq 0: \quad \Delta\gamma_{ave}(\%) = 0.326\, e^{3.466\,\bar{N}} \tag{5.8}$$

Equations 5.7 and 5.8 can be combined with Equation 5.6 to estimate $\Delta\bar{u}$ from γ_c or $\Delta\gamma_{ave}$, respectively:

$$\tau_{ave}=0: \quad \Delta\bar{u} = 0.413\, [\ln (\frac{\gamma_c}{0.127})]^{0.623} \tag{5.9}$$

$$\tau_{ave}\neq 0: \quad \Delta\bar{u} = 0.433\, [\ln (\frac{\Delta\gamma_{ave}}{0.326})]^{0.623} \tag{5.10}$$

5.6.3 Prediction of Cyclic Behavior of Normally Consolidated Resedimented Boston Blue Clay

This section presents a method for predicting the behavior of a normally consolidated sample of resedimented Boston Blue Clay when subjected to undrained stress-controlled cyclic direct simple shearing.

If the average shear stress τ_{ave}, the cyclic shear stress τ_c, and the vertical consolidation stress $\bar{\sigma}_{vc}$ are known, then the excess pore pressure Δu and shear strain (γ_c in the case of $\tau_{ave}=0$ and $\Delta\gamma_{ave}$ in the case of $\tau_{ave}\neq 0$) can be estimated as follows:

1. Determine Δu_f from Equation 5.3, and N_f from Figure 5.46;

2. At any shearing cycle N, calculate the normalized cycle number $\bar{N}=N/N_f$, hence determine the normalized excess pore pressure, $\Delta\bar{u}$, from either Figure 5.47 or Figure 5.48, and the accumulated shear strain (γ_c or $\Delta\gamma_{ave}$) from either Figure 5.49 or Figure 5.50;

3. Calculate $\Delta u = \Delta\bar{u} \cdot \Delta u_f$.

This method applies for normally consolidated RBBC samples with no previous cyclic history. It is restricted to combinations of $\tau_{ave}/s_u(NC)$

and $\tau_c/s_u(NC)$ above the threshold shear stress boundary shown in Figure 5.44, and for undrained cycling with a period of 10 seconds.

5.7 BEHAVIOR OF NORMALLY CONSOLIDATED CLAY UNDER VARIABLE CYCLIC LOADING

In order to investigate the effect of storm loading which is variable in nature, three cyclic undrained DSS tests were performed with variable cyclic shear stress ratios. The three tests, which are listed in Table 5.4, were performed on normally consolidated samples of resedimented Boston Blue Clay, with zero average shear stress τ_{ave}. For each test, the table gives the test number, the vertical consolidation stress $\bar{\sigma}_{vc}$, the average shear stress ratio $\tau_{ave}/s_u(NC)$ which equals zero for all tests, the cyclic shear stress ratio $\tau_c/s_u(NC)$ which varies between 0.5 and 0.7, and information at failure including the number of cycles, the excess pore pressure, and the average shear strain $\gamma_{ave}(\%)$.

5.7.1 Results of test C-28

Test C-28 consists of two phases. During the first, cycling was performed at $\tau_c/s_u(NC)=0.57$ for the first 29 cycles, then in phase two, the cyclic stress ratio was increased to $\tau_c/s_u(NC)=0.70$ and maintained at this level until sample failure. Results of test C-28 are presented in Figure 5.51, and show the following trends:

1. During phase one, the excess pore pressure versus cycle number shows a trend similar to normally consolidated samples, namely a sharp increase followed by a more gradual one. There is a discontinuity in excess pore pressure at the interface of the two phases (end of cycle 29) resulting from the increase in cyclic shear stress ratio. During phase

two, the excess pore pressure curve is concave upward (as opposed to concave downward in phase one), due to an increasingly faster rate of excess pore pressure generation. At failure, the excess pore pressure reaches a final value of $\Delta u/\overline{\sigma}_{vc}$=0.72.

2. The shear strain increases slowly with cycle number during phase one, then quickly in phase two, due to the higher cyclic stress ratio. There is an instantaneous increase in strain due to the jump in τ_c/s_u(NC) at cycle number 30. The sample fails due to accumulation of cyclic shear strain γ_c(%), with almost zero average shear strain.

3. The normalized shear stress $\tau/\overline{\sigma}_{vc}$ versus cycle number curves shows larger hysteresis loops resulting in smaller secant modulus with increasing number of cycles.

4. The effective stress path clearly shows the variable nature of the cyclic loading. The stress path migrates towards the origin with increasing cycle number until failure occurs at N_f=53 by reaching the maximum obliquity line (close to 30°). This is the same failure criterion as tests with constant cyclic stress ratio. At failure, the cyclic shear strain exceeds 3% as shown in Figure 5.51(b).

5.7.2 Results of test C-37

Test C-37 consists of two phases, the first is from cycle number 1 to 62 with a cyclic shear stress ratio τ_c/s_u(NC)=0.50, and the second from cycle number 62 to failure with τ_c/s_u(NC)=0.64. The results are plotted in Figure 5.52, and show identical trends to results of test C-28.

1. The excess pore pressure curve is discontinuous at cycle 62, which corresponds to the increase in cyclic stress ratio. The pore pressure increases slowly, with a concave downward curve in phase one, then

very rapidly, with a concave upward curve in the second phase.

2. The cyclic shear strain increases with cycle number, and at failure, $\gamma_c(\%)$ exceeds 3%. There is a jump in cyclic shear strain at cycle 62 because of the increase in the cyclic stress ratio.

3. The secant modulus decreases with increasing cycle number as shown in Figure 5.52(c).

4. The effective stress path migrates towards the origin as cycling progresses. Failure occurs at maximum obliquity, after 112 cycles.

5.7.3 Results of test C-38

Test C-38 consists of three phases with different values of cyclic shear stress ratio. The test sample was first subjected to 265 cycles at $\tau_c/s_u(NC)=0.50$, followed by 10 cycles at $\tau_c/s_u(NC)=0.70$, after which the cyclic stress ratio was decreased to $\tau_c/s_u(NC)=0.56$ until failure. The results are shown in Figure 5.53, and indicate similar trends to those of tests C-28 and C-37.

1. In the first phase up to cycle 265, the excess pore pressure increases gradually, in a manner similar to tests with constant cyclic stress ratio, with a concave downward curve. Then, during the 10 cycles with $\tau_c/s_u(NC)=0.70$, the pore pressure increases very rapidly, with a concave upward curve. In the third phase, after decreasing the cyclic shear stress ratio to $\tau_c/s_u(NC)=0.56$, the excess pore pressure continues to increase until failure, but at a lower rate, resulting in a concave downward curve.

2. The cyclic shear strain increases slowly in the first phase up to cycle 265. There is a sudden increase in cyclic shear strain at cycle 266

due to the increase in $\tau_c/s_u(NC)$, and there is a sudden decrease in cyclic shear strain at cycle 276 due to the decrease in $\tau_c/s_u(NC)$. At failure, the cyclic shear strain is greater than 3%, and the average shear strain is small.

3. The normalized shear stress versus shear strain curves are plotted in Figure 5.53(c), and show hysteresis loops. The secant modulus constantly decreases with cycle number as the size of the loops increases.

4. The effective stress path shows three distinct levels of cyclic shear stress ratio. The vertical effective stress decreases, and hence the stress path migrates towards the origin, with increasing number of cycles. At failure, the stress path reaches the maximum obliquity line (30°), after a total of 303 cycles.

5.7.4 Summary of Tests with Variable Cyclic Loading

Results of three tests with zero τ_{ave} and variable $\tau_c/s_u(NC)$ indicate similar trends to results of tests with constant cyclic stress ratios. Failure occurs when maximum obliquity is reached, at which point the cyclic shear strain exceeds 3%, and the average shear strain is very small. The normalized excess pore pressure at failure, $\Delta u_f/\bar{\sigma}_{vc}$, can be estimated using either equation 5.2 or 5.3, with τ_c equal to the last value of cyclic shear stress applied prior to failure.

The rate of increase in excess pore pressure varies with the cyclic shear stress ratio. This gives the excess pore pressure curve a concavity which is upward following an increase in cyclic shear stress ratio, and a concavity which is downward following a decrease in $\tau_c/s_u(NC)$.

The cyclic shear strain is proportional to the cyclic stress level,

and changes suddenly when the cyclic stress ratio is changed. Any increase (or decrease) in $\tau_c/s_u(NC)$ results in an instantaneous increase (or decrease) in $\gamma_c(\%)$.

A method of predicting the results of tests with variable cyclic loading, using results of tests with constant cyclic stress ratio, is presented in Chapter 7. The method is then evaluated using the results of tests C-28, C-37 and C-38.

TABLE 5.1

SUMMARY OF UNDRAINED CYCLIC DSS TESTS
WITH τ_{ave}=0 ON NORMALLY CONSOLIDATED BBC

				γ_c = 3(%)		
TEST NO.	$\bar{\sigma}_{vc}$ Kg/cm^2	$\frac{\tau_{ave}}{s_u(NC)}$	$\frac{\tau_c}{s_u(NC)}$	N	$\frac{\Delta u}{\bar{\sigma}_{vc}}$	γ_{ave} (%)
C-2	4.0	0	0.50	525	0.72	0.70
C-5	6.13	0	0.56	160	0.78	0.35
C-6	4.08	0	0.70	43	0.67	0
C-7	4.08	0	0.85	11	0.59	0.05
C-29	4.00	0	0.56	No failure in 29 cycles		
C-30	8.01	0	0.56	139	0.82	1.1

TABLE 5.2

SUMMARY OF UNDRAINED CYCLIC DSS TESTS
WITH $\tau_{ave} \neq 0$ ON NORMALLY CONSOLIDATED BBC

				γ_{ave} = 15(%)		
TEST NO.	$\bar{\sigma}_{vc}$ Kg/cm^2	$\frac{\tau_{ave}}{s_u(NC)}$	$\frac{\tau_c}{s_u(NC)}$	N	$\frac{\Delta u}{\bar{\sigma}_{vc}}$	γ_c (%)
C-8	4.09	0.45	0.46	427	0.76	1.2
C-9	4.08	0.45	0.46	275	0.77	1.7
C-10	4.08	0.69	0.40	300	0.63	0.56
C-11	4.09	0.69	0.40	312	0.65	0.61
C-12	6.13	0.49	0.40	1827	0.73	0.73
C-13	6.12	0.59	0.40	801	0.67	0.59
C-14	6.13	0.59	0.41	532	0.68	0.67
C-15	6.14	0.59	0.50	80	0.64	0.81
C-16	6.13	0.49	0.60	47	0.69	1.64
C-18	6.13	0.39	0.60	66	0.73	2.91
C-19	6.00	0.50	0.51	73	0.69	1.73
C-20	6.00	0.40	0.51	156	0.74	1.82

TABLE 5.3

SUMMARY OF UNDRAINED CYCLIC DSS TESTS
NOT REACHING FAILURE ON NORMALLY CONSOLIDATED BBC

TESTS WITH $\tau_{ave}=0$

TEST NO.	$\bar{\sigma}_{vc}$ Kg/cm^2	$\frac{\tau_{ave}}{s_u(NC)}$	$\frac{\tau_c}{s_u(NC)}$	AT END OF CYCLING		
				N	$\frac{\Delta u}{\bar{\sigma}_{vc}}$	γ_c (%)
C-22	6.01	0	0.25	10000	0.15	0.05
C-23	6.01	0	0.35	10000	0.27	0.15

TESTS WITH $\tau_{ave}\neq 0$

TEST NO.	$\bar{\sigma}_{vc}$ Kg/cm^2	$\frac{\tau_{ave}}{s_u(NC)}$	$\frac{\tau_c}{s_u(NC)}$	AT END OF CYCLING			
				N	$\frac{\Delta u}{\bar{\sigma}_{vc}}$	γ_{ave} (%)	γ_c (%)
C-17	6.12	0.59	0.30	10000	0.24	2.93	0.1
C-25	6.01	0.35	0.35	15000	0.37	1.80	0.1
C-39	6.02	0.15	0.38	100000	0.54	0.90	0.3
C-40	6.01	0.80	0.20	30000	0.20	4.40	0.1

TABLE 5.4

SUMMARY OF UNDRAINED CYCLIC DSS TESTS
WITH τ_{ave}=0 AND VARIABLE τ_c
ON NORMALLY CONSOLIDATED BBC

					Failure: Max. Obliquity		
TEST NO.	$\bar{\sigma}_{vc}$ Kg/cm^2	$\frac{\tau_{ave}}{s_u(NC)}$	$\frac{\tau_c}{s_u(NC)}$	Range of N	N_f	$\frac{\Delta u}{\bar{\sigma}_{vc}}$	γ_{ave} (%)
C-28	6.01	0	0.56 0.71	1 to 29 30 to failure	53	0.72	-0.56
C-37	6.00	0	0.50 0.64	1 to 62 62 to failure	112	0.75	-2.39
C-38	6.01	0	0.50 0.70 0.56	1 to 265 265 to 275 275 to failure	303	0.76	-2.54

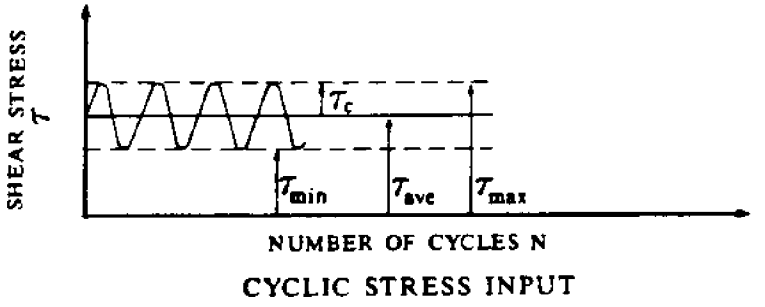

CYCLIC STRESS INPUT

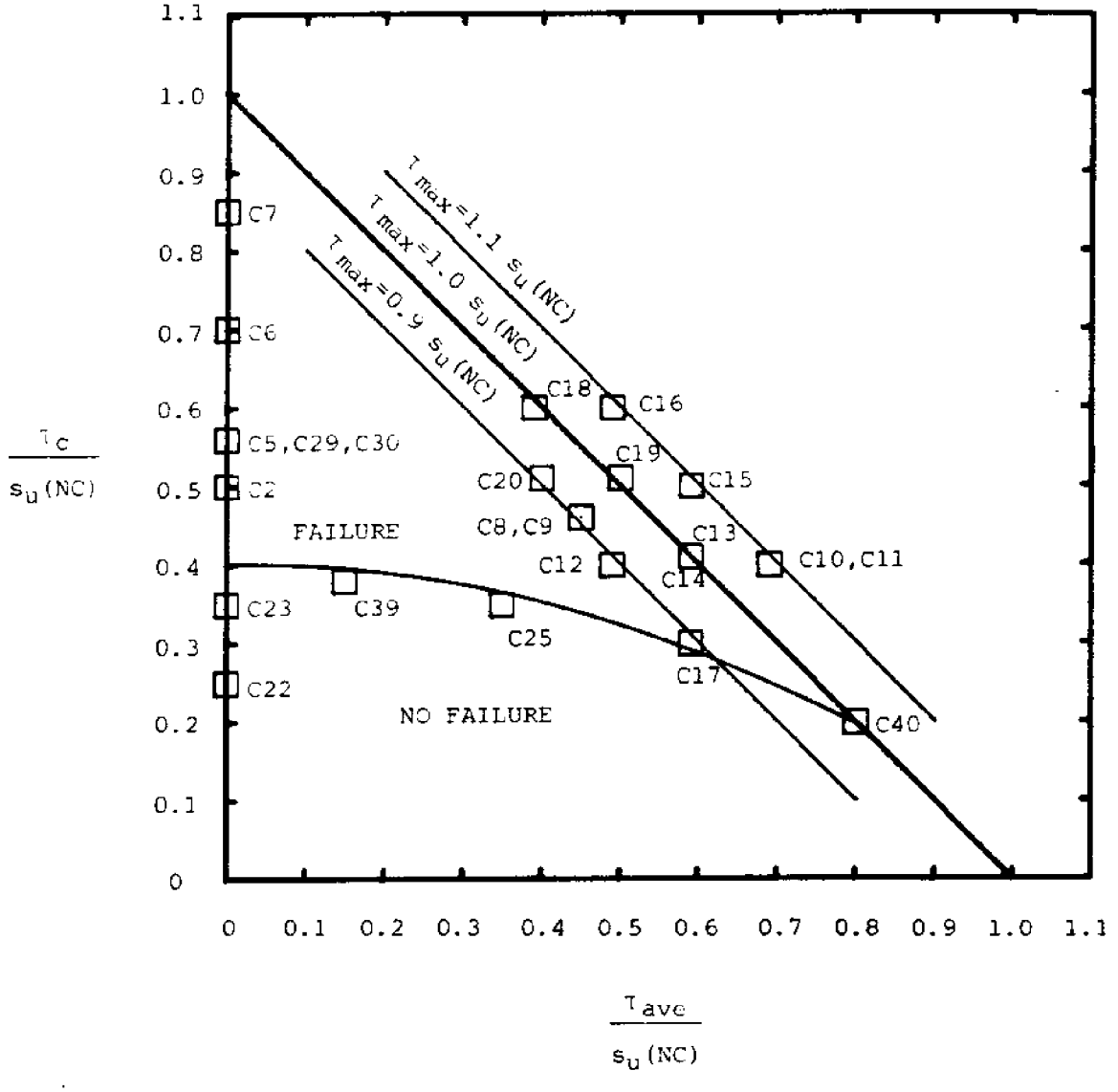

Figure 5.1 Summary of Stress-Controlled Cyclic CK_oUDSS Tests on N.C. BBC

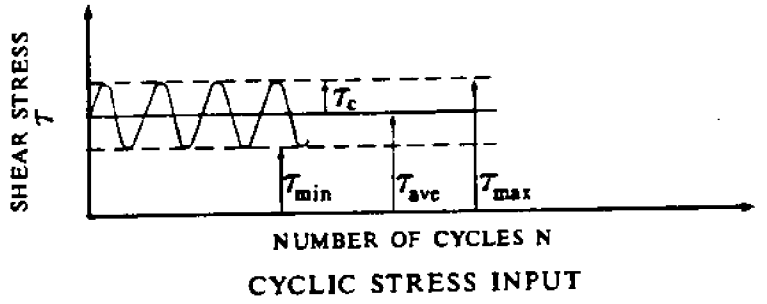

CYCLIC STRESS INPUT

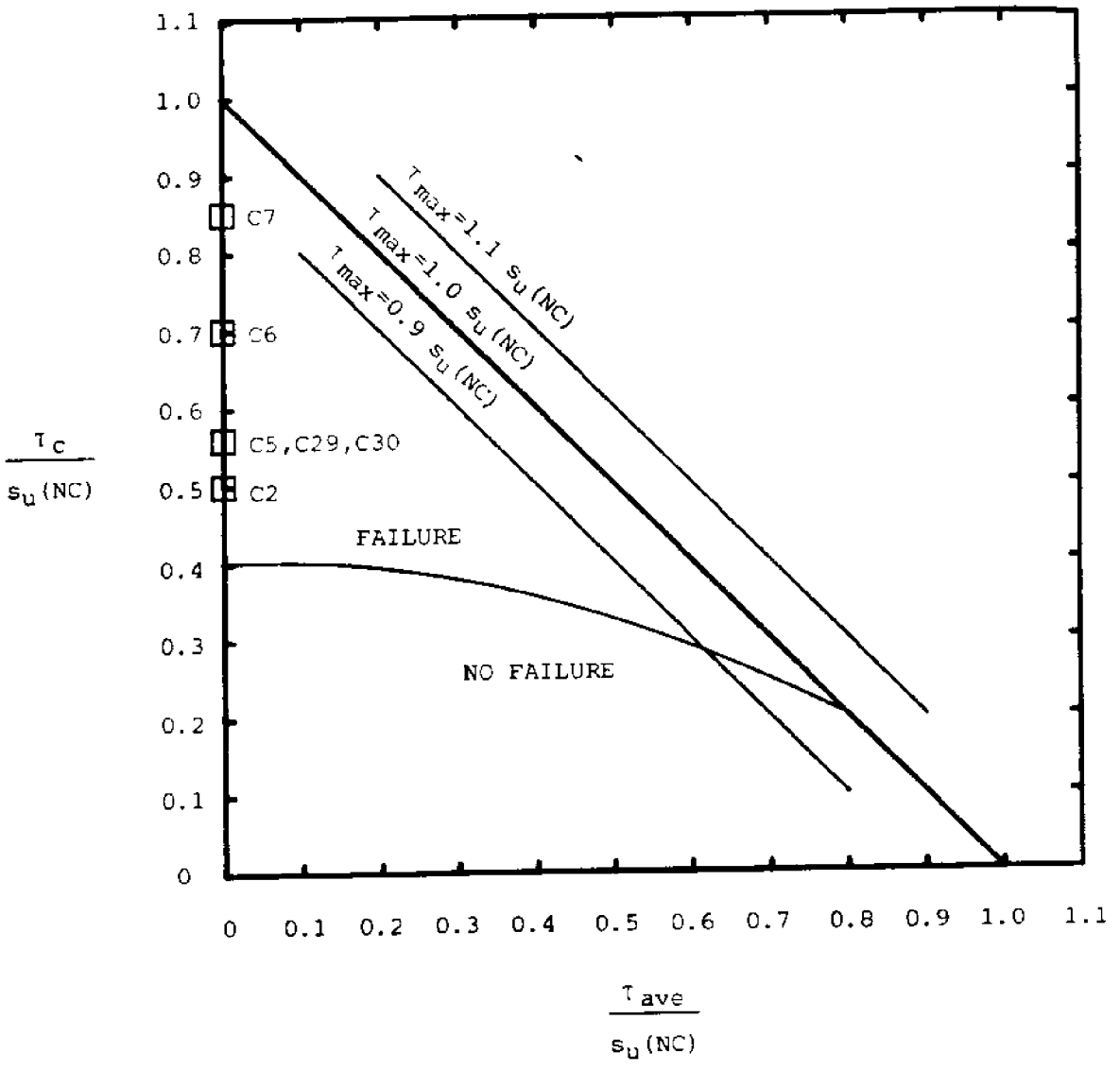

Figure 5.2 Summary of Cyclic CK_oUDSS Tests with $\tau_{ave} = 0$

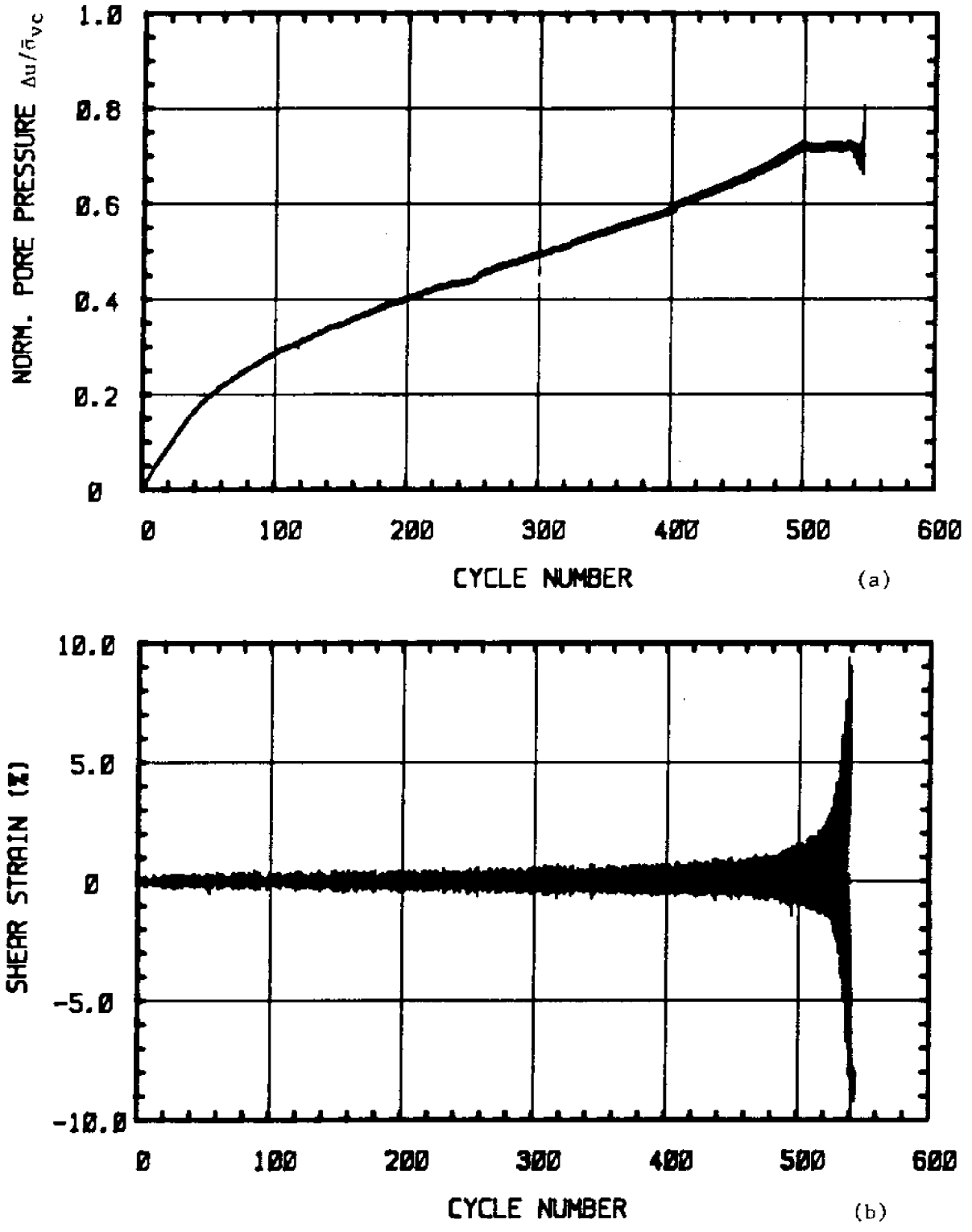

Figure 5.3 Test C-2: N.C. BBC, τ_{ave} = 0, τ_c/s_u(NC) = 0.50
a) Normalized Excess Pore Pressure versus Cycle Number
b) Shear Strain versus Cycle Number

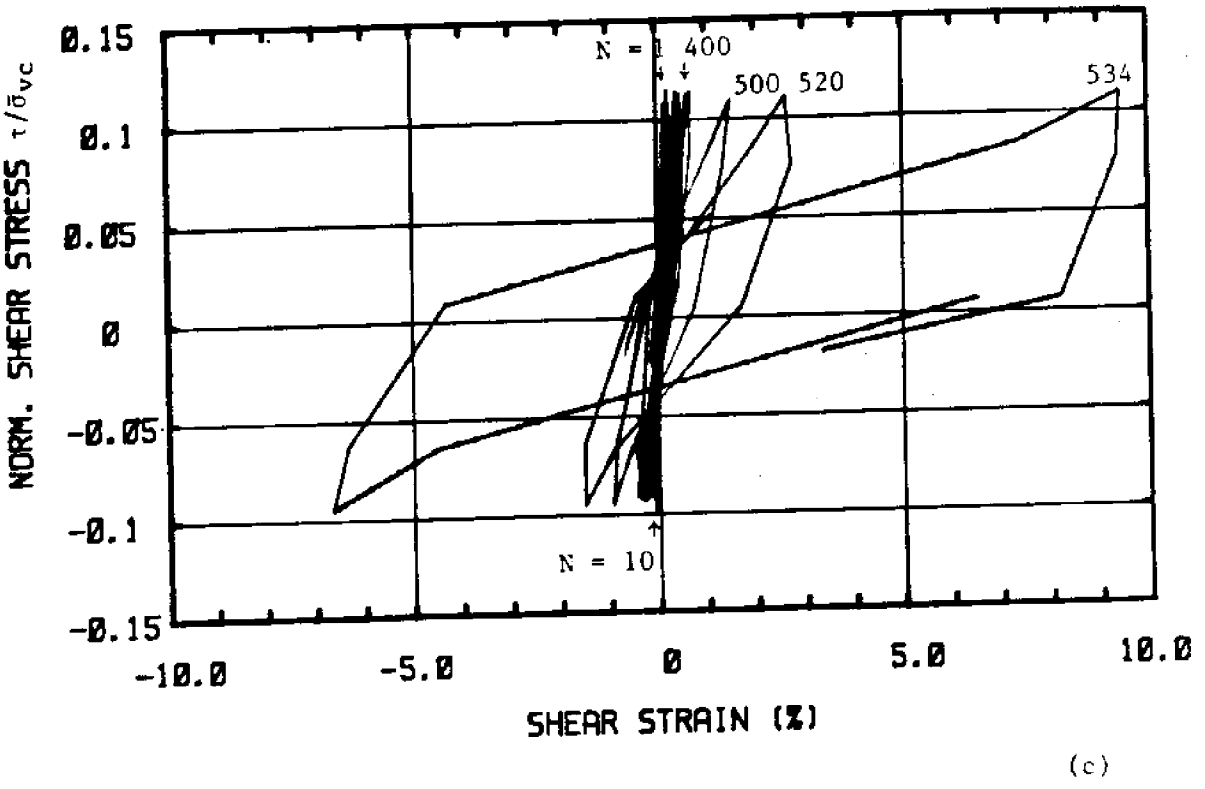

(c)

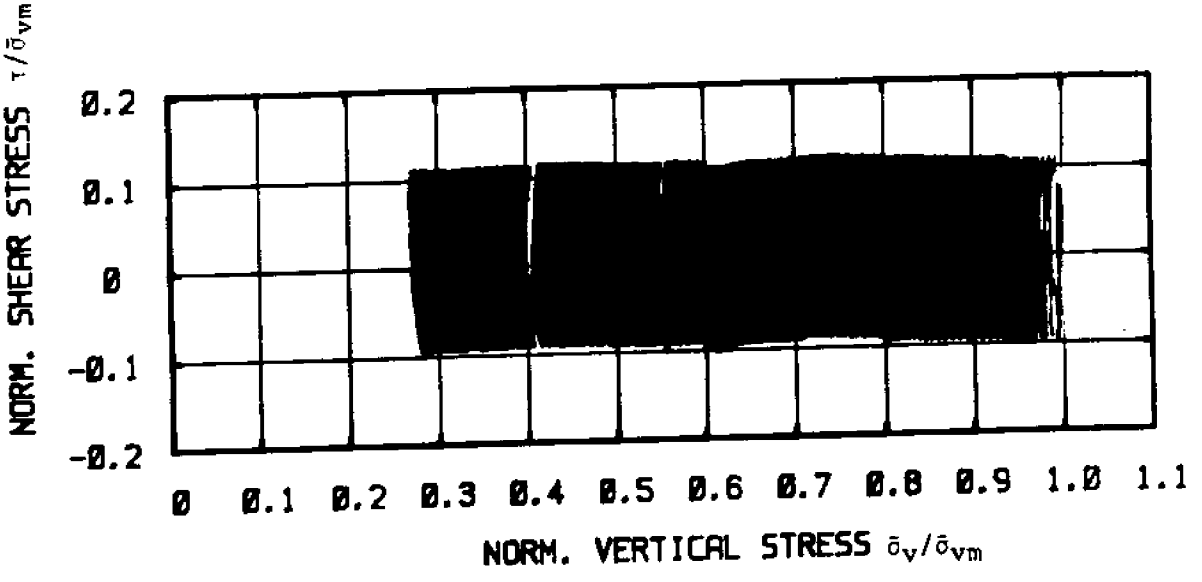

(d)

Figure 5.3 Test C-2: N.C. BBC, $\tau_{ave} = 0$, $\tau_c/s_u(NC) = 0.50$
c) Normalized Shear Stress versus Shear Strain
d) Normalized Stress Path

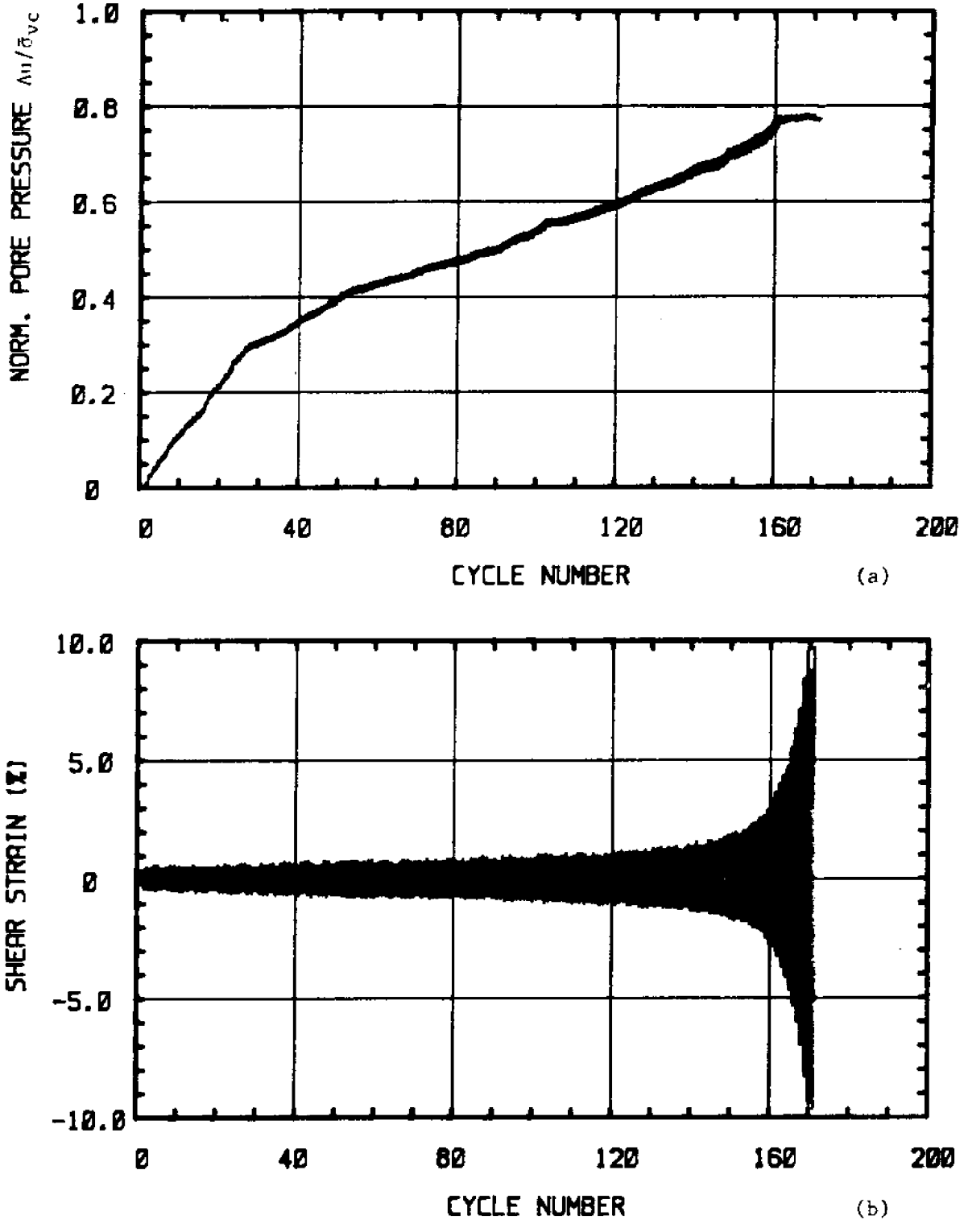

Figure 5.4 Test C-5: N.C. BBC, $\tau_{ave} = 0$, $\tau_c/s_u(NC) = 0.56$
a) Normalized Excess Pore Pressure versus Cycle Number
b) Shear Strain versus Cycle Number

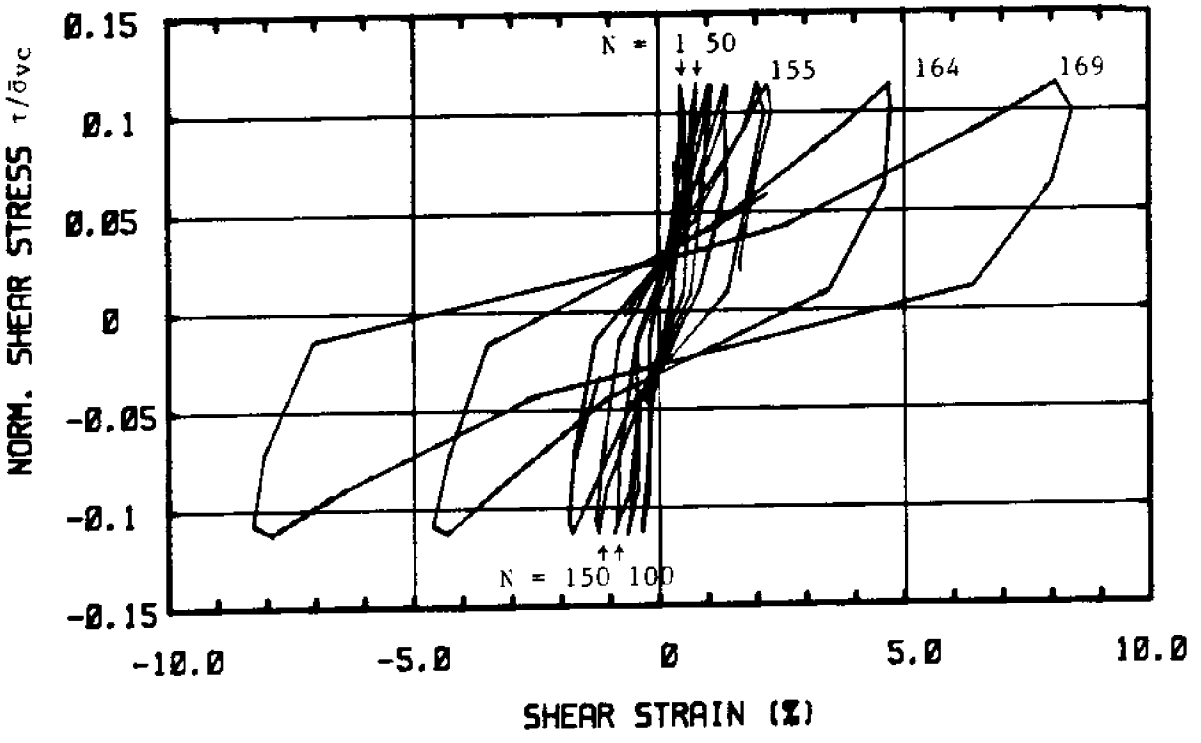

(c)

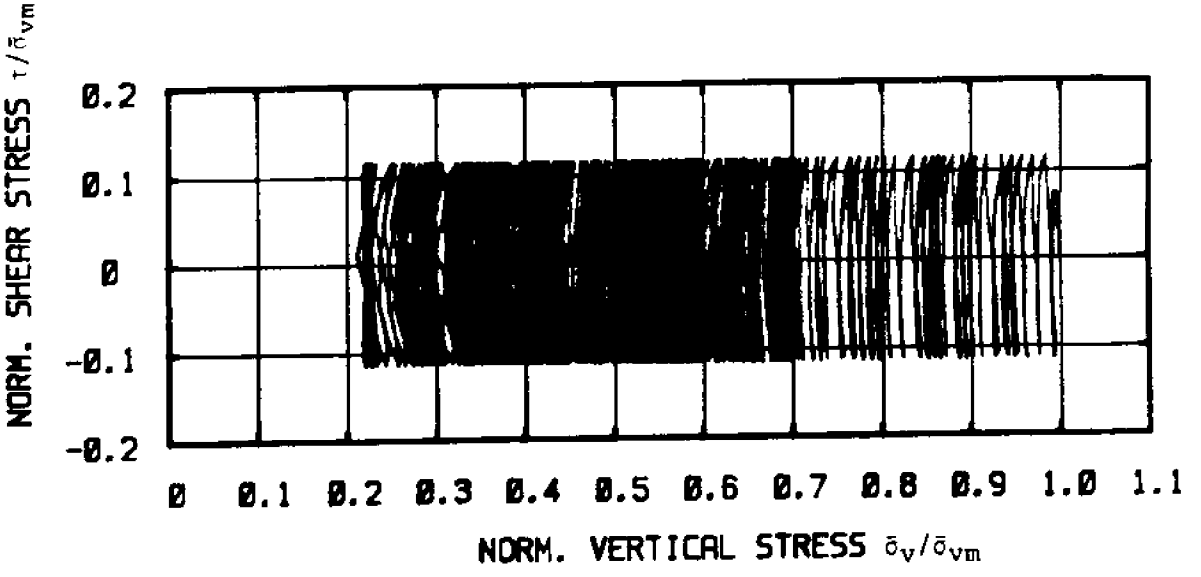

(d)

Figure 5.4 Test C-5: N.C. BBC, $\tau_{ave} = 0$, $\tau_c/s_u(NC) = 0.56$
c) Normalized Shear Stress versus Shear Strain
d) Normalized Stress Path

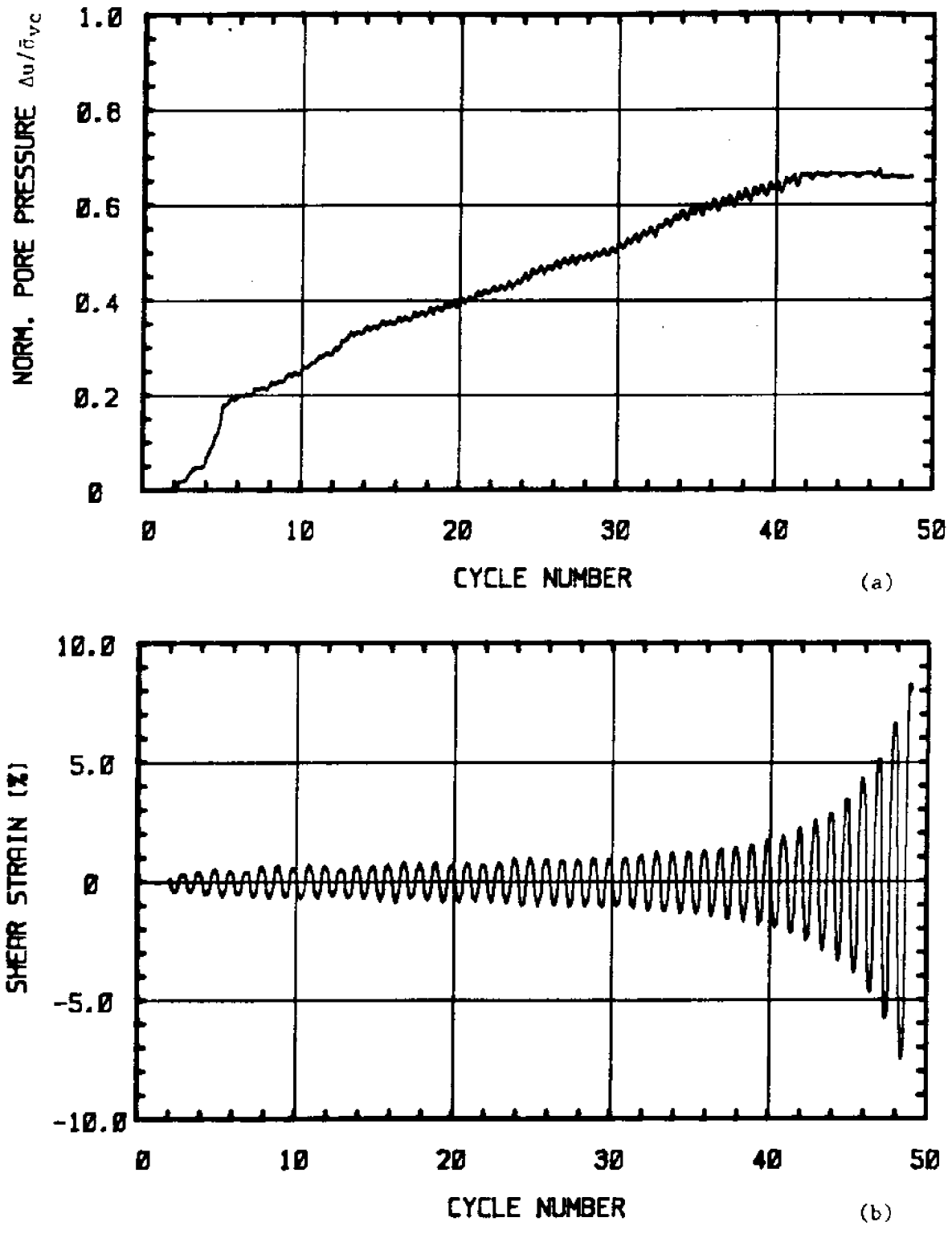

Figure 5.5 Test C-6: N.C. BBC, $\tau_{ave} = 0$, $\tau_c/s_u(NC) = 0.70$
a) Normalized Excess Pore Pressure versus Cycle Number
b) Shear Strain versus Cycle Number

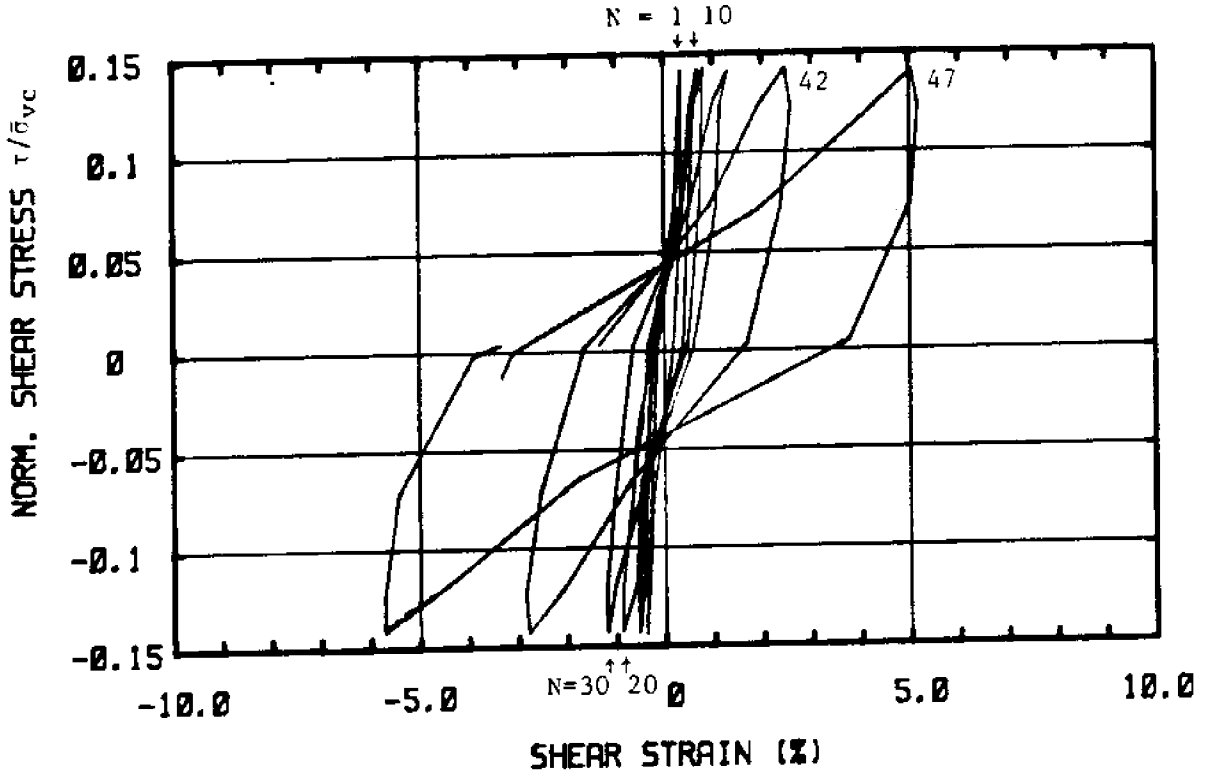

(c)

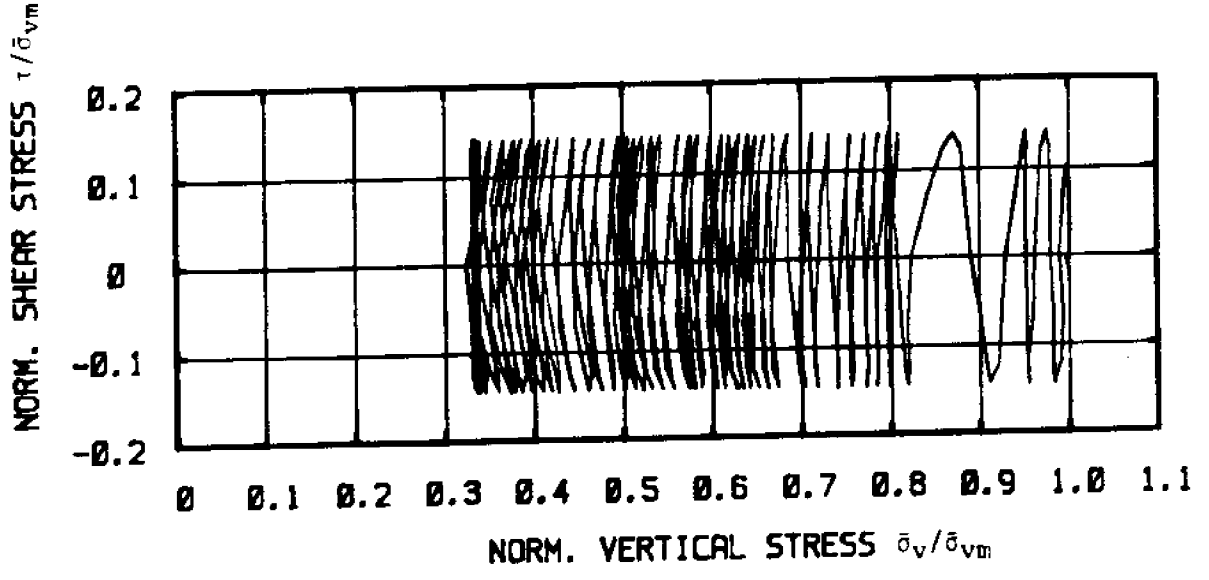

(d)

Figure 5.5 Test C-6: N.C. BBC, $\tau_{ave} = 0$, $\tau_c/s_u(NC) = 0.70$
c) Normalized Shear Stress versus Shear Strain
d) Normalized Stress Path

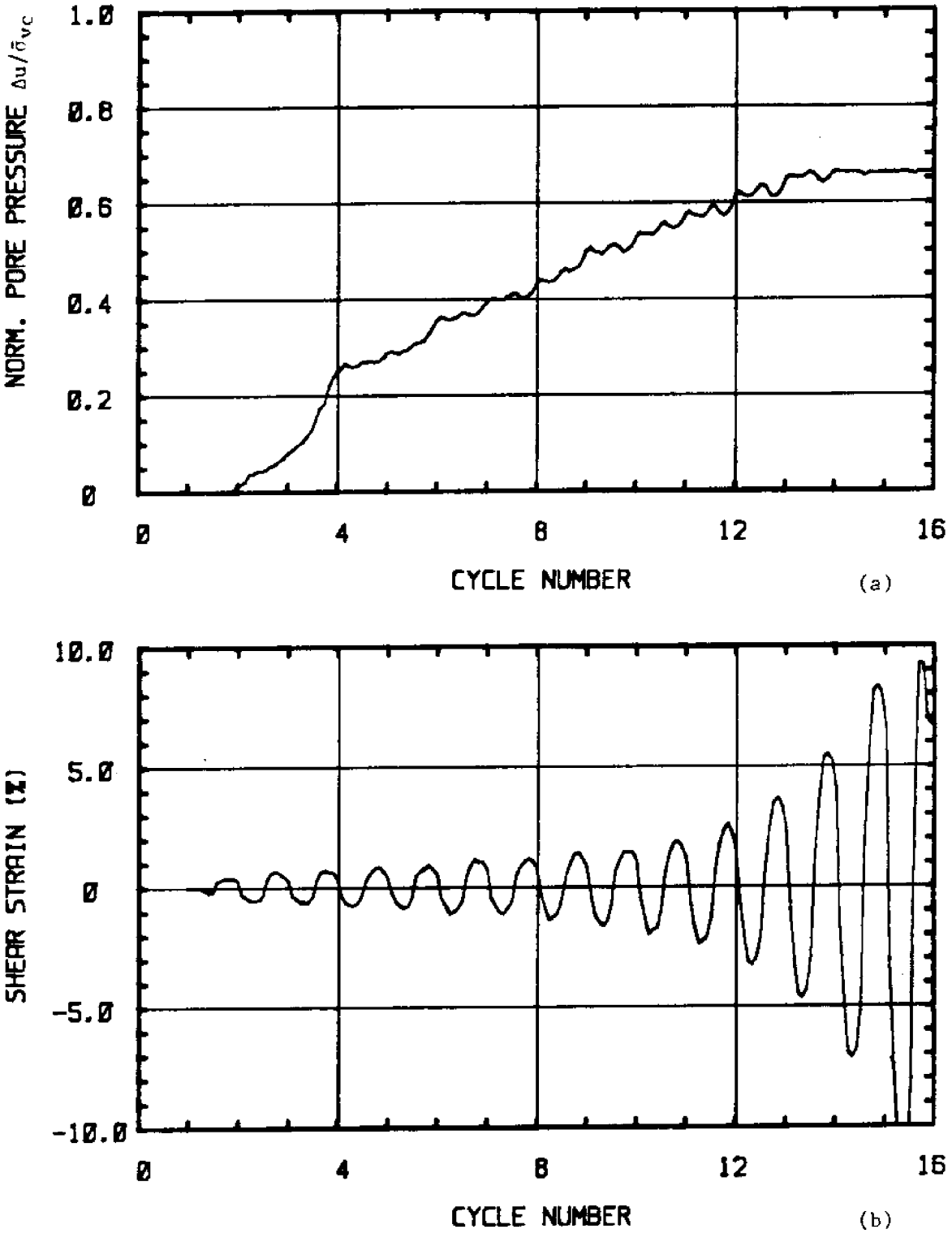

Figure 5.6 Test C-7: N.C. BBC, τ_{ave} = 0, $\tau_c/s_u(NC)$ = 0.85
a) Normalized Excess Pore Pressure versus Cycle Number
b) Shear Strain versus Cycle Number

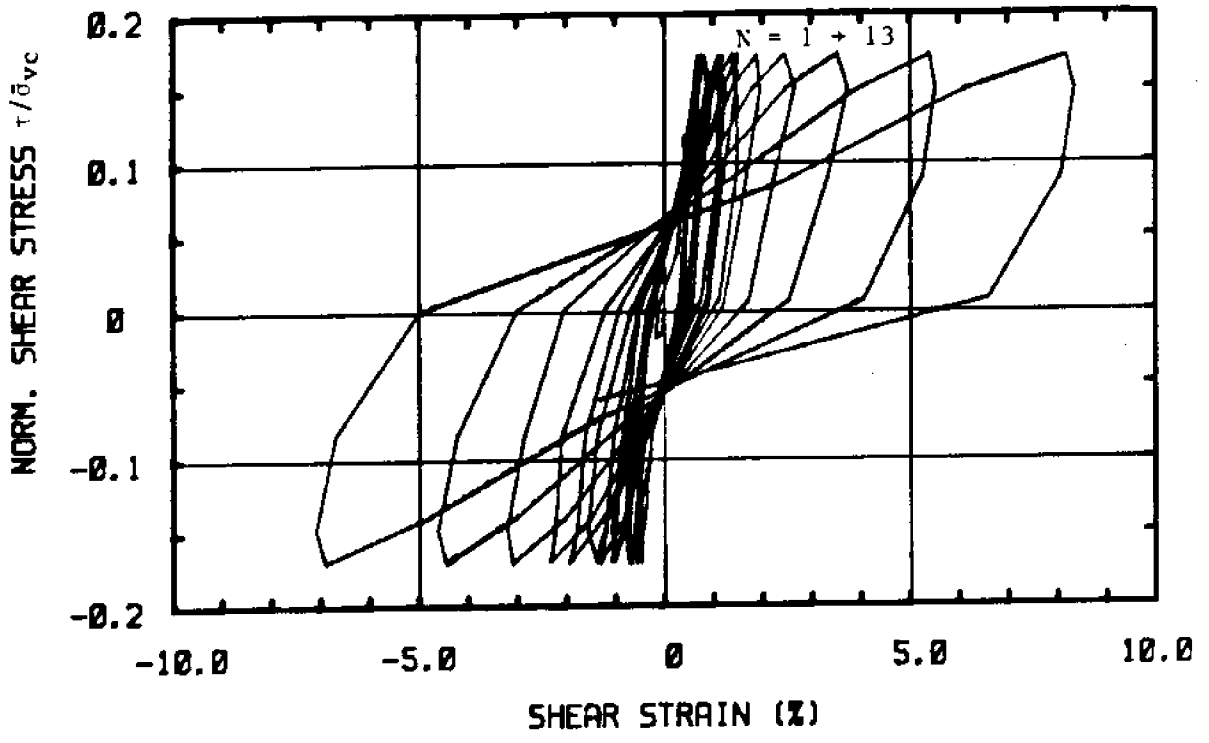

(c)

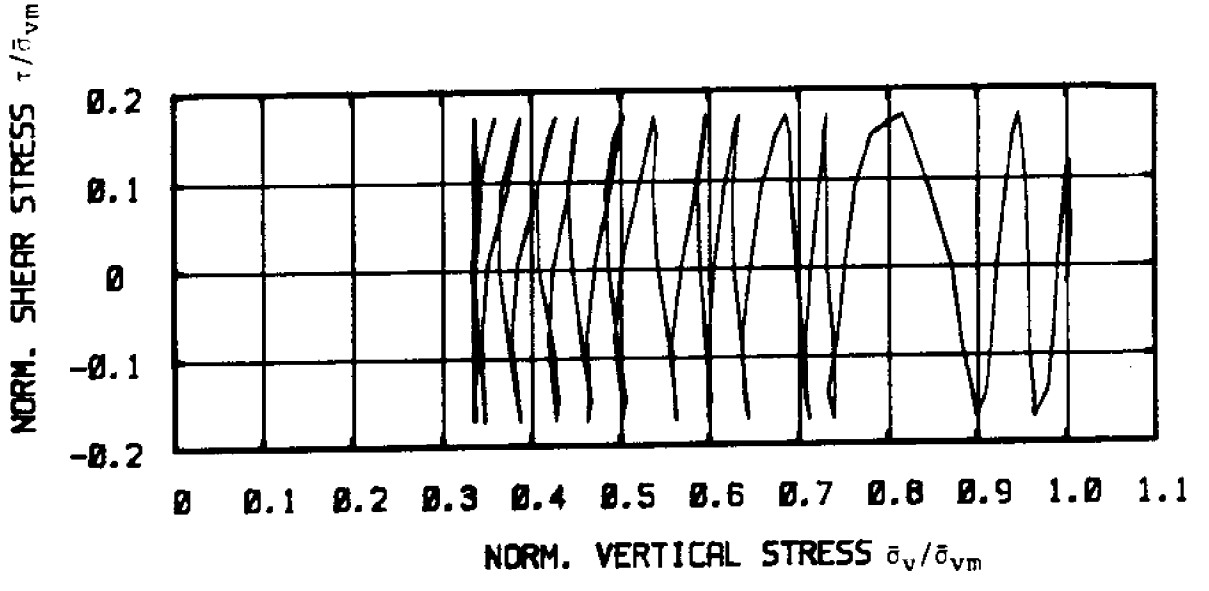

(d)

Figure 5.6 Test C-7: N.C. BBC, τ_{ave} = 0, τ_c/s_u(NC) = 0.85
c) Normalized Shear Stress versus Shear Strain
d) Normalized Stress Path

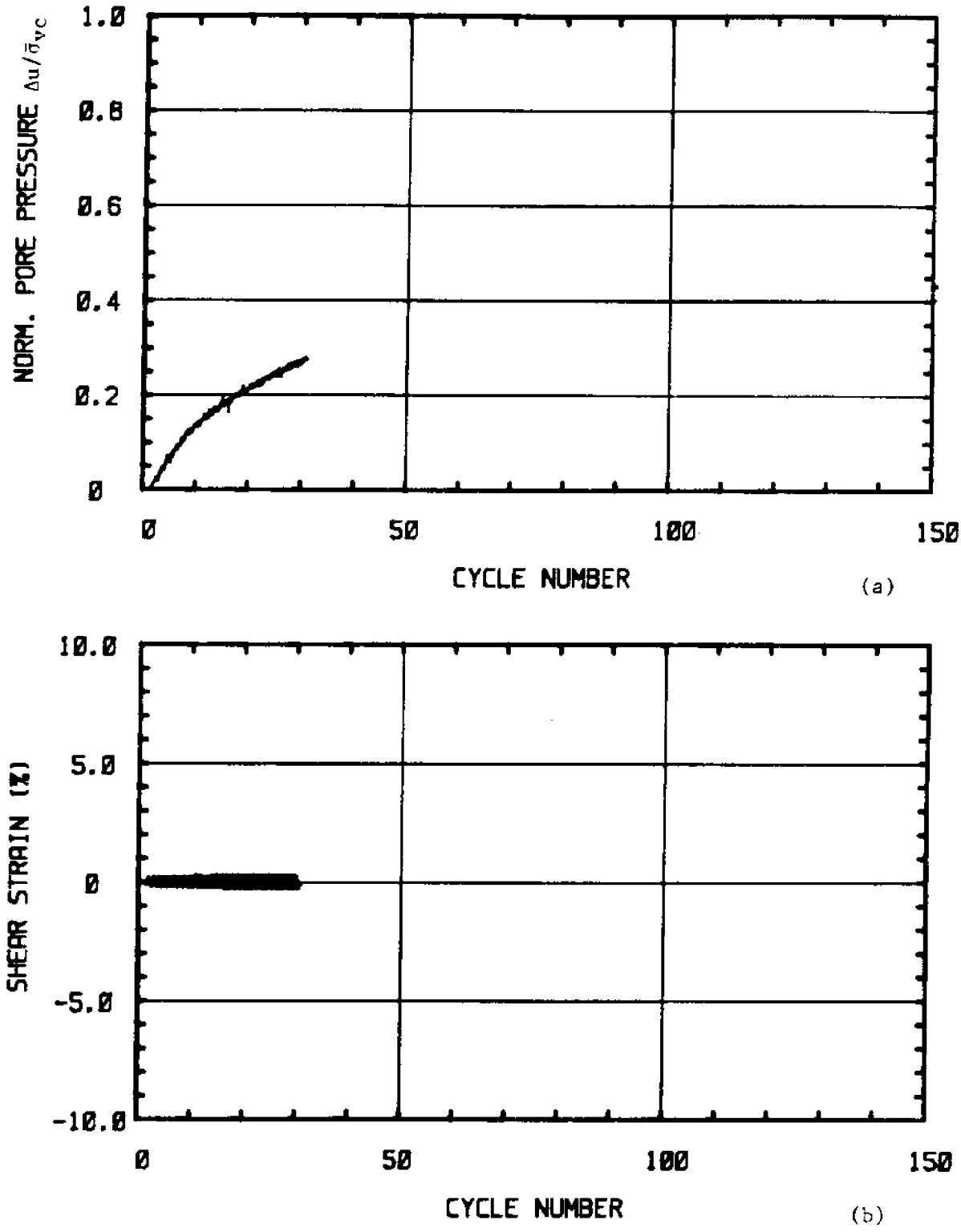

Figure 5.7 Test C-29: N.C. BBC, $\tau_{ave} = 0$, $\tau_c/s_u(NC) = 0.56$
a) Normalized Excess Pore Pressure versus Cycle Number
b) Shear Strain versus Cycle Number

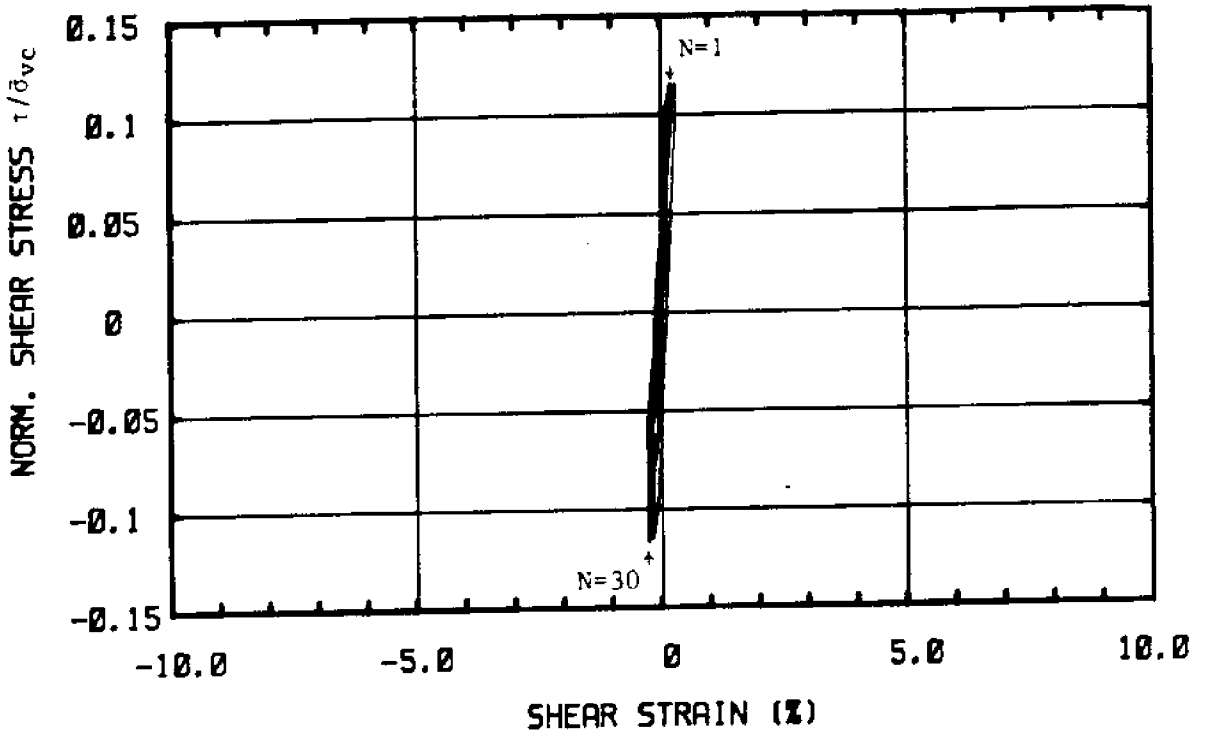

(c)

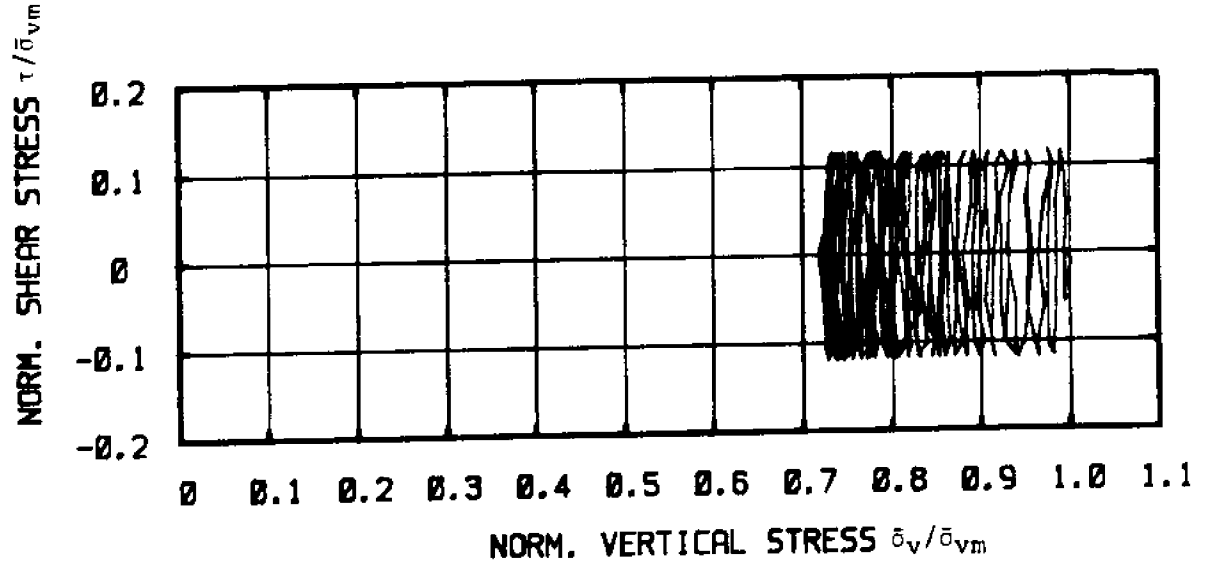

(d)

Figure 5.7 Test C-29: N.C. BBC, $\tau_{ave} = 0$, $\tau_c/s_u(NC) = 0.56$
c) Normalized Shear Stress versus Shear Strain
d) Normalized Stress Path

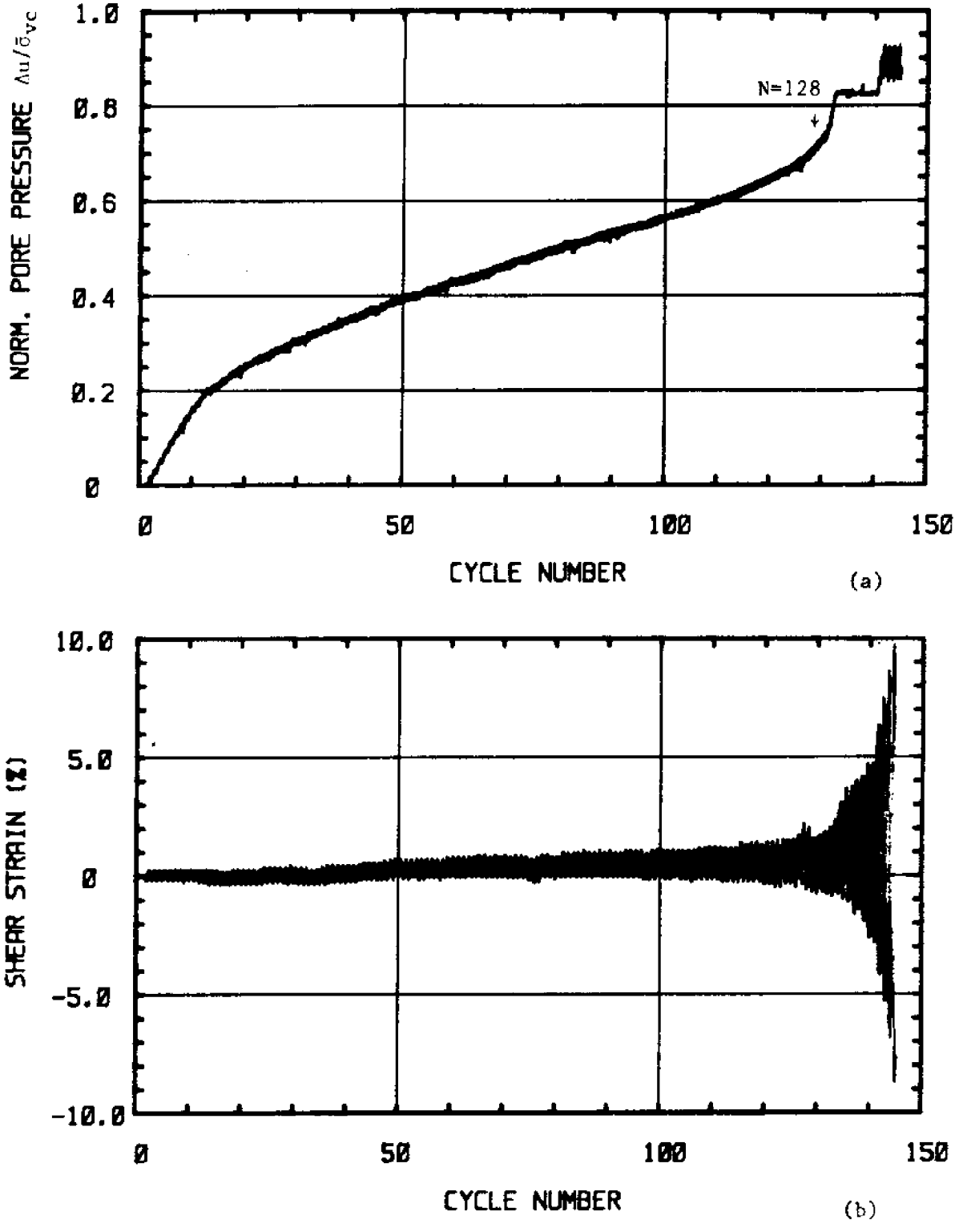

Figure 5.8 Test C-30: N.C. BBC, $\tau_{ave} = 0$, $\tau_c/s_u(NC) = 0.56$
a) Normalized Excess Pore Pressure versus Cycle Number
b) Shear Strain versus Cycle Number

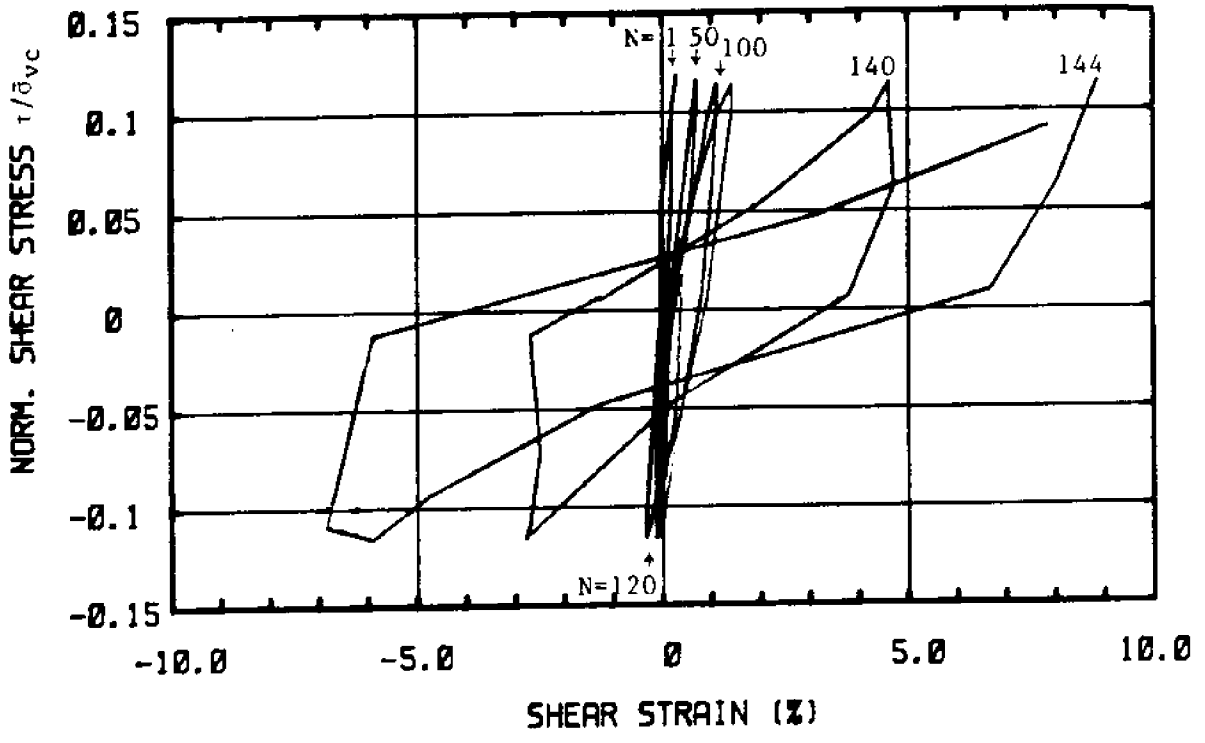

(c)

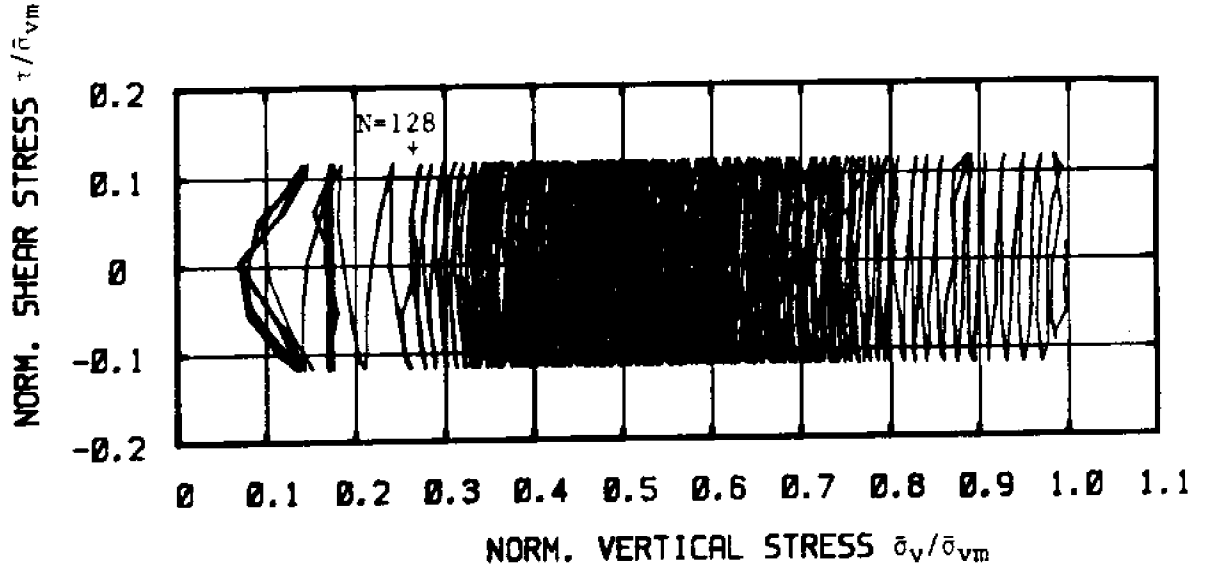

(d)

Figure 5.8 Test C-30: N.C. BBC, $\tau_{ave} = 0$, $\tau_c/s_u(NC) = 0.56$
c) Normalized Shear Stress versus Shear Strain
d) Normalized Stress Path

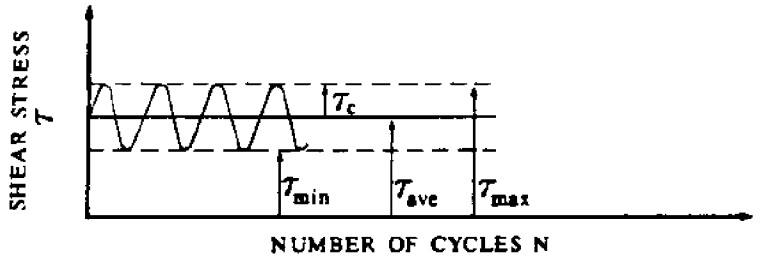

CYCLIC STRESS INPUT

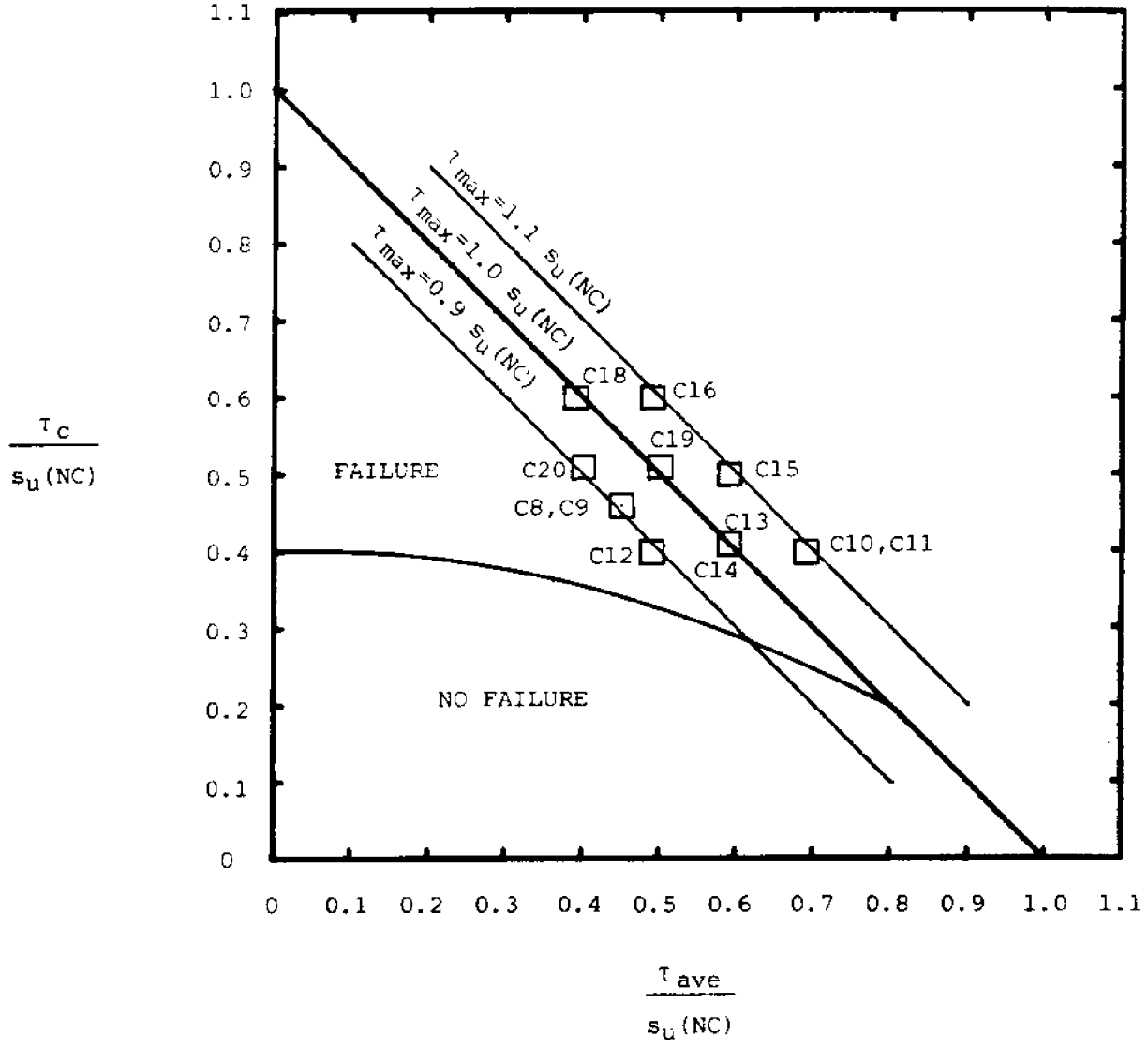

Figure 5.9 Summary of Cyclic CK_oUDSS Tests with $\tau_{ave} \neq 0$

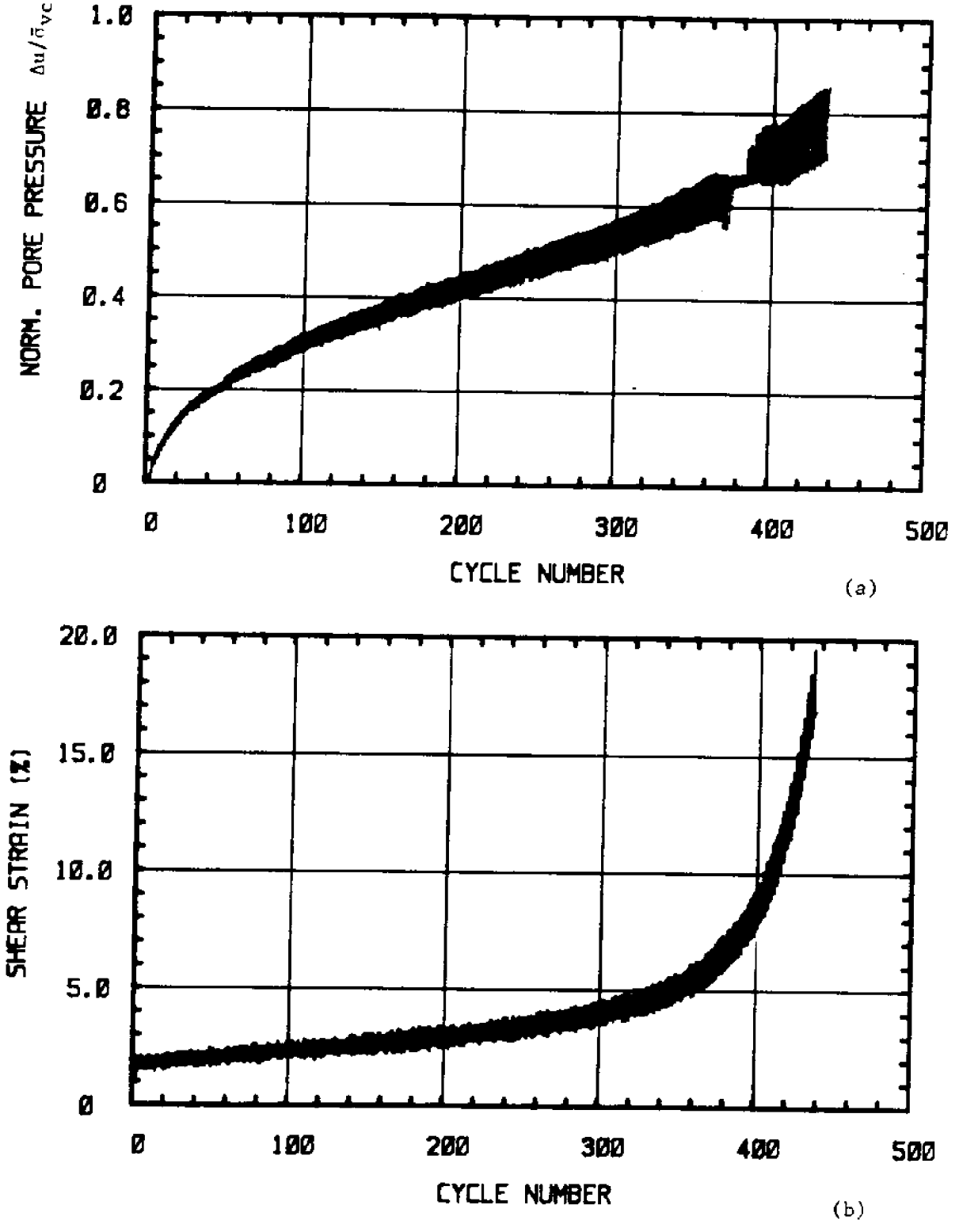

Figure 5.10 Test C-8: N.C. BBC, $\tau_{ave}/s_u(NC) = 0.45$, $\tau_c/s_u(NC) = 0.46$
a) Normalized Excess Pore Pressure versus Cycle Number
b) Shear Strain versus Cycle Number

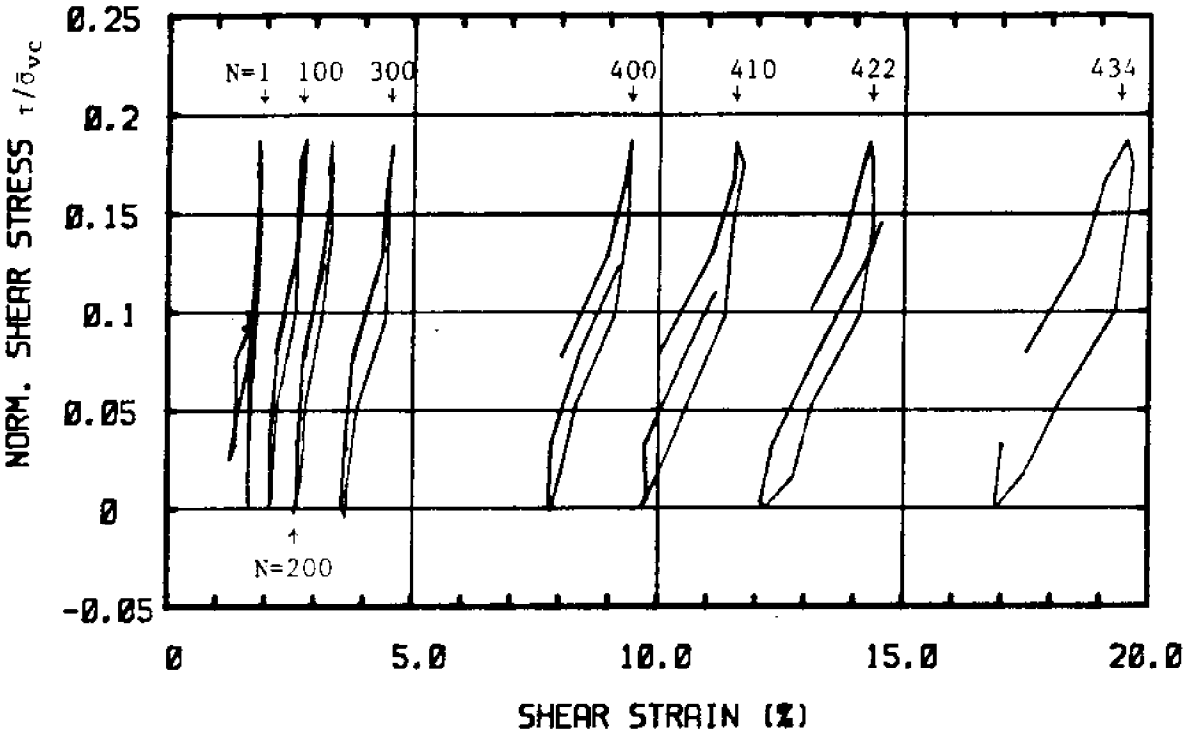

(c)

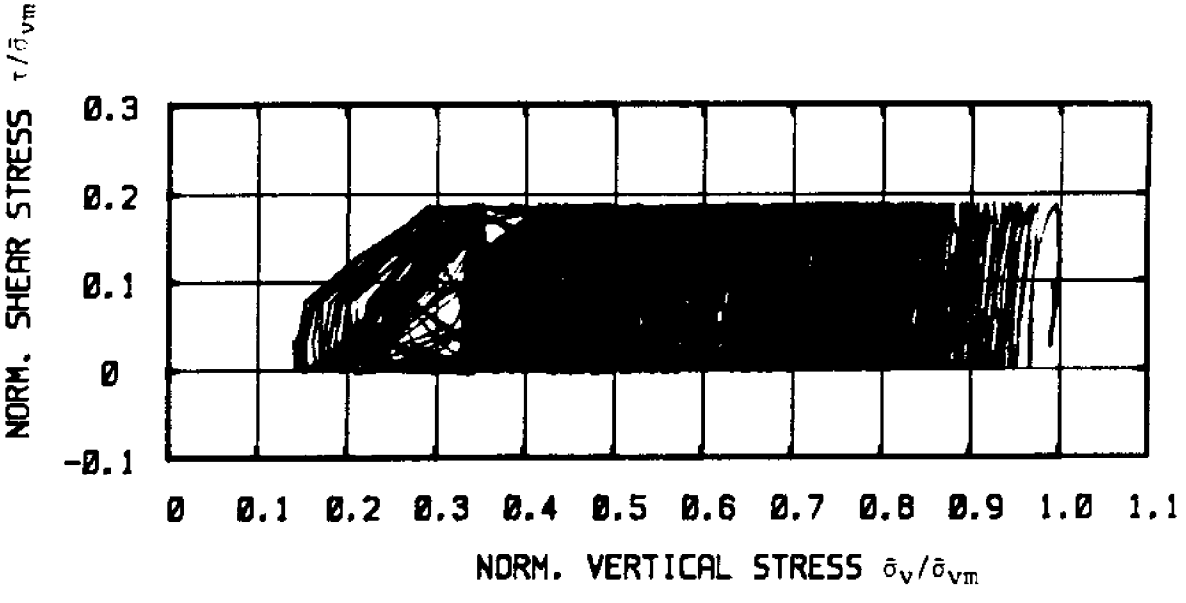

(d)

Figure 5.10 Test C-8: N.C. BBC, $\tau_{ave}/s_u(NC) = 0.45$, $\tau_c/s_u(NC) = 0.46$
c) Normalized Shear Stress versus Shear Strain
d) Normalized Stress Path

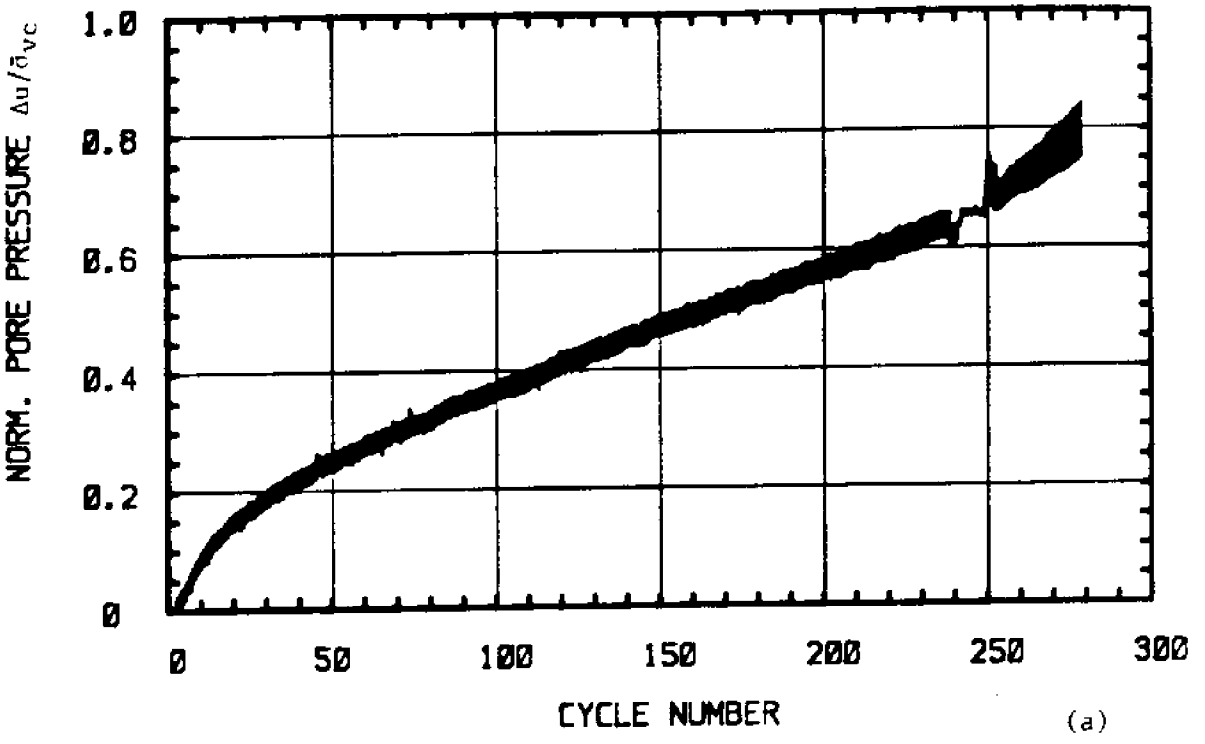

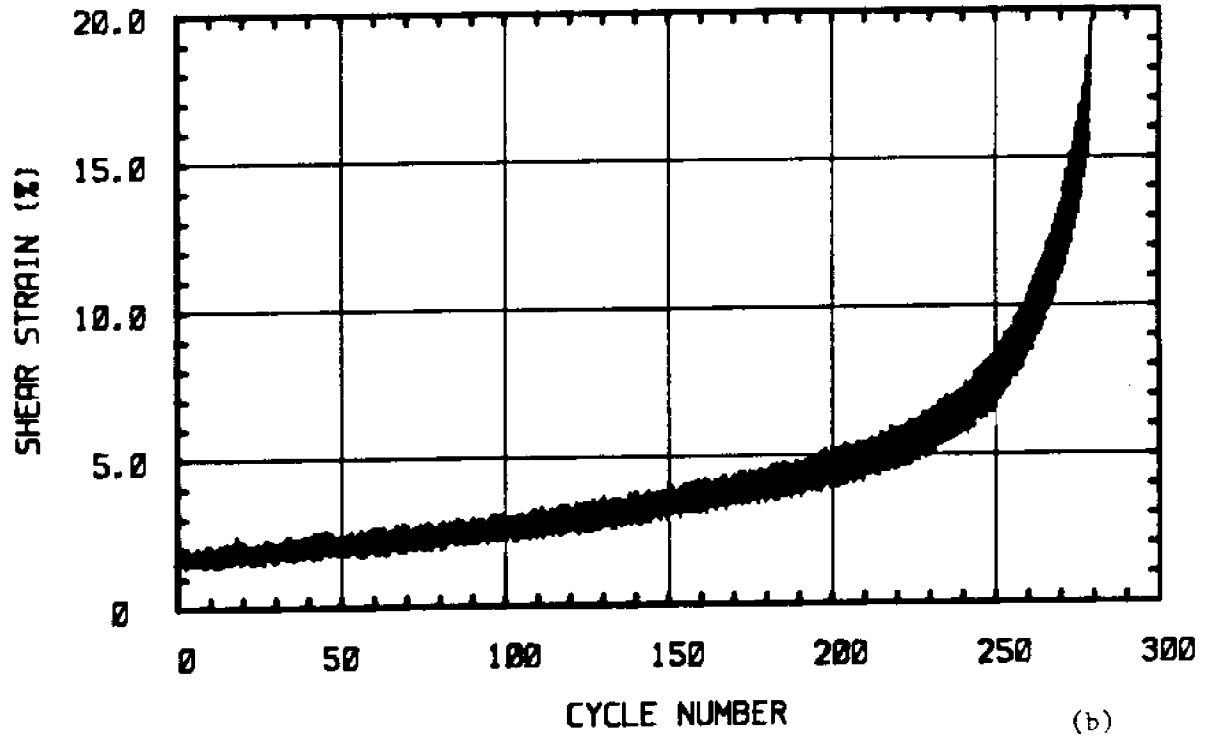

Figure 5.11 Test C-9: N.C. BBC, $\tau_{ave}/s_u(NC) = 0.45$, $\tau_c/s_u(NC) = 0.46$
a) Normalized Excess Pore Pressure versus Cycle Number
b) Shear Strain versus Cycle Number

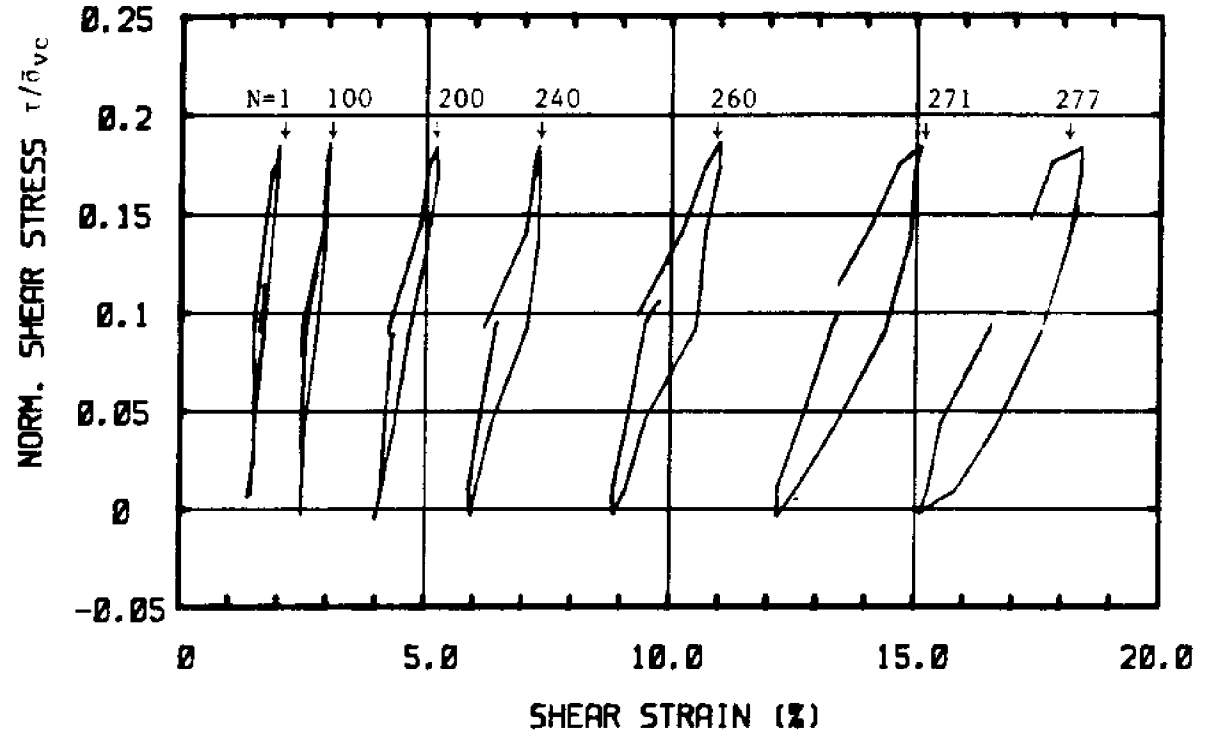

(c)

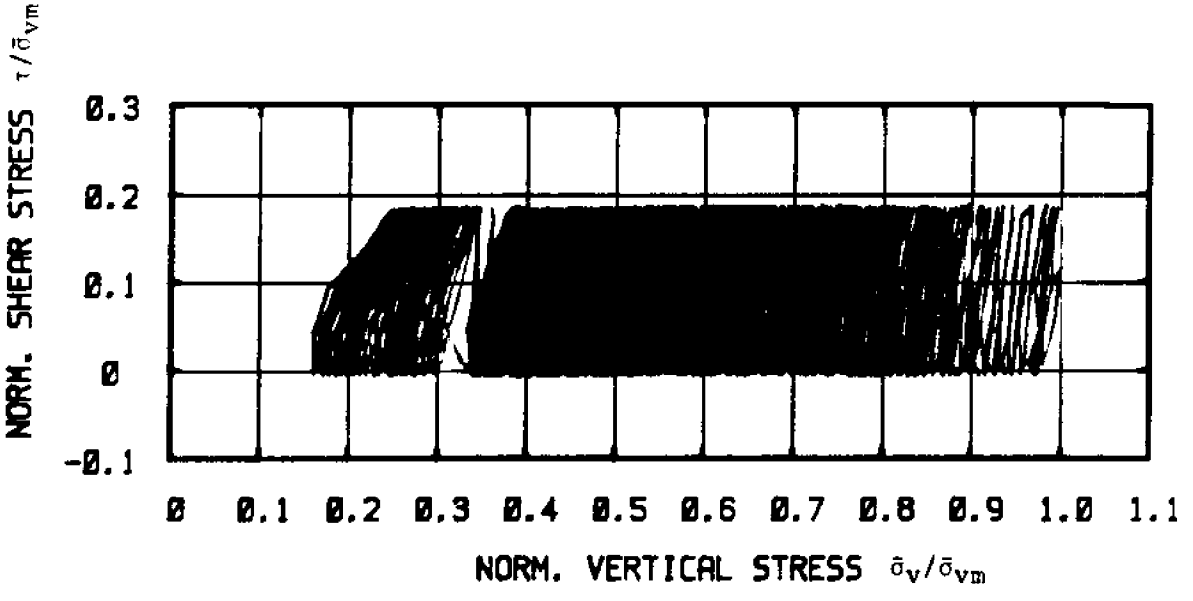

(d)

Figure 5.11 Test C-9: N.C. BBC, $\tau_{ave}/s_u(NC) = 0.45$, $\tau_c/s_u(NC) = 0.46$
c) Normalized Shear Stress versus Shear Strain
d) Normalized Stress Path

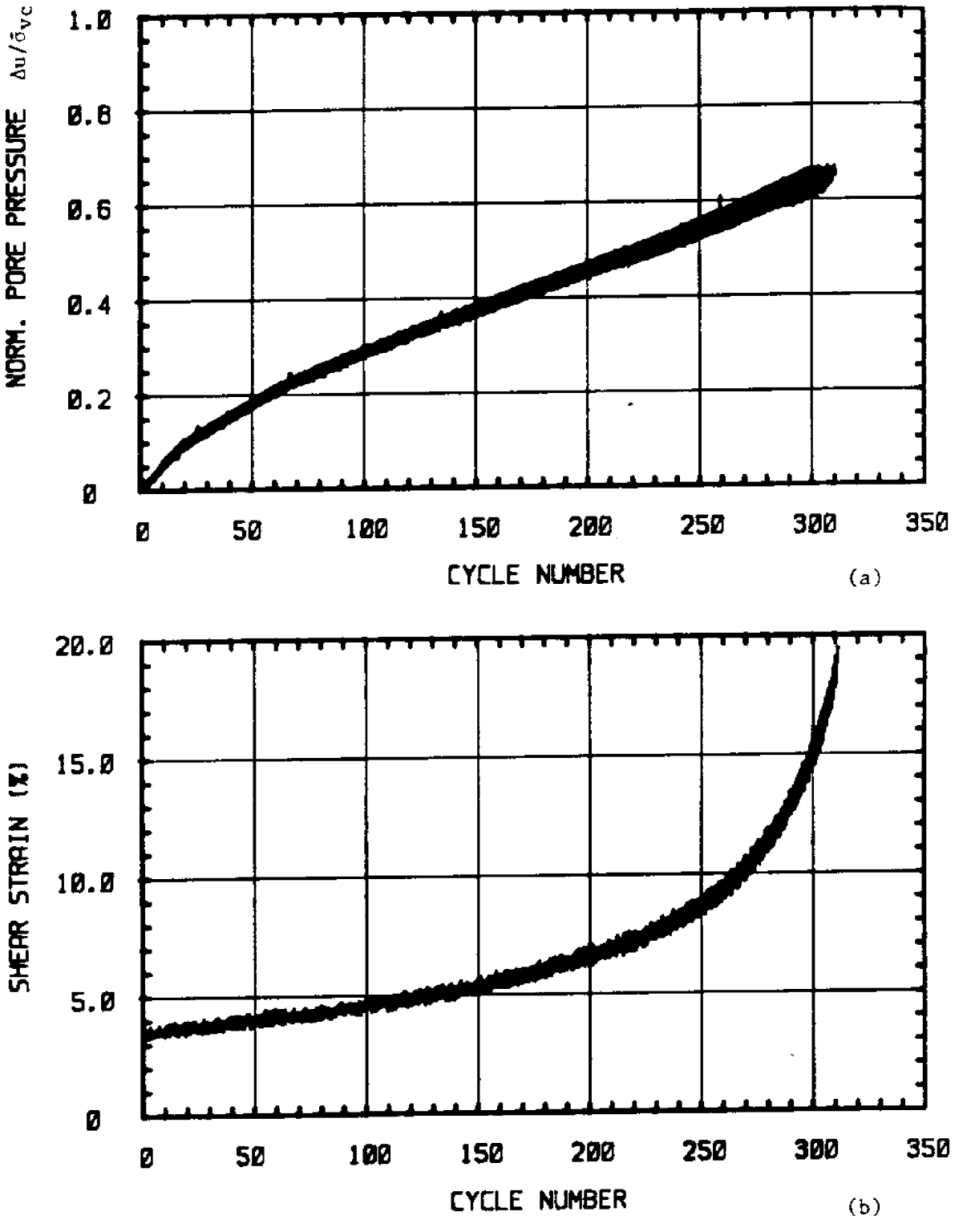

Figure 5.12 Test C-10: N.C. BBC, $\tau_{ave}/s_u(NC) = 0.69$, $\tau_c/s_u(NC) = 0.40$
a) Normalized Excess Pore Pressure versus Cycle Number
b) Shear Strain versus Cycle Number

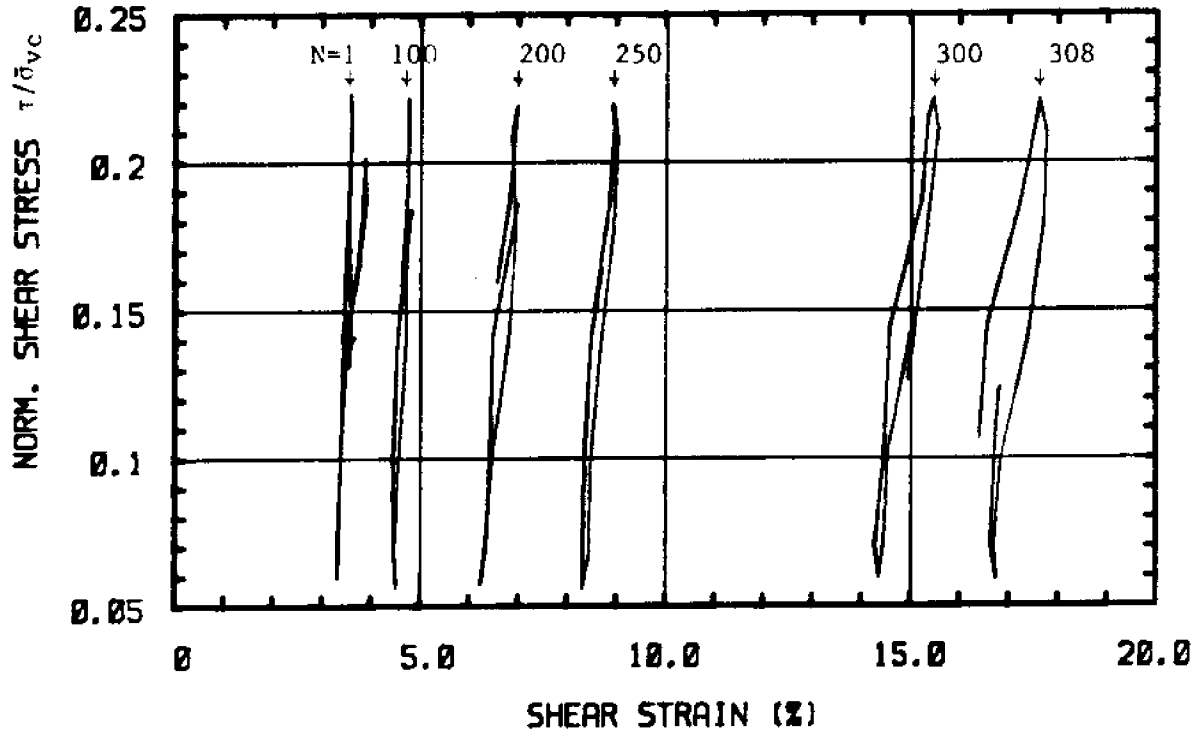

(c)

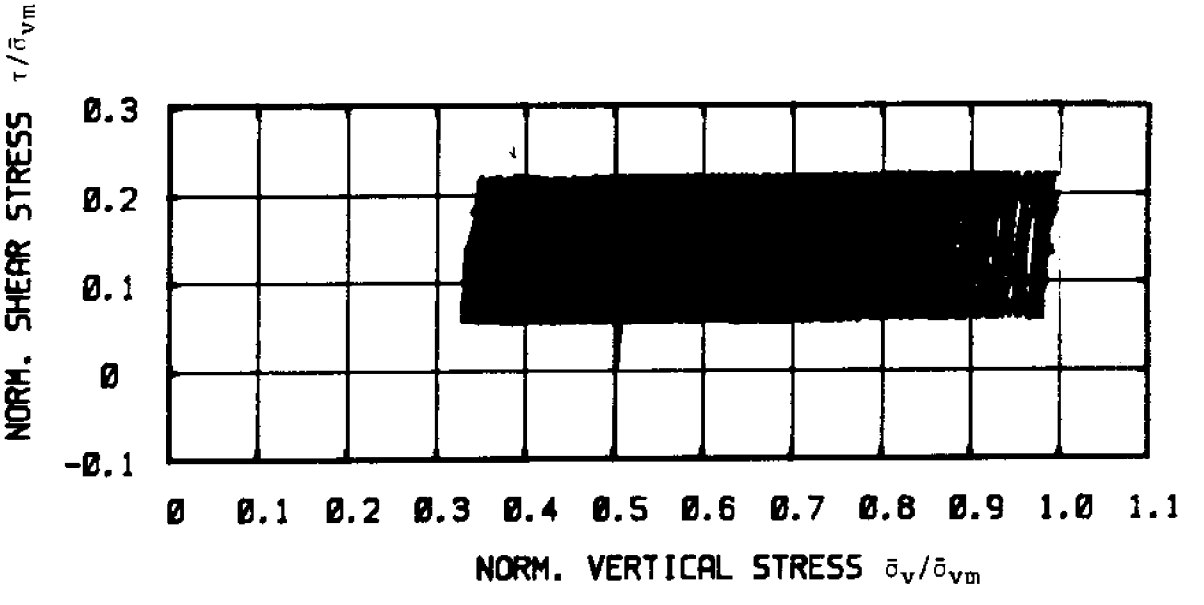

(d)

Figure 5.12 Test C-10: N.C. BBC, $\tau_{ave}/s_u(NC) = 0.69$, $\tau_c/s_u(NC) = 0.40$
c) Normalized Shear Stress versus Shear Strain
d) Normalized Stress Path

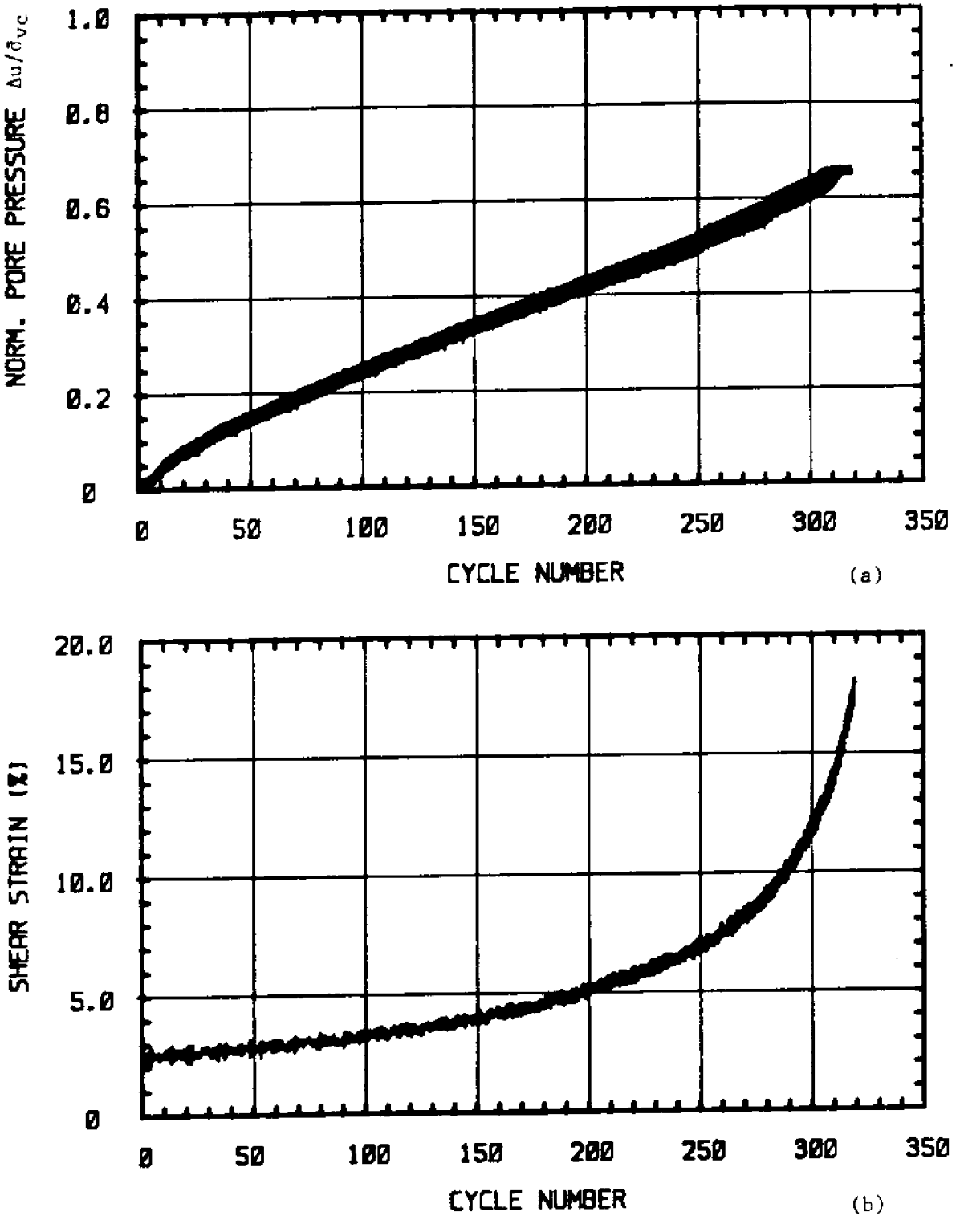

Figure 5.13 Test C-11: N.C. BBC, $\tau_{ave}/s_u(NC) = 0.69$, $\tau_c/s_u(NC) = 0.40$
a) Normalized Excess Pore Pressure versus Cycle Number
b) Shear Strain versus Cycle Number

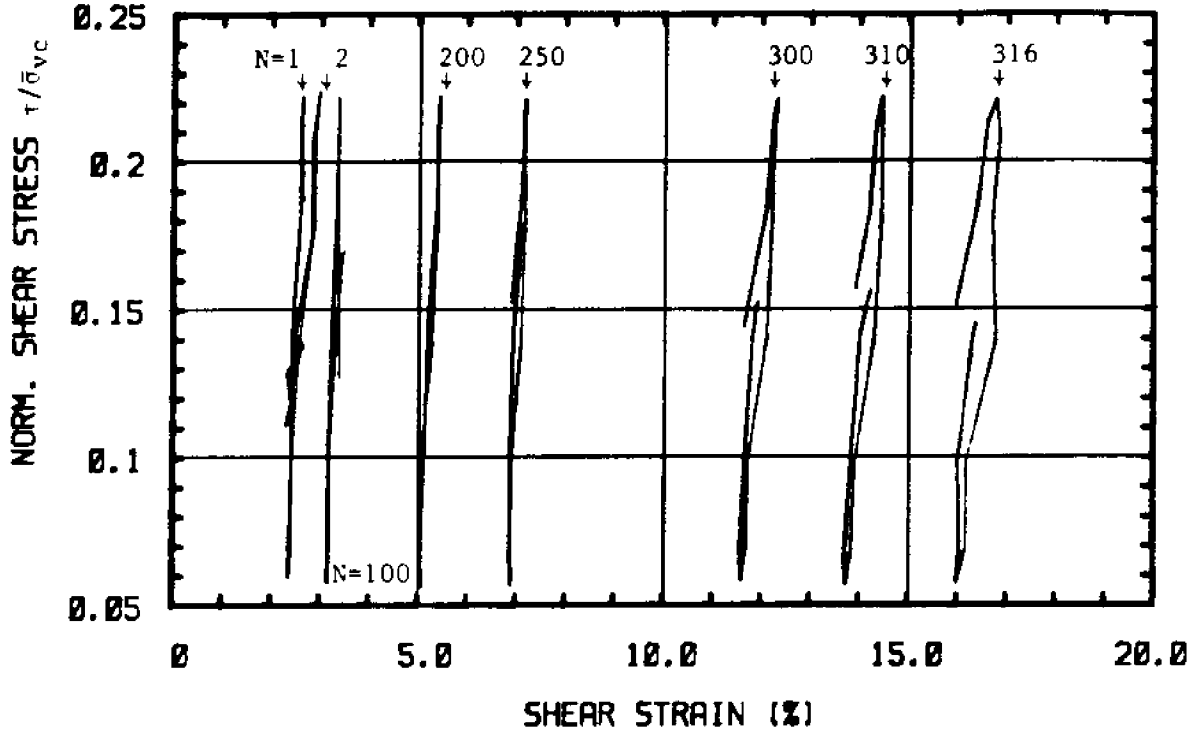

(c)

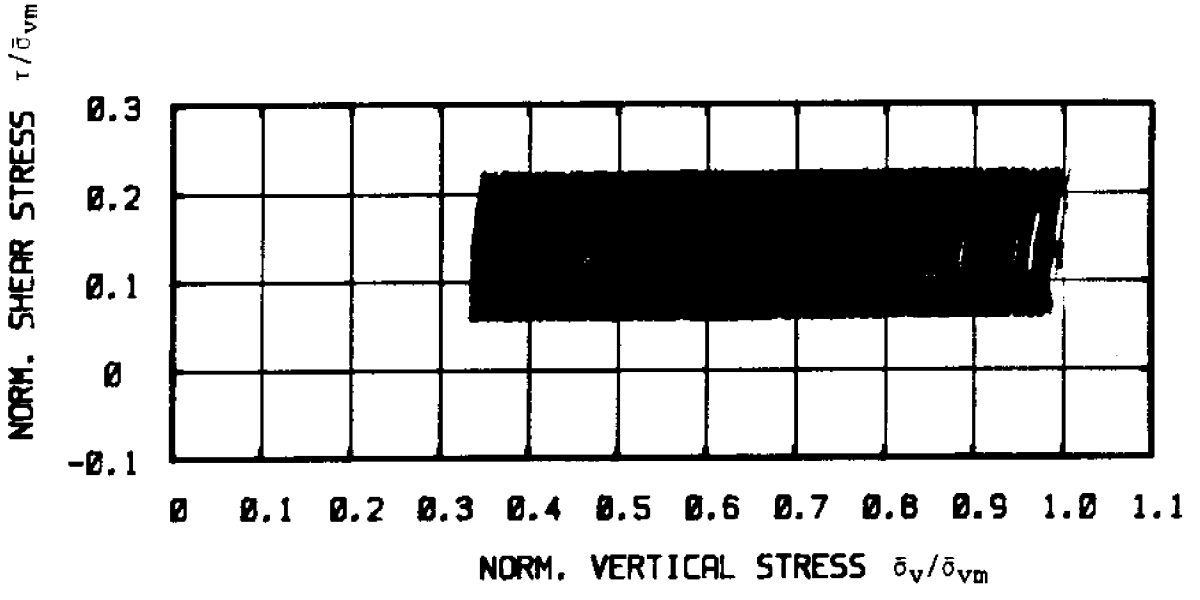

(d)

Figure 5.13 Test C-11: N.C. BBC, $\tau_{ave}/s_u(NC) = 0.69$, $\tau_c/s_u(NC) = 0.40$
c) Normalized Shear Stress versus Shear Strain
d) Normalized Stress Path

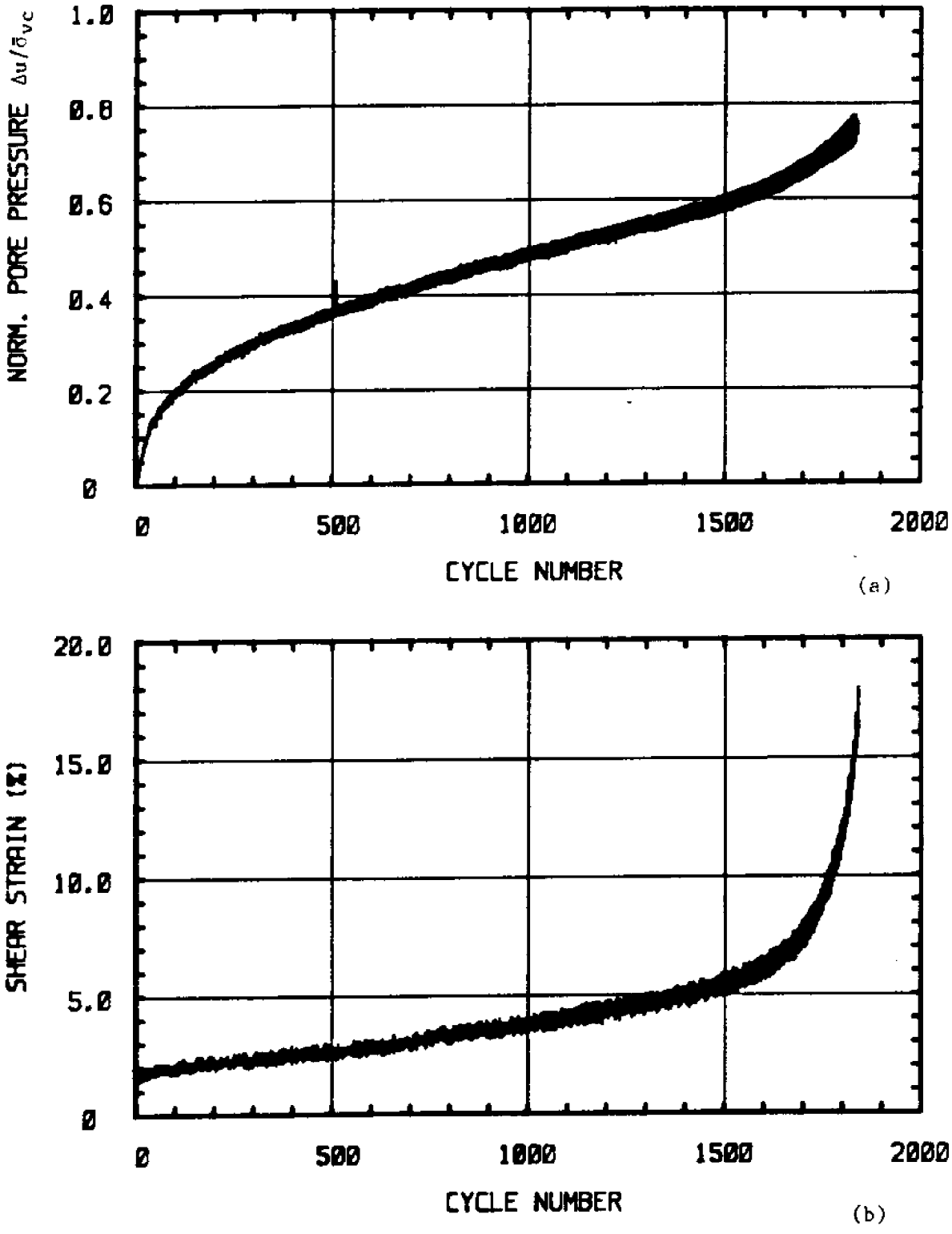

Figure 5.14 Test C-12: N.C. BBC, $\tau_{ave}/s_u(NC) = 0.49$, $\tau_c/s_u(NC) = 0.40$
a) Normalized Excess Pore Pressure versus Cycle Number
b) Shear Strain versus Cycle Number

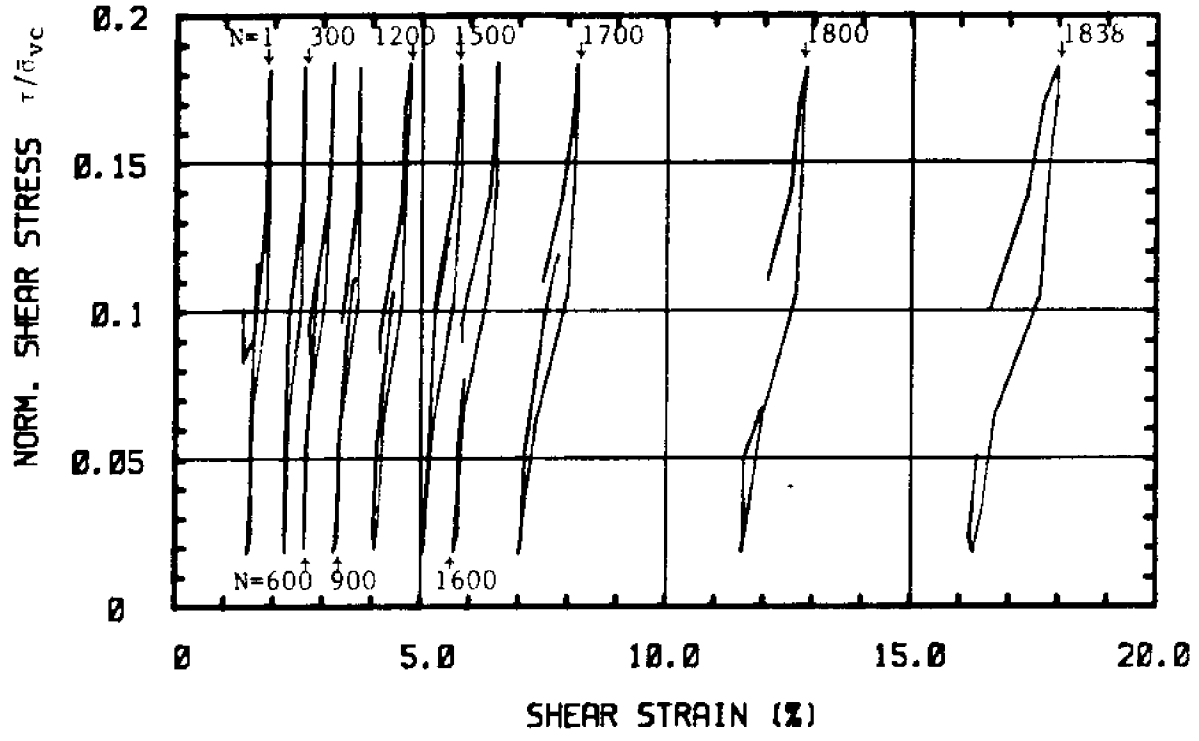

(c)

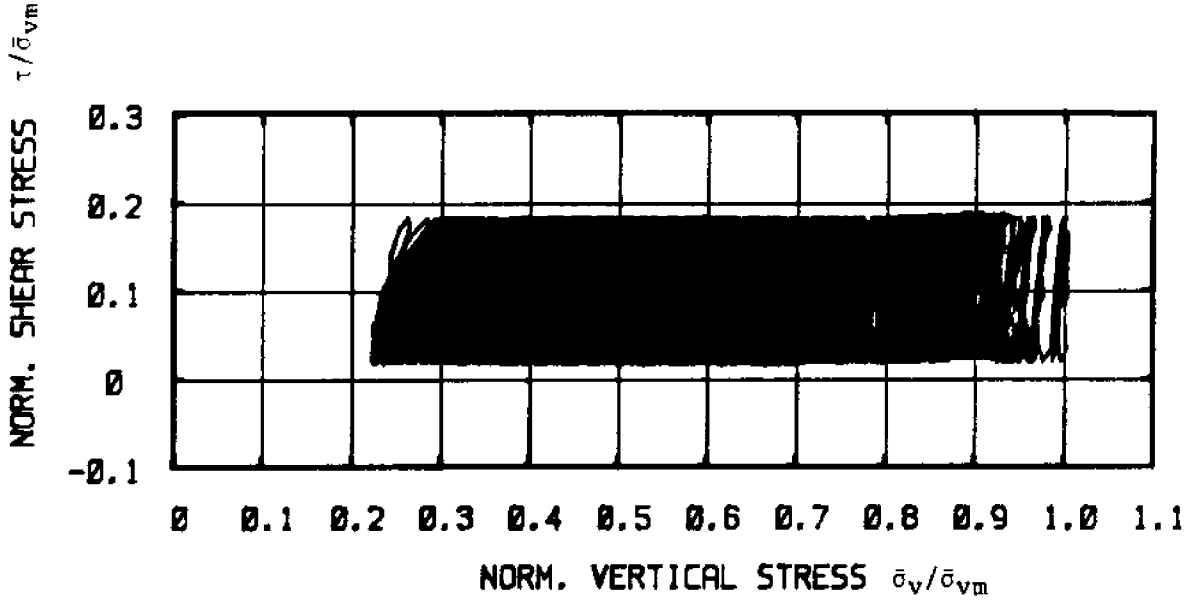

(d)

Figure 5.14 Test C-12: N.C. BBC, $\tau_{ave}/s_u(NC) = 0.49$, $\tau_c/s_u(NC) = 0.40$
c) Normalized Shear Stress versus Shear Strain
d) Normalized Stress Path

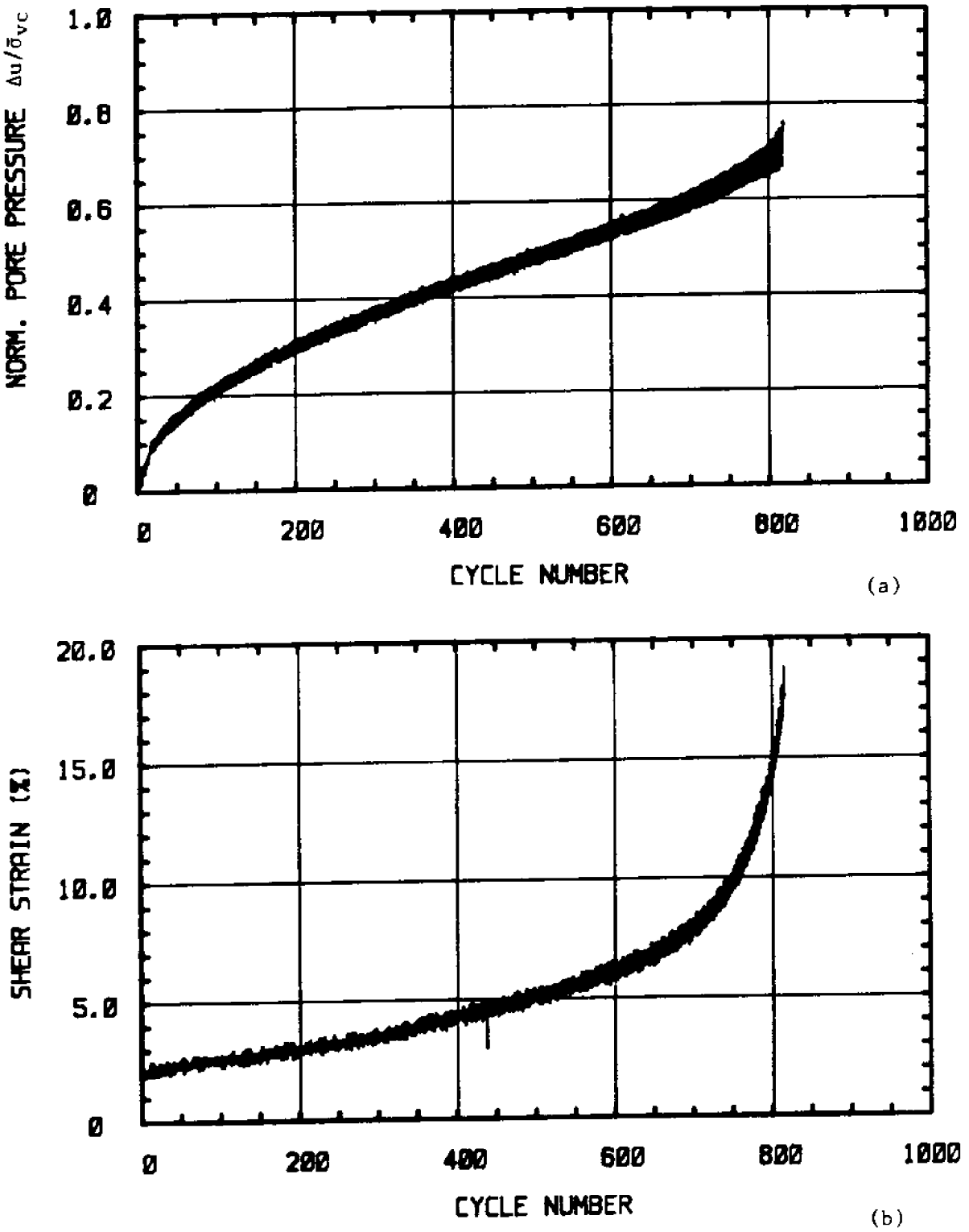

Figure 5.15 Test C-13: N.C. BBC, $\tau_{ave}/s_u(NC) = 0.59$, $\tau_c/s_u(NC) = 0.40$
a) Normalized Excess Pore Pressure versus Cycle Number
b) Shear Strain versus Cycle Number

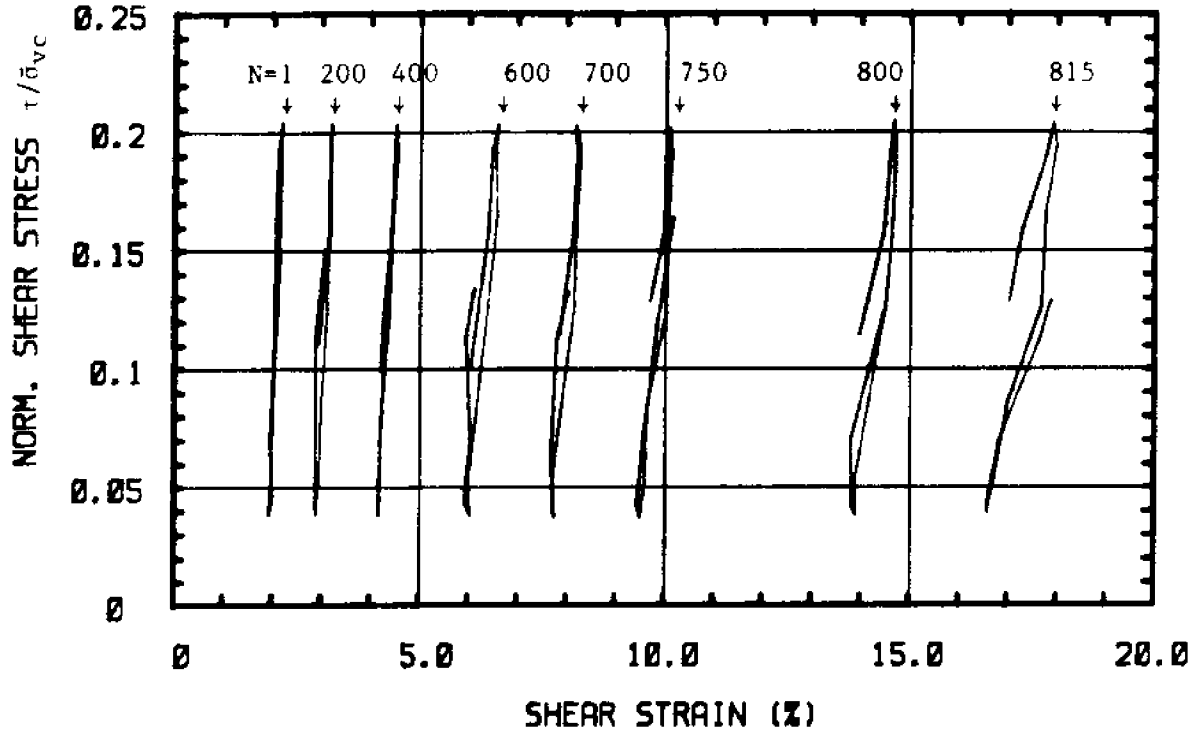

(c)

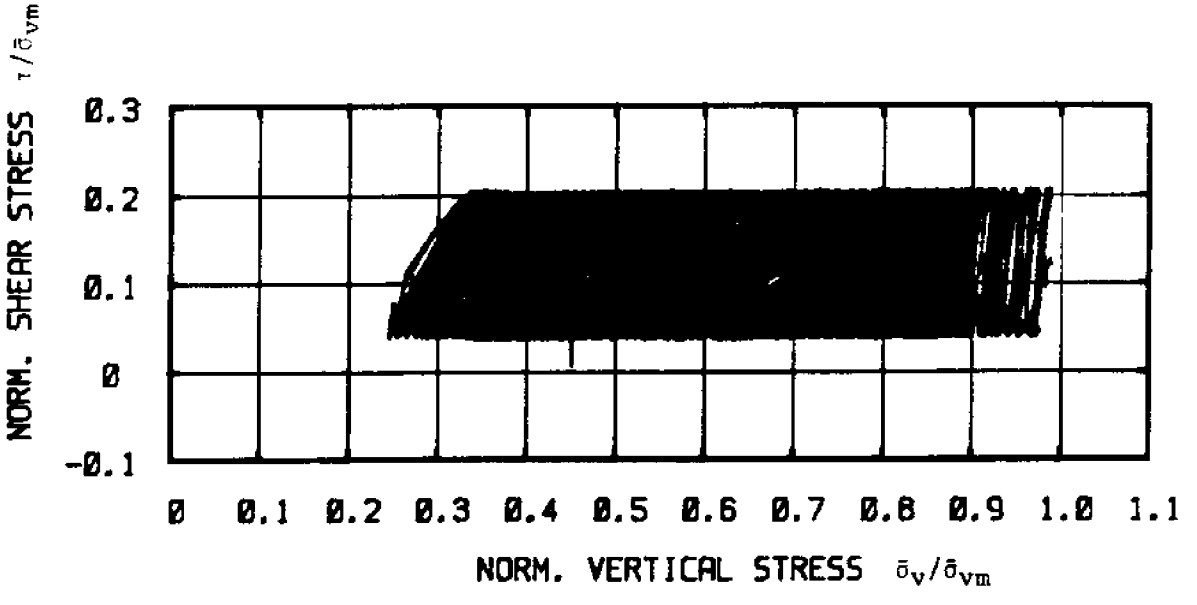

(d)

Figure 5.15 Test C-13: N.C. BBC, $\tau_{ave}/s_u(NC) = 0.59$, $\tau_c/s_u(NC) = 0.40$
c) Normalized Shear Stress versus Shear Strain
d) Normalized Stress Path

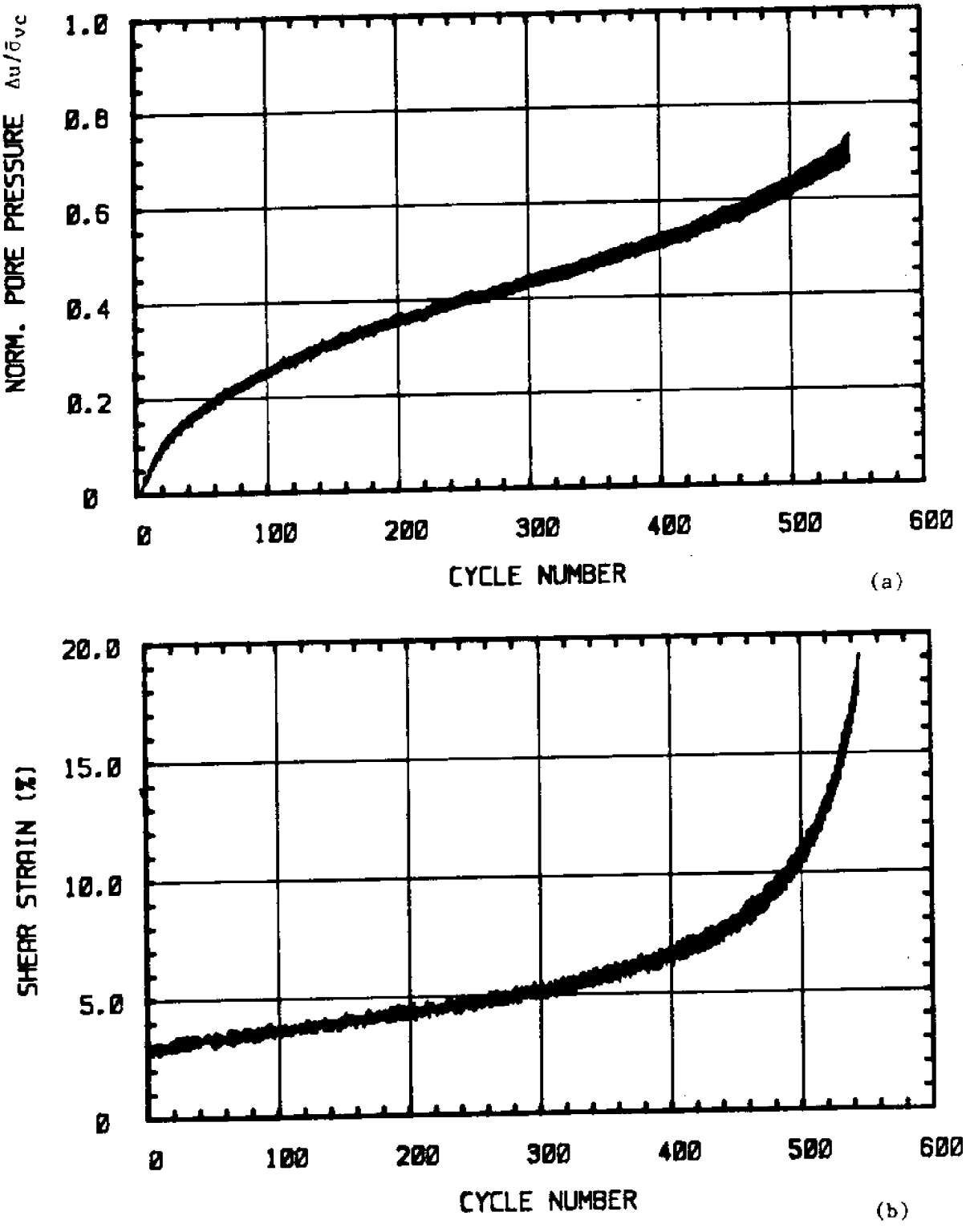

Figure 5.16 Test C-14: N.C. BBC, $\tau_{ave}/s_u(NC) = 0.59$, $\tau_c/s_u(NC) = 0.41$
a) Normalized Excess Pore Pressure versus Cycle Number
b) Shear Strain versus Cycle Number

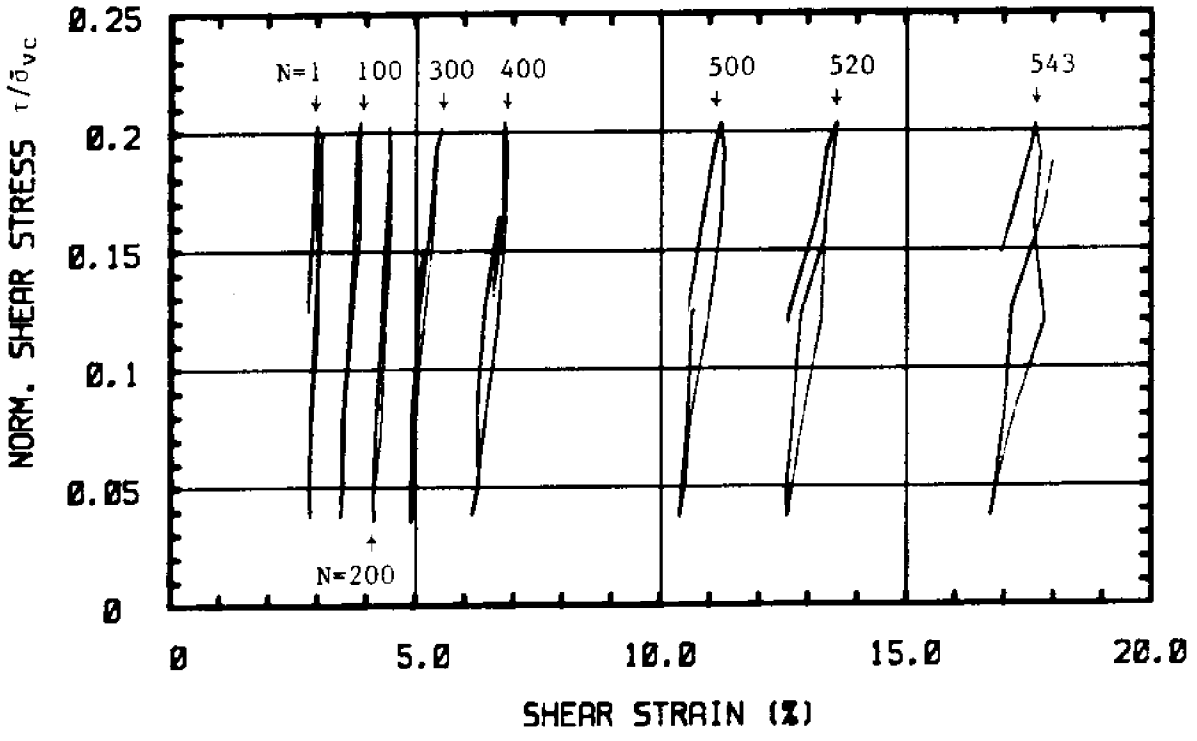

(c)

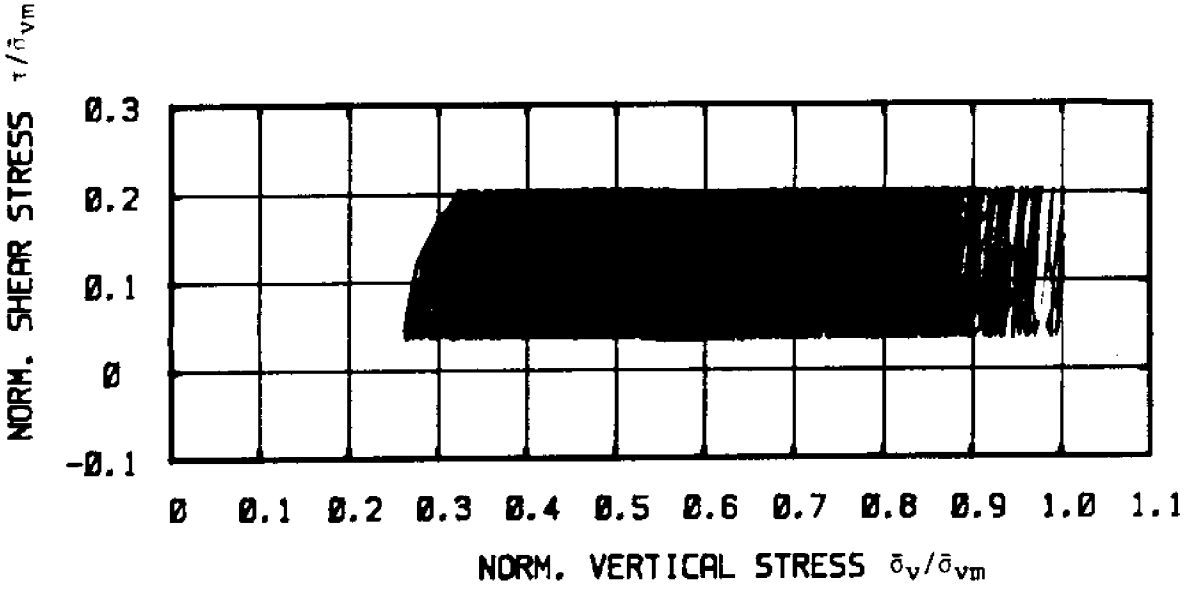

(d)

Figure 5.16 Test C-14: N.C. BBC, $\tau_{ave}/s_u(NC) = 0.59$, $\tau_c/s_u(NC) = 0.41$
c) Normalized Shear Stress versus Shear Strain
d) Normalized Stress Path

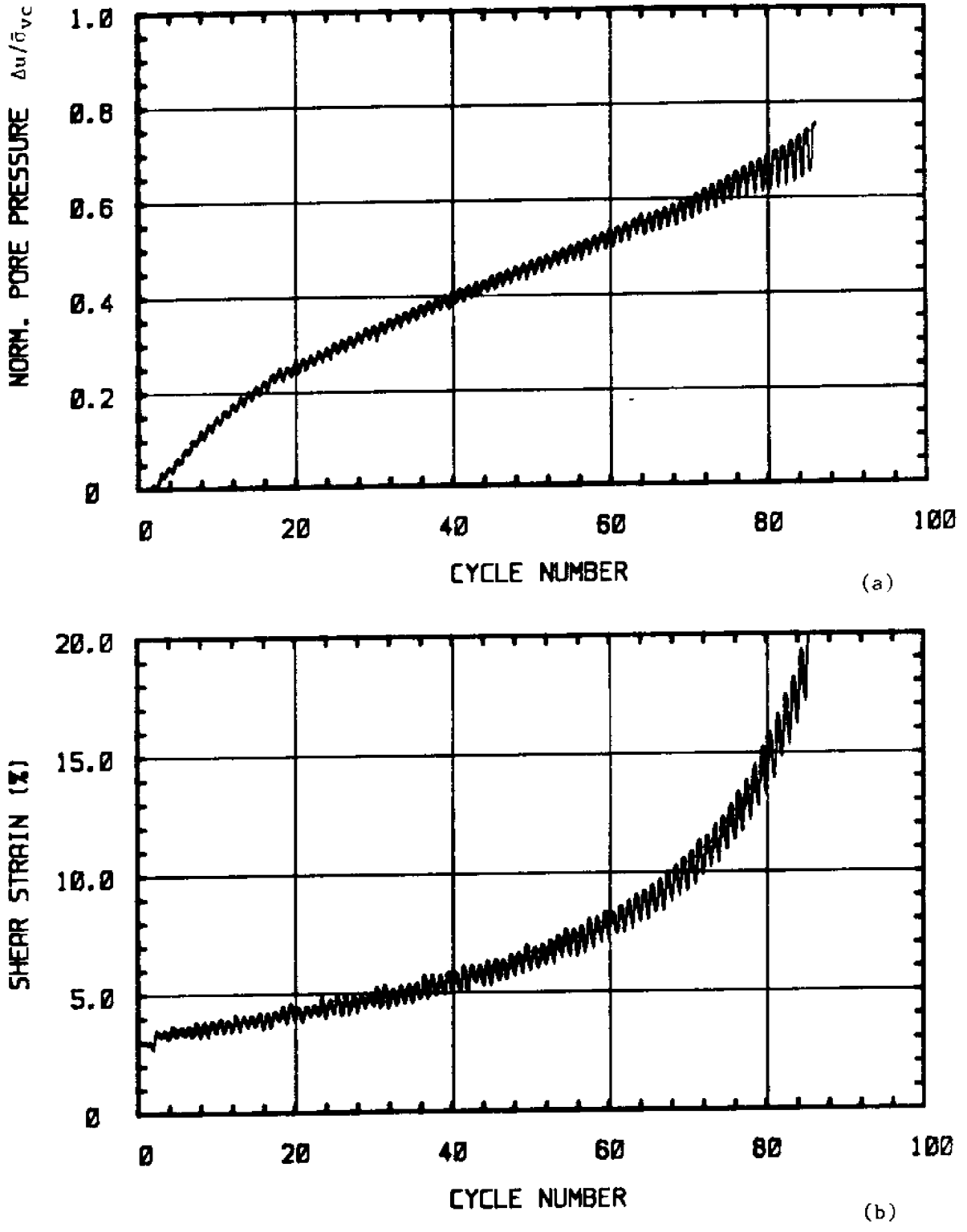

Figure 5.17 Test C-15: N.C. BBC, $\tau_{ave}/s_u(NC) = 0.59$, $\tau_c/s_u(NC) = 0.50$
a) Normalized Excess Pore Pressure versus Cycle Number
b) Shear Strain versus Cycle Number

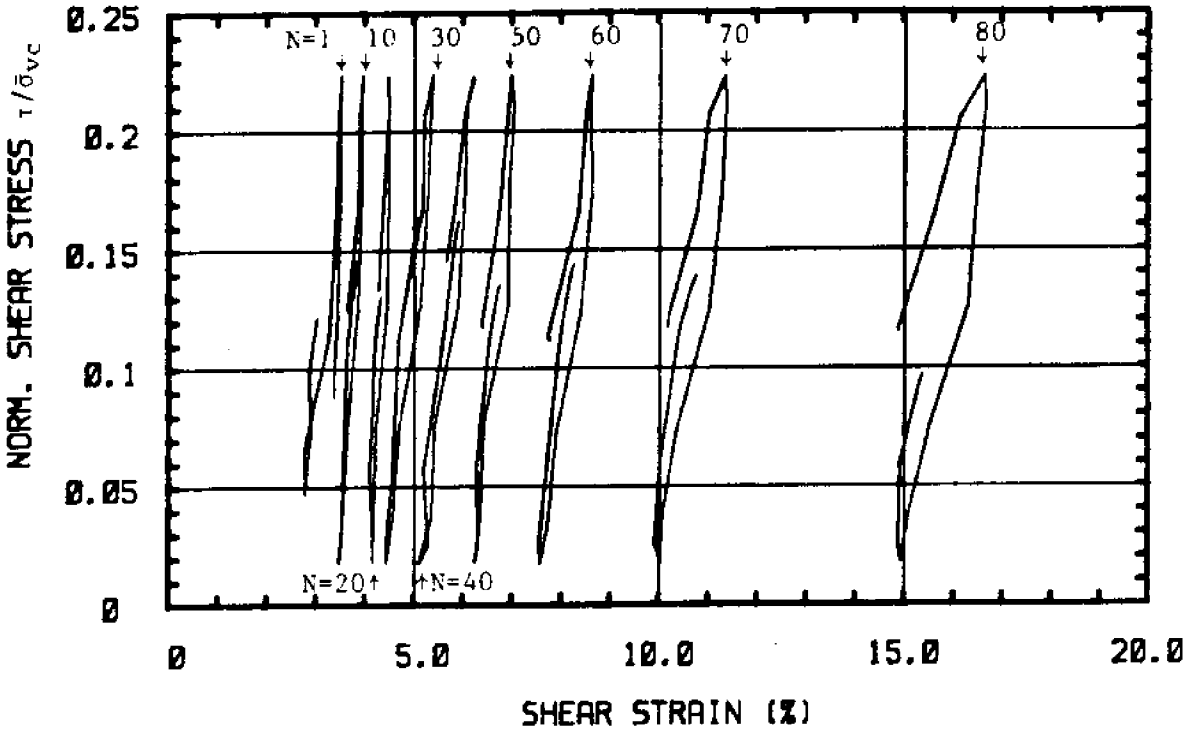

(c)

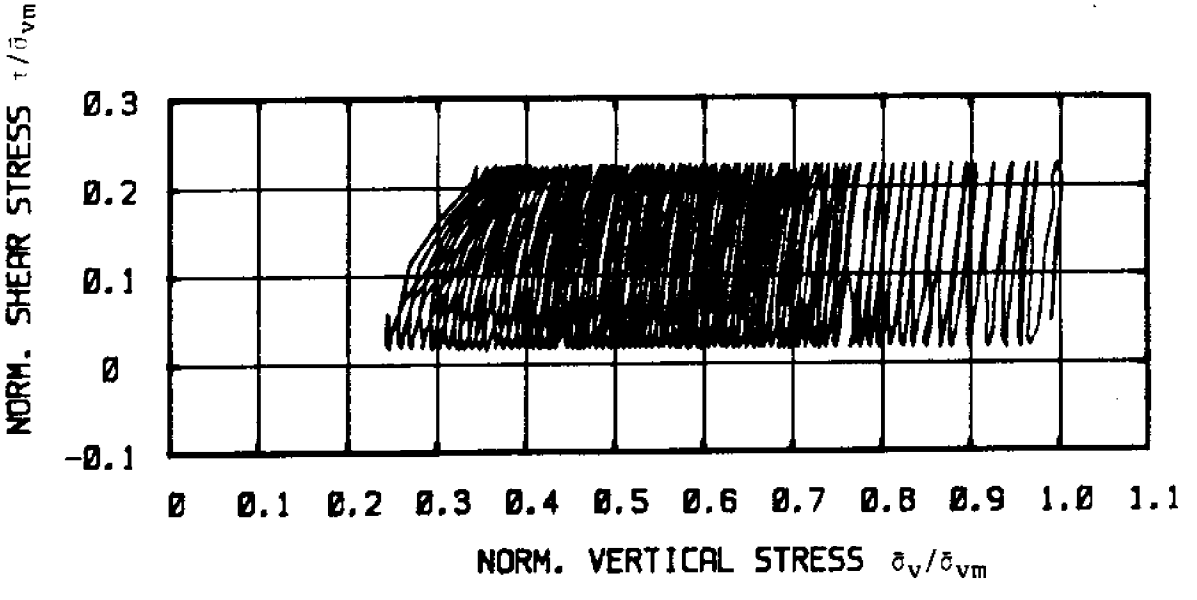

(d)

Figure 5.17 Test C-15: N.C. BBC, $\tau_{ave}/s_u(NC) = 0.59$, $\tau_c/s_u(NC) = 0.50$
c) Normalized Shear Stress versus Shear Strain
d) Normalized Stress Path

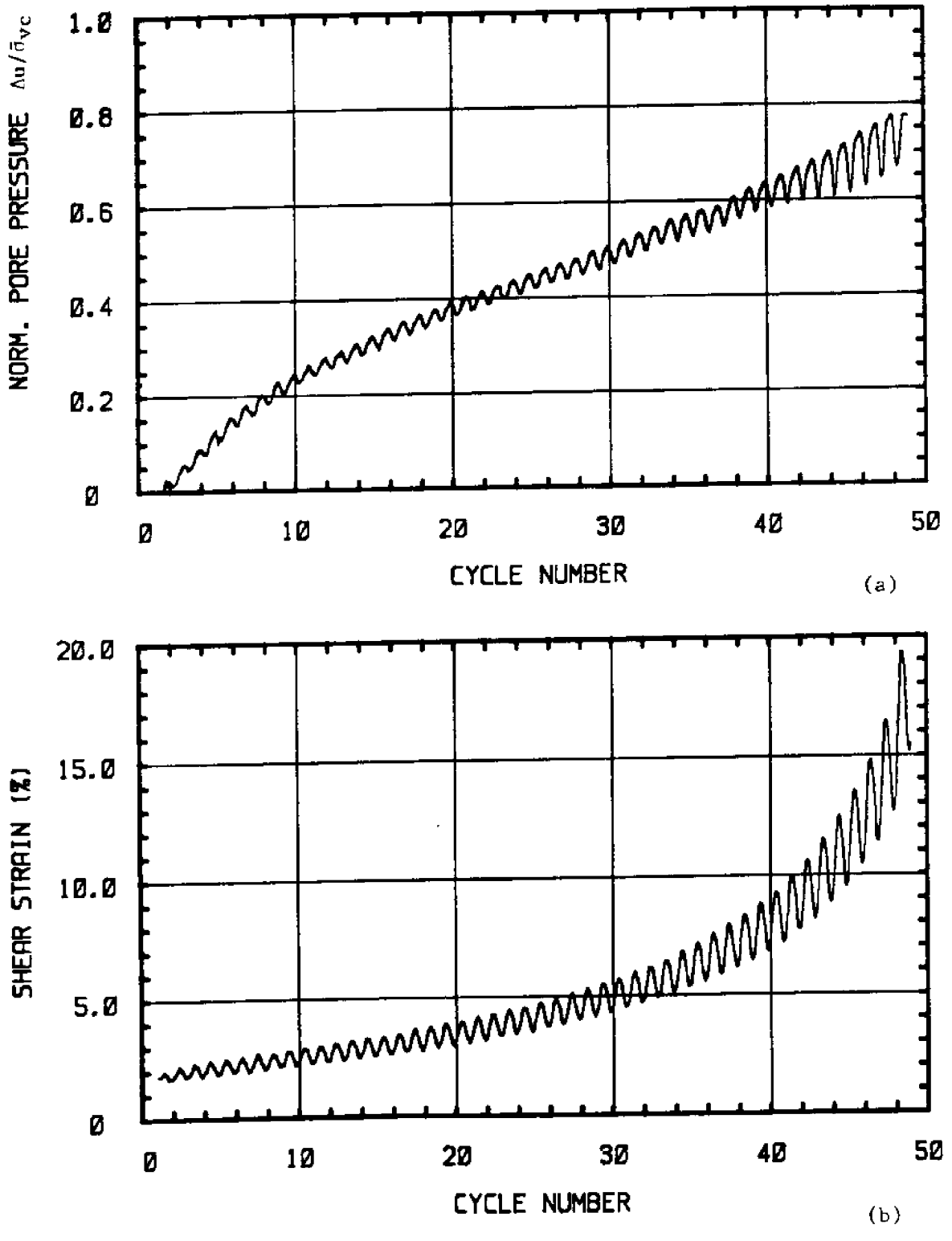

Figure 5.18 Test C-16: N.C. BBC, $\tau_{ave}/s_u(NC) = 0.49$, $\tau_c/s_u(NC) = 0.60$
a) Normalized Excess Pore Pressure versus Cycle Number
b) Shear Strain versus Cycle Number

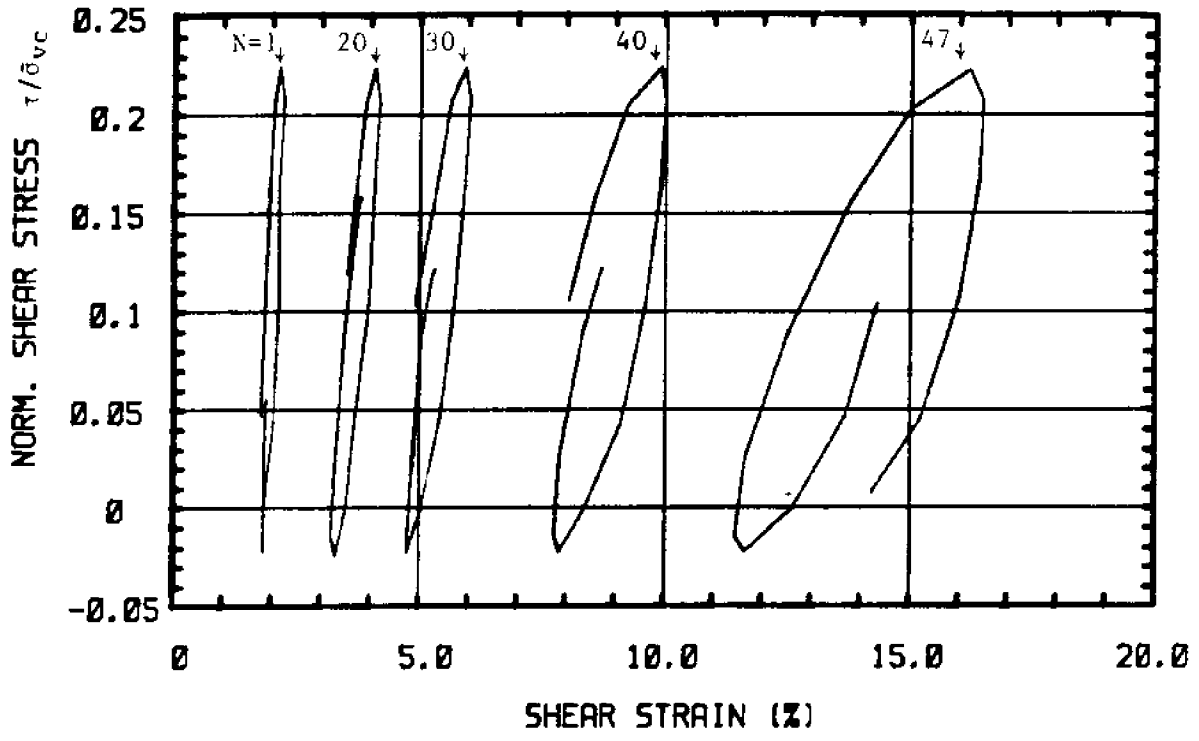

(c)

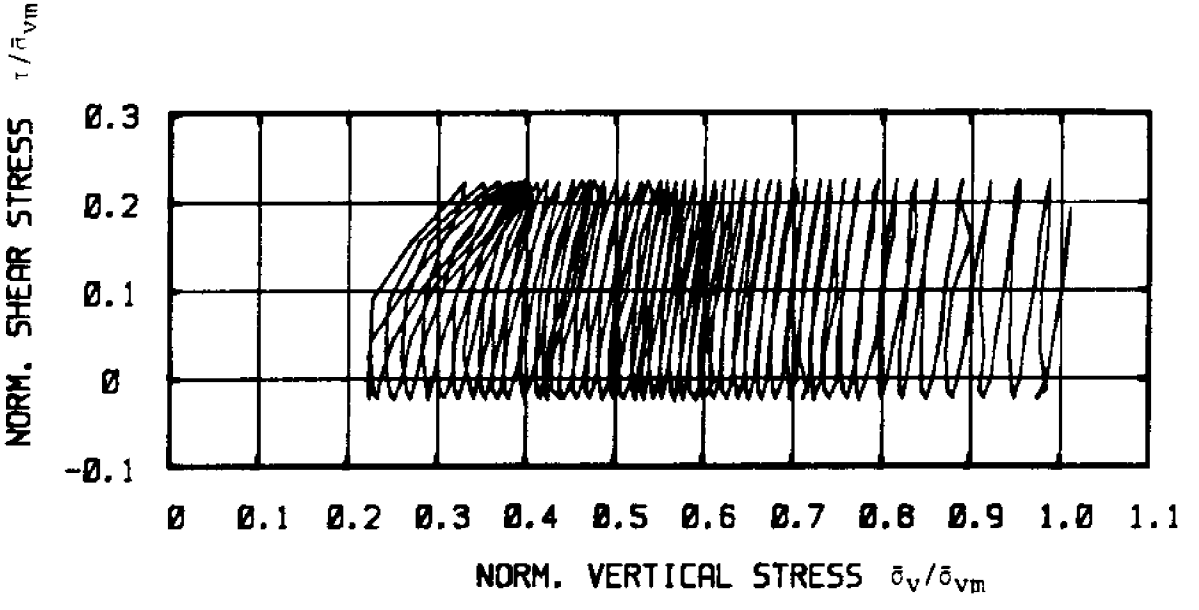

(d)

Figure 5.18 Test C-16: N.C. BBC, $\tau_{ave}/s_u(NC) = 0.49$, $\tau_c/s_u(NC) = 0.60$
c) Normalized Shear Stress versus Shear Strain
d) Normalized Stress Path

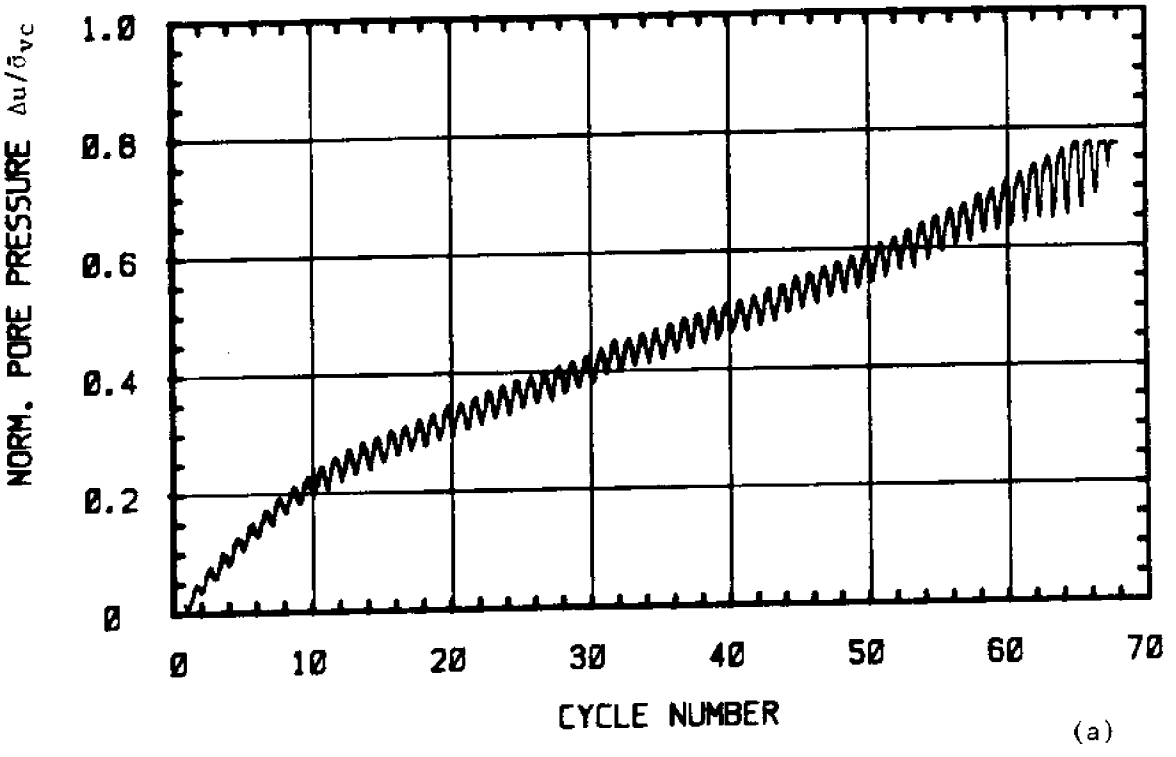

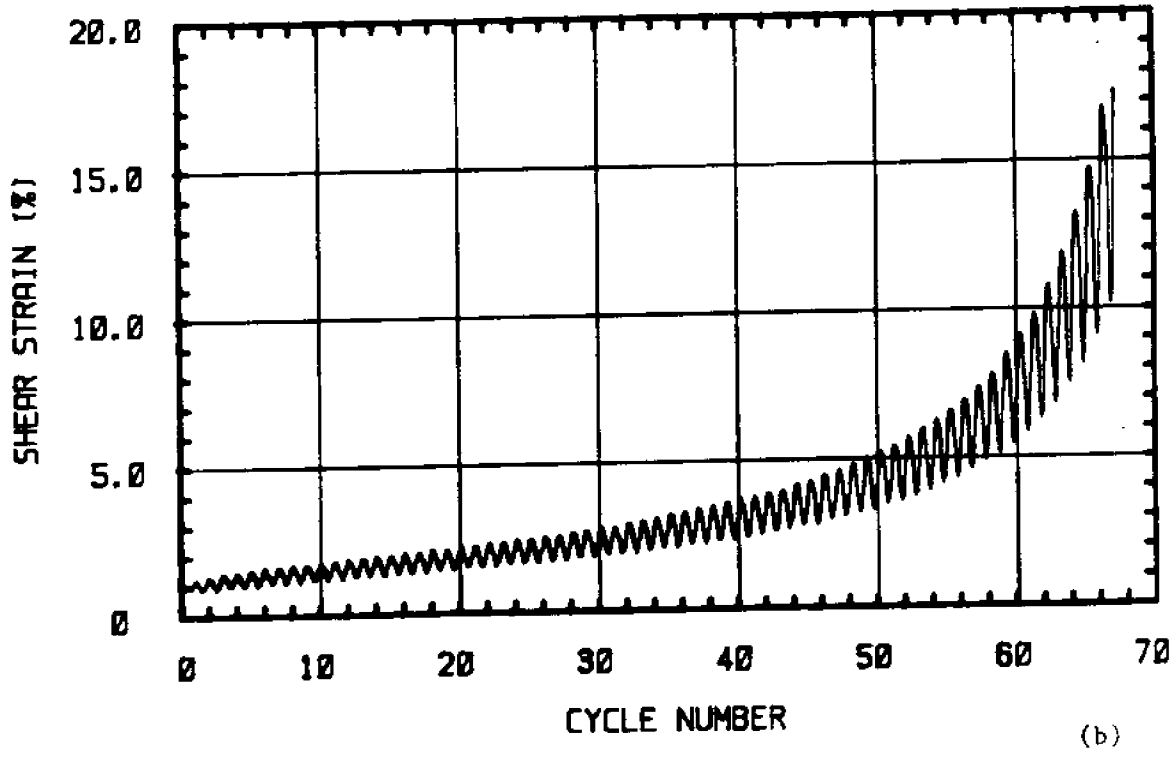

Figure 5.19 Test C-18: N.C. BBC, $\tau_{ave}/s_u(NC) = 0.39$, $\tau_c/s_u(NC) = 0.60$
a) Normalized Excess Pore Pressure versus Cycle Number
b) Shear Strain versus Cycle Number

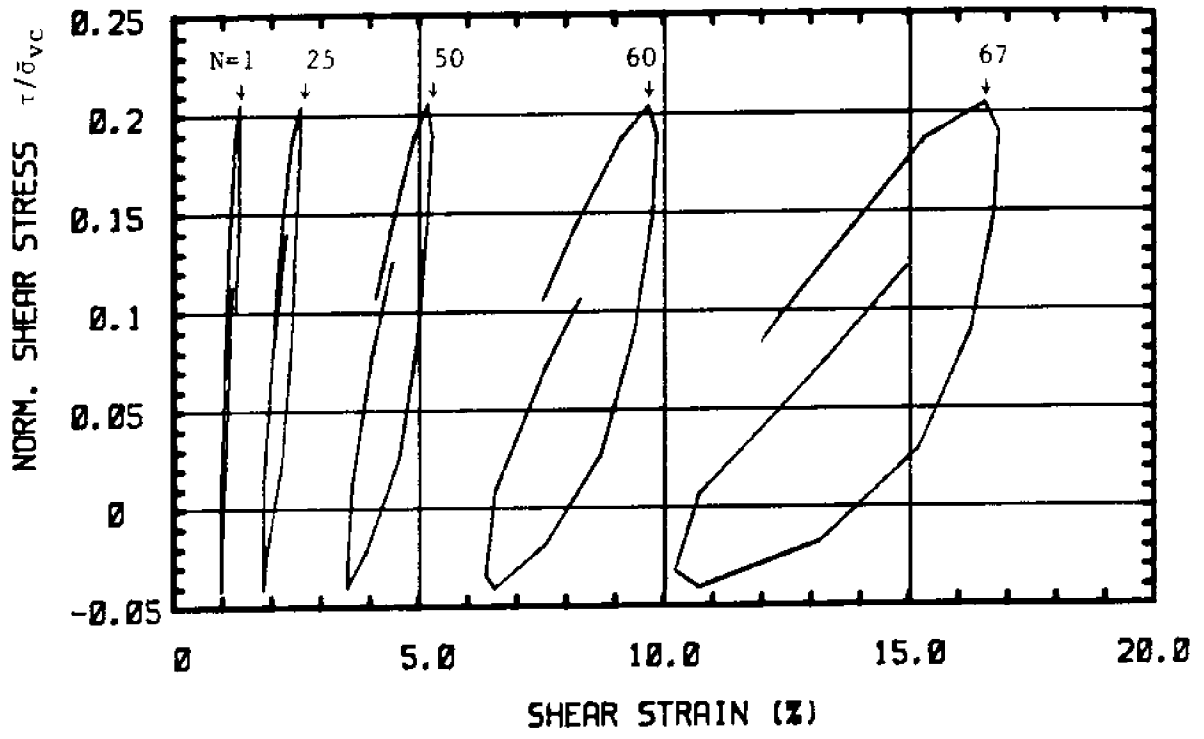

(c)

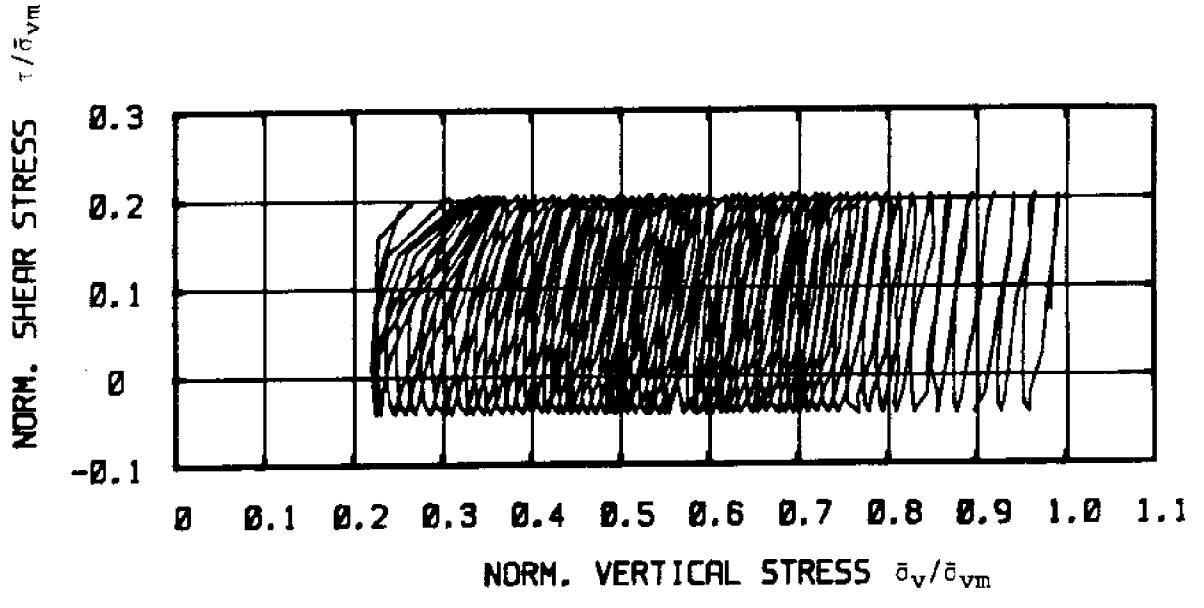

(d)

Figure 5.19 Test C-18: N.C. BBC, $\tau_{ave}/s_u(NC) = 0.39$, $\tau_c/s_u(NC) = 0.60$
c) Normalized Shear Stress versus Shear Strain
d) Normalized Stress Path

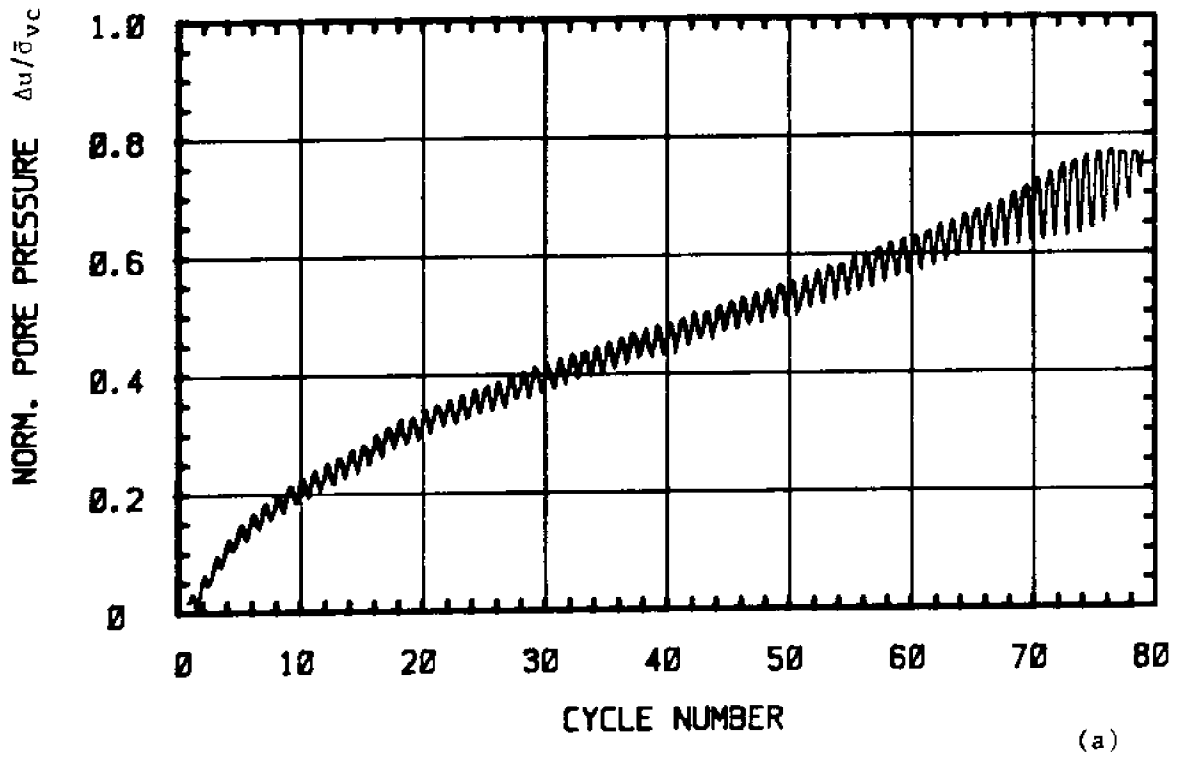

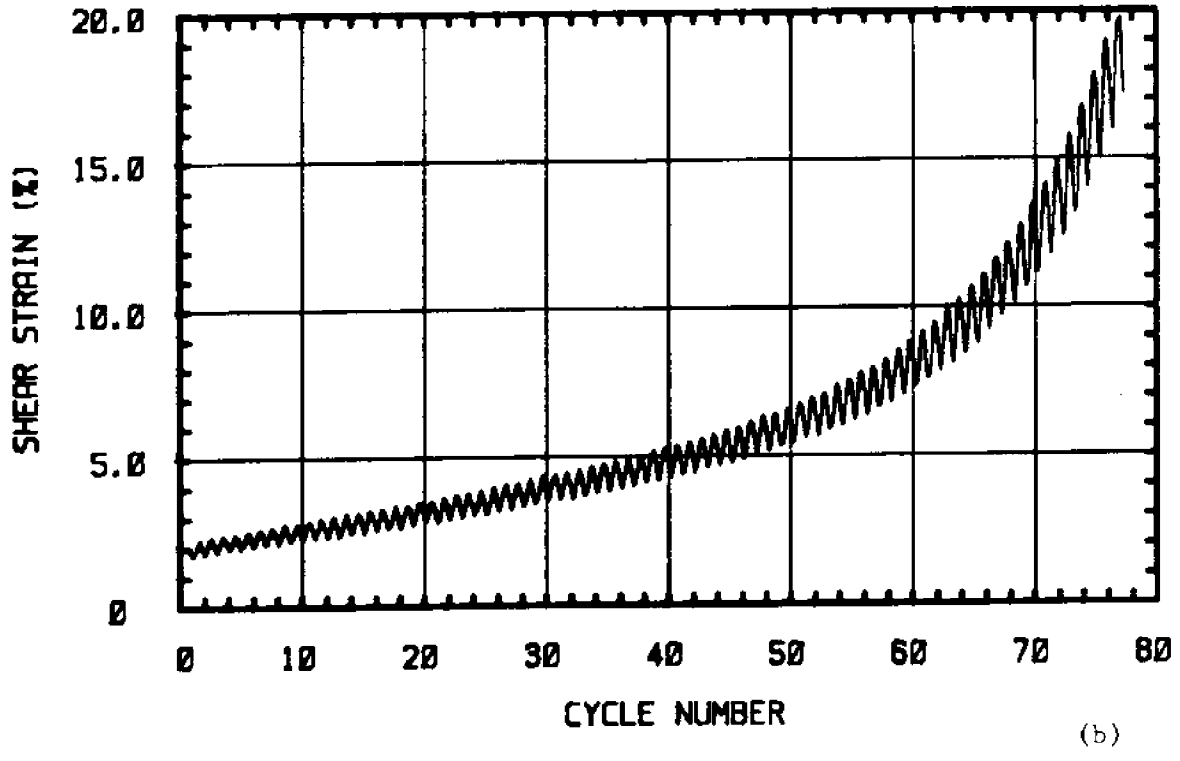

Figure 5.20 Test C-19: N.C. BBC, $\tau_{ave}/s_u(NC) = 0.50$, $\tau_c/s_u(NC) = 0.51$
a) Normalized Excess Pore Pressure versus Cycle Number
b) Shear Strain versus Cycle Number

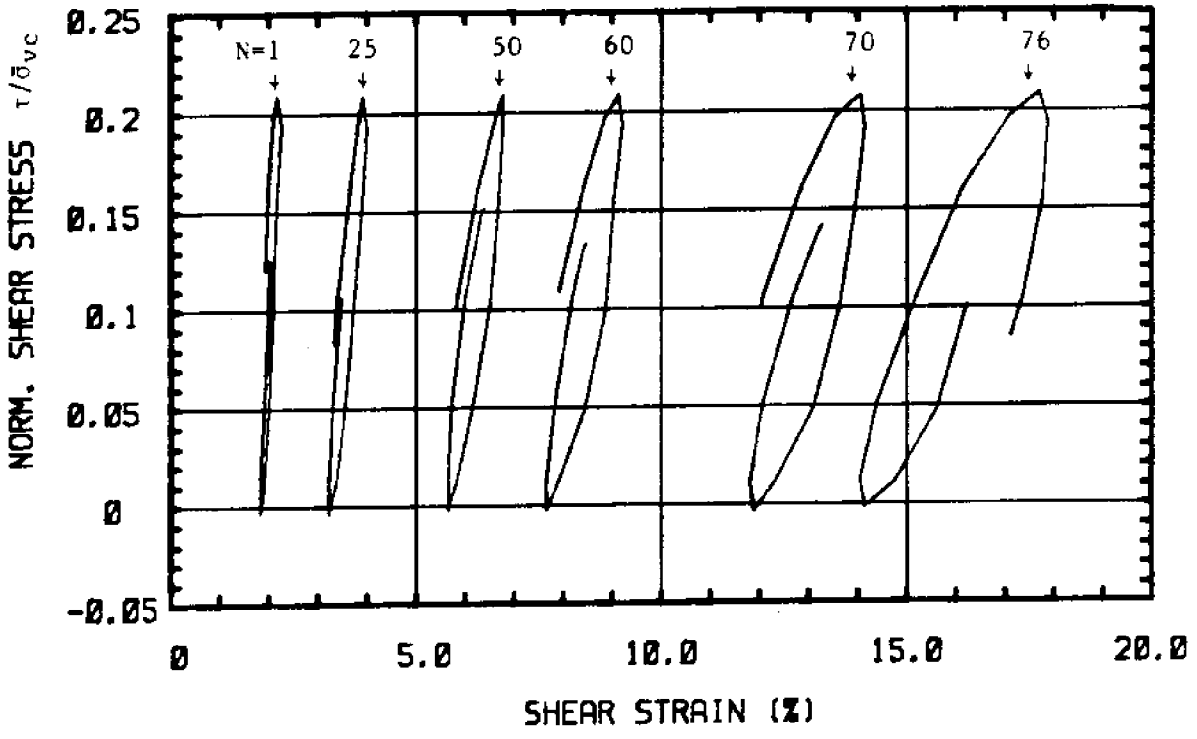

(c)

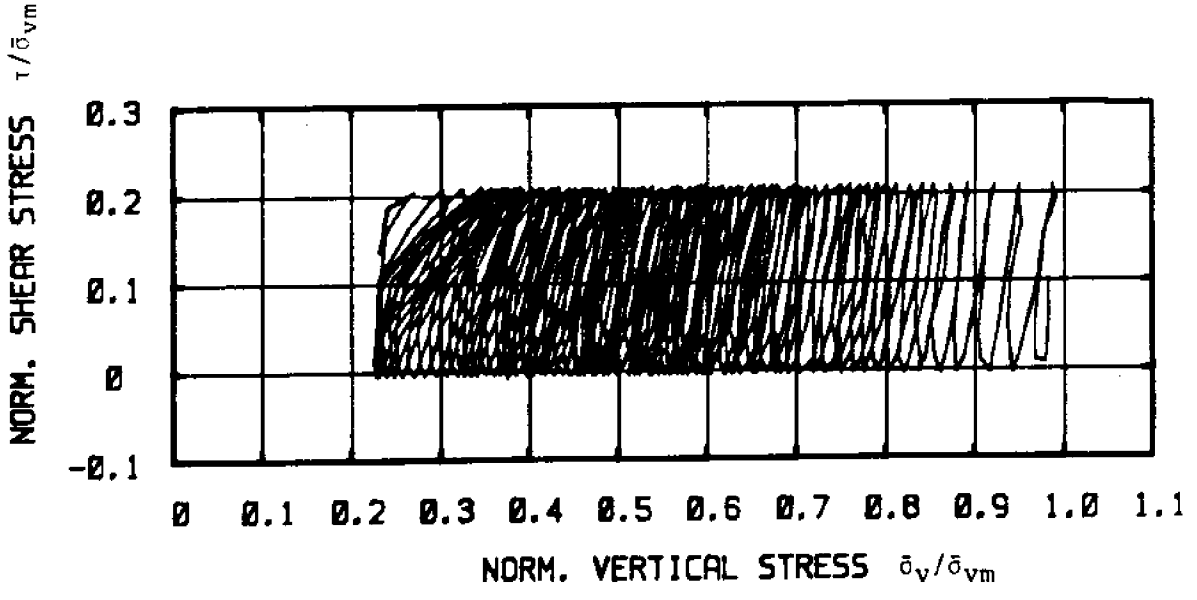

(d)

Figure 5.20 Test C-19: N.C. BBC, $\tau_{ave}/s_u(NC) = 0.50$, $\tau_c/s_u(NC) = 0.51$
c) Normalized Shear Stress versus Shear Strain
d) Normalized Stress Path

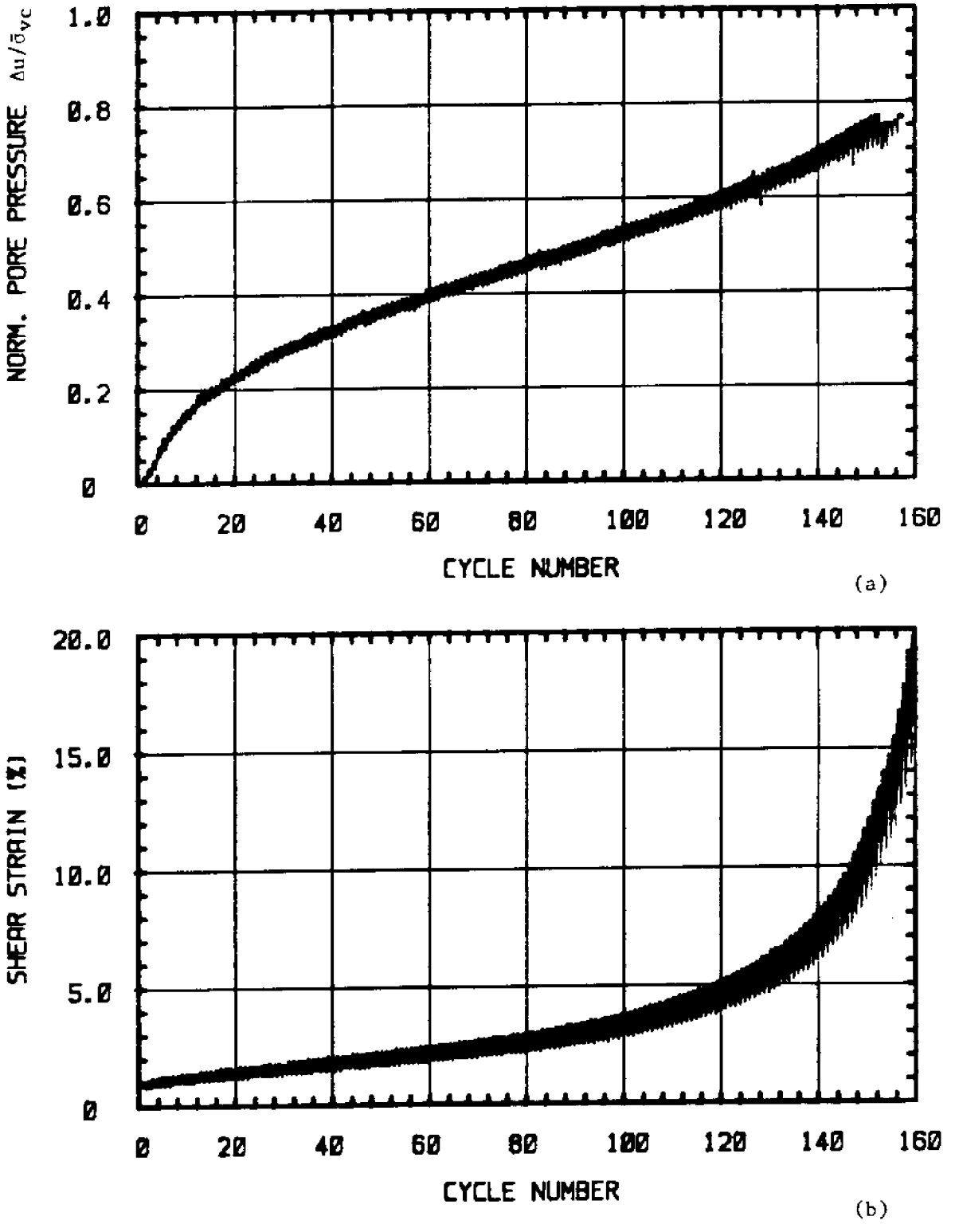

Figure 5.21 Test C-20: N.C. BBC, $\tau_{ave}/s_u(NC) = 0.40$, $\tau_c/s_u(NC) = 0.51$
a) Normalized Excess Pore Pressure versus Cycle Number
b) Shear Strain versus Cycle Number

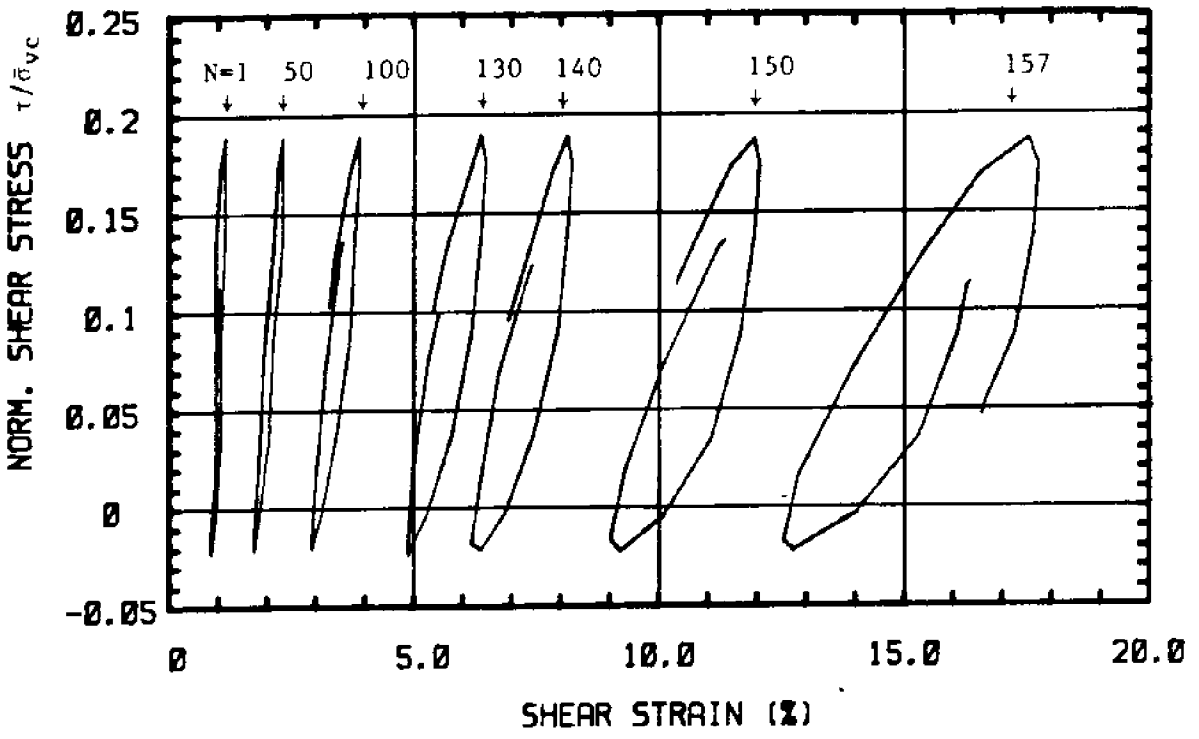

(c)

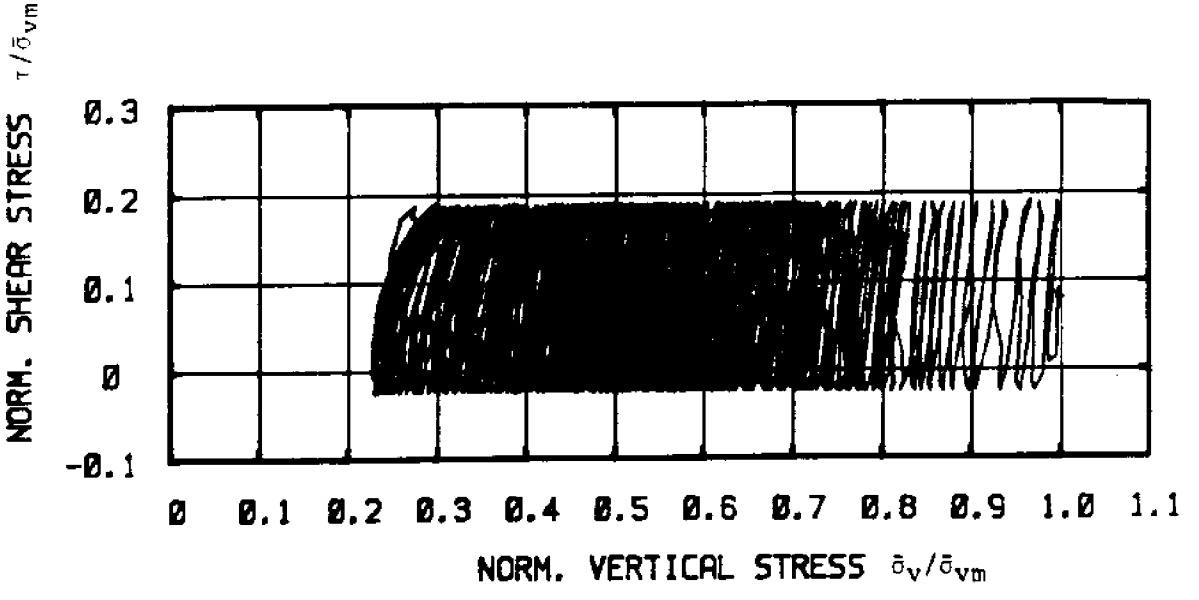

(d)

Figure 5.21 Test C-20: N.C. BBC, $\tau_{ave}/s_u(NC) = 0.40$, $\tau_c/s_u(NC) = 0.51$
c) Normalized Shear Stress versus Shear Strain
d) Normalized Stress Path

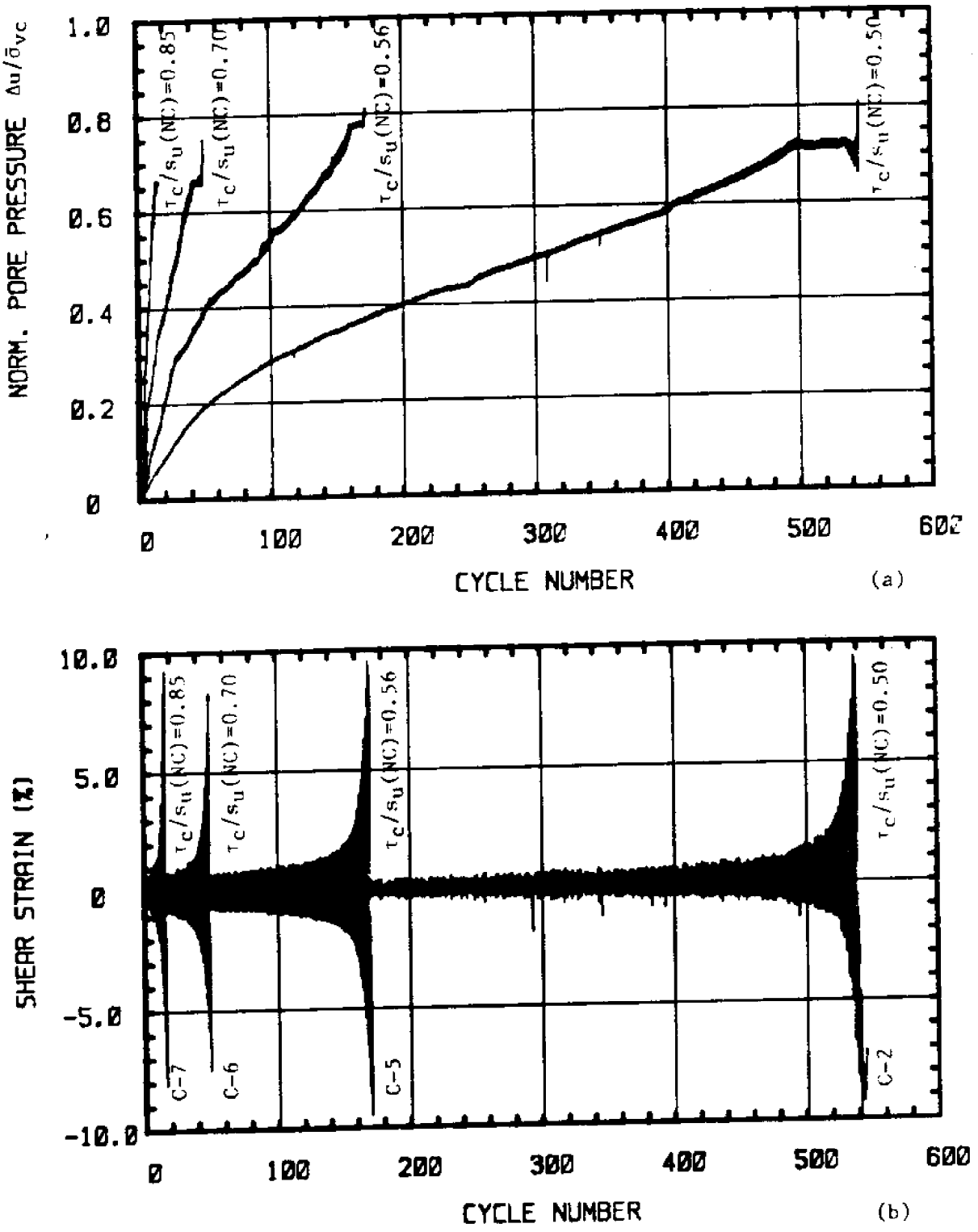

Figure 5.22 Effect of $\tau_c/s_u(NC)$ on Cyclic Behavior, $\tau_{ave} = 0$
a) Normalized Excess Pore Pressure versus Cycle Number
b) Shear Strain versus Cycle Number

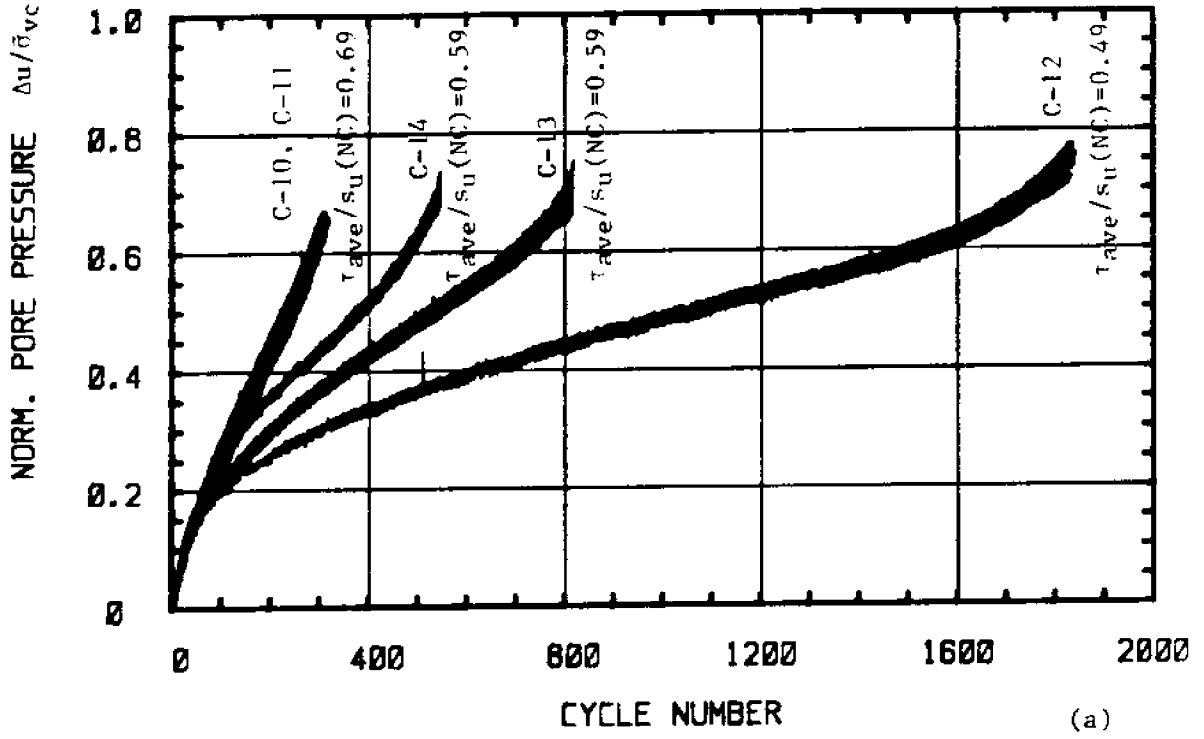

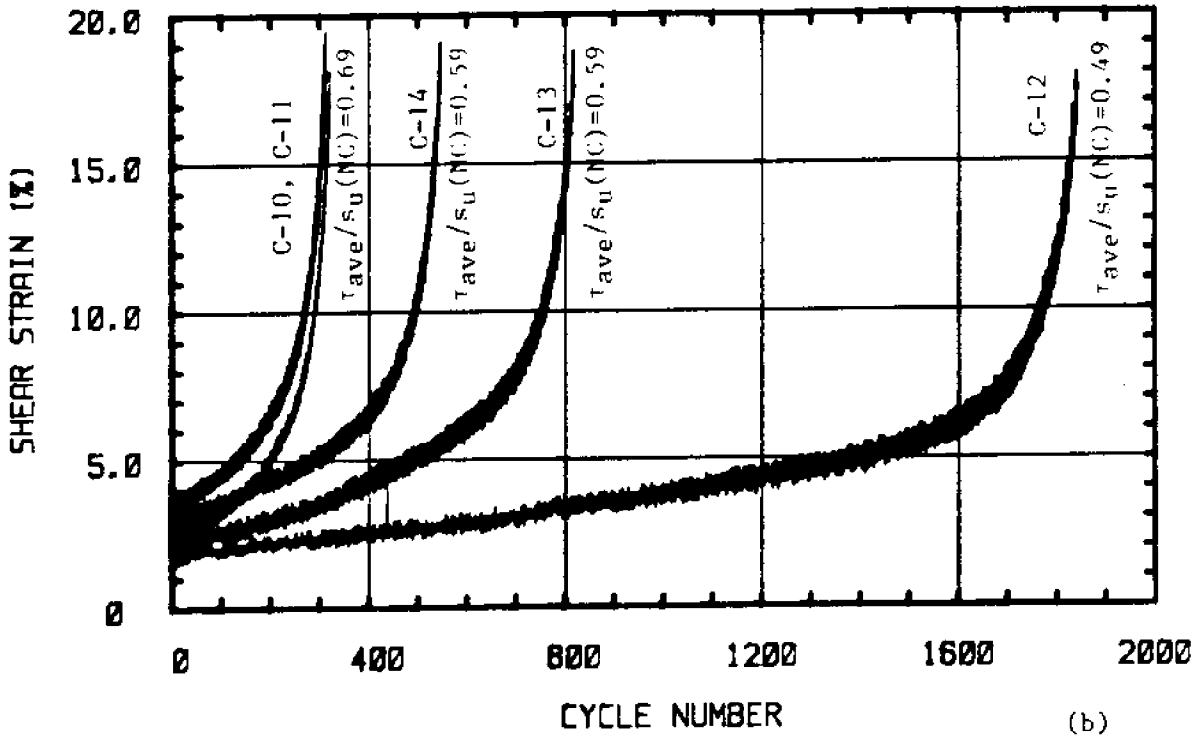

Figure 5.23 Effect of $\tau_{ave}/s_u(NC)$ on Cyclic Behavior, $\tau_c/s_u(NC)=0.40$
a) Normalized Excess Pore Pressure versus Cycle Number
b) Shear Strain versus Cycle Number

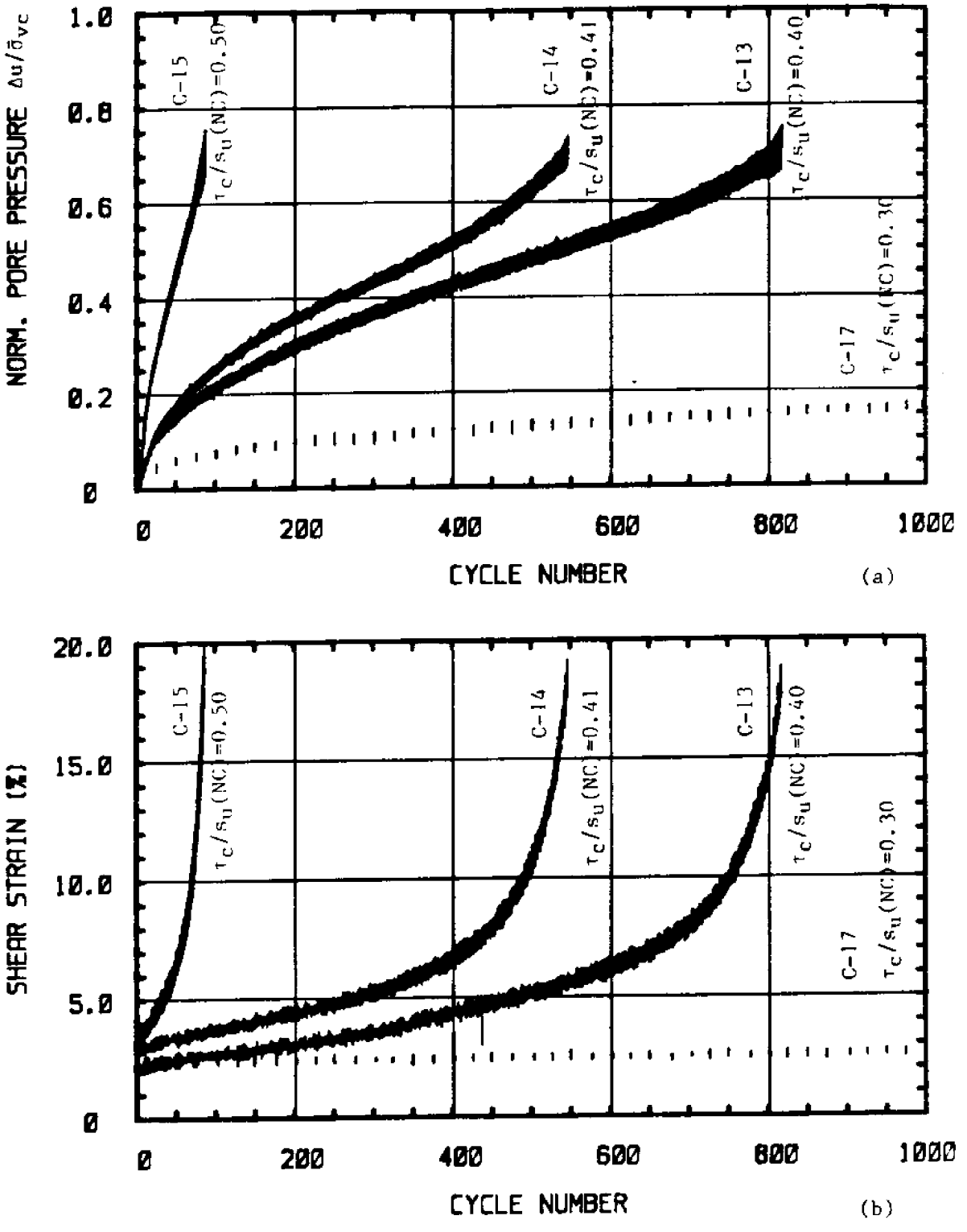

Figure 5.24 Effect of $\tau_c/s_u(NC)$ on Cyclic Behavior, $\tau_{ave}/s_u(NC)=0.59$
a) Normalized Excess Pore Pressure versus Cycle Number
b) Shear Strain versus Cycle Number

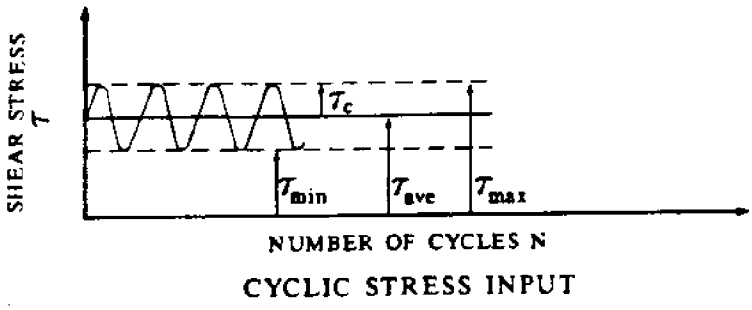

CYCLIC STRESS INPUT

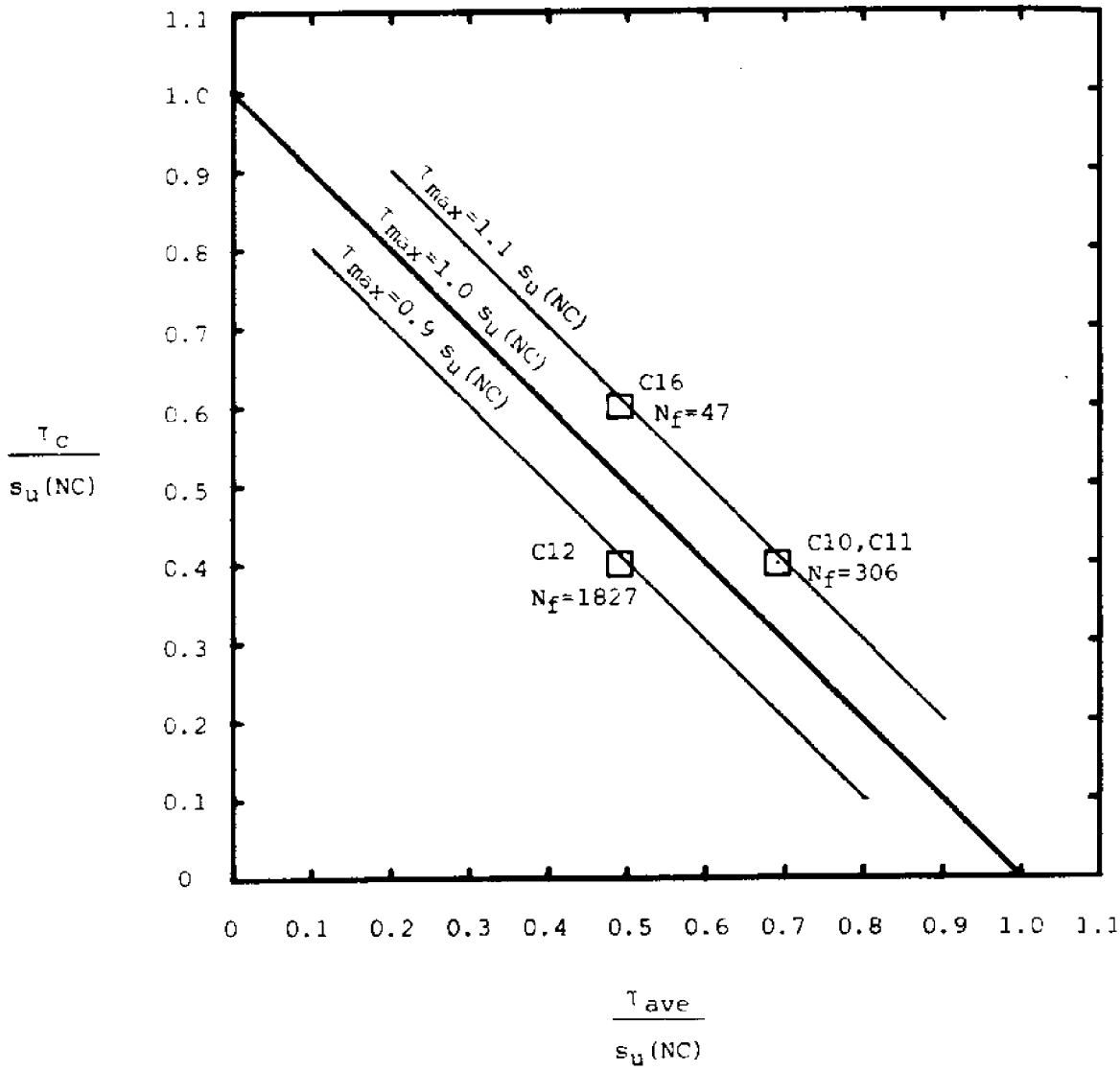

Figure 5.25 Comparison of the Effect of $\tau_{ave}/s_u(NC)$ and $\tau_c/s_u(NC)$ on Number of Cycles at Failure

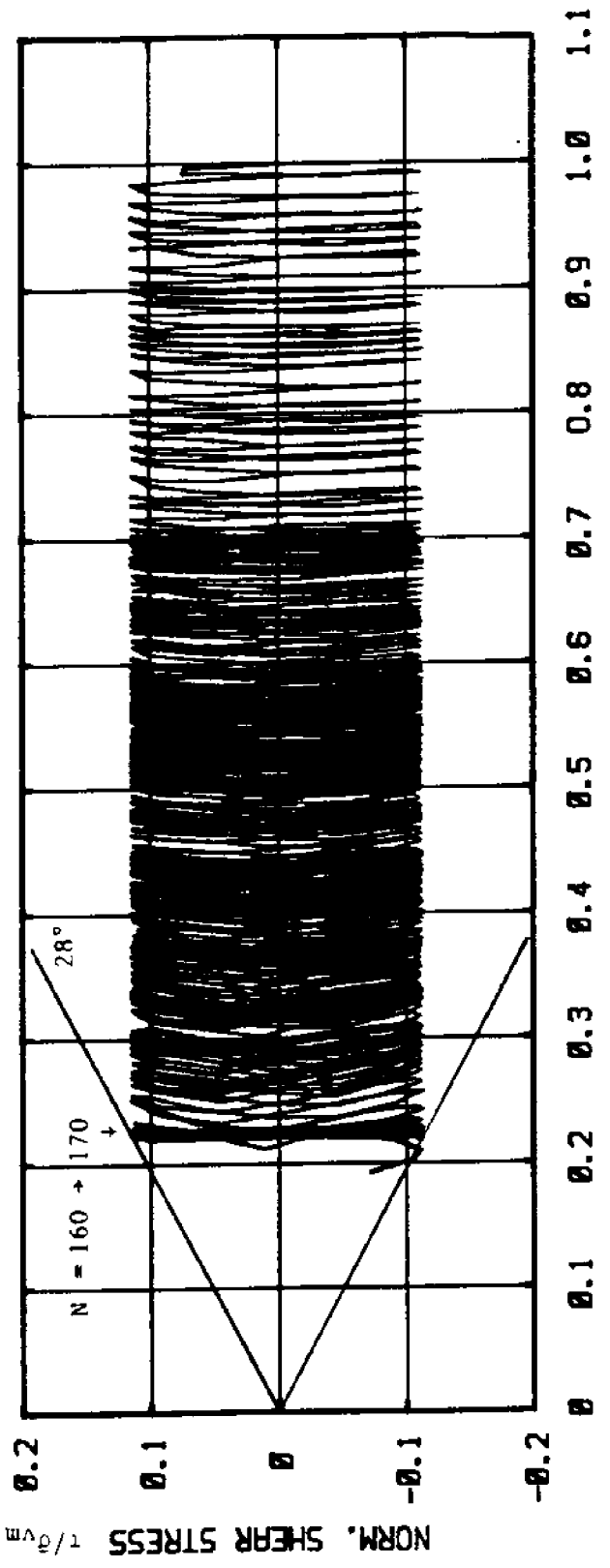

Figure 5.26 Normalized Stress Path and Obliquity at Failure
Test C-5: N.C. BBC, τ_{ave} = 0, $\tau_c/s_u(NC)$ = 0.56

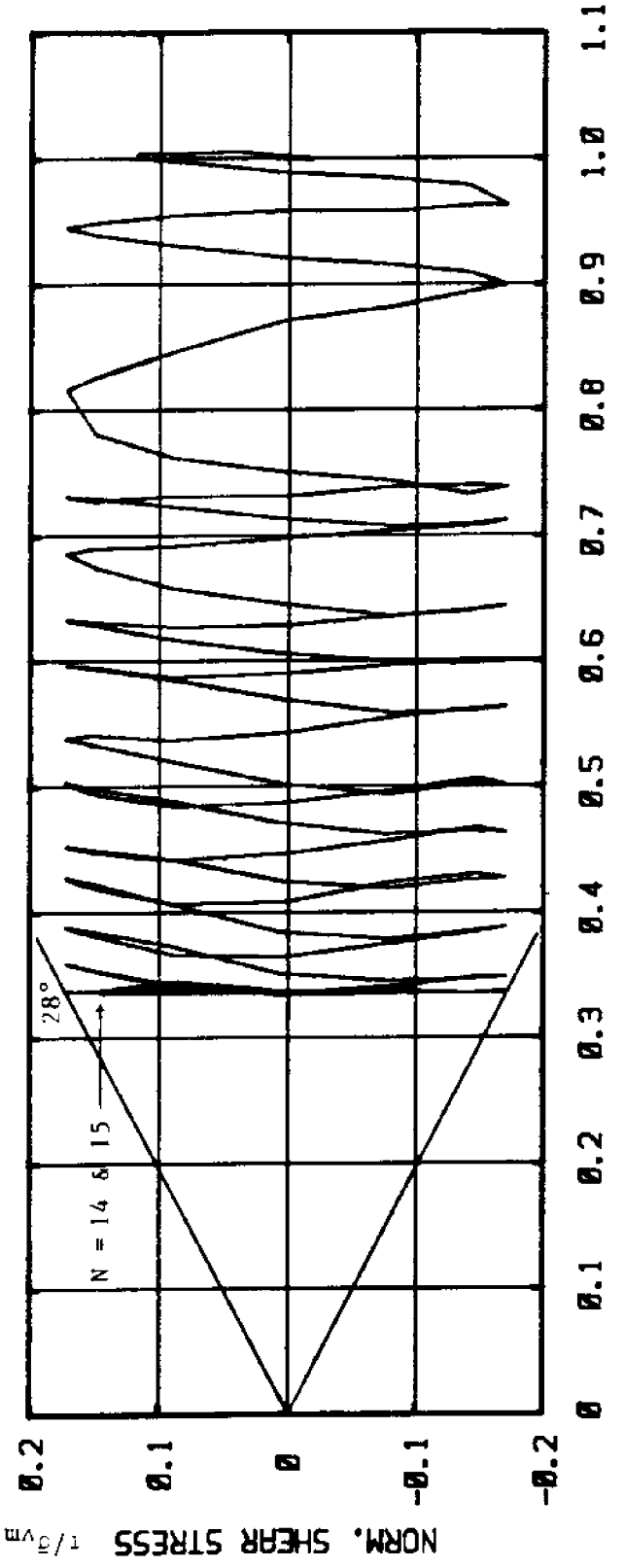

Figure 5.27 Normalized Stress Path and Obliquity at Failure
Test C-7: N.C., BBC, $\tau_{ave} = 0$, $\tau_c/s_u(NC) = 0.85$

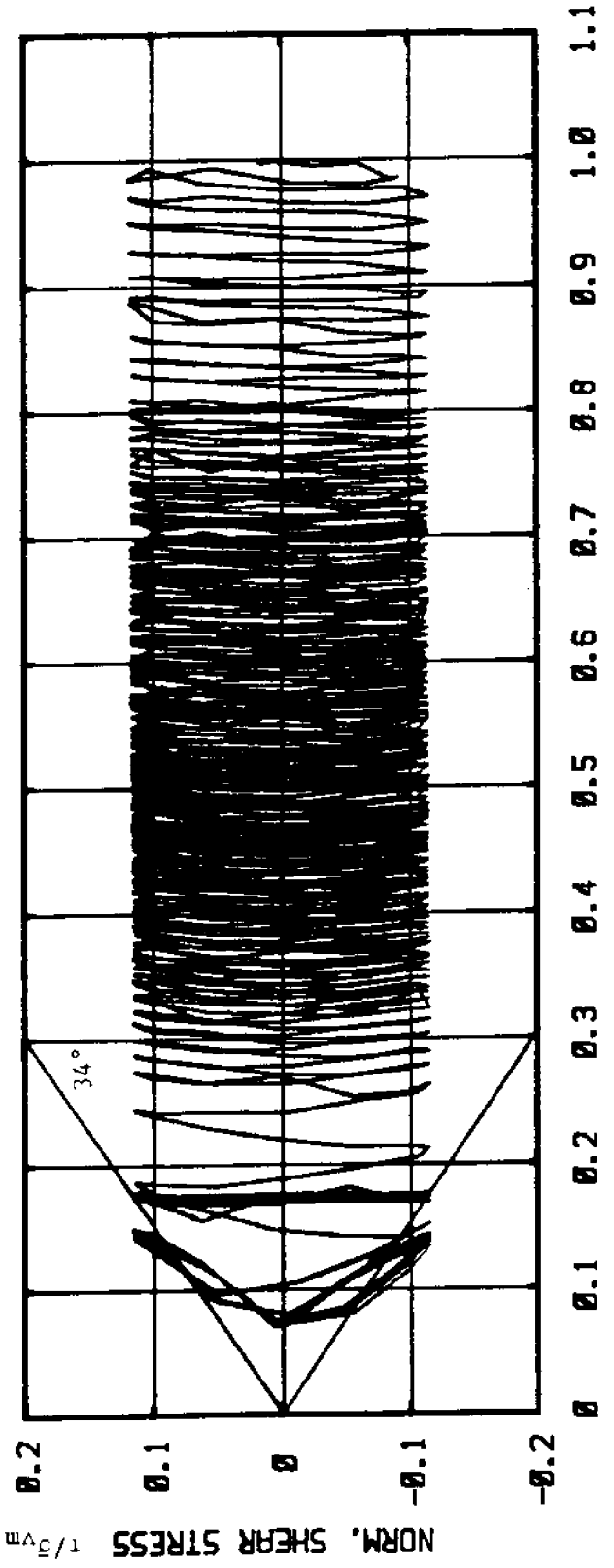

Figure 5.28 Normalized Stress Path and Obliquity at Failure
Test C-30: N.C. BBC, $\tau_{ave} = 0$, $\tau_c/s_u(NC) = 0.56$

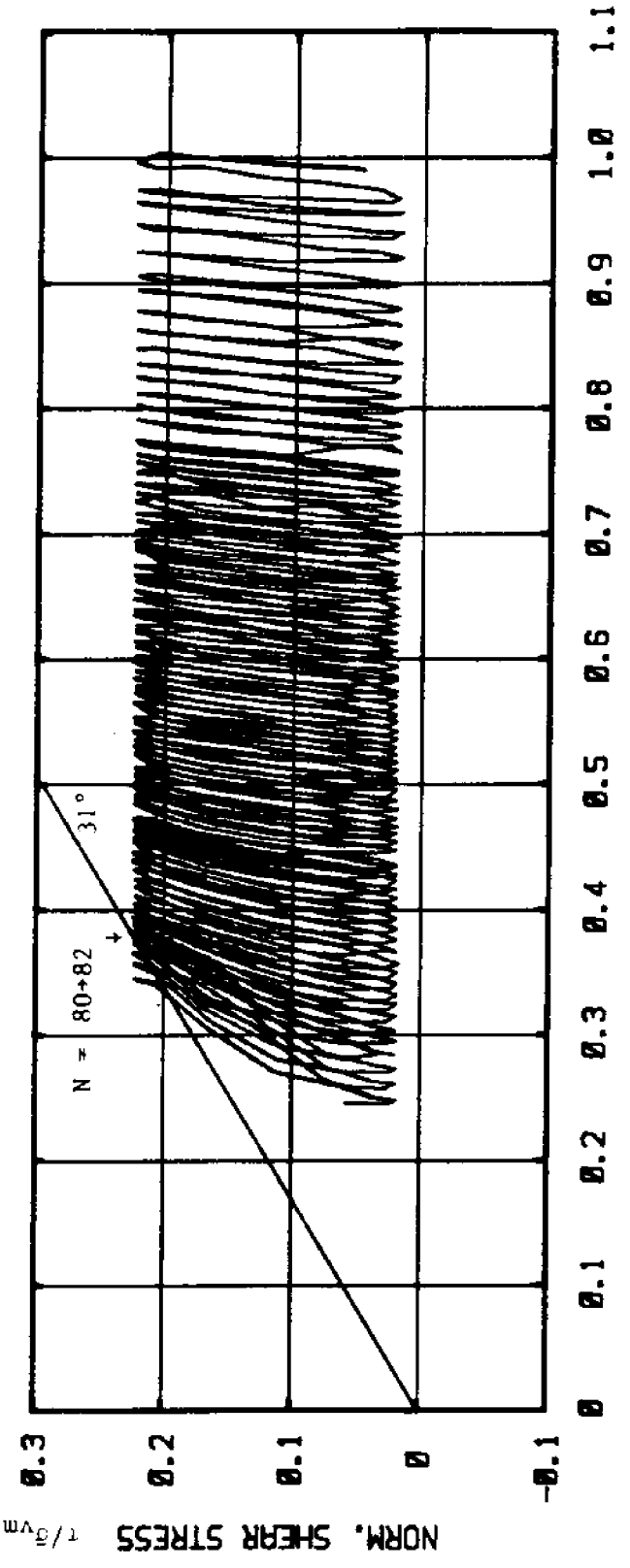

Figure 5.29 Normalized Stress Path and Obliquity at Failure
Test C-15: N.C. BBC, $\tau_{ave}/s_u(NC) = 0.59$, $\tau_c/s_u(NC) = 0.50$

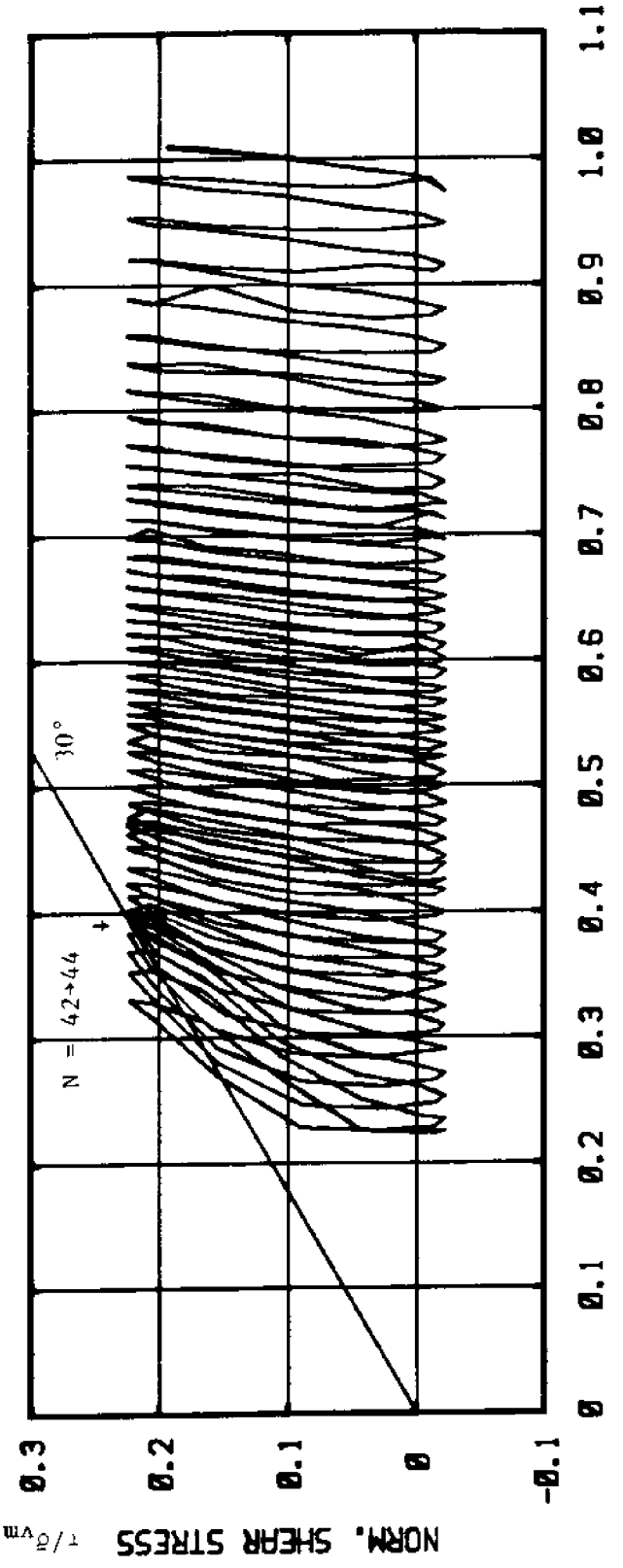

Figure 5.30 Normalized Stress Path and Obliquity at Failure
Test C-16: N.C. BBC, $\tau_{ave}/s_u(NC) = 0.49$, $\tau_c/s_u(NC) = 0.60$

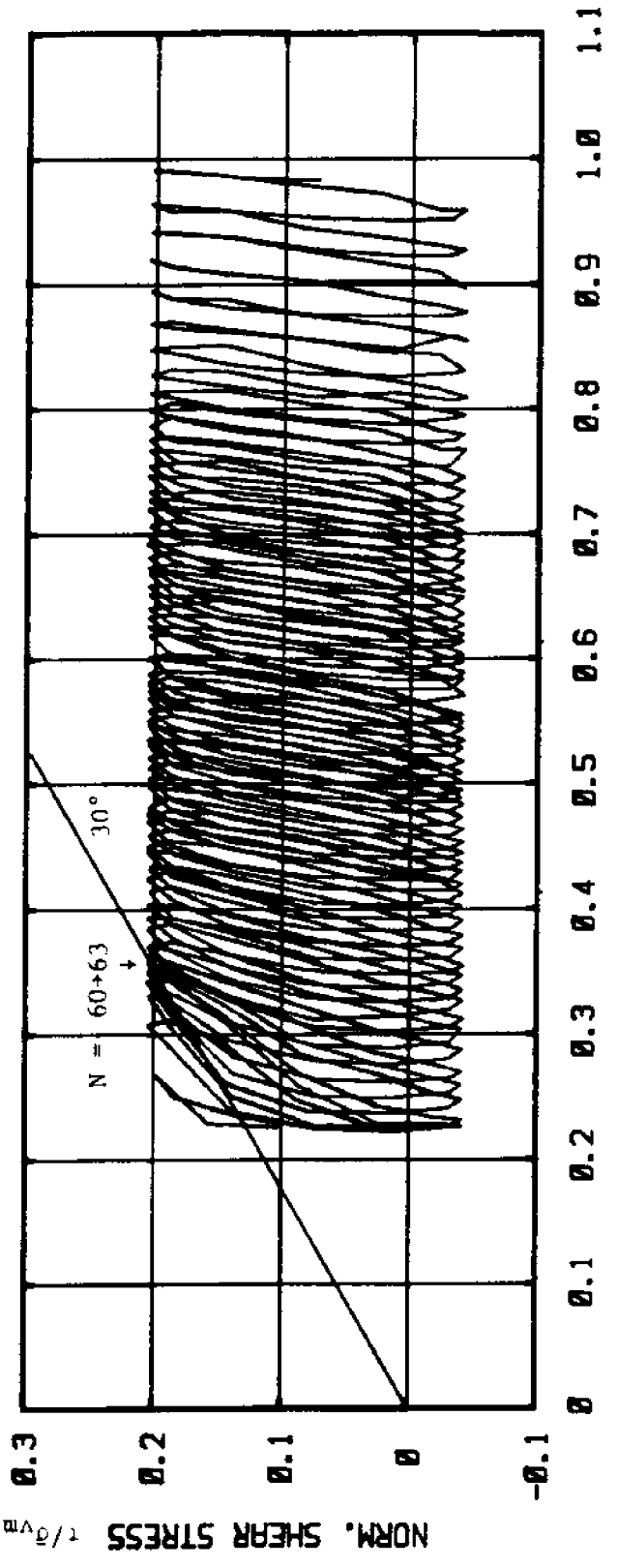

Figure 5.31 Normalized Stress Path and Obliquity at Failure
Test C-18: N.C. BBC, $\tau_{ave}/s_u(NC) = 0.39$, $\tau_c/s_u(NC) = 0.60$

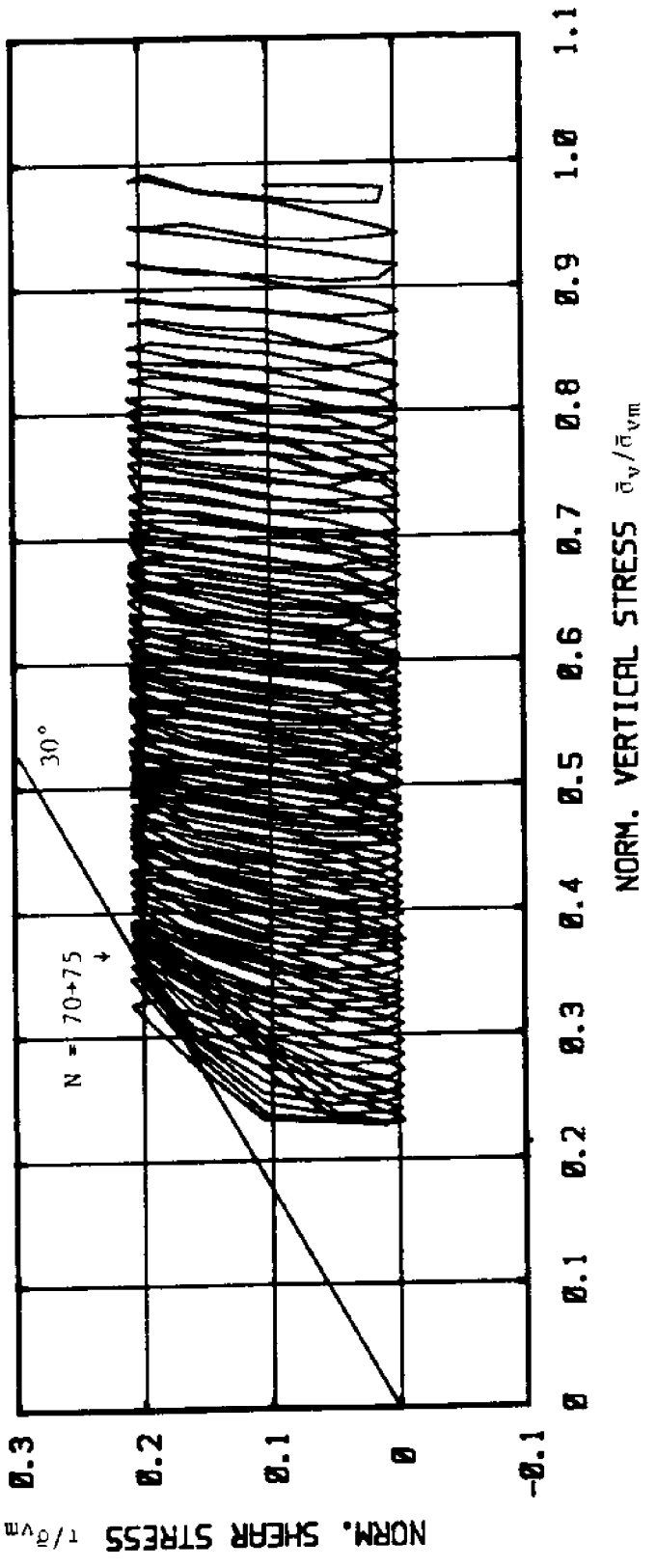

Figure 5.32 Normalized Stress Path and Obliquity at Failure
Test C-19: N.C. BBC, $\tau_{ave}/s_u(NC) = 0.50$, $\tau_c/s_u(NC) = 0.51$

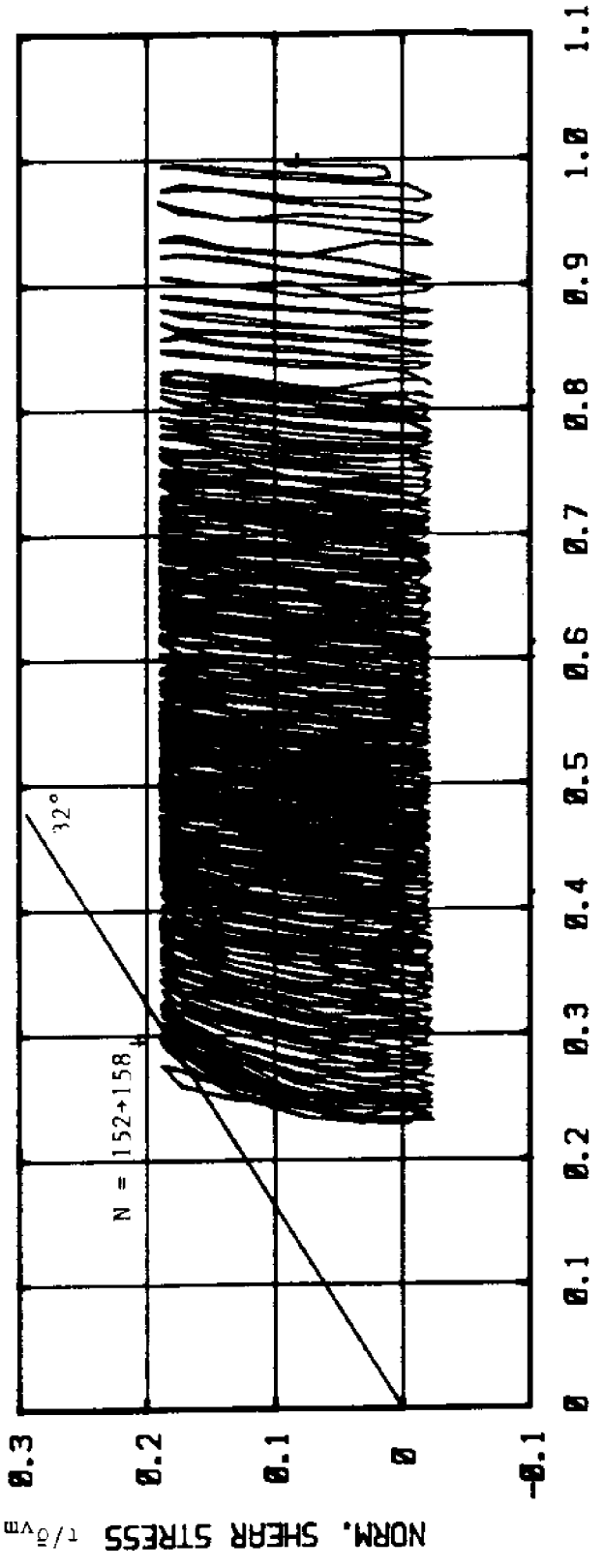

Figure 5.33 Normalized Stress Path and Obliquity at Failure
Test C-20: N.C. BBC, $\tau_{ave}/s_u(NC) = 0.40$, $\tau_c/s_u(NC) = 0.51$

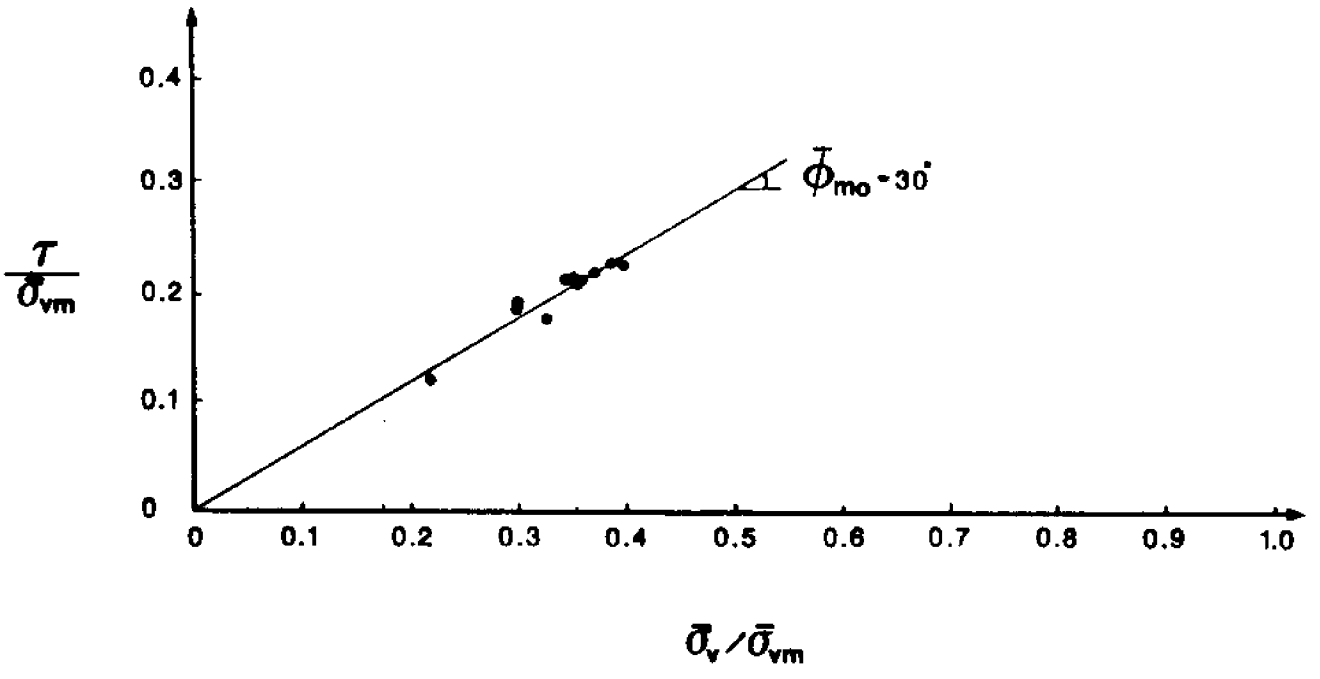

Figure 5.34 Obliquity at Failure from Various Cyclic DSS Tests with $\tau_{ave} = 0$ and $\tau_{ave} \neq 0$ on N.C. BBC

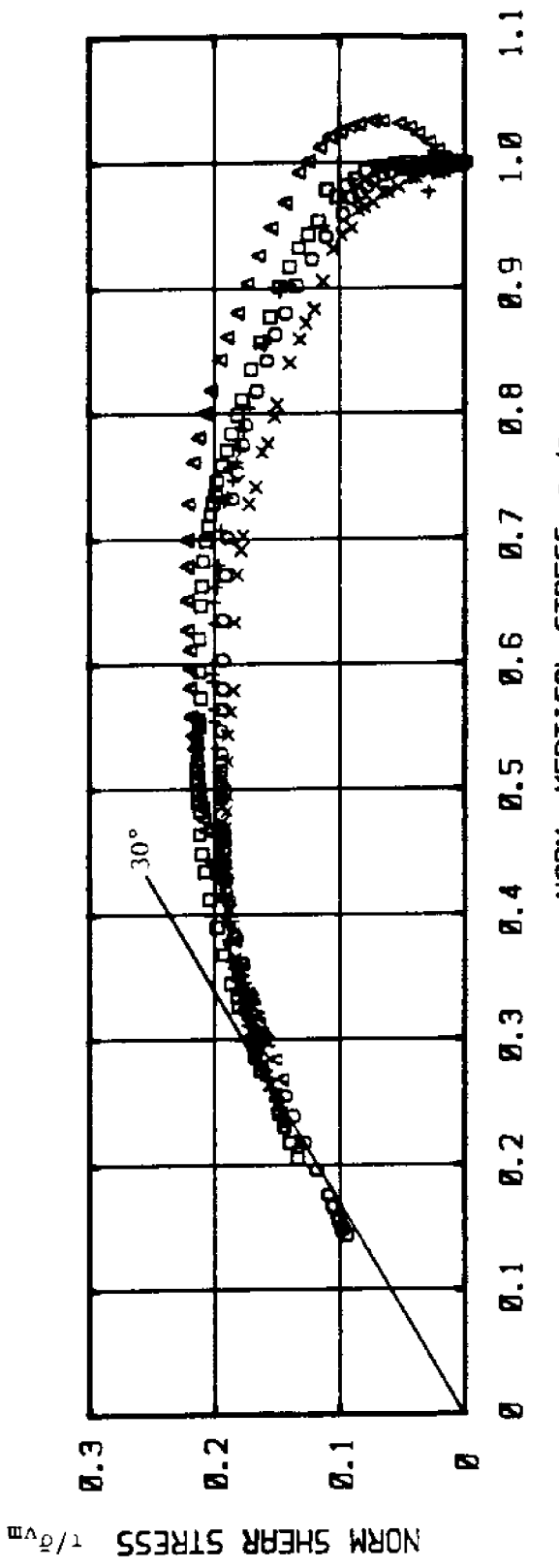

Figure 5.35 Normalized Stress Paths from Monotonic CK_0UDSS Tests, Showing the Maximum Obliquity Line

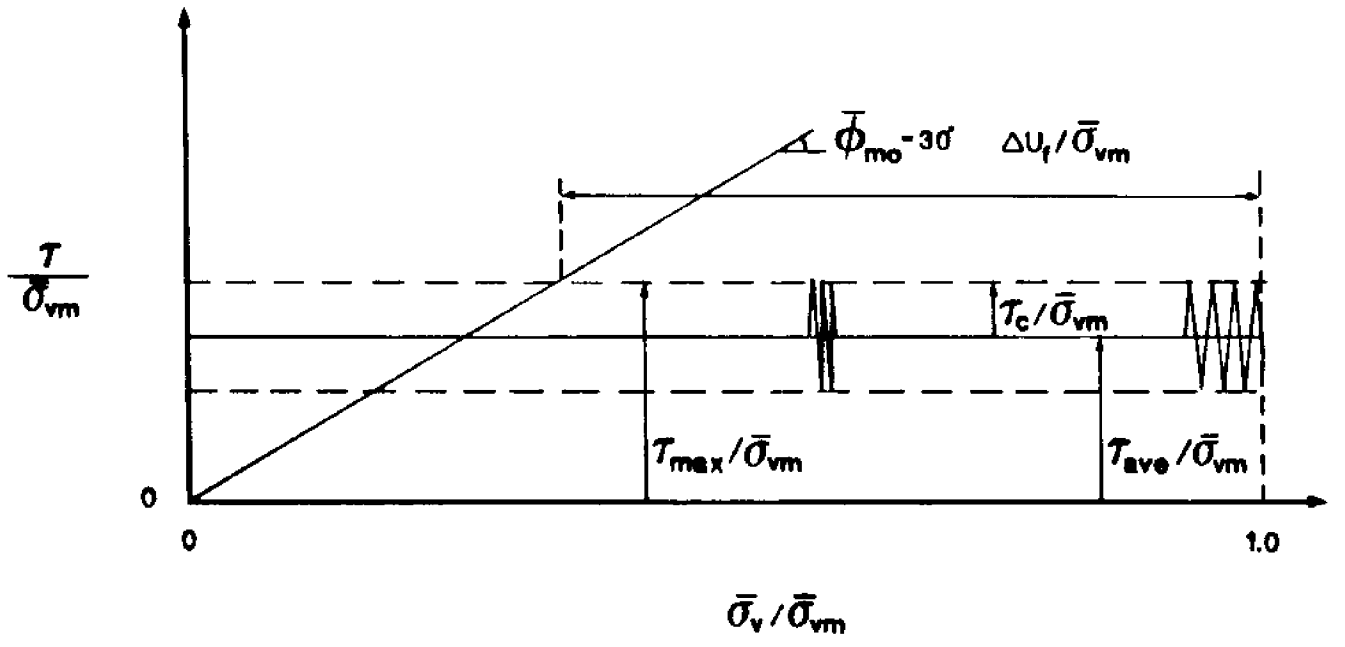

$$\frac{\Delta u_f}{\bar{\sigma}_{vm}} = 1 - \frac{\tau_{max}}{\bar{\sigma}_{vm} (\tan \bar{\Phi}_{MO})} \quad ; \quad \bar{\Phi}_{MO} = 30°$$

Figure 5.36 Excess Pore Pressure at Failure in Undrained Cyclic CK_oUDSS Tests Normally Consolidated BBC

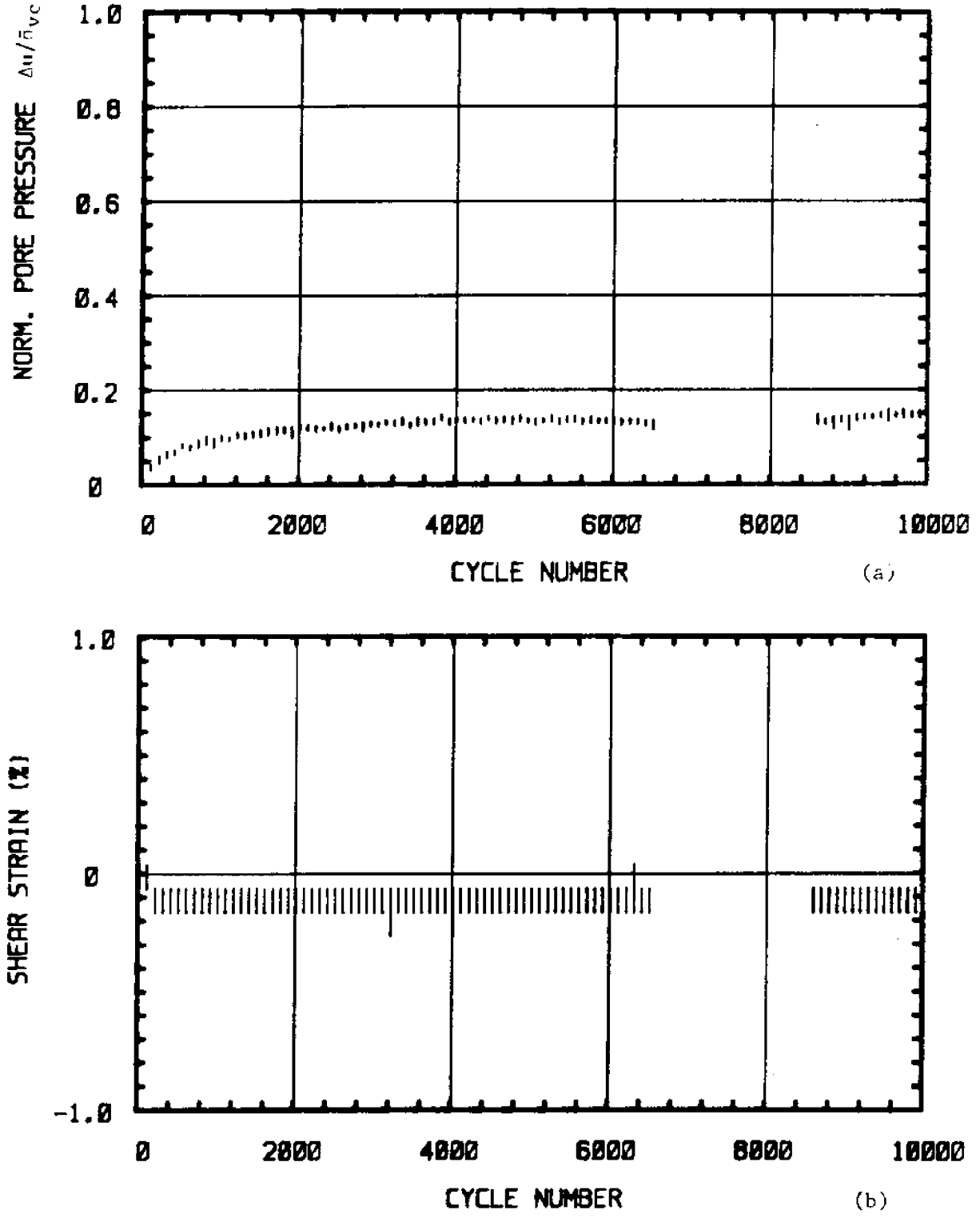

Figure 5.37 Test C-22: N.C. BBC, $\tau_{ave} = 0$, $\tau_c/s_u(NC) = 0.25$
a) Normalized Excess Pore Pressure versus Cycle Number
b) Shear Strain versus Cycle Number

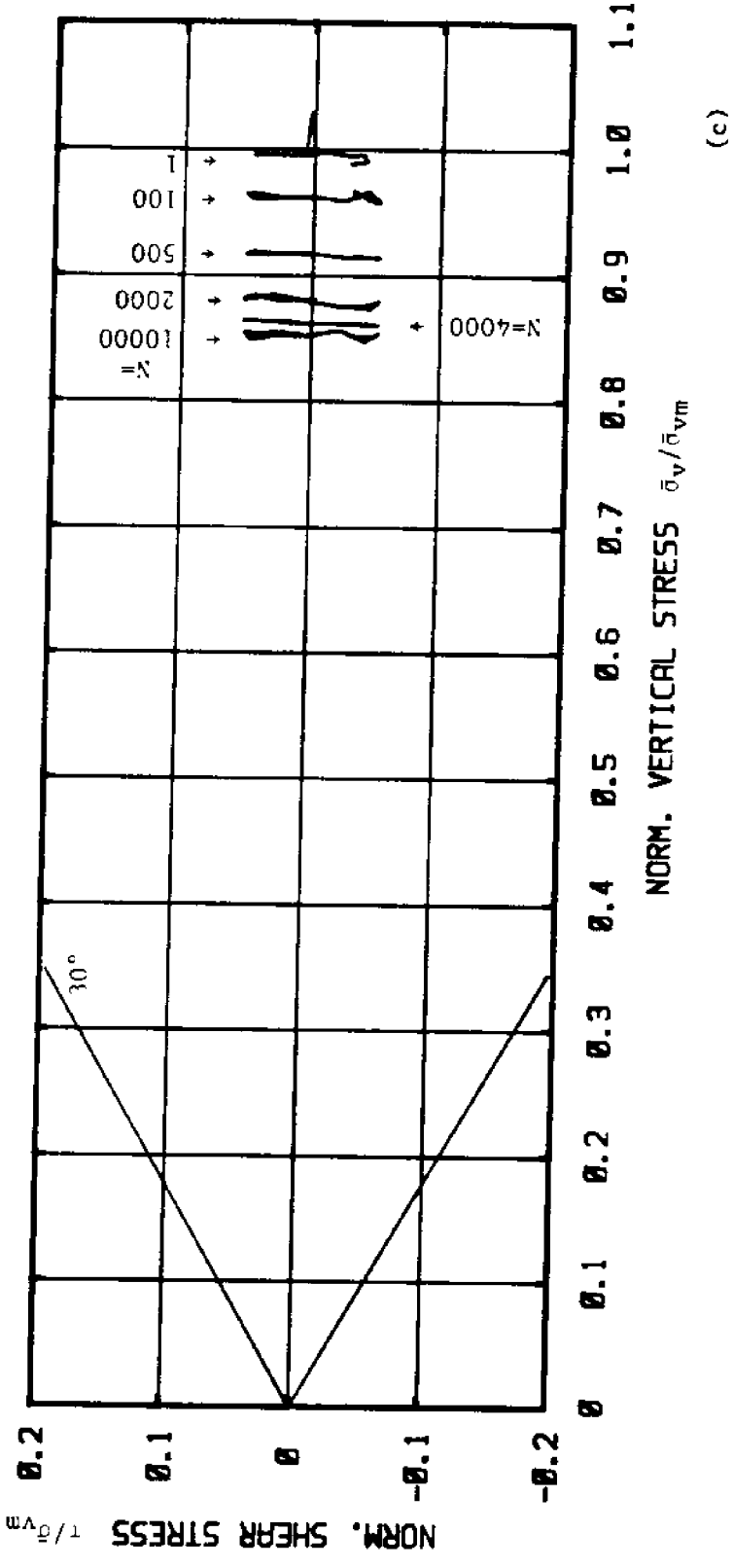

(c)

Figure 5.37 Test C-22: N.C. BBC, $\tau_{ave} = 0$, $\tau_c/s_u(NC) = 0.25$
c) Normalized Stress Path at Selected Cycles

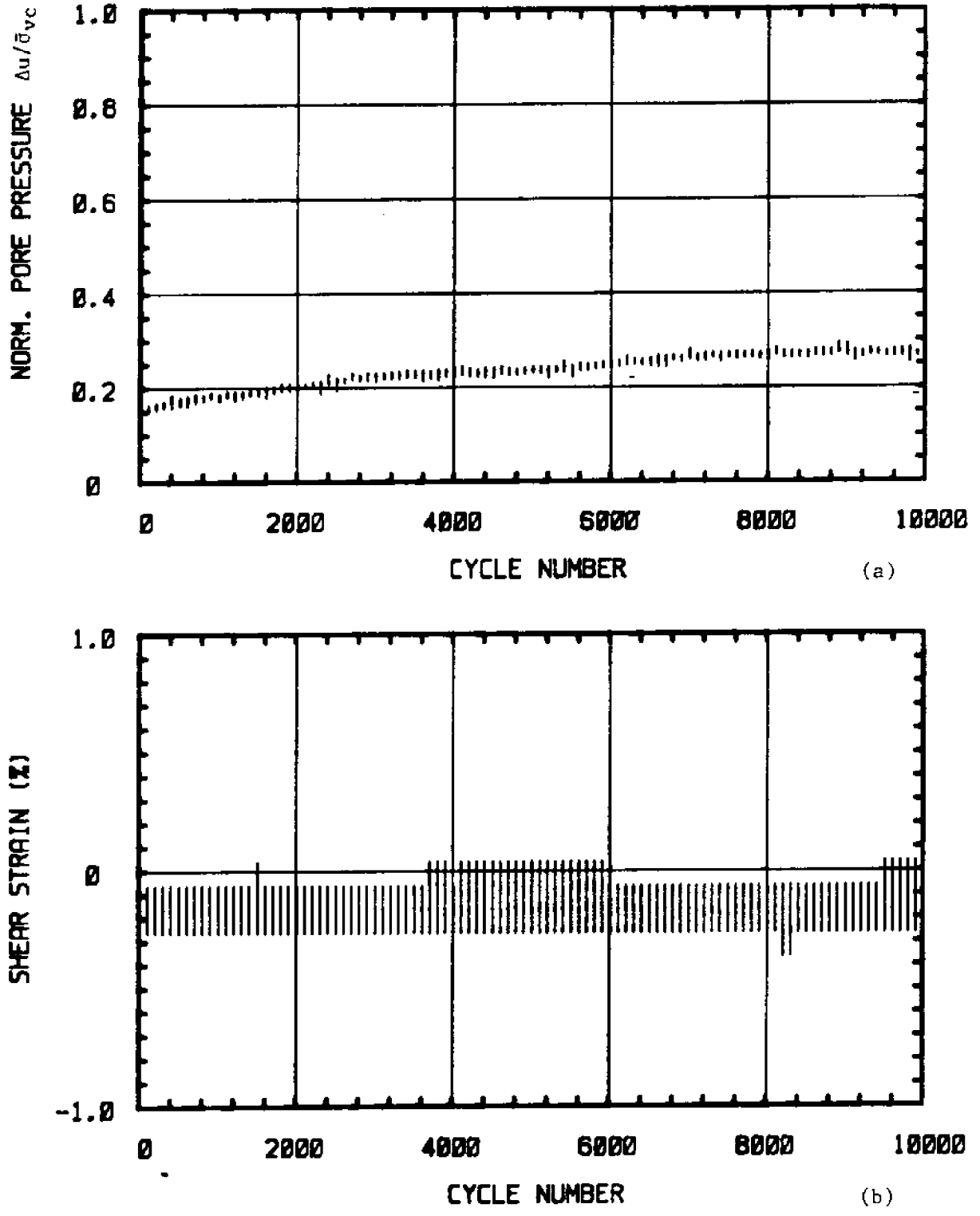

Figure 5.38 Test C-23: N.C. BBC, $\tau_{ave} = 0$, $\tau_c/s_u(NC) = 0.35$
a) Normalized Excess Pore Pressure versus Cycle Number
b) Shear Strain versus Cycle Number

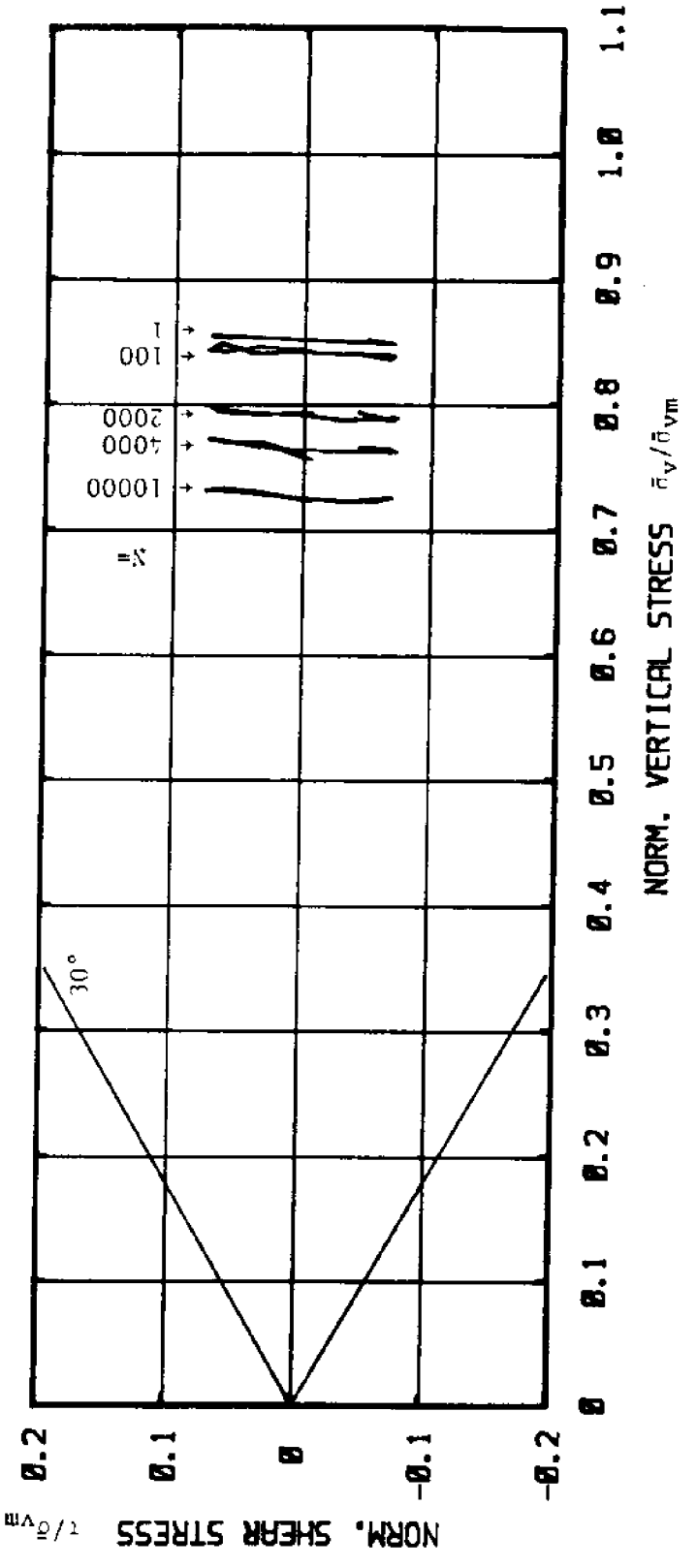

(c)

Figure 5.38 Test C-23: N.C. BBC, $\tau_{ave} = 0$, $\tau_c/s_u(NC) = 0.35$
c) Normalized Stress Path at Selected Cycles

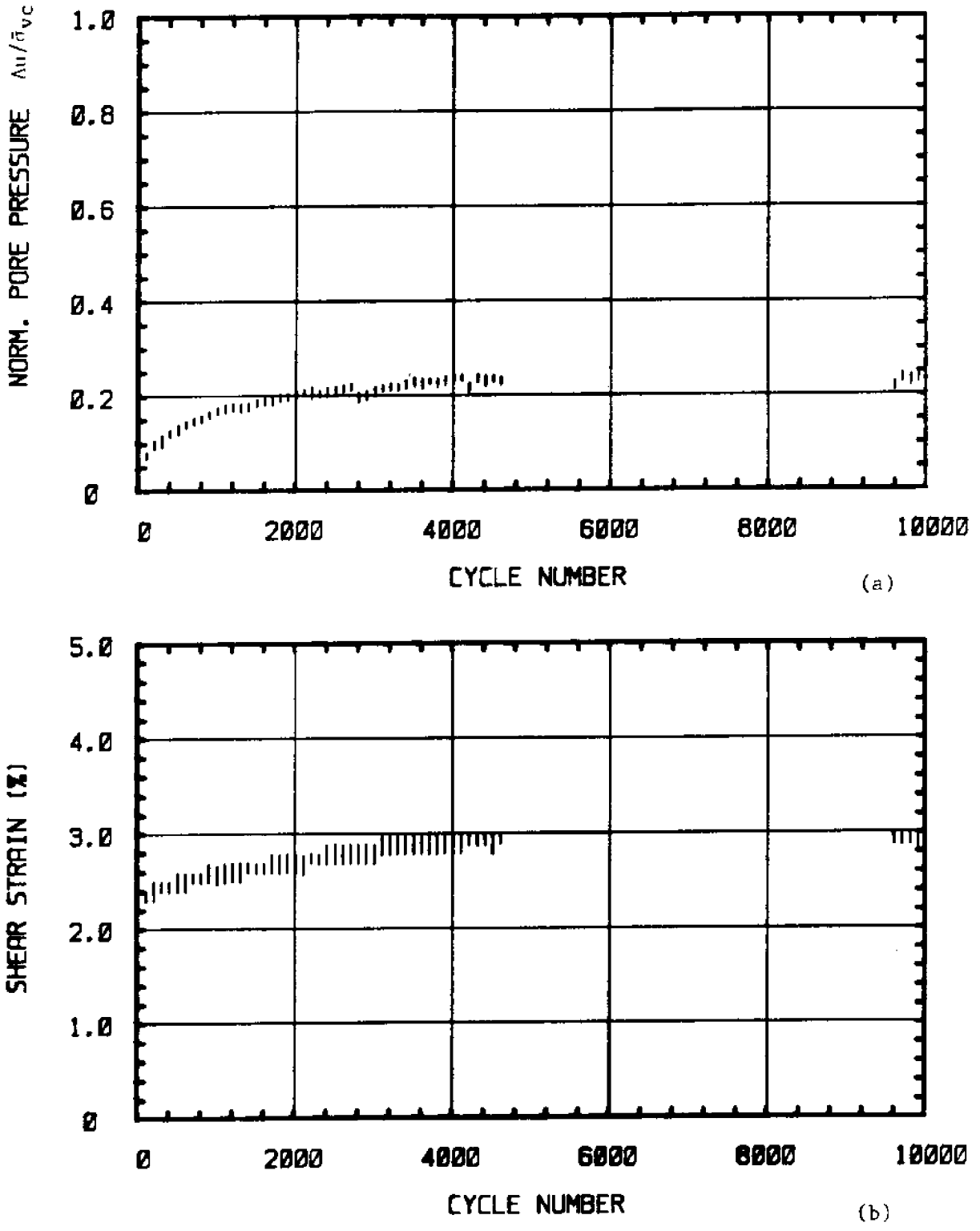

Figure 5.39 Test C-17: N.C. BBC, $\tau_{ave}/s_u(NC) = 0.59$, $\tau_c/s_u(NC) = 0.30$
a) Normalized Excess Pore Pressure versus Cycle Number
b) Shear Strain versus Cycle Number

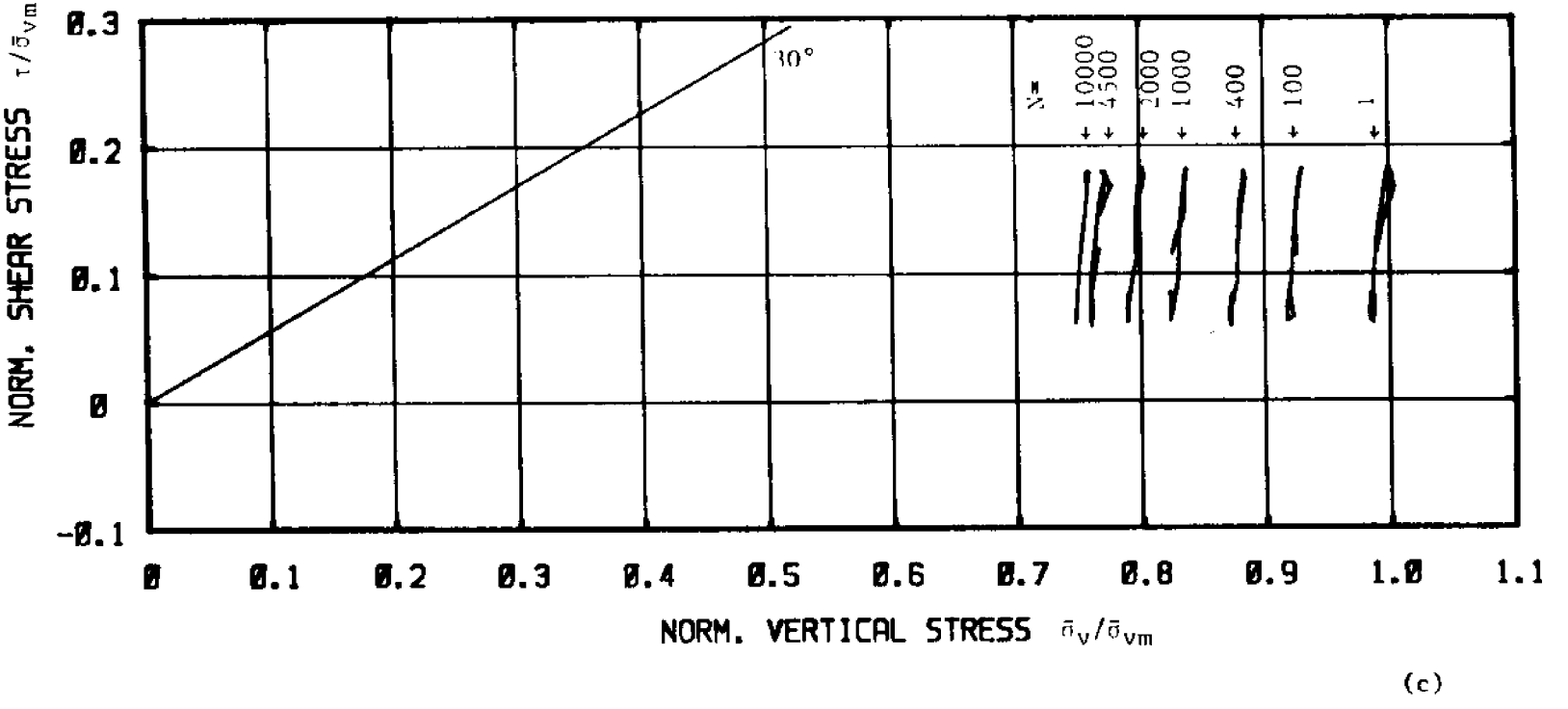

(c)

Figure 5.39 Test C-17: N.C. BBC, $\tau_{ave}/s_u(NC) = 0.59$, $\tau_c/s_u(NC) = 0.30$
c) Normalized Stress Path at Selected Cycles

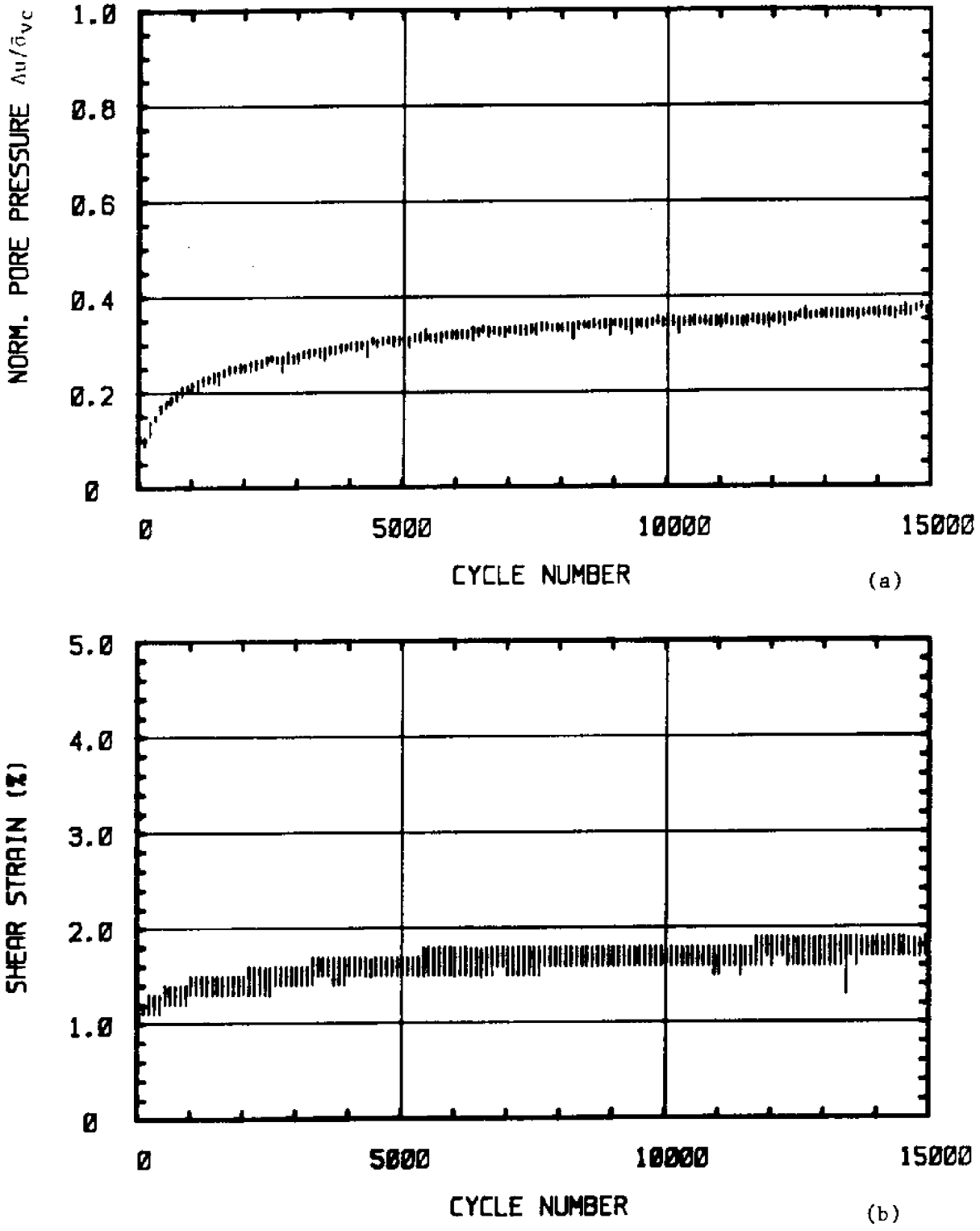

Figure 5.40 Test C-25: N.C. BBC, $\tau_{ave}/s_u(NC) = 0.35$, $\tau_c/s_u(NC) = 0.35$
a) Normalized Excess Pore Pressure versus Cycle Number
b) Shear Strain versus Cycle Number

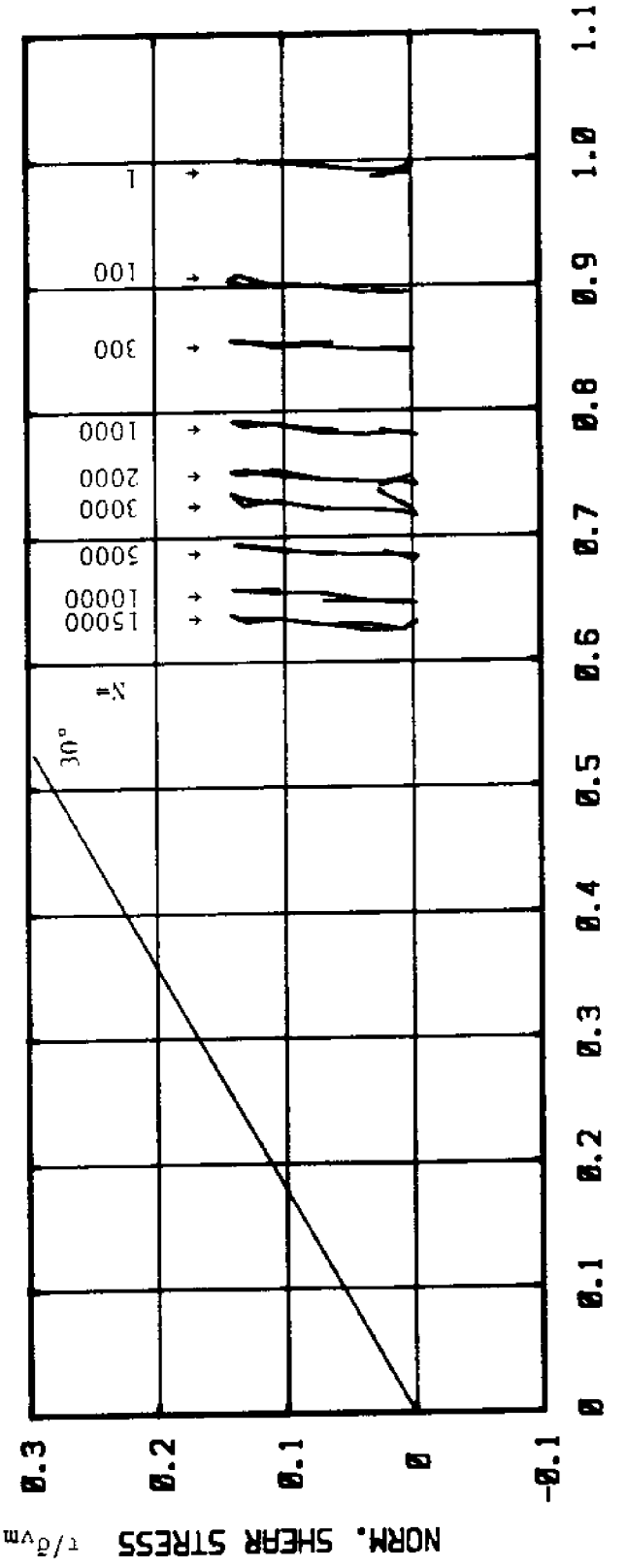

(c)

Figure 5.40 Test C-25: N.C. BBC, $\tau_{ave}/s_u(NC) = 0.35$, $\tau_c/s_u(NC) = 0.35$
c) Normalized Stress Path at Selected Cycles

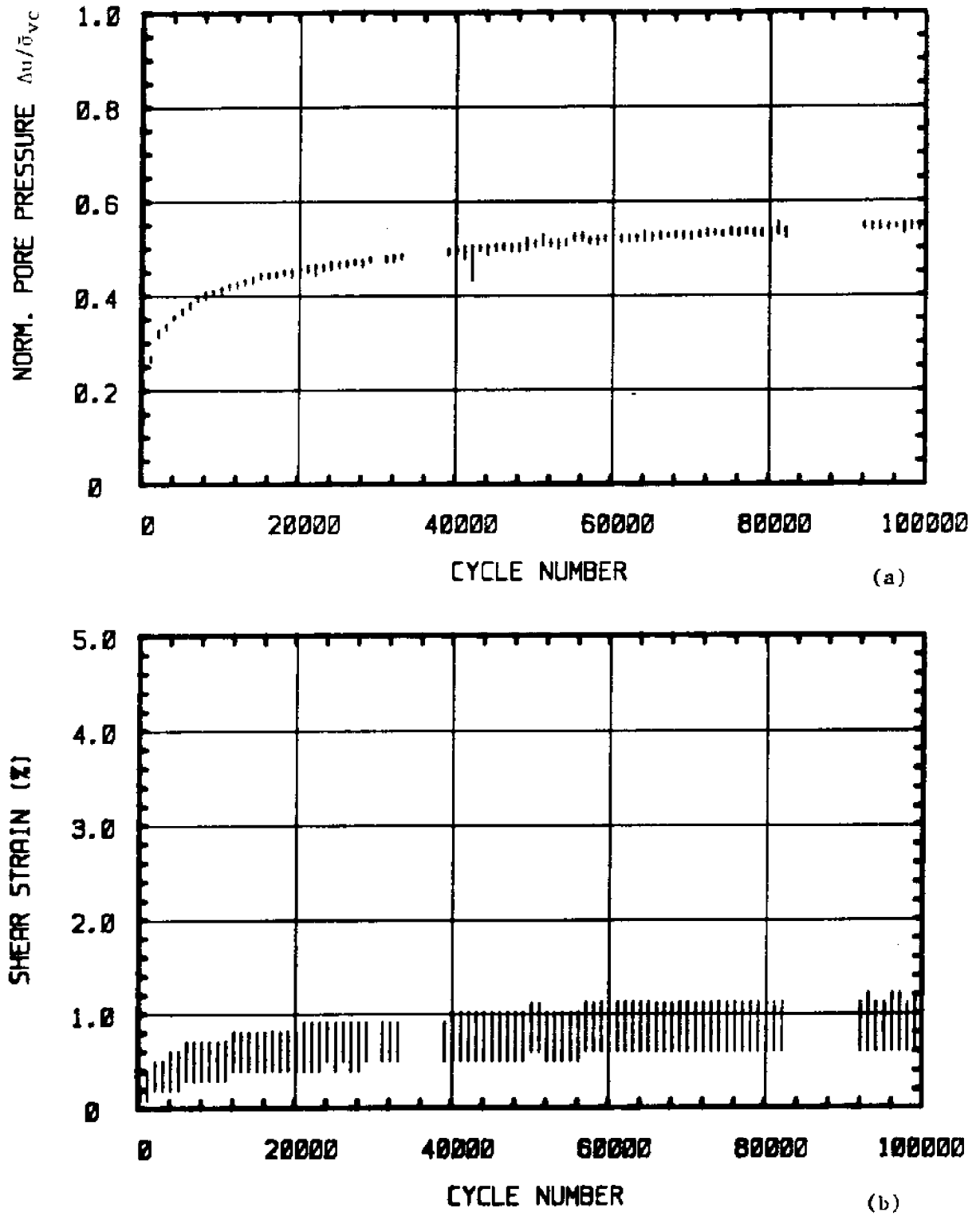

Figure 5.41 Test C-39: N.C. BBC, $\tau_{ave}/s_u(NC) = 0.15$, $\tau_c/s_u(NC) = 0.38$
a) Normalized Excess Pore Pressure versus Cycle Number
b) Shear Strain versus Cycle Number

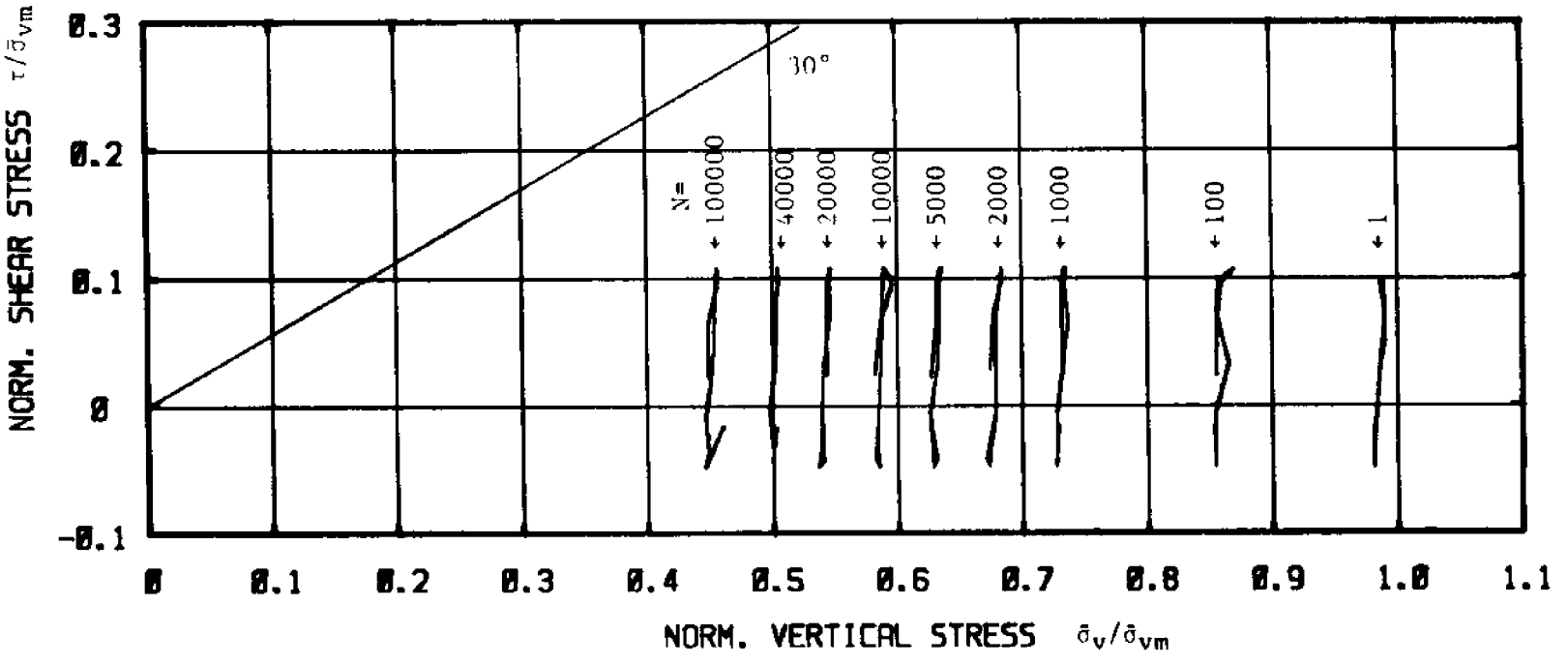

(c)

Figure 5.41 Test C-39: N.C. BBC, $\tau_{ave}/s_u(NC) = 0.15$, $\tau_c/s_u(NC) = 0.38$
c) Normalized Stress Path at Selected Cycles

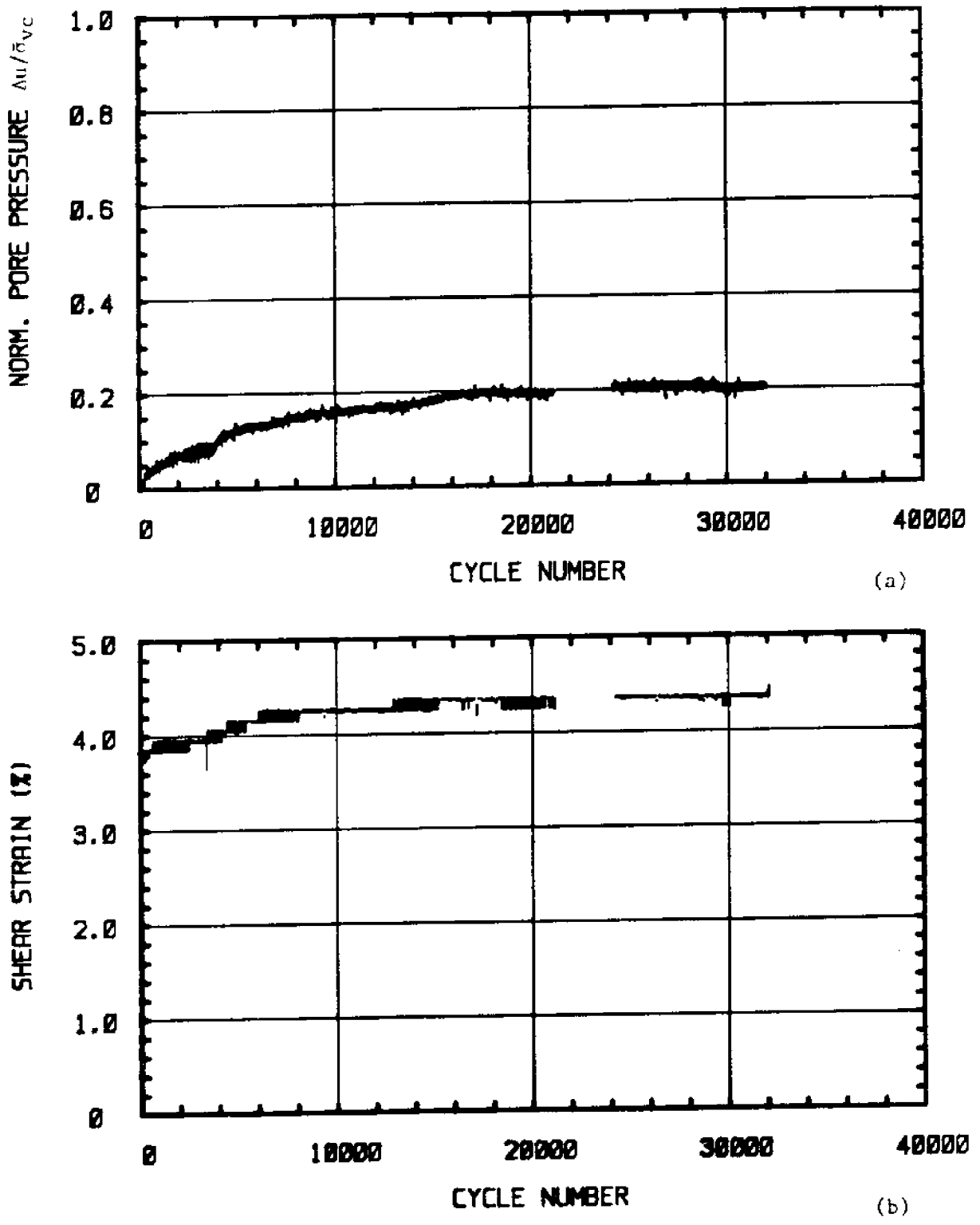

Figure 5.42 Test C-40: N.C. BBC, $\tau_{ave}/s_u(NC) = 0.80$, $\tau_c/s_u(NC) = 0.20$
a) Normalized Excess Pore Pressure versus Cycle Number
b) Shear Strain versus Cycle Number

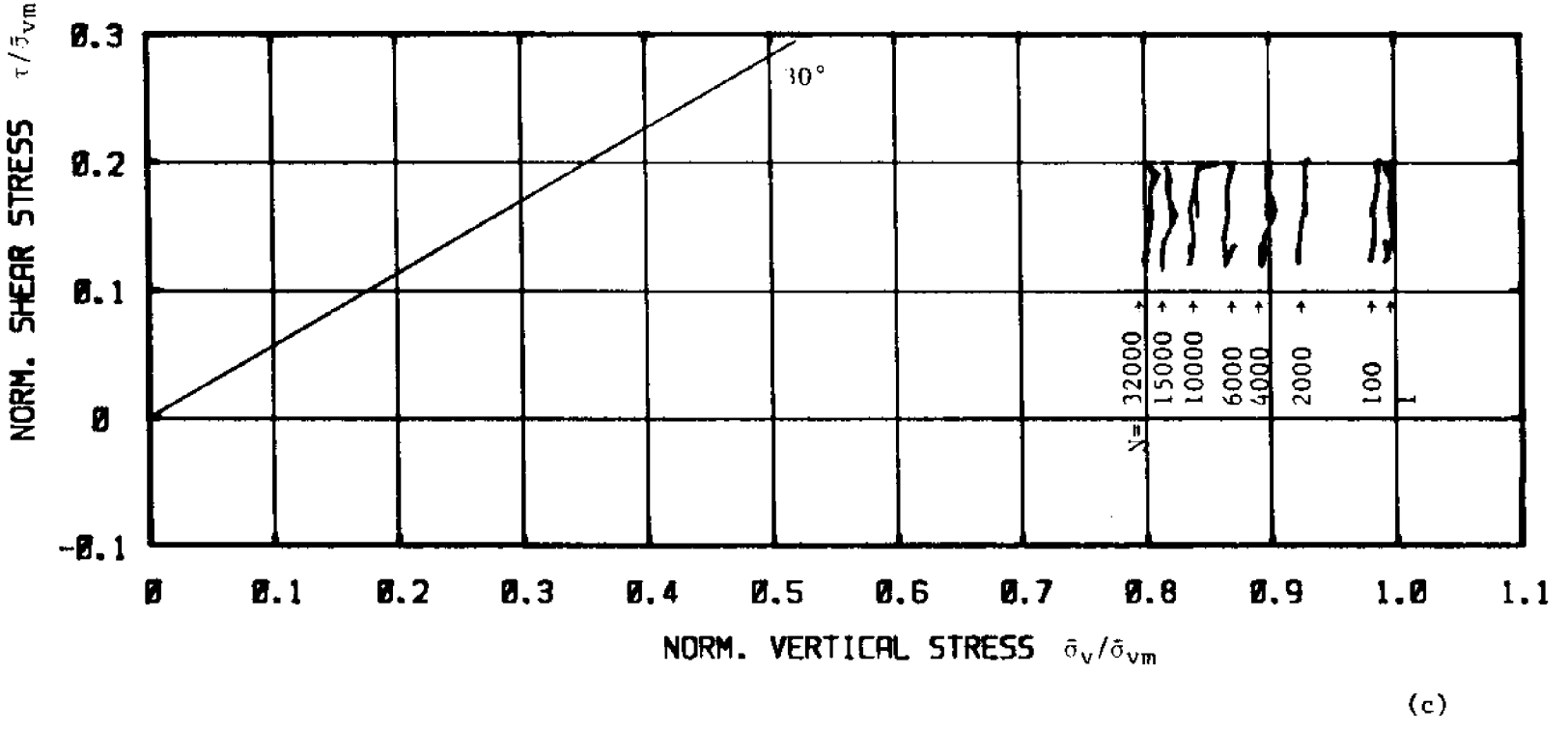

Figure 5.42 Test C-40: N.C. BBC, $\tau_{ave}/s_u(NC) = 0.80$, $\tau_c/s_u(NC) = 0.20$
c) Normalized Stress Path at Selected Cycles

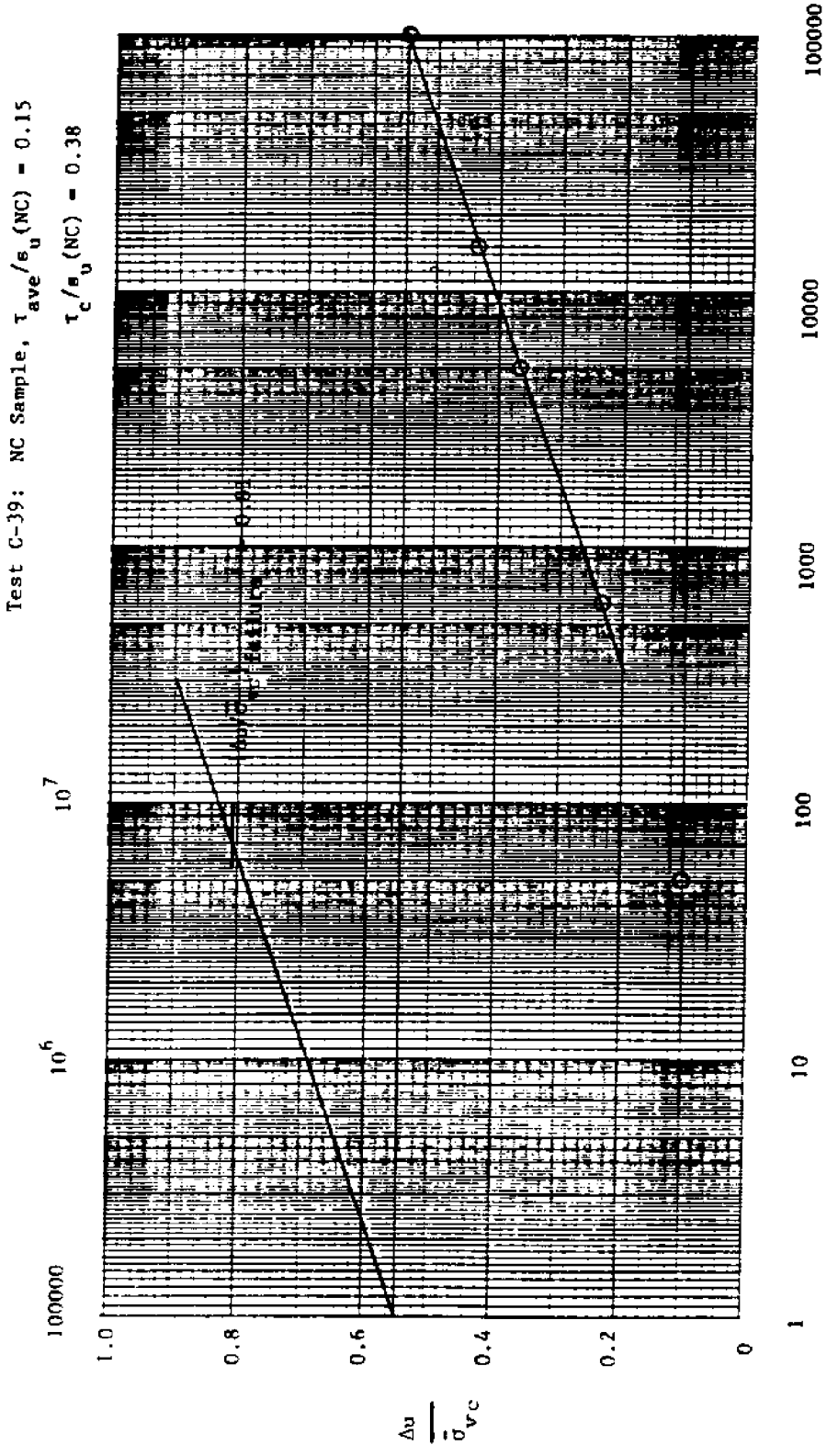

Figure 5.43 Excess Pore Pressure versus LOG N, Test C-39

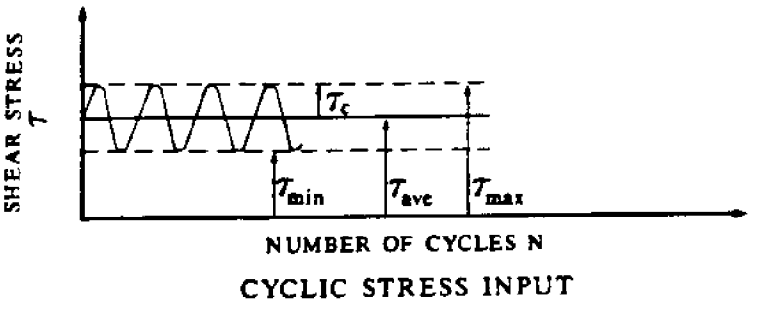

CYCLIC STRESS INPUT

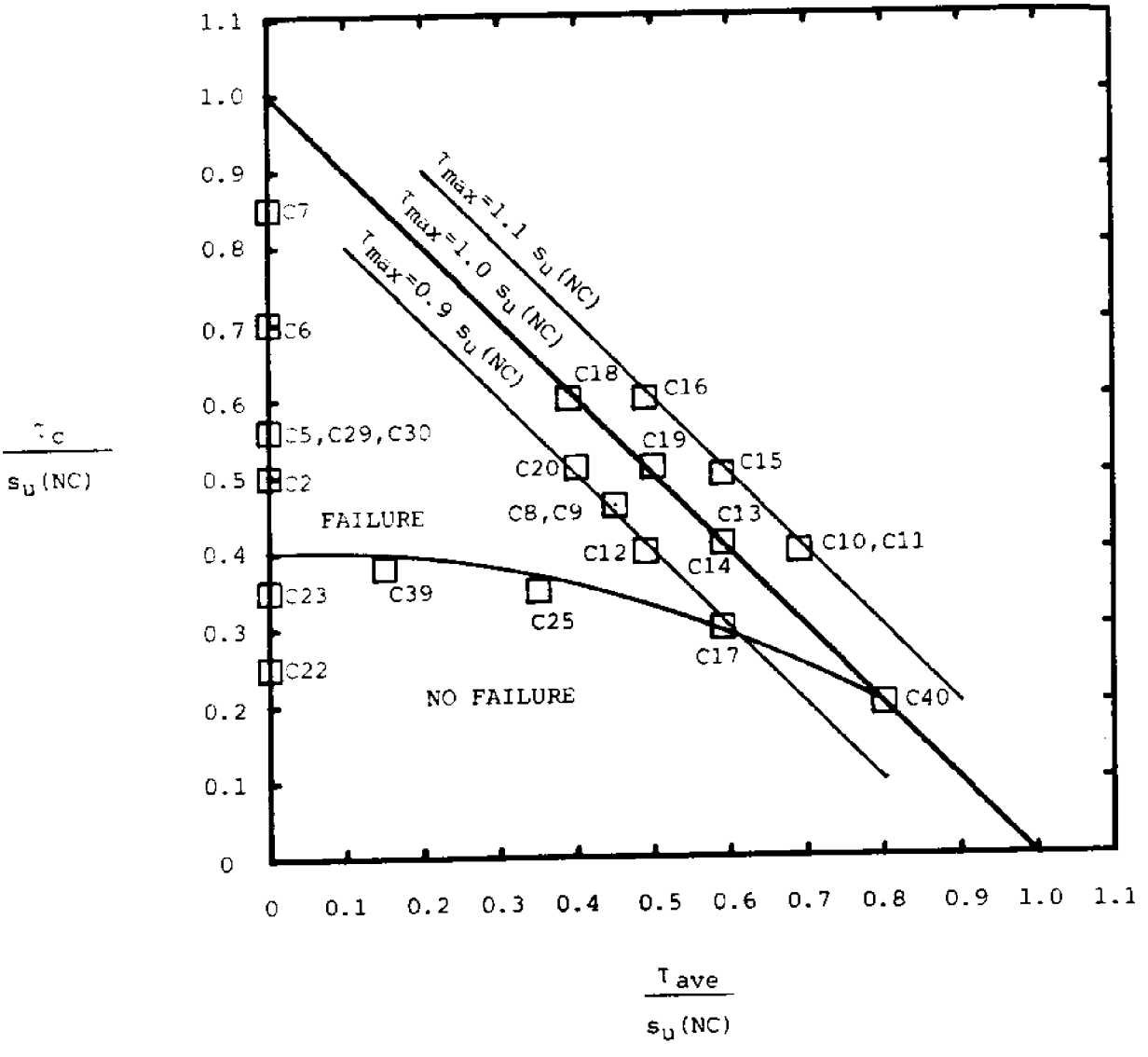

Figure 5.44 Threshold Shear Stress Boundary

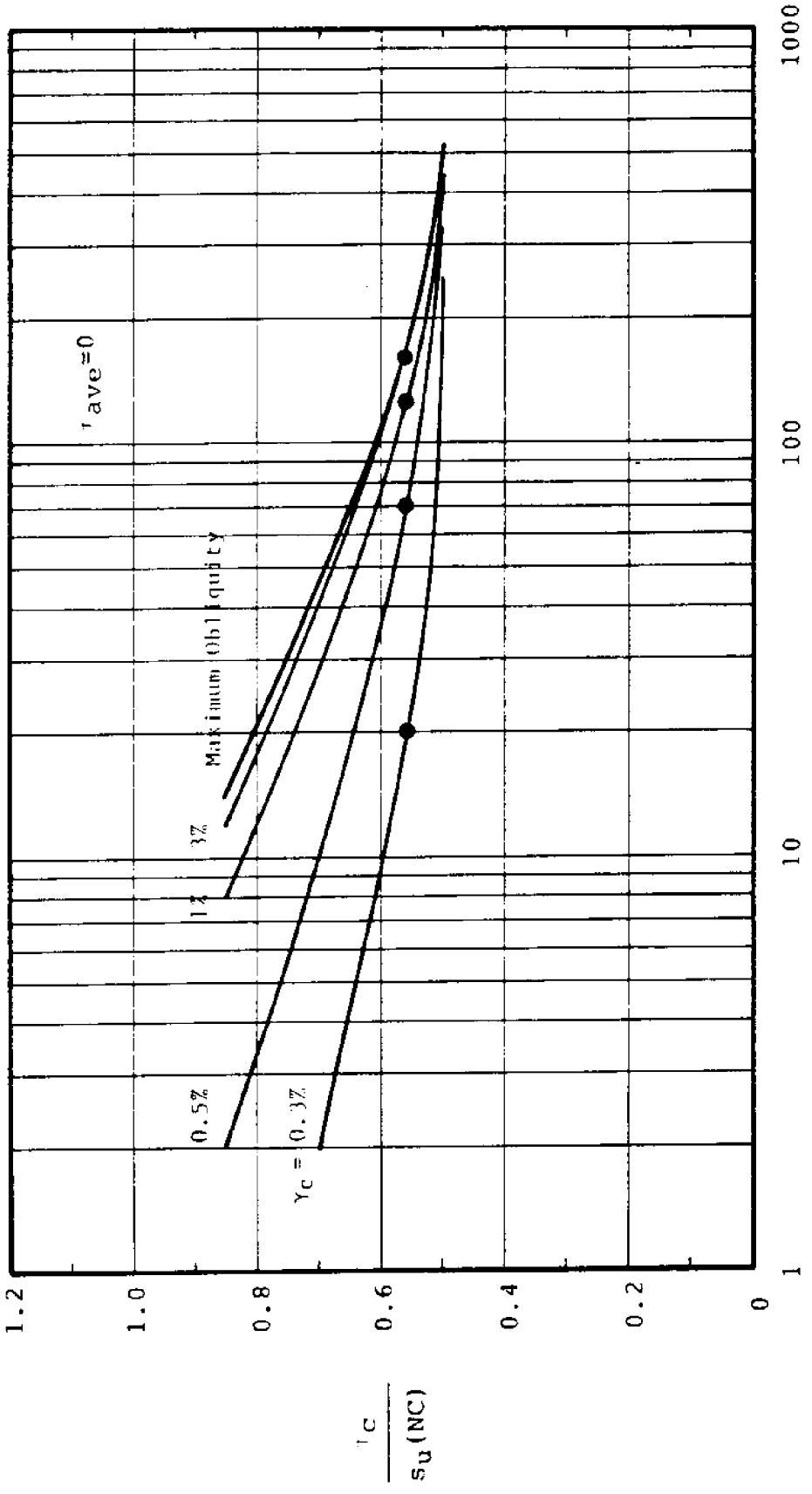

Figure 5.45 S-N Curves: Cyclic Stress Ratio versus Log Number of Cycles
Normally Consolidated BBC, τ_{ave} = 0

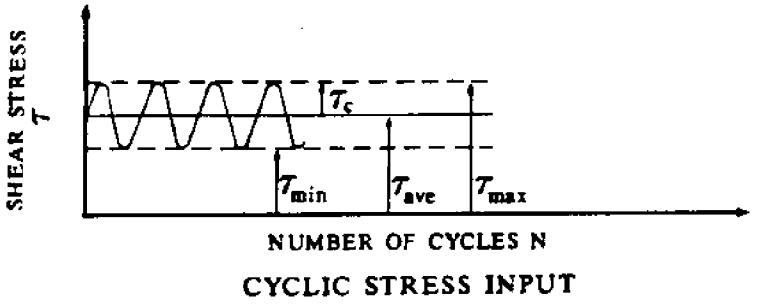

CYCLIC STRESS INPUT

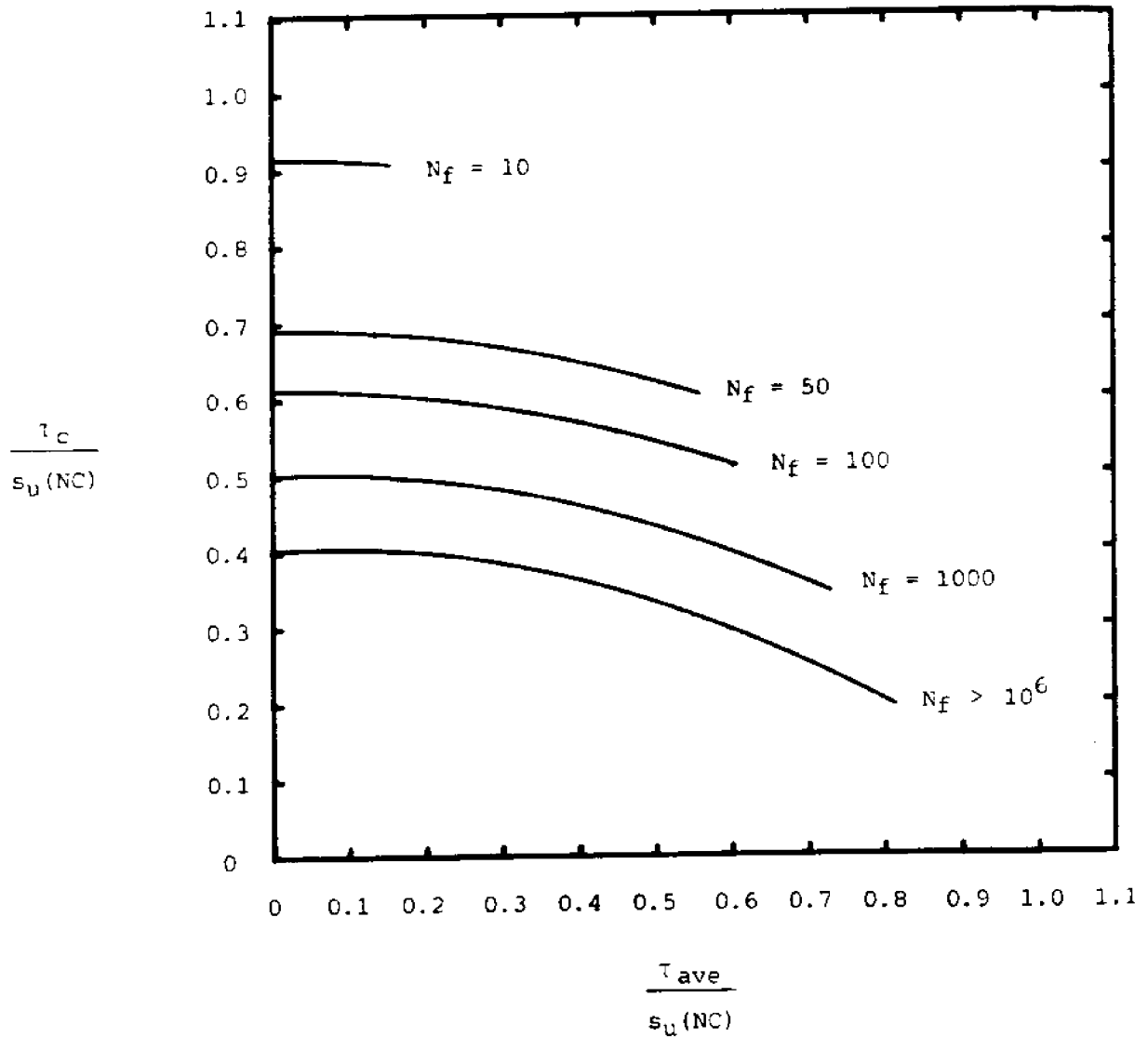

Figure 5.46 Iso-N_f Contours

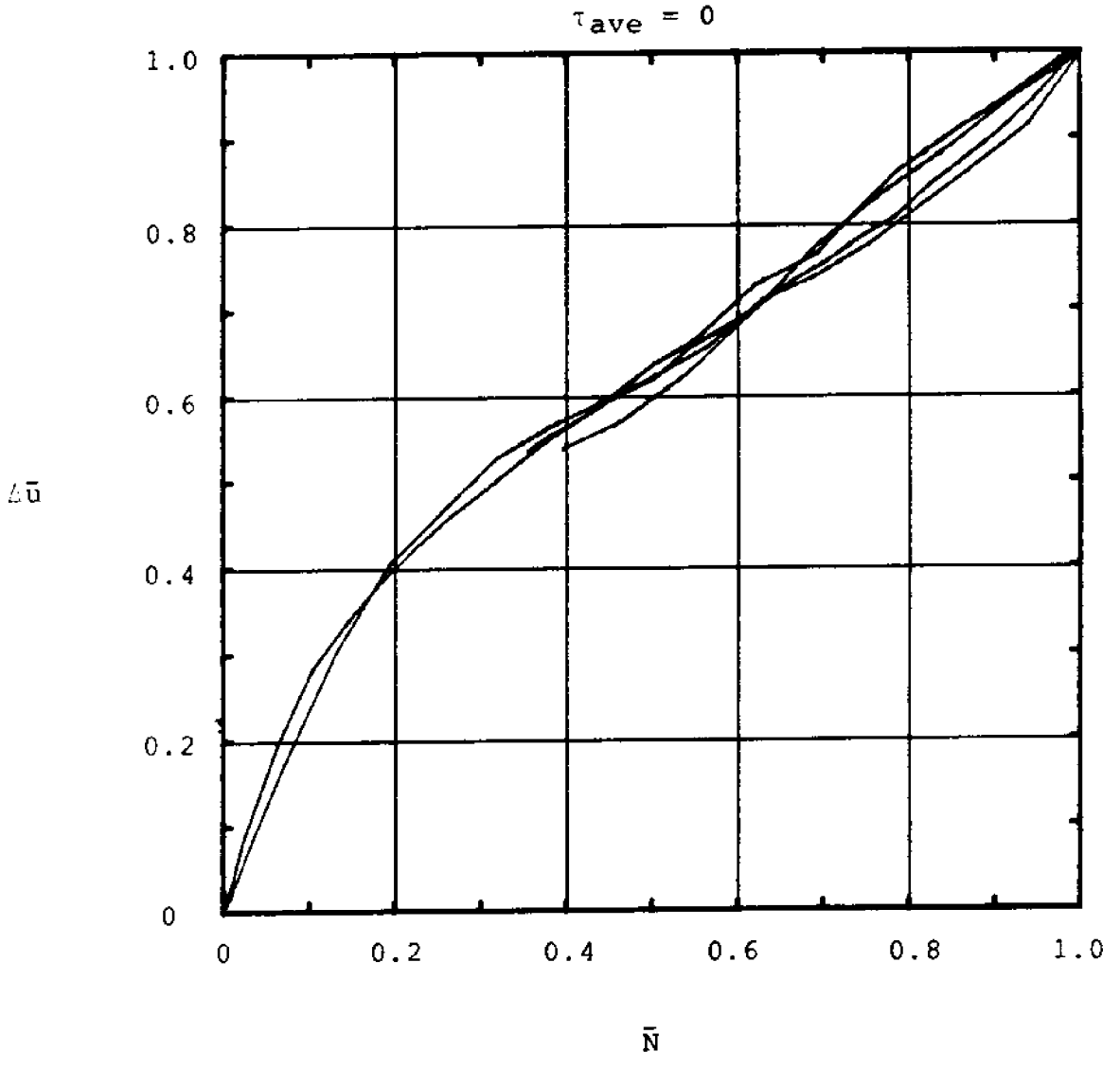

Figure 5.47 Normalized Excess Pore Pressure $\Delta\bar{u}$ versus Normalized Cycle Number $\bar{N}$ for Tests with $\tau_{ave} = 0$

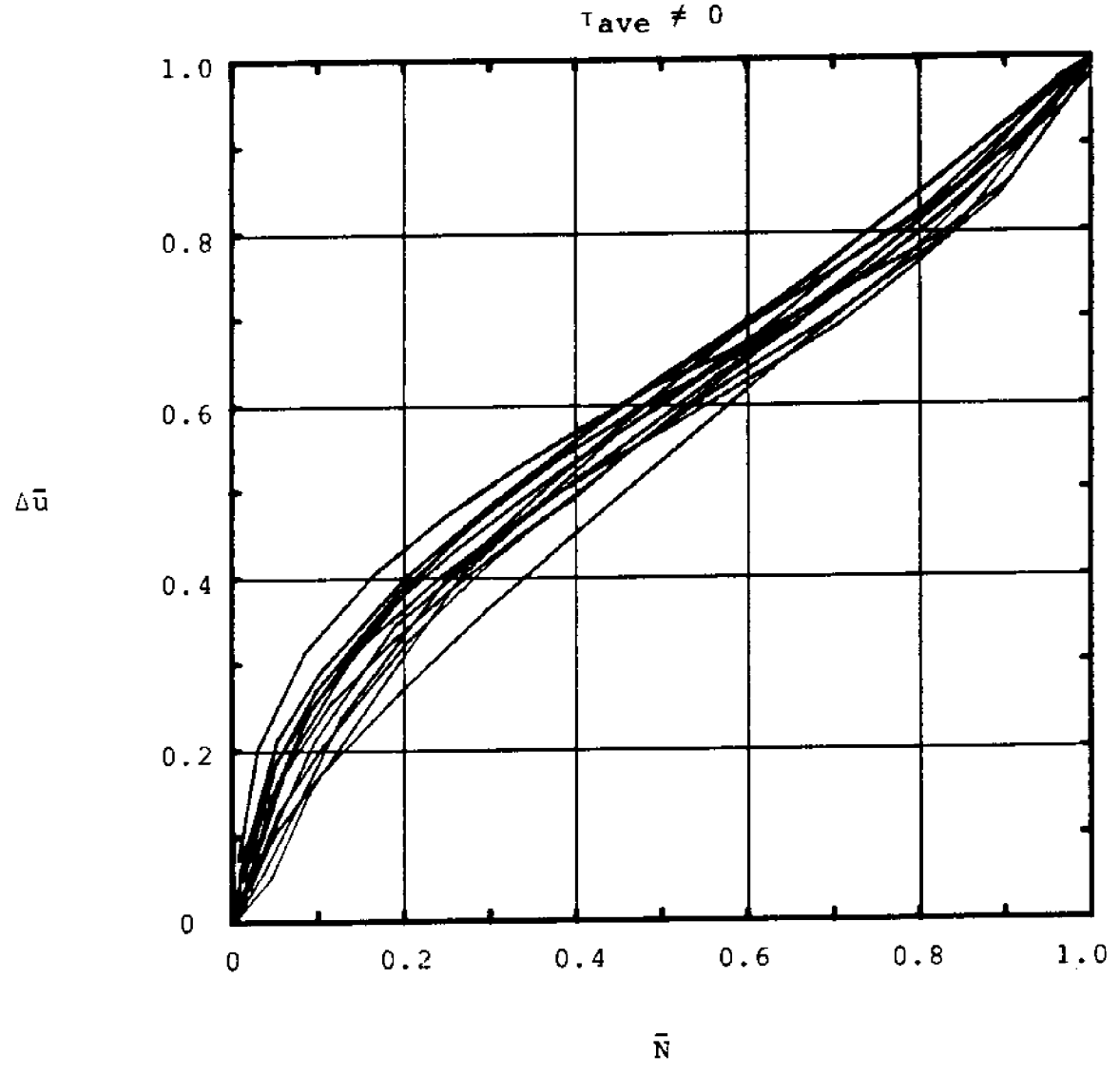

Figure 5.48 Normalized Excess Pore Pressure $\Delta\bar{u}$ versus Normalized Cycle Number $\bar{N}$ for Tests with $\tau_{ave} \neq 0$

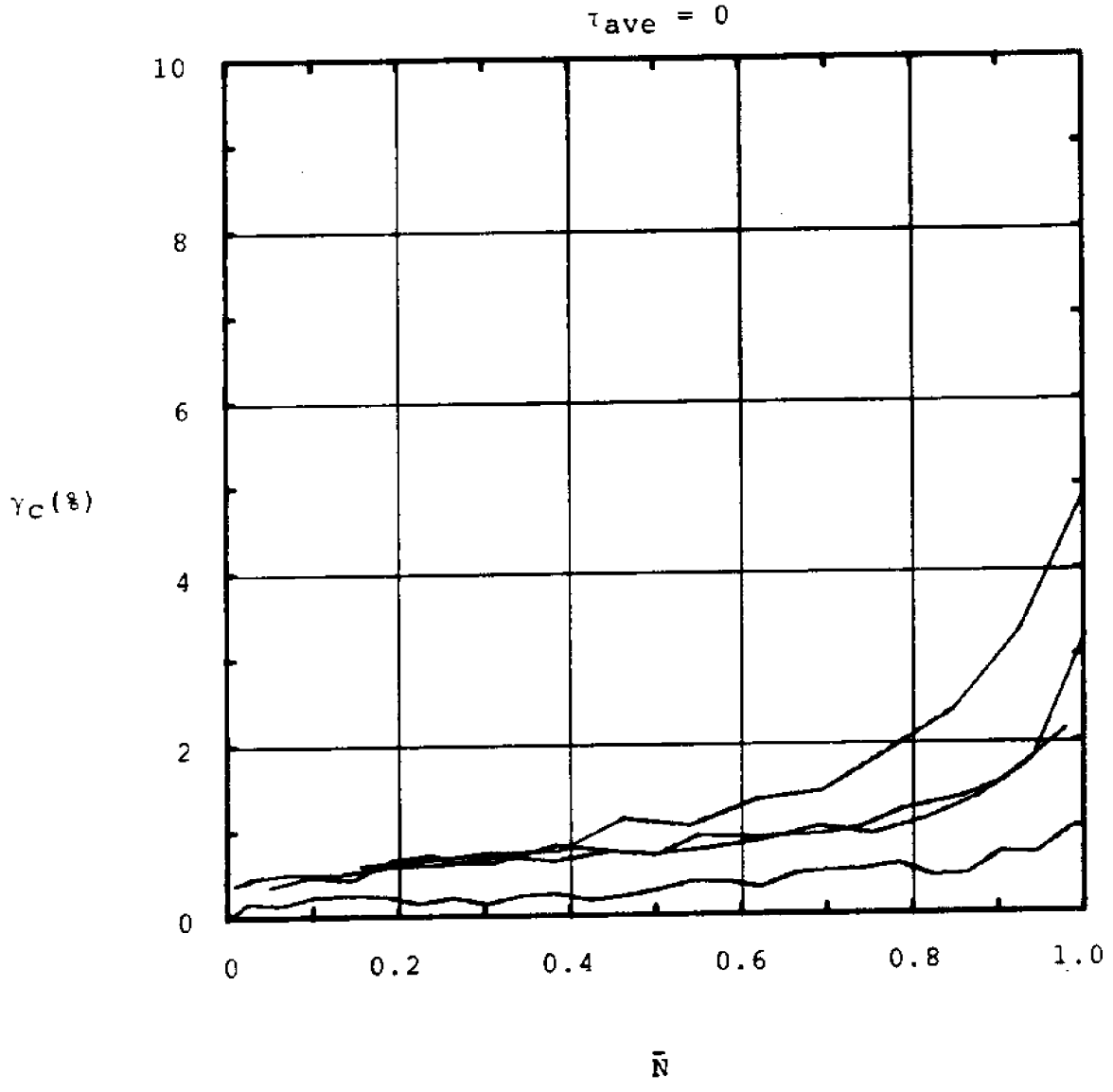

Figure 5.49 Cyclic Shear Strain $\gamma_c(\%)$ versus Normalized Cycle Number $\bar{N}$ for Tests with $\tau_{ave} = 0$

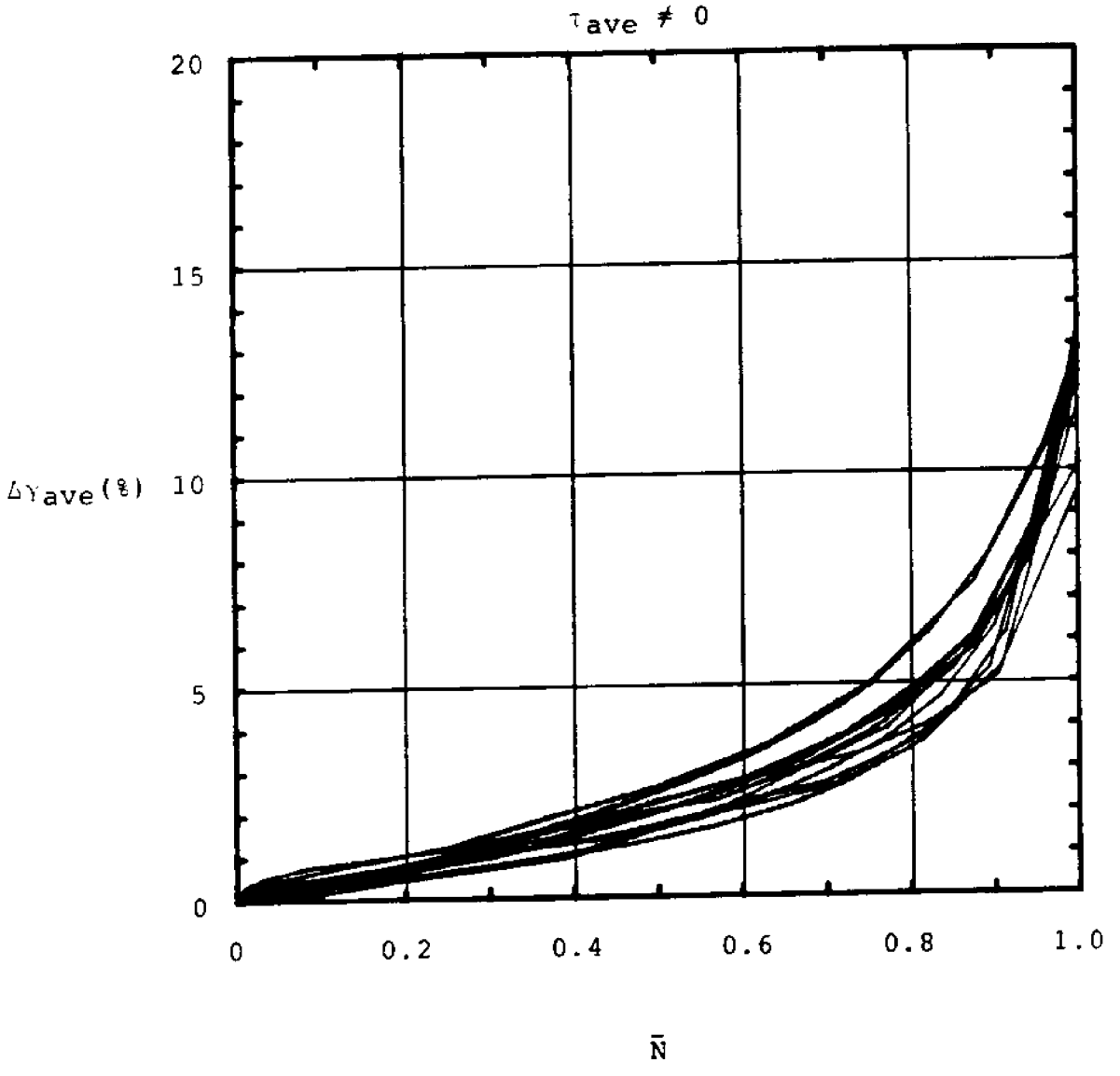

Figure 5.50 Average Shear Strain $\Delta\gamma_{ave}(\%)$ versus Normalized Cycle Number $\bar{N}$ for Tests with $\tau_{ave} \neq 0$

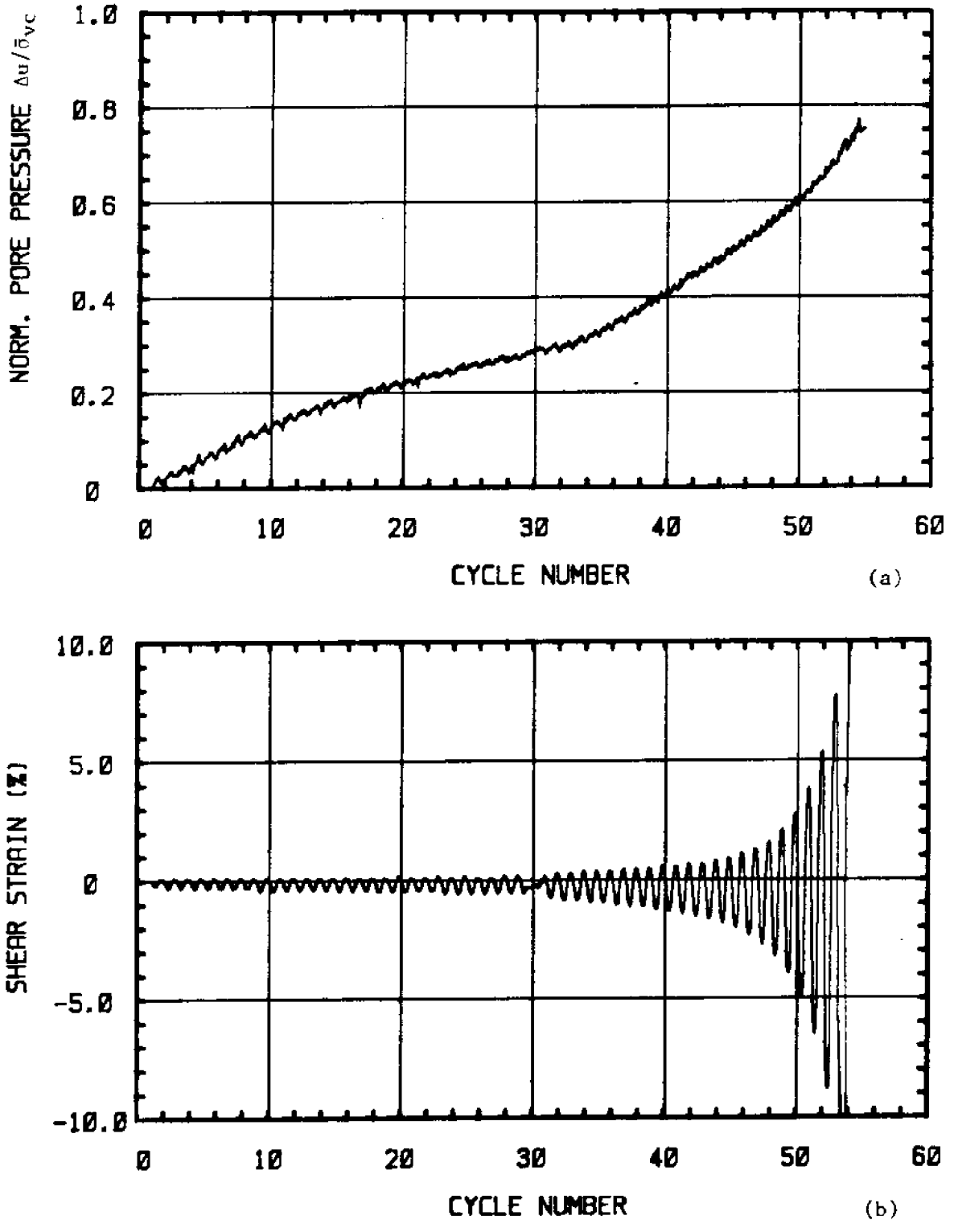

Figure 5.51 Test C-28: N.C. BBC, $\tau_{ave} = 0$, $\tau_c/s_u(NC) = 0.56, 0.71$
a) Normalized Excess Pore Pressure versus Cycle Number
b) Shear Strain versus Cycle Number

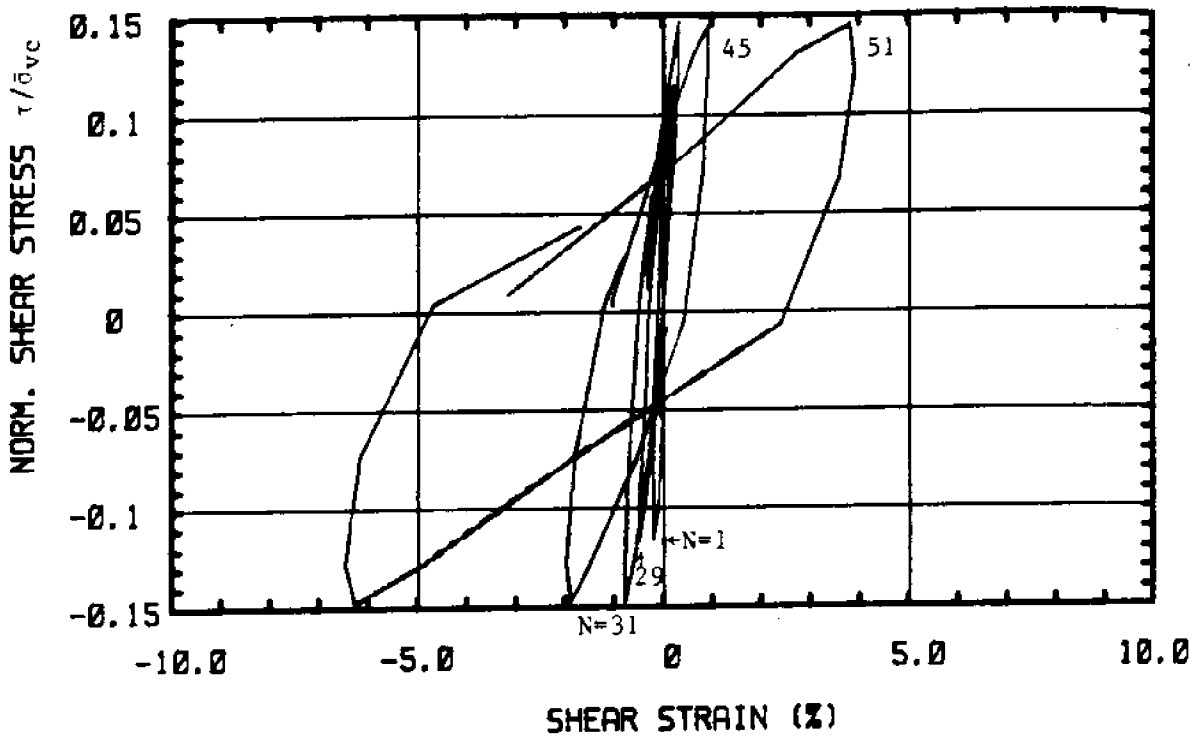

(c)

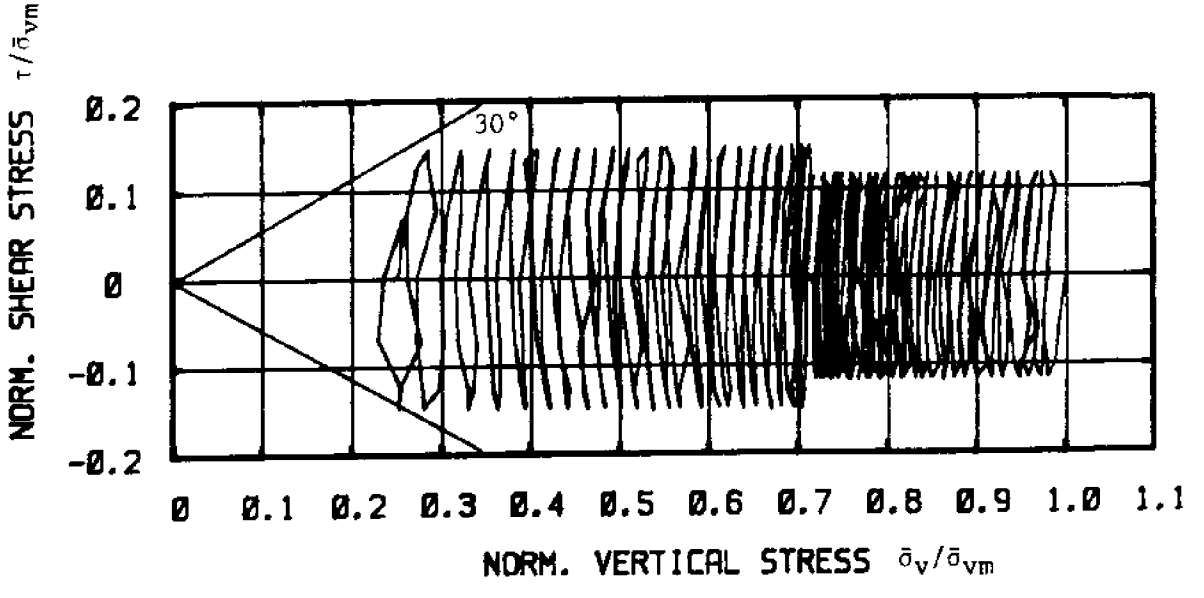

(d)

Figure 5.51 Test C-28: N.C. BBC, τ_{ave} = 0, τ_c/s_u(NC) = 0.56, 0.71
c) Normalized Shear Stress versus Shear Strain
d) Normalized Stress Path

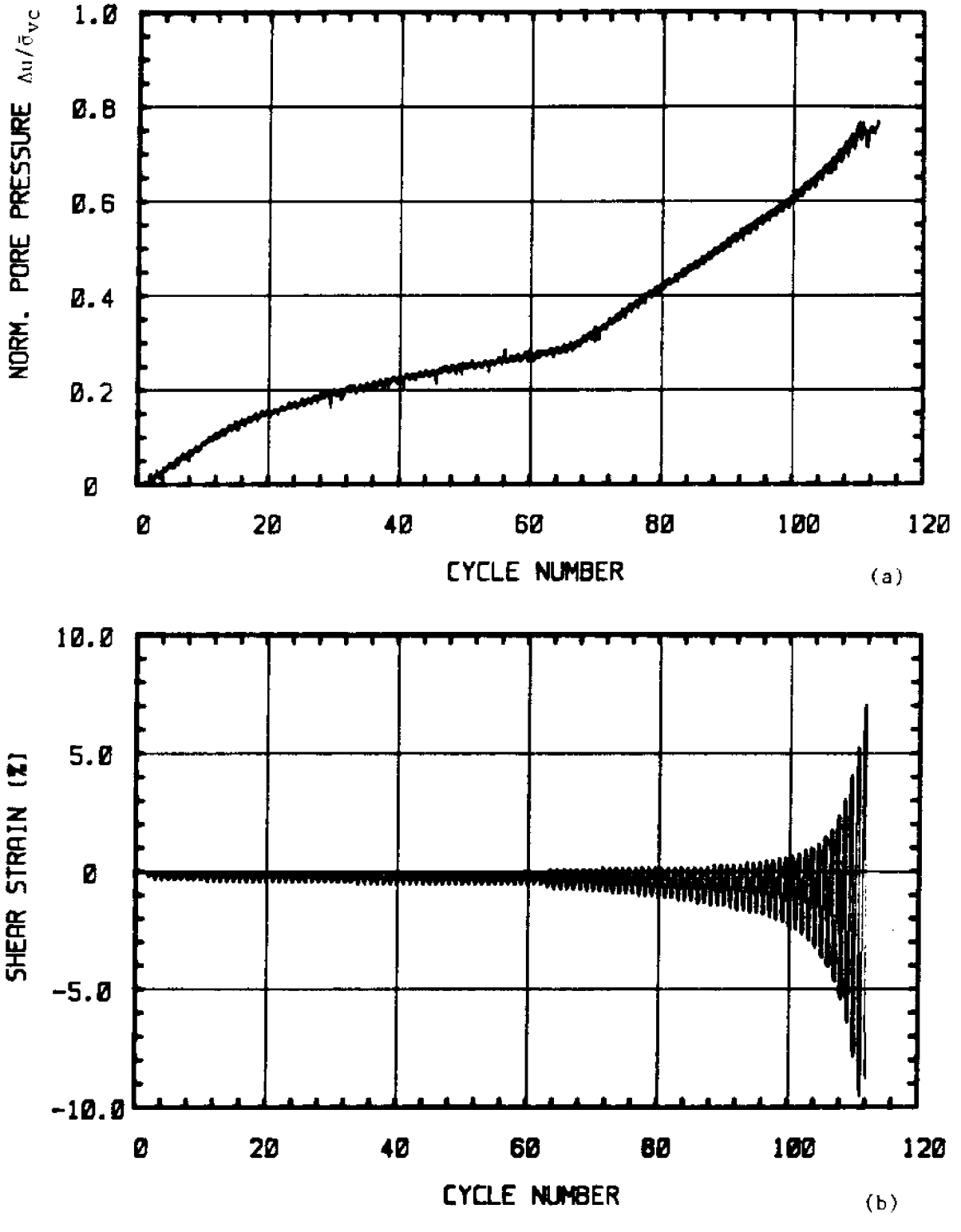

Figure 5.52 Test C-37: N.C. BBC, $\tau_{ave} = 0$, $\tau_c/s_u(NC) = 0.50, 0.64$
a) Normalized Excess Pore Pressure versus Cycle Number
b) Shear Strain versus Cycle Number

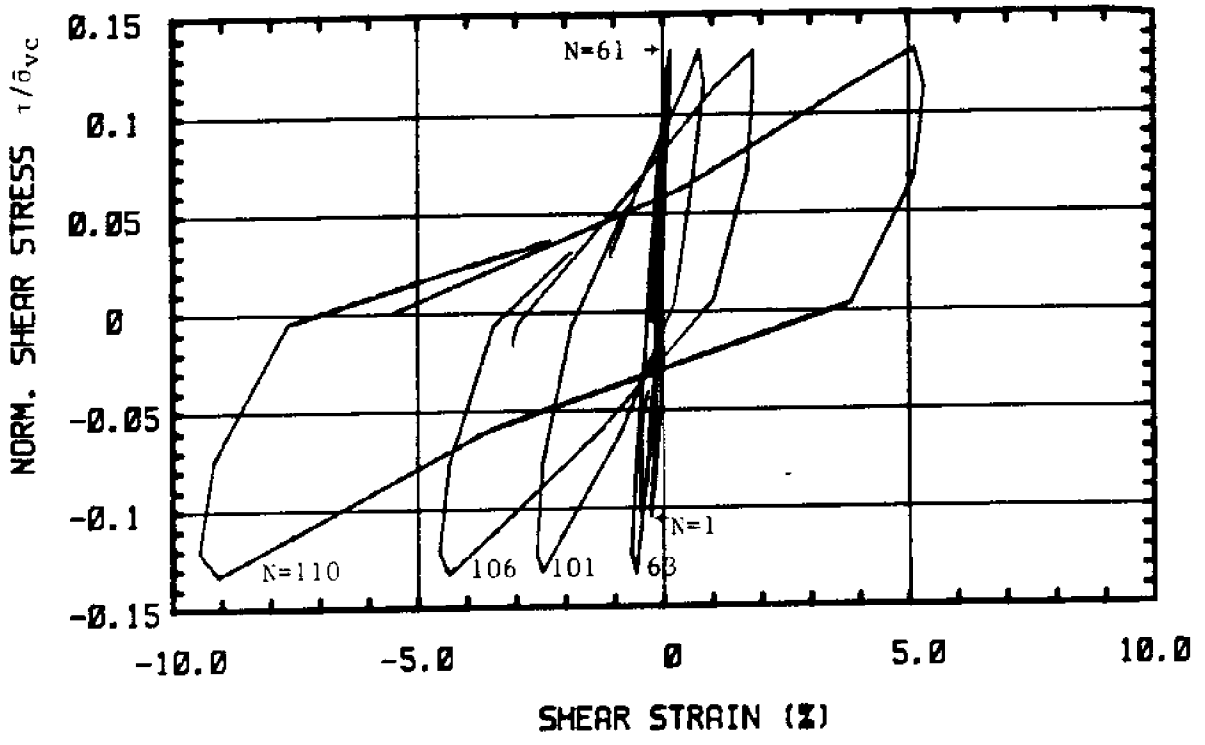

(c)

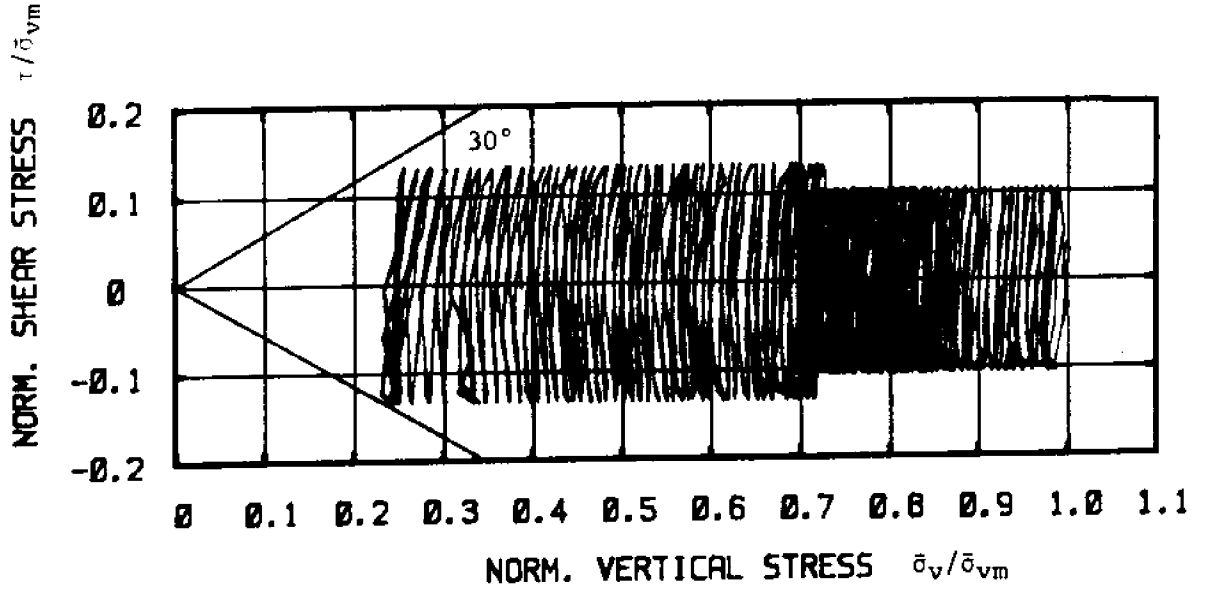

(d)

Figure 5.52 Test C-37: N.C. BBC, $\tau_{ave} = 0$, $\tau_c/s_u(NC) = 0.50, 0.64$
c) Normalized Shear Stress versus Shear Strain
d) Normalized Stress Path

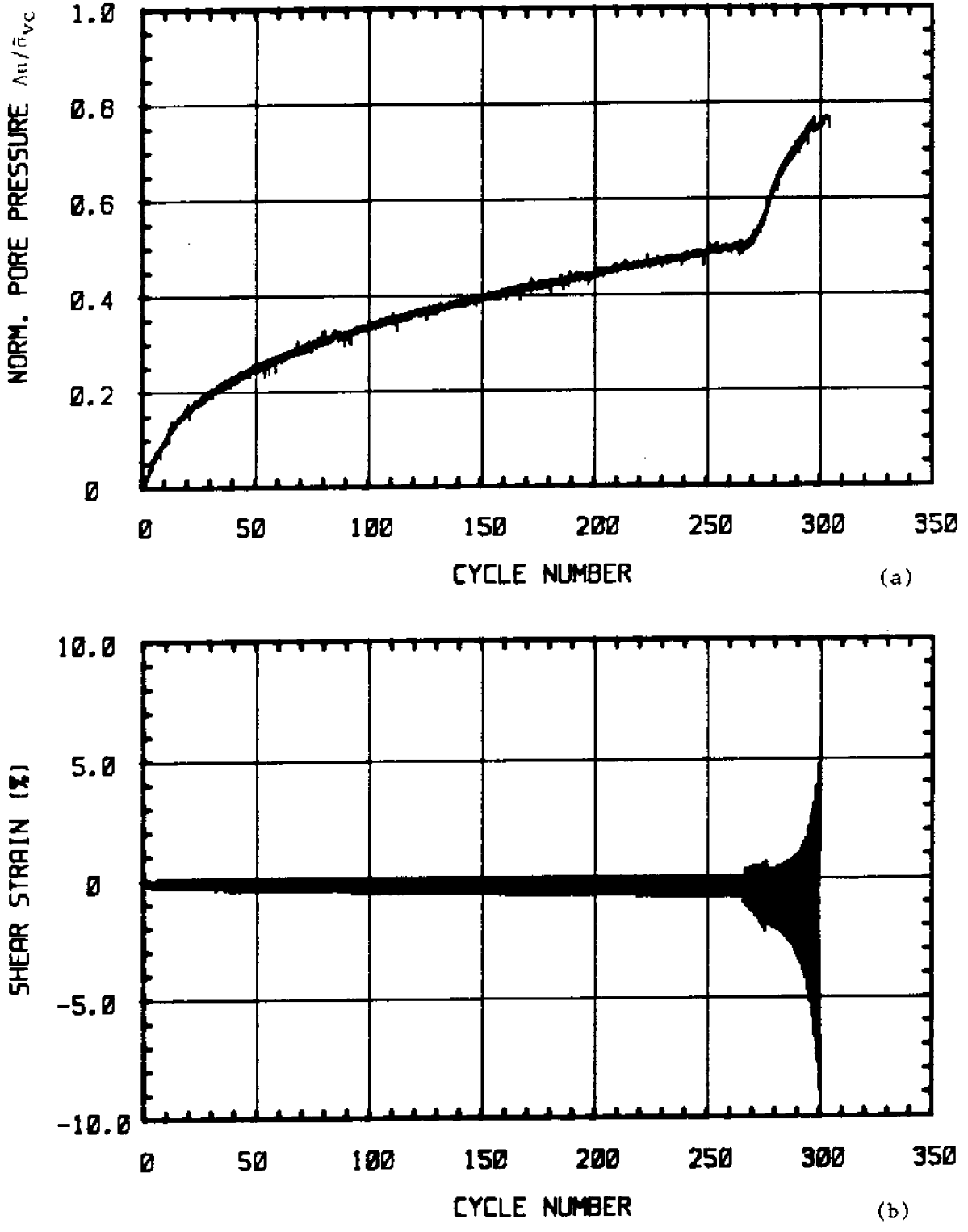

Figure 5.53 Test C-38: N.C. BBC, τ_{ave} = 0, τ_c/s_u(NC) = 0.50, 0.70, 0.56
a) Normalized Excess Pore Pressure versus Cycle Number
b) Shear Strain versus Cycle Number

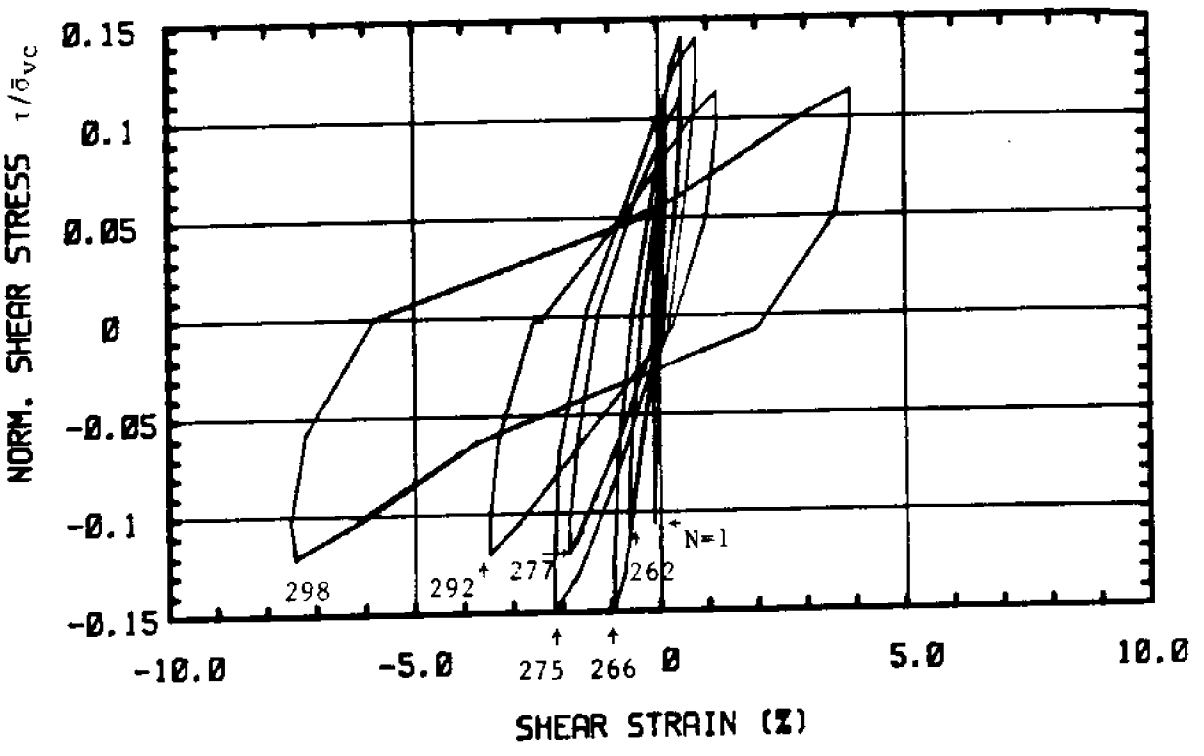

(c)

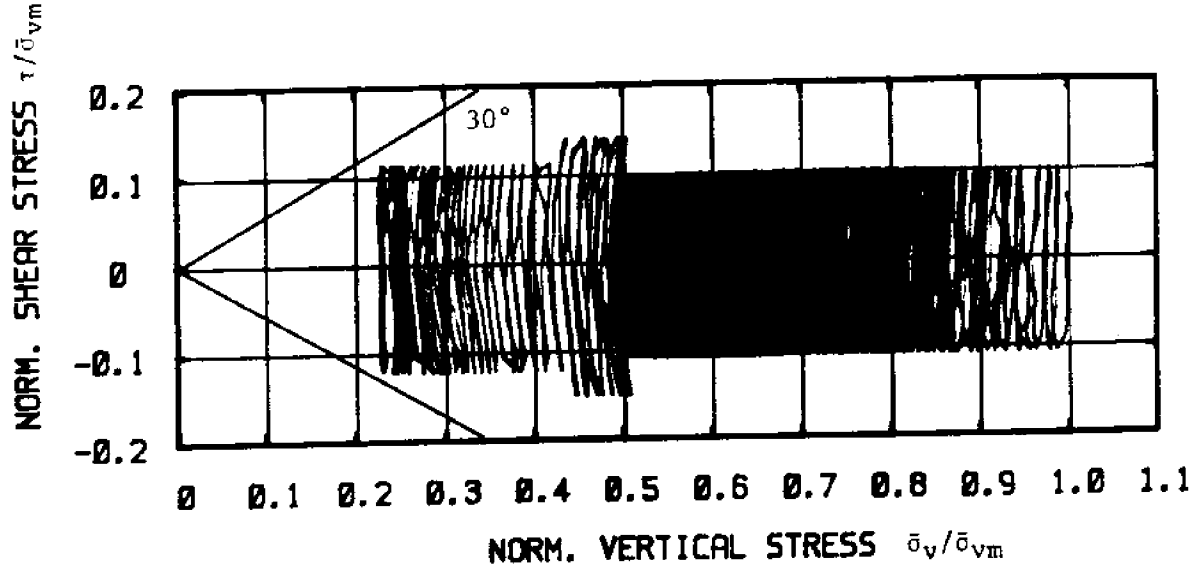

(d)

Figure 5.53 Test C-38: N.C. BBC, τ_{ave} = 0, τ_c/s_u(NC) = 0.50, 0.70, 0.56
c) Normalized Shear Stress versus Shear Strain
d) Normalized Stress Path

CHAPTER 6

UNDRAINED CYCLIC BEHAVIOR OF OVERCONSOLIDATED RESEDIMENTED BOSTON BLUE CLAY

This chapter presents results of cyclic undrained DSS tests on overconsolidated samples of resedimented Boston Blue Clay (RBBC), up to OCR=4. A summary of monotonic shearing is given first, followed by the results of the cyclic DSS tests. Finally, a hypothesis regarding Apparent Overconsolidation (AOCR) caused by undrained cycling is presented. The AOCR hypothesis enables predictions of the behavior of overconsolidated clays during undrained cyclic shearing to be made on the basis of test results on normally consolidated soil. In addition, the AOCR hypothesis allows predictions of clay response due to cyclic shearing with variable intensities.

6.1 OVERCONSOLIDATED BEHAVIOR UNDER UNDRAINED MONOTONIC SHEARING

Figures 6.1, 6.2, and 6.3 present results of eight undrained monotonic CK_oUDSS tests performed on RBBC samples with overconsolidation ratios ranging from 1 to 8, as reported by Ladd & Edgers (1972). The samples in these tests were first consolidated under K_o conditions to a value $\bar{\sigma}_{vm}$ in the virgin compression range and then the vertical effective stress was decreased to $\bar{\sigma}_{vc}$ in order to reach the desired $OCR=\bar{\sigma}_{vm}/\bar{\sigma}_{vc}$. The samples were then sheared in an undrained mode at a constant rate of strain.

Figure 6.1 shows the stress paths from these tests at OCR values of

1,2,4 and 8. Compared to the normally consolidated (NC) soil, the overconsolidated (OC) samples show a tendency for swelling as shearing starts, as indicated by the increase in $\bar{\sigma}_v/\bar{\sigma}_{vm}$. For high OCR values, (OCR=8), this tendency of $\bar{\sigma}_v/\bar{\sigma}_{vm}$ to increase continues until the peak resistance is reached. For medium values of OCR (OCR=2-4), the initial increase in $\bar{\sigma}_v/\bar{\sigma}_{vm}$ is followed by a decrease until peak. After the peak strength is reached, strain softening of the soil occurs at all OCRs. Both $\bar{\sigma}_v/\bar{\sigma}_{vm}$ and $\tau/\bar{\sigma}_{vm}$ tend to decrease and the stress paths approach the maximum obliquity line with $\bar{\phi}_{MO}=30°$. The peak normalized strength $s_u/\bar{\sigma}_{vm} = \tau_{max}/\bar{\sigma}_{vm}$ decreases with increasing OCR as is shown in the figure.

Figure 6.2 presents normalized shear stress and normalized pore pressure vs. shear strain. Both τ and Δu are normalized by $\bar{\sigma}_{vc}$, the vertical effective stress prior to undrained shearing. The stress vs. strain curves show an increase in $\tau_{max}/\bar{\sigma}_{vc}$ with increasing OCR (not to be confused with the decrease in $\tau_{max}/\bar{\sigma}_{vm}$ with OCR). The pore pressure vs. strain curves show a decrease in $\Delta u/\bar{\sigma}_{vc}$ (negative pore pressures) followed by an increase. The higher the OCR, the more negative the pore pressures, and the smaller the final value of $\Delta u/\bar{\sigma}_{vc}$.

Figure 6.3 plots the peak undrained strength ratio $s_u/\bar{\sigma}_{vc}$ vs. OCR. The data points can be fitted by the equation:

$$\frac{s_u(OC)}{\bar{\sigma}_{vc}(OC)} = \frac{s_u(NC)}{\bar{\sigma}_{vc}(NC)} (OCR)^m \qquad m = 0.8 \qquad (6.1)$$

which can be used to estimate the undrained DSS strength for any OCR value.

6.2 OVERCONSOLIDATED BEHAVIOR UNDER UNDRAINED CYCLIC SHEARING

Eight undrained cyclic DSS tests were performed in this study on overconsolidated samples of RBBC, and are listed in Table 6.1. Two tests were performed at OCR=1.38, four at OCR=2, and two at OCR=4, and all had zero average shear stress, $\tau_{ave}=0$. For each test, the table gives the test number, the maximum consolidation stress $\overline{\sigma}_{vm}$, the vertical effective consolidation stress $\overline{\sigma}_{vc}$, the overconsolidation ratio OCR, the average shear stress ratio $\tau_{ave}/s_u(OC)$, where $s_u(OC)$ is the undrained monotonic DSS strength at the proper OCR for each test, the cyclic shear stress ratio $\tau_c/s_u(OC)$ which ranges between 0.5 and 0.85, and finally information at failure (or maximum obliquity), including the cycle number at failure, the normalized excess pore pressure $\Delta u/\overline{\sigma}_{vc}$, and the average shear strain $\gamma_{ave}(\%)$.

6.2.1 Results at OCR=1.38

Tests C-26 and C-27 were performed on slightly overconsolidated samples with OCR=1.38. The test samples were first consolidated into the virgin compression range to $\overline{\sigma}_{vm}=6.0$ Kg/cm^2, then the vertical stress was decreased to $\overline{\sigma}_{vc}=4.36$ Kg/cm^2, and undrained cyclic shearing was performed with $\tau_{ave}=0$ and $\tau_c/s_u(OC)=0.60$ and 0.76, respectively.

Figures 6.4 and 6.5 show results of tests C-26 and C-27. Each figure includes:

(a) normalized excess pore pressure $\Delta u/\overline{\sigma}_{vc}$ versus number of cycles N;

(b) shear strain $\gamma(\%)$ versus the number of cycles N;

(c) normalized shear stress $\tau/\overline{\sigma}_{vc}$ versus shear strain $\gamma(\%)$ at selected cycles;

(d) effective stress path, which plots normalized shear stress $\tau/\bar{\sigma}_{vm}$ versus normalized vertical effective stress $\bar{\sigma}_v/\bar{\sigma}_{vm}$.

The results indicate generally similar trends:

1. The normalized excess pore pressure $\Delta u/\bar{\sigma}_{vc}$ is cyclic and does not increase sharply in the first cycles, as in the case of normally consolidated samples, but remains very small for the first couple of cycles and then starts increasing slowly with continued cyclic shearing until failure is reached and the pore pressure stabilizes.

2. The shear strain versus number of cycle plots show identical trends to those of normally consolidated samples. The cyclic shear strain $\gamma_c(\%)$ increases with number of cycles, while the average strain component remains zero, and the sample fails by increasing cyclic strain.

3. The normalized shear stress versus shear strain plots show hysteresis loops increasing in size with cycle number, which leads to a decreasing secant modulus with cycle number. At failure in test C-26, the modulus reaches 6% of the initial value at cycle one, and in test C-27, it reaches 10% of the initial value.

4. The stress paths start from a value of $\bar{\sigma}_v/\bar{\sigma}_{vm}=0.73$ corresponding to an OCR=1.38, and $\tau/\bar{\sigma}_{vm}$ varies between the specified peaks while the stress path migrates towards the origin. At failure, the stress path reaches the maximum obliquity line with $\bar{\phi}_{MO}=30.0° \pm 1.2°$, and the cyclic shear strain $\gamma_c(\%)$ is close to ± 3% as for normally consolidated samples.

Tests C-26 (OCR=1.38) and test C-5 (OCR=1) have the same value of $\tau_c/\bar{\sigma}_{vm}=0.117$, but different values of the cyclic shear stress ratio τ_c/s_u due to differences in the $s_u/\bar{\sigma}_{vc}$ values resulting from the different overconsolidation ratios. Test C-26 has a cyclic shear stress ratio τ_c/s_u (OCR=1.38)=0.60 which is higher than the cyclic shear stress ratio

$\tau_c/s_u(NC)=0.56$ of test C-5, and thus has a lower number of cycles at failure ($N_f=140$) than test C-5 ($N_f=160$). Also, tests C-27 (OCR=1.38) and C-6 (OCR=1) have the same values of $\tau_c/\bar{\sigma}_{vm}=0.144$, but different values of cyclic shear stress ratio. Test C-27 has τ_c/s_u (OCR=1.38)=0.76, and test C-27 has $\tau_c/s_u(NC)=0.70$, which also results in a lower number of cycles at failure for the overconsolidated sample ($N_f=37$ for test C-27 versus $N_f=43$ for test C-6).

6.2.2 Results at OCR=2

Tests C-33 through C-36 were performed on samples with OCR=2. The test samples were first consolidated to $\bar{\sigma}_{vm}=6.0$ Kg/cm^2, then unloaded to $\bar{\sigma}_{vc}=3.0$ Kg/cm^2, and sheared under undrained cyclic loading with $\tau_{ave}=0$ and $\tau_c/s_u(OC)$ ranging between 0.56 and 0.85.

Figures 6.6 through 6.9 show results of the four tests which indicate the following:

1. The normalized excess pore pressure, $\Delta u/\bar{\sigma}_{vc}$, is cyclic. During early cycles, it decreases and reaches a maximum negative value of -0.05. However, it gradually increases and becomes positive with increasing numbers of cycles until failure.

2. The shear strain versus cycle number plots indicate increasing cyclic strain $\gamma_c(\%)$ with cycle number, until failure occurs by increasing $\gamma_c(\%)$, while $\gamma_{ave}(\%)$ remains zero.

3. The secant modulus decreases with increasing cycle number, and at failure, the modulus is typically equal to 8% to 11% of the initial value at cycle one.

4. The effective stress path starts at $\bar{\sigma}_v/\bar{\sigma}_{vm}=0.5$, corresponding to OCR=2, and moves away from the origin (corresponding to negative excess

pore pressures) in the beginning of the tests, then it migrates towards the origin as positive excess pore pressures are generated, until failure is reached at the maximum obliquity line.

Tests C-33 and C-35 involve identical loading. Comparison of their results, which are shown in Figures 6.6 and 6.8, shows very good agreement, hence presents another confirmation of test repeatability. The major difference is a 10% change in the cycle number at failure (N_f=264 for test C-33 and 240 for test C-35), which is small and negligible. These two tests have the same value of $\tau_c/\bar{\sigma}_{vm}$=0.10, which almost equals that of test C-2 with OCR=1. However, the overconsolidated tests have a higher value of τ_c/s_u(OCR=2)=0.56 than the normally consolidated test with τ_c/s_u(NC)=0.50, and thus a smaller number of cycles at failure (N_f=252 for tests C-33 and C-35 versus N_f=525 for tests C-2).

6.2.3 Results at OCR=4

Tests C-31 and C-32 were performed on samples with OCR=4. The samples were consolidated to $\bar{\sigma}_{vm}$=6.0 Kg/cm^2, then unloaded to $\bar{\sigma}_{vc}$=1.5 and cycled undrained with τ_{ave}=0 and τ_c/s_u(OC)=0.55 and 0.50 respectively. The results are shown in Figures 6.10 and 6.11, and indicate the following trends:

1. The normalized excess pore pressure, $\Delta u/\bar{\sigma}_{vc}$, is cyclic and initially starts with large negative values (up to a maximum of -0.15), then becomes positive and increases very rapidly until failure. Test C-31 experienced problems with the height adjustment, causing a jump in excess pore pressure at cycle 56.

2. The shear strain versus cycle number shows a gradual increase in cyclic shear strain until failure by increased cyclic strain, and zero

average shear strain.

3. The normalized shear stress versus shear strain shows hysteresis loops increasing in size, as the secant modulus decreases with cycle number, and at failure, it reaches 8% to 6% of the initial value at cycle one.

4. The effective stress path starts at $\bar{\sigma}_v/\bar{\sigma}_{vm}$=0.25, and moves to the right to about $\bar{\sigma}_v/\bar{\sigma}_{vm}$=0.28 before it starts migrating towards the origin. At failure, the stress path reaches maximum obliquity $\bar{\phi}$=30° ± 1.2°. The sudden decrease in vertical effective stress in Figure 6.10(d) due to the experimental problem mentioned above.

6.2.4 Summary of Overconsolidated Behavior

Undrained cyclic DSS tests on eight samples of overconsolidated resedimented Boston Blue Clay, with zero average shear stress indicate the following:

1. The failure mechanism and criterion are the same as for normally consolidated samples, namely that failure occurs when the effective stress path reaches the maximum obliquity line, at which point the cyclic shear strain γ_c(%) reaches large values, and the average shear strain remains zero.

2. The rate of excess pore pressure generation differs for overconsolidated samples. At the beginning of cyclic testing, the excess pore pressures are negative, with increasingly negative values for higher OCR values. At failure, the excess pore pressures are positive, and can be estimated from:

$$\frac{\Delta u_f}{\bar{\sigma}_{vc}} = 1 - \frac{\tau_{ave} + \tau_c}{\bar{\sigma}_{vc}(\tan \bar{\Phi}_{MO})} \qquad (6.2)$$

which is obtained from the geometry in Figure 6.12, and is identical to Equation 5.2 for normally consolidated clay samples.

For RBBC with $\frac{s_u(OC)}{\bar{\sigma}_{vc}(OC)} = 0.205\ (OCR)^{0.8}$, and $\bar{\phi}_{MO}=30°$, equation 6.2 can be rewritten as:

$$\Delta u_f = \left[1 - \frac{0.205\ (OCR)^{0.8}\left(\tau_{ave}/s_{u(OC)} + \tau_c/s_{u(OC)}\right)}{\tan 30°}\right] \qquad (6.3)$$

which reduces to equation 5.3 for normally consolidated samples.

3. For the same values of $\tau_c/\bar{\sigma}_{vm}$, overconsolidated samples fail at smaller number of cycles N_f than normally consolidated samples. However, overconsolidated samples are stronger and fail at larger N_f values than normally consolidated ones when subjected to the same value of $\tau_c/\bar{\sigma}_{vc}$.

4. S-N curves at maximum obliquity for OCR values of 1.38, 2, and 4 are shown in Figure 6.13. These curves are drawn from the knowledge of $\tau_c/s_u(OC)$ and the number of cycles at failure N_f for each of the tests listed in Table 6.1. The curves for OCR=1.38 and 2 are very close, and plot slightly higher than the normally consolidated S-N curve at maximum obliquity. However, the curve corresponding to OCR=4 plots below the normally consolidated curve. Andersen (1975) performed cyclic undrained DSS tests with $\tau_{ave}=0$ at varying OCR values. Figure 6.14 shows Andersen's S-N curves at failure (defined as ± 3% cyclic shear strain) at OCR=1, 4, and 10, and indicates a trend of lower S-N curves at failure with increasing OCR. Comparison of Figures 6.13 and 6.14 shows good agreement at OCR=4, namely that the S-N curve at failure for OCR=4 is lower than the S-N curve at failure for N.C. clay. However, no data are reported by Andersen to allow comparisons at lower OCR values. The results at low OCR values of 1.38 and 2, in Figure 6.13, seem to indicate a contradiction in

the expected trend with OCR. However, before such a conclusion is made, a more careful examination of the data is required, and is presented in the next paragraph.

The S-N curves in Figure 6.13 were constructed using the cyclic stress ratios listed in Table 6.1. These were computed based on the overconsolidated undrained monotonic DSS strength $s_u(OC)$ given by Equation 6.1, which is an average fit of the experimental data shown in Figure 6.3. There is scatter in the overconsolidated strength, which induces an equivalent scatter in the cyclic shear stress ratio, resulting in a scatter in the position of the S-N curves. Figure 6.15(a) and (b) plot the range of S-N curves at failure corresponding to the scatter in undrained strength at OCR values of 2 and 4 for Boston Blue Clay. Figures 6.15(a) and (b) show that, depending on the value of $s_u(OC)$ used, the S-N curves for OCR=2 and 4 can be either above or below the normally consolidated S-N curve. Therefore, a definite trend with OCR cannot be expected, and would be very difficult to see at low OCR values because of the high sensitivity of the S-N curves to the undrained strength, and the high sensitivity of number of cycles at failure to the cyclic stress ratio.

The important conclusion from Figures 6.13 through 6.15 is that there is a general trend of lower S-N curves at failure with increasing OCR. However, the position of the S-N curves is very sensitive to the undrained strength value used in computing the cyclic stress ratio, which might mask this trend.

6.3 APPARENT OVERCONSOLIDATION CAUSED BY UNDRAINED CYCLIC SHEARING

The results in Chapter 5 and previous sections of Chapter 6 showed that undrained cyclic shearing causes excess pore pressures in the soil, hence changes in effective stresses as well as changes in soil properties. This section investigates the effects of undrained cyclic shearing on subsequent undrained monotonic clay behavior. Various researchers have studied this problem, and some of their results which are of particular interest to the current research are summarized below.

6.3.1 Results of Andersen (1975)

Andersen (1975) at the Norwegian Geotechnical Institute (NGI) reports results of several undrained monotonic shear tests which were performed at NGI using both the triaxial and the direct simple shear devices, on Drammen clay samples which were presheared cyclically in an undrained fashion for a prescribed number of cycles. The triaxial samples were subjected to one way cycling, and the DSS samples to two way cycling (τ_{ave}=0) before they were sheared monotonically. Figure 6.16 shows the stress paths during subsequent undrained monotonic shearing of these samples and indicates the following:

> "Normally consolidated samples which are subjected to undrained cyclic loading of some severity...behave as overconsolidated in a subsequent static (monotonic) test."
>
> "The reason why the effective stress paths for static loading on normally consolidated samples which have been subjected to undrained cyclic loading approach the failure envelope for overconsolidated clays, is most probably the reduction in effective stresses due to the generation of pore water pressure during [undrained] cyclic loading. This effective stress reduction has the same effect as if the effective stresses had been reduced by a real unloading which will increase the OCR of the clay sample."
>
> "On the average, the effective stress path for static loading on overconsolidated clay ends up at the same effective strength envelope

whether the clay has been subjected to previous undrained cyclic loading or not. However, there is a tendency for the cohesion intercept to be larger for samples with a low cyclic stress level than for those with high stress level."[1]

Figure 6.17 shows the stress-strain and pore pressure curves during undrained static loading, with and without undrained cyclic preshearing, for DSS samples with OCR=1 and 4. The results indicate:

"the deformation modulus has decreased due to cyclic loading, and it seems like the decrease in modulus is a function of the amount of cyclic shear strain that the clay sample has experienced."

"..the samples which have been subjected to undrained cyclic loading are not able to mobilize as high horizontal shear stresses at failure as samples without previous undrained cyclic loading. This behavior is also in agreement with the effective stress paths..."[2]

In conclusion, research at NGI has indicated that undrained cyclic loading of normally consolidated samples leads to a decrease in effective stress which has the same effect as overconsolidation in subsequent monotonic shearing.

6.3.2 Results of Researchers at the University of Chile

Ortigosa et al. of the University of Chile report results on the behavior of Quilicura clay subjected to cyclic triaxial testing. Part of their research involved the performance of monotonic undrained triaxial tests on clay samples which were previously cycled in an undrained fashion. The clay samples, which exhibit normalized behavior, were first consolidated into the normally consolidated range to $\bar{\sigma}_{cmax}$, then subjected to undrained cyclic loading with constant, as well as variable cyclic shear

---

[1]K.H. Andersen, Research Report, Repeated Loading on Clay: Summary and Interpretation of Test Results, NGI Report No. 74037-9, 15 October 1975, pp. 10-1, 10-2.

[2]Ibid, p. 10-3.

stresses. At the end of cycling, an increase in excess pore pressure, equal to the decrease in effective stress from $\bar{\sigma}_{cmax}$ to $\bar{\sigma}_c$, was measured. The pore pressures were allowed to equilibrate, and then the sample was sheared in undrained monotonic loading. The measured undrained shear strength normalized by the effective confining stress at the end of cyclic shearing is plotted in Figure 6.18 versus the "quasi-overconsolidation ratio" equal to $\bar{\sigma}_{cmax}/\bar{\sigma}_c$. The figure also plots the range of normalized strength with increasing OCR, for typical clays obeying normalized behavior. This range is given by:

$$s_u(OC)/\bar{\sigma}_{vc}(OC) = s_u(NC)/\bar{\sigma}_{vc}(NC) \cdot (OCR)^m \qquad (6.4)$$

where $m = 0.8 \pm 0.1$.

There is good agreement between the experimental data and the range of overconsolidated strength values obtained from the equation. Therefore, it seems that normally consolidated samples of Quilicura clay, subjected to previous undrained cycling of either constant or variable magnitude, behave as overconsolidated samples when sheared in undrained monotonic loading.

6.3.3 Apparent Overconsolidation in Resedimented Boston Blue Clay

First Observation

Test C-21 was performed on a normally consolidated RBBC sample. The test was the only strain-controlled test in the series and consisted of applying a cyclic shear strain $\gamma_c = \pm 0.5\%$ with $\Delta\gamma_{ave}=0$ (two way cycling). The results are shown in Figure 6.19 and indicated that there is a gradual decrease in cyclic shear stress (and therefore in modulus), and after 8500 cycles, failure had not occured, and the stress path had moved from initial values of $\bar{\sigma}_v/\bar{\sigma}_{vm}=1$ and $\tau/\bar{\sigma}_{vm}=0.15$ to final values of $\bar{\sigma}_v/\bar{\sigma}_{vm}=0.25$ and

$\tau/\overline{\sigma}_{vm}$=0.06, which is below the maximum obliquity line of 30° ± 1.2°.

After cycling had stopped, the sample was sheared in an undrained monotonic fashion and results are shown in Figure 6.20. In discussing these results note that, due to cyclic shearing, the vertical effective stress decreased from a value of $\overline{\sigma}_v/\overline{\sigma}_{vm}$=1 to 0.25 and hence resulted in an "Apparent Overconsolidation Ratio," AOCR=4. Comparison of results in Figure 6.20 with results of a "mechanically overconsolidated" sample of OCR=4 in Figures 6.1 and 6.2, shows the following:

1) The effective stress paths (in the normalized $\tau/\overline{\sigma}_{vm}$ vs. $\overline{\sigma}_v/\overline{\sigma}_{vm}$ plane) are very similar in shape (compare Figure 6.20(a) and 6.1);

2) The peak shear strength for the cycled sample to AOCR=4 is given by $s_u/\overline{\sigma}_{vm}$=0.155. This value is very close to the $s_u/\overline{\sigma}_{vm}$= 0.15 (± 0.01) given by the mechanically overconsolidated samples with OCR=4 (see Figure 6.2(a) and note that for OCR=4, $\overline{\sigma}_{vm}/\overline{\sigma}_{vc}$=4) or values calculated by means of Equation 6.1;

3) The stress-strain behavior of the cycled sample to AOCR=4 (Figure 6.20(b)) is very similar to overconsolidated samples having OCR=4 (Figure 6.2(a)) such that the peak strength is reached at the same strain level γ=10%.

In summary, undrained cyclic DSS shearing of normally consolidated RBBC appears to develop an apparent overconsolidation of the clay as reported in previous NGI and other studies. Furthermore, the monotonic undrained shear behavior following undrained cycling loading is very similar to clays mechanically overconsolidated to the same Apparent Overconsolidation Ratio AOCR (= $\overline{\sigma}_{vm}/\overline{\sigma}_v$). In particular, this means that the shear strength, s_u, of a cyclically sheared sample can be estimated at any stage of cyclic loading by means of Equation 6.1.

Second Observation

Results of a triaxial test on RBBC (Lutz, 1985) are shown in Figure 6.21. This test consists of first shearing a K_o-normally consolidated sample in compression to an axial strain of +1%, then shearing it in extension to -1% axial strain. Following this load-unload cycle to ± 1%, the sample was finally sheared to 10% axial strain in compression.

The stress path and the stress-strain response are shown in Figures 6.21(a) and (b), respectively. The stress path indicates that after the loading-unloading cycle, (Path AB) the sample has an apparent OCR and behaves like a mechanically overconsolidated sample. Moreover, the stress-strain curve shows that the second compression loading resulted in a value of $s_u/\overline{\sigma}_{vm}$=0.25 which is lower than that of the first compression $s_u/\overline{\sigma}_{vm}$=0.320. Also, in the second compression loading, the stiffness has decreased. The values of $\overline{p}/\overline{\sigma}_{vm}$ and $q/\overline{\sigma}_{vm}$ at the beginning of the first compression (point A) when the sample was normally consolidated, and those at the beginning of the second compression loading (point B) when the sample was apparently overconsolidated (due to the one cycle of cyclic strain) can be used to compute the AOCR, which equals AOCR= 5.2 (see Figure 6.21). Using the apparent OCR and Equation 6.1, a value of the peak $s_u/\overline{\sigma}_{vm}$ for the second compression loading of the test can be estimated, and equals 0.230.

The estimated value of 0.230 is close to the measured value of 0.25 (the error is 8%), which further supports the apparent overconsolidation observation.

6.3.4 Apparent Overconsolidation Hypothesis

For purposes of estimating the undrained behavior of clays subjected

to complicated (and often unknown) stressing or straining histories which might involve cyclic (or variable) loading around TLP piles, results described above suggest that "Reasonable predictions of the undrained stress-strain-strength behavior of clays can be obtained on the basis of: 1) the effective stress state prior to undrained shearing, and 2) the maximum past pressure to which the soil has been subjected."

This simplifying hypothesis avoids insurmountable difficulties by neglecting the detailed history of straining of a soil element adjacent to a TLP pile. On the other hand, the hypothesis contradicts well established concepts of soil behavior, e.g. the unique relationship between void ratio and undrained strength. A careful evaluation of this hypothesis and its limitations is therefore needed.

TABLE 6.1

SUMMARY OF UNDRAINED CYCLIC DSS TESTS
WITH τ_{ave}=0 ON OVERCONSOLIDATED BBC

						Failure: at Maximum Obliquity		
TEST NO.	$\bar{\sigma}_{vm}$ Kg/cm^2	$\bar{\sigma}_{vc}$ Kg/cm^2	OCR	$\frac{\tau_{ave}}{s_u(OC)}$	$\frac{\tau_c}{s_u(OC)}$	N_f	$\frac{\Delta u}{\bar{\sigma}_{vc}}$	γ_{ave} (%)
C-26	6.00	4.36	1.38	0	0.60	140	0.66	-0.94
C-27	6.01	4.36	1.38	0	0.76	37	0.60	-1.03
C-31	6.00	1.50	4	0	0.55	80	0.43	-1.08
C-32	6.00	1.50	4	0	0.50	150	0.48	-1.69
C-33	6.01	3.01	2	0	0.56	264	0.65	-0.83
C-34	6.01	3.01	2	0	0.70	50	0.57	-0.76
C-35	6.01	3.00	2	0	0.56	240	0.67	-0.63
C-36	6.00	3.00	2	0	0.85	15	0.44	0.52

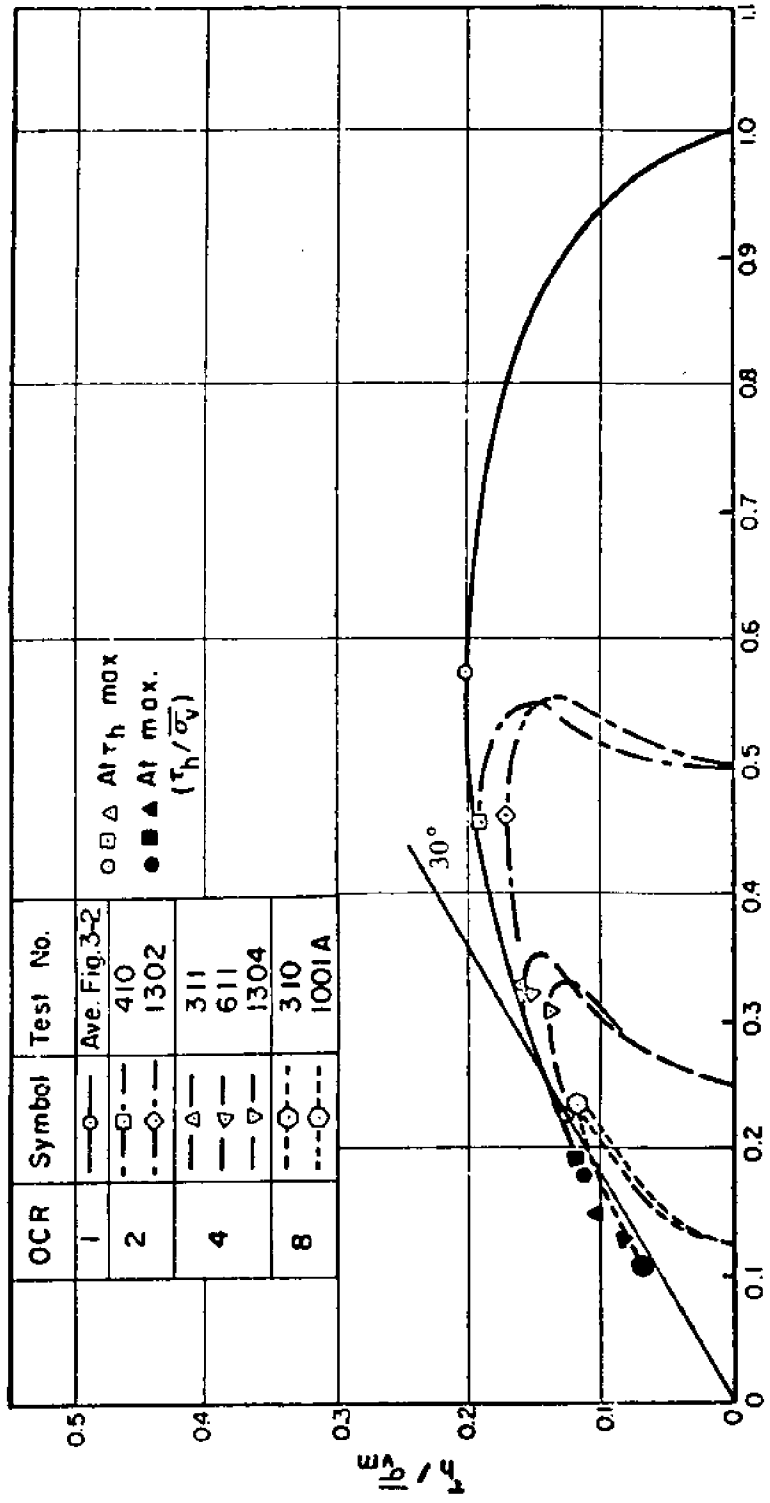

Figure 6.1 Normalized Effective Stress Paths from Monotonic CK_oUDSS Tests (from Ladd and Edgers, 1972)

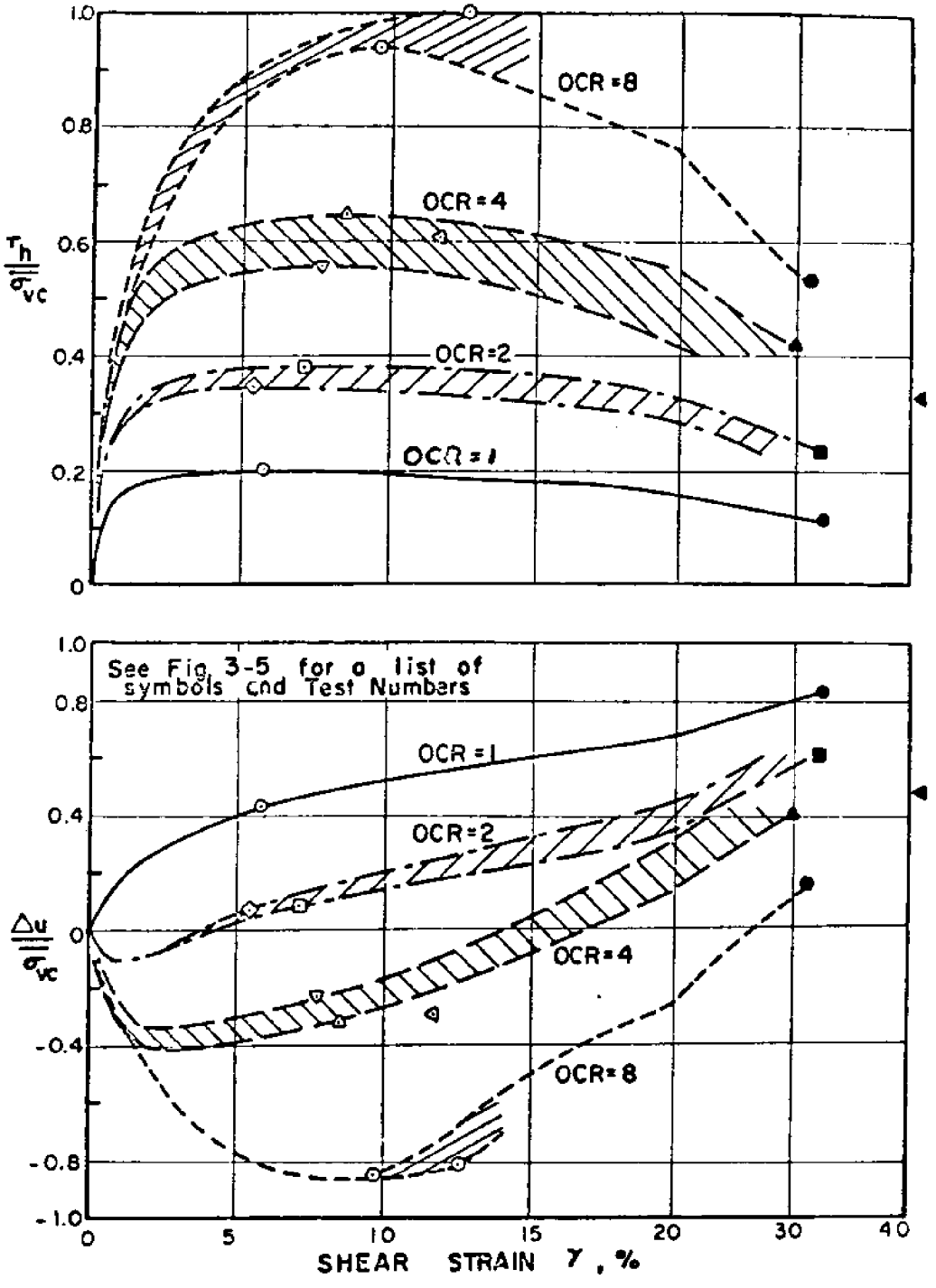

NORMALIZED STRESS VS STRAIN FROM $\overline{CK_oUDSS}$ TESTS ON BOSTON BLUE CLAY AT OCR = 1, 2, 4 AND 8

Figure 6.2 Normalized Stress-Strain and Excess Pore Pressure versus Shear Strain Curves from Monotonic CK_oUDSS Tests (from Ladd and Edgers, 1972)

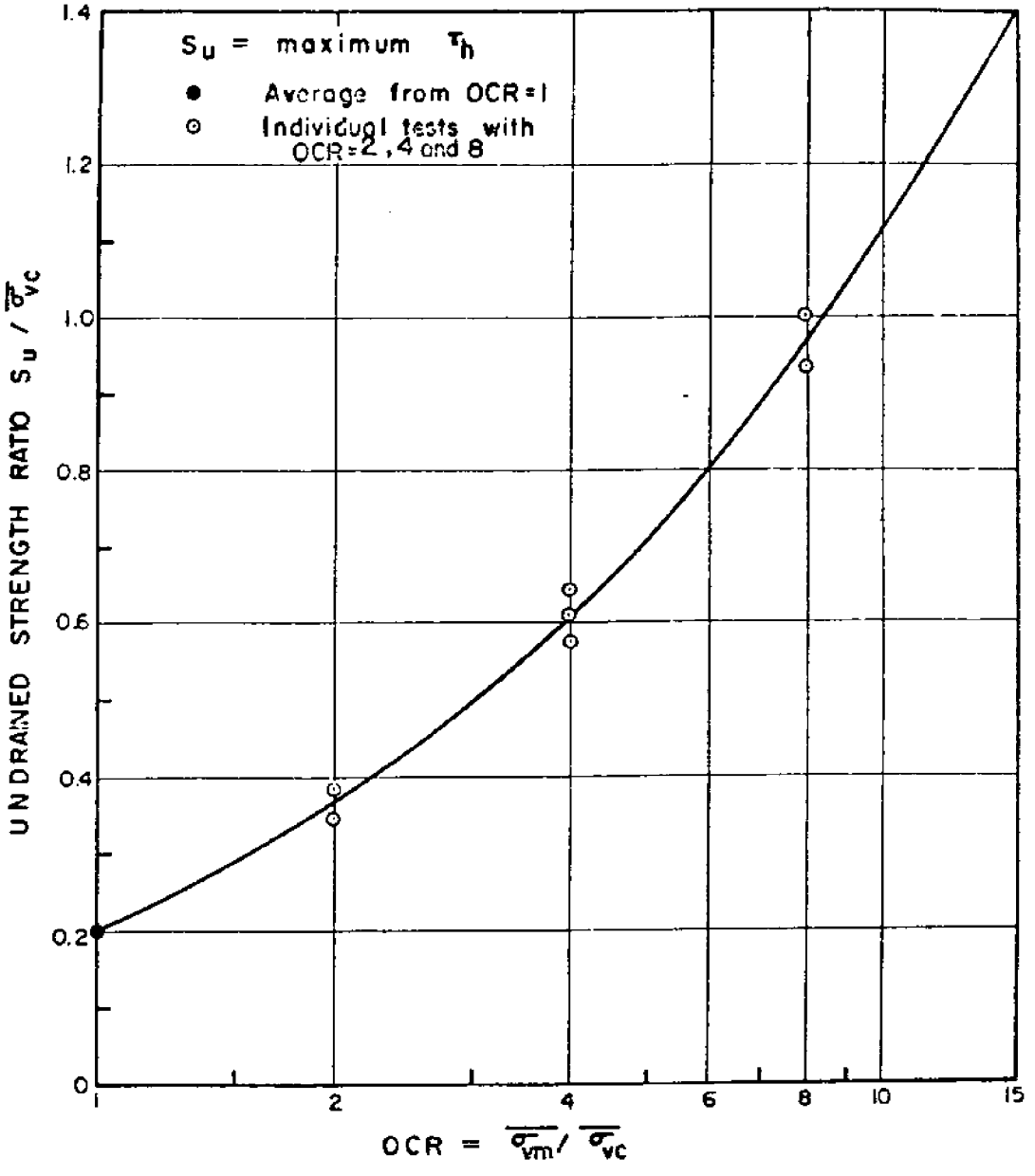

UNDRAINED STRENGTH RATIO VS OVERCONSOLIDATION RATIO FROM $\overline{CK_0UDSS}$ TESTS ON BOSTON BLUE CLAY

Figure 6.3 Undrained Strength Ratio versus OCR from Monotonic CK_0UDSS Tests (from Ladd and Edgers, 1972)

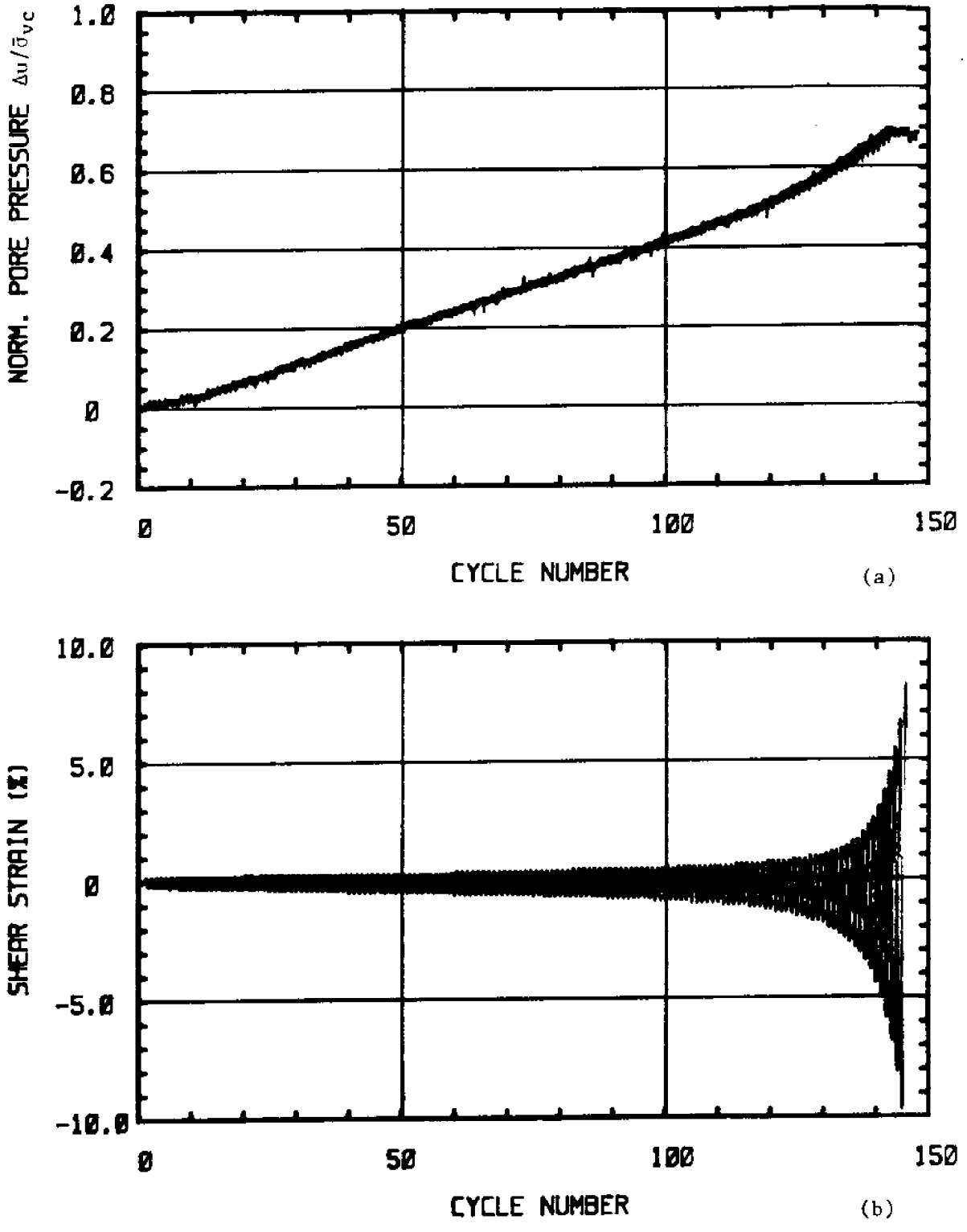

Figure 6.4 Test C-26: OCR = 1.38, τ_{ave} = 0, τ_c/s_u(OC) = 0.60
a) Normalized Excess Pore Pressure versus Cycle Number
b) Shear Strain versus Cycle Number

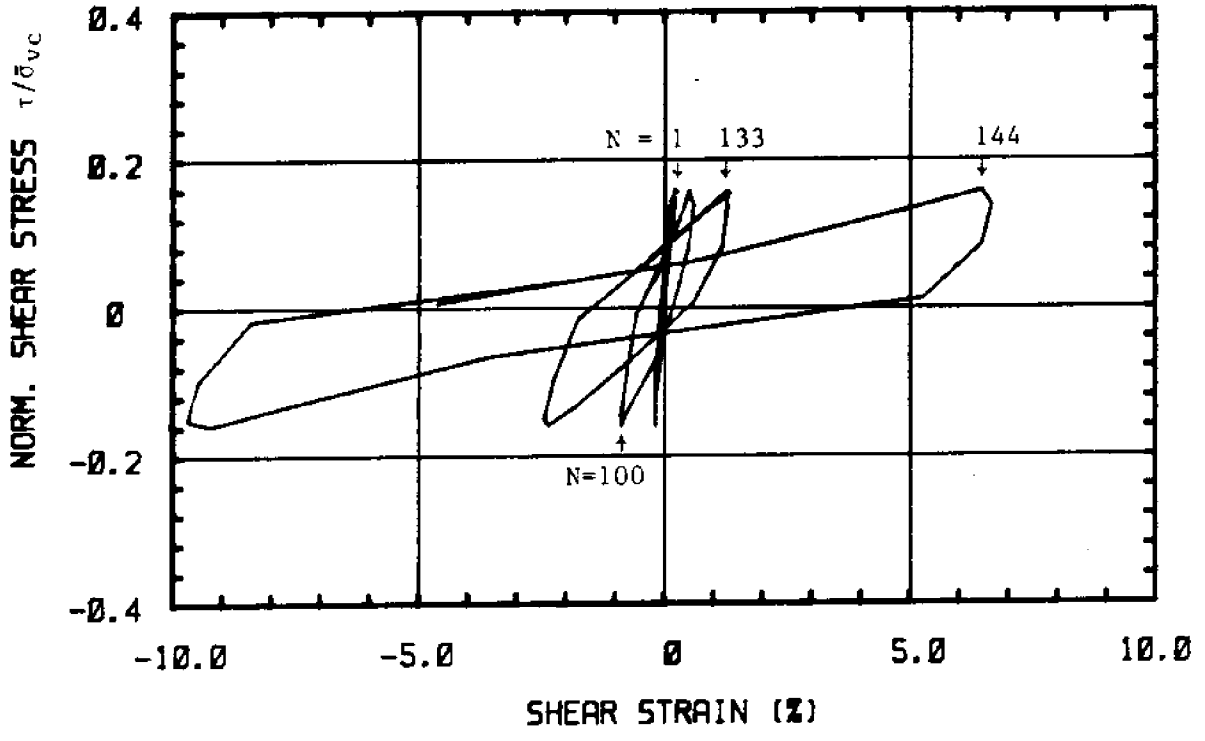

(c)

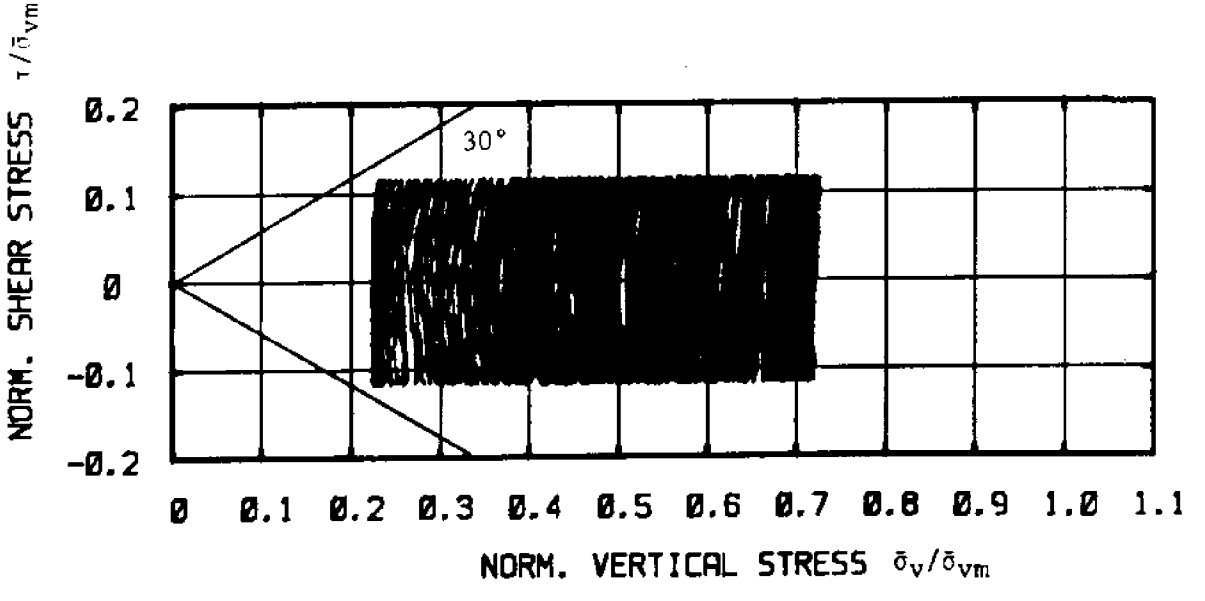

(d)

Figure 6.4 Test C-26: OCR = 1.38, τ_{ave} = 0, $\tau_c/s_u(OC)$ = 0.60
c) Normalized Shear Stress versus Shear Strain
d) Normalized Stress Path

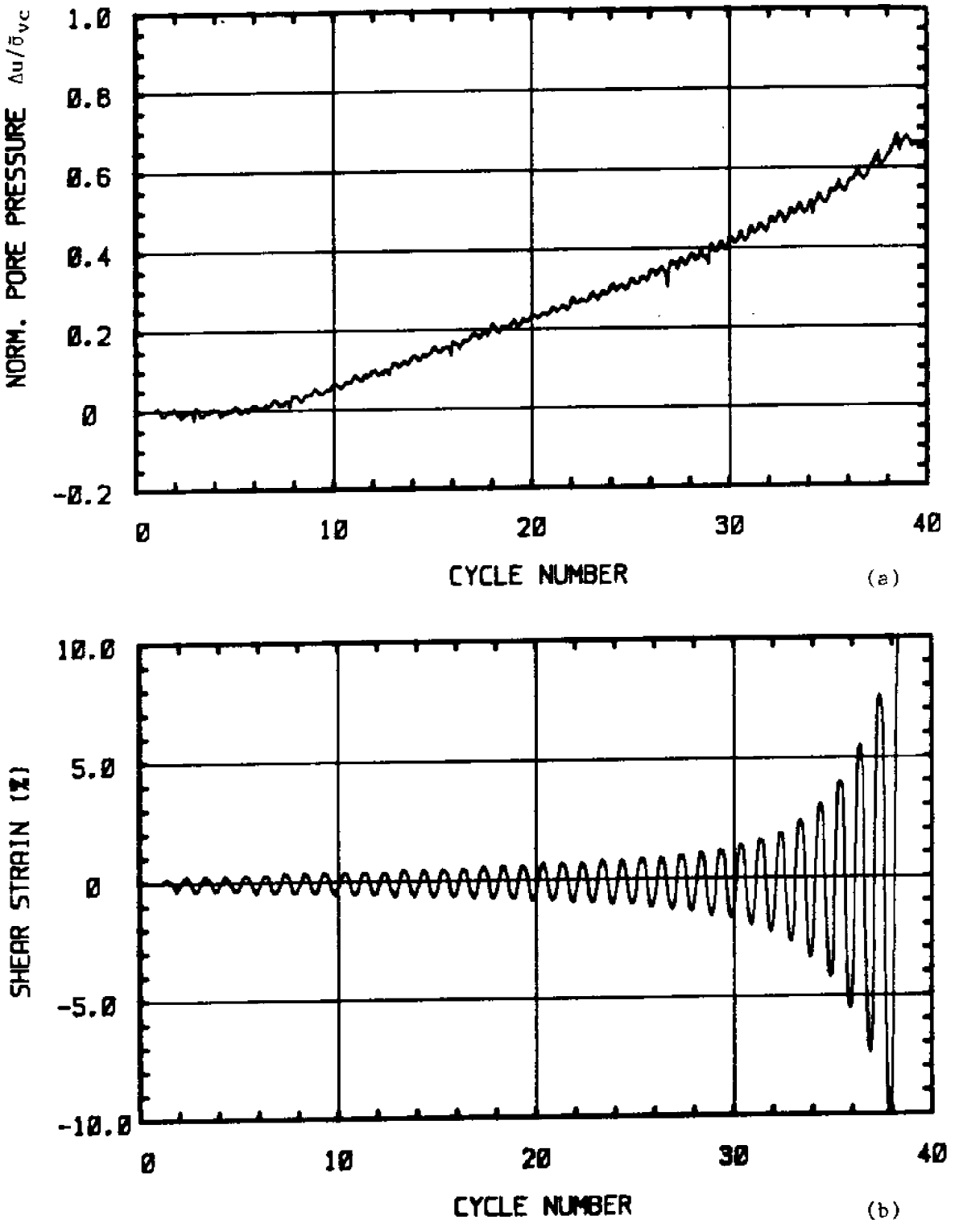

Figure 6.5 Test C-27: OCR = 1.38, τ_{ave} = 0, $\tau_c/s_u(OC)$ = 0.76
a) Normalized Excess Pore Pressure versus Cycle Number
b) Shear Strain versus Cycle Number

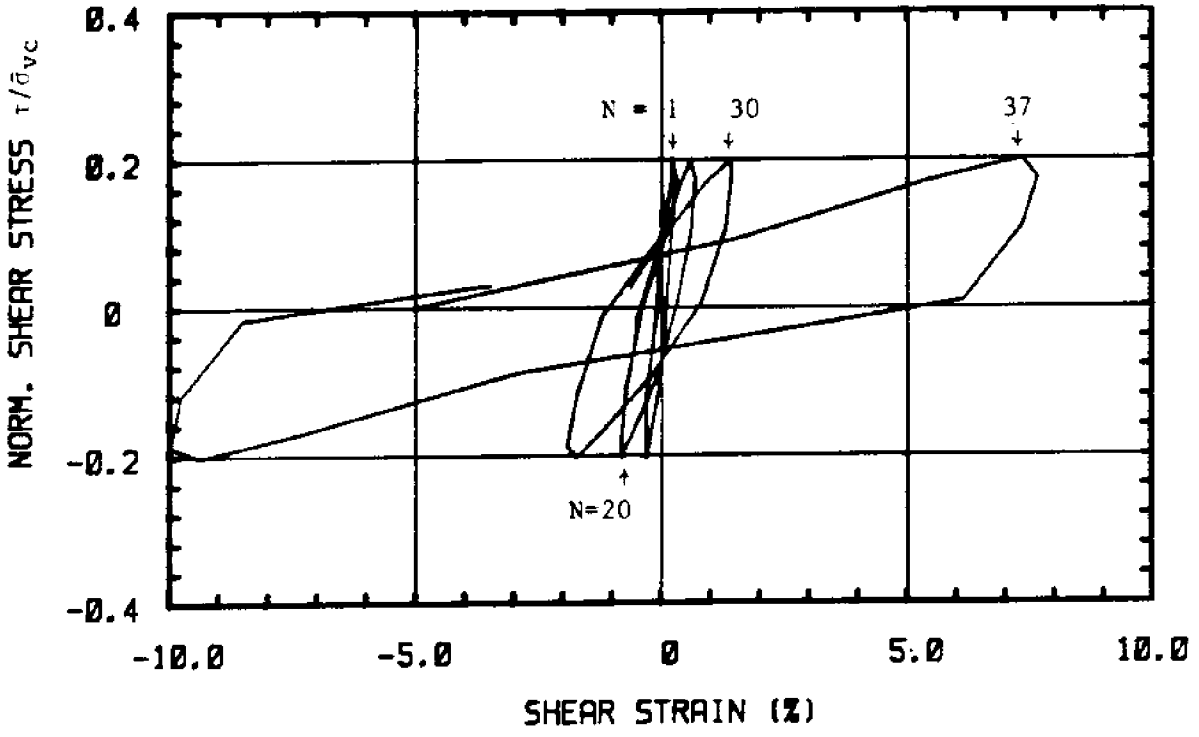

(c)

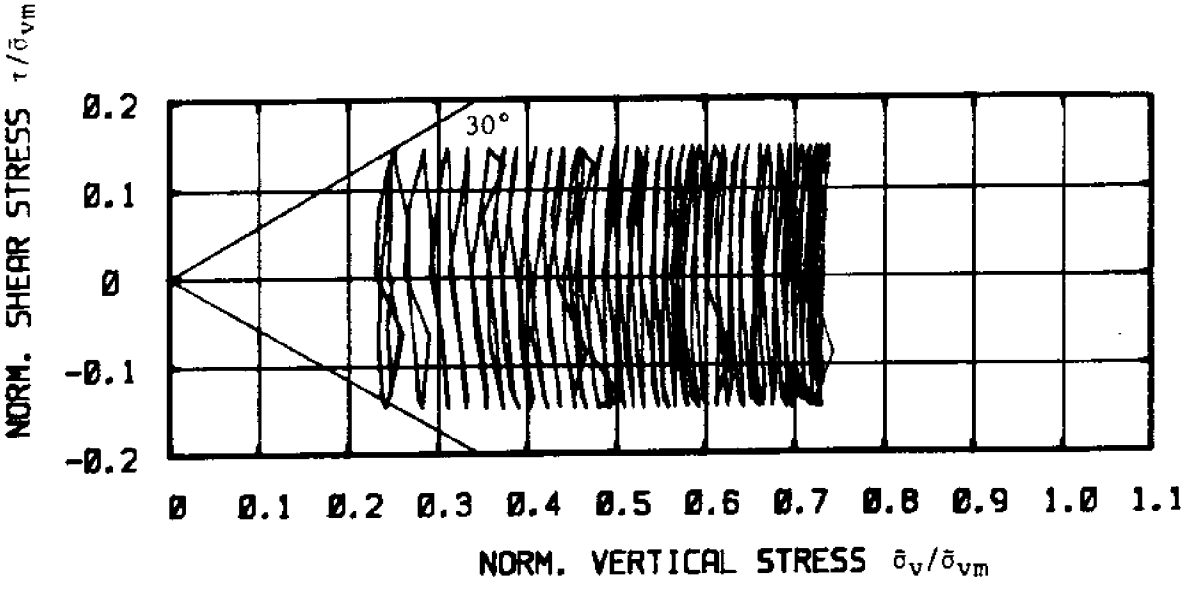

(d)

Figure 6.5 Test C-27: OCR = 1.38, τ_{ave} = 0, τ_c/s_u(OC) = 0.76
c) Normalized Shear Stress versus Shear Strain
d) Normalized Stress Path

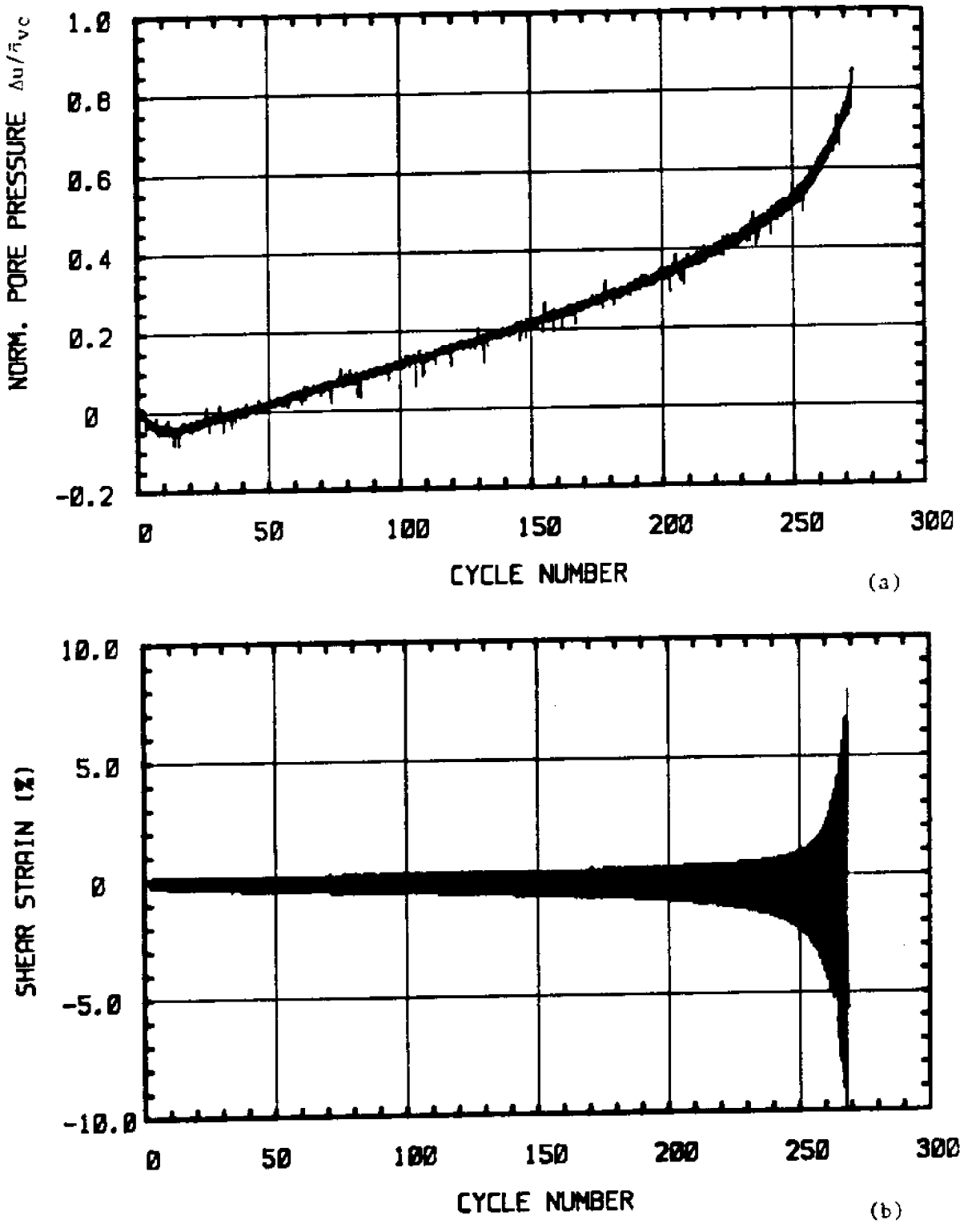

Figure 6.6 Test C-33: OCR = 2, τ_{ave} = 0, $\tau_c/s_u(OC)$ = 0.56
a) Normalized Excess Pore Pressure versus Cycle Number
b) Shear Strain versus Cycle Number

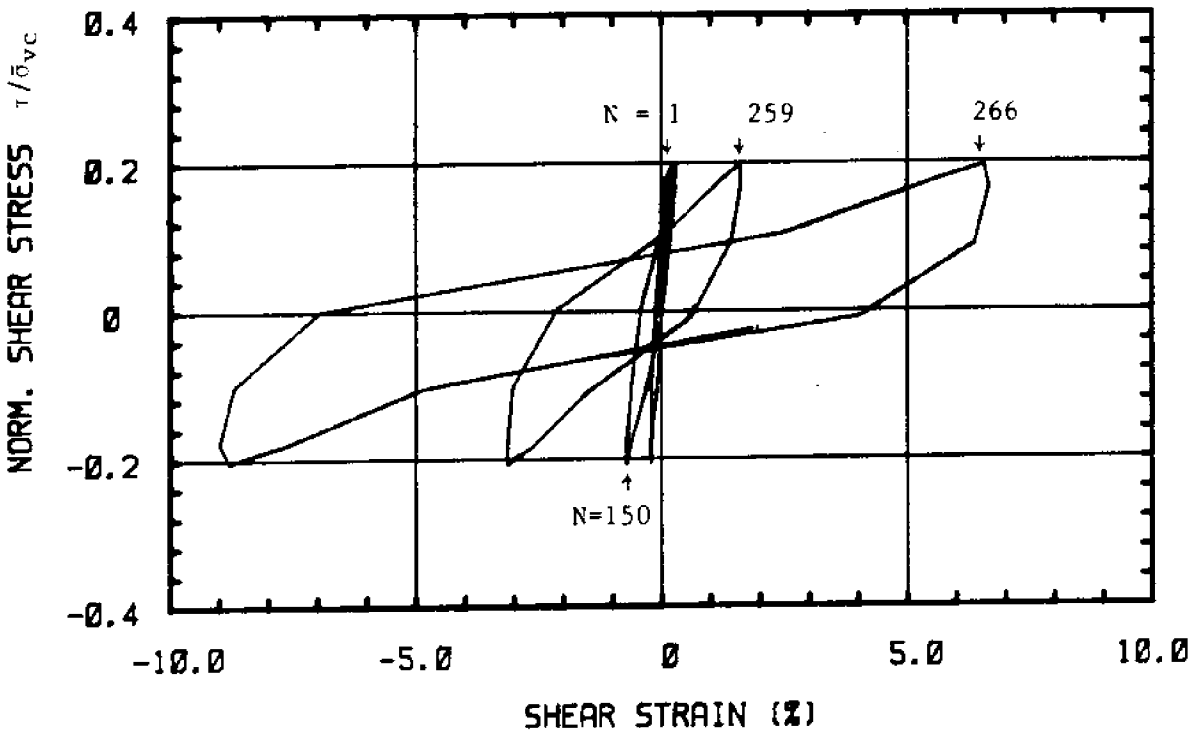

(c)

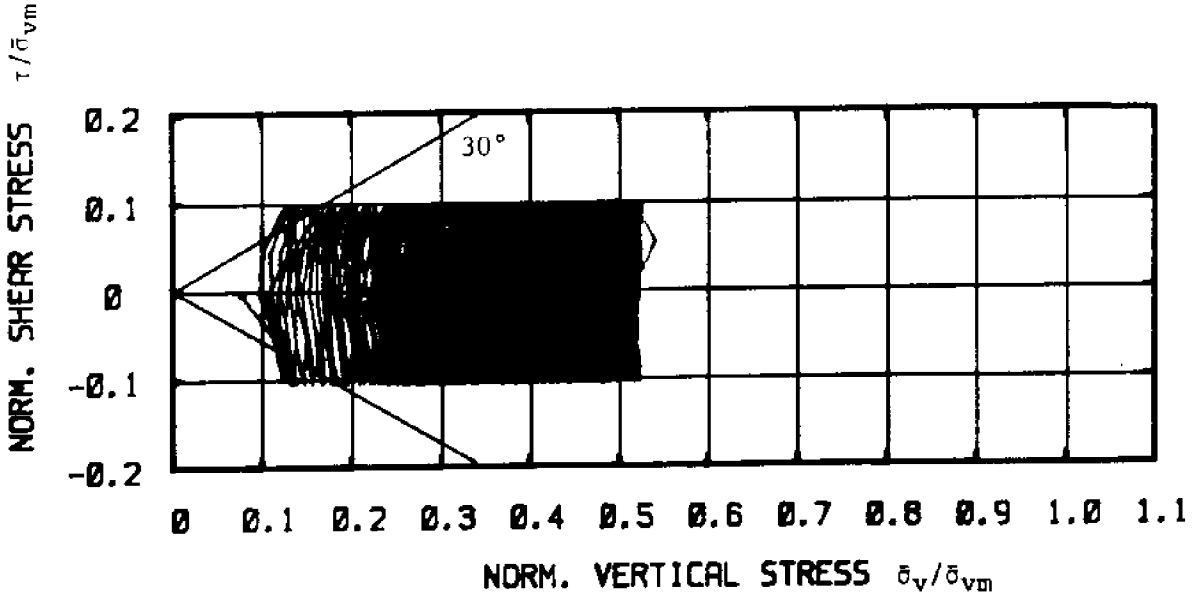

(d)

Figure 6.6 Test C-33: OCR = 2, τ_{ave} = 0, $\tau_c/s_u(OC)$ = 0.56
c) Normalized Shear Stress versus Shear Strain
d) Normalized Stress Path

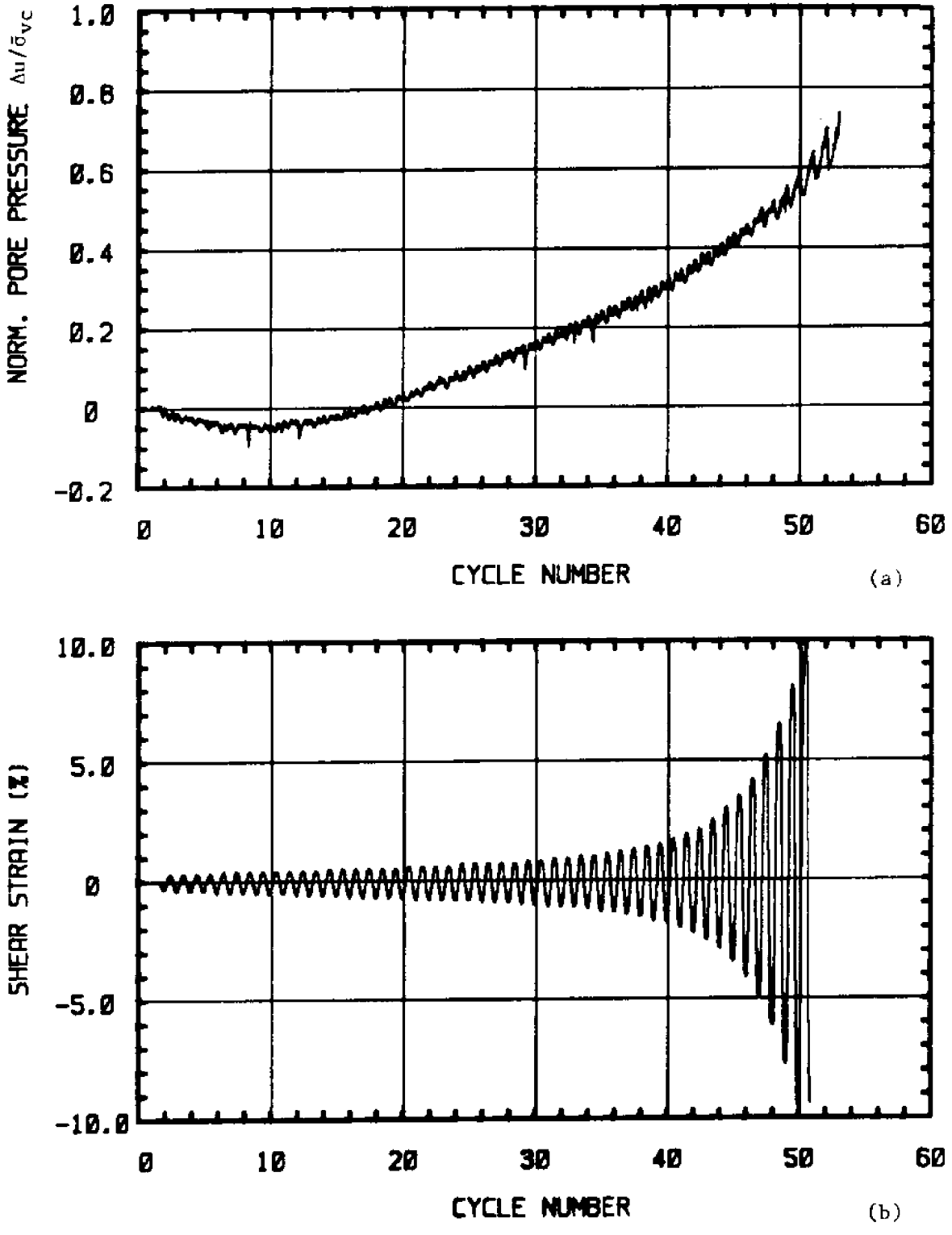

Figure 6.7 Test C-34: OCR = 2, τ_{ave} = 0, $\tau_c/s_u(OC)$ = 0.70
a) Normalized Excess Pore Pressure versus Cycle Number
b) Shear Strain versus Cycle Number

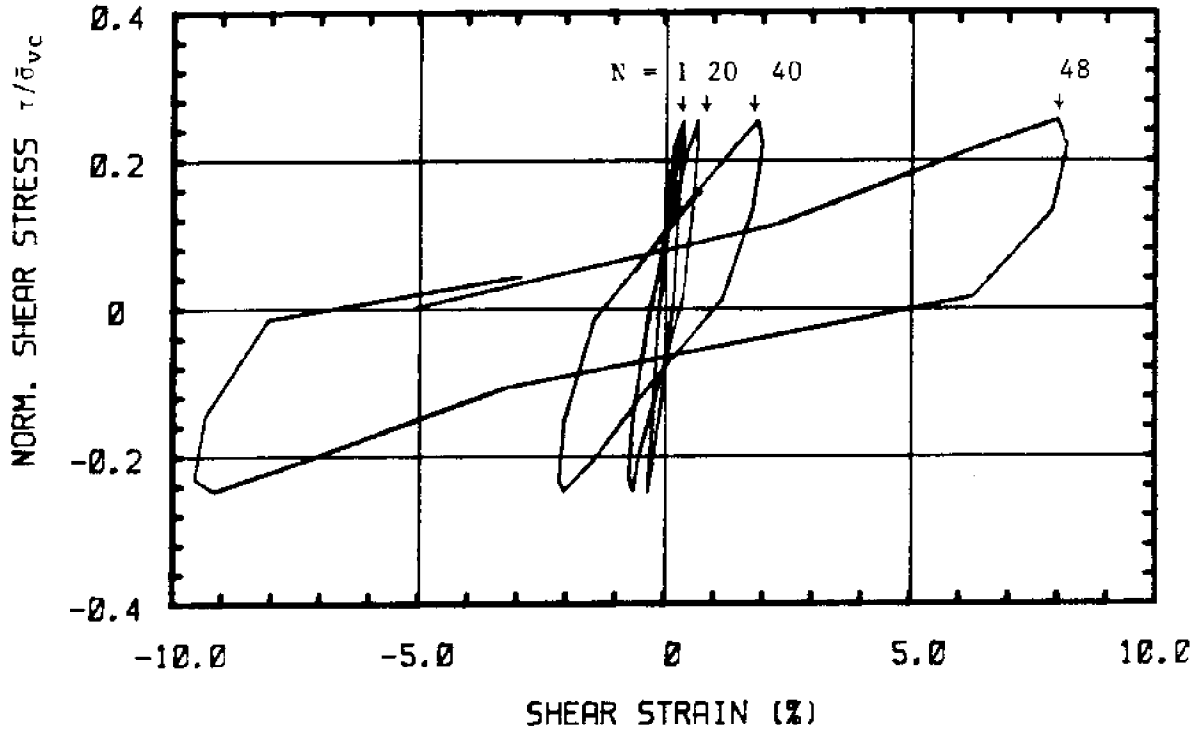

(c)

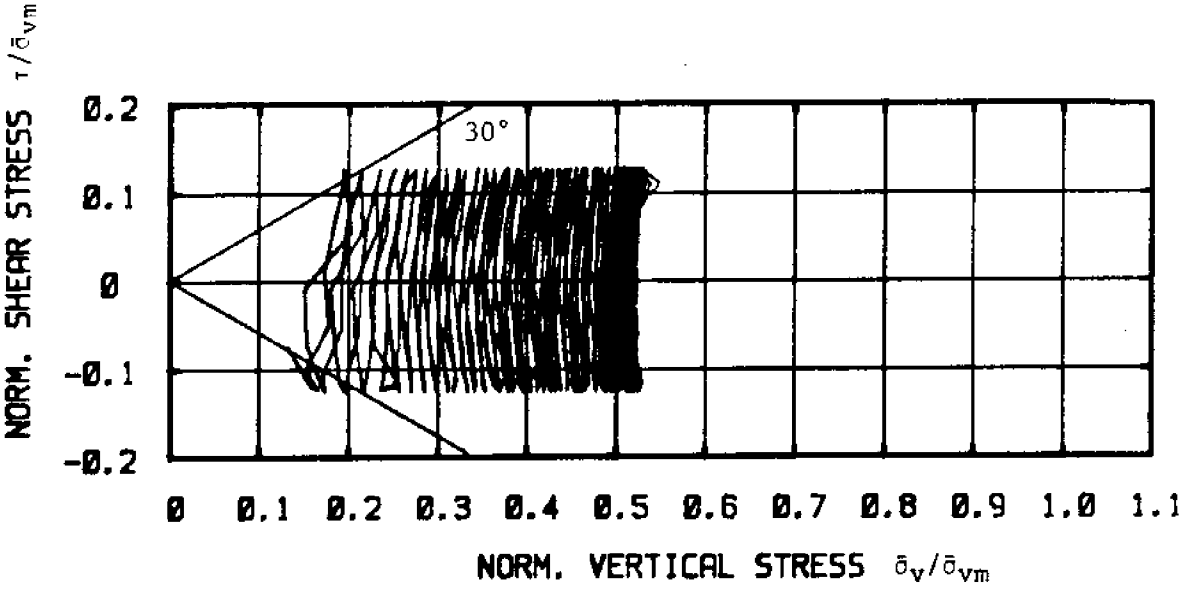

(d)

Figure 6.7 Test C-34: OCR = 2, τ_{ave} = 0, $\tau_c/s_u(OC)$ = 0.70
c) Normalized Shear Stress versus Shear Strain
d) Normalized Stress Path

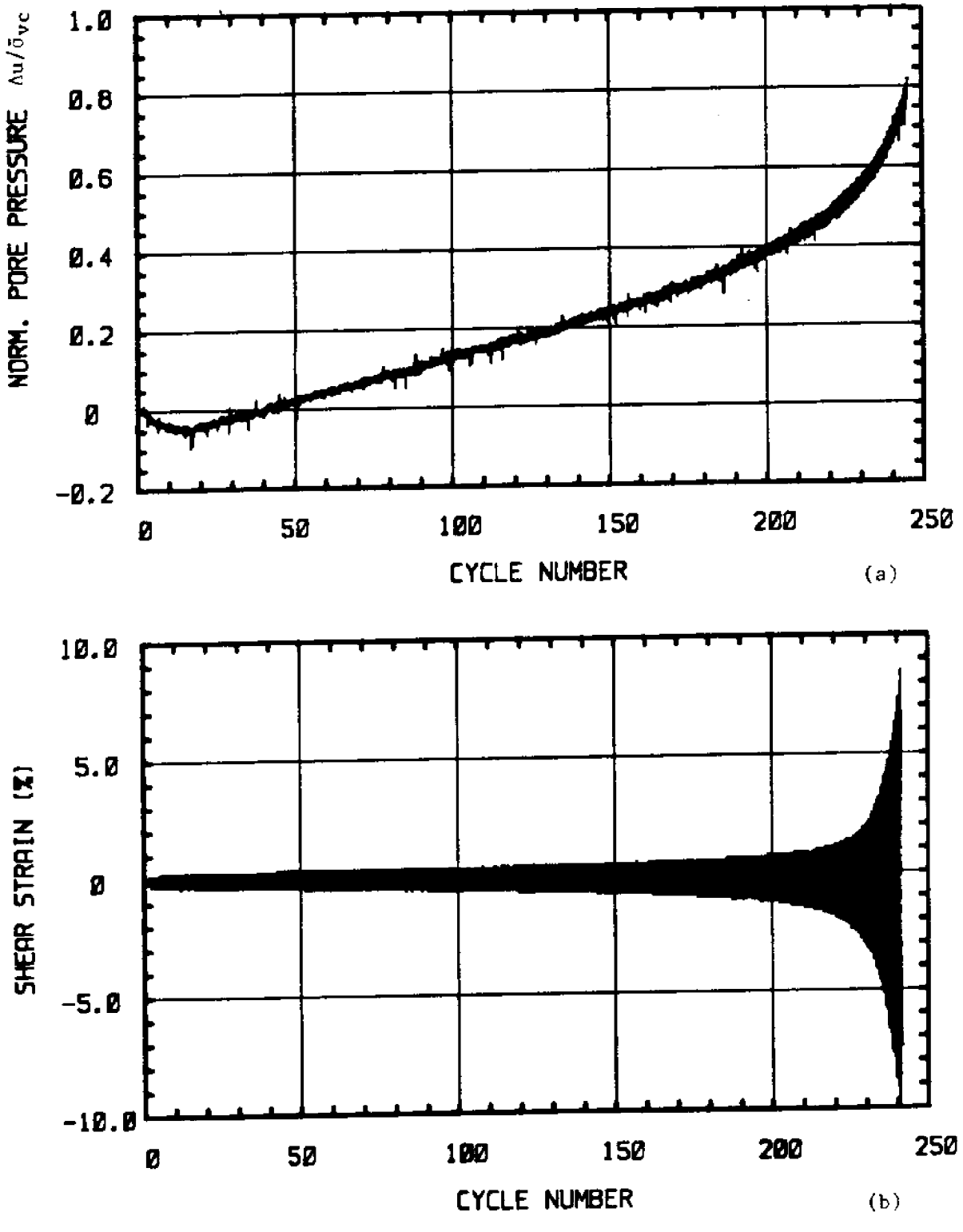

Figure 6.8 Test C-35: OCR = 2, τ_{ave} = 0, $\tau_c/s_u(OC)$ = 0.56
a) Normalized Excess Pore Pressure versus Cycle Number
b) Shear Strain versus Cycle Number

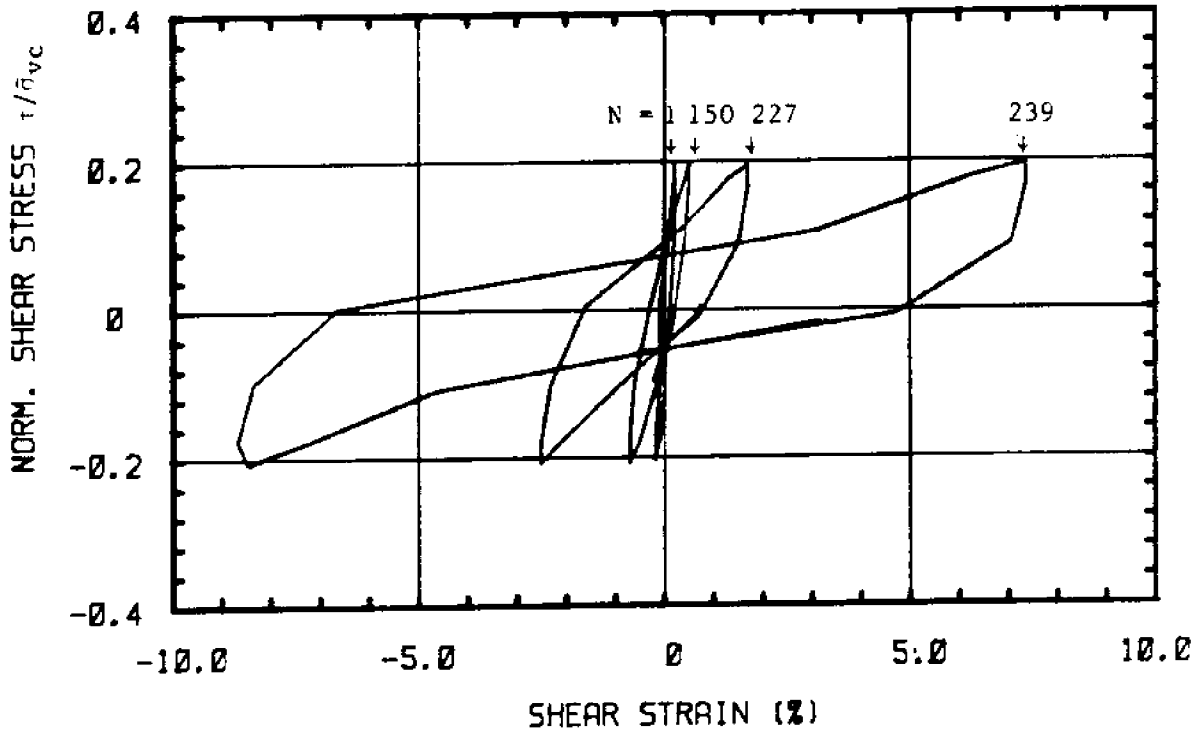

(c)

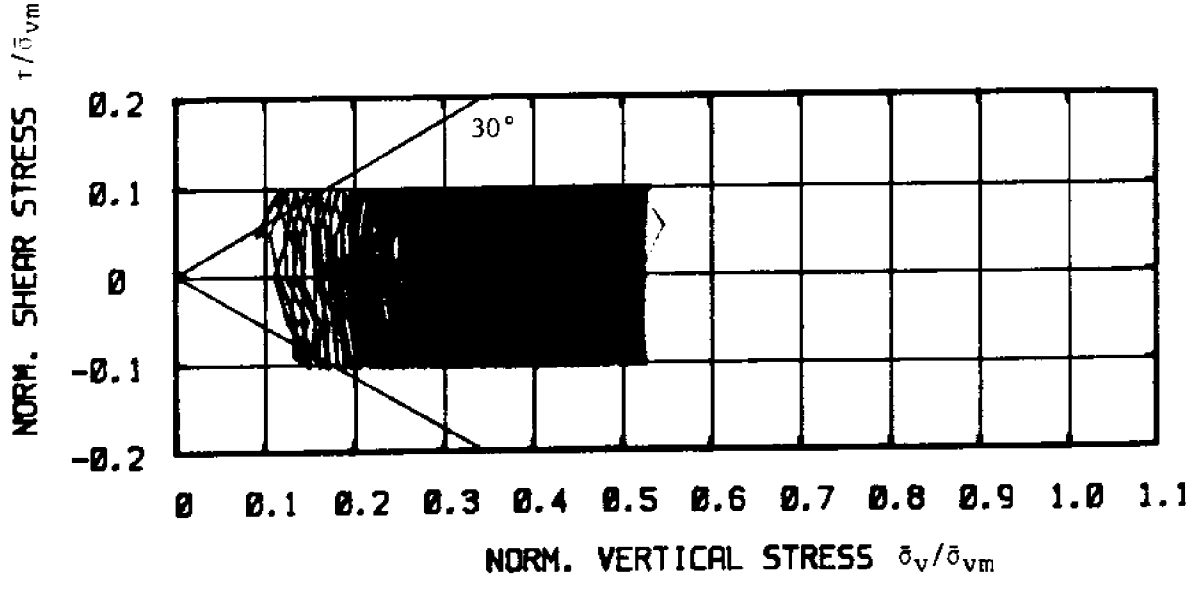

(d)

Figure 6.8 Test C-35: OCR = 2, τ_{ave} = 0, τ_c/s_u(OC) = 0.56
c) Normalized Shear Stress versus Shear Strain
d) Normalized Stress Path

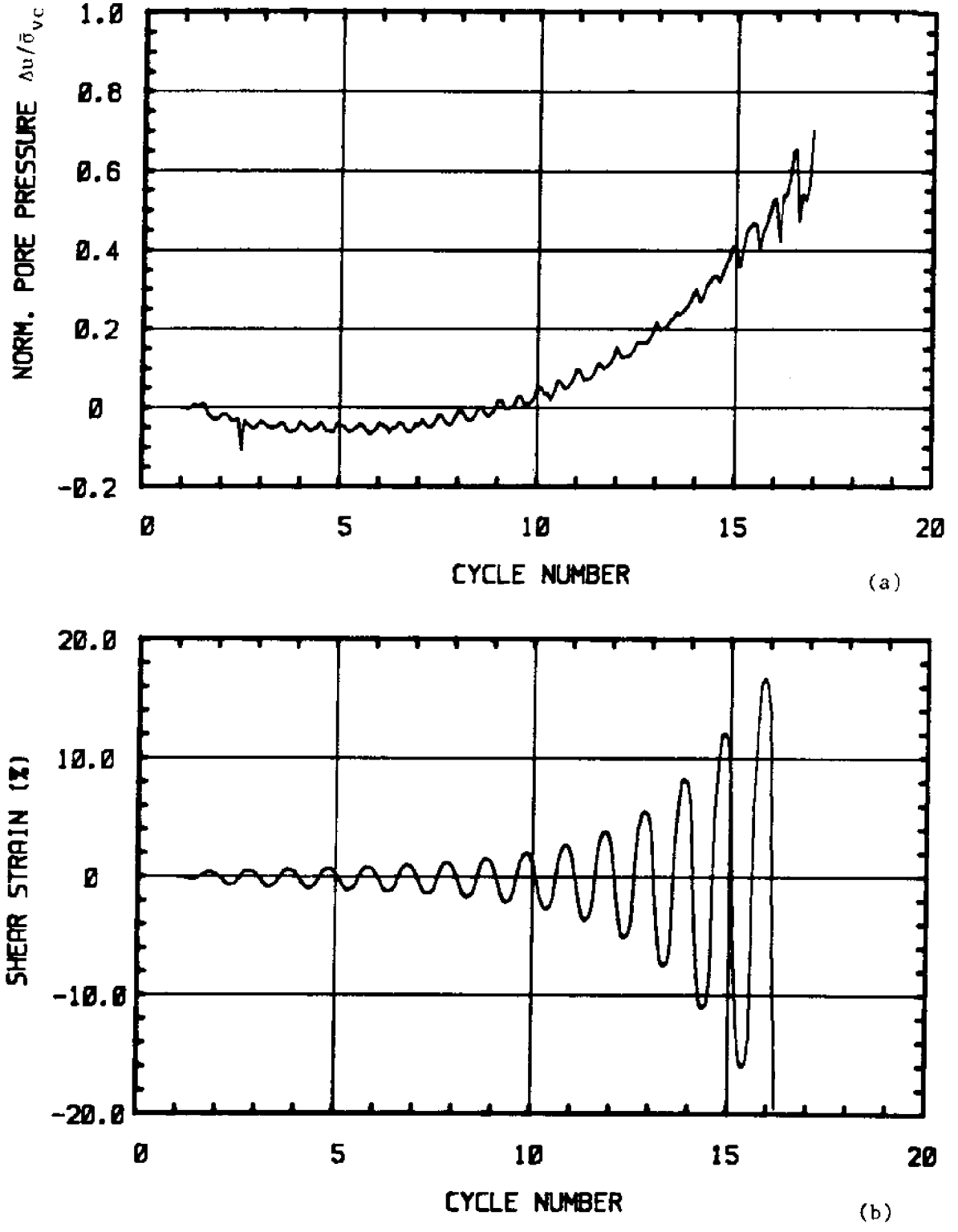

Figure 6.9 Test C-36: OCR = 2, τ_{ave} = 0, τ_c/s_u(OC) = 0.85
a) Normalized Excess Pore Pressure versus Cycle Number
b) Shear Strain versus Cycle Number

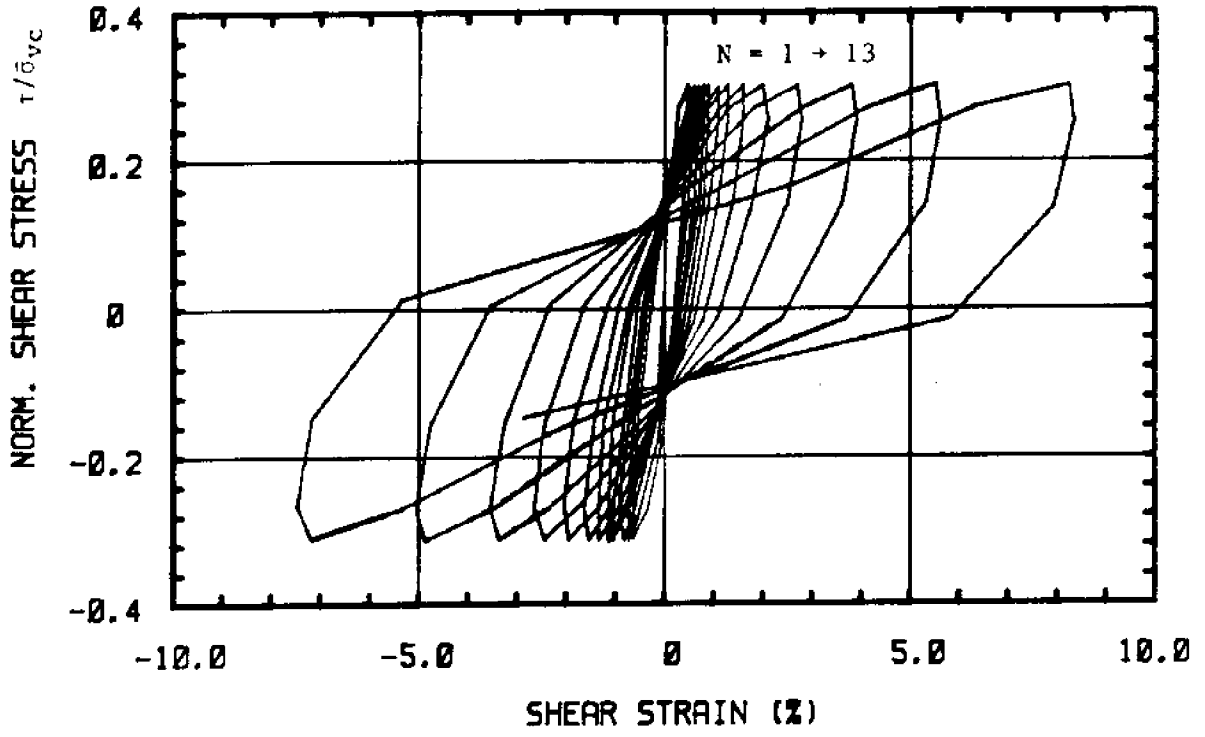

(c)

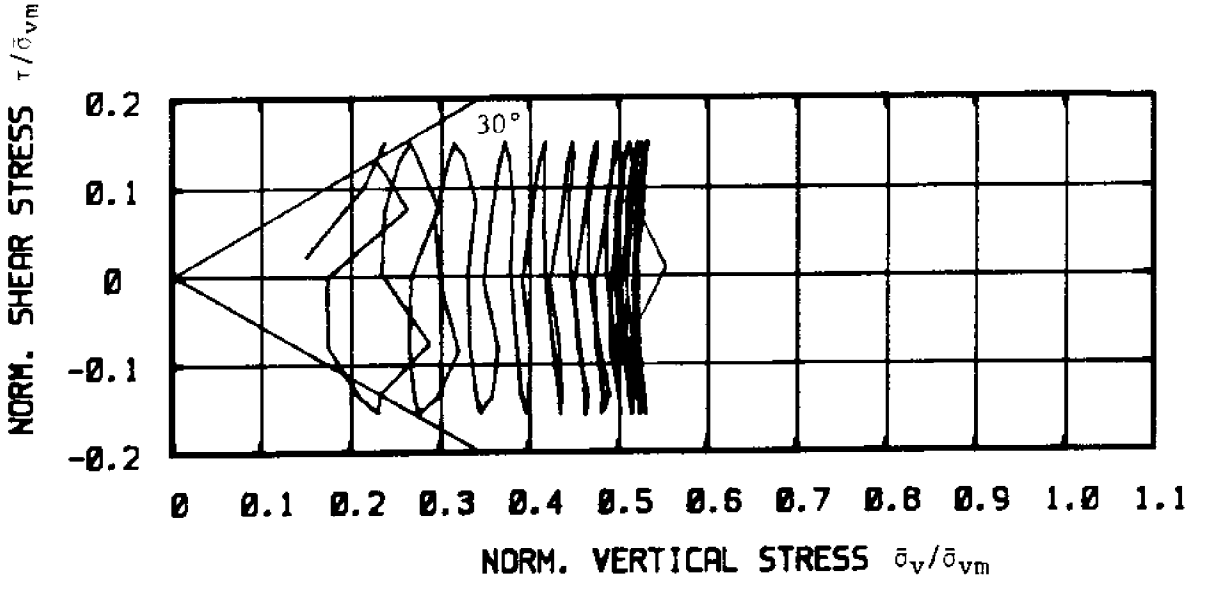

(d)

Figure 6.9 Test C-36: OCR = 2, τ_{ave} = 0, τ_c/s_u(OC) = 0.85
c) Normalized Shear Stress versus Shear Strain
d) Normalized Stress Path

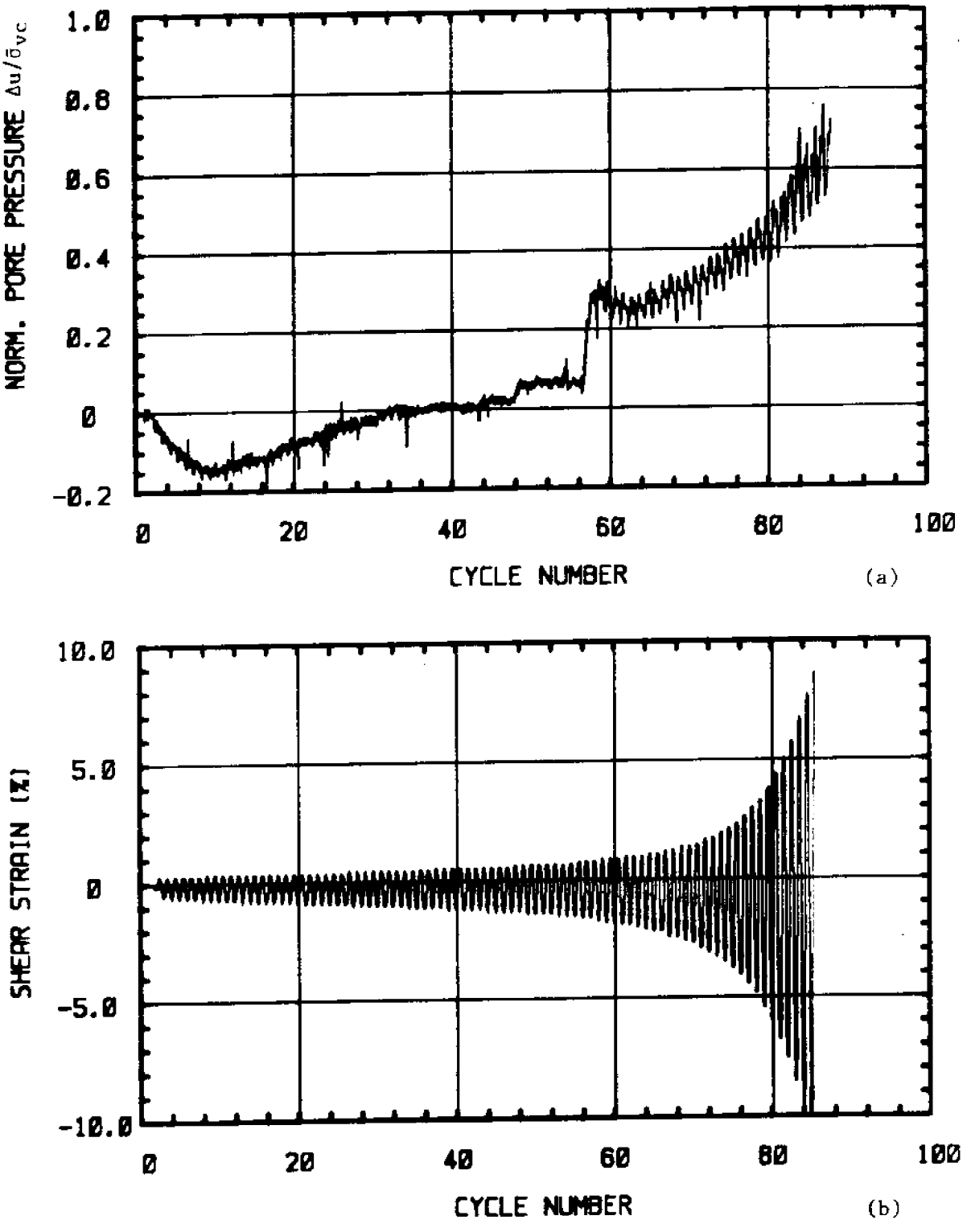

Figure 6.10 Test C-31: OCR = 4, τ_{ave} = 0, $\tau_c/s_u(OC)$ = 0.55
a) Normalized Excess Pore Pressure versus Cycle Number
b) Shear Strain versus Cycle Number

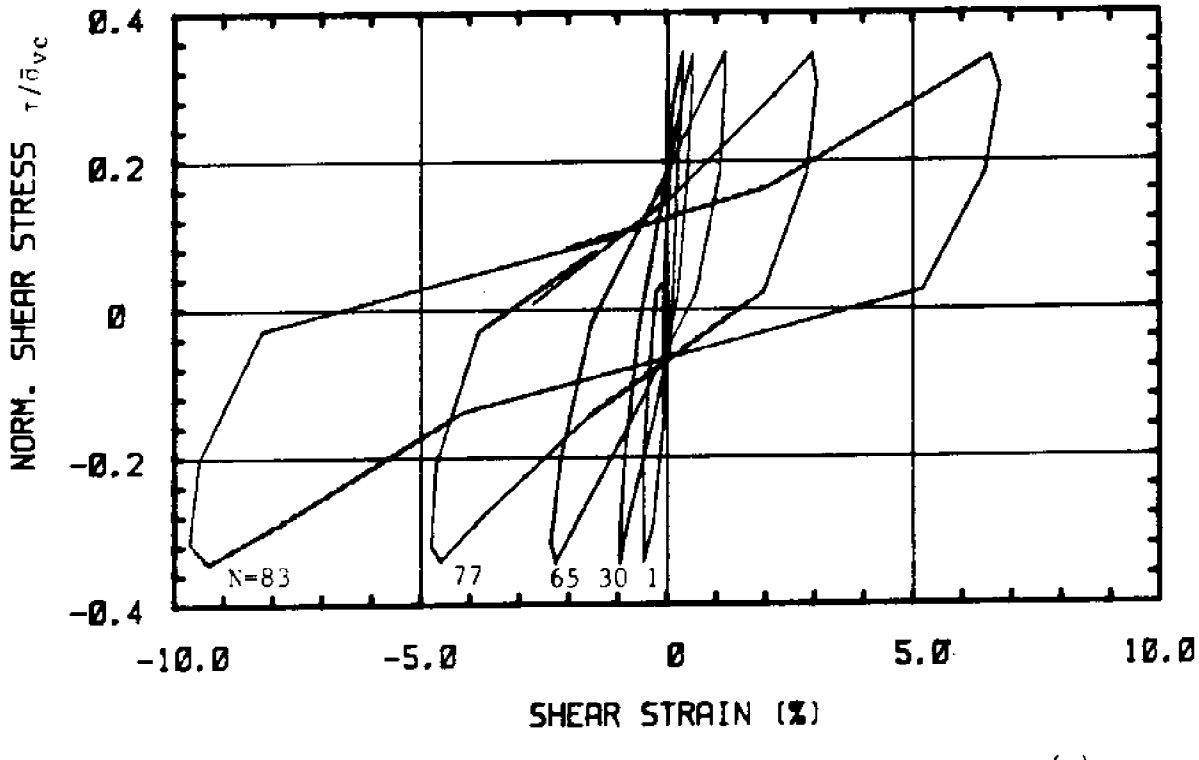

(c)

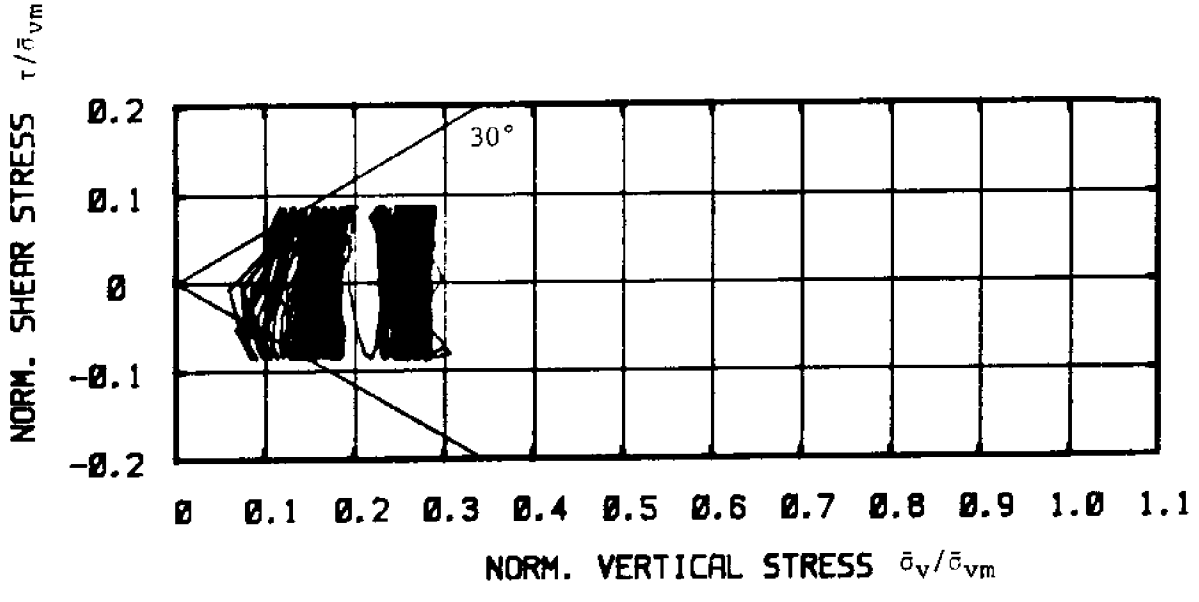

(d)

Figure 6.10 Test C-31: OCR =4, τ_{ave} = 0, τ_c/s_u(OC) = 0.55
c) Normalized Shear Stress versus Shear Strain
d) Normalized Stress Path

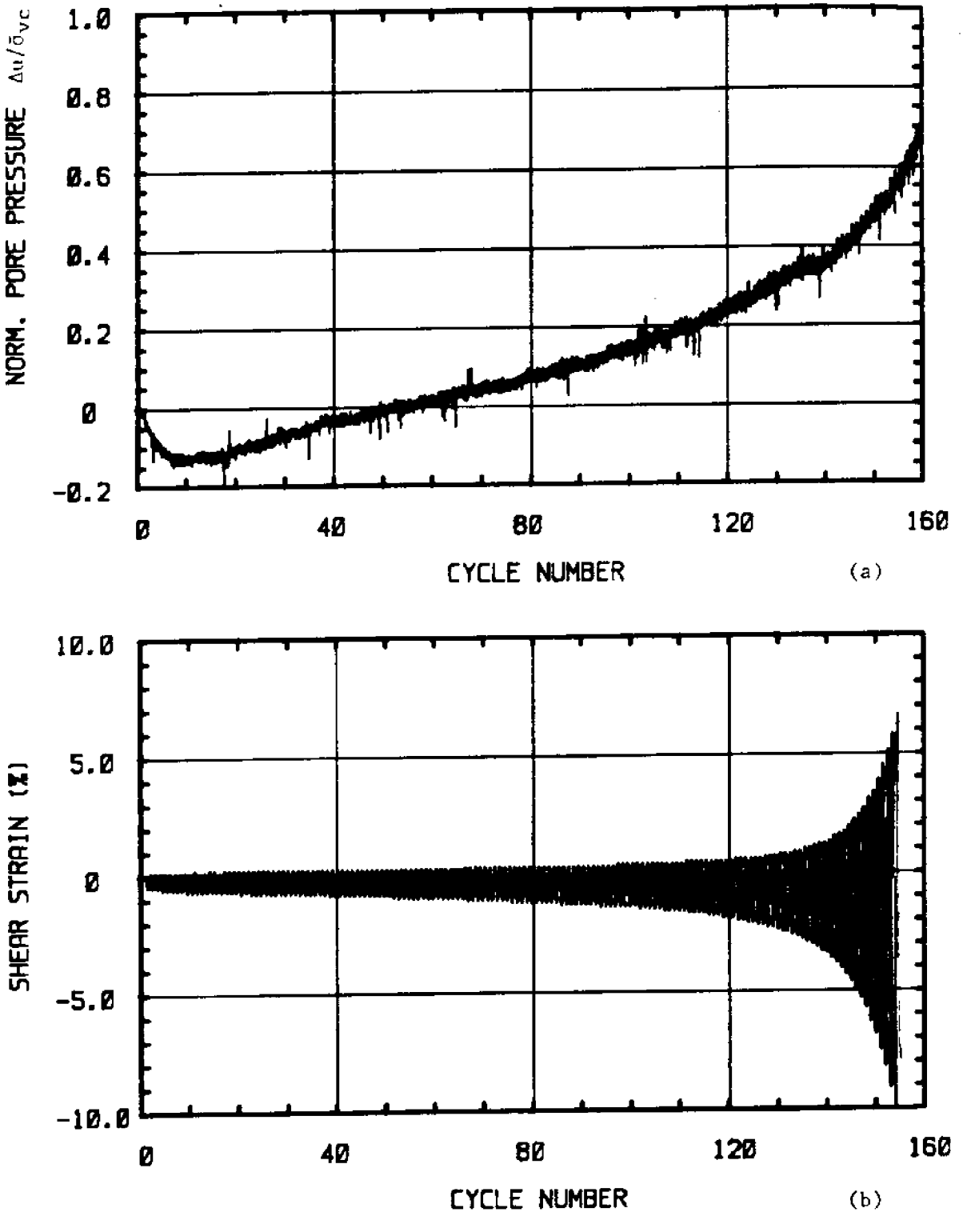

Figure 6.11 Test C-32: OCR = 4, τ_{ave} = 0, $\tau_c/s_u(OC)$ = 0.50
a) Normalized Excess Pore Pressure versus Cycle Number
b) Shear Strain versus Cycle Number

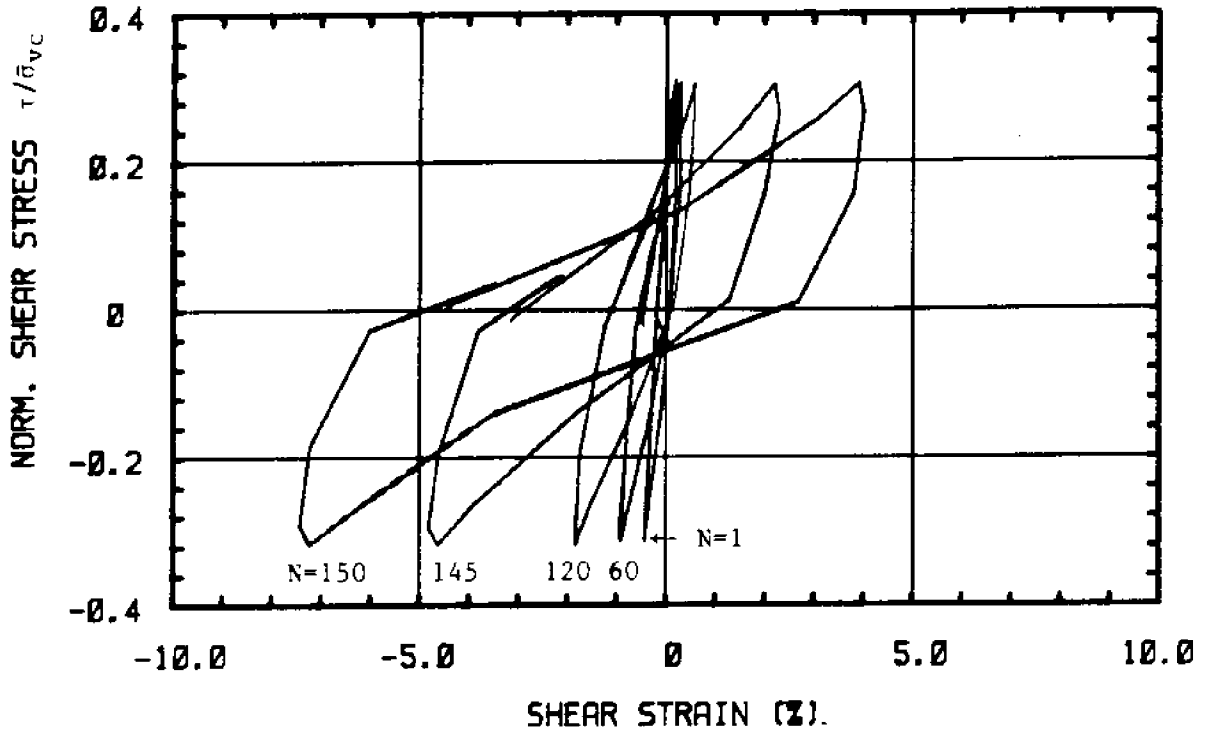

(c)

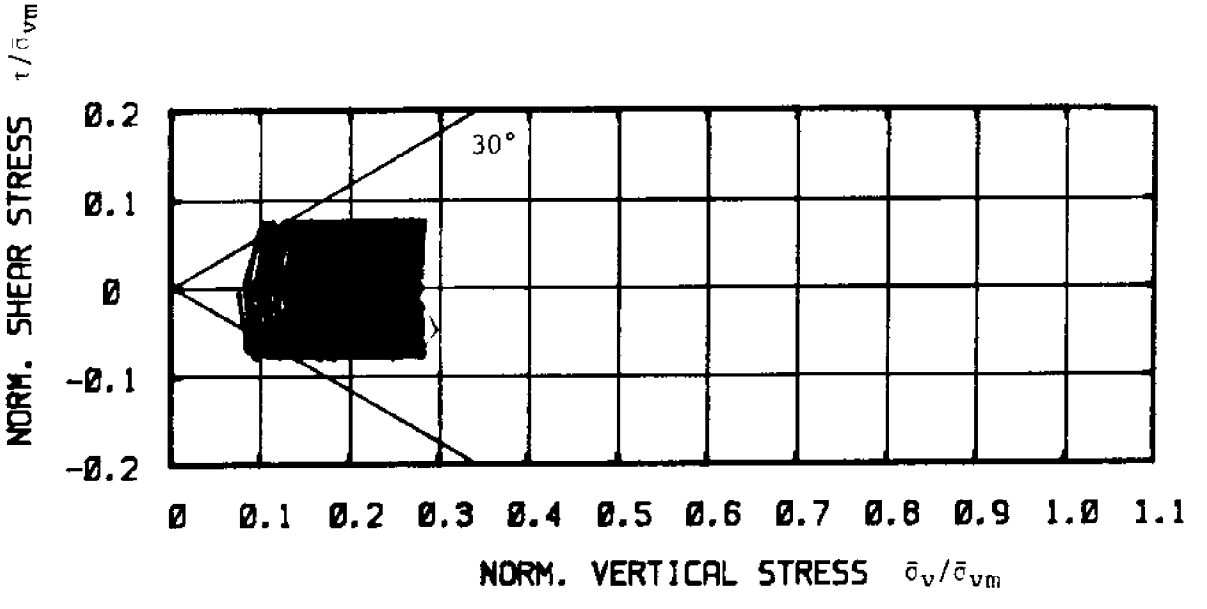

(d)

Figure 6.11 Test C-32: OCR = 4, τ_{ave} = 0, $\tau_c/s_u(OC)$ = 0.50
c) Normalized Shear Stress versus Shear Strain
d) Normalized Stress Path

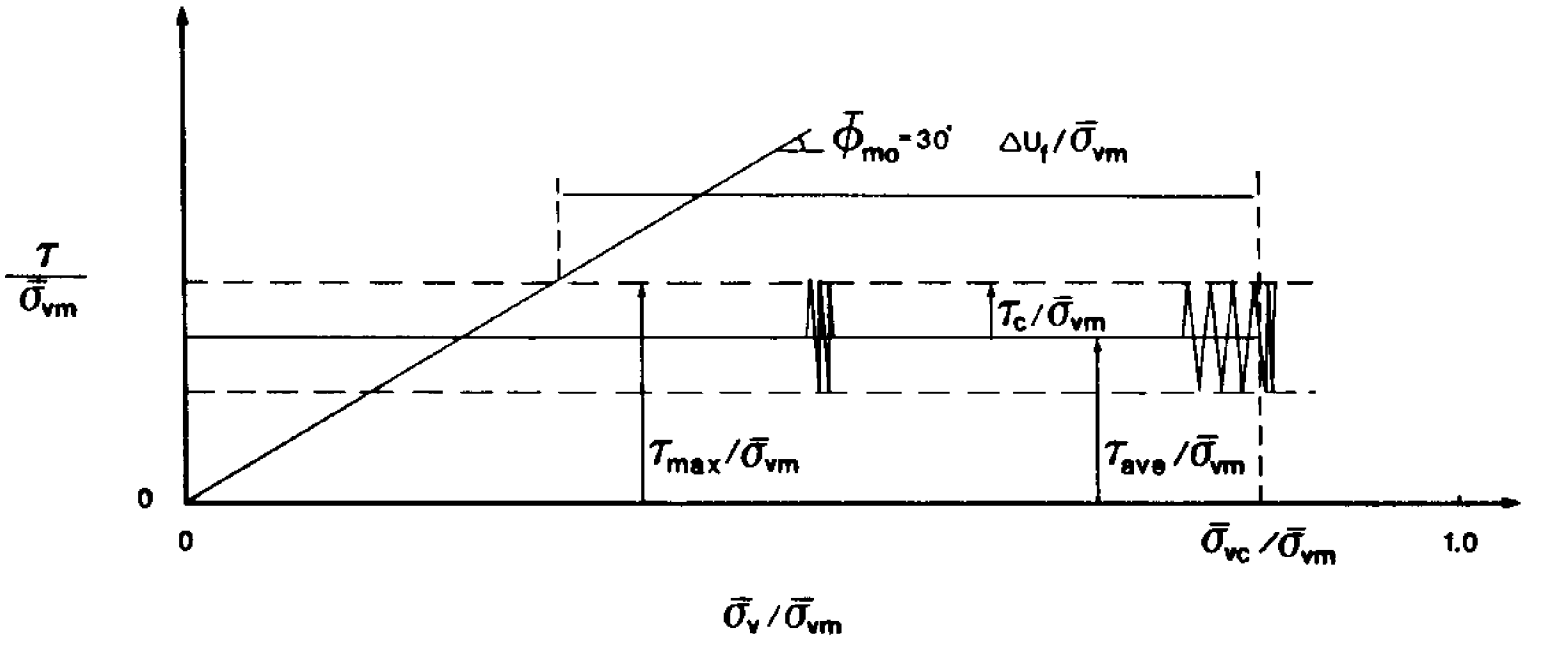

$$\frac{\Delta u_f}{\bar{\sigma}_{vm}} = \frac{\bar{\sigma}_{vc}}{\bar{\sigma}_{vm}} - \frac{\tau_{max}}{\bar{\sigma}_{vm}\ (\tan\ \bar{\Phi}_{MO})} \quad ; \quad \bar{\Phi}_{MO} = 30°$$

$$\frac{\Delta u_f}{\bar{\sigma}_{vc}} = 1 - \frac{\tau_{max}}{\bar{\sigma}_{vc}\ (\tan\ \bar{\Phi}_{MO})}$$

Figure 6.12 Excess Pore Pressure at Failure in Undrained Cyclic CK_oUDSS Tests Overconsolidated BBC

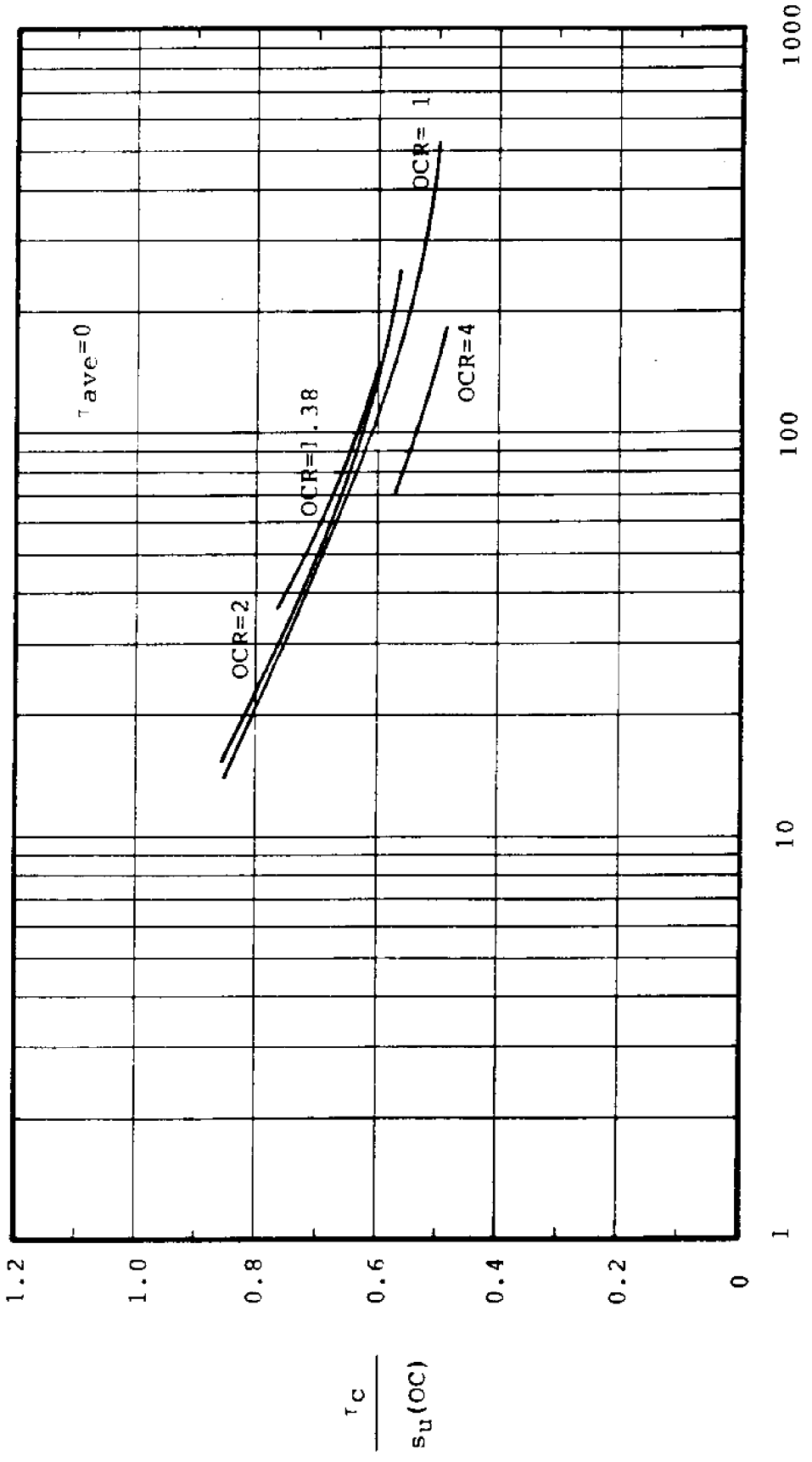

Figure 6.13 S-N Curves at Maximum Obliquity for BBC at OCR=1, 1.38, 2, and 4

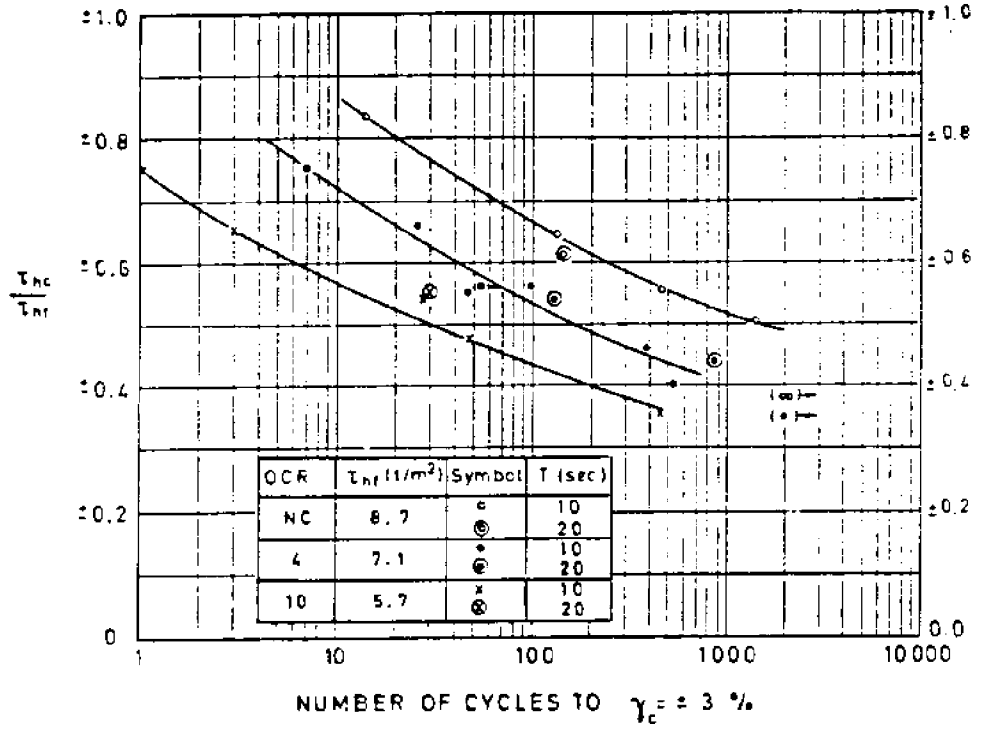

Figure 6.14 S-N Curves at γ_c = 3% (Failure) for Drammen Clay with OCR=1, 4, and 10 (from Andersen, 1975)

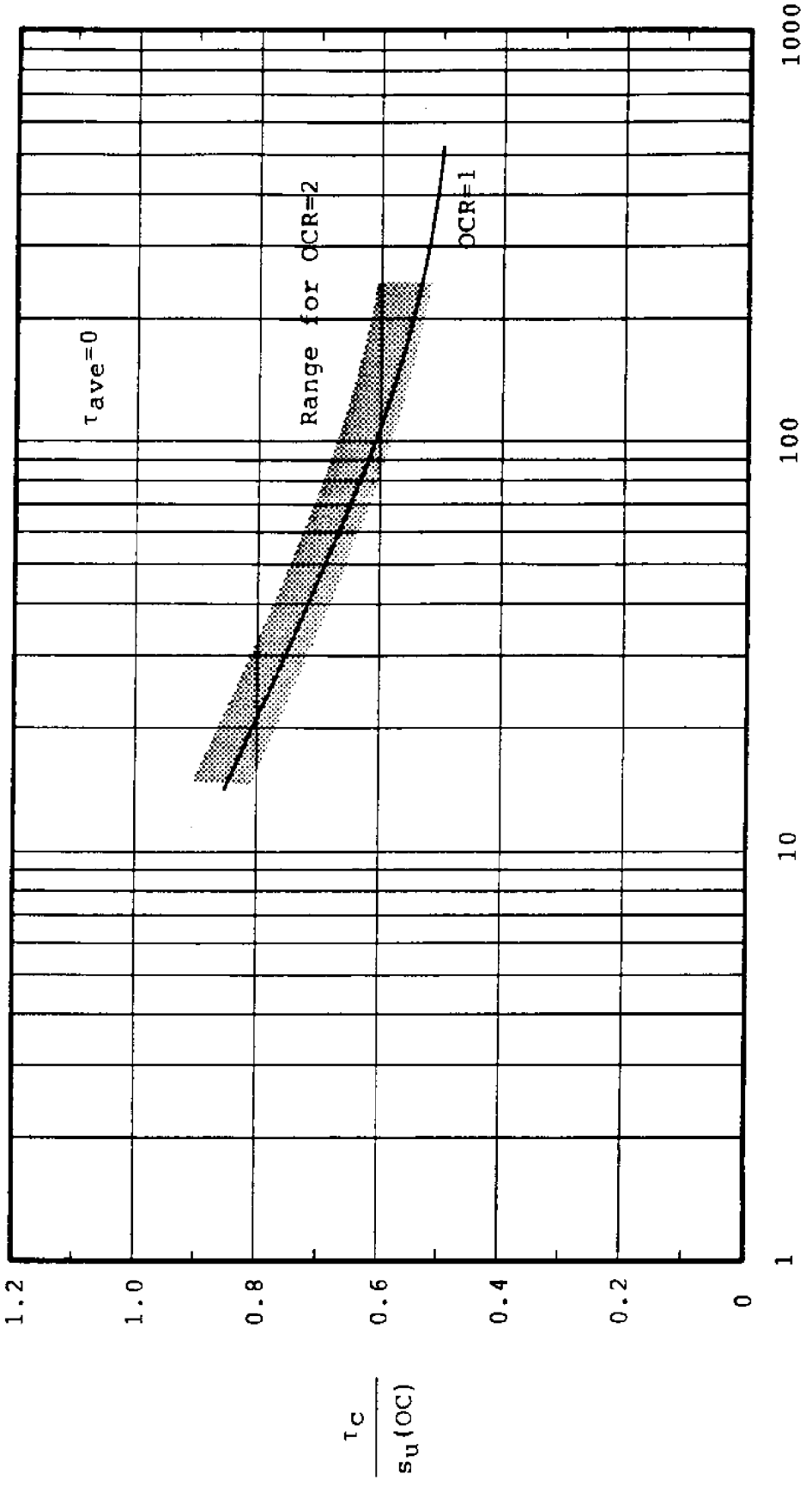

Figure 6.15 a) S-N Curve at Maximum Obliquity for OCR=1 and Range of S-N Curves at Maximum Obliquity for OCR=2 for BBC

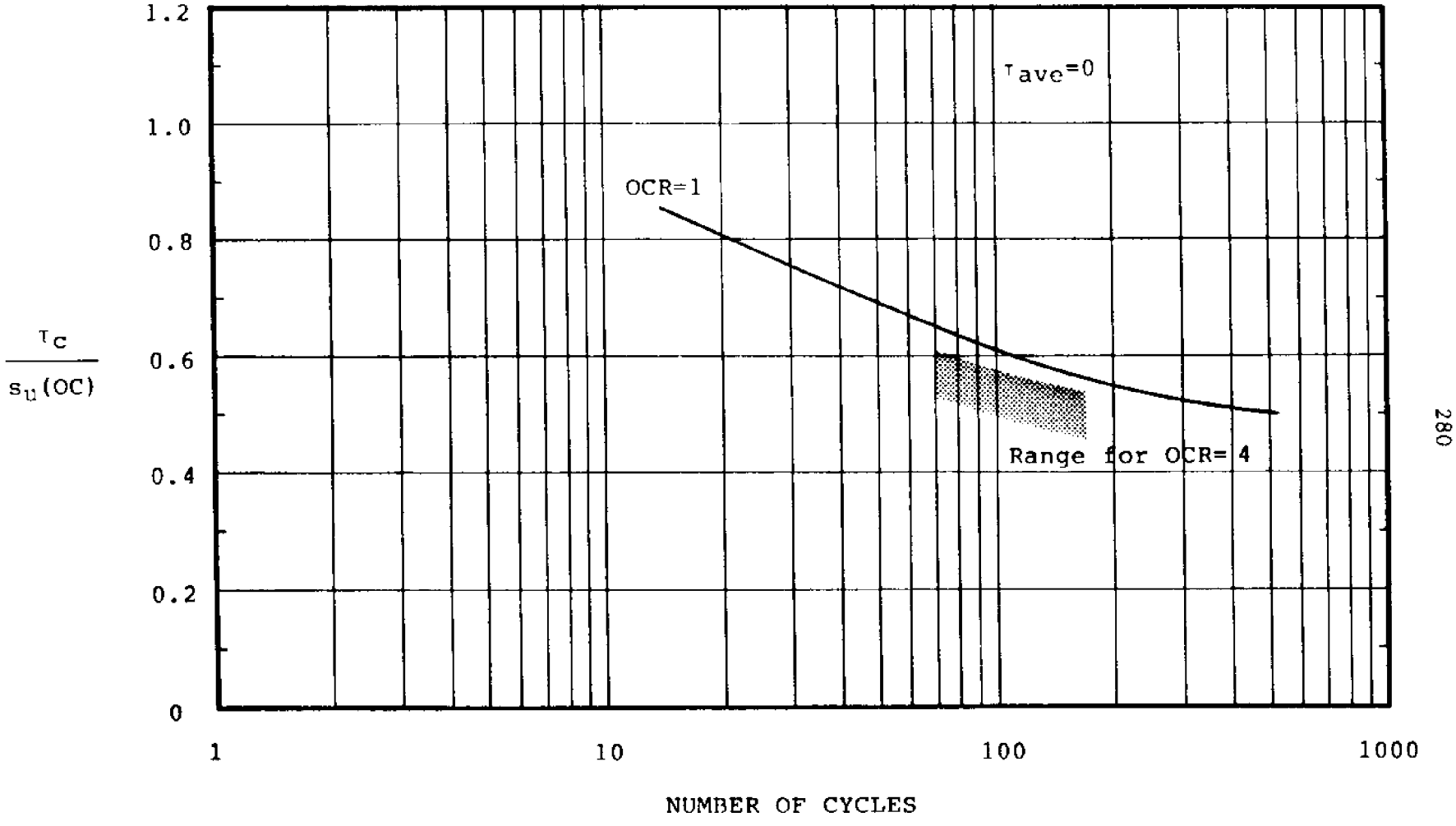

Figure 6.15 b) S-N Curve at Maximum Obliquity for OCR=1 and Range of S-N Curves at Maximum Obliquity for OCR=4 for BBC

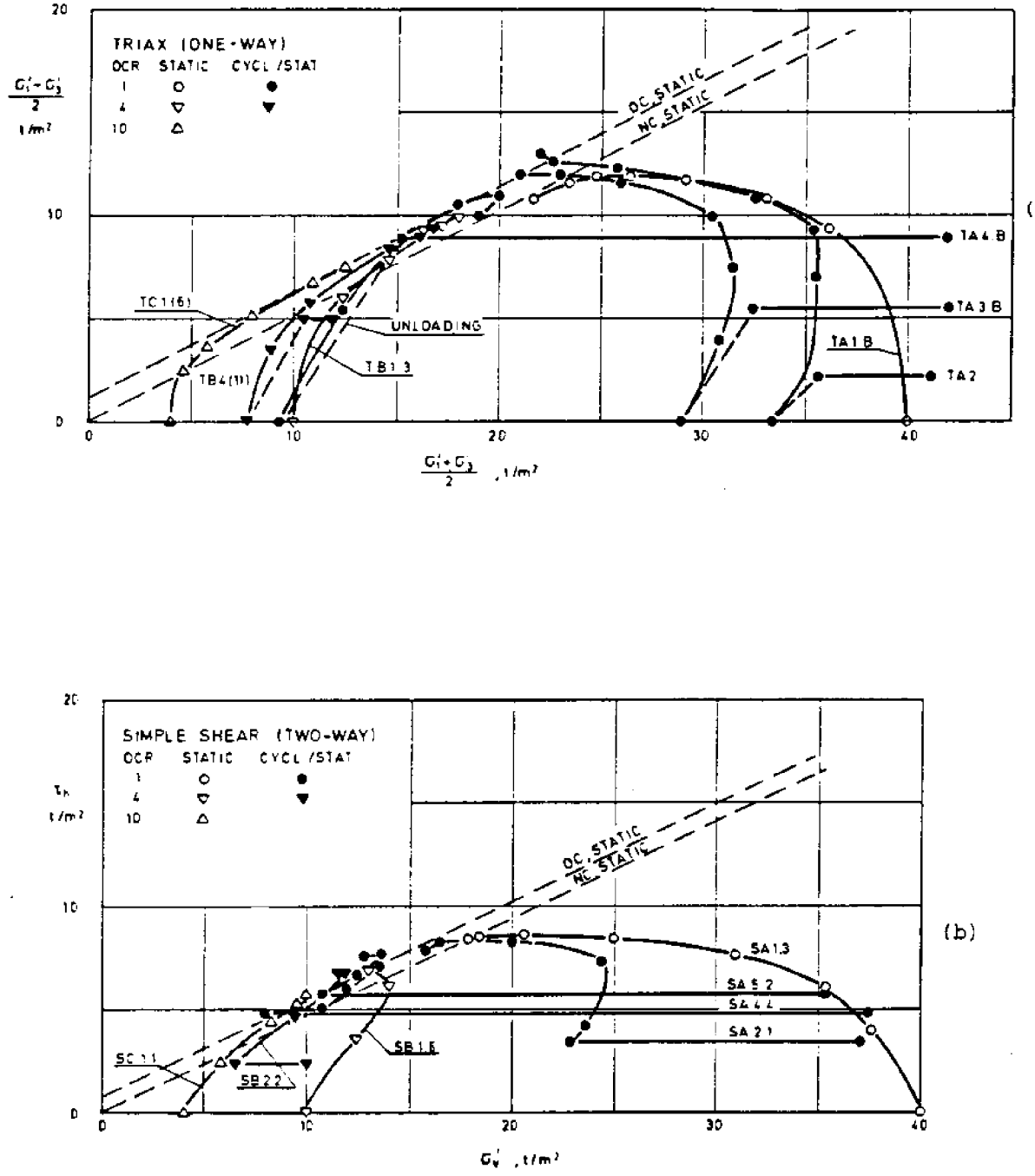

Figure 6.16 Effective Stress Paths from Static Undrained Shearing of Drammen Clay in:
a) Triaxial Tests Following One-Way Cyclic Loading
b) Simple Shear Tests Following Two-Way Cyclic Loading
(from Andersen, 1975)

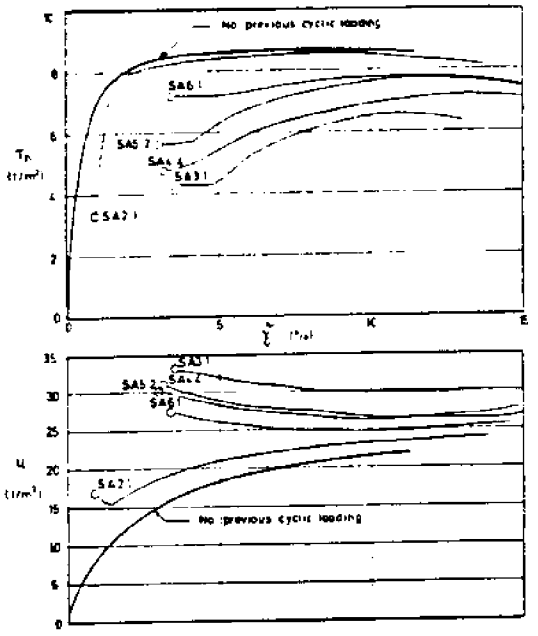

(a) OCR=1

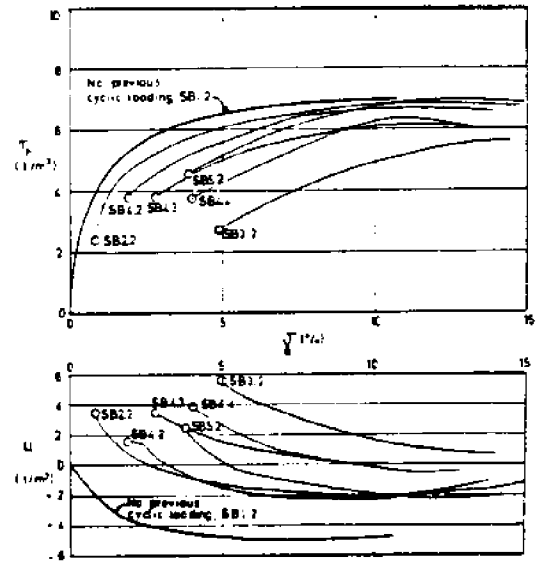

(b) OCR=4

Figure 6.17 Results of Undrained Static DSS Tests, with and without Previous Undrained Cyclic Loading
a) OCR = 1
b) OCR = 4
(from Andersen, 1975)

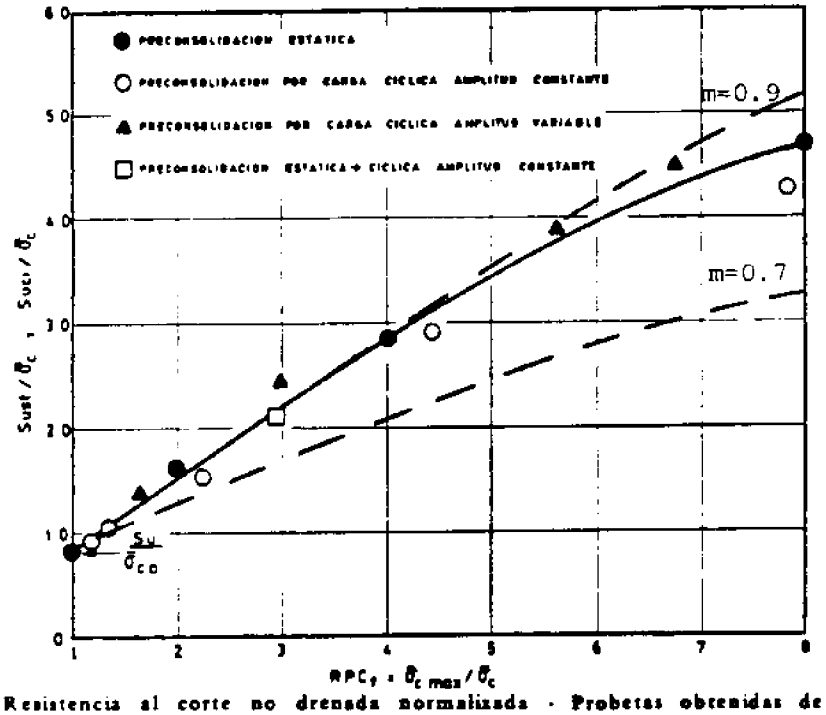

Fig. 7. Resistencia al corte no drenada normalizada - Probetas obtenidas de un slurry con $RPC_0 = 1$.

---- using $s_u(OC)/\bar{\sigma}_{vc}(OC) = s_u(NC)/\bar{\sigma}_{vc}(NC) \cdot (OCR)^m$

Figure 6.18 Undrained Strength Ratio versus OCR from:
Mechanically Overconsolidated Samples (solid circles)
Apparently Overconsolidated Samples Due to Cyclic Loading
(other symbols) (from Ortigosa et al., 1983)

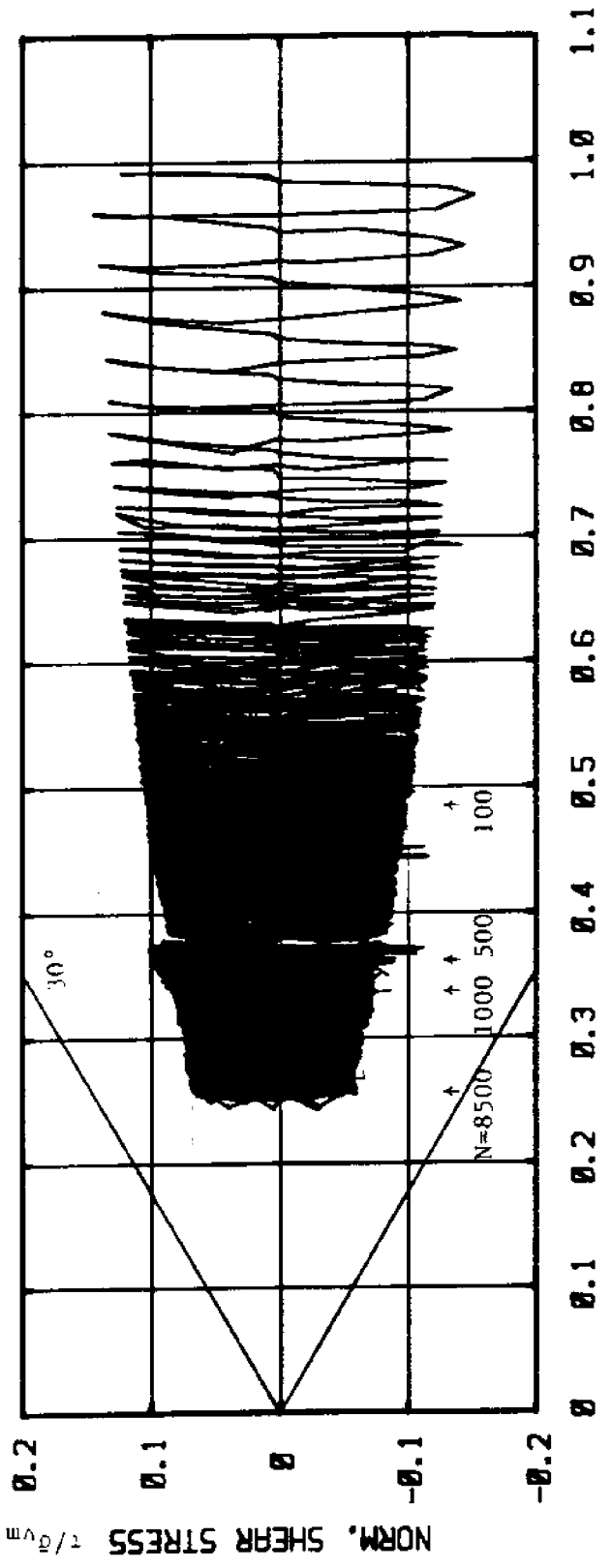

Figure 6.19 Normalized Effective Stress Path from Strain-Controlled Test C-21: N.C. BBC, $\bar{\sigma}_{vc}$=6.0 Kg/cm^2, γ_c=±0.5%

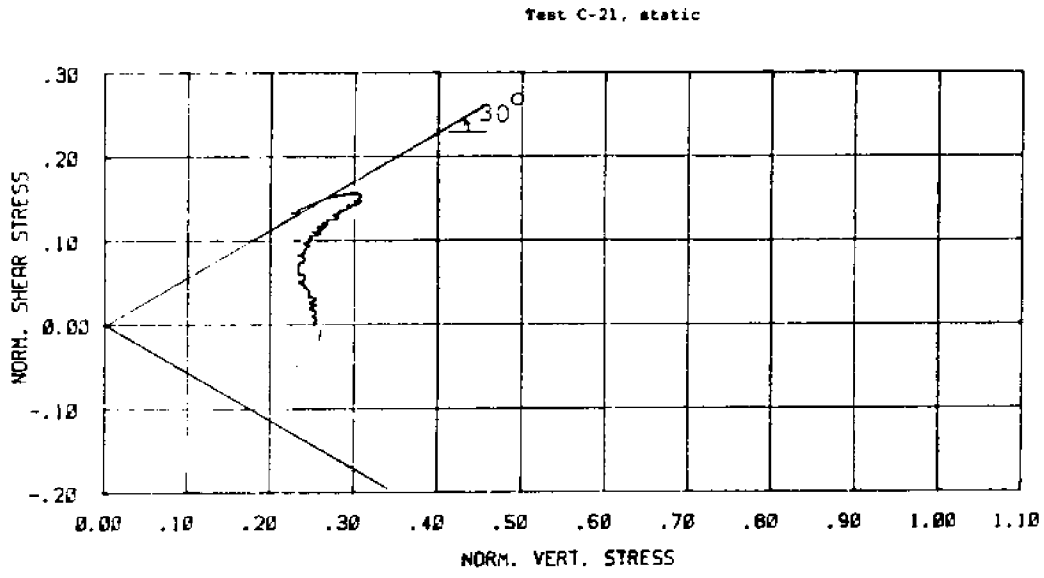

(a)

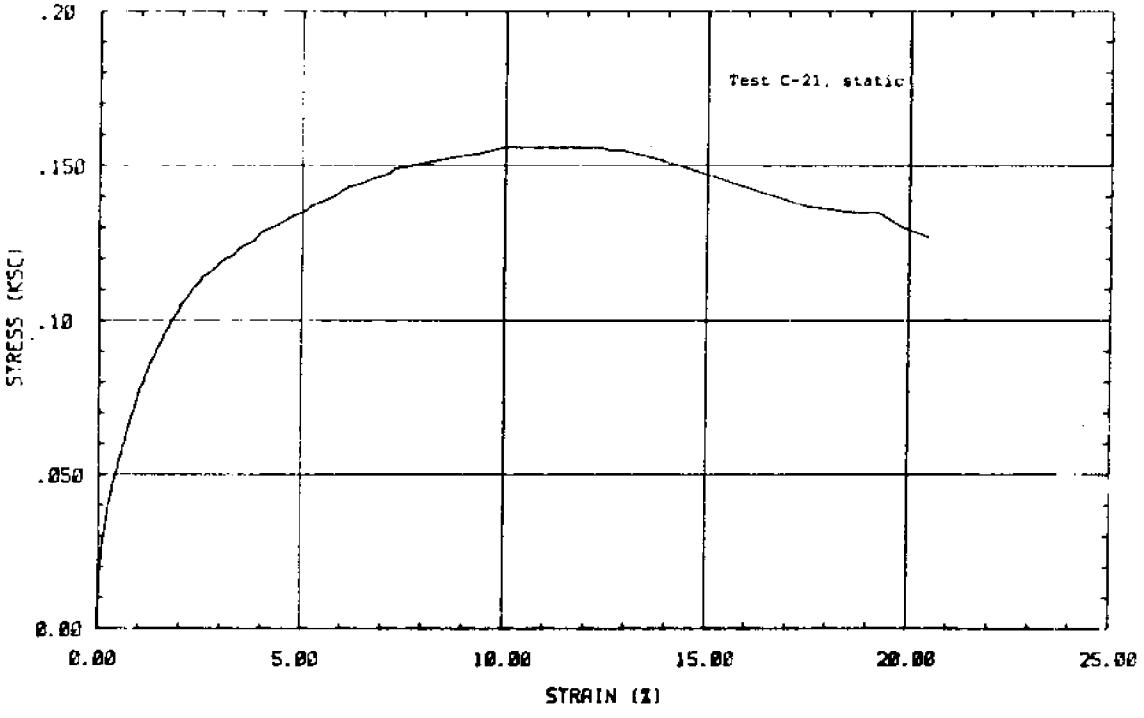

(b)

Figure 6.20 Normalized Effective Stress Path and Stress-Strain Curve from Undrained Monotonic DSS Test on BBC Sample Previously Cycled in Test C-21

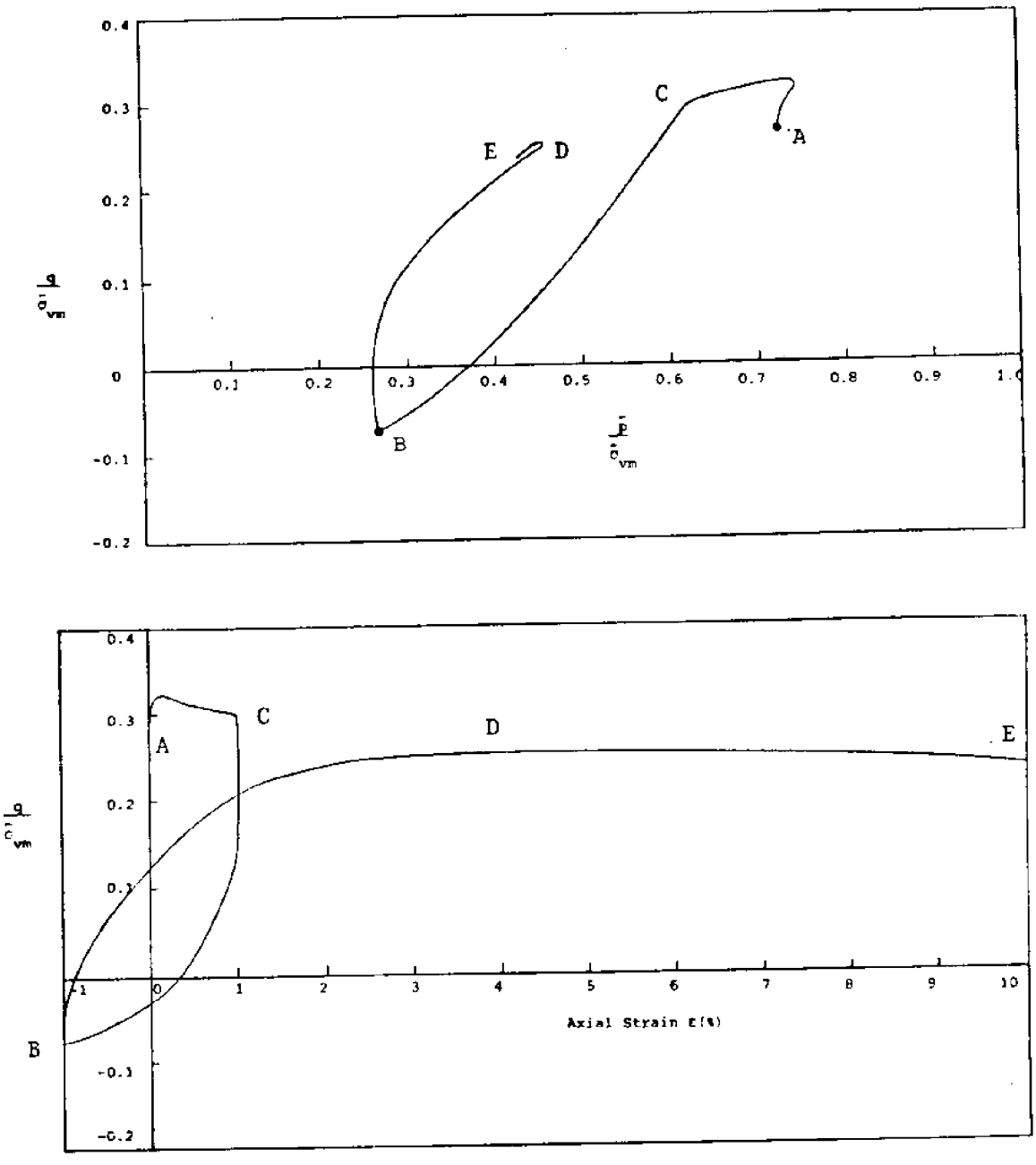

Point A: $\bar{p}/\bar{\sigma}_{vm} = 0.725$, $q/\bar{\sigma}_{vm} = 0.260$ → $\bar{\sigma}_v/\bar{\sigma}_{vm} = 0.493$ → AOCR = 5.2

Point B: $\bar{p}/\bar{\sigma}_{vm} = 0.265$, $q/\bar{\sigma}_{vm} = -0.075$ → $\bar{\sigma}_v/\bar{\sigma}_{vm} = 0.095$

Figure 6.21 Apparent Overconsolidation in Triaxial Testing on BBC After One Cycle of ε=±1%

CHAPTER 7

IMPLICATIONS OF THE APPARENT OVERCONSOLIDATION HYPOTHESIS

Chapter 6 has shown that undrained cyclic shearing of normally consolidated clay samples causes apparent overconsolidation in their subsequent monotonic shearing behavior. The term "apparent overconsolidation" is used rather than "overconsolidation" because the latter requires changes in water content in the sample as the effective consolidation stress is unloaded, which is not the case in samples undergoing overconsolidation due to undrained cyclic shearing. The major consequence of apparent overconsolidation is that it will allow prediction of overconsolidated cyclic clay behavior from results of cyclic tests on normally consolidated samples, as well as predictions of clay response due to cyclic loading with variable intensities, as will be described in the following sections. This is an important finding since it reduces the number of necessary tests in any cyclic testing program.

7.1 EFFECT OF APPARENT OVERCONSOLIDATION ON RESULTS OF NORMALLY CONSOLIDATED CLAYS

Having recognized that undrained cyclic loading causes an apparent overconsolidation, it is necessary to redefine the cyclic stress ratio to take into account the effects of apparent overconsolidation. As undrained cycling takes place, the initially normally consolidated sample goes to an apparently overconsolidated state, with the AOCR increasing as the number of cycles N increases. After N cycles, the normally consolidated

monotonic undrained strength, $s_u(NC)$, no longer has any physical significance, and should be replaced by $s_u(AOCR)$ which is the undrained monotonic strength at OCR=current AOCR induced by N cycles, and which is given by:

$$s_u(AOCR) = s_u(NC)\ (AOCR)^{m-1} \qquad m=0.8 \tag{7.1}$$

The cyclic stress ratio is redefined as $\tau_c/s_u(AOCR)$, and equals the cyclic shear stress normalized by the instantaneous undrained strength at any cycle N. For a test with a constant τ_c applied, $\tau_c/s_u(AOCR)$ increases with N since $s_u(AOCR)$ decreases with increasing AOCR. The following equation gives the expression of the new cyclic stress ratio as a function of the AOCR:

$$\frac{\tau_c}{s_u(AOCR)} = \frac{\tau_c}{s_u(NC)}\ (AOCR)^{1-m} \qquad m=0.8 \tag{7.2}$$

Figure 7.1 shows the S-N curves based on the cyclic stress ratio $\tau_c/s_u(AOCR)$, for tests with $\tau_{ave}=0$ on normally consolidated samples of resedimented Boston Blue Clay, using the same data utilized to construct Figure 5.45. The curves of equal γ_c and of maximum obliquity are shown as well as a family of curves, each corresponding to a test with constant τ_c but increasing $\tau_c/s_u(AOCR)$, intersecting the iso-γ_c curves.

Figure 7.1 can be used to predict N_f and γ_c versus number of cycles given the initial stress ratio $\tau_c/s_u(NC)$. First, the starting point is located (N=1 and $\tau_c/s_u(AOCR=1)=\tau_c/s_u(NC)$), then a curve is drawn parallel to the family of curves with constant τ_c. The intersection of this newly drawn curve with the M.O. line gives the number of cycles to failure N_f, and its intersection with the various iso-γ_c curves gives the

corresponding N.

Figures 7.1 and 5.45 give the same information as far as the cyclic shear strain $\gamma_c(\%)$ versus cycle number, and the number of cycles at failure. However, Figure 7.1 contains additional information about the apparent overconsolidation caused by undrained cyclic shearing. For any test with zero τ_{ave} and a given cyclic stress ratio $\tau_c/s_u(NC)$, the apparent overconsolidation ratio at an intermediate cycle number N can be estimated by obtaining $\tau_c/s_u(AOCR)$ from the figure and using the following relationship:

$$AOCR = \left[\left(\frac{\tau_c}{s_u(AOCR)}\right) / \left(\frac{\tau_c}{s_u(NC)}\right)\right]^{\frac{1}{1-m}} \qquad m = 0.8 \qquad (7.3)$$

This apparent overconsolidation at intermediate cycles is the key to the method described in the next section, which is aimed at predicting overconsolidated cyclic results from results of normally consolidated samples.

7.2 USE OF APPARENT OVERCONSOLIDATION IN PREDICTING OVERCONSOLIDATED CYCLIC BEHAVIOR

The Apparent Overconsolidation Hypothesis allows us to predict the undrained cyclic behavior of a mechanically overconsolidated clay sample based on the results of tests performed on normally consolidated samples. A method of prediction in the case of τ_{ave}=0 is presented, and the results of six mechanically overconsolidated tests, at OCR values of 1.38 and 2, are compared to the predictions based on the AOCR hypothesis.

7.2.1 Methodology

Figure 7.2 shows the S-N curves based on $\tau_c/s_u(AOCR)$ for tests on normally consolidated samples with $\tau_{ave}=0$. The heavily drawn curve corresponds to a cyclic test with $\tau_{ave}=0$ and $\tau_c/s_u(AOCR=1)\Big|_{N=1}=0.56$ (or 56% of $s_u(NC)$). The test starts at point A and ends at point F where failure occurs. Point S on the curve corresponds to $N_S=70$, $\tau_c/s_u(AOCR)=0.64$ and $\gamma_{cS}=0.5\%$. Using equation 7.2, the apparent OCR at point S can be estimated and is equal to 2. Furthermore, according to the apparent overconsolidation hypothesis, apparent overconsolidation is equivalent to mechanical overconsolidation, and therefore point S represents the start of a cyclic test on a mechanically overconsolidated sample to OCR=2 with $\tau_c/s_u(OCR=2)\Big|_{N=1}=0.64$ (or 64% of the $s_u(OC)$). The portion S-F of the heavy curve can therefore be used to predict the number of cycles to failure and the γ_c vs. N for the mechanically overconsolidated sample described above, except that the initial values N_S and γ_{cS} should be subtracted. The following table gives an example to illustrate this prediction method.

N.C. sample	Mechanically O.C. sample OCR=2
Point S:	Point S: start of test on OC sample
$N_S=70$ $\tau_c/s_u(AOCR)=0.64$ $\gamma_{cS}=0.5\%$	$N=1$ $\tau_c/s_u(OCR=2)=0.64$ $\gamma_c(OC)=0\%$
Point F: failure of NC sample	Point F: failure of OC sample
$N_F=165$ $\gamma_c \geq 3\%$	$N_f(OC)=N_F-N_S=165-70=95$ $\gamma_c \geq 3\%$
Point B: intermediate point	Point B: intermediate point
$N_B=100$ $\gamma_{cB}=0.75\%$	$N=N_B-N_S=100-70=30$ cycles $\gamma_c(OC)_B=\gamma_{cB}-\gamma_{cS}=0.75=0.5=0.25\%$

Point B is an intermediate point which corresponds to 30 cycles with $\tau_c/s_u(OCR=2)=0.64$ on a sample mechanically overconsolidated to OCR=2. The value of γ_c after 30 cycles is estimated at 0.25%.

The number of cycles at failure of the overconsolidated test is estimated using:

$$N_f(OC) = N_F - N_S \; ; \tag{7.4}$$

and the cyclic shear strain at any intermediate point B is estimated using:

$$\gamma_c(OC)_B = \gamma_{cB} - \gamma_{cS} \tag{7.5}$$

The excess pore pressure at failure can be estimated using equation 6.2 which gives equation 6.3 for RBBC and is rewritten below:

$$\Delta u_f(OC) = \left[1 - \frac{0.205(OCR)^{0.8}\,(\tau_{ave}/s_u(OC) + \tau_c/s_u(OC))}{\tan 30^\circ}\right] \bar{\sigma}_{vc} \tag{7.6}$$

The pore pressure $\Delta u(OC)$ versus N for the mechanically overconsolidated sample can be predicted using Figures 7.2 and 5.47 and the method outlined below. For any intermediate point such as point B, the cycle number corresponding to the overconsolidated tests is estimated using:

$$N(OC)_B = N_B - N_S \tag{7.7}$$

Also at point B, $\bar{N}_B=100/165=0.606$ is estimated, and yields a value of $\Delta\bar{u}_B=0.7$ (see Figure 5.47). For the mechanically overconsolidated sample at point B, the excess pore pressure can be estimated from:

$$\Delta u(OC)_B = \left(\frac{\Delta\bar{u}_B - \Delta\bar{u}_S}{\Delta\bar{u}_F - \Delta\bar{u}_S}\right) \Delta u_f(OC) \qquad (7.8)$$

where $\Delta\bar{u}_B$, $\Delta\bar{u}_S$ and $\Delta\bar{u}_F$ are the $\Delta\bar{u}$ values obtained from Figure 5.47 at $\bar{N}_B$, $\bar{N}_S$, and $\bar{N}_F$ corresponding to points B, S, and F respectively, and $\Delta u_f(OC)$ is obtained from equation (7.6).

The method outlined above is based on the apparent overconsolidation hypothesis, and gives predictions of N_f, Δu_f, γ_c vs. N, and Δu vs. N for overconsolidated clays based on the results of normally consolidated samples. The accuracy of this method is now checked by comparing predictions with measurements on mechanically overconsolidated samples. This evaluation is achieved by means of results of tests C-26 and C-27 with OCR=1.38, and C-33, C-34, C-35 and C-36 with OCR=2.

7.2.2 Evaluation at OCR=1.38

7.2.2.1 Test C-26

Test C-26 was performed on an overconsolidated sample of resedimented Boston Blue Clay, with OCR=1.38, τ_{ave}=0, and $\tau_c/s_u(OCR=1.38)|_{N=1} = 0.60$. This section predicts the results of test C-26 using the methodology outlined in the previous section.

The S-N curve to be used in prediction is the one corresponding to a test on a normally consolidated sample with:

$$\tau_c/s_u(NC) = (\tau_c/s_u(OCR)) \cdot (OCR)^{m-1} \qquad m=0.8 \qquad \text{(from Eq. 7.2)}$$

$$= (0.60) \cdot (1.38)^{-0.2}$$

$$= 0.56.$$

This curve is drawn heavily in Figure 7.3, and starts from a value of $\tau_c/s_u(AOCR=1)|_{N=1}$=0.56 which increases with cycle number N.

• Point S, which is located at $\tau_c/s_u(AOCR)=0.60$, indicates the beginning of test C-26, and corresponds to a number of cycles $N_S=29$, and a cyclic shear strain $\gamma_c=0.35\%$.

• Point F, indicates the failure point of test C-26, and corresponds to a cycle number $N_F=165$, and a cyclic shear strain $\gamma_c>3\%$.

• Point B is an intermediate point with $N_B=90$ and $\gamma_c=0.65\%$.

The following table gives the parameters necessary for prediction, with $\bar{N}=N/N_F$, and $\Delta\bar{u}$ obtained from Figure 5.47.

POINT	CYCLE NUMBER	$\gamma_c(\%)$	$\bar{N}$	$\Delta\bar{u}$
S	29	0.35	0.18	0.38
F	165	> 3	1.00	1.00
B	90	0.65	0.55	0.68

• Using equation 7.4, the number of cycles at failure in test C-26 is estimated: $N_f = 165-29 = 136$.

• Using equation 7.6, the excess pore pressure at failure in test C-26 is estimated:

$$\Delta u_f(OC) = \left[1 - \frac{(0.205)\ .\ (1.38)^{0.8}\ .\ (0.60)}{\tan(30^\circ)}\right] \bar{\sigma}_{vc}$$

$$= 0.72\ \bar{\sigma}_{vc}$$

• Using equation 7.7, the cycle number at point B corresponding to test C-26 is estimated: $N(OC)_B = 90-29 = 61$

• The cyclic shear strain at point B, corresponding to cycle number 61 in test C-26, is estimated using equation 7.5:

$$\gamma_c(OC)_B(\%) = 0.65 - 0.35 = 0.30\%$$

• The excess pore pressure at point B, corresponding to cycle number 61

in test C-26, is estimated using equation 7.8:

$$\Delta u(OC)_B = \left(\frac{0.68 - 0.38}{1.00 - 0.38}\right) \cdot (0.72)\ \bar{\sigma}_{vc}$$

$$= 0.35\ \bar{\sigma}_{vc}$$

The following table compares the predicted values with the actual measured ones.

TEST C-26 OCR=1.38

	MEASURED VALUES	PREDICTED VALUES	ERROR
N_f	138	136	2%
Δu_f	$0.70\ \bar{\sigma}_{vc}$	$0.72\ \bar{\sigma}_{vc}$	3%
γ_c at N=61	0.44%	0.35%	20%
Δu at N=61	$0.25\ \bar{\sigma}_{vc}$	$0.35\ \bar{\sigma}_{vc}$	40%

7.2.2.2 Test C-27

Test C-27 was performed on an overconsolidated sample of resedimented Boston Blue Clay, with OCR=1.38, τ_{ave}=0, and $\tau_c/s_u(OCR=1.38)|_{N=1}$=0.76. This section predicts the results of test C-27 using the method based on the apparent overconsolidation hypothesis. The details of the procedure are similar to those of test C-26, and therefore, only a summary and a comparison of the results with measured data are presented.

The S-N curve used in prediction is heavily drawn in Figure 7.4. It corresponds to a normally consolidated test with:

$\tau_c/s_u(NC) = (0.76) \cdot (1.38)^{-0.2}$ (from equation 7.2)

$= 0.71.$

Figure 7.4 shows point S corresponding to the first cycle in test C-27, point F corresponding to failure, and point B at an intermediate cycle number. The following table gives the parameters required for prediction.

POINT	CYCLE NUMBER	γ_c(%)	$\overline{N}$	$\overline{\Delta u}$
S	11	0.55	0.26	0.46
F	42	> 3	1.00	1.00
B	25	1.00	0.59	0.71

Using the above parameters and equations 7.4 through 7.8, predictions of results of test C-27 are made, and the following table compares the predictions to the measured data.

TEST C-27 OCR=1.38

	MEASURED VALUES	PREDICTED VALUES	ERROR
N_f	34	31	9%
Δu_f	0.65 $\overline{\sigma}_{vc}$	0.65 $\overline{\sigma}_{vc}$	0%
γ_c at N=14	0.55%	0.45%	18%
Δu at N=14	0.13 $\overline{\sigma}_{vc}$	0.30 $\overline{\sigma}_{vc}$	131%

7.2.3 Evaluation at OCR=2

7.2.3.1 Tests C-33 and C-35

Tests C-33 and C-35 are identical tests on overconsolidated samples of resedimented Boston Blue Clay with OCR=2, $\tau_{ave}=0$, and $\tau_c/s_u(OCR=2)|_{N=1}=0.56$. The S-N curve used to predict their results is drawn heavily in Figure 7.5, and corresponds to a normally consolidated test with:

$$\tau_c/s_u(NC) = (0.56) \cdot (2)^{-0.2} \qquad \text{(from equation 7.2)}$$

$$= 0.49.$$

The starting point S corresponding to cycle one of tests C-33 and C-35 is shown in Figure 7.5, and is located at a value of $\tau_c/s_u(AOCR) = 0.56$, as well as the failure point F, and an intermediate point B. The list of parameters used in the prediction is shown below.

POINT	CYCLE NUMBER	$\gamma_c(\%)$	N	Δu
S	370	0.20	0.62	0.73
F	600	> 3	1.00	1.00
B	480	0.50	0.80	0.88

Using the above parameters and equations 7.4 through 7.8, the following predictions of tests C-33 and C-35 are made and compared with the average data from the two tests.

TESTS C-33 AND C-35 OCR=2

	MEASURED VALUES	PREDICTED VALUES	ERROR
N_f	252	230	9%
Δu_f	0.66 $\bar{\sigma}_{vc}$	0.65 $\bar{\sigma}_{vc}$	1.5%
γ_c at 110 cycles	0.42%	0.30%	29%
Δu at 110 cycles	0.14 $\bar{\sigma}_{vc}$	0.36 $\bar{\sigma}_{vc}$	160%

7.2.3.2 Test C-34

Test C-34 was performed on an overconsolidated sample with OCR=2, $\tau_{ave}=0$, and $\tau_c/s_u(OCR=2)|_{N=1}=0.70$. The S-N curve used to predict the results of the test is shown in Figure 7.6, and corresponds to a normally consolidated test with:

$$\tau_c/s_u(NC) = (0.70) \cdot (2)^{-0.2} \qquad \text{(from equation 7.2)}$$

$$= 0.61.$$

Point S (at $\tau_c/s_u(AOCR)=0.70$), point F at failure, and intermediate point B are shown in the Figure. The following parameters are used in the prediction.

POINT	CYCLE NUMBER	γ_c(%)	$\bar{N}$	$\bar{\Delta u}$
S	50	0.75	0.50	0.64
F	100	> 3	1.00	1.00
B	70	1.00	0.70	0.80

The above parameters yield the following predictions.

TEST C-34 OCR=2

	MEASURED VALUES	PREDICTED VALUES	ERROR
N_f	50	50	0%
Δu_f	0.57 $\bar{\sigma}_{vc}$	0.57 $\bar{\sigma}_{vc}$	0%
γ_c at 20 cycles	0.60%	0.25%	58%
Δu at 20 cycles	0.02 $\bar{\sigma}_{vc}$	0.25 $\bar{\sigma}_{vc}$	1150%

7.2.3.3 Test C-36

Test C-36 was performed on a sample with OCR=2, τ_{ave}=0, and $\tau_c/s_u(OCR=2)|_{N=1}$=0.85. Figure 7.7 shows the S-N curve used for predicting the results test C-36, and corresponds to a test on a normally consolidated sample with:

$$\tau_c/s_u(NC) = (0.85) \cdot (2)^{-0.2} \qquad \text{(from equation 7.2)}$$

$$= 0.74.$$

Point S (at $\tau_c/s_u(AOCR)$=0.85), point F at failure, and intermediate point B are shown in Figure 7.7, and give the following parameters used in the prediction.

POINT	CYCLE NUMBER	γ_c(%)	$\bar{N}$	$\bar{\Delta u}$
S	18	1.00	0.56	0.68
F	32	> 3	1.00	1.00
B	24	2.00	0.75	0.84

The above parameters yield the following predictions.

TEST C-36 OCR=2

	MEASURED VALUES	PREDICTED VALUES	ERROR
N_f	15	14	7%
Δu_f	0.48 $\bar{\sigma}_{vc}$	0.45 $\bar{\sigma}_{vc}$	6%
γ_c at 8 cycles	1.6%	1.0%	38%
Δu at 8 cycles	-0.03 $\bar{\sigma}_{vc}$	0.23 $\bar{\sigma}_{vc}$	850%

7.2.4 Accuracy of the Prediction Method

A method for predicting the behavior of overconsolidated clay samples from results of normally consolidated samples, using the apparent overconsolidation hypothesis, was outlined in section 7.2.1 and evaluated for OCR values of 1.38 and 2 in sections 7.2.2 and 7.2.3 respectively.

The method seems to predict very well the number of cycles at failure and the excess pore pressure at failure, with a maximum error less than 10%. The estimates of cyclic shear strain γ_c(%) at intermediate cycles are reasonable, with a maximum error of about 60%, which increases with OCR. However, estimates of excess pore pressure at intermediate cycle numbers are poor with errors up to 1200%. This is mainly due to the fact that overconsolidated samples experience negative excess pore pressures in the initial phase of cycling, a feature which cannot be predicted, since the normally consolidated excess pore pressure curves which were used in Figure 5.47 show no negative pore pressures.

Despite the lack of accuracy in the predicted excess pore pressures

at intermediate cycles, the method allows very good estimates of N_f and Δu_f, and fair estimates of $\gamma_c(\%)$ at intermediate cycles. It should be noted that the method is limited to an overconsolidation ratio smaller than 2, with decreasing accuracy as OCR increases.

7.3 A SUPERPOSITION METHOD FOR PREDICTING CLAY BEHAVIOR UNDER VARIABLE CYCLIC LOADING

This section presents a superposition method aimed at predicting the results of undrained cyclic DSS tests with variable cyclic loading history. Such a superposition method is crucial for predicting the cyclic clay behavior under variable storm loading from the results of tests with constant cyclic loading, which were presented in Chapter 5.

Andersen (1975) has presented a superposition scheme, which was described in Section 3.3.2 of the report. His method is based on S-N curves from DSS tests with τ_{ave}=0 and constant $\tau_c/s_u(NC)$, and assumes that at any point in the history of cycling, knowledge of the current cyclic shear strain is sufficient to predict all aspects of subsequent behavior. While his method gives good predictions, it neglects the effects of apparent overconsolidation resulting from undrained cycling, and therefore it does not incorporate changes in the stress history which occur during cycling. Hence, a modified procedure, which utilizes S-N curves corrected for apparent overconsolidation, is introduced herein in order to achieve more accurate predictions.

The following sections will present predictions of the results of tests C-28, C-37, and C-38, performed with τ_{ave}=0 and variable $\tau_c/s_u(NC)$.

Predictions, using the original Andersen superposition procedure, and the new proposed procedure accounting for apparent overconsolidation, will be compared.

7.3.1 Prediction of Results of Test C-28

The results of test C-28 were presented in section 5.7.1, and are summarized in the following table. The sample was first subjected to 29 cycles at $\tau_c/s_u(NC)=0.56$, at the end of which the cyclic shear stress ratio was increased to $\tau_c/s_u(NC)=0.71$ and kept at this level until failure.

TEST C-28, $\tau_{ave}=0$

MEASURED DATA

	CYCLE NUMBER		
$\tau_c/s_u(NC)=0.56$	1 to 29		
	at N=29	γ_c = 0.35%	$\Delta u/\bar{\sigma}_{vc}=0.29$
$\tau_c/s_u(NC)=0.71$	29 to end		
	at N=30	γ_c = 0.50%	$\Delta u/\bar{\sigma}_{vc}=0.30$
	at $N_f=53$	γ_c > 3%	$\Delta u/\bar{\sigma}_{vc}=0.72$

7.3.1.1 Predictions Using the Andersen Superposition Method

Figure 7.8, which plots the S-N curves for Boston Blue Clay, shows the steps involved in Andersen's procedure for predicting the results of test C-28. Line AB corresponds to the first phase of the test with $\tau_c/s_u(NC)=0.56$. At point B, the cycle number is 29 and the cyclic shear strain is estimated by curve BC which corresponds to $\gamma_c=0.35\%$. Path BCD corresponds to the transition from $\tau_c/s_u(NC)=0.56$ to $\tau_c/s_u(NC)=0.71$. BC

is a constant cyclic shear strain path corresponding to the state of the sample immediately after the end of phase one (point B) or immediately before the start of phase two (point C). Path CD corresponds to the immediate increase in shear strain, $\Delta\gamma_{c1}(\%)$, due to the increase in cyclic shear stress ratio from 0.56 to 0.71. $\Delta\gamma_{c1}$ is obtained from Figure 7.9 which plots shear stress ratio, $\tau_c/s_u(NC)$ versus cyclic shear strain $\gamma_{c1}(\%)$ in the first cycle. The figure is constructed from the results of normally consolidated cyclic DSS tests C-2, C-5, C-6, C-7, C-29, and C-30 with $\tau_{ave}=0$. $\Delta\gamma_c$ is estimated at 0.1%, which brings the sample to the iso-γ_c curve corresponding to 0.45% (point D). Path DF corresponds to the second phase, with the sample failing when point F is reached, at maximum obliquity. The predicted number of cycles during the second phase is therefore

$$N_F - N_D = 43 - 6 = 37,$$

and the predicted total number of cycles for test C-28 is

$$N_B + (N_F - N_D) = 29 + 37 = 66.$$

The following table compares the predicted versus measured values of the number of cycles at failure N_f, and the cyclic shear strain at points B and D corresponding to the end of the first phase and the beginning of the second phase respectively.

PREDICTIONS BASED ON THE

ANDERSEN SUPERPOSITION METHOD

	Cycle Number	Measured γ_c(%)	Predicted γ_c(%)	Error in γ_c(%)
Point B	29	0.35	0.35	0
Point D	30	0.50	0.45	10%

	γ_c(%)	Measured N_f	Predicted N_f	Error in N_f
Failure	>3%	53	66	25%

There is good agreement in the number of cycles at failure, N_f which is predicted within 25%, and in the cyclic shear strain values, which show a maximum error of 10%.

7.3.1.2 Predictions Using the Modified Andersen Superposition Method

The new modified Andersen procedure is identical to the regular Andersen procedure except that it uses S-N curves modified for apparent overconsolidation, and plots of cyclic stress ratio τ_c/s_u(AOCR) versus cyclic shear strain γ_{c1}(%) at cycle one, at the appropriate apparent overconsolidation ratio.

Figure 7.10 shows the prediction of test C-28 using the new superposition method. The sample starts at point A with τ_c/s_u(AOCR)=0.56 until point B is reached. At point B, the sample has an apparent overconsolidation ratio which is estimated using equation 7.3 and the values of τ_c/s_u(AOCR) at points A and B:

$$AOCR_B = (0.6 / 0.56)^{(1/(1-0.8))} = 1.41.$$

Path BC corresponds to constant γ_c=0.35%, and constant AOCR+1.41. Hence, at point C, the new cyclic stress ratio is computed using equation 7.2 and the value of $\tau_c/s_u(NC)$=0.71 and AOCR=1.41:

$$\tau_c/s_u(AOCR) = (0.71) \cdot (1.41)^{(1-0.8)} = 0.76.$$

Path CD corresponds to the immediate increase in cyclic shear strain, which occurs at constant τ and constant AOCR, and hence at constant $\tau_c/s_u(AOCR)$. The increase in cyclic shear strain $\Delta\gamma_{cl}$ is estimated from Figure 7.11 which plots the cyclic shear stress ratio $\tau_c/s_u(AOCR)$ versus γ_{cl}(%) at OCR values of 1, 2, and 4. This plot is obtained using the data of cyclic tests on mechanically overconsolidated BBC with OCR=1, 2, and 4. The increase in γ_{cl} at AOCR=1.41 due to increasing $\tau_c/s_u(AOCR)$ from 0.6 to 0.76 is estimated by interpolation between the curves corresponding to OCR=1 and 2, and equals 0.17%. Point D is therefore on the iso-γ_c curve corresponding to 0.52%, with N_D=10. The total number of cycles is estimated as follows:

$$N_B + (N_F - N_D) = 29 + (39 - 10) = 58.$$

The prediction based on the new modified Andersen method are summarized below.

PREDICTIONS BASED ON THE

MODIFIED ANDERSEN SUPERPOSITION METHOD

	Cycle Number	Measured γ_c(%)	Predicted γ_c(%)	Error in γ_c(%)
Point B	29	0.35	0.35	0
Point D	30	0.50	0.52	4%

	γ_c(%)	Measured N_f	Predicted N_f	Error in N_f
Failure	>3%	53	58	9%

There is excellent agreement between the number of cycles at failure N_f, with an error of 9% which is within the scatter range in N_f values caused by test variability at identical cyclic stress ratio. The intermediate strain at points B and D is very well predicted, with a maximum error of 4%.

7.3.2 Predictions of Test C-37

The results of test C-37 were presented in section 5.7.2, and are summarized in the following table. The sample was first subjected to 62 cycles at $\tau_c/s_u(NC)=0.50$, at the end of which the cyclic shear stress ratio was increased to $\tau_c/s_u(NC)=0.64$ and kept at this level until failure.

TEST C-37, τ_{ave}=0

MEASURED DATA

	CYCLE NUMBER		
$\tau_c/s_u(NC)$=0.50	1 to 62		
	at N=62	γ_c = 0.25%	$\Delta u/\bar{\sigma}_{vc}$=0.28
$\tau_c/s_u(NC)$=0.64	62 to end		
	at N=63	γ_c = 0.35%	$\Delta u/\bar{\sigma}_{vc}$=0.28
	at N_f=112	γ_c > 3%	$\Delta u/\bar{\sigma}_{vc}$=0.75

7.3.2.1 Predictions Using the Andersen Superposition Method

Figure 7.12 shows the steps used in the prediction process. The end of the first phase is indicated by point B, with N_B=62 and a predicted value of γ_c=0.25%. Path CD corresponds to the immediate increase in γ_c caused by the increase in cyclic shear stress ratio, and is estimated from Figure 7.9, and equals 0.08%. Hence, point D, which corresponds to the start of phase two of the test, lies on the iso-γ_c curve equal to 0.33%. The predicted number of cycles at failure is estimated as follows:

$$N_B + (N_F - N_D) = 62 + (75 - 6) = 131.$$

The following table summarizes the predicted versus measured values of N_f and γ_c.

PREDICTIONS BASED ON THE

ANDERSEN SUPERPOSITION METHOD

	Cycle Number	Measured γ_c(%)	Predicted γ_c(%)	Error in γ_c(%)
Point B	62	0.25	0.25	0
Point D	63	0.35	0.33	5.7%

	γ_c(%)	Measured N_f	Predicted N_f	Error in N_f
Failure	>3%	112	131	17%

As for test C-28, there is good agreement between predicted and measured data, with a 17% error in number of cycles at failure, and a maximum error of 6% in γ_c.

7.3.2.2 Predictions Using the Modified Andersen Superposition Procedure

Figure 7.13 shows the prediction procedures for test C-37 using the modified Andersen superposition method. At point B, the sample has an apparent overconsolidation ratio which is estimated using equation 7.3 and the values of τ_c/s_u(AOCR) corresponding to points A and B:

$$AOCR_B = (0.52 \;/\; 0.50)^{(1/(1-0.8))} = 1.22.$$

Path BC corresponds to constant γ_c=0.25%, and constant AOCR=1.22. Hence, at point C, the new cyclic stress ratio is computed using equation 7.2 and the value of τ_c/s_u(NC)=0.64 and AOCR=1.22:

$$\tau_c/s_{u(AOCR)} = (0.64) \cdot (1.22)^{(1-0.8)} = 0.67.$$

The increase in cyclic shear strain $\Delta\gamma_{c1}$ at AOCR=1.22, due to increasing τ_c/s_u(AOCR) from 0.52 to 0.67, is estimated using Figure 7.11

and interpolating between the curves corresponding to OCR=1 and 2. $\Delta\gamma_{cl}$ is estimated at 0.09%, and therefore, Point D is on the iso-γ_c curve corresponding to 0.34%, with N_D=6. The total number of cycles is estimated as follows:

$$N_B + (N_F - N_D) = 62 + (70 - 6) = 126.$$

The prediction based on the new modified Andersen superposition method are summarized below, and indicate excellent agreement.

PREDICTIONS BASED ON THE MODIFIED ANDERSEN METHOD

	Cycle Number	Measured γ_c(%)	Predicted γ_c(%)	Error in γ_c(%)
Point B	62	0.25	0.25	0
Point D	63	0.35	0.34	3%

	γ_c(%)	Measured N_f	Predicted N_f	Error in N_f
Failure	>3%	112	126	13%

7.3.3 Predictions of Test C-38

The results of test C-38 were presented in section 5.7.3, and are summarized in the following table. The test sample was first subjected to 265 cycles at τ_c/s_u(NC)=0.50, at the end of which the cyclic stress ratio was increased to τ_c/s_u(NC)=0.70 for 10 cycles, followed by a final decrease in cyclic shear stress ratio to τ_c/s_u(NC)=0.56, until failure.

TEST C-38, τ_{ave}=0

MEASURED DATA

	CYCLE NUMBER		
$\tau_c/s_u(NC)$=0.50	1 to 265		
	at N=265	γ_c = 0.41%	$\Delta u/\bar{\sigma}_{vc}$=0.51
$\tau_c/s_u(NC)$=0.70	266 to 275		
	at N=266	γ_c = 0.71%	$\Delta u/\bar{\sigma}_{vc}$=0.51
	at N=275	γ_c = 1.47%	$\Delta u/\bar{\sigma}_{vc}$=0.56
$\tau_c/s_u(NC)$=0.56	276 to end		
	at N=276	γ_c = 1.11%	$\Delta u/\bar{\sigma}_{vc}$=0.58
	at N_f=303	γ_c > 3%	$\Delta u/\bar{\sigma}_{vc}$=0.76

7.3.3.1 Predictions Using the Andersen Superposition Method

Figure 7.14 shows the S-N curves and the steps involved in Andersen's procedure for predicting the results of test C-38. Line AB corresponds to the first phase of the test with $\tau_c/s_u(NC)$=0.50. At point B, the cycle number is 265 and the cyclic shear strain is estimated by curve BC, which corresponds to γ_c=0.33%. Path BCD corresponds to the transition from $\tau_c/s_u(NC)$=0.50 to $\tau_c/s_u(NC)$=0.70. Path CD corresponds to the immediate increase in cyclic shear strain, $\Delta\gamma_{c1}$(%), due to the increase in cyclic shear stress ratio from 0.50 to 0.70. $\Delta\gamma_{c1}$ is obtained from Figure 7.9 which plots shear stress ratio, $\tau_c/s_u(NC)$, versus cyclic shear strain, γ_{c1}(%) in the first cycle. $\Delta\gamma_c$ is estimated at 0.12%, which brings the sample to the iso-γ_c curve corresponding to 0.45% (Point D). Path DE corresponds to the second phase, consisting of 10 cycles at $\tau_c/s_u(NC)$=0.70, at the end of which γ_c reaches at value of 0.71% (point E). Path EFG corresponds to the decrease in $\tau_c/s_u(NC)$ from 0.70 to 0.56,

with FG giving the immediate decrease in cyclic shear strain $\Delta\gamma_{c1}$. The latter is estimated from Figure 7.9, and equals -0.1% which puts point G on the iso-γ_c curve equal to 0.61%, with N_G=80. Path NG corresponds to the last phase of the test, with failure occuring at point H with N_H=170. The predicted total number of cycles at failure for test C-38 is

$$N_B + (N_E - N_D) + (N_H - N_G) = 265 + 10 + (170 - 80) = 365.$$

The following table compares the predicted versus measured values of the number of cycles at failure N_f, and the cyclic shear strain at points B, D, E, G, and at failure.

PREDICTIONS BASED ON THE

ANDERSEN SUPERPOSITION METHOD

	Cycle Number	Measured γ_c(%)	Predicted γ_c(%)	Error in γ_c(%)
Point B	265	0.41	0.33	20%
Point D	266	0.71	0.45	37%
Point E	275	1.47	0.71	52%
Point G	276	1.11	0.61	45%
	γ_c(%)	Measured N_f	Predicted N_f	Error in N_f
Failure	>3%	303	365	21%

There is good agreement in the number of cycles at failure, N_f, which is predicted within 21%, and average agreement in the cyclic shear strain values at the intermediate points, with an error ranging between 20% to 52%.

7.3.3.2 Predictions Using the Modified Andersen Superposition Method

Figure 7.15 shows the prediction of test C-38 using the modified Andersen superposition method. The sample starts at point A with $\tau_c/s_u(AOCR)=0.50$ until point B is reached. At point B, the sample has an apparent overconsolidation ratio which is estimated using equation 7.3 and the values of $\tau_c/s_u(AOCR)$ at points A and B:

$$AOCR_B = (0.56 \;/\; 0.50)^{(1/(1-0.8))} = 1.76.$$

Path BC corresponds to constant $\gamma_c=0.33\%$, and constant AOCR=1.76. Hence, at point C, the new cyclic stress ratio is computed using equation 7.2 and the value of $\tau_c/s_u(NC)=0.70$ and AOCR=1.76:

$$\tau_c/s_u(AOCR) = (0.70) \cdot (1.76)^{(1-0.8)} = 0.78.$$

Path CD corresponds to the immediate increase in cyclic shear strain, $\Delta\gamma_{c1}(\%)$, due to the increase in cyclic shear stress level. Figure 7.11 is used to estimate $\Delta\gamma_{c1}$ for AOCR=1.76, and $\tau_c/s_u(AOCR)$ increasing from 0.56 to 0.78, by interpolation between the curves corresponding to OCR=1 and 2. $\Delta\gamma_{c1}$ equals 0.27%, and therefore point D is on the iso-γ_c curve corresponding to 0.60%, with $N_D=10$. Path DE corresponds to the second phase of the test (10 cycles at $\tau_c/s_u(NC)=0.70$), with point E on the iso-γ_c curve corresponding to 0.95%, and having $N_E=20$. The apparent OCR at point E is estimated using equation 7.3 with the value of $\tau_c/s_u(AOCR)$ at point E, and $\tau_c/s_u(NC)=0.70$:

$$AOCR_E = (0.82 \;/\; 0.70)^{(1/1-0.8)} = 2.2.$$

Path EFG corresponds to the decrease in cyclic shear stress ratio from $\tau_c/s_u(NC)=0.70$ to $\tau_c/s_u(NC)= 0.56$. Path EF corresponds to constant

γ_c=0.95%, and constant AOCR=2.2. Hence, at point G, the new cyclic stress ratio is computed using equation 7.2 and the value of τ_c/s_u(NC)=0.56 and AOCR=2.2:

$$\tau_c/s_u(AOCR) = (0.56) \cdot (2.2)^{(1-0.8)} = 0.66.$$

Path FG corresponds to the immediate decrease in cyclic shear strain, $\Delta\gamma_{c1}$, due to the decrease in cyclic shear stress level. Figure 7.11 is used to estimate $\Delta\gamma_{c1}$ for AOCR=2.2, and τ_c/s_u(AOCR) decreasing from 0.82 to 0.66, by interpolation between the curves corresponding to OCR=2 and 4. $\Delta\gamma_{c1}$ equals -0.27%, and therefore, point G is on the iso-γ_c curve corresponding to 0.68%, with N_G=70. Path GH corresponds to the last phase of the test, with the sample failing at point H with N_H=135. From the above, the total number of cycles to failure is estimated as follows:

$$N_B + (N_E - N_D) + (N_H - N_G) = 265 + 10 + (135 - 70) = 340.$$

The following table compares the predicted versus measured values of the number of cycles at failure N_f, and the cyclic shear strain at points B, D, E, G, and at failure.

PREDICTIONS BASED ON THE

MODIFIED ANDERSEN METHOD

	Cycle Number	Measured γ_c(%)	Predicted γ_c(%)	Error in γ_c(%)
Point B	265	0.41	0.33	20%
Point D	266	0.71	0.60	15%
Point E	275	1.47	0.95	35%
Point G	276	1.11	0.68	39%
	γ_c(%)	Measured N_f	Predicted N_f	Error in N_f
Failure	>3%	303	340	12%

There is good agreement in the number of cycles at failure, N_f, with an error of 12% which is within the scatter range in N_f values caused by test variability at identical cyclic stress ratio. The strain at intermediate points is well predicted, with a maximum error of 29%.

7.3.4 Discussion of the Superposition Methods

The new modified Andersen superposition method consistently gives better estimates of the number of cycles at failure, N_f, and the cyclic shear strain γ_c, at cycle number less than N_f, than the original Andersen method. This is a direct result of using the apparent overconsolidation hypothesis, which allows to follow the changes in stress history in the clay sample as the cyclic shear stress level is varied.

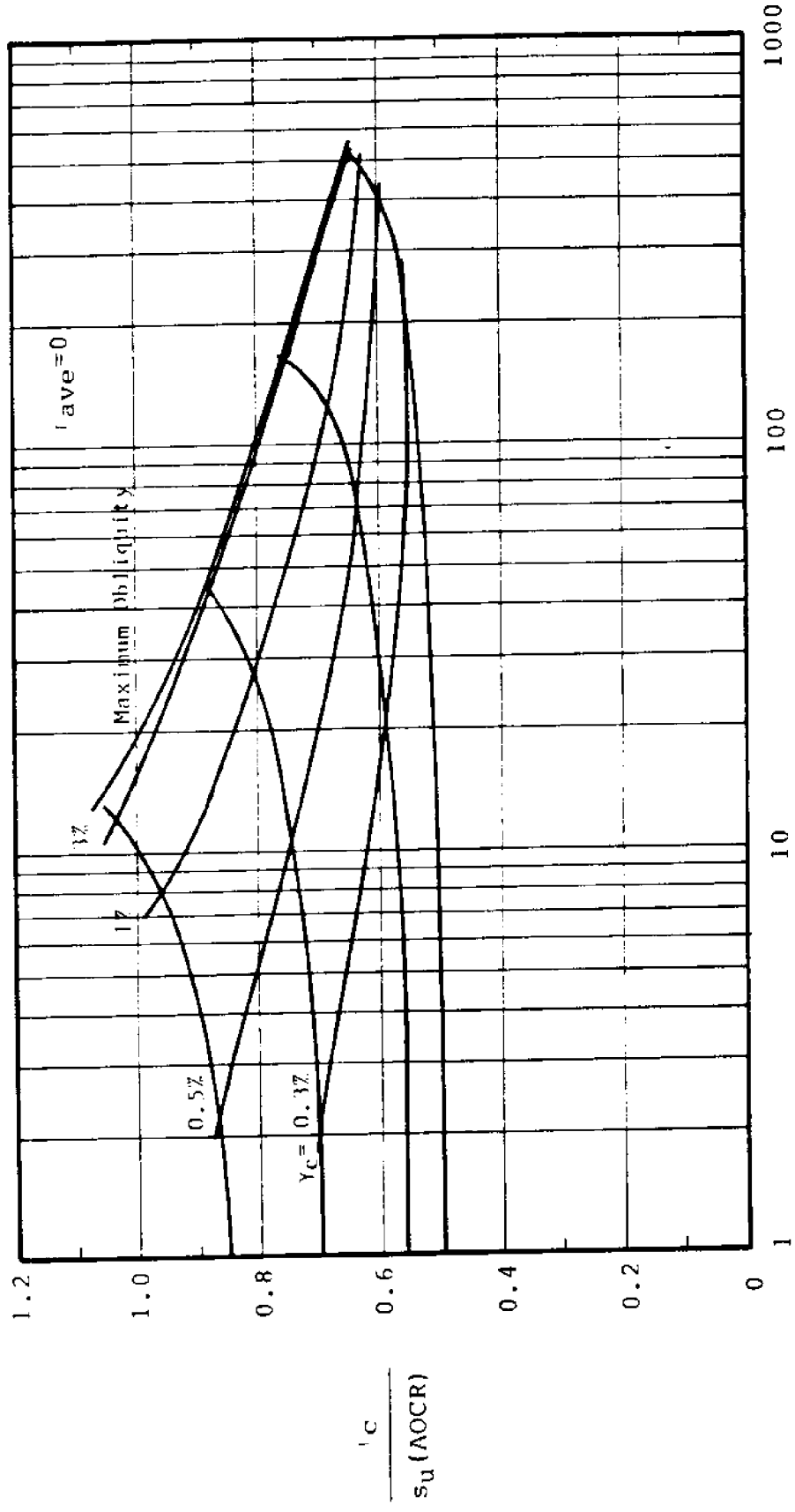

Figure 7.1 S-N Curves Modified for Apparent Overconsolidation, Tests with τ_{ave} = 0

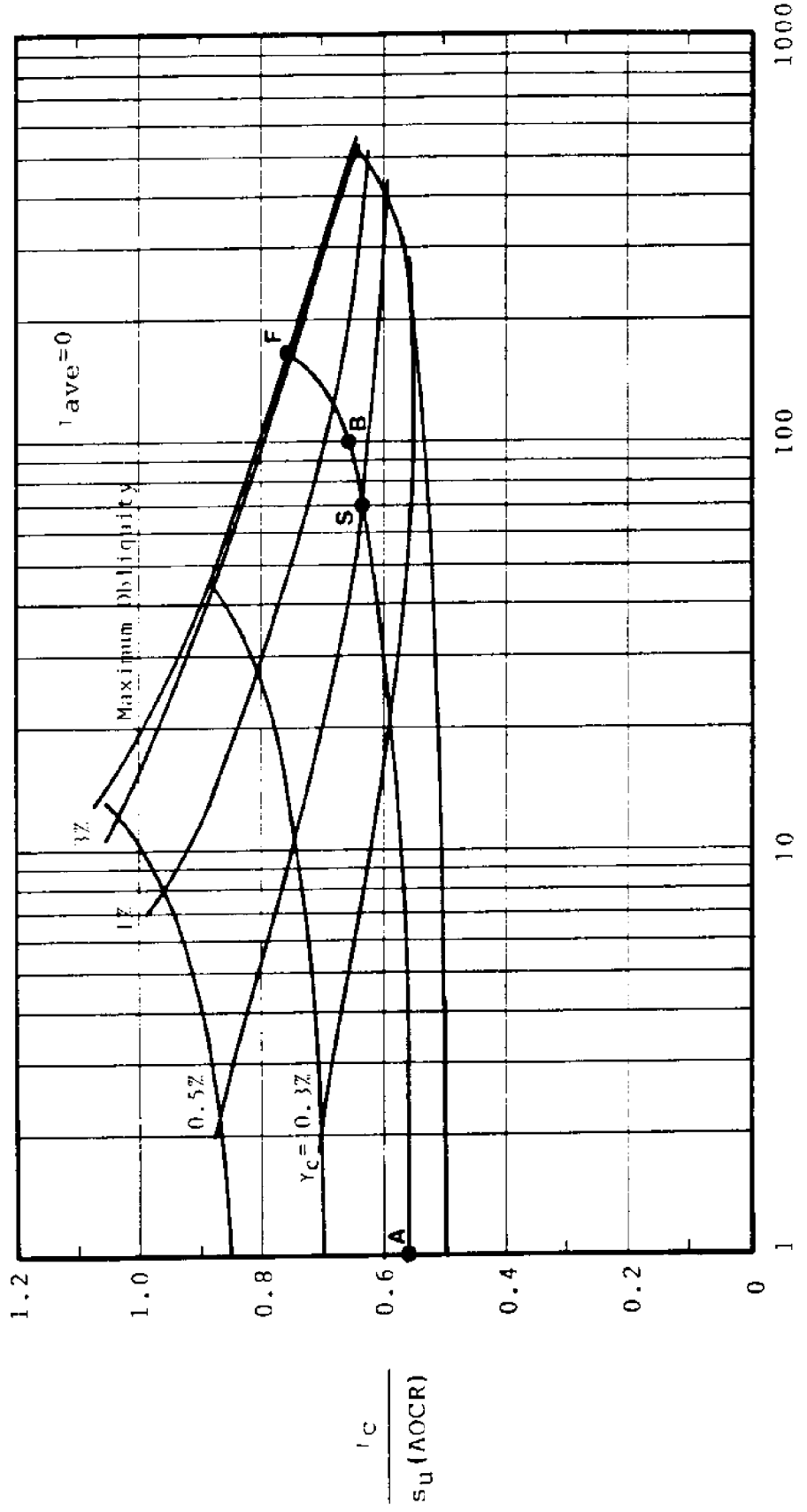

Figure 7.2 Example of an S-N Curve Used In Predicting Overconsolidated Cyclic Behavior

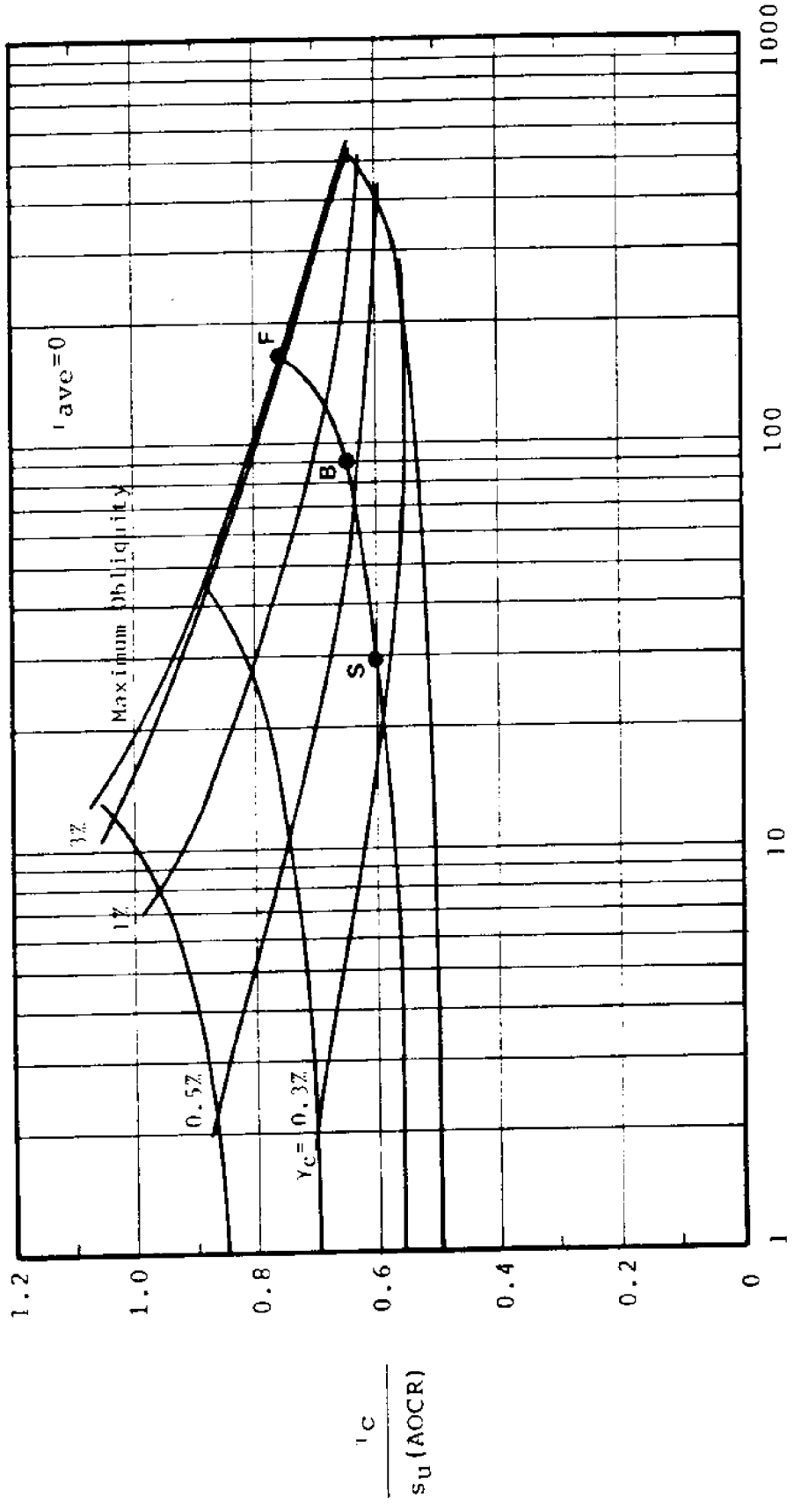

Figure 7.3 S-N Curve Used in Predicting Results of Test C-26: BBC, OCR=1.38, $\tau_{ave}=0$, $\tau_c/s_u(OC)=0.60$

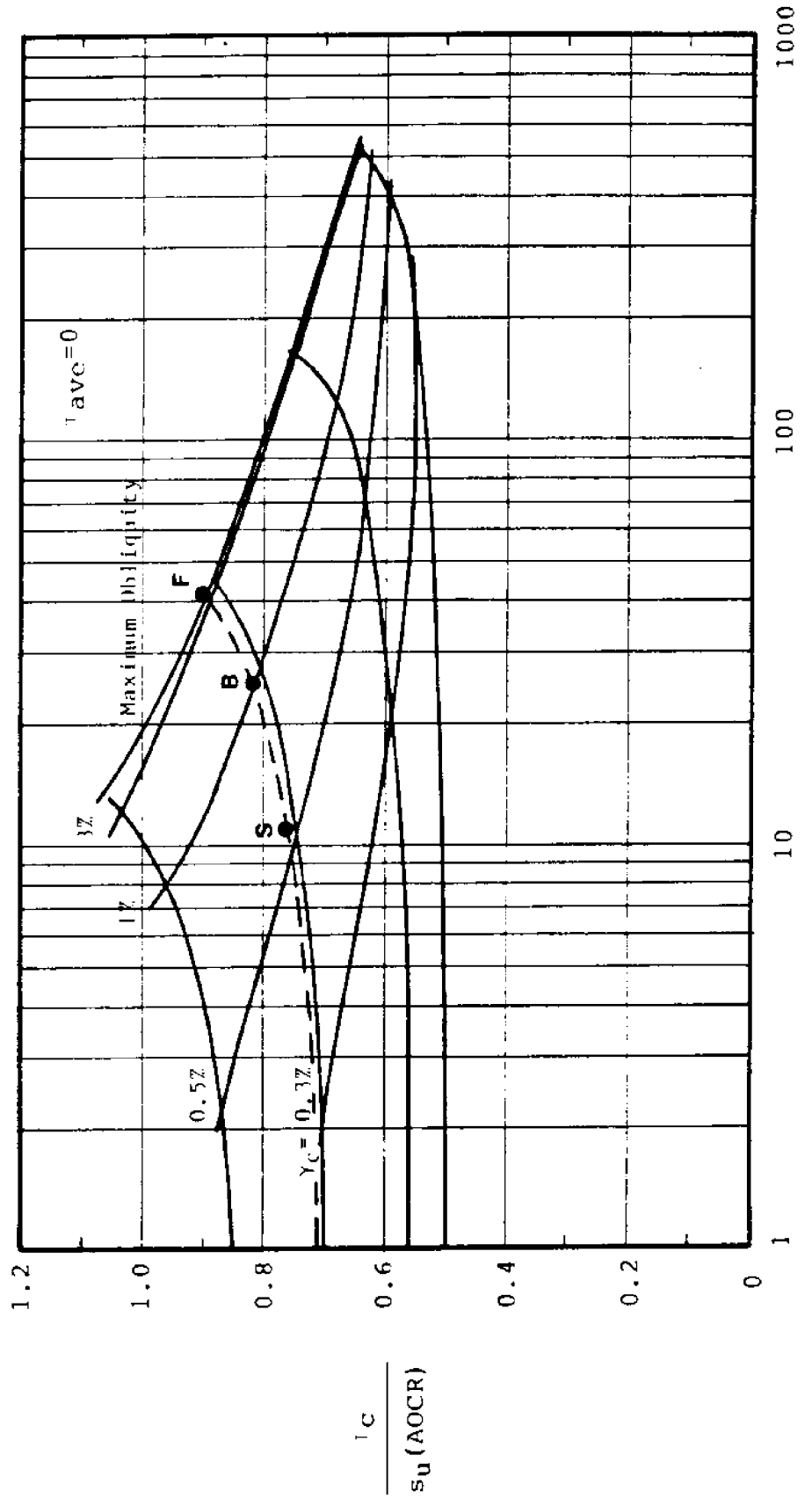

Figure 7.4 S-N Curve Used in Predicting Results of Test C-27: BBC, OCR=1.38, $\tau_{ave}=0$, $\tau_c/s_u(OC)=0.76$

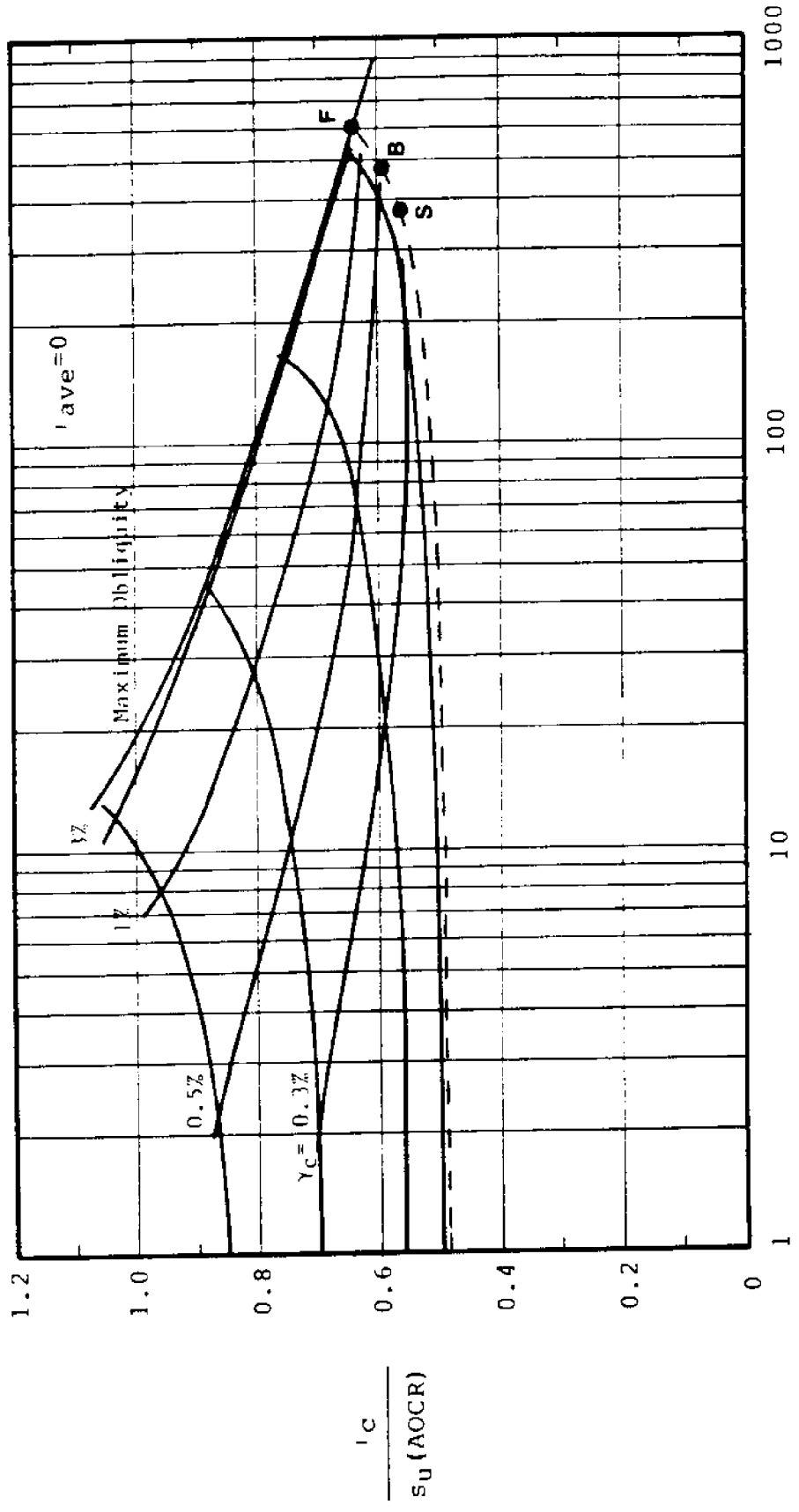

Figure 7.5 S-N Curve Used in Predicting Results of Tests C-33 and C-35, both with: BBC, OCR=2, τ_{ave}=0, $\tau_c/s_u(OC)$=0.56

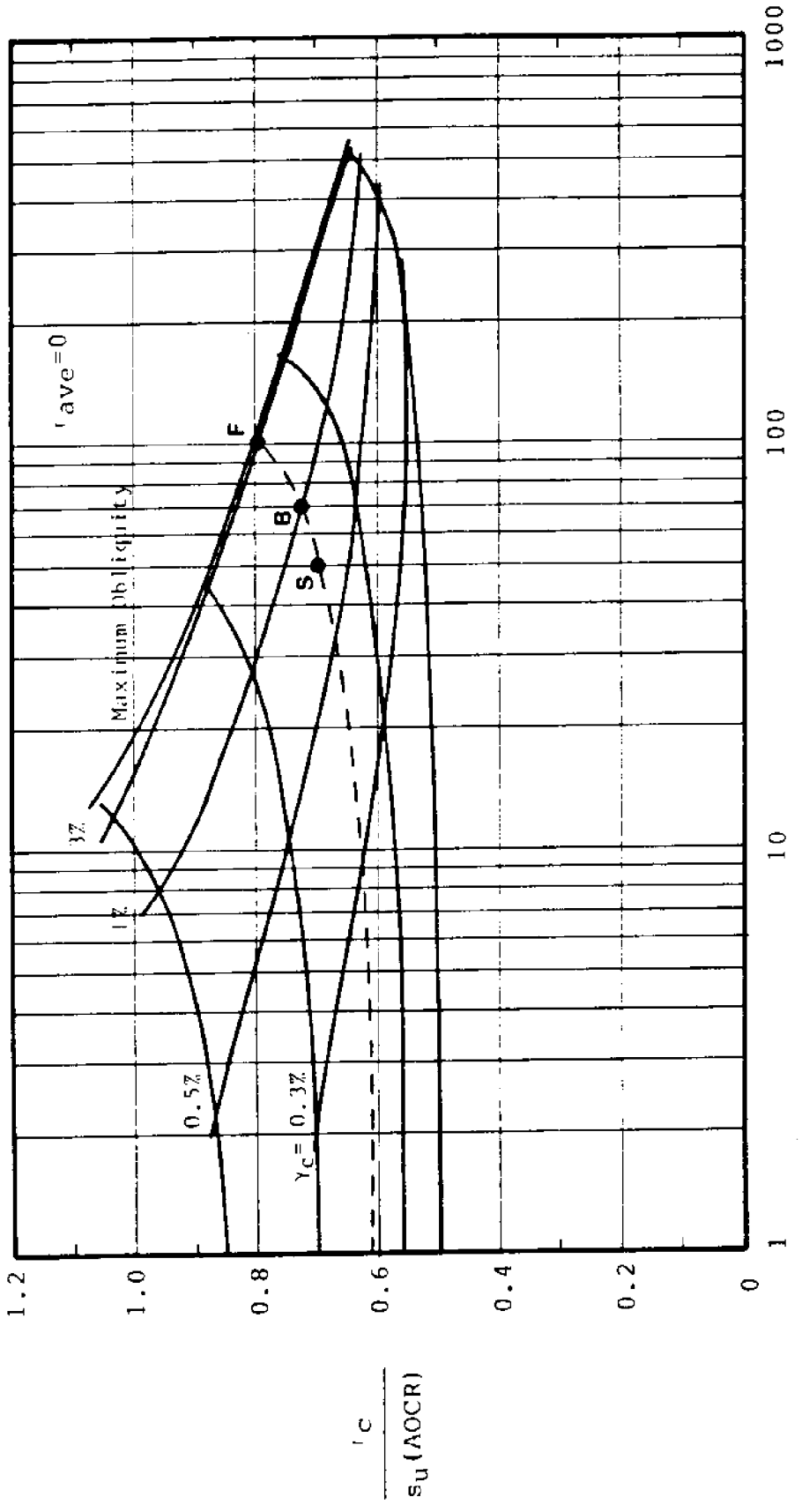

Figure 7.6 S-N Curve Used in Predicting Results of Test C-34: BBC, OCR=2, $\tau_{ave}=0$, $\tau_c/s_u(OC)=0.70$

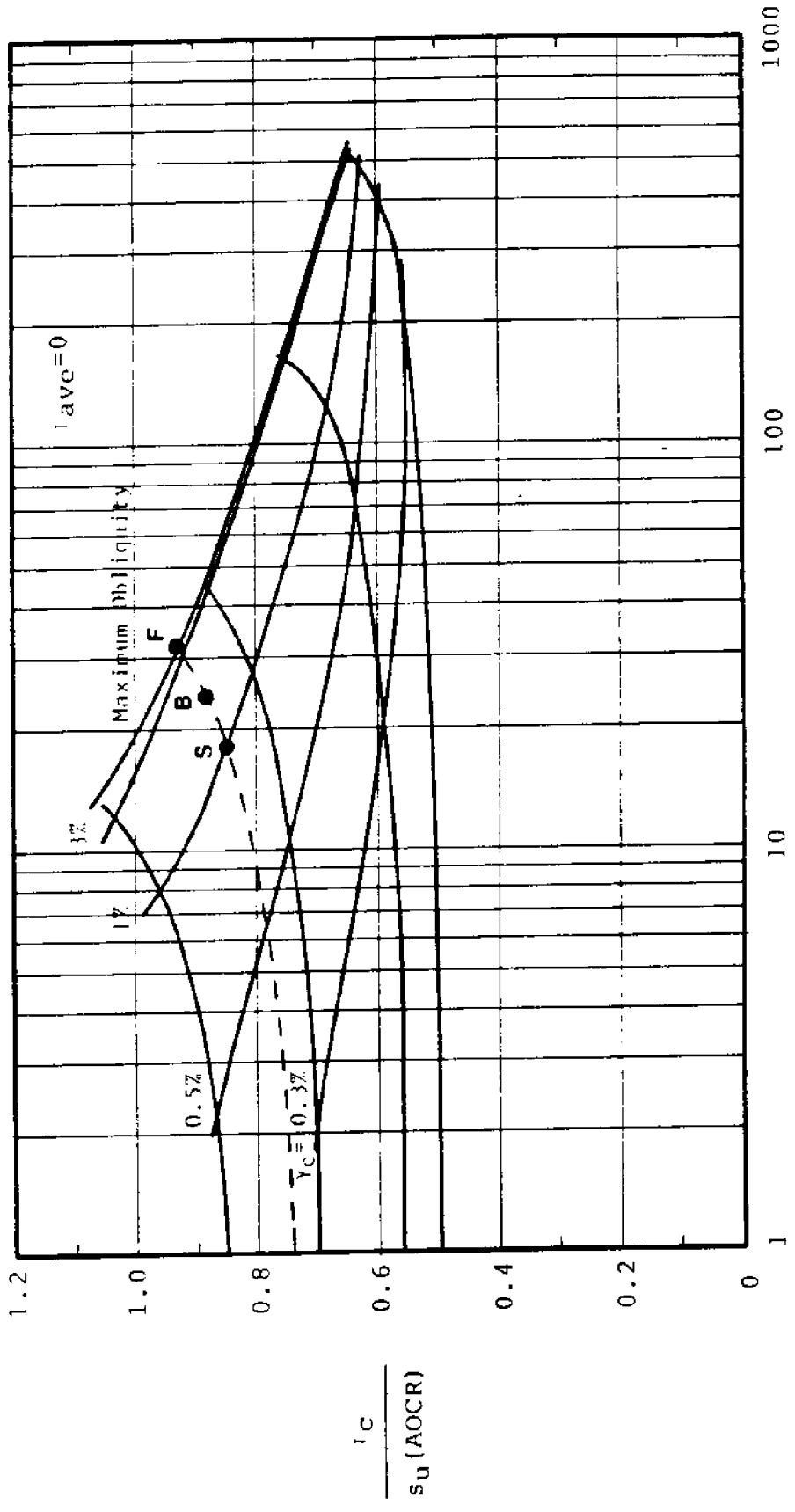

Figure 7.7 S-N Curve Used in Predicting Results of Test C-36: BBC, OCR=2, $\tau_{ave}=0$, $\tau_c/s_u(OC)=0.85$

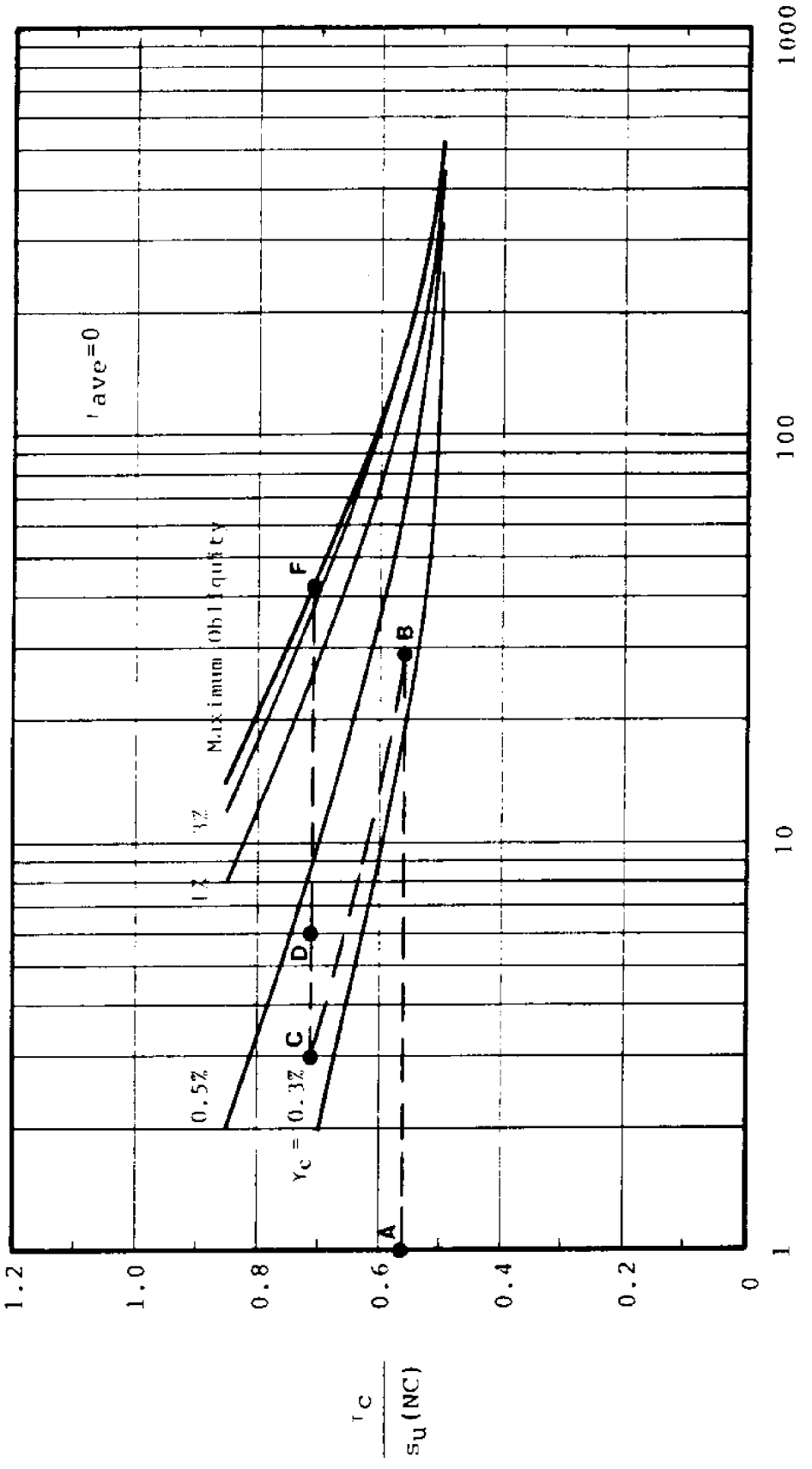

Figure 7.8 Prediction of Results of Test C-28: N.C. BBC, $\tau_{ave}=0$, $\tau_c/s_u(NC)=0.56$, 0.71, Using Andersen's Procedure

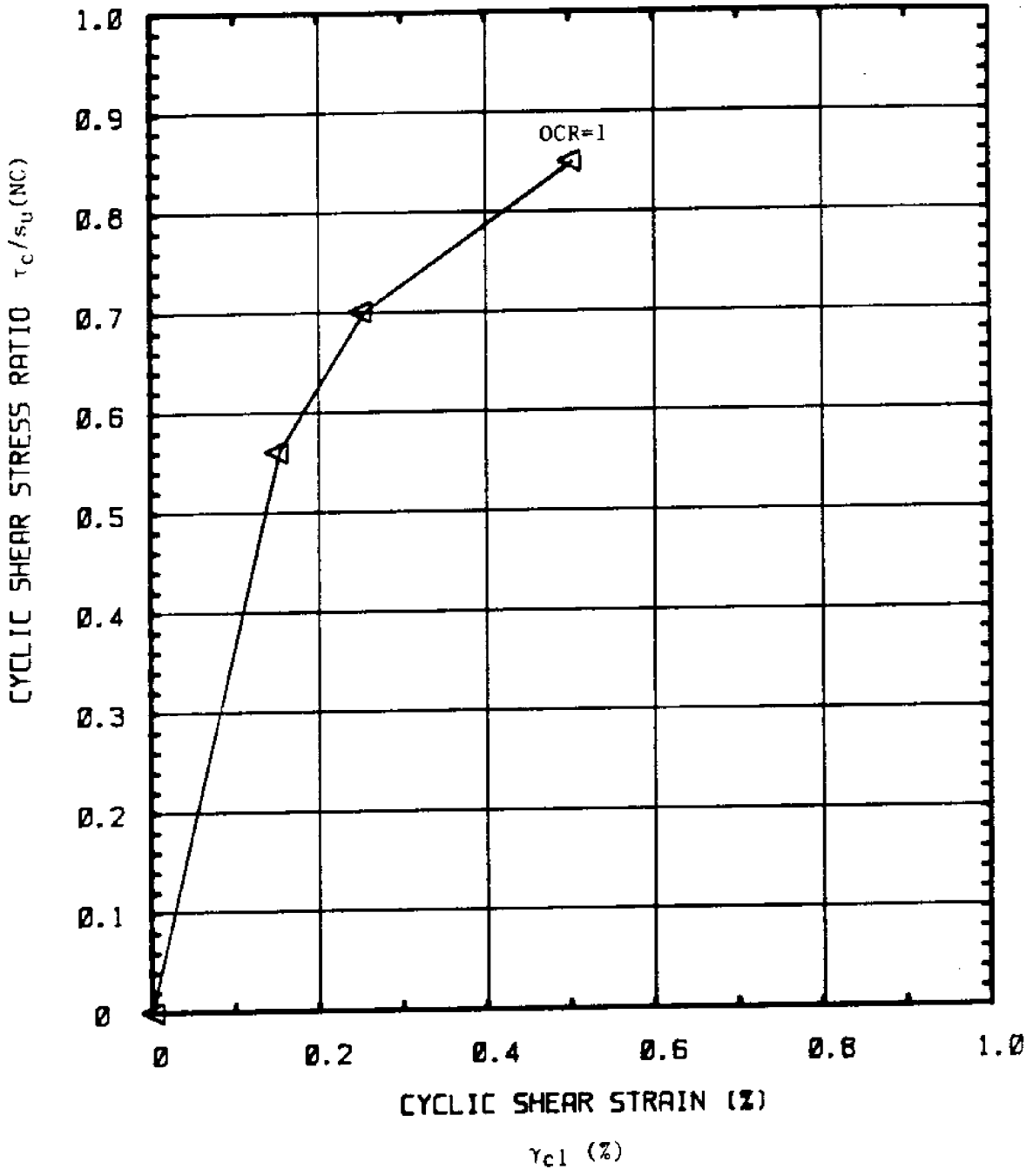

Figure 7.9 Cyclic Shear Stress Ratio $\tau_c/s_u(NC)$ versus Cyclic Shear Strain in the First Cycle, $\gamma_{c1}(\%)$ for N.C. BBC

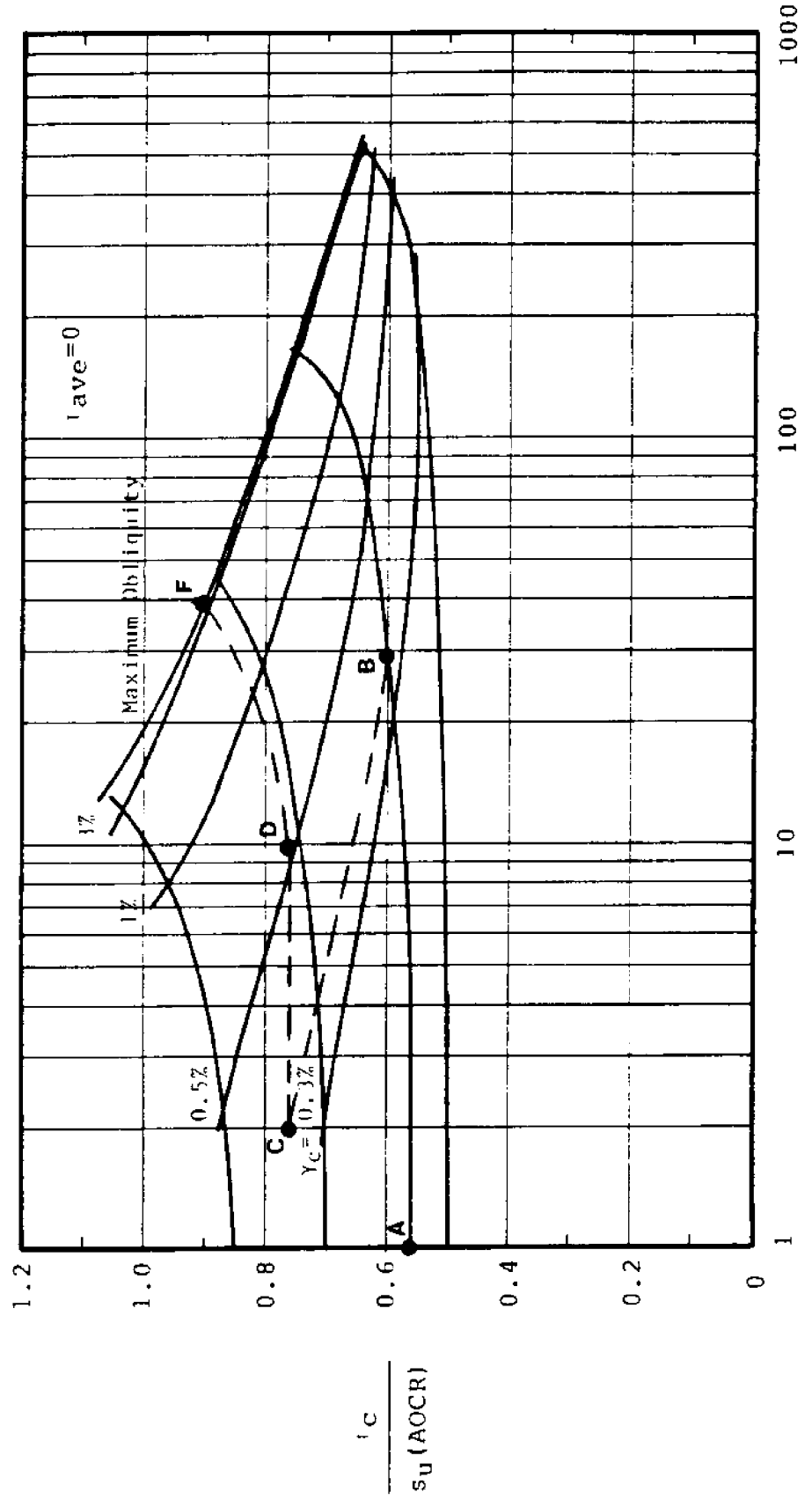

Figure 7.10 Prediction of Results of Test C-28: N.C. BBC, $\tau_{ave}=0$, $\tau_c/s_u(NC)= 0.56, 0.71$, Using the New Modified Andersen Procedure

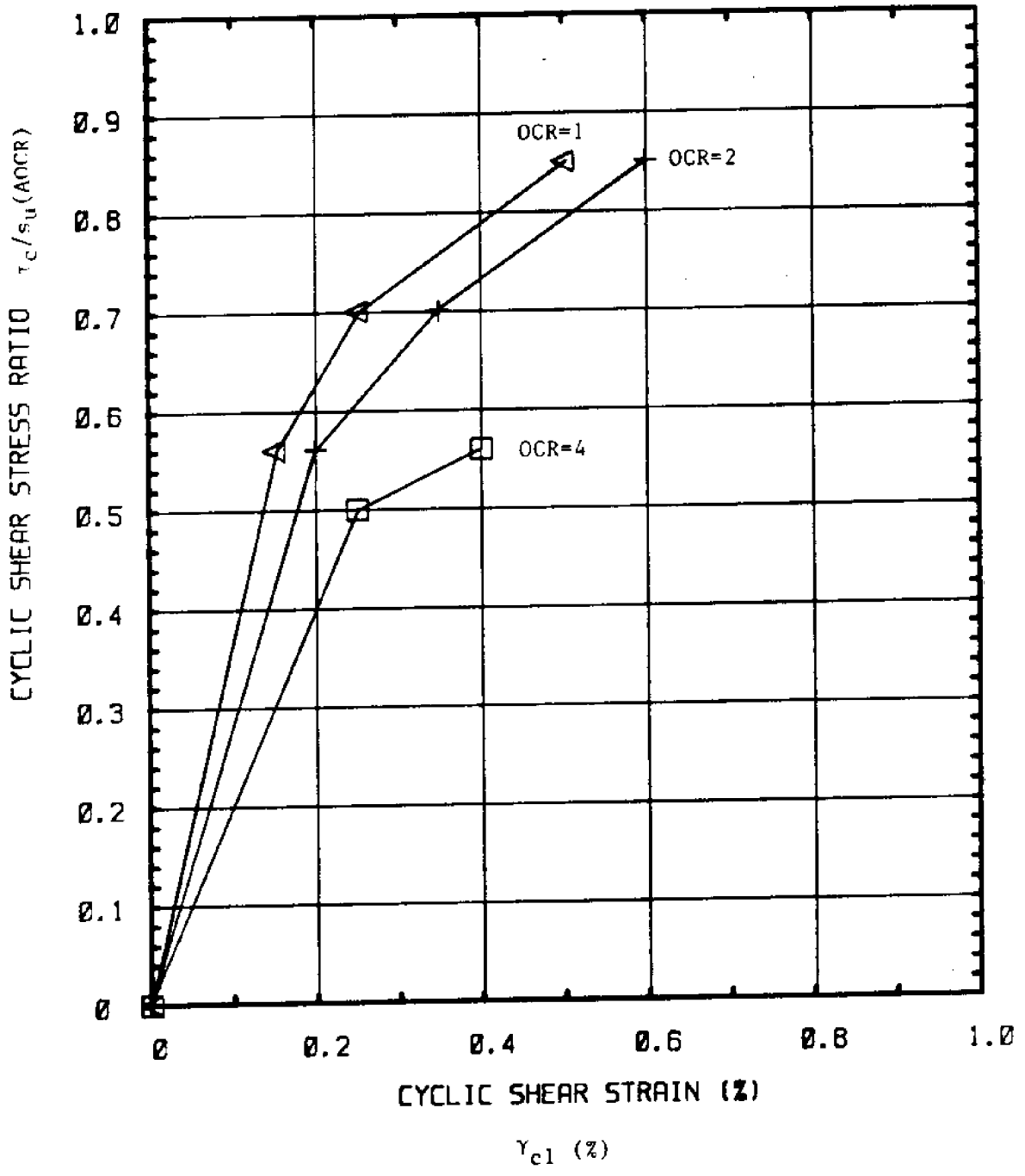

Figure 7.11 Cyclic Shear Stress Ratio τ_c/s_u(AOCR) versus Cyclic Shear Strain in the First Cycle, γ_{c1}(%) for BBC with OCR=1, 2, and 4

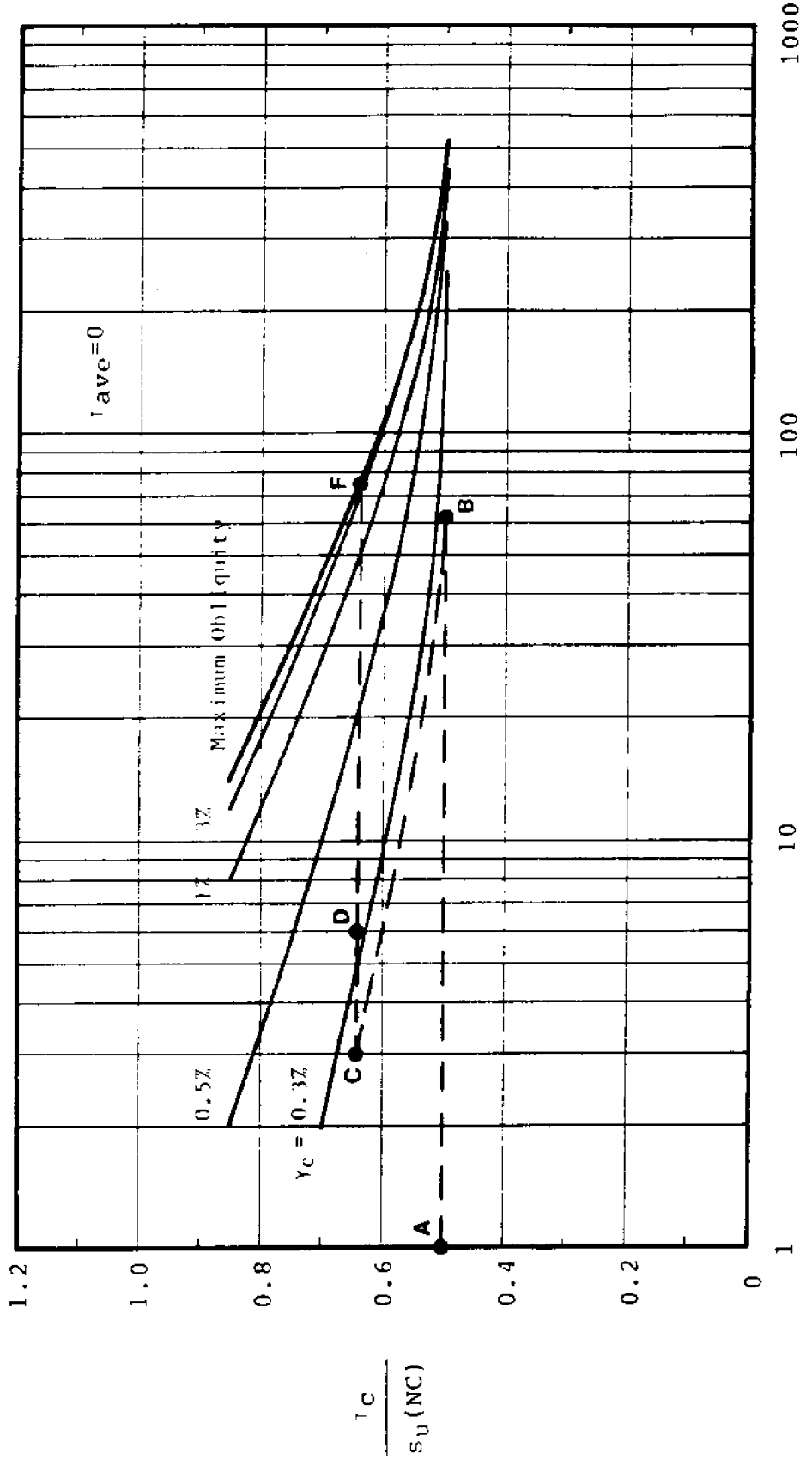

Figure 7.12 Prediction of Results of Test C-37: N.C. BBC, $\tau_{ave}=0$, $\tau_c/s_u(NC)=0.50$, 0.64, Using Andersen's Procedure

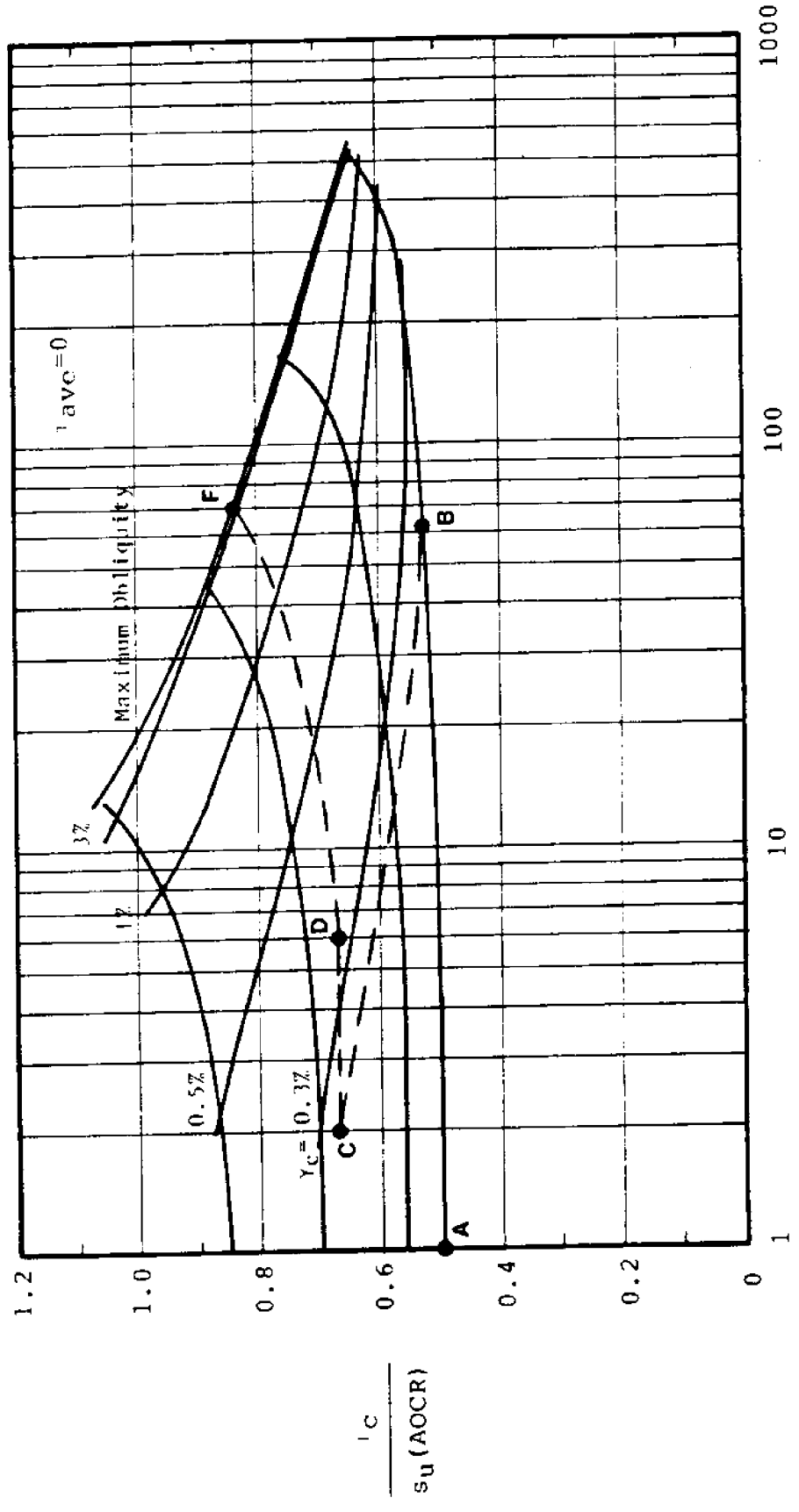

Figure 7.13 Prediction of Results of Test C-37: N.C. BBC, $\tau_{ave}=0$, $\tau_c/s_u(NC)=0.50$, 0.64, Using the New Modified Andersen Procedure

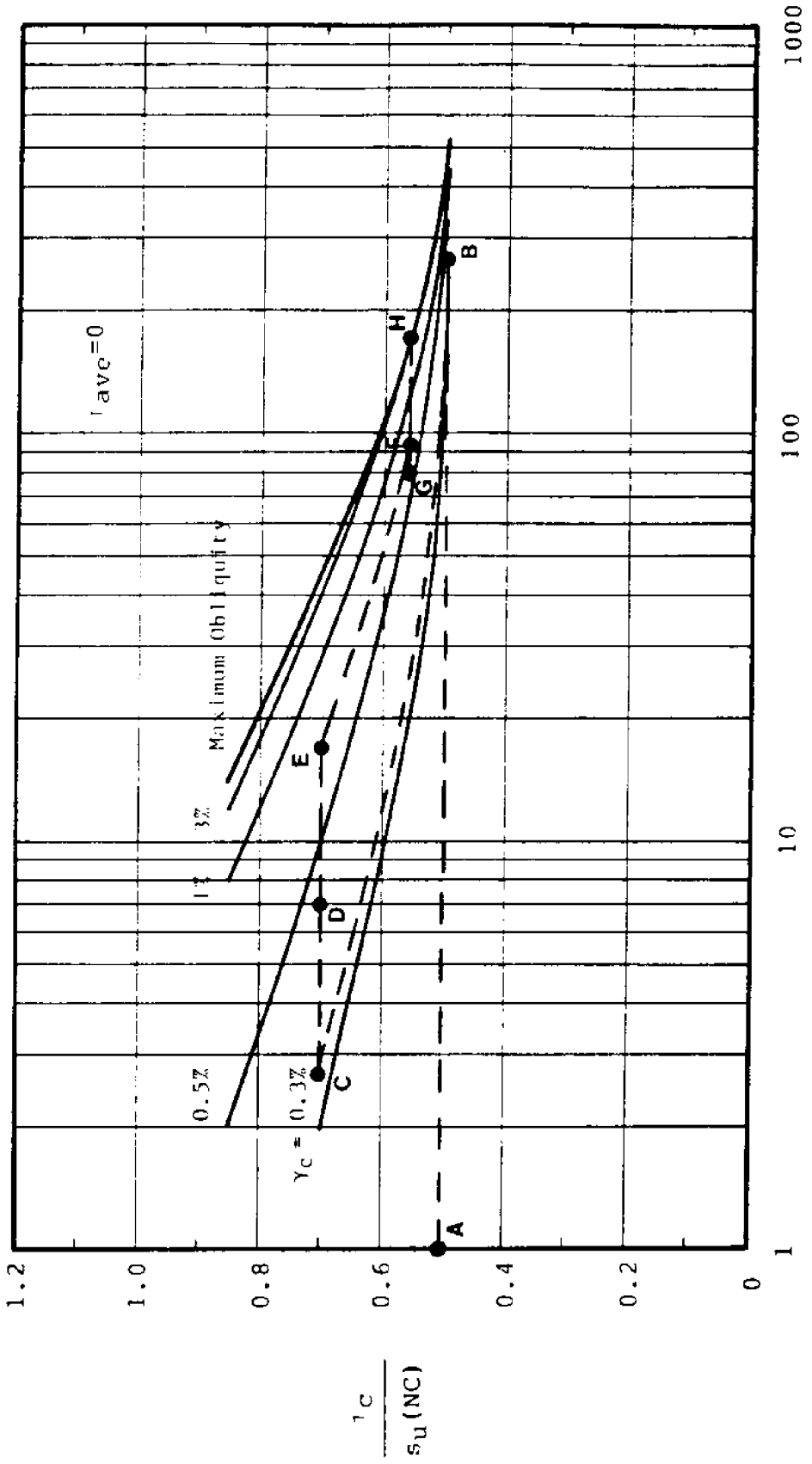

Figure 7.14 Prediction of Results of Test C-38: N.C. BBC, $\tau_{ave}=0$, $\tau_c/s_u(NC)=0.50$, 0.70, 0.56, Using Andersen's Procedure

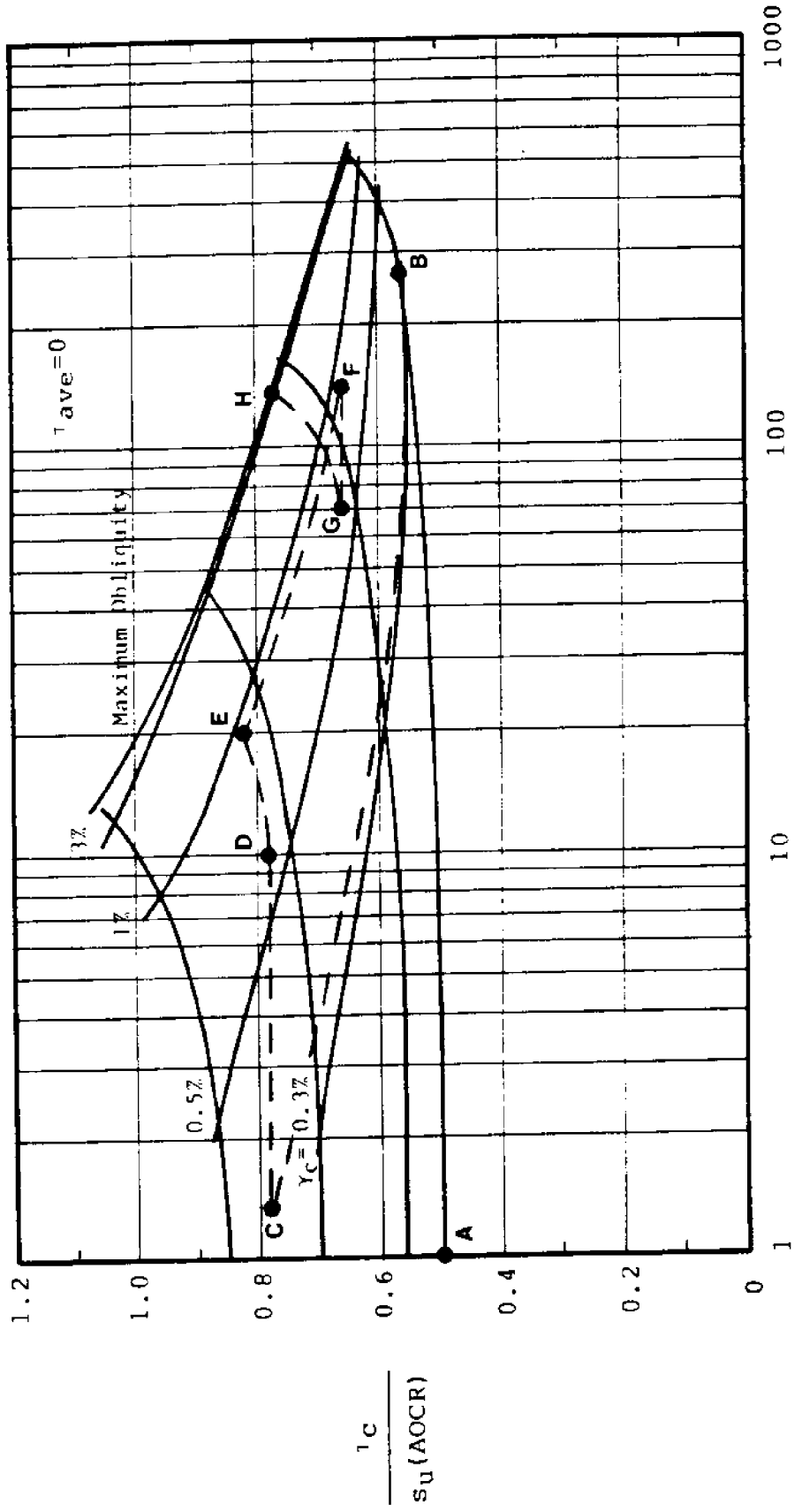

Figure 7.15 Prediction of Results of Test C-38: N.C. BBC, $\tau_{ave}=0$, $\tau_c/s_u(NC)=0.50$, 0.70, 0.56, Using the New Modified Andersen Procedure

CHAPTER 8

CONCLUSIONS

The objective of this report is to contribute to the understanding of the behavior of clays under the complex loading imposed by deep water compliant offshore structures. More specifically, the research attempts to identify and evaluate the effect of important factors on the behavior of clays subjected to cyclic loading in order to achieve more rational and reliable design and prediction methods for friction piles supporting Tension Leg Platforms (TLP).

An extensive laboratory testing program consisting of the design and development of equipment and the performance of stress-controlled K_o-consolidated undrained cyclic direct simple shear tests (CK_oUCDSS), was conducted on Boston Blue Clay in order to determine the undrained cyclic behavior of a soil element next to the TLP pile. The testing procedures and the stresses imposed on the laboratory DSS samples were chosen to simulate the stresses imposed on soil elements at the walls of long TLP piles. Most samples were normally consolidated, with a few tests performed on overconsolidated samples up to OCR=4.

The testing procedure consisted of first consolidating the samples under K_o conditions to the desired OCR, then applying an average shear stress, τ_{ave}, in a drained fashion, in order to simulate the mooring stress, τ_m, on the TLP pile. Twenty-four hours after the application of τ_{ave}, the sample was sheared to failure by applying an undrained cyclic shear stress with an amplitude τ_c and a constant period of 10 seconds.

Cyclic shearing was undrained because it represents the most critical condition for soft clays. Storm loading was simulated by undrained cyclic shearing, because most storms have limited duration, hence allow little or no drainage to occur in the soil.

8.1 RESULTS

The testing program considered the effects of the following factors on the performance of TLP piles subjected to cyclic loading:

- The mooring shear stress $\tau_m = \tau_{ave}$
- The cyclic shear stress τ_c
- Variable amplitudes of the cyclic shear stress τ_c
- OCR
- Undrained cyclic shearing on subsequent monotonic behavior.

Test results indicated the following:

1) There is a unified definition of failure in undrained cyclic DSS mode of shearing, which is independent of whether cycling is one-way ($\tau_{ave} \neq 0$) or two-way ($\tau_{ave} = 0$). Samples with OCR=1, 1.4, 2, and 4 which were sheared cyclically under various combinations of τ_{ave} and τ_c (constant or variable), reached failure when the effective stress path approaches the maximum obliquity line from monotonic undrained DSS testing, with $\bar{\phi}_{MO} = 30° \pm 1.2°$. This definition of failure is different from previous definitions introduced by Andersen (1975) for the case of $\tau_{ave} = 0$, and by Goulois (1982) for the case of $\tau_{ave} \neq 0$, in undrained cyclic DSS testing. Andersen described failure as the condition leading to

cyclic shear strain $\gamma_c=\pm 3\%$ for two-way cyclic shearing whereas Goulois defined failure through the average shear strain reaching $\gamma_{ave}=15\%$ in one-way cycling. Clearly, previous definitions of failure based on shear strain rather than effective stresses introduced an artificial distinction between tests with $\tau_{ave}=0$ versus those with $\tau_{ave}\neq 0$. In contrast, when failure is defined in terms of effective stresses, test results indicate a continuous and smooth transition from cases involving $\tau_{ave}=0$ to those with $\tau_{ave}\neq 0$.

2) At failure, samples with $\tau_{ave}=0$ experience large cyclic shear strains in excess of $\gamma_c=\pm 3\%$, with the average shear strain γ_{ave} very close to zero. Also at failure, samples with $\tau_{ave}\neq 0$ experience large average shear strain values close to $\gamma_{ave}=15\%$, with a relatively small cyclic shear strain ($\gamma_c = < \pm 3\%$ depending on the value of τ_c). This was observed for all samples tested having an initial OCR ≤ 4.

3) The unified definition of failure in terms of effective stresses allows estimates of the average excess pore pressure at failure, Δu_f, to be calculated directly from the geometry of the effective stress path. This can be done for any OCR value, and for constant as well as variable cyclic shear stress levels.

4) The cyclic shear stress ratio τ_c/s_u has a more important effect on the failure of soft clays than the average shear stress ratio τ_{ave}/s_u. This means that the number of cycles to failure is more sensitive to changes in τ_c/s_u than τ_{ave}/s_u.

5) For normally consolidated samples, there is a threshold shear stress level, defined as the combination of average and cyclic shear stress ratios in a $\tau_{ave}/s_u(NC)$ versus $\tau_c/s_u(NC)$ space, below which failure in undrained cyclic DSS shearing does not occur. The existence of this

no-failure region at sufficiently small levels of shearing is crucial to the feasibility and design of TLP piles. Some tests were carried out to 100,000 cycles without reaching failure which is far more severe than any real storm.

6) For normally consolidated clay samples sheared with $\tau_{ave}=0$, S-N curves were presented. These plots can be used to determine the number of cycles at failure, N_f, for any given cyclic shear stress ratio, as well as the cyclic shear strain, γ_c, at any cycle, N.

7) For normally consolidated samples, contours of equal number of cycles at failure, N_f, were presented in a $\tau_c/s_u(NC)$ versus $\tau_{ave}/s_u(NC)$ space. These iso-N_f contours are parallel to the threshold curve, and therefore, can be constructed from the knowledge of the S-N curves (which give the starting point at $\tau_{ave}=0$), and from the knowledge of the shape of the threshold curve.

8) For normally consolidated samples, plots of the normalized excess pore pressure, $\Delta u/\Delta u_f$, versus normalized number of cycles, N/N_f, are shown to be independent of the cyclic shear stresses τ_c and τ_{ave}. Hence these normalized plots can be used, along with the iso-N_f contours, to estimate the excess pore pressure at any cycle number, N, for any value of τ_{ave}/s_u, and τ_c/s_u.

9) For normally consolidated samples, undrained cyclic shearing develops positive excess pore pressures, hence an "apparent overconsolidation" of the clay such that when it is subsequently subjected to monotonic shearing, it behaves as an overconsolidated soil. This observation was extended herein to subsequent cyclic shearing to form the basis of the "apparent overconsolidation hypothesis," AOCR, which is then used to develop a method for predicting the undrained cyclic shearing

behavior of slightly overconsolidated clay samples, from test results on normally consolidated samples.

10) An evaluation of the AOCR hypothesis by means of comparisons between predictions and test results on samples with initial OCR values up to 2 shows good agreement with respect to the number of cycles at failure, N_f, the excess pore pressure at failure, Δu_f, and the cyclic shear strain, γ_c, at intermediate cycles, N. However, the method cannot provide accurate predictions of the excess pore pressures, Δu, vs N.

11) The AOCR hypothesis has been incorporated in the original Andersen superposition procedure in order to predict the effect of variable cyclic loading using the test results with constant τ_c/s_u. The proposed method not only keeps track of the strain history of the sample as the cyclic shear stress level is varied, but can also realistically incorporate the changes in vertical effective stress, hence excess pore pressure development with N, as given by the change in apparent overconsolidation with increasing number of cycles. An evaluation of the proposed superposition method by means of three tests with variable τ_c indicates a better prediction of the number of cycles to failure, N_f, and a better prediction of the cyclic shear strain, γ_c versus N, than the original Andersen procedure.

8.2 RESEARCH LIMITATIONS AND PROPOSED FUTURE WORK

The research program did not consider several secondary parameters of cyclic loading on clay elements adjacent to the TLP pile shaft. These parameters, listed below, are candidates for future research in order to

increase the overall understanding of cyclic clay behavior with application to TLP piles:

1) Effect of τ_m different from τ_{ave}. The average shear stress during storm loading, τ_{ave}, is usually higher than the mooring shear stress τ_m. In this study, it was assumed that $\tau_m=\tau_{ave}$. Hence, future research needs to consider the effect of increasing the average shear stress, in an undrained fashion from τ_m to τ_{ave} on the undrained cyclic clay behavior in the DSS mode of shearing.

2) Effect of cyclic frequency. In this study, a fixed cyclic period, T_c=10 seconds was used because it is typical of storm loading. Future studies must consider the effect of T_c on clay behavior.

3) Effect of drainage. All tests performed in this research were conducted in an undrained mode. No consideration was given for partial drainage during the cyclic loading, or for partial or full drainage following a given storm. For a better representation of storm loading, the effect of partial drainage should be taken into account.

4) Storm effects, with variable average shear stress τ_{ave}, as well as variable τ_c. The new modified Andersen superposition method, incorporating AOCR, is only applicable for the case of zero average shear stress, which is not the case for TLP piles. Goulois (1982) has presented a modified Andersen superposition method with a fit on γ_{ave}, which gave good estimates of tests with variable τ_{ave} and τ_c. Goulois' method should be evaluated further, and improved by modifying it to incorporate the apparent overconsolidation.

REFERENCES

Note: The following abbreviations are used:

ASCE	American Society of Civil Engineers
BOSS	Behavior of Offshore Structures
ICSMFE	International Conference on Soil Mechanics and Foundation Engineering
JGED	Journal of the Geotechnical Engineering Division
NGI	Norwegian Geotechnical Institute
OTC	Offshore Technology Conference

Airey, D.W. and Wood, D.M. (1987), "An Evaluation of Direct Simple Shear Tests on Clay," Geotechnique, Vol. 37, No. 1, pp. 25-35.

Andersen, K.H. (1975), "Repeated Loading on Clay. Summary and Interpretation of Test Results," NGI Research Report #74037-9, October.

Andersen, K.H. (1976), "Behavior of Clay Subjected to Undrained Cyclic Loading," Proceedings, BOSS 1976, Vol. 1, pp. 392-403.

Andersen, K.H. and Aas, P.M. (1981), "Foundation Performance," NGI Publication No. 137.

Andersen, K.H., Hansteen, O.E., Hoeg, K., and Prevost, J.H. (1978), "Soil Deformations due to Cyclic Loads on Offshore Structures," NGI Publication No. 120.

Andersen, K.H., Lacasse, S., Aas, P.M., and Andenaes, E. (1982), "Review of Foundation Design Principles for Offshore Gravity Platforms," Proceedings, BOSS 1982, MIT, Vol. 1, pp. 243-261.

Andersen, K.H., Pool, J.H., Brown, S.F., and Rosenbrand, W.F. (1980), "Cyclic and Static Laboratory Tests on Drammen Clay," ASCE, JGED, Vol. 106, No. GT5, May, pp. 499-529.

Annaki, M. and Lee, K.L. (1977), "Equivalent Uniform Cycle Concept for Soil Dynamics," ASCE, JGED, Vol. 103, No. GT6, June, pp. 549-564.

Azzouz, A.S. and Baligh, M.M. (1984), "Behavior of Friction Piles in Plastic Empire Clays," Research Report R84-14, MIT, Departement of Civil Engineering, 619 p.

Baligh, M.M. (1985), "Strain Path Method," ASCE, JGED, Vol. 111, No. 9, September, pp. 1108-1136.

Bea, R.G., Dover, A.R. and Audibert, J.M.E. (1982), "Pile Foundation Design Considerations for Deepwater Fixed Structures," Proceedings, BOSS 1982, M.I.T., Cambridge, MA, Vol. 1, pp. 125-140.

Bensari, J.E. (1984), "Stress-Strain Characteristics from Undrained and Drained Triaxial Tests on Resedimented Boston Blue Clay," S.M. Thesis, Department of Civil Engineering, MIT, Cambridge, MA, July, 193 p.

Bjerrum, L. and Landva, A. (1966), "Direct Simple Shear Tests on a Norwegian Quick Clay," Geotechnique, Vol. 16, pp. 1-20.

Bradshaw, H., Stokes, E.G., and Leece, M.J. (1985), "Hutton TLP Installation," Proceedings, Seventeenth OTC, Houston, Texas, Vol. 2, Paper No. 4913.

Brown, S.F., Lashine, A.K.F., and Hyde, A.F.L. (1975), "Repeated Load Triaxial Testing of a Silty Clay," Geotechnique, Vol. 25, No. 1, pp. 95-114.

Budhu, M. (1984), "Nonuniformities Imposed by Simple Shear Apparatus," Canadian Geotechnical Journal, Vol. 20, pp. 125-137.

Budhu, M. (1984), "On Comparing Simple Shear and Triaxial Test Results," Technical Note, ASCE, JGED, Vol. 110, No. 12, December, pp. 1809-1814.

Castro, G. and Christian, J.T. (1976), "Shear Strength of Soils and Cyclic Loading," ASCE, JGED, Vol. 102, No. GT9, Sept., pp. 887-894.

Donovan, N.C. (1971), "A Stochastic Approach to the Seismic Liquefaction Problems," Proceedings of the First International Conference on Applications of Statistics and Probability to Soils and Structural Engineering, Hong Kong University Press, Hong Kong, September, pp. 513-535.

Dyvik, R. and Zimmie T.F. (1981), "Strain and Pore Pressure Behavior of Fine Grained Soils Subjected to Cyclic Shear Loading," Deptartment of Civil Engineering, Rensselaer Polytechnic Institute, Troy, NY, July, 335 p.

Dyvik, R., Zimmie T.F., and Floess, H.L. (1981), "Lateral Stress Measurements in Direct Simple Shear Device," Laboratory Shear Strength of Soil, ASTM STP 740, Yong & Townsend, Eds., ASTM, pp. 191-206.

Eide, O. (1974), "Marine Soil Mechanics," NGI Publication No. 103.

Ellis, W. and V.B. Hartman (1967), "Dynamic Soil Strength and Slope Stability," ASCE, JSMFD, Vol. 93, No. SM4, July, pp. 355-375.

Faccioli, E. (1973), "A Stochastic Model for Predicting Seismic Failure in a Soil Deposit," Earthquake Engineering and Structural Dynamics, Vol. 1, 1973, pp. 193-207.

Fay, C.E. (1985), "Platform Alternatives for the Troll Field," Proceedings of the 4th International Conference on Behavior of Offshore Structures," Delft, The Netherlands, Vol. 2.

Fayad, P.H. (1986), "Aspects of the Volumetric and Undrained Behavior of Boston Blue Clay," S.M. Thesis, MIT, Cambridge, MA, September, 273 p.

Fisher, J.A., Koutsoftas, D.C. and Lu, T.D. (1976), "The Behavior of Marine Soils under Cyclic Loading," Proceedings, BOSS 1976, Vol. 2, pp. 407-417.

France, J.W. (1976), "An Investigation of the Effects of Drainage on the Repeated Load Behavior of Soils," Thesis submitted to the Departement of Civil Engineering at Cornell University, NY, Geotechnical Engineering Report 76-2, January, 227 p.

France, J.W. and Sangrey, D.A. (1977), "Effects of Drainage in Repeated Loading of Clays," ASCE, JGED, Vol. 103, No. GT7, July, pp. 769-785.

Geer, R. L. (1982), "Engineering Challenges for Off-Shore Exploration and Production in the '80's," Proceedings, BOSS 1982, MIT, Cambridge, MA, Vol. 2 Supplement.

Germaine, J.T. (1982), "Development of the Directional Shear Cell for Measuring Cross Anisotropic Clay Properties," Sc.D. Thesis, MIT, Department of Civil Engineering, Cambridge, MA, 530 p.

Glasscock, M.S. et al. (1984), "Design of the Lena Guyed Tower," Proceedings of the Sixteenth Annual Off-Shore Technology Conference, Houston, Texas, Vol. 1, Paper No. 4650.

Goulois, A. M. (1982), "Contribution to the Study of Tension Piles under Cyclic Loading," Ph.D. thesis, Department of Civil Engineering, MIT, Cambridge, MA, 399 p.

Halbouty, M. T. (1981), "Petroleum Still Leader in the Energy Race," Offshore, 20 June, pp. 49-52.

Herrmann, H.G. and Houston, W.N. (1976), "Response of Seafloor Soils to Combined Static and Cyclic Loading," Proceedings, 8th OTC, Houston, Texas, Paper #2428.

Herrmann, H.G. and Houston, W.N. (1978), "Behavior of Seafloor Soils Subjected to Cyclic Loading," Proceedings, 10th OTC, Houston, Texas, Paper #3260.

Houston, W.N. and Herrmann, H.G. (1980), "Undrained Cyclic Strength of Marine Soils," ASCE, JGED, Vol. 106, No. GT6, June, pp. 691-712.

Huslid, J.M., Gudmestod, O.T., and Alm-Pauken, A. (1982), "Alternate Deep Water Concepts for North Sea Extreme Conditions," Proceedings of the Third International Conference on Behavior of Offshore Structures, MIT, Cambridge, MA, Vol. 1, pp. 18-49.

Hyde, A.F.L. and Brown, S.F. (1976), "The Plastic Deformation of a Silty Clay Under Creep and Repeated Loading," Geotechnique, Vol. 26, No. 1, pp. 173-184.

Kavvadas, M. (1982), "Non-Linear Consolidation Around Driven Piles in Clays," Sc.D. Thesis, Department of Civil Engineering, MIT, Cambridge, MA, 666 p.

Kelland, C.D., Pearce, C.D., and Williams, P.V. (1985), "The Role of Accoustics for Monitoring and Controlling Subsea Operations During the Development of the Hutton Field," Proceedings, OTC, Vol. 2.

Koutsoftas, D.C. (1978), "Effect of Cyclic Loads on Undrained Strength of Two Marine Clays," ASCE, JGED, Vol. 104, No. GT5, May, pp. 609-620.

Ladd, C.C. (1964), "Stress-Strain Behavior of Saturated Clay and Basic Strength Principles," Research Report R64-17, Research on Earth Physics, Department of Civil Engineering, MIT, Cambridge, 112 p.

Ladd, C.C. and Lambe, T.W. (1963), "The Strength of Undisturbed Clay Determined from Undrained Tests," NRC-ASTM Symposium on Laboratory Shear Testing of Soils, STP No. 361.

Ladd, C.C., Bovee, R.B., Edgers, L., and Rixner, J.J. (1971), "Consolidated-Undrained Plane Strain Shear Tests on Boston Blue Clay," Research Report R71-13, No. 273, Department of Civil Engineering, MIT, Cambridge, 243 p.

Ladd, C.C. and Edgers, L. (1972), "Consolidated-Undrained Direct-Simple Shear Tests on Saturated Clays," MIT Research Report 72-82, Department of Civil Engineering, MIT, Cambridge, MA.

Lawson, M. and Tuchman, J. (1987), "Gulf Platforms Head for Record Depths," Engineering News Record, Vol. 218, No. 11, 12 March, p. 10.

Lee, G.C. (1982), "Design and Construction of Deep Water Jacket Platforms," Proceedings, BOSS 1982, MIT, Cambridge, MA, Vol. 1, pp. 3-17.

Lee, K.L. (1976), "Cyclic Strength of Outardes 2 Clay," Confidential Report.

Lee, K.L. (1979), "Cyclic Strength of a Sensitive Clay of Eastern Canada," Canadian Geotechnical Journal, Vol. 16, pp. 163-176.

Lee, K.L. and Chan, K. (1972), "Number of Equivalent Significant Cycles in Strong Motion Earthquakes," Proceedings, International Conference on Micro-Zonation, Vol ii, Seattle, Washington, October 1972, pp. 609-627.

Lee, K.L. and Focht, J.A. (1975), "Cyclic Testing of Soil for Ocean Wave Loading Problems," Proceedings, 7th OTC, May, Houston, Texas, paper #2183.

Lee, K.L. and Focht, J.A. (1975), "Liquefaction Potential at The Ekofisk Tank in the North Sea," ASCE, JGED, Vol. 101, No. GT1, January, pp. 1-18.

Lee, K.L. and Focht, J.A. (1976), "Strength of Clay Subjected to Cyclic Loading," Marine Geotechnology, Vol. 1, No. 3, pp. 165-185.

Levadoux, J.N. (1980), "Pore Pressure in Clays Due to Cone Penetration," Ph.D. Thesis, Department of Civil Engineering, MIT, Cambridge, MA, 752 p.

Lucks, A.S., Christian, J.T., Brandow, G.E., and Hoeg, K. (1972), "Stress Conditions in NGI Simple Shear Test," ASCE, JSMFD, Vol. 98, SM1, January, pp. 155-160.

Lutz, D.G. (1984), "Predictions of the Axial Capacity of Friction Piles in Empire Clays by Means of the Piezo-Lateral Stress Cell," S.M. Thesis, Department of Civil Engineering, MIT, Cambridge, MA.

Matsui, T., O'Hara, H., and Ito, T. (1980), "Cyclic Stress-Strain History and Shear Characteristics of Clay," ASCE, JGED, Vol. 106, No. GT10, October, pp. 1101-1120.

Miner, A.M. (1945), "Cumulative Damage in Fatigue," Transactions, American Society of Mechanical Engineering, NY, Vol. 67, 1945, pp. A159-A164.

Mitchell, R.J. and King, R.D. (1976), "Cyclic Loading of an Ottawa Area Champlain Sea Clay," Canadian Geotechnical Journal, Vol. 14, pp. 52-63.

Morrison, M.J. (1984), "In Situ Measurements of Model Piles," Ph.D. Thesis, Department of Civil Engineering, MIT, Cambridge, MA.

O'Neill, D.A. (1985), "Undrained Strength Anisotropy of an Overconsolidated Thixotropic Clay," S.M. Thesis, Department of Civil Engineering, MIT, Cambridge, MA, 359 p.

Ortigosa, P., Solsilli, R., Musante, H., and Retamal, E. (1983), "Comportamiento de Arcillas Sometidas a Cargas Ciclicas," Revista del Indien, Universidad De Chile, Vol. 22, No. 1, May, pp. 17-36.

Palmgren, A. (1924), "Die Lebensdauer Von Kugella Geru," (Life and Times of Ball Bearings)," ZVDI, Vol. 68, No. 14, April, pp. 339-341.

Proctor, D.C. and Khaffaf, J.H. (1984), "Cyclic Triaxial Tests on Remolded Clays," ASCE, JGED, Vol. 110, No. 10, October, pp. 1431-1445.

Randolph, M.F. and Wroth, C.P. (1981), "Application of the Failure State in Undrained Simple Shear to the Shaft Capacity of Driven Piles," Geotechnique, Vol. 31, No. 1, pp. 143-157.

Raymond, G.P., Gaskin, P.N., and Addo-Abedi, F.Y. (1979), "Repeated Compressive Loading of Leda Clay," Canadian Geotechnical Journal, Vol. 16, No. 1, pp. 1-10.

Salig, E.T. and Chang, C.S. (1981), "Soil Failure Modes in Undrained Cyclic Loading," ASCE, JGED, Vol. 107, No. GT5, May, pp. 539-551.

Sangrey, D.A., Castro, G., Poulos, S.J., and France, J.W. (1978), "Cyclic Loading of Sands, Silts and Clays," Proceedings, Specialty Conference on Earthquake Engineeering and Soil Dynamics, Pasadena, CA, June, pp. 836-851.

Sangrey, D.A., Henkel, D.J. and Esrig, M.I. (1969), "The Effective Stress Response of a Saturated Clay Soil to Repeated Loading," Canadian Geotechnical Journal, Vol. 6, pp. 241-252.

Seed, H.B., McNeill, R.L., and de Guenin, J. (1958), "Increased Resistance to Deformation of Clay caused by Repeated Loading," ASCE, JSMFD, Vol. 84, No. SM2, May, pp. 1645-1, 1645-28.

Seed, H.B. and Chan, C.K. (1966), "Clay Strength under Earthquake Loading Conditions," ASCE, JSMFD, Vol. 92, No. SM2, March, pp. 53-78.

Seed, H.B. and Idriss, I.M. (1967), "Analysis of Soil Liquefaction Niigata Earthquake," ASCE, JSMFD, Vol. 93, No. SM3, May, pp. 83-108.

Seed, H.B. and Idriss, I.M. (1971), "A Simplified Procedure for Evaluating Soil Liquefaction Potential," ASCE, JSMFD, Vol. 97, No. SM9, September, pp. 249-274.

Seed, H.B., Lee, K.L., and Idriss, I.M., (1969) "Analysis of the Sheffield Dam Failure," ASCE, JSMFD, Vol. 95, No. SM6, November, pp. 1453-1490.

Seed, H.B., et al. (1975), "Representation of Irregular Stress Time Histories by Equivalent Uniform Stress Series in Liquefaction Analyses," Report No. EERC 75-29, Department of Civil Engineering, University of California, Berkeley, CA, October.

Shen, C.K., Sadigh, K. and Hermann. L.R. (1978), "An Analysis of NGI Simple Shear Apparatus for Cyclic Soil Tetsing: Dynamic Geotechnical Testing," ASTM, STP 654, pp. 148-162.

Thiers, G.R. and Seed, H.B. (1968), "Cyclic Stress-Strain Characteristics of Clay," ASCE, JSMFD, Vol. 94, No. SM2, March, pp. 555-568.

Vucetic, M. and Lacasse, S. (1982), "Specimen Size Effect in Simple Shear Test," ASCE, JGED, Vol. 108, GT12, December, pp. 1567-1585.

Whittle, A.J. (1987), "A Constitutive Model for Overconsolidated Clays and Cyclic Loading of Friction Piles," Sc.D. Thesis, Department of Civil Engineering, MIT, Cambridge, MA.

Wilson, N.E. and Greenwood, J.R. (1974), "Pore Pressures and Strains after Repeated Loading of Saturated Clay," Canadian Geotechnical Journal, Vol. 11, pp. 269-277.

Wissa, A.E.F. and Heiberg, S.A. (1969), "New One-Dimensional Consolidation Test," MIT Research Report 69-9, Soils Publication No. 229.

Wright, D.K., Gilbert, P. and Saada, A.S. (1978), "Shear Devices for Determining Dynamic Soil Properties," Proceedings, ASCE, Specialty Conference on Earthquake Engineering and Soil Dynamics, Pasadena, Vol. 2, pp. 1056-1075.

APPENDIX A

APPENDIX A

PREVIOUS STUDIES OF THE RESPONSE OF CLAYS SUBJECTED TO CYCLIC LOADING

(1) Seed, McNeill and de Guenin (1958), "Increased Resistance to Deformation of Clay Caused by Repeated Loading."

The authors investigated the influence of repeated loading on the foundation clay of highway pavements, in particular the increased resistance to deformations due to cycling. Partially saturated compacted silty clay samples were tested in triaxial compression. Samples were first cycled undrained, with the average deviatoric stress equal to the cyclic one (i.e. no stress reversals), using a period of 3 seconds. The deviator stress was large enough to cause 1% to 2% permanent axial strain after the application of 80,000 to 180,000 cycles. After cycling, the samples were removed and placed in triaxial cells that allow drainage and sheared in a drained fashion.

For specimens with moderate degrees of saturation (60%), the drained strength of previously cycled samples was found to be higher than that of uncycled ones, the increase in strength being larger for larger levels of cycling. Also the stiffness was increased, and the samples exhibited strain softening to a residual strength approximately equal to that of the previously uncycled specimens. Samples with higher degrees of saturation (86%) were stiffer than previously uncycled ones, but did not consistently have higher strengths. Furthermore, there was no increase in resistance to deformations once the permanent strain exceeded 4%.

A series of tests were conducted at various water contents and densities in order to determine the significance of a density increase on compacted clay behavior. Results of the tests indicated that the increase in stiffness and sometimes in strength resulting from previous cycling

cannot be attributed simply to an increase in density during repeated loading.

Tests were also conducted in order to study the effect of sustained confining pressure during the testing period on subsequent strength. The results indicated that the stiffening due to the application of a sustained confining pressure is partially responsible for the increased stiffness observed in previously cycled samples, which were considerably stronger and stiffer.

The test data indicated that specimens subjected to greater deformations during repeated loading subsequently have greater resistance to deformation. However, the magnitude and the number of applications of the repeated stress, rather than the resulting strain are primarily responsible for the increased stiffness of the samples. A large number of lighter stress applications has a greater effect on subsequent behavior of a soil than a smaller number of applications of a higher stress, both samples having the same strain at the end of the repeated loading.

Possible causes of increased resistance to deformation might be: 1) changes in moisture distribution or structural arrangement of the soil grains, 2) thixotropy. Their effects however are cancelled if the soil deforms appreciably (greater than 4%).

(2) Seed and Chan (1966), "Clay Strength Under Earthquake Loading Conditions."

The authors studied the effects of various combinations of sustained (average) and pulsating (cyclic) stresses on strength and deformation

characteristics of clays. Samples were tested in a triaxial cell capable of applying one-directional and two-directional cyclic loads, at a frequency of 2 Hz. The tests included unconsolidated undrained, as well as isotropically and anisotropically consolidated triaxial compression tests, sheared in a stress-controlled fashion. Changes in pore pressure were not measured during shearing.

One-directional cyclic shearing was performed on samples of undisturbed San Francisco Bay Mud (medium sensitivity, W_L=88%, w_P=43%). Symmetrical as well as unsymmetrical stress pulses were applied in compression only (no stresses in extension even in the case of a non-zero sustained shear stress). Unconsolidated undrained triaxial tests with various average and cyclic stress components were performed and yielded curves of equal number of cycles at failure, or iso-N_f curves in a pulsating versus sustained shear stress space. The cyclic shear stress ranged from 0% to 160% of the conventional UU strength, and the average shear stress from 0% to 100%.

Two-directional cyclic shearing in the triaxial apparatus were also performed and their results presented in the form of iso-N_f curves. The reversal in direction of the shear stresses is a far more severe condition than that caused by one-way stress pulses of equal magnitudes.

The shape of the stress pulses was varied, and it was found that pulses with flat peaks are more destructive than pointy ones.

The effect of anisotropic consolidation was investigated and the results differ very little (5%) from those of isotropically consolidated samples, assuming that the sustained and pulsating stresses are expressed as a percentage of the appropriate s_u (s_u from CIUTC tests in the case of isotropic consolidation, and s_u from CAUTC tests in the case of anisotropic

consolidation).

Soil deformation during cycling can be estimated using curves of equal axial strain. Equal strain contours are presented as a function of pulsating and sustained stresses, and for various number of cycles.

(3) Ellis and Hartman (1967), "Dynamic Soil Strength and Slope Stability."

The authors presented results of undrained cyclic triaxial tests, performed on compacted and undisturbed clays. The paper was not clear in describing whether the apparatus could apply one-directional or two-directional loading, therefore, it is assumed that testing was one-directional. The frequency of loading was 2 Hz., and the sustained and pulsating stresses were varied over a wide range (expressed as a percentage of conventional strength).

Contours of cycles at failure N_f (failure being defined as 15% axial strain) were drawn in an impulse versus sustained stress space. Also, the data were rearranged to give contours of equal axial strain at the end of 30 pulses as a function of impulse and sustained stresses. This plot can be used in design, and yields the maximum cyclic stress that an element of soil can sustain, given the pre-earthquake average stress and the maximum level of strain that can be tolerated in the earthquake. This procedure assumes that a typical earthquake record contains 30 pulses at maximum acceleration.

(4) Thiers and Seed (1968), "Cyclic Stress-Strain Characteristics of Clay."

The authors presented results of cyclic simple shear tests which were used in analyzing surface ground motion during earthquakes. Surface ground motions are due primarily to the upward propagation of shear waves, from an underlying rock formation, which subjects soil elements to cyclic simple shearing.

The testing apparatus was an NGI direct simple shear machine modified to run cyclic tests. The samples used were 8 cm in diameter by 2 cm high and were surrounded by a wire reinforced membrane with sire clamps at the top and bottom caps to prevent drainage. The top cap was held fixed while the bottom moved horizontally under the action of an oil driven reciprocating piston, with a frequency of 1 Hz. The samples were sheared cyclically in a strain-controlled fashion, at a constant cyclic strain value, for a maximum of 200 cycles. The applied cyclic strain was varied up to 4% (8% peak to peak).

The test results indicate that the stress-strain curves during cycling can be approximated by a bilinear model with parameters G_1, G_2, and γy (G_1 and G_2 being the two moduli, and γy being the yield strain). During undrained cycling, pore pressures are generated, and therefore the stress-strain curves become flatter with increasing number of cycles. By fitting the bilinear model to the experimental curves, the variation of the moduli and the yield strain with number of cycles was obtained at various cyclic strains. For any given applied cyclic strain, G_1 and G_2 decrease by about 30% during the first 50 cycles and then remain fairly constant. The yield strain γy does not vary with number of cycles, but is proportional to the applied cyclic strain.

The effect of cycling on static strength was obtained by performing undrained static tests on samples which were previously subjected to 200 cycles of cyclic shear strain (no drainage allowed between the two tests). Static strength was found to be unaffected by 200 cycles of straining as long as the applied cyclic strain remained less than 1.5% (3% peak to peak). A cyclic strain of 3% reduced strength by only 10%. The static secant modulus at 1% was reduced by 20% for an applied strain of about 1%, and reduced by 50% for a strain of 3%.

(5) Sangrey, Henkel and Esrig (1969), "The Effective Stress Response of a Saturated Clay Soil to Repeated Loading."

The authors summarized results of previous research on cyclic clay testing which indicate that "repeated loading, at a particular stress level, leads to larger deformations than are obtained for a single cycle of loading." Previous testing also indicated that total collapse or failure can occur at stress levels below the maximum that can be supported by one cycle, and that cycling below a "critical level of repeated stress" can be tolerated indefinitely.

The authors' testing program consisted of undrained cyclic triaxial tests, with pore pressure measurements, on block samples of low plasticity Newfield, N.Y. clay. The samples were backpressured in order to achieve a high degree of saturation. Most were isotropically consolidated, few were anisotropically consolidated, and some were overconsolidated from an isotropic normally consolidated state. Static triaxial compression and extension tests indicated that pore pressure equilization was achieved when the strain rate used did not exceed 0.0002%/min. This strain rate was then

used in the undrained cyclic tests, which required 10 hours per cycle. After consolidation, cycling was performed between fixed values of minimum and maximum deviator stress, which were applied undrained, with the average deviator stress equal to the cyclic deviator stress (no stress reversal), until either a failure or a non failure condition was reached (non failure being defined as a state where the stress-strain and the pore pressure-strain curves follow closed hysteresis loops). The "single loading to failure test" was used as a control test.

For isotropically normally consolidated samples, it was observed that a sample (#T2) failed after 10 cycles of shearing at an average deviator stress equal to the cyclic deviator stress equal to 43% of the static stress deviator at failure. Another sample (#T3) sheared at 24% of the static stress deviator at failure does not fail, and hysteresis loops form after 6 cycles, and do not change up to 100 cycles (41 days). In the case of T2, the stress path hits the failure envelope after 2 cycles, whereas in that of T3, pore pressure buildup causes migration of the stress path until stabilization occurs. Results of many tests reaching the no-failure condition indicate that the stress path migrates to a terminal position which is a function of the applied stress level. The locus of stress path peaks defines an equilibrium line, there is "a linear relationship between the level of cycled stress and the pore water pressure at the peak of the nonfailure equilibrium cycle." The intersection of this equilibrium line with the failure envelope gives the maximum stress level which must not be exceeded in order to ensure no failure. For the Newfield clay, and for undrained cycling with $q_{ave}=q_c$, the threshold stress level $(q_{ave} + q_c)_{max} = 2/3\ q_{ult}$.

The threshold value for anisotropically consolidated samples was found

to be higher than that for isotropically consolidated ones.

(6) Wilson and Greenwood (1974), "Pore Pressures and Strains After Repeated Loading of Saturated Clay."

Repeated and sustained loading tests on undrained samples of normally consolidated clay were used to prove the existence of a relationship between pore pressure and strains.

Isotropically consolidated undrained cyclic triaxial tests with pore pressure measurements were performed on Hamilton, Ontario lacustrine clay (medium sensitivity, low plasticity). The static compressive strength, σ_s, was obtained from CIUTC tests. Cycling was performed at one cycle per minute, between 0 and σ_r (repeated deviator stress, expressed as a percentage of σ_s).

During cycling, there are two components of pore pressure: an elastic, recoverable one, and a plastic nonrecoverable one. Also, there are two components of strain: elastic, recoverable strain, and a plastic, nonrecoverable one. For small applied deviator stresses, below a threshold value of 37% of the compressive strength σ_s, the strains and pore pressures are small and elastic, and the sample does not fail. For stresses above the threshold, failure occurs and the pore pressures and strains are nonrecoverable. By plotting pore pressure versus strain for tests below the threshold, the authors found a linear relationship between the elastic pore pressure and the elastic strains, as well as a linear relationship between plastic pore pressures and plastic strains. The elastic recoverable pore pressure component is thought to be attributed to the elastic deformation of the soil skeleton, whereas the plastic nonrecoverable pore pressure component is due to a partial collapse of the

soil grain structure with subsequent transfer of stresses from the failed grain contacts to the pore pressure.

(7) Eide (1974), "Marine Soil Mechanics," NGI Publication No. 103.

The paper is a reprint of a lecture presented at "Offshore North Sea" Technology Conference and Exhibition, Stavanger, Norway, Sept. 1974. The author reviewed some of the most important topics in offshore foundation engineering, which included soil investigations, soil conditions (specifically in the North Sea), pile design, and finally, foundation problems related to offshore gravity structures, which include: contact between structure and sea floor, stability against sliding and overturning under static loading, installation, settlement, displacements under static loading, effect of cyclic loading, dynamic behavior, scour, and instrumentation. Only the discussion about the effects of cyclic loading on gravity offshore platforms is summarized herein.

According to the author, it is not enough to check the stability of the structure under the maximum force due to the 100-year wave acting as a static force, but one must determine to what extent previous cyclic wave loads have reduced the shear strength of the soil, a trend observed in the laboratory.

In the case of sands, cycling under constant total stresses causes the pore pressure to increase. A linear relationship between the shear stress level and the average pore pressure generated per cycle is given. Under severe cycling, all the total stress can be transferred to pore pressure, and liquefaction occurs. The author stresses the importance of the previous stress history since small storms with small cyclic stress levels followed by drainage cause the sandy soil to densify, leading to improved

factor of safety. Also, the effect of drainage during the storm must be taken into consideration because it affects the magnitude of pore pressure buildup.

In the case of clays, research at NGI indicates that strain is the basic parameter. Strain during cyclic loading has been found to decrease the undrained shear strength of clays. Having estimated the accumulated strain from the design storm, the decrease in undrained strength can be estimated by using plots of reduction in undrained strength versus peak cyclic shear strain presented by Thiers and Seed, 1968 (paper #4). This revised undrained strength is then used in the stability calculation for the 100-year storm. The author finally concludes that much research work is needed in order to better understand the cyclic behavior of clays.

(8) Andersen (1975), NGI Research Report 74037-9. See Chapter 2.

(9) Brown, Lashine and Hyde (1975), "Repeated Load Triaxial Testing of a Silty Clay."

The authors present results of undrained cyclic triaxial tests on overconsolidated samples of Keuper marl (silty clay, PI=14%). The samples were resedimented and isotropically consolidated in the triaxial device, and then rebounded to OCR values of 2, 4, 10 and 20.

Cycling was performed in a stress-controlled fashion, with the sinusoidal deviator stress $q_r = q_{ave} + q_c$ applied at a frequency of 10 Hz., with $q_{ave} = q_c$. Because of the high frequency of cycling, only the average pore pressure could be measured.

Previous work by Lashine using the same clay, testing apparatus and procedure, but on normally consolidated samples gave the following

conclusions:

a) there is no frequency effect for cycling between 0.1 Hz. and 10 Hz.

b) Failure in cyclic testing did not occur, after 10^6 cycles, when the deviator stress $q_r = q_{ave} + q_c$ was less than 75% of the undrained strength (failure being defined as the point where the rate of strain starts to increase, and undrained strength being obtained from "quick undrained triaxial tests").

c) failure did occur when q_r was greater than 80% of the undrained strength.

d) there was a 50% chance of failure for q_r between 75% and 80%.

Test results on the overconsolidated samples included only three failure situations. Samples that did not fail were still accumulating permanent strains after 10^6 cycles.

Under comparable applied stress conditions, the permanent strains after 10^6 cycles were considerably larger than those in the static test. In both tests, pore pressures levelled out, with larger values (both positive and negative) occuring in the cyclic tests under comparable shear stress conditions. Under the same conditions of deviator stress and pore pressure, similar permanent strains occurred in both tests.

Information about modulus degradation was given. Refer to paper for more information.

(10) Lee and Focht (1976), "Cyclic Testing of Soil for Ocean Wave Loading Problems."

The authors illustrate the 1976 state of the art methods for evaluating the strength of soil, especially clays, to be used in foundation stability analyses of large offshore structure and embankments subjected to severe wave loading.

Because the governing loads are due to wave forces, it is important to use realistic wave time histories in design. The most useful form of wave data is an envelope of peak wave heights throughout the duration of the design storm, as well as distributions of wave heights and frequencies within half or quarter-day increments during the storm. This information can be obtained by oceanographers for any given site from wind, water depth, and geography data, as well as previous history. Typical storm records indicate that the wave height is random, but the frequency is approximately constant at 12 seconds per cycle. Hydraulic and analytical models use the wave data as input, and give forces acting on the structure, which in turn lead to estimates of the cyclic stresses acting on the foundation soil. The stresses acting on the soil are cyclic at approximately the same frequency as the waves, and their amplitude is proportional to the wave height.

Ideally, laboratory tests can apply such storm loading histories to an element of soil in order to obtain its cyclic behavior. However, this is not done since the most severe time history wave pattern is not known in advance. Instead, an equivalent uniform cyclic loading pattern is applied to the laboratory soil sample. Usually, the "significant wave" height and frequency are used, and are probabilistic rather than deterministic values. The "significant wave" height is defined as the average of the highest 1/3 of the waves in a group. The average period is called the "significant period." The height of the maximum single wave in the group can be up to

1.5 to 2 times the significant wave height, and it usually occurs near the middle of the storm.

The stresses applied to elements of foundation soil are not known exactly, and are very difficult to reproduce in the lab. They include static normal and shear stresses as well as cyclic normal and shear stresses. The direct simple shear and the triaxial tests are used in the laboratory to study the cyclic soil behavior, but both of them cannot reproduce the exact field stresses. Samples tested in direct simple shear are subjected to non-uniform stress distributions (because vertical complementary stresses are not possible), and cannot be subjected to changing lateral normal stresses. This results in the fact that the most critical failure plane is always horizontal. The triaxial test is limited since it can only give results in the case of either compression or extension, and not any other intermediary state. The authors did not express any preference towards either test.

Typical cyclic testing procedures are given as well as typical cyclic stress-strain curves and strain versus number of cyclic curves. The effects of undrained cycling on subsequent undrained strength (with no drainage allowed in between) are also given. The following effects are noted:

- cyclic strains increase with number of cycles and with the magnitude of the applied cyclic stress;

- the average strain may develop in a preferred direction if the loading is not symmetrical, or if the strength is anisotropic;

- there is a reduction in static strength following undrained cyclic loading (no drainage in between), and there is an increase in strain required to develop the maximum static strength after cyclic loading.

At the element level, the cyclic test data is usually presented in the form of S-N curves which are lines of equal strain in a cyclic stress ratio versus number of cycles space (the cyclic stress ratio being defined as the ratio of the applied cyclic stress to the undrained cyclic strength).

At the element level, a method of converting irregular field loads to equivalent uniform cycles is presented. It is based on the Miner (1945) damage potential and the procedure given by Lee and Chan (1972). Because storm loading can occur over several days, it is convenient to estimate the equivalent uniform cycle N_{eq} at stress level Se for various parts of the storm (quarter or half daily increments). The Se-N_{eq} curve for the entire storm can be plotted in a stress ratio versus number of cycles space by doing the following. First, plot the Se-N_{eq} curve for each increment of storm (20%, 40%,...100%) using the Lee and Chan procedure. Second, locate the point on each curve corresponding to the number of cycles, in the portion of the actual record, with magnitudes greater than a threshold value below which no significant strains occur after large number of cycles. The line connecting these points is the Se-N_{eq} curve for the entire storm, which can give, when superimposed with the S-N curves, the history of strain accumulation at the element level due to the storm.

(11) Ficher, Koutsoftas and Lu (1976), "The Behavior of Marine Soils Under Cyclic Loading."

The authors present results of two series of cyclic triaxial tests on the foundation soil of a rockfill breakwater, off the coast of New Jersey. The first series was on a clay material and the second on a sandy soil

encountered in the foundation.

The offshore clay is an overconsolidated Holocene clay with OCR ranging between 3.5 and 9. Normally consolidated behavior was obtained by running cyclic tests on isotropically consolidated samples to an effective stress equal to 1.5 to 2 times the maximum past pressure. Sinusoidal, cyclic, stress controlled tests were performed at a frequency of 1 Hz. Overconsolidated samples, with OCR=4 were also tested at two different frequencies (1 Hz. and 1/15 Hz.). These samples were first consolidated up to 1.5 to 2 times the maximum past pressure before being unloaded to OCR=4. No specific details were given about whether the tests were undrained, or whether the loading was one-way or two-way. However, from certain comments in the paper, one can infer that cycling was undrained, and of two-way symmetric nature.

The test results are given in terms of S-N curves, or normalized peak cyclic shear stress ratio τ_c/s_{ust} versus logarithm of the number of cycles required to induce double amplitude strain of 1, 2.5, 5 and 10 percent. The static undrained strength s_{ust} was obtained from undrained triaxial compression tests performed on specimens consolidated in the same manner as those in the corresponding cyclic tests. The samples developed much larger strains in extension than in compression, and most of them failed in extension. Overconsolidated samples suffered larger strains than normally consolidated ones subjected to similar loading conditions (same τ_c/s_{ust}, and same number of cycles). At both OCR=1 and OCR=4, the silty clay has lower dynamic strength than the plastic clay, that is it develops larger strains at the same stress ratio and the same number of cycles. Comparison of the results of two tests with the same consolidation history and cyclic stress ratio, but with different frequencies (1 Hz. versus 1/15 Hz.) shows

that the slower tested specimen experienced more strain than the fast one, especially in extension. This can be explained by the fact that the static undrained clay strength in extension is 30% to 40% less than that in compression (strength anisotropy), and that the magnitude of the cyclic shear stress is the same in compression and in extension (the soil is closer to failure in the extension part). Because the rotation of principal stresses in the field are less severe than in the triaxial test, the authors believe that results of cyclic triaxial tests may be too conservative.

In conclusion, cyclic shear strength of clays obtained at high frequency loading are significantly greater than those obtained at low frequency loading. In contrast, the cyclic shear strength of sands is not significantly affected by the frequency of loading.

(12) Andersen (1976), "Behavior of Clay Subjected to Undrained Cyclic Loading."

The author recognizes that the behavior of clay subjected to cyclic loading is the most important problem in the design of offshore gravity structures due to the enormous cyclic forces applied by these structures on the foundation soil. This behavior may be separated into a short-term or undrained situation, and a long-term or drained situation. This paper is concerned with the short-term condition, and presents the results of undrained cyclic triaxial and direct simple shear (DSS) tests, with a cyclic period of 10 seconds, on Drammen clay samples overconsolidated to an OCR of 4.

Undrained cycling causes the pore pressure to increase and the effective stress path to move towards the origin until the failure envelope is reached and the soil element experiences large strains and fails in cyclic loading. Two-way cyclic DSS tests indicate that the permanent pore pressure increases with increasing number of cycles, with small variations within each cycle. The cyclic strains are approximately symmetrical with almost zero average shear strain. One-way triaxial testing indicates the existence of a permanent strain in addition to the cyclic strain. Both components of shear strain increase with increasing number of cycles.

For two-way cyclic DSS testing, the number of cycles to failure (defined as reaching + or -3% cyclic shear strain) increases rapidly with decreasing cyclic shear stress level (defined as a percentage of the static strength). The results also seem to indicate that cyclic loading has a negligible effect on clay behavior, below a certain cyclic stress level which depends on clay type, overconsolidation ratio, and type of cyclic loading.

OCR affects the number of cycles to failure. For the same cyclic stress level τ_c/s_u (s_u being the static undrained strength of a normally consolidated sample), normally consolidated clay is more resistant than overconsolidated clay.

The shear modulus decreases with increasing number of cycles, and this decrease is especially significant at high cyclic shear stress levels.

The results of static DSS tests on clay samples subjected to previous undrained cyclic loading indicate a reduction in stiffness and shear strength which increase with increasing cyclic shear strains and number of cycles.

Based on tests with constant cyclic shear stresses, a method for

predicting clay behavior under variable cyclic stresses (as in the case of storm loading) was presented. The method is based on accumulated cyclic strains, and was found to be successful.

(13) Herrmann and Houston (1976), "Response of Seafloor Soils to Combined Static and Cyclic Loading."

The authors present results of stress-controlled cyclic triaxial tests on two deep ocean soils: a hemipelagic organic silt or turbidite, which is a cohesive soil of slight sensitivity, and a calcareous ooze, which is a non-plastic sand with fines. "Undisturbed" box core samples were tested in the triaxial apparatus. After K_o consolidation, a static deviator stress is applied undrained, followed by an undrained cyclic component of deviator stress. Cycling was continued until 300,000 cycles or failure. The static and cyclic deviator stresses were such that stress reversal did not occur. A frequency of 2 Hz. was used. Samples which did not fail during the cyclic loading phase were cyclically loaded again after a rest period up to three times. Therefore, not all tests were performed on "virgin" samples, which makes interpretation of the results difficult. Static control tests were also performed to determine the static undrained strength. During static shearing of normally consolidated samples, the turbidite developed positive pore pressures whereas the calcareous ooze developed negative pore pressures due to dilation.

Results of cyclic tests on the turbidite indicate no failure after 300,000 cycles even when the shear stresses cycled between 63% and 95% of the undrained strength. The pore pressure during cycling decreased first then increased. The secant modulus decreased with number of cycles. The

results of tests on the calcareous ooze are similar except for more negative pore pressure during shear.

(14) Lee and Focht (1976), "Strength of Clay Subjected to Cyclic Loading."

The authors present a state-of-the-art literature review of the 1975 data on cyclic clay behavior. They arrive at the following conclusions concerning the effect of cyclic loading on clay strength.

"1. The strength is significantly less with reversing cyclic stress than with one directional pulsating loading.

2. Cyclic loading leads to a buildup of excess pore pressure. Large strains develop especially if the combination of excess pore pressure and cyclic stress results in an effective stress failure condition defined by $(\sigma'_1/\sigma'_3)_{max}$.

3. Cyclic strength deterioration is best explained as a strain dependent phenomenon. Soft samples with low initial static tangent modulus and large static strain to failure will be weaker under cyclic loading than stiff samples, because every stress cycle on a soft sample causes more strain and hence more remolding than for a stiff sample.

4. Because of the strain dependency, and because clay soil creeps under load, cyclic loading conditions that produce the longest duration of high sustained load per cycle will lead to the greatest amount of cyclic strength deterioration. Thus, low frequencies and flat top load forms lead to the lowest cyclic strengths. Laboratory tests should be performed using the load

shape and frequency representative of the field loading conditions.

5. On a cyclic/static strength ratio basis, the cyclic strength of a clay appears not to be affected by soil anisotropy or test method, provided both the cyclic and static tests are performed using the same procedures. This suggests that the laboratory tests results can be used directly for field conditions.
6. Cyclic strength data from a wide range of clay soils form a broad band but consistent pattern of strength ratio versus number of cycles. All data suggests that for 1000 or more cycles the cyclic stress needed to cause significant strains will be only 20-50% of the static undrained strength.
7. The available data suggests that on an effective stress ratio basis overconsolidated clays are stronger than normally consolidated and normally consolidated clays have cyclic strengths similar to saturated sands. However, on a cyclic/static strength basis, overconsolidated clays appear to suffer more rapid cyclic strength deterioration than normally consolidated clays.
8. In static loading following a cyclic test the strength is less and the strain to failure is greater than for the same soil before cyclic loading. However the change is small provided that the cyclic loading produces cyclic strains less than half of the normal static strain to failure. It is suggested that this may be a useful design criterion, in which case the appropriate failure criterion under cyclic loading would be half the strain to failure in a corresponding static test on an undisturbed sample.
9. Few data are available concerning the effect of sustained shear

stress prior to the cyclic loading for cyclic stress reversing conditions. More information is needed on this topic."

(15) Hyde and Brown (1976), "The Plastic Deformation of a Silty Clay Under Creep and Repeated Loading."

The authors carried out tests in order to establish a relationship between plastic strains developed under creep and those under cyclic loading conditions in the sub-failure region. The materials and experimental techniques were similar to those of Brown et al. (1975). Reconsolidated Keuper marl samples were isotropically consolidated, in a triaxial cell, to different stresses in the normally-consolidated range, and then unloaded to OCR's of 4, 10 and 20, and to the same consolidation stress values. Filter paper side drains were used, and the pore water pressure measured using a 1 cm ceramic probe connected to a transducer at the base of the sample. Loading was applied with a servo-controlled electro-hydraulic apparatus. Creep loading as well as repeated loading were carried out using the same equipment. Sinusoidal cycling was done at a frequency of 10 Hz. with $q_{ave}=q_c$. Some drift (up to 10%) occured during creep testing due partly to a sticky servo-valve.

Analysis of the results shows that for OCR=10, the pore pressure varied from positive to negative with increasing time. The final equilibrium pore pressure value was greater for creep or repeated loading, for a given q value, than that obtained in a strain-controlled test. Pore pressure variation with time for both creep and repeated loading tests were very similar, with higher peaks during creep testing. For both creep and repeated loading tests, plots of log strain rate versus log time yielded

reasonably straight parallel lines, with the parallel lines representing different deviator stresses. The mean slopes of these lines were found to be the same for both creep and repeated loading, but they were dependent on the sample stress history (OCR). The above data can be replotted using log strain rate versus deviator stress, and yields parallel lines at different times.

A method for predicting the strain rate in a cyclic test after a certain time (or number of cycles), using the results of creep tests, is given. The method is based on breaking the sinusoidal loading in a repeated test into a finite number of creep stress increments, obtaining the strain rate for each increment (from creep test plots of log strain rate versus deviator stress for given elapsed time), and finally taking the average value of strain rate as the sinusoidal strain rate. The method gave good predictions.

Finally, tests performed with rest periods between sets of loadings indicated no effect on the accumulation of plastic strain.

(16) Castro and Christian (1976), "Shear Strength of Soils and Cyclic Loading."

The authors discuss the effect of undrained cyclic shearing on subsequent monotonic strength, with no drainage allowed in between. While undrained cycling increases both pore pressure and strain, its effect on strength is not obvious. "It is completely misleading to compute the available undrained shear strength on the basis of the Mohr-Coulomb relation for effective stress from the values of effective confining stress

that exists in the soil immediately after cyclic loading. Such an approach ignores the changes in pore pressure that take place during undrained shear." Previous work indicates that subsequent undrained strength is much larger than what Mohr-Coulomb would predict, mainly because significant negative pore pressure changes occur during shearing.

Undrained stress-controlled cyclic triaxial tests with symmetric loading (zero average deviator stress), followed by undrained compressive monotonic tests (no drainage in between), were performed by the authors. Their results indicate that "the static undrained shear strength is equal to or very close to the static undrained shear strength for samples that failed without initial cyclic loading. Possible exceptions to this statement are sensitive clays and very loose sands." The results also indicate that "the modulus of deformation can be greatly reduced" by cycling, and that the effect of cycling must be included in estimates of deformations.

(17) France (1976), "An Investigation of the Effects of Drainage on the Repeated Load Behavior of Soils."

See summary of paper No. 20.

(18) Lee (1976), "Cyclic Strength of Outardes 2 Clays." Confidential Report.

See summary of paper No. 25.

(19) Mitchell and Douglas King (1976), "Cyclic Loading of an Ottawa Area Champlain Sea Clay."

The authors investigated the cyclic properties of Champlain Sea clay. The clay is highly sensitive (sensitivity=15 to 25), and has a liquidity index of unity. Block samples were used in undrained triaxial testing with back pressure. Static tests were performed at 0.5%/hour to establish the static failure envelope. Samples were consolidated isotropically for 24 hours prior to testing at effective confining pressures less than the preconsolidation pressure, therefore all samples tested were overconsolidated.

Most cyclic triaxial tests were loaded with $q_{ave}=q_c$, and most had values of $q_{max}=q_{ave} + q_c$ of 70% of static strength, at different consolidation stresses up to 88% of the preconsolidation stress. Most samples were cycled at 2 cycles/min and some at 15 cycles/min. The frequency of loading had a marginal effect on the behavior of similar samples. The number of cycles to failure is a function of the deviator stress level as well as the confining stress, and varied between 100 to 20000. "Failure under cyclic loading results from continued pore water pressure increases, causing a migration of the effective stress path until the failure envelope is attained." The rate of pore pressure increase depends on the "initial state of stress, the cyclic stress level, and the magnitude of the cyclic stress increment." Large distortional strains accompanied the pore pressure buildup to failure, and samples "appeared to reach an equilibrium stage (closed hysteresis loop in axial strains) between 500 and 1000 cycles, after which the strains increased until the samples failed.

The equilibrium conditions (no failure) under cyclic loading were

investigated by performing tests with q_c ranging between 25 and 55% of the static undrained strength, q_{max} not exceeding 70% of the static strength. The effective confining stress was varied between 15 and 88% of the preconsolidation pressure. All of these tests did not fail, but reached closed hysteresis condition of elastic equilibrium after more than 2000 cycles. "At low initial confining stresses, early increases in pore water pressure due to cyclic loading were followed by pore water pressure decreases prior to reaching an equilibrium condition." This behavior can be explained by the existence of two components of pore pressure: a decrease in pore pressure due to dilation caused by the closely spaced weakness planes in the soil, and an increase in pore pressure due to structural disturbance. "At higher confining stresses the pore water pressure increases gradually terminated, creating an equilibrium condition." The tests indicate that q_{max} of 70% of undrained static strength can be imposed on this sensitive soil without failure as long as q_c does not exceed 50% of static strength.

(20) France and Sangrey (1977), "Effects of Drainage in Repeated Loading of Clays."

Having recognized that drainage occurs in practical cyclic loading schemes, such as drainage between storms, the authors present a descriptive model for the response of clays subjected to repeated loading with drainage periods.

Cyclic triaxial compression tests were performed on laboratory sedimented and aged illite clay (PI=31%). Conventional undrained monotonic

compression tests on both isotropically normally consolidated and overconsolidated samples were done in order to provide a reference frame for dynamic behavior. Stress controlled multistage undrained cyclic compression tests were performed on isotropically normally consolidated samples. The test consists of cyclically loading the specimen at two or more successively higher deviator stress levels. At each level, cycling was applied until either failure occured or a state of nonfailure equilibrium was reached. Stress controlled semidrained cyclic compression tests were performed on isotropically normally consolidated, anisotropically normally consolidated, and isotropically overconsolidated specimens. This test consisted of repeatedly applying undrained load-unload cycles of constant deviator stress and allowing complete drainage of all residual pore pressures during the unload portions. Cycling was continued until either failure occured or a state of nonfailure equilibrium was reached. In all cyclic tests, the deviator stress was varied between a specified maximum value and a value which is essentially zero (for stability in the loading apparatus, a value of 4.9 kN/m^2 was applied instead of zero). It follows that the average component of deviator stress was equal to the cyclic component of deviator stress which equaled half of the maximum value of deviator stress. In semidrained tests, drainage periods were long enough for complete dissipation of excess pore pressures. No frequency of loading was mentioned, but the authors state that in the case of undrained multi-stage cyclic tests, "both the loaded and unloaded stresses were maintained for at least t_{95}...of the last consolidation increment." In the case of semi-drained cyclic tests, "the time intervals for loading, unloading and drainage were always at least equal to t_{95}...of the last consolidation increment." However, in both

kinds of tests, the loading intervals were reduced in later cycles when the pore pressure and strain response became more rapid.

Contractive soils. These are normally consolidated soils which tend to decrease in volume when sheared, and therefore produce positive pore pressures when sheared undrained. Isotropically as well as anisotropically normally consolidated samples were tested.

Multistage undrained cyclic compression tests confirmed the previous results of Sangrey et al. (paper No. 5), namely that undrained cycling below a "critical level of repeated loading" produces hysteretic nonfailure equilibrium. It was also found as reported by Sangrey et al. that "the peak points on the nonfailure stress path loops defined a straight equilibrium line...that intersected the failure envelope at the critical level of repeated loading" (in a Cambridge type p-q diagram). Based on the work of Sangrey et al., the critical levels of repeated loading were assumed to represent the remolded undrained compressive strengths of the soil, or critical state.

Semidrained cyclic compression tests on five isotropically consolidated samples reached a nonfailure equilibrium state. After 10 to 12 cycles, the residual pore pressures were almost zero and the peak pore pressures had declined to almost constant values. Also, the rate of strain and volume change accumulation decreased rapidly. After 5 cycles, the strain reached 80% of the total accumulated strain, and 70% of the total volume change had taken place. During the drainage phase, the excess pore pressures dissipate and lead to a decrease in water content. Subsequent monotonic shear of the specimens after reaching the equilibrium phase indicate an increase in undrained monotonic strength by about 30% over the original undisturbed undrained strength.

Semidrained compressive tests on two anisotropically consolidated specimens exhibited nonfailure equilibrium behavior. Their behavior is similar to the isotropically consolidated samples except that the increase in subsequent strength is only 15%.

In summary, for normally consolidated clay, "when drainage is introduced into the repeated loading history, the soil tends towards an equilibrium behavior as long as undrained failure does not occur prior to drainage." Also, "if drainage is allowed, the water content decreases and the undrained shear strength increases to the undisturbed strength at the new water content."

Dilative soils. These are overconsolidated soils that tend to increase in volume when sheared. Under undrained shearing, negative excess pore pressures are generated. Samples with OCR value of 8 were tested.

Semidrained cyclic compression loading tests were performed on six specimens of isotropically overconsolidated clay. The maximum deviator stress ranged between 40% and 88% of the undrained compressive strength. Failure was observed at the four highest stress levels, while nonfailure equilibrium occured at the others. These results indicate the existence of a critical level of semidrained repeated loading above which failure occurs, and below which there is equilibrium. By plotting the stress path on a Cambridge type p-q space, it appears that for OCR=8, failure occurs under semidrained conditions when the point corresponding to repeated loading failure lies above the normally consolidated failure envelope. On the other hand, nonfailure occurs when the peak point of the nonfailure hysteresis loop lies below the normally consolidated failure envelope. From this study, it appears that this level of critical repeated loading is given by the intersection of the undrained monotonic stress path for OCR=8

and the normally consolidated failure envelope.

(21) Herrmann and Houston (1978), "Behavior of Seafloor Soils Subjected to Cyclic Loading."

The authors present the results of cyclic triaxial tests on eight different soils. Five were deep marine soils, with water depths ranging between 1000 meters and 5400 meters, and were sampled using either the box core sampler or the piston core sampler. These marine soils range from clayey sand to clayey silt to silty clay to clay. The other soils included an artificially consolidated clayey silt, and San Francisco Bay Mud, a highly plastic clayey silt. Stress controlled undrained cyclic triaxial tests were performed on isotropically as well as anisotropically consolidated samples. Cycling was sinusoidal in nature with a frequency of 2 Hz., and was continued to 300,000 cycles or failure which is defined as axial strain greater than 10%. Cyclic tests with zero average stress deviator, having symmetrical stress reversals, as well as tests with non zero average stress deviator or "static bias", with or without stress reversal depending on the relative magnitude of the average and cyclic shear stress components. The average stress deviator was applied undrained, followed by undrained cyclic deviator stresses in the case of tests with static bias. Finally, monotonic undrained triaxial tests were performed under the same consolidation conditions in order to obtain the undrained static strength for normalization purposes.

Results of about 125 stress controlled consolidated undrained cyclic triaxial tests gave the following trends. Plots of axial strain versus the logarithm of the number of cycles indicate sudden failure in tests with

zero average deviator stress and a more gradual failure with gradual strain accumulation in tests where the average shear deviator stress is nonzero. This is due to the different nature of axial strain in both kinds of tests, cyclic axial strain in the case of zero average deviator stress, and cyclic+average axial strain in the case where the average deviator stress is nonzero. Tests that did not fail after 300,000 cycles show very small or zero strain accumulation. The number of cycles at failure was found to decrease as the cyclic stress level was increased.

In tests reaching failure, the secant modulus was found to decrease to small value, and in some case to almost zero. In tests that did not fail, the modulus decreases initially due to breaking of bonds between particles, followed by a subsequent modulus increase or stiffening. Plots of pore pressure versus the logarithm of the number of cycles indicate significant pore pressure increases as failure is approached.

Cyclic strain threshold values were identified for the various soils. The higher the plasticity, the larger the values of the threshold strain below which significant modulus degradation and failure will not likely occur. Stress levels (expressed as a percentage of the static undrained strength) as high as 50% average deviator stress and 25% cyclic deviator stress did not cause failure in 300,000 cycles. For plastic soils, strain accumulation was insignificant for specimens with average deviator stress less than 25% as long as the cyclic deviator stress is kept below 75%. These threshold values can be used in design to prevent excessive strains or failure.

(22) Koutsoftas (1978), "Effect of Cyclic Loads on Undrained Strength of

Two Marine Clays."

Fischer, Koutsoftas and Lu, in paper No. 12, presented results of cyclic tests on two marine clays. The author, in this paper, presents a summary of triaxial tests conducted to determine the behavior of the clay following a series of cyclic loadings.

One of the clays is "plastic" with a PI of 40%, a sensitivity ranging from 2 to 5, and an OCR ranging from 3.5 to 6. The second is a "silty clay" with a PI of 18%, a sensitivity between 8 and 10, and an OCR varying between 5 and 9. Tests were conducted on both normally consolidated and overconsolidated samples at OCR=4. The clays exhibited normalized behavior, and therefore, in order to minimize the sample disturbance, testing conformed to the SHANSEP technique. Normally consolidated samples were obtained by isotropically consolidating the specimens to 1.5 to 2 times the in situ preconsolidation stress. Overconsolidated samples were obtained by subsequent unloading to OCR=4. One cycle of secondary compression was allowed at the final consolidation stress, before shearing. Cyclic loading followed, and consisted of sinusoidally varying stress-controlled two-way loading at 1 Hz. All normally consolidated samples were subjected to a "cyclic stress ratio" of 75%, whereas all overconsolidated samples were subjected to a ratio of 50%, until a prescribed double amplitude strain developed. The cyclic stress ratio is defined here as q/s_u where s_u is the undrained shear strength from a consolidated undrained triaxial compression test. The specimens were then left to cure for 24 hours at zero shear stresses in order to allow the pore pressures to equilibrate. The specimens were then monotonically sheared undrained until failure occurred. A number of consolidated undrained static triaxial compression tests were performed in order to provide a

basis for interpretation. These specimens were cured for the same amount of time as the cyclic ones, prior to static shear, in order to account for the creep effects during the cure period.

The results for both clays indicate that "the undrained shear strength after cyclic loading decreases and the strain at failure increases as the double amplitude strain at the end of cyclic loading increases." Also, "at all stress levels, the secant and tangent moduli decrease significantly as the double amplitude strain at the end of cyclic loading increases." The results also indicate that "the excess pore pressures induced in normally consolidated specimens are larger than those for overconsolidated specimens." The author summarized the results on plots similar to those used by Thiers and Seed (paper No. 4). These are plots of cyclic strength ratio (strength after cyclic loading/static strength) versus cyclic strain ratio (peak cyclic strain/failure strain in static test). The plots indicate that as the strain ratio increases, the reduction in undrained shear strength increases. Whereas Thiers and Seed reported a large reduction in undrained strength for strain ratios exceeding 0.5 (up to 50% reduction for a strain ratio of 0.8), the author reports relatively small reductions (10%-20%) a large strain ratios (up to 0.8). This smaller reduction in strength is also confirmed by Castro and Christian (paper No. (15).

Having recognized that the excess pore pressures induced by cyclic loading cause a reduction in effective stress, which can be viewed as having an effect similar to that of overconsolidation, the author defines an overconsolidation ratio due to cyclic loading. OCR_{cy} equals the ratio of maximum effective stress before cycling to the effective stress measured after cyclic loading and immediately prior to undrained shear. Comparison

of the undrained shear strength ratio versus OCR plot as obtained from static tests with that of the undrained shear strength after cycling versus OCR_{cy} plot shows great similarity, and indicates that "excess pore water pressures induced during cyclic loading have an effect similar to that of overconsolidation."

Finally, the results indicate that there is a dramatic reduction in modulus with cyclic loading, as reported by previous researchers. This reduction in modulus is perhaps of much more practical significance than the reduction in undrained shear strength.

(23) Sangrey, Castro, Poulos, and France (1978), "Cyclic Loading of Sands, Silts and Clays."

Based on available laboratory data, the authors present a "behavioral model...based on critical void ratio and critical state concepts."

For contractive clays, "cyclic loading leads to failure when the excess pore pressures result in an effective stress condition at the cyclic limit state for the soil...Laboratory data indicate that the cyclic limit state coincides with the remolded strength state for clays." There is a "critical level for repeated loading" (CLRL) below which no failure occurs.

For dilative clays, "the rates of accumulation of strain are relatively small for maximum cyclic stress levels less than approximately 85 percent of the undrained compressive strength." The authors believe that "for dilative clays there are no data available indicating strength reduction or continuous deformation induced by cyclic loading at cyclic stress levels less than 90 to 100 percent of the monotonic undrained

compressive strength. Therefore, it appears that for dilative clays the undrained CLRL and the undrained shear strength after cyclic loading are approximately equal to the undrained monotonic shear strength."

(24) Gaskin and Abbo-Abedi (1979), "Repeated Compressive Loading of Leda Clay."

The authors present a study of the behavior of sensitive, weak, saturated Leda clay under undrained repeated compressive triaxial loading. The clay sensitivity ranges between 11 and 15, the plasticity index equals 46%, and the natural water content equals 91% well above the liquid limit of 66%. Repeated triaxial loading was performed drained at a frequency of 1 Hz., on isotropically consolidated specimens obtained from block samples. The repeated axial stress difference or stress deviator varied between zero and a specified maximum value (the average component of stress deviator equals the cyclic component), and cycling was continued until failure or 100,000 cycles were reached.

An axial stress difference factor was introduced, and is defined as the ratio of the repeated axial stress difference to the axial stress difference that causes failure in a static drained test at the same confining pressure. A threshold axial stress difference factor was observed and equals 54%. Stress difference factors above 54% caused the rate of permanent axial as well as volumetric strains to increase until failure occurred. Failure was sudden with a well defined failure plane. At failure, permanent axial strains were small and less than 2%, and the permanent volumetric strains were smaller than 0.15%. Values of axial stress difference factors below 54% resulted in no sudden failure up to

100,000 cycles, and permanent deformations continued to increase. Plotting the permanent axial and volumetric strains versus the stress difference factor for all the tests indicates the following. At about the threshold stress factor, the axial and volumetric strains are similar which indicates no lateral strain. Below the threshold, the lateral strain was compressive (decrease in diameter), and above the threshold, the lateral strain was negative (increase in diameter). Such a plot can be used to give a good definition of the threshold stress value.

Plots of resilient modulus (or stress difference divided by recoverable strain) versus cycle number at various stress difference factors were presented. For each test, the modulus dropped slightly first before increasing to an almost constant value at 100,000 cycles. A nonlinear relationship was given between the stress difference factor and the resilient modulus at 100,000 cycles for values of stress difference below the threshold.

As mentioned earlier, soils that were cycled above the threshold stress failed without much volume change. This can be explained by the fact that, even though the tests were carried out under drained conditions, dissipation of excess pore pressures during the early cycles would have been minimal at a frequency of 1 Hz. for such a low permeability soil. For stress factors above the threshold, failure was probably induced by excessive buildup of pore pressures as evidenced by the fact that volumetric strains at failure were small, of the order of 0.1%, indicating that a great portion of the applied stresses were carried by the pore pressure. For stress levels below the threshold, the initial increase in pore pressure is not large enough to cause failure, and dissipation occurs after continued cycling.

Leda clay has a flocculated structure with cementation bonds at the particle contacts. In early cycles, part of the cementation is broken, leading to a more deformable structure, which explains why the resilient modulus decreases first at very small volume changes. The increase in modulus is observed after appreciable volumetric compression, and was probably due to the particles coming closer together, thus increasing the stiffness.

(25) Lee (1979), "Cyclic Strength of a Sensitive Clay of Eastern Canada."

The author presents a summary of a comprehensive cyclic testing program on very sensitive Champlain clays (sensitivity index between 380 and 35). Specimens were obtained from block samples from two distinct locations.

Cyclic triaxial undrained tests on isotropically and anisotropically consolidated samples were performed, as well as undrained simple shear tests. In triaxial tests, both clays failed by liquefying along one or more thin well defined shear planes after reaching single amplitude cyclic strains between 2% and 6%. The failed specimens remained strong, firm, and brittle away from the shear plane. This failure mechanism (development of a shear plane) is in contrast with the behavior of less sensitive clays which fail by bulging or necking after accumulating strains. The author states that the traditional definition of failure (3% single amplitude cyclic strain) is consistent with the failure definition based on development of shear planes to within a few cycles difference.

The results indicate that cyclic strength decreases as the loading becomes more nearly symmetrical in nature. Also, the cyclic strength

obtained from both the simple shear and the triaxial test are almost identical, as reported by Thiers and Seed (1969).

Static loading tests, on samples which were subjected first to cyclic undrained loading without failure, indicated subsequent static strength close to 80% of the undisturbed monotonic value.

(26) Andersen, Pool, Brown, and Rosenbrand (1980), "Cyclic and Static Laboratory Tests on Drammen Clay." See Chapter 2.

(27) Matsui, Ohara and Ito (1980), "Cyclic Stress-Strain History and Shear Characteristics of Clay."

The authors present results of undrained stress-controlled cyclic triaxial tests on normally and overconsolidated clays. Cycling is performed by varying both the vertical stress and cell pressure so as to keep the mean total principal stress constant. This makes pore pressure interpretation more convenient since it eliminates the contribution, to pore pressure generation, of the isotropic stress component. The pore pressure generated during cycling is only due to deviatoric stress changes. During cycling, the stress deviator varies between + or - 1.5 times the peak change in vertical stress (symmetrical two way loading, with zero average deviator stress). The clay used was Senri clay, with PI of 55%. The samples were prepared by remolding above the liquid limit in a large container. Normally consolidated samples were prepared by isotropic consolidation for 1 day under the desired stress. Overconsolidated samples were isotropically consolidated then rebounded for 1 day to the desired

OCR. The samples were backpressured to ensure saturation.

The testing program investigated the effects of various parameters. A summary of the results is presented below.

The effect of loading frequency on excess pore pressure and strain was obtained by conducting four tests on normally consolidated samples at frequencies ranging from 0.2 to 0.5 Hz. (or periods ranging from 2 to 50 seconds) at the same cyclic stress ratio (+ or - 42%). The results indicated that for a given number of cycles, higher excess pore pressures and axial strains are generated at lower frequencies. The clay exhibits normalized behavior in cyclic loading, and the effective confining pressure has no effect on the pore pressure versus number of cycles relationship.

The effect of cyclic shear stress ratio on excess pore pressure generation was investigated for both normally and overconsolidated clay samples. It was found that the pore pressure increases more rapidly with increasing cyclic stress ratio. For normally consolidated Senri clay, there exists a lower bound for the cyclic stress ratio equal to 20% (single peak amplitude) below which no pore pressure develops (same as for Drammen clay). The results of overconsolidated clays are similar in trends except that for OCR=2, negative pore pressures develop in early cycles and increase gradually to positive values. The effect of the overconsolidation ratio was also determined, and the higher the OCR, the more negative the pore pressure at early cycles, and the less positive at larger number of cycles. At OCR values less than 1.5, negative pore pressures are negligible. The residual excess pore pressure was found to increase with increasing maximum cyclic shear strain and with decreasing OCR, and a formula expressing this relationship was given.

The authors recognize that undrained cycling leads to an increase in

pore pressure, therefore to a decrease in effective stress, define an equivalent overconsolidation ratio due to cycling. By running monotonic tests on previously cycled normally consolidated samples, without drainage of the residual pore pressure, the authors conclude that overconsolidation due to cycling is similar in strength to tradiational overconsolidation (same results as Koutsoftas, paper No. 21). By running monotonic tests on previously cycled normally consolidated samples, after allowing drainage of the residual pore pressure, it is concluded that in spite of the temporary loss of strength and modulus immediately after cyclic loading, the dissipation of pore pressures leads to a higher strength and modulus than initially. This implies that cyclic stress-strain history can be one of the factors causing natural deposits to become lightly overconsolidated.

(27) Dyvik and Zimmie (1981), "Strain and Pore Pressure Behavior of Fine Grained Soils Subjected to Cyclic Shear Loading." See Chapter 2.

(28) Selig and Chang (1981), "Soil Failure Modes in Undrained Cyclic Loading."

The authors describe the various cyclic triaxial tests which include two main categories, one in which the cyclic deviator stress is symmetrically varied around an isotropic stress state (zero average shear stress), and another in which the cyclic deviator stress is symmetrically varied around an anisotropic non-zero stress state. In the anisotropic case, the cyclic deviator stress can be greater than the average deviator stress in which case shear stress reversal occurs, or the cyclic deviator

stress can be less than the average deviator stress with no shear stress reversals. The strain and pore pressure behavior of a saturated soil element subjected to undrained cyclic loading depends upon which of these three categories the tests is being conducted. Using experimental data from other references, and mainly from triaxial tests on sand samples, the authors offered the following conclusions. Failure can be defined by a specified magnitude of strain in the sample. Two distinctly different failure modes occur, the first is by increased cyclic strain and the second by increased permanent strain. Shear stress reversal is the governing factor, and the permanent shear strain failure mode governs when no shear stress reversals occur. The pore pressures generated during cycling with shear stress reversals were larger than those generated during cycling without stress reversals. Only for the case of shear stress reversal can the pore pressure ratio reach 100%, and thus the effective stress reach zero.

(29) Goulois (1982), "Contribution to the Study of Tension Piles Under Cyclic Loading." See Chapter 2.